MONITORING AND PREDICTION OF DAMAGE IN FILAMENT WOUND COMPOSITE PIPES UNDER PRESSURE LOADING

by

Guillermo Ramirez, B.S., M.S.E.

Dissertation

Presented to the Faculty of the Graduate School of

the University of Texas at Austin

in Partial Fulfillment

of the Requirements

for the Degree of

Doctor of Philosophy

The University of Texas at Austin

May, 1999

MONITORING AND PREDICTION OF DAMAGE IN FILAMENT WOUND COMPOSITE PIPES UNDER PRESSURE LOADING

Approved by
Dissertation Committee:

To my Father

To my Mother

To my brother and sister

ACKNOWLEDGEMENTS

At the end of a long trek as this doctoral work was, it is difficult to place a value or recognition to all the people that helped in the process. There are always small details, people and situations that make life and work bearable, and that cannot be credited in all fairness. My stay in Austin was a combination of a large number of very good times and, a few bad times. Both combined to make this part of my life one of the most creative and memorable experiences that I will miss with all my heart.

One of the best friends I made in this time was my supervisor Michael D. Engelhardt. I cannot say enough about his professionalism as a teacher, researcher and engineer that is not already known in the field. I can however, say praises about his personality and class, probably the two strongest and most important traits that any person can wish. I can only hope that I will be able to treat my students with the same dedication and style he showed me. I cannot think of a better legacy of a supervisor to a student than the one that he has passed on to me. To Dr. Karl Frank who helped me, along with Dr. Engelhardt, to understand what integrity in work and research mean. Dr. Frank helped me learn to look at data with an honest eye to conclude only what it really showed, and not what I wanted so desperately to see. To my brother Dr. Julio Ramirez, I have always been very proud of you and your example, I hope this is an indication of how much.

To my special friends Paul Ziehl and Yajai Promboon, two of the smartest people I have ever meet. I have no words that will clearly express how I feel about our friendship and what you have meant to me. Paul helped remind me how much fun life can and should be. Even in the most difficult times, he managed to pull me out of the frustration with pearls of wisdom about life and relationships that unfortunately cannot be replicated here. Yayai, there is nothing I can say that you already do not know. Thank you for showing me how perfect life can be for me. I wish you good luck and happiness.

To my good friends: Trey Hamilton, Todd Helwigg, John Myers, Shawn Gross and Jenny Gross, Reagan Herman, Jeff West, David Jauregui, John Grove and Charlie-Andy

Barnes, I will miss not been around them all the time. The help of the other members of the doctoral committee, Dr. Jose Roesset, Dr. John Tassoulas, Dr. Richard Shappery and Dr. Fowler is also greatly appreciated. The help and friendship of my two undergraduate assistants Mark Clarke and John D. Nelson will always be remembered and appreciated. To the Ferguson Lab staff, quite a unique grouping of individuals, also thanks are due. Blake and Wayne, who make all the difference at FSEL, thank you very much.

Last, but obviously not least, my family. Mother Martha, sister Maine, brother Julio and nephews (Erika and Ses), I could not have asked for a better moral and personal support.

To my Dad, who I miss so much and hope that is seeing this from heaven and smiling.

Guillermo Ramirez
Austin, Texas May 1999

MONITORING AND PREDICTION OF DAMAGE IN FILAMENT WOUND COMPOSITE PIPES UNDER PRESSURE LOADING

Publication No. _____

Guillermo Ramirez, Ph.D.
The University of Texas at Austin, 1999

Supervisor: Michael D. Engelhardt

A number of pressure loading tests were conducted on large-scale filament wound composite pipes. The objective of the program was to assess the effectiveness of existing failure criteria in predicting several limit states and to develop methods based on nondestructive evaluation techniques to monitor damage growth and predict residual capacity of composite pipes. The program consisted of internal pressure tests under static and fatigue pressure loading on specimens constructed following the ASME RTP-1 specifications for pressure vessels for corrosive or hazardous fluids. An external pressure test on a full-scale specimen constructed of carbon fiber was also part of the program. Finally,

a series of impact tests on fiberglass pipe specimens were also performed. Acoustic emission (AE) and other nondestructive evaluation (NDE) monitoring techniques were used as part of the program. The AE method was selected for further study because of its applicability to existing structures and relative economy in its use. Results of the program indicated that AE may be used as a tool for predicting fatigue endurance of pressure vessels under internal loading. In addition, acoustic emission showed promising results as a tool for predicting residual capacity on impact damaged fiberglass pipes. In the external pressure (collapse) portion of the test program, AE monitoring presented with supporting and additional information for the interpretation of other measured data during a test where visual inspection at the time of loading was not possible. An analytical phase followed the experimental tests, in an effort to evaluate existing tools and their accuracy in predicting measured behavior. Results of the analysis are compared to the measured responses and limiting factor in their applicability are enumerated.

ACKNOWLEDGEMENTS

At the end of a long trek as this doctoral work was, it is difficult to place a value or recognition to all the people that helped in the process. There are always small details, people and situations that make life and work bearable, and that cannot be credited in all fairness. My stay in Austin was a combination of a large number of very good times and, a few bad times. Both combined to make this part of my life one of the most creative and memorable experiences that I will miss with all my heart.

One of the best friends I made in this time was my supervisor Michael D. Engelhardt. I cannot say enough about his professionalism as a teacher, researcher and engineer that is not already known in the field. I can however, say praises about his personality and class, probably the two strongest and most important traits that any person can wish. I can only hope that I will be able to treat my students with the same dedication and style he showed me. I cannot think of a better legacy of a supervisor to a student than the one that he has passed on to me. To Dr. Karl Frank who helped me, along with Dr. Engelhardt, to understand what integrity in work and research mean. Dr. Frank helped me to look at my data with an honest eye to conclude only what it really showed, and not what I wanted so desperately to see. To my brother Dr. Julio Ramirez, I have always been very proud of you and your example, I hope this is an indication of how much.

To my special friends Paul Ziehl and Yajai Promboon, two of the smartest people I have ever meet. I have no words that will clearly express how I feel about our friendship and what you have meant to me. Paul helped remind me how much fun life can and should be. Even in the most difficult times, he managed to pull me out of the frustration with pearls of wisdom about life and relationships that unfortunately cannot be replicated here due to censorship.

Yayai, there is nothing I can say that you already do not know. Thank you for showing me how perfect life can be for me. If only for a few moments, I was the happiest person alive. I wish you good luck and happiness.

To my good friends: Trey Hamilton, Todd Helwigg, John Myers, Shawn Gross and Jenny Gross, Reagan Herman, Jeff West, David Jauregui, John Grove and Charlie-Andy Barnes, I will miss not been around them all the time. The help of the other members of the doctoral committee, Dr. Jose Roesset, Dr. John Tassoulas, Dr. Richard Shappery and Dr. Fowler is also greatly appreciated. The help and friendship of my two undergraduate assistants Mark Clarke and John D. Nelson will always be remembered and appreciated. To the Ferguson Lab staff, quite a unique grouping of individuals, also thanks are due. Blake and Wayne, who make all the difference at FSEL, thank you very much.

Last, but obviously not least, my family. Mother Martha, sister Maine, brother Julio and nephews (Erika and Ses), I could not have asked for a better moral and personal support. To my Dad, who I miss so much and hope that is seeing me from heaven and smiling.

That is it Mom! no more school after this. Can I start dating now?

TABLE OF CONTENTS

LIST OF TABLES

LIST OF FIGURES

CHAPTER 1

INTRODUCTION AND BACKGROUND

The recent drop in demand for composite materials in the aerospace and defense industries has helped increase research efforts to find suitable applications for composites in other fields. One such field is the oil and gas industry where composite materials may provide several advantages over more traditional construction materials [1.1]. Adaptation of composite materials to offshore applications has been the subject of several studies in the US and abroad. Some of the potential advantages offered by composites to the oil industry are:

i. Corrosion resistance

ii. High strength-to-weight ratio

iii. Fatigue resistance characteristics

iv. The ability to tailor the material combinations to the structural and geometrical demands

Corrosion resistance and damage repair is a costly aspect of maintenance of offshore platforms. In addition, the recent move towards deep-water exploration has made composites a more attractive option to the traditional materials. Even though the offshore industry had been using fiberglass composites in secondary structural applications for more than 30 years, it is only until recently that the use of advanced composites for primary structures has been studied.

1.1. APPLICATIONS OF COMPOSITE TUBULARS IN OFFSHORE STRUCTURES

Table 1.1 shows a comparison of material densities normalized to the density of steel. As can be seen, some of the most common combinations of composite materials

are from 4 to 6 times lighter than steel. In addition, the strength of the fibers per unit area is on the order of 5 to 10 times greater than steel depending on the fiber used.

The lightweight of composites may offer important advantages in the case of tension leg platforms and other moored compliant structures. In general, savings of a ton of component weight will result in a two-ton saving in the rest of the structure [1.1]. Lighter structures require smaller forces and foundation components to stay buoyant.

Some potential applications of composite materials in offshore structures include, but not limited to:

Material description	*Normalized Density to Steel*
Steel	1.00
Kevlar/Epoxy	0.17
Glass/Epoxy	0.24
Graphite/Epoxy	0.20

Table 1.1 Material density comparison

i) Composite tethers - These are ropes fabricated mainly through the pultrusion method. All fibers are aligned parallel to their axis to provide high axial stiffness and strength.

ii) Composite production riser - Smaller diameter tubing located inside a larger tube (riser) carry oil and gas to the platform. In addition to their lightweight, the lower axial stiffness may be use to eliminate the need of the tensioners on the platform.

iii) Composite drilling riser - Drilling in deep water is conducted using heavy drill pipe that is rotated inside a drilling riser. This is another potential candidate for using composites to reduce weight.

iv) Composite tubing - Composites can be designed to provide near zero thermal expansion coefficients. By using different winding angles in the fabrication process composites can be tailored so that extreme changes in temperature can be tolerated by the tubing without significant deformations.

v) Glass Reinforced Plastic (GRP) cores sample tube - Once again the lightweight nature of the composite plays and important part in the selection process. It is important during exploratory drilling to retrieve undisturbed core samples of the rock formations. The lightweight property makes GRP core sample holders easier to handle.

vi) Mooring rope - Changing the mooring ropes from steel to a material like Kevlar™ and other synthetic materials may permit increasing the water depth at which these platforms operate.

vii) GRP facilities - In general, the offshore industry is exploring the use of materials that provide a combination of properties that will result in reduced maintenance costs and weight savings. Because of their chemical inertness, composite materials present possible advantages to corrosion and material handling challenges of the oil industry. In the past, the use of GRP components has been a common situation for the industry in the form of line pipes, downhole tubing, storage tanks, gratings etc. Finally environmental concerns steer the industry towards the use of materials that will minimize the use of chemicals such as the corrosion inhibitors required to protect steel components.

1.1.1. NEED FOR LARGE SCALE TESTING

As suggested by the listing above, many of the possible applications of composites in the offshore industry are in the form of a tubular section. Further, many material characterization tests on composites are often made on tubular samples for a well-defined state of stress and the elimination of edge effects. Due to the high cost in the material and fabrication of research specimens, much of the research geared towards specific applications has been performed on small-scale thin walled specimens. Previous work has shown that there can be scale effects in composite material specimens and components [1.21]. In order to achieve an adequate level of confidence in test results for use in design of prototype structures, large-scale specimens are needed. Also, in

order to accurately calibrate analytical models to results of test of small-scale specimens it is necessary to quantify this scaling effect.

1.2. TESTING APPROACHES

1.2.1. MATERIAL CHARACTERIZATIONS TESTS

ASTM provides a number of test standards for material characterization of fiber reinforced composite elements. The following table shows the most common of the ASTM standards in material characterization tests:

MATERIAL CONSTANT REQUIREMENTS BY ASTM

Constant name	Symbol	ASTM Specification	Comments
Longitudinal modulus	E_L	ASTM D3039	The modified version of this standard allows the use of a tubular specimen
Transverse modulus	E_t	ASTM D3039	Tubular specimen may me used also.
Major Poisson ratio	ν_L	ASTM D3039	Tubular specimen may me used also.
Shear modulus	G	ASTM D3518	Tubular specimen may me used also.
Longitudinal Tensile strength	X	ASTM D3039	Tubular specimen may me used also.
Longitudinal compressive strength	X_c	ASTM D3410	No modifications to standard for use of tubular specimens
Transverse tensile strength	Y	ASTM D3039	Tubular specimen may me used also.
Transverse compressive strength	Y_c	ASTM D3410	No modifications to standard for use of tubular specimens

Shear strength	S	ASTM D3518	Tubular specimen
Longitudinal tensile strain limit	X_ε	N/A	X / E_L
Longitudinal compressive strain limit	$X_{c\varepsilon}$	N/A	X_c / E_L
Transverse tensile strain limit	Y_ε	N/A	Y / E_T
Transverse compressive strain limit	$Y_{c\varepsilon}$	N/A	Y_c / E_T
Shear strain limit	S_ε	ASTM D3518	or S/G for elastic limit
Testing of Pressure vessels in Tension	General	ASTM D2585	Size limitations on specimen are enforced; good for biaxial tension loading.
Testing of Pressure vessels in Compression	General	ASTM D2586	Requirements on maximum specimen size and profile

Table 1.2 ASTM test methods for composites

Development of new test methods is continuing and there are several initiatives underway to establish a consistent set of procedures that will be applicable to a wide range of materials. One of these agencies is the CRAG in England (Composite Research Advisory Group). Their procedures are awaiting a validation program before formal adoption. The following table shows a list of these procedures.

Shear Test Methods	Method 100	Interlaminar Shear Strength
	Method 101	In-plane shear strength and modulus
	Method 102	Lap shear strength
Flexural Test Methods	Method 200	Flexural strength and modulus
Tensile Test Methods	Method 300	Longitudinal tensile strength and modulus of unidirectional composites
	Method 301	Transverse tensile strength and modulus of unidirectional composites
	Method 302	Tensile strength and modulus of multidirectional composites

	Method 303	Notched tensile strength of multidirectional composites
Compression Test Methods	Method 400	Longitudinal compression strength and modulus of unidirectional composites
	Method 401	Longitudinal compression strength and modulus of multidirectional composites
	Method 402	Notched compression strength of multidirectional fiber composites
	Method 403	Residual compression strength of multidirectional composites
Methods of test for fatigue properties	Method 500	Test specimens for the measurement of fatigue properties
Methods of test for toughness	Method 600	Interlaminar fracture toughness
Methods of test for bearing properties	Method 700	Bearing properties of multidirectional composites
Physical Test Methods	Method 800	Density
	Method 801	Coefficient of linear thermal expansion
	Method 802	Outgassing properties
Environmental effects	Method 900	Background information on environmental effects
	Method 901	Diffusivity properties
	Method 902	Conditioning under hot/wet environments
Miscellaneous Tests	Method 1000	Fiber volume fraction
	Method 1001	Void volume faction by ultrasonic scanning

Table 1.3 CRAG test methods [1.8]

1.2.2. TEST STANDARDS FOR COMPOSITE TUBULAR STRUCTURES AND COMPONENTS

Testing of large-scale composites has been governed by the agencies associated with their intended application. Unfortunately, most of the tests prescribed are directed towards proofing for their target design loads rather than behavior characterization. For this, they can only serve as a starting point when structuring a testing program for

tubular composites. In addition, most of the applications to date for the composite tubulars has been centered around pressure vessels. Conditions of external and internal pressure are covered by these agencies. However, less is covered for the case of more complex loading conditions.

Common sources of information for design and testing of tubular and pressure vessel specimens are:

- **The American Society of Mechanical Engineers (ASME) Pressure Vessel Code, Section X, "Fiber Reinforced Plastic Vessels"** [1.3]**.** This particular Section applies for pressure vessels containing non dangerous fluids with a maximum pressure of 3000 psi

- **ASME RTP-1, "Reinforced Thermoset Corrosion Resistance Equipment"** [1.6]**.** In essence, this code covers the design of "one of a kind vessels" that do not fall within the purview of other sections or codes. There is nevertheless a scope of application for this code in the maximum pressure that these vessels can hold. That is 15 psig internal pressure plus hydrostatic head or 15 psig of external pressure.

- **American Water Works Association Standard C950, "Fiberglass Pressure Pipe"**[1.4]**.** This code applies for water pipes with maximum pressures of equal or less of 250 psi.

- **API (American Petroleum Institute) Specs 15LR, 15HR and, 15TR** [1.5]. The letter acronyms stand for low pressure (LR), high pressure (HR) and, tubing (TR). The largest limitation of this standard is that it was developed and accepted for pipes of no more than 4.5" in diameter.

- **ASTM D 2992, "Obtaining Hydrostatic or Pressure Design Basis for Fiberglass Pipe and Fittings,"** and **ASTM D 2837, "Obtaining**

Hydrostatic Design Basis for Thermoplastic Pipe Materials.“ [1.7] These Standards were developed for thin walled pipes.

A final source still in development at the time of writing is the **“Military Handbook of Polymer Matrix Composites**”, Department of Defense, Vol. 1 and Vol. 2 [1.9]**.** Although, still largely in the development phase, this handbook is a compendium of the most common testing standards in composite materials. When finished, it should provide with a thorough database in testing procedures and material characterization approaches.

As is can be noted in all of theses codes and standards, most of the information available is on thin walled specimens. This does not preclude the standards from being a reliable starting point in the development of a testing program.

1.2.3. ISSUES IN SPECIMEN GRIPPING, REINFORCING AND, SEALING

A key difficulty encountered when testing thick walled tubular composite specimens is providing adequate grips at the ends of the tube for application of load to the specimen. The grips typically introduce stress concentrations that can cause premature failure of the specimen at the grip location, and consequently make interpretation of test results difficult. A similar problem is encountered when sealing the tube ends for internal or external pressure tests. Stress concentrations can develop at the seal locations causing the specimen to fail prematurely at these locations. To alleviate problems associated with stress concentrations at grips and seals, specimen ends are often reinforced.

Methods to properly grip, seal and reinforce the ends of composite tubular members have been developed for thin walled specimen [1.10]. However, such methods are not well developed for thick walled specimens. Consequently, developing appropriate grips, seals and end reinforcing can pose a significant challenge in testing of thick walled composite tubular specimens.

1.3. MEASUREMENTS AND INSTRUMENTATION

Instrumentation used for testing fiber composites often differs from that used for testing metals or other materials. Conventional instrumentation, such as foil strain gages, is frequently used. However, other less conventional types of instrumentation and measurement systems can often provide additional valuable insights into the behavior and response of fiber composites. This includes items such as acoustic emission monitoring, thermal emission monitoring, leak detection monitoring, and others. Following is a brief description and discussion of some of the key instrumentation and measurement systems that can be used when testing composites.

1.3.1. FOIL STRAIN GAGES

The use of foil strain gages is a common technique for instrumenting composite components and materials. Such gages can provide reliable information on the strains at the surface of the component where the gage is mounted, are relatively inexpensive. A limitation of strain gages is that they only provide data on surface strains. For thick walled specimens, significant strain gradients can occur through the thickness of the wall, which cannot be measured by surface mounted gages. An additional limitation on the use of strain gages is that they may not provide a reliable indication on the development of important damage mechanisms in the composite. For example, as a composite is loaded, damage mechanisms such as matrix cracking and delamination can occur. In some cases, these events may have a relatively small effect on the specimen's stiffness, and therefore may be quite difficult to detect from strain gage data. To detect the development of such forms of damage as a composite is loaded, other measurement techniques, such as acoustic emission monitoring, may be more useful. Nonetheless, strain gages can still provide a great deal of useful information on the response of a test specimen.

In general, the use of strain rosettes (either 120^o or 45^o) are preferred in composite materials in order to characterize the complete state of strain at a point. Also, the use of a relatively viscous epoxy bonding agent is preferred when installing the gage. The surface of fiber reinforced composite elements may have pronounced ridges and valleys. Strain gages must be placed on smooth flat areas to ensure good bond to the material. A common solution is the use of an initial layer of the same epoxy to be used to attach the strain gage. This epoxy will fill whatever valleys and voids are present at the surface and can later be sanded to a flat smooth finish without damaging the fibers of the composite. Whenever preparing the surface of the composite care must be exercised to avoid damaging the outermost fibers. Strain gage manufactures have technical literature on the use of foil gages on composite materials. An example of such literature is Ref 1.12.

1.3.2. ACOUSTIC EMISSION MONITORING

Acoustic emission (AE) is the elastic energy released by materials when they undergo deformation. This energy release results in transient elastic waves that propagate through the material and are detected by sensors mounted on the surface of the material. In composites, acoustic emission can be caused by a number of mechanisms, including fiber fracture, fiber-matrix debonding, matrix crazing and cracking and delamination.

One of the principal advantages of AE is the ability to monitor a large area in a short amount of time and with a limited number of sensors. Figure 1.1 AE sensors monitoring a pipe specimen. The number of sensors and location is dependent on the information sought during testing. Unlike ultrasonic scanning, where a single transducer is mechanically scanned over the structure, an array of AE sensors once installed can be used instantly to survey the entire component. In addition, the sensors can be left in place during loading stages of the test.

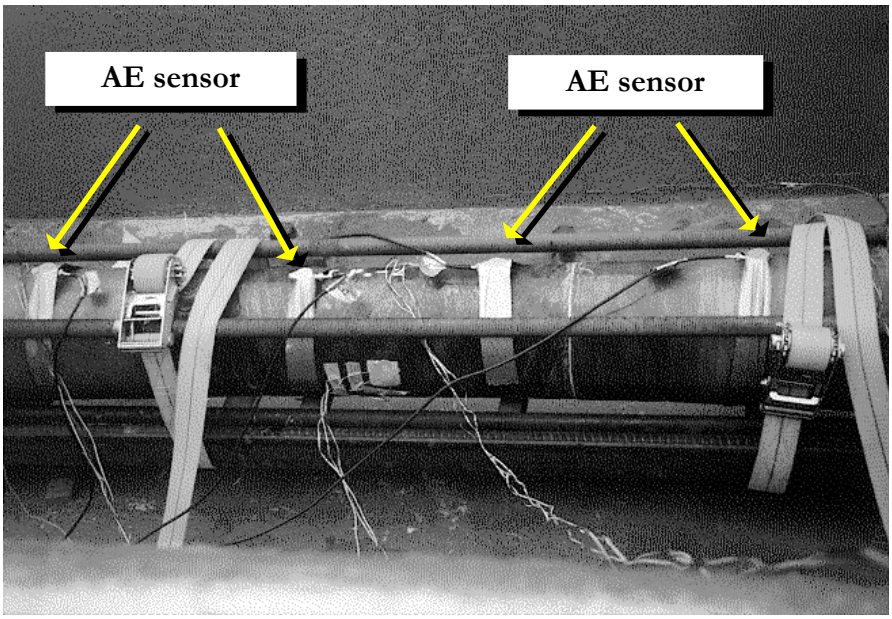

Figure 1.1 Typical acoustic emission sensor layout

Some of the most common terms associated with Acoustic Emission and as defined by the Committee on Acoustic Emission from Reinforced Plastics (CARP) and that will be consistently referred to here are:

- Acoustic Emission Count (count, emission count) – The number of times the acoustic emission signal exceeds a preset threshold during any selected portion of the test

- Acoustic Emission Event (event, emission event) – A local material change giving rise to acoustic emission (ASTM E 1316)

- Acoustic Emission Signal Amplitude – The peak voltage (measured in decibels) of the largest excursion attained by the signal waveform from an emission event (ASTM E 1316)

- Acoustic Emission Source – See event

- High Amplitude Hits – Hits having an amplitude greater than or equal to the reference amplitude threshold

- Historic Index – A measure of the change in signal strength throught a test. And it is defined by the formula:

$$H(t) = \frac{N}{N-K}\left(\frac{\sum_{i=K+1}^{N} Soi}{\sum_{i=1}^{N} Soi}\right)$$

Where

N ~ Number of hits up to time (t)

$S_o i$ ~ Signal strength of i^{th} hit

for composites, the value of K is defined by the following table [3.13, 3.14]:

# OF HITS	**K**
Less that 100	Not applicable
101 to 500	0.8 * N
> 500	N - 100

The values for K change depending on the type of material in question, the ones shown here are specifically for composite materials.

- Hit duration (duration) – The time from the first threshold crossing to the last threshold crossing of the signal or envelope of the linear voltage time signal. Hit duration does not include the hit definition time at the end of a hit.

- Intensity – A measure of the structural significance of an acoustic emission source. An intensity analysis compares the change in signal strength throughout the test (historic index) with hits having large signal strength values (severity). For purposes of analysis, intensity can be measured per channel basis or as a group.

- MARSE – Measured area of the rectified signal envelope. A measurement of the area under the envelope of the rectified linear voltage time signal from the sensor (ASME Section V, Article, 12).

- Signal Strength – The area under the envelope of the linear voltage time signal from the sensor. The signal strength will normally include the absolute area of both the positive and negative envelopes. For purposes of this dissertation, MARSE was used as the approximation of signal strength

- Severity – A measure of hits having large signal strength values. Severity is the average signal strength for a predefined number of hits having the largest numerical value of signal strength. The formula used to define the values of severity is as follows:

$$S_r = \frac{1}{J}\sum_{m=1}^{m=j} S_{Om}$$

Where:

S_{om} is the signal strength of the **m***th* hit. **m** is ordered on the magnitude of the signal strength with m=1 being the hit having the largest signal strength. **J** is an empirical derived constant that depends on the material. For composites, **J** is as shown in the following table

# OF HITS	J
< 20	Not applicable
> 20	20

Other definitions will be presented as necessary during the course of this dissertation. However, as a final point in the description of commonly used terms in acoustic emission, Figure 1.2 shows a typical waveform for a resonant sensor and the common features extracted from it.

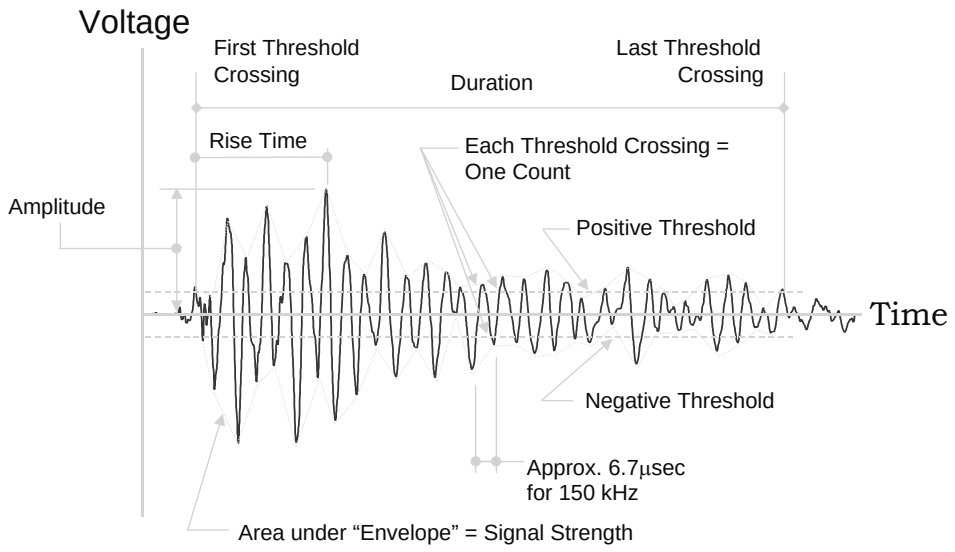

Figure 1.2 Common AE features from captured signal

Part of the evaluation process for AE data is developed based on the loading profile used in the monitoring. In the case of composite materials, differences on the emission obtained during the first time loading, subsequent loading and, emissions

during load holds are correlated with extent of damage, damage progression and serviceability levels of the structure being tested.

Loading profiles selected for AE monitoring take into account behavioral aspects of composite structures. Typically, composite structures have several possible sources of emission. In some cases, these sources are not directly related to the main structural performance of the system but more to initial redistribution of load paths in areas of discontinuities, or in some cases in the general body of the structure. In order to evaluate the importance of the AE records obtained during loadings, the profiles have several instances of load holds and load drops. Previous work has shown that the use of a stepped loading profile with load drops and holds will allow for the proper identification of critical AE in a structure. The possibility exist that emission during a first loading is the result of a "shakedown" of the structural component, and the creation of alternate load paths in the structure. Therefore, evaluation of AE data from first loading is sometimes ignored when compared to subsequent loadings in the evaluation of structures using AE. This is recognized by Codes and Specifications [1.2, 1.3], which allows the use of AE technique for the inspection of structures.

The development of high sampling rate digitizing cards small enough to fit on a PC system has provided the acoustic emission technology with an economical option. This is that not only can you extract the features from an analog signal captured by the sensors, but also you can digitize the complete waveform associated with the signal for later analysis. The use of broadband piezoelectric sensors, or sensors that have a flat response through a range of frequencies has also being explored for AE analysis. This allows for the analysis of the frequency content of the generated waveform in the material. This additional information however, comes with a price in the associated sensitivity of these broadband sensors when compared to single frequency resonant sensors. This loss of sensitivity is typically in the order of 12 to 18 dB. In an effort to improve the sensitivity of sensors capturing broadband information, new developments have been produced in the area of optical sensors. These are laser based sensors that measure the surface deformations produced by the traveling waves in the material and

that do not suffer of the lower sensitivity of the piezoelectric sensors when compared to narrow band resonant sensors.

1.3.2.1. GEOMETRIC AND PHYSICAL LIMITATION OF AE

There are, of course, limitations to AE applicability to composite materials. Although AE can detect fiber breakage and other events, determining the location of these events is difficult. Although theoretically plausible, precise source location is impractical in full-scale specimens, even within highly controlled laboratory environments. Current research is addressing methods for improved source location. At present, however, determining the approximate location of AE sources in the general vicinity of sensors is the best that can usually be accomplished.

There is a difficulty associated with testing a curved surface as in the case of a cylindrical specimen. As shown in Figure 1.3, the smaller the diameter of the pipe, the more pronounced the surface curvature where the sensors must be attached.

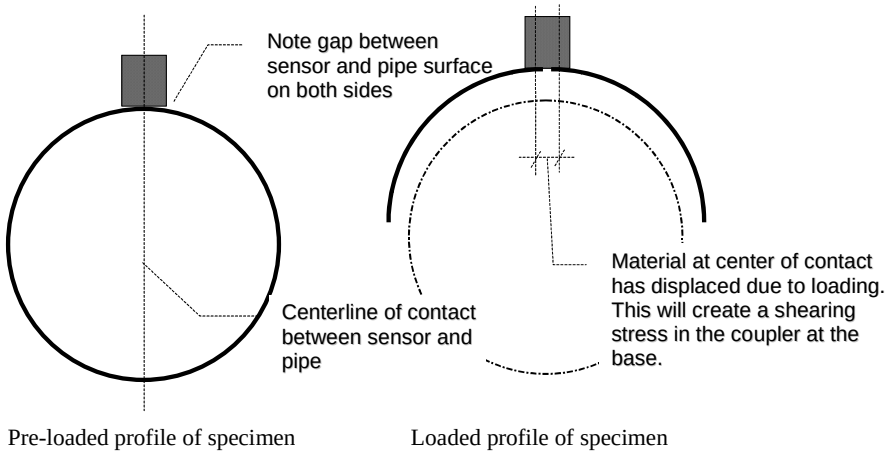

Figure 1.3 Problems with AE sensors in pipes

Sensors have a flat surface at the point of contact with the composite. This surface cannot conform to the curvature of the pipe, therefore creating the geometrical mismatch shown in the figure. As the pipe is loaded and deformed the sensor may tend to displace with respect to the surface and therefore change the contact characteristics with the pipe. This will lead to changes in the readings during testing making data analysis more difficult. Unfortunately, there is very little that can be done to minimize the problem. The use of a smaller diameter sensor is a possibility, however this will only reduce the impact of the curvature it will not eliminate the problem completely. Another possibility is the use of a mechanical attachment of the sensor to the pipe itself. The use of a contact gel between the sensor and the pipe surface will fill the air left by the curvature of the pipe. The task then becomes to ensure no new gap is created between the sensor-gel-pipe interfaces. A mechanical attachment with spring loading of the sensor will ensure sensor attachment to the pipe will maintain the sensor at the relative same location with respect to the pipe.

Precise determination of the size, geometry and orientation of the defect or flaw is another current limitation of AE monitoring. This does not preclude its usefulness in determining the extent of damage and impact on the overall behavior of the specimen, as it will be shown later. The limitation comes when it is desired to determine, for example, the extent of cracking and size of cracks and location; or if once a characteristic signal for delamination is detected and it is desired to determine the size of the delamination.

1.3.2.2. DETERMINATION OF EXTENT OF DAMAGE IN COMPOSITES WITH ACOUSTIC EMISSIONS

Determination of the structural significance of damage in composites using AE is a function of loading history and damage growth during load holds. Two useful concepts used in the analysis of AE data in this regard are the Kaiser and Felicity effects.

First discovered in the 1950's, the Kaiser effect (Fig 1.4) was noted as the lack of acoustic emission activity, which was observed during initial sample loading to a level of stress, until the previous maximum applied stress was reached. This phenomenon has been utilized for structures as an estimate of the maximum load that the structure has experienced in its service environment. Nevertheless, subsequent research has shown that the Kaiser effect is not a universal phenomenon [1.16].

Unless the sample is metallic, unflawed, and the reloading is immediate, the Kaiser effect may not be observed. This is the case of composite materials. Researchers have made use of this observation as means for estimating damage in composites. This gave rise to the Felicity ratio (Fig 1.5) developed by Fowler [1.16, 1.17]. It is defined as follows:

$$Felicity\ ratio = \frac{load\ at\ which\ AE\ is\ first\ observed\ on\ reloading}{previously\ applied\ \mathrm{max}imum\ load}$$

The Felicity ratio has been found to provide a means of monitoring damage development in fiber reinforced composites. Felicity ratios less than 1.0 generally indicate that damage has occurred within the composite.

The use of AE monitoring is facilitated by the use of specific loading profiles. These generally involve a series of loading, unloading and reloading sequences that permit evaluation of the Kaiser effect and the Felicity ratio. Periods where the load is held constant, i.e., load holds, are also generally included. Continued emission during load holds is generally indicative of damage. Several agencies have a set of required loading profiles in their specifications for AE testing. Some of these agencies are MonPac Plus, ASME codes and the CARP [1.6]. In general, the loading profile will consist of discrete pre-defined load increments followed by load holds of about 2 minutes while AE data is been recorded.

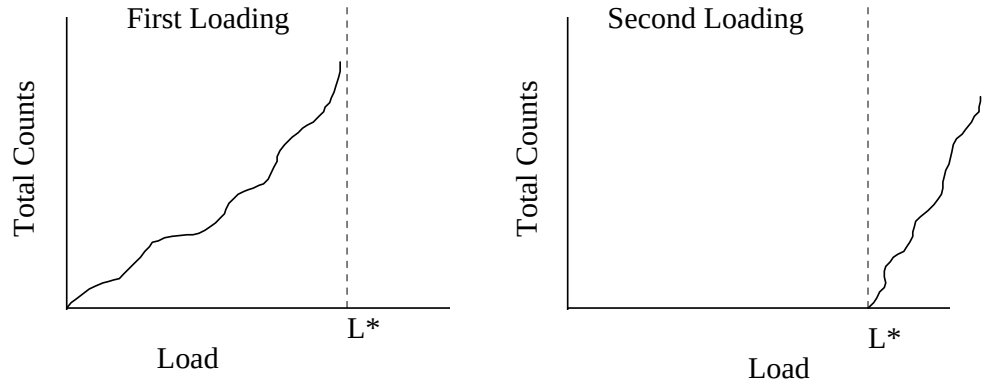

No AE activity until the applied load exceeds previous load maximum (L*)

Figure 1.4 Kaiser effect

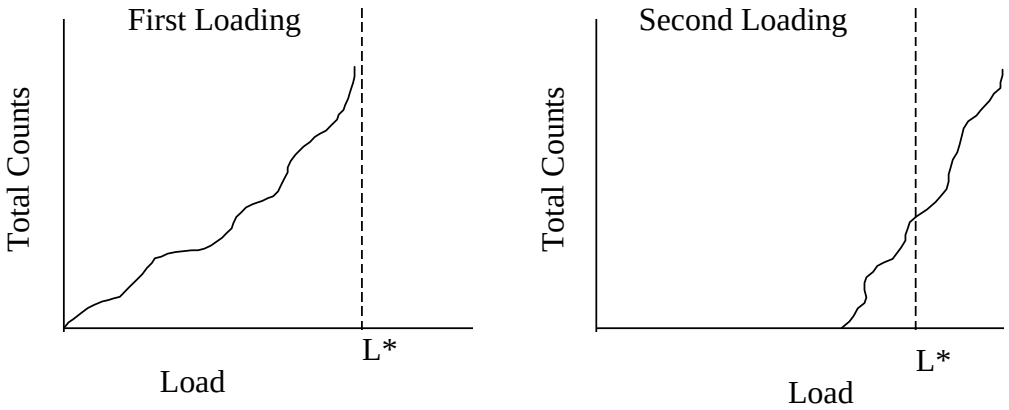

AE activity begins at load L < L*

Felicity Ratio = $\frac{L}{L^*}$

Figure 1.5 Felicity effect

1.3.3. THERMAL EMISSION MONITORING

When matter is dilated, a change in temperature takes place. This temperature change, although small, is detectable by optic methods like infrared radiometers as long as the material is cycled at a rate that high enough to preclude heat transfer between elements of the material and their surrounding. The temperature will vary following the same time variation used in the cyclic loading. These temperature changes can be related to strains and then to stresses following the theory of thermoelasticity. A well-known apparatus that uses this principle in measurement of stress and strain is called the SPATE™ marketed by a company named OMETRON Inc.

The now called SPATE technique has been successfully used in homogenous and heterogeneous materials to evaluate stress and strain fields in a non-contact manner. The SPATE setup used in this research program on testing of composite pipes is presented in Fig. 1.6. The cyclic straining was provided by means of an applied cyclic

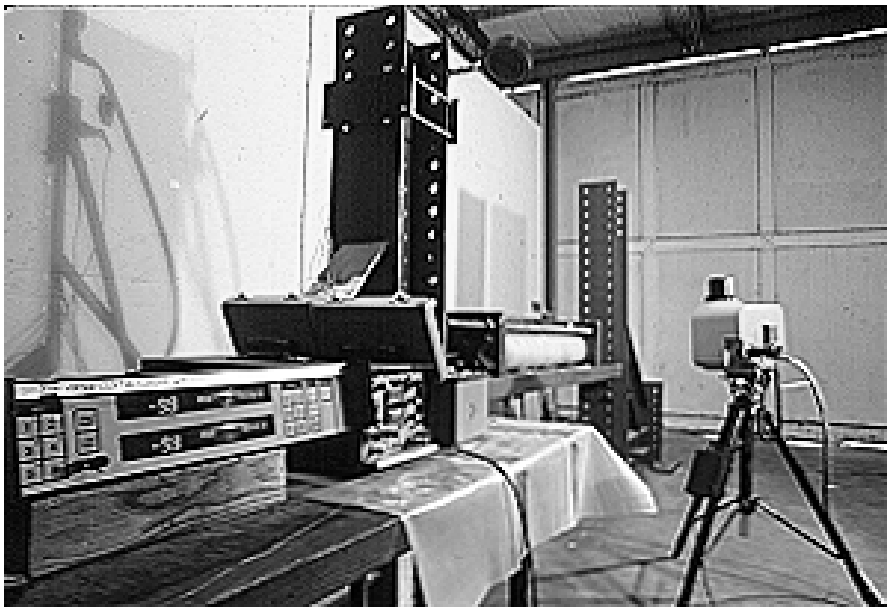

Figure 1.6 SPATE setup for fiberglass pipe monitoring

internal pressure. The load versus time profile followed a sine function, using a function generator that controlled a set of accumulators and a hydraulic pump.

Following is a brief description of how the SPATE technique works. The SPATE machine consists of a scanning infrared photon detector with a lock-in amplifier and a controlling computer. The computer will control all the movements and setting of the camera with the detector. The camera scans the specimen in discrete points under the control of the operator. The profile of the loading curve must be inputted into the computer so that the program can discriminate between sporadic changes and true readings. The correlator (lock in amplifier) performs the job of discrimination. The smallest area that can be scanned is approximately a 0.5-mm diameter circle. The scanning time is influenced by two main factors: the number of points to be scanned within the area of interest and the time spent performing the readings at each point. These are operator controllable and their selection is of outmost importance in composite material research, more so than in any other material. Further information on the SPATE technique, including theoretical background, can be found in a number of publications [1.14, 1.19].

There are inherent difficulties in using the SPATE technique in thick walled composites. The obvious one is that SPATE measurements are most sensitive to the deformations of the outermost ply on the surface observed. Since the strains and associated temperature changes of all the layers in a thick walled composite of plies with different orientation will differ from one another a post-test analytical interpretation is required. This interpretation will require the knowledge or the stacking sequence in the laminate and will be highly dependent on the accuracy of ply property estimation. In addition, this extrapolation of strains is only accurate if the plies remain bonded together throughout the test and subsequent measurements. So far the only reliable results of the SPATE technique in composite layered materials have resulted from tests in unidirectional ply coupons in tensile loading [1.19].

A final difficulty in the use of the SPATE technique in cylindrical specimens is the geometry constraints. The distance between the specimen and the camera is critical for the uniformity of the readings. Due to the natural curvature of the pipe the distance between camera and specimen changes in the vertical direction. As a result, area scans become difficult to perform and interpret. Line scans in the horizontal direction are not affected by this problem. Selection of the scan frame size for area studies on pipes is specimen dependent and must be small enough to minimize the effect of curvature. Another possible solution, is the post-test manipulation of spate data, to correct readings for the effect of the curvature. Nevertheless, this correction will require full knowledge of the theory of thermoelasticity and post-processor software.

In general, fiber dominated specimens are the most difficult to examine with the SPATE technique due to their low temperature change during cyclic loading. Following is a review of the most common procedures for obtaining repeatable and quality data from fiber composites developed of experiences resulting from this program in conjunction with recommendations made by the manufacturer and other researchers [1.19].

As stated, one of the factors influencing the quality and usability of the SPATE acquired information is the integrity of the plies during cyclic loading. Therefore, unless otherwise specified or needed, for proper determination of elastic properties of the specimen, one should maintain a load that does not cause damage growth during the scan. Also, the overall range of loading must be maintained within the linear elastic range of the material. Some authors recommend a sinusoidal load with a maximum of 30-40% of the tensile strength of the specimen as determined by a static load test and a load ratio (min/max) of 0.15. The frequency of the applied load is another factor that influences the accuracy and reliability of the readings. It has been determined that frequencies between 3 and 15 Hz are adequate. Higher frequencies may result in false readings and estimated gradients.

Even though the use of a Krylon™ ultra-flat black paint is recommended by the SPATE manual, in the case of composites is recommended to avoid its use when possible. Investigators have found that the use of paint in some cases attenuates the signal at high frequencies and with increasing paint thickness. Epoxy-matrix composites that have a diffuse surface finish do not require any surface preparation. Sample times of 0.3 to 3 sec are typical in the study of fiber composites leading to very long scan times.

The usefulness of the SPATE technique in the study of thick walled composite pipes becomes apparent when used in conjunction with other methods of monitoring and data acquisition. By itself, SPATE is still too dependent on estimates of specimen properties and post-processing calculations. It is still necessary to backup numbers obtained through the SPATE technique by means of other measurements, but by no means should the technique be dismissed as impractical. In the experience of the writer, the SPATE has proved to be a solid and reliable tool for general estimation of the condition of a cylindrical specimen. Critical delaminations, areas of stress concentrations and general surface damage are detectable by SPATE readings. Through thickness flaws that are large enough to change the stress distribution in its surrounding areas can be also detected with the SPATE.

1.3.4. LEAK MONITORING

Use of conductive layers placed within the thickness of the pipe is another method of damage detection in composite materials. These layers can be placed at discrete locations within the pipe wall to monitor progression of liquids and some gases through the wall. A proprietary leak detection system used in this research program is called CRBD^3 (Corrosion Resistant Barrier Deterioration and Damage Detection, CRIBBED™ for short). Thomas F. Anderson of Anderson Consultants in Texas optimized the meter used with the system [1.21].

The principle behind leak monitoring using conductive layers rests in an electrical process in which a special type of condenser is set up. If the chemicals (or liquid) used are conductive and an electrical charge is placed in the circuit between the conductive layer and the conductive liquid, the condenser circuit is set up. As contact between the liquid contained in the pipe and the layer increases (crack propagation and opening) the electrical characteristics of the condenser will change. Figure 1.7 shows a typical layout of a conductive layer monitoring system. Note how it is important to have two connections between the individual conductive layers so that circuit continuity can be regularly checked. Also, a connection must be carried between the liquid or gas contained in the pipe and the exterior. This can be accomplished by connecting to a metal surface in contact with the liquid or gas. In the case of the figure shown here, the connection was made to the seal plates used in the setup during testing of the pipe. The contacts to the conductive layer can be carried out by the use of wires of stainless steel, titanium and tantalum.

Care should be exercised when selecting the wires so that their inherent

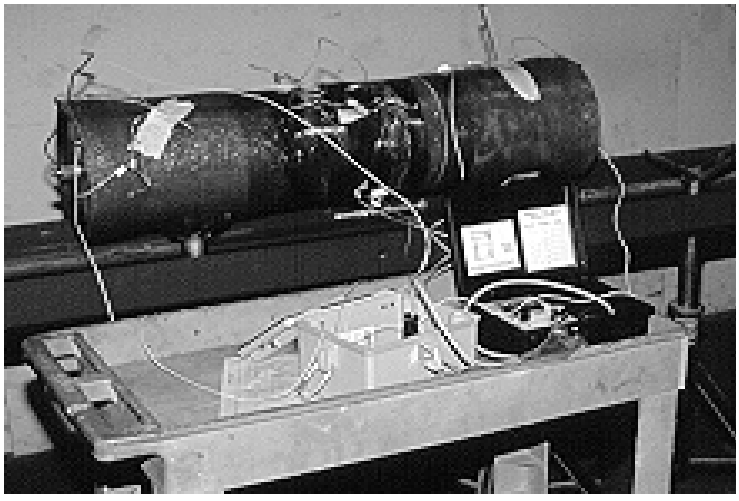

Figure 1.7 Leak monitoring

electrical resistant does not affect the accuracy of the readings. A physical connection between the sensitive layer and the wire is needed. For short pipe specimens, this can be carried out by exposing the conductive layer at the end of the pipe and with the use of epoxy "gluing" the wire to the layer. The selection of the material used for the conductive layer is also of critical importance for proper behavior of the specimen. The ideal material should provide of the following properties:

- It must have good conductivity as provided by a thin layer
- It should not interfere with the bond between the layers of the composite pipe
- It should be able to be placed exactly where the conductivity is needed without spreading around to insulating areas
- It should be resistant to the liquid to be used in the test

The results of a study performed in 1994 [1.21] on the conductivity of several types of carbon and graphite layers are presented in the following Table 1.4.

Material Used	**Conductivity Ω/Π**	**Handling**	**Cost $/ft²**
Graphite Cloth	0 - 1	Slippery, hard to cut, comes apart, stray fibers, some bond problems	2.00 - 3.00
Carbon Veil	3 to 1000	Buckles, fragile, stray fibers, springy, breaks up, some bond problems	0.50 - 0.90
Conductive Nexus®	1000 - 2000	Strong, pliable, cuts easily, does not come apart in laminating	0.35 - 0.40
Conductive Nylon	>100,000 Unacceptable	Good handling, not tested for bond	0.45 - 0.70

Table 1.4 Conductive layer information

® Nexus is a polyester veil proprietary of Precision Fabrics Group, Inc. Formed Fabrics division, 301 N. Elm St., Greensboro, NC 27401, 910-279-8071

All of these materials except for the conductive Nylon provide conductivity values that are appropriate to work with. Once contacts have been made to the layer and the test media, readings can be taken either by the use of ohmmeters if the desired information is within the capabilities of the units, or with the use of the CRIBBED system if a wider range is desired.

1.3.5. OTHER TECHNIQUES

Other methods of data acquisition are available for testing of composite materials. Although not as common as those indicated previously, they also provide information useful in the interpretation of test results. Limitations in their applicability as well as cost are some of the main reasons why they are not as yet commonly used.

1.3.5.1. LIQUID METAL STRAIN GAGES

Certain composites exhibit such low stiffness, due to their highly compliant matrix material, that conventional strain gages cannot be used to take quantitative strain measurements. The greater stiffness of the strain-gage material causes a localized stiffening effect, which drastically reduces the measured strain magnitudes relative to the actual ones. Also some materials with poor hear dissipation properties allow the temperature to build up in the area beneath the current-carrying resistance strain gage.

As shown in Fig.1.8, the liquid metal strain gage (LMSG) consists of a column of liquid mercury contained in a compliant tubular casing with lead wires attached to each end. A wide variety of contact-wire materials have been used. Ordinary copper wire is satisfactory, however there is a corrosion problem since mercury attacks copper. As a result, the shelf life of a LMSG is limited. To mount the gage, the Teflon end tubes should be bonded to the specimen using a flexible adhesive, such as silicon-rubber adhesive, rather than an epoxy. Since it offers very low resistance, it must be connected

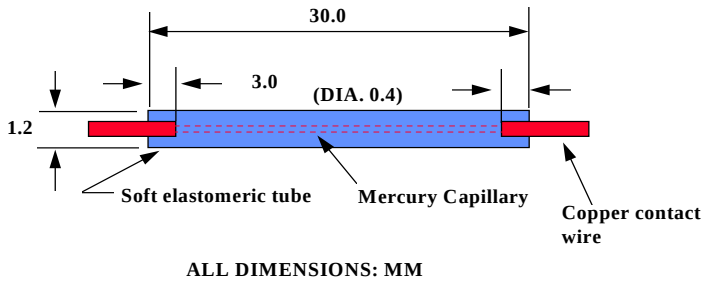

Figure 1.8 Liquid metal strain gages

to a conventional strain indicator in series with a large resistor (typically 120 ohms). Their principal disadvantages are short shelf life and nonlinear a calibration curve.

1.3.5.2. ULTRASONIC TESTING

A widely used method of flaw detection in materials is ultrasonic testing. It is based on the attenuation of high frequency sound passing through the specimen. This attenuation results from three sources: viscoelastic effects in the resin matrix, geometric dispersion caused by material heterogeneity, and geometric attenuation caused by internal defects such as delaminations and cracks. The effects of the latter are maximized by proper selection of the sound-wave frequency.

In the use of UT for thick walled pipes with fiber reinforced material, control of the attenuation variables is difficult. The use of ultrasonic scanning in thin composites has provided promising results [1.20]. However when used on thicker material, more sophisticated equipment may be needed. In the aerospace industry large UT scanners are used in the inspection of components where the more common single sensor equipment has proven impractical. Of outmost difficulty is calibration of the signal when the component is unique in nature and no calibration block has been provided. By nature,

every fabricated composite tubular will be unique, since as a result of fabrication procedures, properties change from one winding to another.

Sensor selection is also critical in the use of UT inspection for composites. As a result of the high attenuation of the material high penetration sensors are required. Tests have shown that a good starting point would be a 1 MHz sensor; this will change depending of the combination of materials used in the tube. The size of the sensors will be determined by taking into account the geometry and size of the composite pipe.

1.3.5.3. FIBER OPTICS

Fiber optics is being used in the development of so called “smart structures” where continuous monitoring is required. Optical fiber can be designed to detect a wide array of physical parameters. The fiber acts as both the transducer and the transmission system - the light being transmitted is modulated by the parameter of interest. The change may take the form of amplitude modulation, phase modulation or reflected signals. Among the variables that can be measured with the appropriate fiber sensor and signal decoder are strain, pressure, rotation, vibration and temperature. Among the advantages of optical fibers offer are:

- The availability of a wide variety of fiber optic measurements techniques especially for monitoring strain and temperature
- The capacity of a single fiber to measure distributions of strain and temperature along its length, thereby eliminating the need for wiring harness.
- The compatibility of the mechanical properties of an optical fiber with those of modern fiber reinforced plastics. In particular an optical fiber will withstand the strain history, which may be imposed upon a modern

composite material. Most other sensing elements fracture before reaching the strain limit of composites.

Location of the fiber optics in the composite laminate is also of critical importance. Depending on the application being sought or the function that the fiber must fulfill, the optical fibers need to be oriented in specific ways with respect of the reinforcing fibers in he laminae. For example, it has been determined that if the OF (optical fibers) are to serve as strain/temperature sensors, they should me mounted, if possible, between collinear plies and be aligned with the reinforcing fibers. Alternatively, if the OF's are acting as damage sensors, then the optimum sensitivity is achieved when the fibers are embedded as close to the surface of maximum tensile strain as possible and sandwiched orthogonally between a pair of collinear plies [1.20].

Reinforcing fibers in composite materials are typically a few microns in diameter. The OF typically is 80 to 125 microns in diameter. Consequently, the optical fiber represents a potentially large inclusion into the composite structure. In response to these considerations, the following basic results have been obtained form experimental work.

- Optical fibers with thin coatings usually embed more satisfactorily that fibers with thick coatings and present better mechanical transfer characteristics

- Of the coatings used both in CFRP and GFRP the polyamide appeared to produce the best results

- An optical fiber laid parallel to the reinforcing fibers caused minimal changes to the mechanical properties of the composite. However, an OF laid perpendicular to the reinforcing fibers could cause significant local stress concentrations in the inevitable local resin rich region.

- The optical fiber should have a diameter, which is significantly less than (say at most 20%) the thickness of the lay-up in a cross ply composite.

There are several other issues to be resolved before selecting the appropriate fiber optic system. It is important to be familiar with the three basic types of fibers and their light transmission characteristics. Also there are three basic types of transducers. The use of these FO transducers as embedded sensors will not be discussed here, but ample literature in their application of the mechanics of stress, strain and deformation is available. The following table presents a summary of optical sensors and potential use in composite material research.

Sensor Type	Properties Measured	Typical Uses (Industry)	Potential use in Composites
Intensity	Mechanical variables Nuclear radiation. Temperature Chemical and medical variables	Electro-Optical transducers Pressure recorders Flow meters Spectrometers	Very High
Polarization	Electrical variables	Current transducers Voltage transducers	Low
Phase (Interferometric)	Strain Pressure Temperature change	Hydrophones Magnetometer Gyroscopes Current Detectors	High

Table 1.5 Summary of optical sensors and potential use in composites

1.3.5.4. COMPARISON OF METHODS

Of the measurement methods presented in this section, none is uniquely better than the other is. They all have characteristic advantages and disadvantages that must be realized if to be used properly. By nature, structural testing of composite materials, and, in this case, large-scale pipes and components are a difficult task. Obtaining as much information as economically and reasonably possible from each test will provide the researcher with the needed tools for interpretation. The following Table 1.6 is a quick reference to the aforementioned systems and their implications to the researcher. It is not meant to be and exhaustive summary of all existing systems, only of those presented here and the experiences gathered during their use. The column with the comments presents the found limitations and advantages of each of the systems individually and not as compared to each other. The combination of any set of these methods would provide with a more complete picture of the behavior of the material.

Table 1.6 Comparison of data acquisition methods

Method	Relative Cost Level	Measurement Location	Comments
Stain Gage	Low	Surface	Good indication of overall deformation. No indications of some type of damage mechanism
Acoustic Emission	Medium	Global	Global monitoring technique. Will react to through thickness damage growth. Difficult to interpret
Spate	High	Surface	Difficult to implement, requires special loading conditions. Typically will not

			react to through thickness flaws
Leak monitoring	Low	Through Thickness	Simple, easy to interpret and implement. Requires coordination at time of specimen fabrication
Embedded Sensors	Low	Through Thickness	Require coordination during fabrication. May alter the properties of the laminate
Fiber Optics	High	Through Thickness	Difficult to implement and not easy to understand
Ultrasonic	Medium	Through Thickness	Capable to locate and determine dimensions of the flaws. Requires calibration to known

1.4. RESEARCH AND TESTING NEEDS

Large scale testing of composite tubes is an area that has received less attention than many other areas of composites related research. As a result, standards and guidelines are still being developed. The use of standards developed for thin walled pipes sometimes are not readily extrapolated to thicker and/or larger specimens. Due to the present costs of fabrication of full-scale components, development of alternative testing methods is an area of interest. The use of more economical experimental results like ring tests to determine strength and behavior, and the development of more accurate analytical models and failure criteria for full-scale components is needed. For many applications, there is a need to properly define behavioral benchmarks and their implications to allowable and ultimate strengths.

One of the most critical issues on proper testing of full-scale composite pipes and tubulars is the design of proper grips. In order to obtain true material data at the ultimate strength stages, it is necessary to develop a grip system that will not cause early failure. Most of the tests performed where grips have been acceptably designed have

been for thin walled elements [1.28 to 1.30]. A review of literature revealed no successfully tested grips systems for testing thick walled composite tubular specimens. Bonded, threaded and integrally wound grip schemes have been insufficient in the axial testing (tension) of composite pipes. Before any failure envelope can be reliably established, a proper gripping/connection system must be developed.

There is a clear need for estimating the scaling effects in composite pipes so that results obtained from smaller and more economical specimens can be used on full-scale structures. On the limited amounts of tests performed on large-scale pipes, it has been observed that even failure mechanisms that dominated a thinner component do not appear on the full-scale one [1.31].

1.5. FAILURE CRITERIA IN COMPOSITE MATERIALS

Failure criteria developed for composite materials have been developed historically to address failure at the ply level. Structural failure is estimated by associating it to a failure condition on a single ply or to a series of failures at the most highly stresses plies. In any case the available criteria are varied and each addresses a separate mode of failure associated with the ply. Strictly speaking, failure criteria can be separated in two groups. One group deals with failure within each ply, the second with failure between plies. We will call the first one, ply failure criteria, and the second laminate failure criteria.

1.5.1. PLY FAILURE CRITERIA

Ply failure criteria can be separated in three families [1.32]. These are: limit criteria, interactive criteria, and separate mode criteria, and are discussed below.

1.5.1.1. LIMIT CRITERIA

Essentially, these criteria will compare the principal stresses resulting form applied stresses and compare them to predetermined critical values without any regard to possible interactions. This form also applies to strains by using the principal strains as calculated from either the applied stresses or measured by the use of strain gages. The general form of this approach is as follows:

$$\frac{\beta_{\alpha}}{S} = 1$$

Where S would be the limit value in either tension or compression for the case of the normal principal stresses and strains, and the limit in shear stress or deformation for the case of maximum shear strains or stresses. β is the applied maximum stress or strain and α are the different directions it can be. Good agreement to this approach has been found in a number of experimental programs.

1.5.1.2. INTERACTIVE CRITERIA

The use of a more involved single polynomial representation is used to determine failure by taking into account interactions between the stresses and/or strains. Usually this criterion is applied by a series of stress/strength ratios.

One of the earliest criteria of this type is the Tsai-Hill. Hill developed a general yield criterion for metals that was later specialized by Tsai of use for the in-plane behavior of composite plies. The resulting expression was:

$$\frac{\sigma_{11}^2}{S_{11}^2} - \frac{\sigma_{11}\sigma_{22}}{S_1^2} + \frac{\sigma_{22}^2}{S_2^2} + \frac{\sigma_{12}^2}{S_1^2} = 1$$

The interaction is proportioned by the strength along the fibers S_1, which is considerably different from S_2. Experiments have show poor agreement from composite materials to this expression [1.20]. Hoffman modified Tsai-Hill by adding linear terms of stresses to account for the strength in tensions and compression separately in one expression.

Tsai-Wu used a power series expansion to express a failure function. Quadratic terms were assumed sufficient to follow the failure locus.

$$F_i \sigma_{ii} + F_{ij} \sigma_{ii} \sigma_{jj} = 1$$

We will not expand the expressions here for in-plane response. However, it can be seen that this is similar to the Hoffman expression except for the additional term in the interaction. Coefficient F_{12} needs to be evaluated from a biaxial strength test. Because of the lack of information available in tests necessary to estimate F_{12}, most researchers assume this value equal to zero which results in the Hoffman expression. Others, like Quinn and Sun, adopted the expression given by Tsai and Hahn, to estimate the value of F_{12}. This, however, will result in similar correlation errors as the Tsai-Hill criterion. Swanson found the criterion to predict data obtained for matrix cracking, if the σ_{11} dependence is omitted [1.10]. He could not, however, get the criterion to agree with his test data of the critical ply failure. Generally, there is agreement that Tsai-Wu criterion can predict first ply failure, like matrix cracking, fairly well [1.31]. The 3D version of this criterion is not used in practice since the tests necessary to determine the coefficients used are not easy to perform. And even when these were somehow obtained, it would be very difficult to verify its applicability.

1.5.1.3. SEPARATE MODE CRITERIA

As the name states, failure modes in the fiber and matrix are treated separately. This does not mean that the interaction between the stresses or strains is neglected. Experimental results have led a number of researchers [1.34-1.36] to emphasize separate criteria for fiber and matrix composites. Hashin and Rotem suggested the following criteria to fit their fatigue data:

$$\frac{\sigma_{11}}{S_1} = 1 \qquad \textit{Fiber failure}$$

$$\left(\frac{\sigma_{22}}{S_2}\right)^2 + \left(\frac{\sigma_{12}}{S_i}\right)^2 = 1 \qquad \textit{Matrix failure}$$

Yamada and Sun argued that at the final stages of loading, plies have already failed in matrix cracking. The suggested the following expression for fiber failure:

$$\left(\frac{\sigma_{11}}{S_1}\right)^2 + \left(\frac{\sigma_{12}}{S_i}\right)^2 = 1$$

Hashin used stress invariant of transverse isotropy to transform the general polynomial expansion previously presented into separate fiber and matrix criteria in tensions and compression. He used experimental observations and general arguments to justify his 3D criteria for practical use.

For fiber mode failure the expressions are:

$$\frac{\sigma_{11}}{S_1^C} = 1 \qquad (Compresion)$$

$$\left(\frac{\sigma_{11}}{S_1^T}\right)^2 + \frac{\sigma_{12}^2 + \sigma_{13}^2}{S_i^2} = 1 \qquad (Tension)$$

For a transverse mode (matrix dominated), the expressions are:

$$\left(\frac{\sigma_{22}}{S_2^T}\right)^2 + \frac{\sigma_{12}^2 + \sigma_{13}^2}{S_i^2} + \left(\frac{\sigma_{23}}{S_\circ}\right) = 1 \qquad (Tension)$$

$$\frac{\sigma_{22}}{S_2^C}\left[\left(\frac{S_2^C}{2S_o}\right)^2 - 1\right] + \left(\frac{\sigma_{22}}{2S_o}\right)^2 + \frac{\sigma_{12}^2 + \sigma_{13}^2}{S_o^2} + \left(\frac{\sigma_{23}}{S_o}\right)^2 = 1 \quad (Compression)$$

where S_o is the out-of-plane shear strength.

Christensen and Swanson suggested strain-based separate criteria. The fiber failure is described by a maximum strain criterion. They reported good agreement with their experimental results. In general, Hashin's is the most widely used criteria in composites.

1.5.1.4. LAMINATE FAILURE CRITERION

Kim and Soni studied experimentally the onset of free edge delamination in laminated composites [1.37, 1.38]. They used a maximum stress-type criterion, as

applied to interlaminar shear, in trying to predict their test data. Chang and Springer [1.39] suggested an interaction criterion accounting for the tensile σ_{33} and the shear stress:

$$\left(\frac{\sigma_{33}}{S_2^T}\right)^2 + \frac{\sigma_{23}^2 + \sigma_{13}^2}{S_o^2} = 1$$

Brewer and Lagace [1.40] suggested a modified version of this expression to account for a compressive stress in the σ_{33} direction

$$\left(\frac{\sigma_{23}}{S_o}\right)^2 + \left(\frac{\sigma_{13}}{S_i}\right)^2 + \left(\frac{\sigma_{33}}{S_2^T}\right)^2 + \left(\frac{\sigma_{33}}{S_2^C}\right)^2 = 1$$

It is assumed in this study that the interface failure mode is not coupled from the in-plane interaction. Hashin has presented arguments supporting this assumption [1.35 and 1.41-1.43]. The general 3-D Tsai-Wu criterion is used to describe this failure mode by retaining terms of stresses acting on the interface only. This would lead to the following expression:

$$\left(\frac{\sigma_{23}}{S_o}\right)^2 + \left(\frac{\sigma_{13}}{S_i}\right)^2 + \frac{\sigma_{33}^2}{S_2^T S_2^C} + \frac{\left(S_2^T + S_2^C\right)\sigma_{33}}{S_2^T S_2^C} = 1$$

It is very important to consider effects of interlaminar shear since it may generate high out of plane shear stresses in certain loading conditions.

1.6. LIMIT STATES FOR OFFSHORE RISER APPLICATIONS

There is a clear distinction between failure modes at the micromechanical level and those at the structural level. Structural failure modes typically will include a combination of material failure modes. Each of the limit states represents a milestone in the behavior of the structural component, and may or may not indicate structural instability or inability to carry additional loads. Depending on the application intended for the structural component, some of this milestones will not apply, however, they are present in one form or another in every failed component made out of fiber composites.

As presented in the previous section, failure criteria designed to predict stresses that will produce a particular mechanism on the material can be used in the determination of the limit states for composite structures. Their application, however, is not an easy task since knowledge of the main material failures associated with the limit states of interest can be complicated depending on the component and its intended application. Following is a brief description of three main limit states as associated with offshore riser applications. This application is used since its part of the theme structure part of the research program for which this work is a part of.

1.6.1. MATRIX CRACKING AND PLY DELAMINATION (LEAKAGE)

This is typically one of the most important limit states in unlined pressure vessels and line pipes systems. This failure mode would signify the end of the operational life of the structure if corrosive or hazardous fluids are being stored or transported in the structure. The main material mechanisms associated with this are, as stated in the heading, matrix cracking and delamination. In addition separation between fiber and matrix will add to the paths available to the fluid for exit.

Of all of the limit states of interest, this one is the most difficult to predict in a manufactured component. It has a high sensitivity to initial flaws in the material like air

bubbles, curing shrinkage cracks, delamination and, thickness variations in the walls. Typically, a regression curve approach is used in determining the maximum allowable pressure in a component fabricated in series. Standard ASTM D2992 outlines the requirements for testing and determining minimum pressures. This type of design limitation is impractical and expensive in applications where only one component is fabricated.

The need for predicting methods for single applications/manufacturing composite structures is needed. Research has been directed towards the use of Non-Destructive Evaluation (NDE) methods in order to predict the expected capacity of composite materials. The need for predicting capacity under repeated and sustain loading is of critical importance before reliable applications of composite materials can be made in civil engineering applications.

1.6.2. FIBER FAILURE (BURST)

Probably the most widely researched subject to this date has been ultimate capacity of fiber composite materials [1.44-1.50]. Test have been performed in elements and components in the shape of plates, coupons and cylinders in order to determine the capacity of the component as related to the fiber failure. Results have demonstrated that most of the ultimate capacity is governed by the fiber capacity in the component. The same researchers have also showed that the burst capacity can be more than double the leakage capacity. It is in very few occasions that typical application of composite pressure vessels will be taken all the way to fiber failure. There are cases, however, where fiber failure will be produced at the same time or even before leakage is reached. Conditions where the component has gone through impact damage, will result in modes where fiber failure is produced. Prediction of residual capacity after impact damage is another of the areas of interest that need to be studied before a complete acceptance of composites is achieved in civil structures.

This limit state constitutes a more catastrophic failure than that of leakage since the structure essentially looses its ability to carry any additional loads through the cross section.

1.6.3. INSTABILITY (COLLAPSE)

Predicting collapse of composite tubes under external pressure is an area where relatively little data is available in the literature, particularly for large size specimens. In addition, experimental results presented here and elsewhere [see Chapter 2 for references] appear to indicate that collapse under external pressure may be more sensitive to scaling effects that the other limit states presented here. As it is known, the stiffness of the fiber reinforced composite structure is dependent on the fibers themselves. The contribution by the matrix to the overall stiffness is small when compared to the contribution of the reinforcement. In components loaded in the strong direction of the fibers, the behavior will seem almost perfectly elastic and linear from beginning to end of the structure. However, influence of initial flaws and irregularities in the material will change as the scale or size of the component changes. Estimating this is difficult since some of the initial flaws occur at random during the fabrication or winding process. The bigger the structure the longer the fabrication process will take place, and therefore the possibility of flaws changes. In addition, surface irregularities, geometrical tolerances and local fiber failures add variables that affect the predictions in capacity. Research in this area for large-scale structures is also needed to answer a number of questions on behavior of composites under external loads.

1.7. SUMMARY

Large scale testing of composite pipes is a difficult and expensive process. For this very reason careful consideration should be exercised in selecting the methods and procedures to be used in the research phase. Most of the methods for testing in the

composite materials field have been developed, either for small-scale specimens or, even when developed for large specimens they have been done based in a particular and unique component for a very specific application. Pipe and/or cylindrical type specimens are a preferred shape for material characterization of fiber reinforced composites. Because of its cost implications, it is very likely the number of specimens available for testing will be more limited as compared to small-scale specimens. Nevertheless, the validity of the results from test of life-size structures is unarguable. There is a clear scaling effect in composites that must be quantified if proper extrapolation of small-scale test results is to be accomplished. The need for test results and development of new testing methods is immediate.

1.8. OVERVIEW OF RESEARCH PROGRAM

The research program described herein involves three sets of experiments, as follows:

1. Testing of a large-scale carbon fiber composite tube under external pressure.
2. Internal pressure tests on fiberglass and glass-carbon hybrid tubes.
3. Internal pressure testing of fiberglass tubes subject to impact damage.

Objectives of these test programs are as follows:

- Develop and document experimental data for each of the three conditions noted above.

  The experimental data is intended to provide insights into the response and failure modes for composite tubular members under internal and external pressure. The data is also intended to provide a benchmark for calibration and verification of analytical models and design models for large size composite tubular members. All specimens in this research program are

relatively large scale. Consequently, the experimental data is also intended to provide a basis for evaluating scale effects.

- Develop improved test methods for large-scale composite tubes subject to internal or external pressure loading.

  Pressure testing of large-scale composite tubes poses significant challenges involving both gripping and sealing of test specimens. Consequently, a major objective of this research program is to investigate and develop methods for gripping and sealing of tubes that will permit collection of meaningful experimental data.

- Investigate methods for nondestructive evaluation (NDE) of composite tube test specimens.

  As described earlier, the use of various NDE methods can significantly enrich the information collected in the test of a composite tube. These techniques include acoustic emission monitoring, thermal emission monitoring, leak monitoring, and others. A major objective of this research program is to evaluate the usefulness of several of these techniques, as applied to laboratory testing of composite tubular members. A significant emphasis has been placed on the use of acoustic emission (AE) monitoring in all the three test series, as a method for detecting damage and predicting the response of the test specimens.

The three test series are described separately in Chapters 2, 3 and 4 of this dissertation. Chapter 5 provides a summary of all three tests series, and provides a summary evaluation of the AE results. Conclusions are provided in Chapter 6. Because of the variability in the materials used for the fabrication of the specimens from each of the series the following Table 1.7 shows a brief summary of the individual make up of the specimens.

Material specifications for specimens tested in the experimental phase		
Series	**Resin**	**Fibers**
External Pressure	Shell Epon 9405 Epoxy	Carbon fibers AS-4 Hexcel™ Glass fibers S2 from Owens Corning
Internal Pressure	Dow Hetron 944 vinylester	E-Glass Verotrex™ Certainteed (fatigue tests) Carbon Fiber Grafil™ Inc. 34 (hybrid specimens)
Impact Evaluation	Off the shelf specimens with Proprietary epoxy mix	E-Glass Verotrex™ Certainteed

Table 1.7 Material Specifications for Experimental Program

CHAPTER 2

BEHAVIOR OF A COMPOSITE TUBE UNDER EXTERNAL PRESSURE

2.1. INTRODUCTION

The move towards exploration and development of petroleum reserves at ever increasing water depth has motivated the development of drilling and production systems that are more efficient than the ones currently in place. This has resulted in the proposed use of alternative materials like advanced fiber reinforced composites. The weight savings offered by these materials is a potentially significant economic advantage in floating deep water offshore platforms, and advanced composites are currently under consideration for a number of applications in the platforms, including drilling and production risers. At present, risers are typically constructed of steel. However, as water depths exceed several thousand feet, the large weight of the riser becomes increasingly difficult and costly to accommodate, thereby motivating interest in lighter weight materials [1.1]. However, before lightweight advanced composites can be applied with confidence for offshore oil production, comprehensive research and testing is needed to develop and verify design criteria.

The cost and time required in the initial development of systems constructed using composite materials makes testing of full size components unique and difficult. Therefore, the majority of the material characterization data comes from tests performed in scaled down specimens whose dimensions are much smaller than the actual components. Nonetheless, a limited number of large-scale tests are valuable as an aid in extrapolating data from small-scale tests, for verifying analytical models and to help identify unanticipated scale effects.

Tests of large-scale cylinders under external pressure have been performed in the past with isotropic homogeneous materials. Testing of fiber composite pipes under external pressure has been mainly focused on thin walled and small diameter specimens [2.2, 2.3] and in some cases to modified ring tests [2.4]. Results from testing of large-scale composite tubular specimens under external pressure to failure are few and not readily available [2.5, 2.6, 2.7]. And most of the information is from tests aimed at proofing of the component rather than collecting experimental data for analytical model verification. The effect of scale and thicker wall construction has not been experimentally studied in detail. Analytical models of the behavior of thick walled and large scale composite tubes under external pressure are available in the literature, these studies however have not been sufficiently verified experimentally for calibration of the models [2.8, 2.9, 2.10, 2.11].

2.1.1. PROGRAM OBJECTIVE

This chapter presents the results of an external pressure test on a carbon fiber composite tube. The specimen represented the main body of a proposed carbon fiber drilling riser, at full scale in diameter and wall thickness. The specimen was tested under external water pressure up to collapse. The test was intended to verify the capability of the specimen to sustain the design external pressure, to establish the actual collapse pressure, and to generate data for verification of analytical collapse pressure predictions. As an unintended added variable, a full length, complete radial delamination was present at mid-thickness at the tube wall as the result of an error during fabrication. Descriptions of the specimen properties as well as the testing system used and results are presented in this chapter. In addition, comparisons to simplified collapse predictions for steel and composite materials are made. A finite element model was developed to verify the records of strains and acoustic emission (AE) events taken during the test. The effect of the delamination in the buckling capacity of this specimen is assessed, along with the ability of AE in monitoring the behavior of this component.

2.2. EXPERIMENTAL PROGRAM DESCRIPTION

This section will present the details of the specimen and the system used in its testing. Information is also provided on the measured initial geometry of the specimen.

2.2.1. SPECIMEN DESCRIPTION

An external pressure test was conducted on a filament wound carbon fiber – epoxy composite tube. The specimen was 15 ft. in length, had an outside diameter of 22.2 inches, and a wall thickness of approximately 1.2 inches. The specimen was intended to model the main body of a carbon fiber composite drilling riser at full scale in diameter. The exact winding sequence for the specimen is proprietary, and is not presented here. However, a general description of the specimen construction can be provided. The tube was constructed with an initial layer of glass veil and a cycle of glass winding. The remainder of the tube was wound with carbon fiber and epoxy, using fiber winding angles of 88^0 and 15^0 with respect to the longitudinal axis of the tube. The materials used in the fabrication of the specimen were AS-4 carbon fiber from Hexcel Co., S2 glass fiber from Owens-Corning, and Shell Epon 9405 epoxy resin.

The test specimen contained a unique unintended feature. During fabrication of the specimen, the filament winding machine broke down after a portion of the wall thickness was wound. The machine was subsequently repaired and winding was continued. However, examination of the completed tube by the manufacturer revealed that when winding was resumed, the new layers apparently did not properly bond with the previously wound layers. Consequently, the tube had a pre-existing delamination at approximately mid-thickness of the wall. This delamination was not repaired. However, the ends the tubes were sealed at the location of the delamination to prevent water from entering the delamination during the external pressure test. Figure 2.1 shows a portion of the tube wall at the end of the tube. The sealed delamination is visible in this photograph.

Figure 2.1 End view of riser

The delaminated layer was located at approximately 0.55 inches from the inside face of the wall. To determine the extent of the delamination, ultrasonic scans were made through the wall thickness. The tube was ultrasonically scanned in arcs of six degree increments around its circumference and continuously along its length. Based on these scans, it was estimated that the delamination extended over the full length and circumference of the tube.

Figure 2.2 shows overall dimensions of the test specimen. Prior to testing, measurements were made of the inside and outside diameter of the tube at the locations shown in Fig. 2.2. These measurements are reported in Tables 2.1 and 2.2. Wall thickness values based on the measured inside and outside diameters are reported in Table 2.3. The specimen ends were labeled as End A and End B for purposes of reporting the location of measurements. The reading locations along the circumference of the tube (Locations 1 to 6 as shown in Fig. 2.2) are numbered in a clockwise order when standing at End A and facing towards End B.

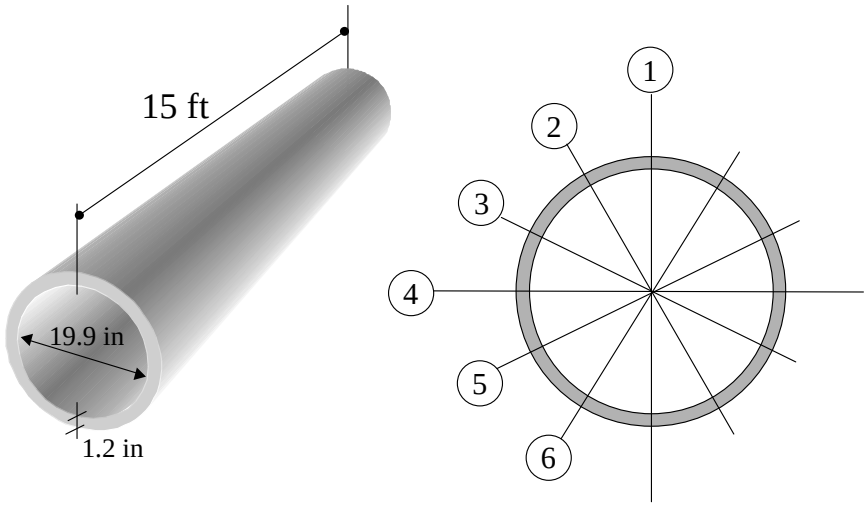

Figure 2.2 Specimen dimensions and diameter measurement locations

Based on the readings of initial outside diameter, the out of roundness of the tube was well below the 0.5% limit established by API standards [2.5] for steel tubes. The out-of-roundness as defined by API specifications can be calculated as:

$$\beta = \frac{D_{\max} - D_{\min}}{D_{nom}} \times 100\%$$

Where D_{max} is the major outer diameter in the cross section. D_{min} is the minor outer diameter in the cross section and D_{nom} is the nominal diameter. This definition is well suited to define the ovalization imperfection. It is not useful, however, to layer waviness imperfection which is critical in cases of thin walled tubes under axial compression.

So, from the data in Table 2.2 we can calculate the out of roundness ratio based on the average diameter and the maximum value as presented in the table for each locations measured. Or for a simplified calculation add the two deviations shown at the

end of each column algebraically and divide them by the average value in the same column.

Location	End A	4 ft. from End B	End B
1	19.821	19.827	19.824
2	19.820	19.825	19.823
3	19.821	19.823	19.823
4	19.822	19.824	19.821
5	19.819	19.824	19.821
6	19.821	19.826	19.824
Average	19.821	19.825	19.823
Deviation of values from the Average	-0.002 +0.001	-0.002 +0.002	-0.002 +0.001

Table 2.1 Internal diameter measurements

Location	End A	¼ L from End A	Middle	¼ L from End B	End B
1	22.196	22.214	22.204	22.214	22.199
2	22.200	22.213	22.204	22.215	22.199
3	22.195	22.217	22.212	22.214	22.195
4	22.197	22.212	22.213	22.213	22.205
5	22.194	22.212	22.213	22.205	22.196
6	22.197	22.214	22.214	22.208	22.207
Average	22.197	22.214	22.210	22.211	22.200
Deviation from the Average	-0.003 +0.003	-0.002 +0.003	-0.006 +0.004	-0.005 +0.004	-0.005 +0.007

Table 2.2 External diameter measurements

Location	End A	End A'	End B	End B'
1	1.197	1.201	1.225	1.210
2	1.194	1.200	1.210	1.218
3	1.199	1.198	1.210	1.210
4	1.199	1.199	1.205	1.227
5	1.199	1.200	1.220	1.215
6	1.204	1.191	1.230	1.215
Average	1.199	1.198	1.217	1.216
Deviation from the Average	-0.005 +0.005	-0.007 +0.003	-0.012 +0.008	-0.006 +0.011
Notes: Primed labels indicate readings made on the diametrically opposite side of the location as shown in Figure 2.4				

Table 2.3 Thickness measurements of pipe

2.2.2. TEST SPECIFICATION AND SETUP

The test performed was part of a prototype verification program for the development of a composite drilling riser for deep-water application. The test was intended to subject the composite tube to a state of pure external pressure, without axial compression stresses. In addition, the assembly had to allow for the free axial deformation of the tube induced by the Poisson effect resulting from the hoop stresses.

Northrop Grumman Marine Systems in Sunnyvale, California fabricated the composite tube for this test. The specimen was then shipped to the University of Texas Ferguson Laboratory in Austin, Texas to be instrumented and prepared for testing. Figure 2.3 shows the specimen as received at the Ferguson Laboratory. The actual

Figure 2.3 Riser in FSEL

external pressure test was then conducted at H.O. Mohr Research and Engineering Company in Houston, Texas. The specimen was subjected to external water pressure in a large chamber that was approximately 5 ft. in diameter and 30 ft. in length. The chamber was rated for pressures up to 5000 psi. Pre-test estimates of the collapse pressure varied from approximately 1100 psi up to approximately 4000 psi. Consequently, the 5000 psi chamber was considered adequate for this test.

The overall configuration of the test specimen is shown in Figure 2.4. Steel end plates were fitted to the tube ends. Seals were placed between the steel plates and the tube wall to prevent water from entering the inside of the tube, and to permit the steel end plates to move freely in the axial direction of the tube. A heavy walled steel pipe was placed inside of the test specimen, and connected to the steel end caps. This steel pipe resisted the axial forces resulting from the water pressure acting on the steel end caps. The anticipated axial force was quite large, so a very heavy steel pipe was required. For example, at 3000 psi, the axial force on the internal steel pipe is approximately 1200 kips. The steel pipe used inside of the specimen was 14 inches in diameter with a 2 inch wall thickness.

Under external water pressure, the test configuration as shown in Fig. 2.4 permitted the composite tube to be subjected to external pressure only, without axial force. Provision was also made to vent air from the inside of the specimen during the test, to prevent internal air pressure from building up in the specimen. Ports were also installed in the steel end plates that permitted strain gage wires to be passed through the end caps. This permitted the use of strain gages on the inside wall of the specimen.

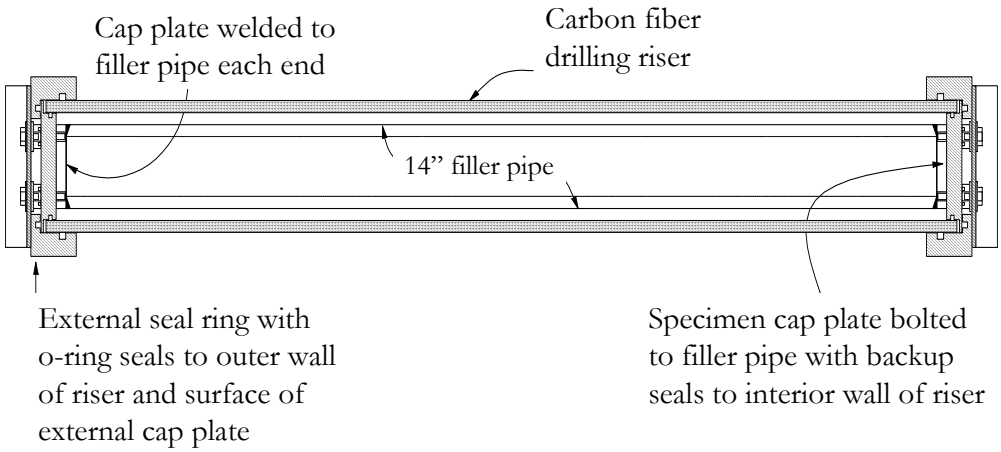

Figure 2.4 Test setup configuration

A major challenge encountered in this test program was developing a seal system at the tube ends to prevent water from entering the inside of the specimen. Two initial attempts at conducting an external pressure test were unsuccessful due to leakage at the seals. The final seal system that proved successful is shown in Fig. 2.5. O-ring seals were used on the outer surface of the tube. In addition, chevron type seals were used on the inner surface as a backup system, in the event that the o-ring seals failed.

Details of the steel end plates are shown in Fig. 2.6. A ledge was machined into these plates that acted as a support for the inner surface of the composite tube, and provided a location to seat the chevron seal against the inner surface of the tube. The ledge on the end plate was also intended to maintain the round shape of the tube ends to prevent failure of the seal system. In the final installation, the steel end plates were bolted to steel cap plates that were welded to the ends of the internal steel pipe, as shown in Fig. 2.4. An outer steel ring was then bolted to the end plate as shown in Fig. 2.5. This outer steel ring supported the o-ring seals on the outer surface of the composite tube. Thus, when the seal system was complete, the tube ends were sealed on both their inner and outer surfaces. Since the tube ends were sandwiched between steel plates, the

tube ends were highly restrained against radial deformations, although they were free to move in the axial direction.

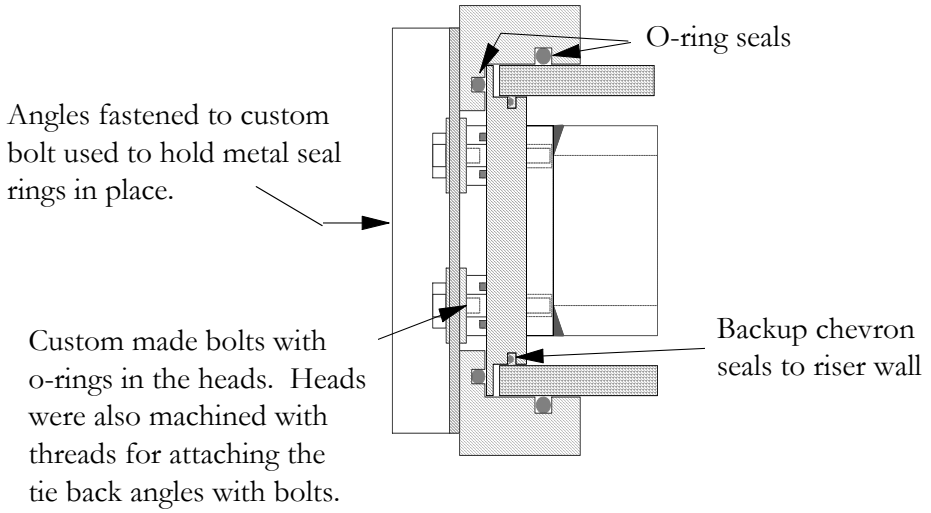

Figure 2.5 Seal detail for external pressure

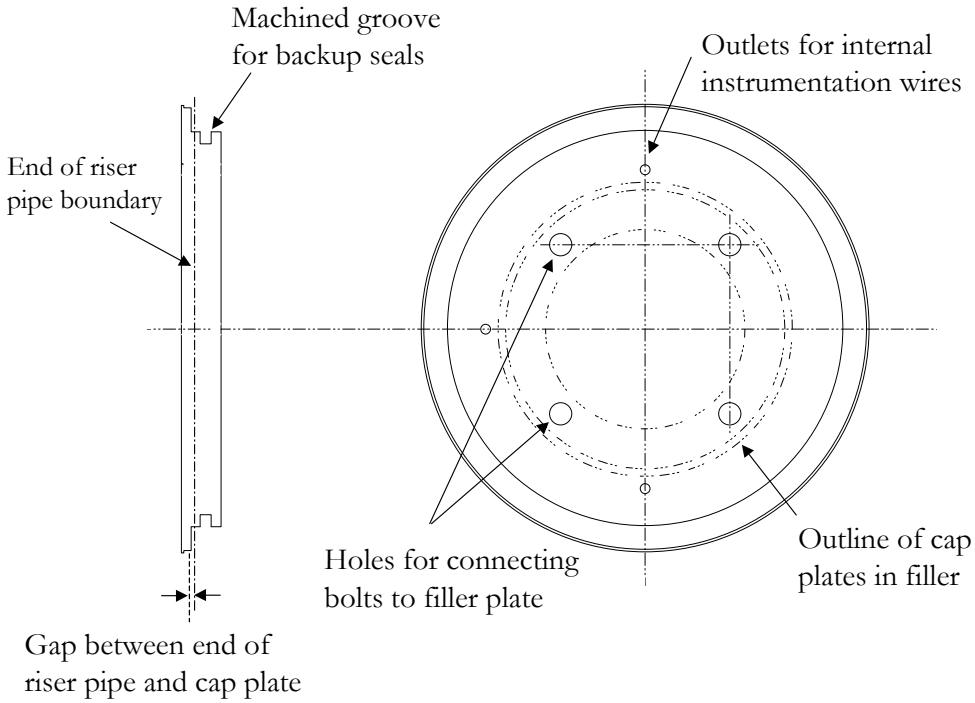

Figure 2.6 End plate detail

The effect of the end restraints, as induced by the seal plates, was studied by finite element modeling and theoretical buckling calculations including stiffeners at regular intervals based on the estimated material properties. It was estimated that end restraints of the type generated by the seal detail would not have an effect for tube lengths exceeding 6 ft. As detailed, the specimen would have a length of 14'-9", therefore eliminating the effects of the end restraint. The elastic finite element model supported this assumption by showing an area of less that one foot as affected by the end restraint. Subsequent non-linear FEA runs of a model with an initial imperfection and, with varying lengths between end plates, also showed no change in the calculated buckling load for tube lengths greater than 4ft.

As described earlier, developing a satisfactory seal system for this specimen proved quite difficult. Consequently, a brief discussion is provided below on some key issues affecting the choice of a seal system for a composite tube of the type tested in this program. Information on the characteristics of various sealing systems for this specimen was obtained from seal manufacturers' literature and from other literature [2.9], from discussions with seal manufacturers and other specialists on seals, and from a trial and error process.

2.2.3. ISSUES RELATED TO CHOICE OF SEAL SYSTEM

The use of chevron seals provided for a means to maintain appropriate sealing in areas where a change in geometry was expected. Although o-ring seals are more forgiving of out-of-roundness geometrical irregularities in the sealing surface, chevron seals have the particular ability of growing or decreasing in size with the surface being sealed. Design issues include the seal type, the seal material, preparation of the tube surface, and reinforcement of the tube wall at the seals if necessary.

Requirements for sealing a composite tube can differ significantly from the requirements for sealing a steel tube. Composite tubes frequently have rougher and more irregular surfaces, and may exhibit a higher degree of out-of-roundness than steel

tubes. Further, the low stiffness of many composites results in greater deformation of the tube in the region of the seals as pressure is applied. The seal system must be capable of accommodating these deformations, or the tube must be reinforced to limit deformations to levels within seal tolerances.

As discussed in Chapter 1 of this dissertation, if the tube surface is not expected to move a great deal relative to the seal, the use of an o-ring can provide a simple and economical solution. Urethane o-rings provide a deformable profile that can help accommodate the rough surfaces often found with composites. On the other hand, o-rings do not have a high tolerance to out-of-roundness irregularities and lose sealing capabilities if the tube surface deforms away from the seal during pressurization. For this test, the ends were supported by the interior seal plate, and therefore were not expected to deform considerably. O-rings were used for the primary sealing in the outer face of the specimen.

Chevron type seals can provide better sealing capability in applications where the surfaces tend to grow apart during testing, and are more tolerant of out-of-roundness. They are not as tolerant of surface roughness as an o-ring, although their tolerance can be improved with proper material and profile selection. Chevron seals are more susceptible to damage while being driven into a pipe. To avoid pinching or damaging the seal, a great deal of care is required during installation. Normally, it will be necessary to taper the composite tube wall slightly to permit proper installation of a chevron seal. Seal manufacturers can provide a recommended slope for the taper, which can then be machined into the tube wall.

Proper preparation of the sealing surface on the composite tube wall is also important. High surface roughness, typical of some fiber reinforced composite materials, can pose problems. For many types of seals, a RMS (root mean square) surface roughness of 15 should not be exceeded for proper functioning of the seal. In most cases, machining of the tube wall with a carbide tip tool will provide an acceptable surface finish, and can help alleviate out-of-roundness irregularities.

Materials selection for the seal is also important for proper performance. Softer urethane materials will perform better when higher levels of surface roughness or out-of-roundness are present. These materials, however, may not perform well at high pressures or in conditions where large radial growth of the tube is expected. Harder materials, like Parker's Polymite [2.9], may perform better under these conditions. Based on the preceding discussion, it should be clear that design of a sealing system for a composite tube requires consideration of a number of opposing requirements, and is not a simple manner. For this project and others in the research program, a considerable amount of trial-and-error was required in developing a seal system, and success was rarely attained on the first attempt. A final issue of concern is the interaction between the tube and the seal. In the case of the collapse pressure test, there was little deformation at the locations where the seals where placed, this simplified the required preparation work in order to ensure proper sealing of the system.

2.2.4. SPECIMEN PREPARATION

There were essentially no modifications made to the specimen after it was received at Ferguson Laboratory prior to seal installation. Two factors were important in this decision; the first was the tolerances in the fabrication of the specimen, the second the size and difficulty involved in making any changes. The surfaces were smooth enough that no special preparation was necessary for the seals. The ends were cut square to each other to a tolerance of 0.1", which was enough for the allowed gap in the design of the setup for free axial growth. The only modification was to the exterior of the riser where the o-ring seals in the final system design were to come in contact. There was a c-glass veil that wrapped the exterior of the riser. This veil was intended to help the specimen keep its round shape as wound during the curing process. It was also intended to maintain the fibers in tight contact with each other through the thickness to maintain a constant resin to fiber proportion. This c-veil layer has a rough texture and it was grounded off in order to provide a smooth surface for the o-ring contact. The grinding was limited to a 5-inch wide band centered in the area of o-ring contact.

Because of the weight of all the components associated with the test, installation of the internal steel pipe and end seal assemblies was made with the specimen in a vertical position and in two stages. The first stage to be completed at Ferguson Laboratory. The second stage was carried out at the testing laboratory owned by H.O. Mohr in Houston Texas. The first stage in the specimen preparation was to assemble the filler pipe and end plates. First the filler pipe was attached to one of the end plates. This was done vertically by temporally attaching the end plate to a floor assembly and picking the filler pipe from one end with the overhead crane. With the filler pipe aligned to the holes in the end plate, the bolts were placed connecting the filler pipe end plate to the end plate in the floor assembly. After bolting was completed, the riser pipe was lowered from the high end of the filler into the bottom end plate. Figure 2.7 show the placing of the specimen into the bottom end plate by lowering along the filler pipe. After setting the specimen into the lower end plate, the filler was aligned (centered) inside the riser pipe and the top end plate was added.

Figure 2.7 Vertical assembly

Figure 2.8 shows the setting of the specimen into the lower and upper end plates. Once the assembly was completed, the specimen was lifted and moved back into its shipping cradle where it was closed and prepared for transportation to Houston. As far as assembly is concerned, the only remaining operation was the assembly and attachment of the outer seal ring into the frame. Figure 2.9 shows how the end ring looked after the assemblies were completed. A constraint in this test was the inability of accessing the specimen once inside the chamber. No visual inspections would be possible during pressurization and only a limited number of wires could be extracted from the chamber once the hatch was closed.

Bottom plate fitting

Top plate fitting

Figure 2.8 Assembly of specimen at Ferguson Laboratory

Figure 2.9 Final setup of specimen before testing

Instrumentation included electrical resistance strain gages located at selected locations on the inner and outer surfaces of the tube. In addition, the use of acoustic emission (AE) monitoring was included during the test in the hope that indications of onset of significant damage mechanisms (matrix cracking, delamination friction/growth, fiber breakage, etc) occurring at various pressure levels would be detectable.

Figure 2.10 shows the locations for the strain rosettes and the location for the AE sensors. The strains rosettes were the 120^{o} type three gage layouts, 120 Ohms resistance foil gages. The gages only provide the strains at the surface of contact. Limitations set by the testing chamber influenced the number of gages available and their distribution. In the final profile, three rosettes were placed in the inside wall of the riser and seven rosettes in the exterior.

The inside gages were located at the bottom section of the riser as placed in the chamber. One rosette at one foot from end A, and B respectively and one in the middle of the specimen length. The exterior gages were placed in similar locations along the length. Two rosettes were placed one foot from each end respectively, two at the middle of the length of the specimen and a single rosettes was placed in the top portion of the riser ¼ length from end A of the riser.

Acoustic emission instrumentation consisted of two sensors exterior to the specimen and located at equal distances from the middle of the pipe. These sensors were specially designed for a pressurized wet environment. The sensors selected for the test program were resonant type R15I sensors (150 kHz peak response) manufactured by Physical Acoustics Inc. (PAC) and custom manufactured for the test. The data acquisition was accomplished with a PAC. model Mistras-2000. During the tests the initial threshold was set at an amplitude of 45dB. Although in the later stages where the either the number of hits as the result of leakage for the preliminary test or storage limitation as in the case of the final test, the threshold was increased to 50dB. Hit definition time was 400 μsec and a band pass filter was set at 20kHz low and 400kHz high. Gains were set to 40 dB in the preamplifiers.

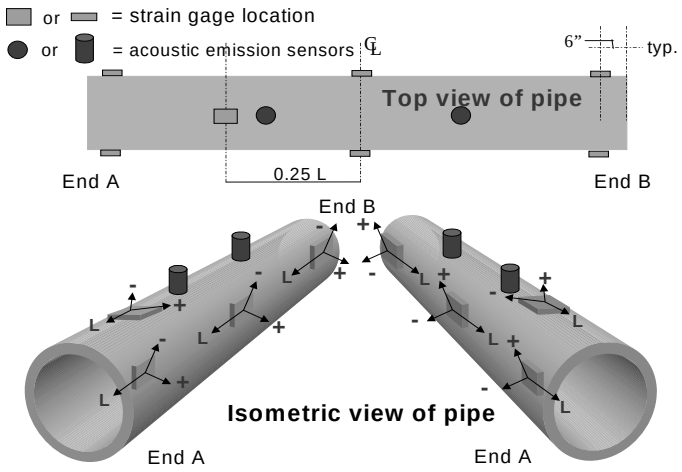

Exterior surface instrumentation

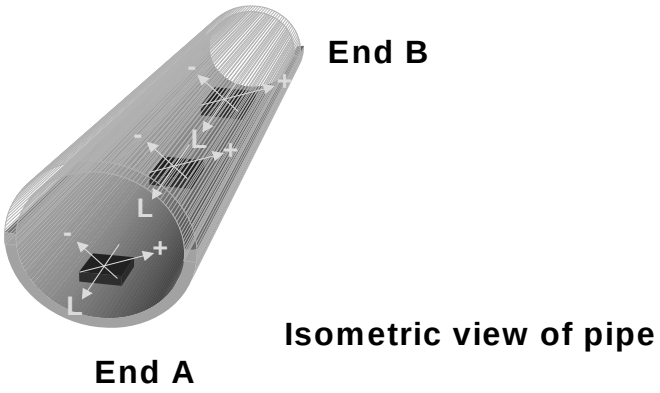

Interior surface instrumentation

Figure 2.10 Location of strain gages and AE sensors

Placing and securing of the AE sensor was performed on-site at H.O. Mohr laboratories. Since the sensor was placed on the exterior surface of the specimen, it was necessary to secure it in a way that would conform to the deformation resulting from the external pressure. The use of elastic bands was selected for this purpose. They provided positive attachment to the surface while keeping tension as the diameter of the riser reduced.

Figure 2.11 AE Calibration

After calibration of the AE sensors (Figure 2.11) one last preparation was made. A secondary concern was that if extensive matrix cracking took place, water would start seeping into the inside cavity of the specimen reducing the possibility of achieving collapse buckling as desired. To account for this, the specimen was wrapped in a triple sheet of plastic film. The intent was not to increase the capacity of the specimen but to bridge any cracks that may form during testing. This proved to be unnecessary since the amount of matrix cracking up to the point of failure was not as extensive, as discussed later.

The specimen was placed horizontally inside the chamber supported only at the ends in a rolling assembly. Figure 2.12 shows views of the specimen as it was before being placed in the chamber and the operation of sliding in to the chamber.

(a) Ready for placing in chamber

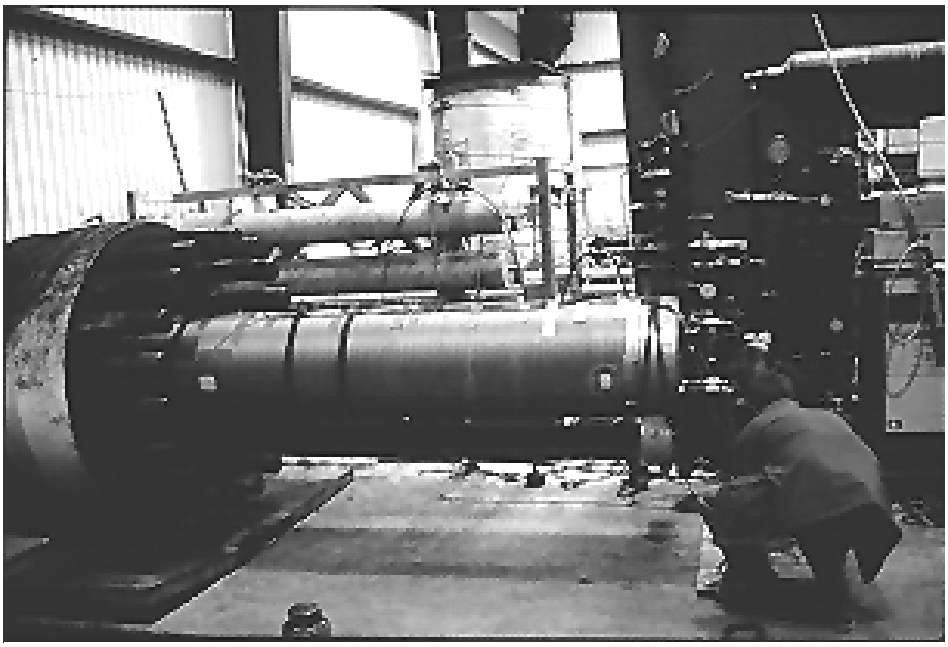

(b) Placing the specimen in chamber

Figure 2.12 Final preparations on-site

2.3. TEST RESULTS

During testing, external water pressure on the specimen was increased in steps, with a number of partial unloading and reloading cycles (Figure 2.13), up to final collapse of the tube. The pressurization sequence was chosen to facilitate acquisition of meaningful acoustic emissions data, and was based on recommendations provided in Reference 2.12. Loading was increased until collapse, which occurred at 3150 psi.

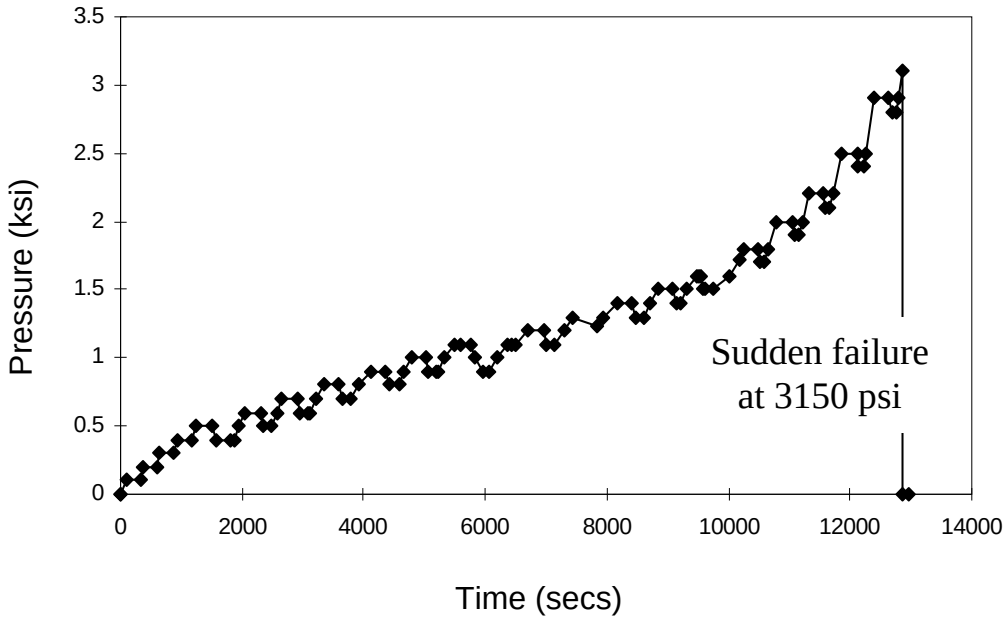

Figure 2.13 Load profile

As a result of seal failure, the specimen was loaded in separate occasions. The maximum loading of the preliminary tests was 700 psi and was followed by a final test with loading to failure. Comparing the measured strains for the tests it was apparent that no permanent deformation was incurred during the preliminary loading.

During the final test, failure occurred suddenly at 3150 psi external pressure. There was no indication of impending collapse from the pressure data or the strain gage data. The energy released during the collapse was enough to shear all four high strength

$1^1/_8$" diameter bolts securing the end cap plates. In addition, the specimen was projected to the far end of the chamber, impacted and rebounded back to the front.

The surface of the specimen after removal from the pressure chamber is shown in Figure 2.14. Damage extended along the entire length of the specimen, starting from about eight inches from each end.

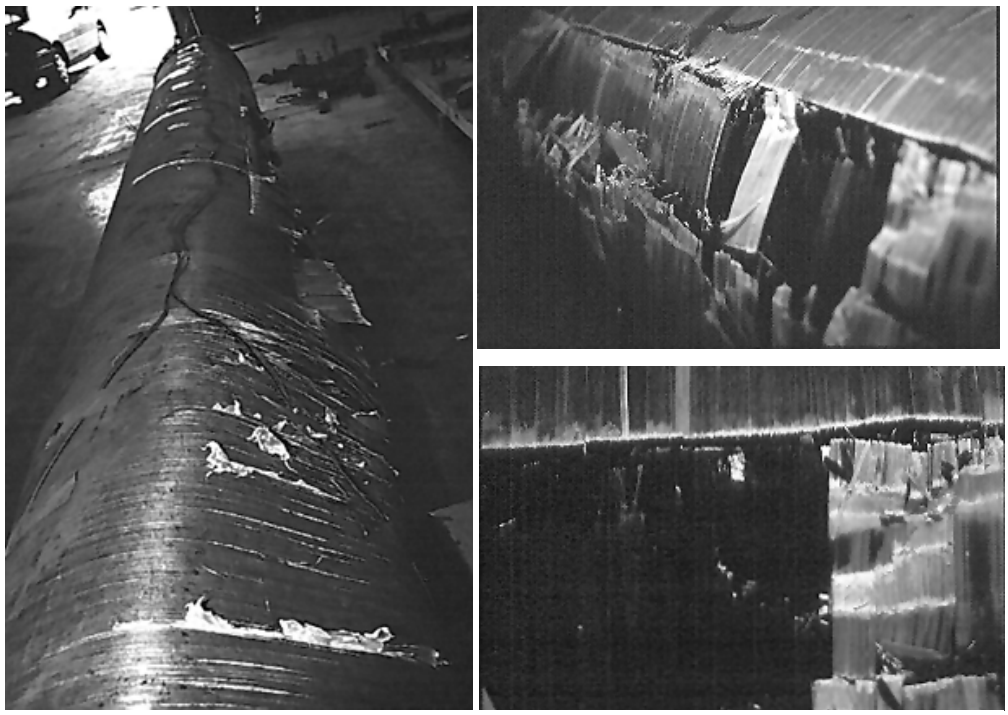

Figure 2.14 Views of tube after testing

Extensive fiber damage was noticeable in the middle third of the length of the specimen. Even though this damage was extensive, it took place only in a band of about one-foot wide. This band was centered along an axis rotated about 45^o degrees counterclockwise from the vertical axis if looking at the specimen from end A to end B as shown in Figure 2.15. The circumferentially opposite side of the specimen did not show signs of such extensive of damage, and no matrix crushing was noted either. For the most part the circumferentially opposite side to the failure surface kept its original

round shape. Unfortunately assessing the extent of damage at the ends of the specimen is difficult since they were severely damaged by the impact against the pressure chamber resulting from the failure energy release. On the interior surface of the specimen no damage was observed other than in the area next to the damage band and on the side of the band. The opposite side of the ID was for the most part as smooth and clear as it had been prior to testing. Figure 2.15 presents schematic representations of the failure profiles of the specimen.

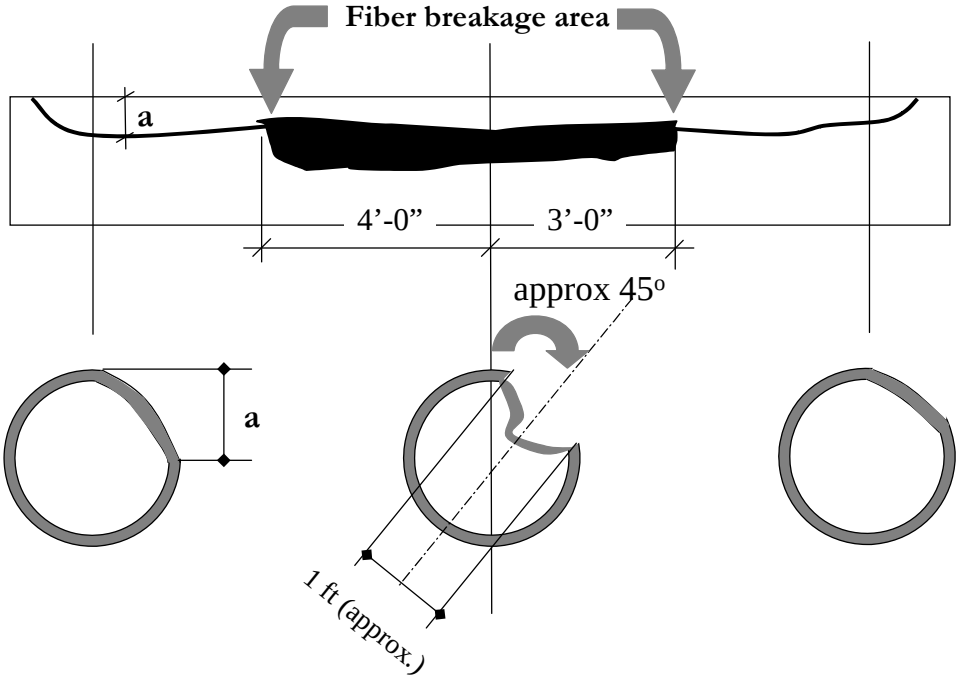

Figure 2.15 Failure profile schematic in riser

The only other visible difference in the outside diameter surface was noted in the side directly opposite to the main failure band. A single crack was noted running longitudinally along the specimen. No secondary cracking was noted in the area around this single long crack. The crack extended for about 5 feet centered on the riser length

and showed only matrix damage with no fiber extruding. No similar damage was observed on the inside diameter in the general location of the isolated crack.

As part of the post buckling study of the specimen, measurements were taken of the diameter of the riser. These readings were taken at seven locations equally spaced from end to end of the specimen. At each of these locations twelve diameter readings were taken as show in Figure 2.16, the spacing between the readings axes was 15 degrees. The results of these readings are presented in Figure 2.17. For the areas where the wall of the specimen was completely destroyed, readings were not taken and they show as a wedge in the profile. As stated earlier, it is interesting to see how only on the side of the final failure a noticeable change in the profile is observed while, the opposite side of the riser is still essentially as it was before the test.

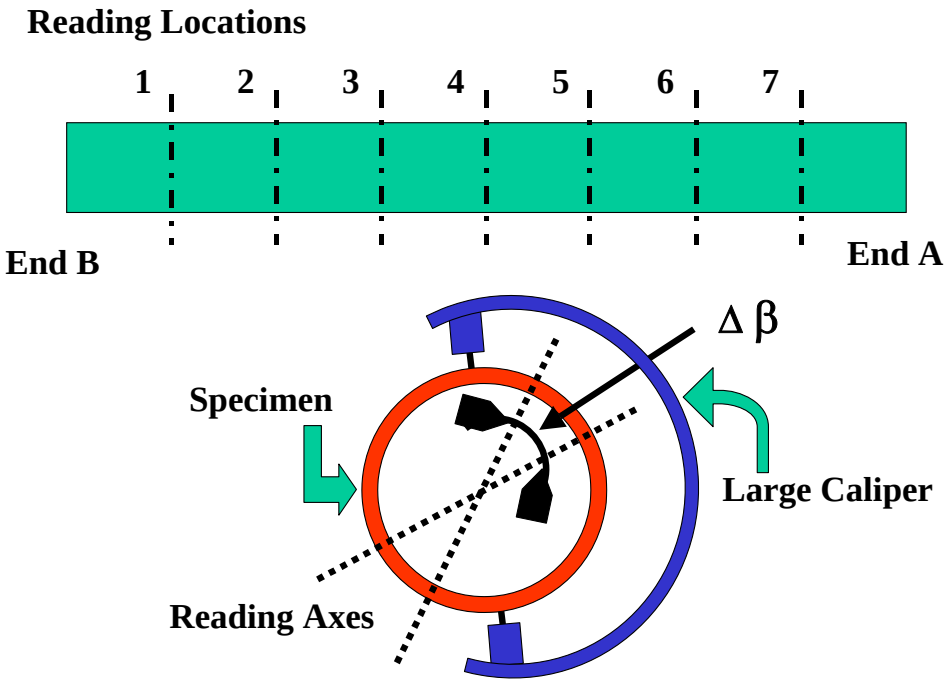

Figure 2.16 Readings at the postbuckled profile

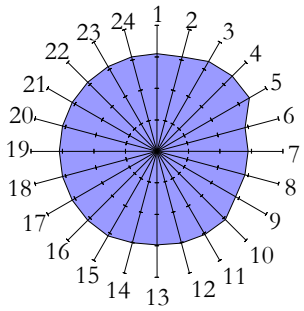

Location 1

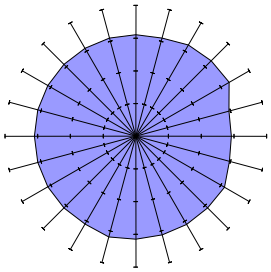

Location 2

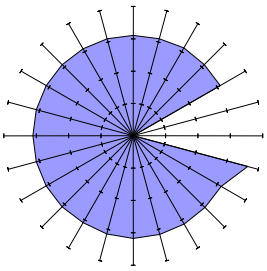

Location 3

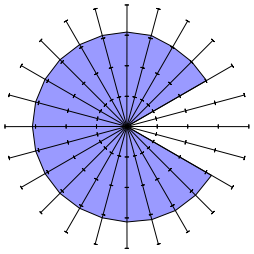

Location 4

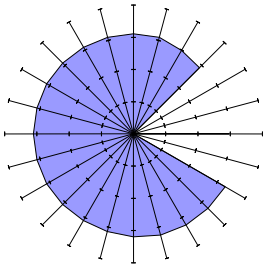

Location 5

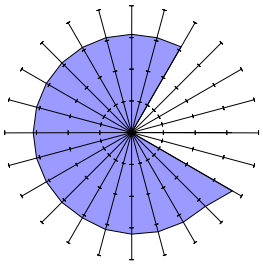

Location 6

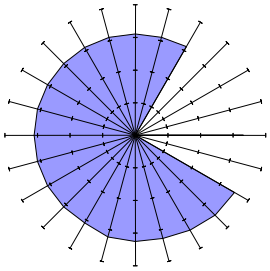

Location 7

Figure 2.17 Deformed profiles after collapse

2.3.1. STRAIN GAGE RECORDS

This sections presents data recorded from strain gages during the external pressure test. Analysis and discussion of this data will be presented in Section 2.4. The strain gage data was obtained from 120^{o} three gage Delta-Rosettes as stated before. These were placed in the specimen so that one of the three gages in the rosette would be aligned with the longitudinal axis of the specimen. Strain readings were taken at each load hold as indicated in the data points of Figure 2.13. Temperature corrections were not judged to be necessary since the test was performed in an unexposed chamber and pressure was slowly increased. The specimen was allowed to stabilize after the chamber was initially filled with water and before pressure beyond the hydrostatic one was applied. Gages were zeroed right before the tests started. In addition to the temperature effects, the gages were selected to minimize the effect of the external pressure applied to the exterior surface gages. Based on the information by the manufacturer and for this application, the effect of this surface pressure would be negligible.

During handling of the specimen a few of the interior gages were damaged. Most of the end gages remained in good working condition throughout the tests. In contrast, the middle axial gage and one of the delta gages in the middle were lost. Since they were inside the assembly, it was not possible to fix or install a replacement gage. Therefore, only one active gage remained in the middle of the pipe on the inside diameter, while all of the exterior gages were active. Between the preliminary and the final test one of the delta-gages from end B was lost. However, at the same time the wiring of one of the delta-gages from end A was repaired. This is the reason why, when looking at the strain records for the preliminary test, an End B Delta (-) gage is seen and for the final plot this is substituted by an End A Delta (-) that was not in the preliminary test results plot. Figure 2.18 shows the recorded data from the strain gages at the interior wall of the specimen, Figure 2.18 (a) shows the data from the preliminary test to 700 psi and, and Figure 2.18 (b) shows the data from the final test to failure. Figure 2.19 (a) presents the recorded strains from the gages on the exterior wall at the middle of the

specimen and at the quarter length of the specimen from the preliminary test. Figure 2.19 (b) presents the recorded strains at the final test loading.

Of the exterior gages in these locations only one was lost completely, and one of the delta gages at the quarter length could not be fixed. However, between the preliminary and final test, one of the delta gages in the middle was recovered after being highly erratic. Figure 2.20 presents the data from the gages located at both ends on the specimen on the exterior surface. Similarly to the other figures, Figure 2.20 (a) shows the data from the preliminary test and the companion view show the data at the same locations from the final test to failure. To understand the gage designations used in this Section refer to Figure 2.10. In this figure the rosettes were indicated with three axes and three symbols. One axis was designated “L”, another “-“ and a last one “+”. So in the figures, the label axial refers to the gage in the rosette oriented in the “L” axis, and the gages labeled Delta, refer to the “+” and “-“ axes respectively.

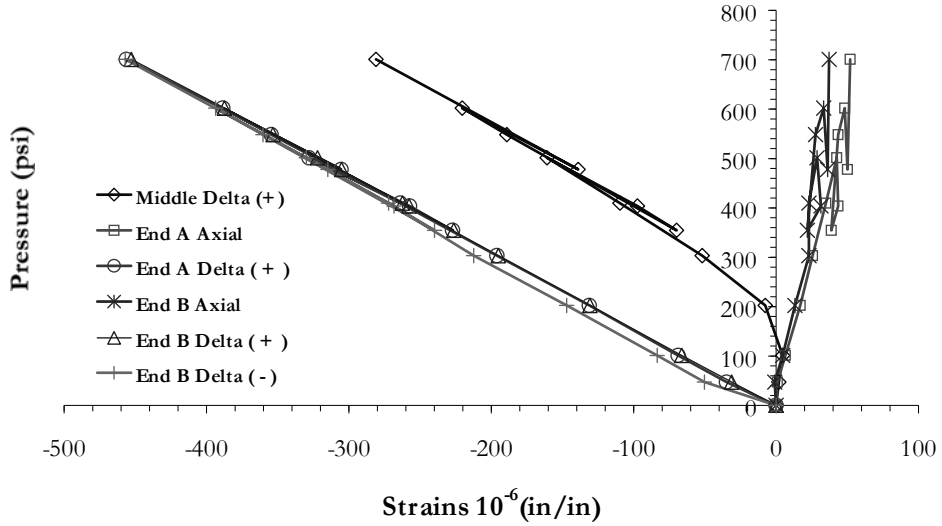

(a) Preliminary test to 700 psi

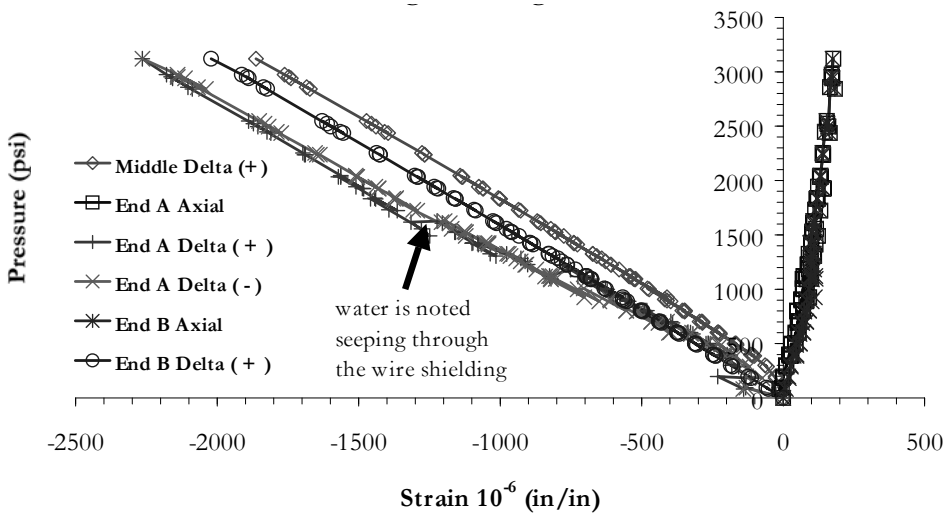

(b) Final test readings

Figure 2.18 Interior gage readings

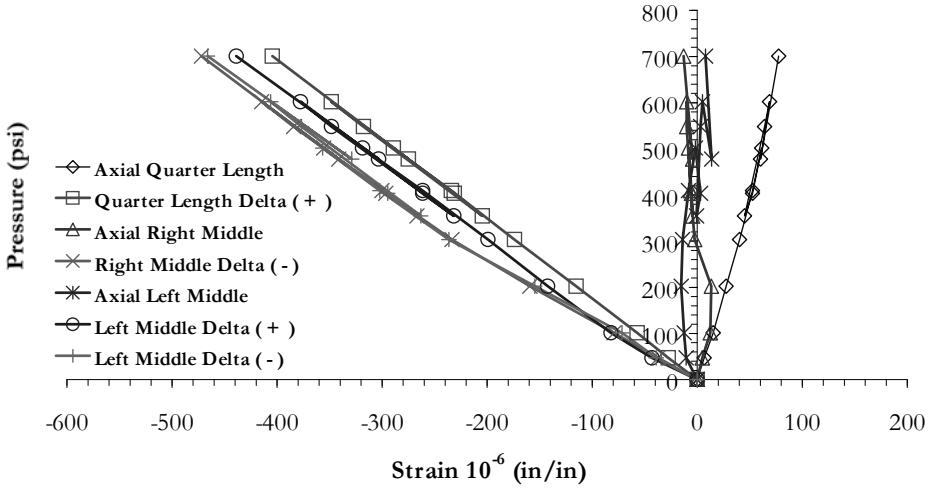

(a) Preliminary Test to 700 psi

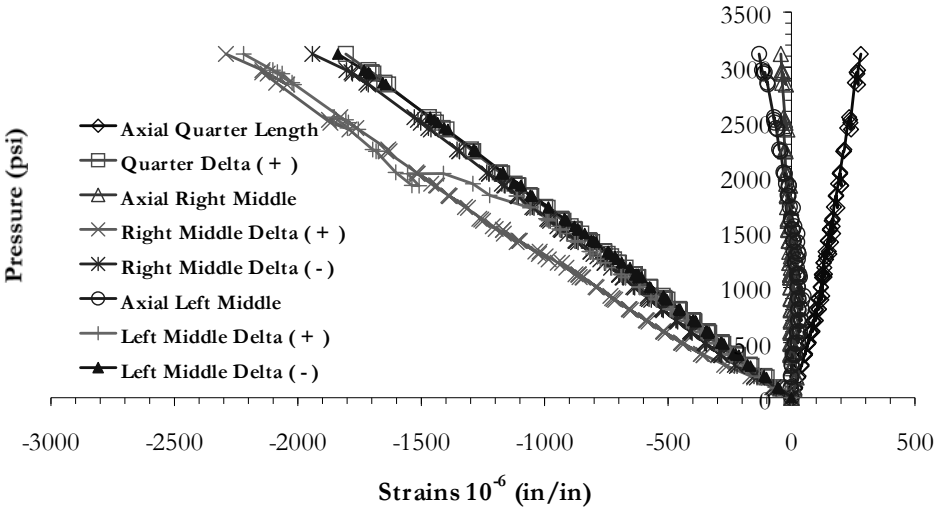

(b) Final Test Readings

Figure 2.19 Exterior gage readings at middle and quarter length locations

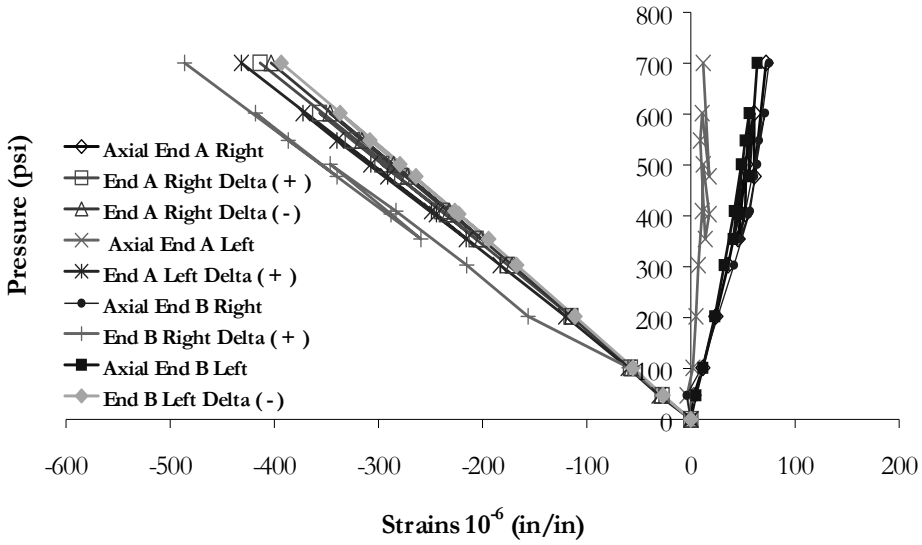

(a) Preliminary test to 700 psi

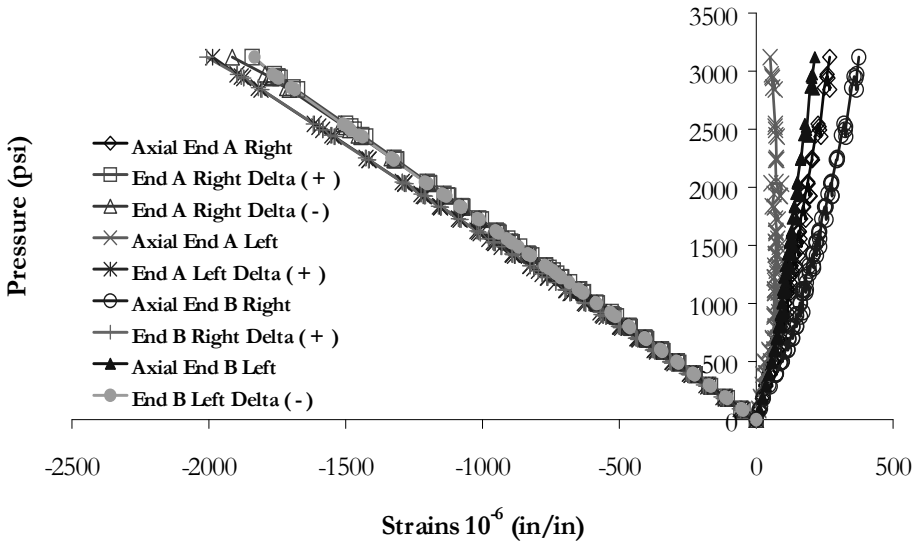

(b) Final test readings

Figure 2.20 Exterior gage readings at ends of specimen

2.3.2. *ACOUSTIC EMISSION RECORDS*

This section presents selected acoustic emission data recorded during the test. Analysis and discussion of this data will be presented in Section 2.4. It is to be noted that the analysis will be focused only on general trends observed during the test. No attempts are made to identify specific damage mechanisms at play during the testing. This work will be performed by others and will be presented on a separate dissertation [2.28]. The equipment used for this test was a PAC Mistras-2000 system with two channels with sensors resonant to 150kHz. The sensors were specifically for operating in a pressurized environment. Figure 2.21 shows the plot of the maximum amplitude shown in decibels (dB) of all of the hits recorded, at both sensors, versus time in seconds for the preliminary test to 700 psi. Superimposed on the same plot, is the loading profile as followed during the test.

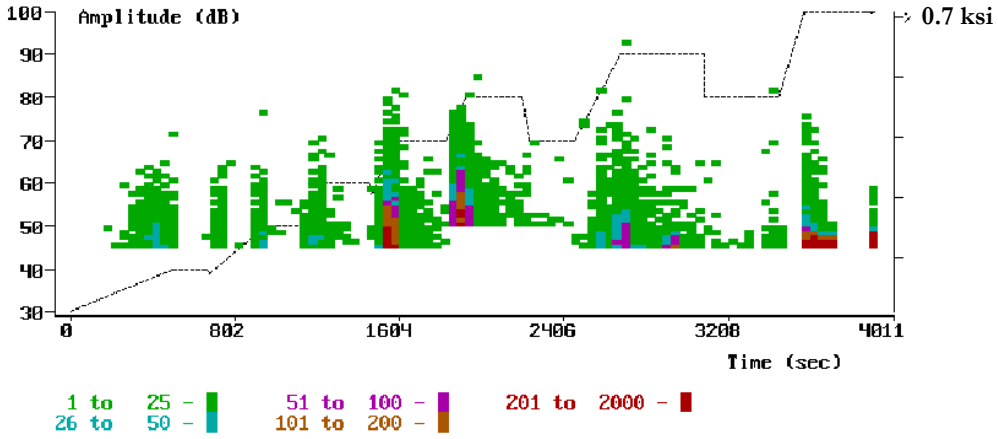

Figure 2.21 Acoustic emission data from preliminary test to 700 psi

Figure 2.22 (a) shows the plot of the duration each hit plotted also in a time scale. Figure 2.22 (b) shows the accumulated signal strength plot.

A significant number of events were recorded right from the beginning of the loading, which is common in thick walled fiber reinforced composite specimens [2.24]. Typically, emissions began during loading and decayed during the load hold until 700 psi was reached, where during the load hold, an increasing number of events were

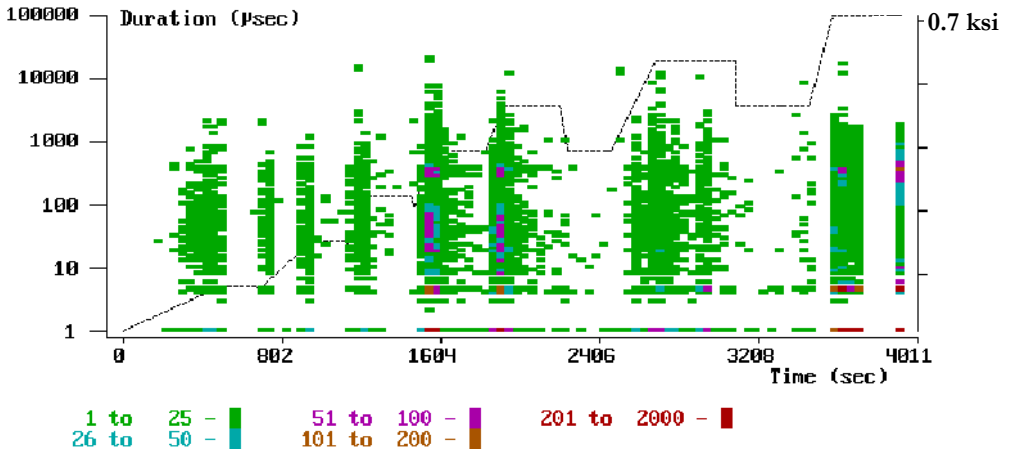

(a) Duration Plot

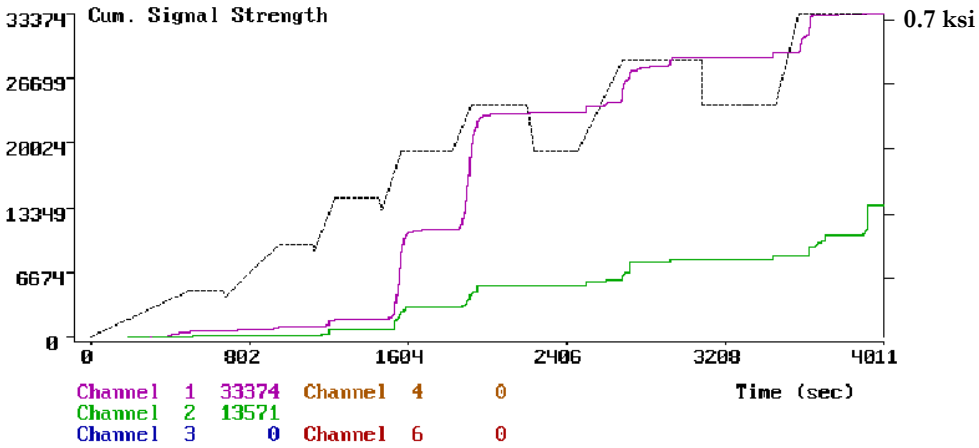

(b) Cummulative Signal Strength

Figure 2.22 Acoustic emission record for preliminary test to 700 psi

recorded. At some point during the 700 psi load hold; the seals began to fail in this test. The seal leaking was detected by the AE and unfortunately masked some of the emission resulting from material changes produced by the applied stress. The increase in emission during load holds became considerable after 500 psi.

Figure 2.23 and 2.24 show the records of emission for the last test during loading from zero to 1,100 psi. No leakage was detected during this test. These records will later be compared to the ones from the first preliminary test. Readings up to this stage will be used to determine the extent of damage as generated during the preliminary loading stage. This is a common practice when evaluating pressure vessels with AE as described in the introduction chapter of this dissertation.

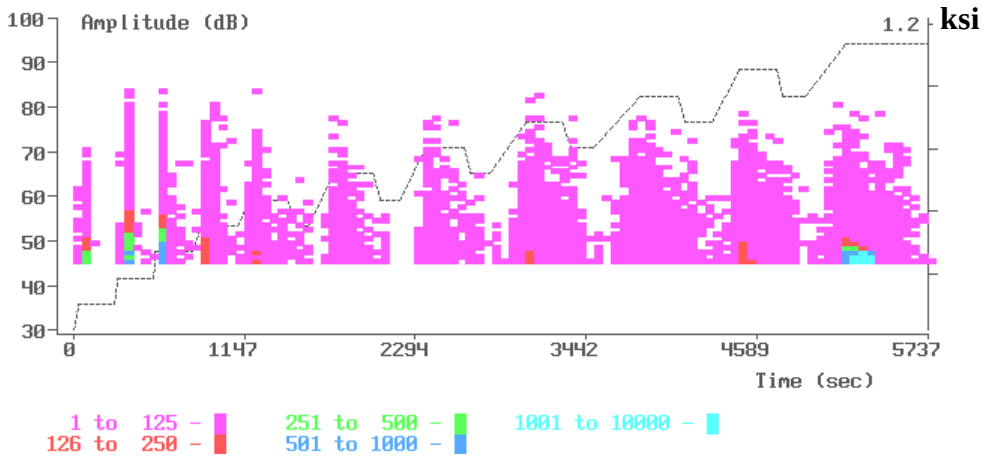

Figure 2.23 Amplitude distribution records for final test for pressure from 0 to 1,100 psi

Next, the AE records from 1,100 psi to 1,600 psi are presented in the Figures 2.25 and 2.26. The reason for separating the AE files in this way is to aid in the interpretations as a set of data is compared to the one immediately before or after the load stage of interest. A file containing all the AE information from initial stage to failure may obscure the first indications of damage as recorded by the AE. Finally the records for the final loading stages are presented. These records correspond to the pressures from 1,600 psi to failure (3150 psi) and are shown in Figures 2.27 to 2.28.

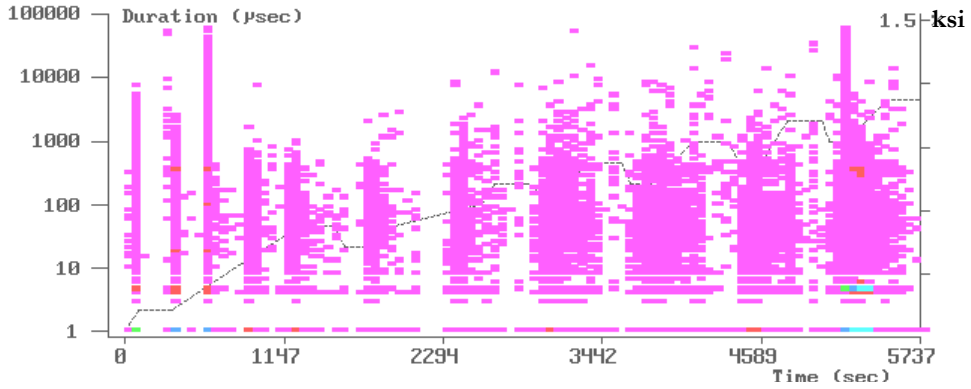

(a) Signal duration

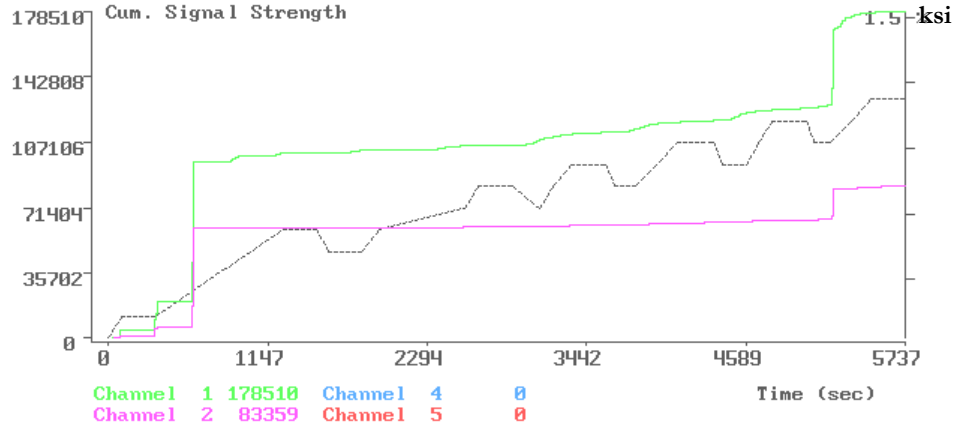

(b) Cummulative signal strength

Figure 2.24 Acoustic emission records for final test for pressures from 0 to 1,100 psi

For composite materials, analysis of AE features when recorded and interpreted correctly have proven quite capable of helping in the understanding of the behavior of a component when used with other methods of data acquisition [2.26].

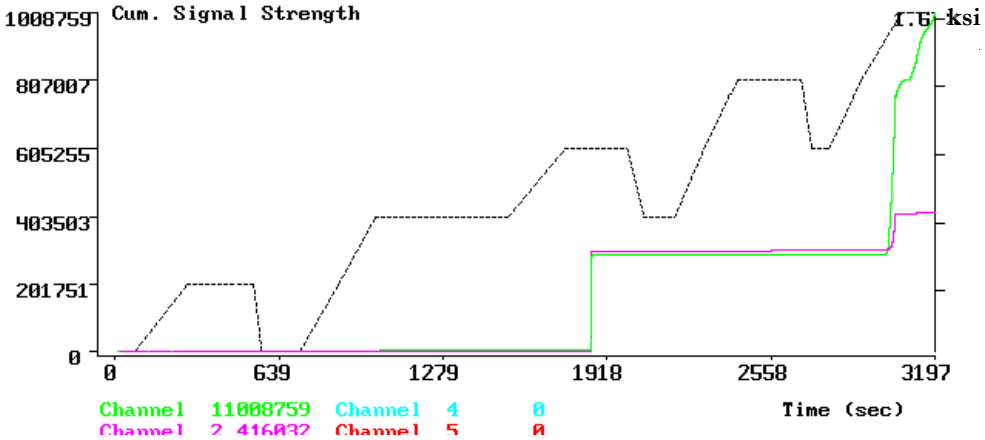

Figure 2.26 Cummulative signal strength for final test for pressures from 1,100 to 1,600 psi

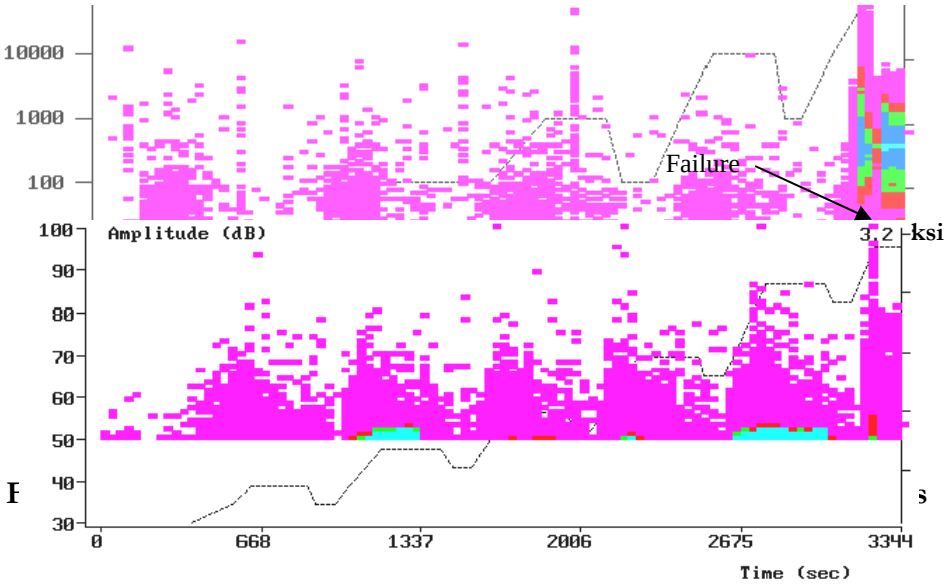

Figure 2.27 Amplitude distribution for final test for pressures from 1,600 to failure

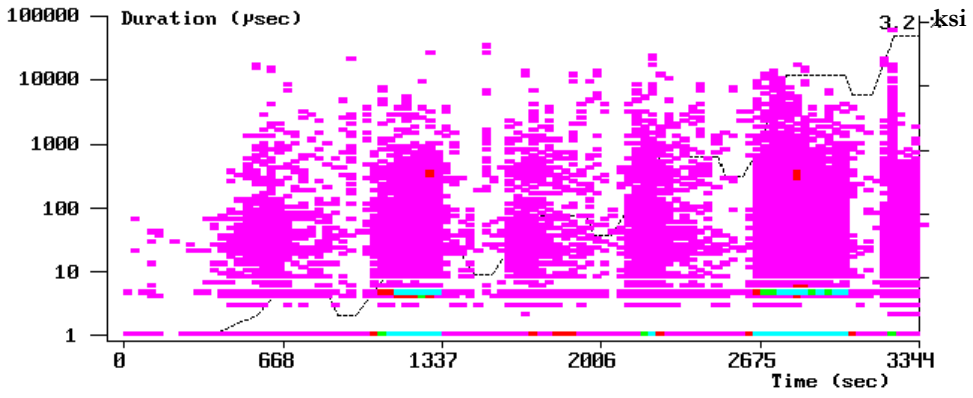

(a) Signal duration

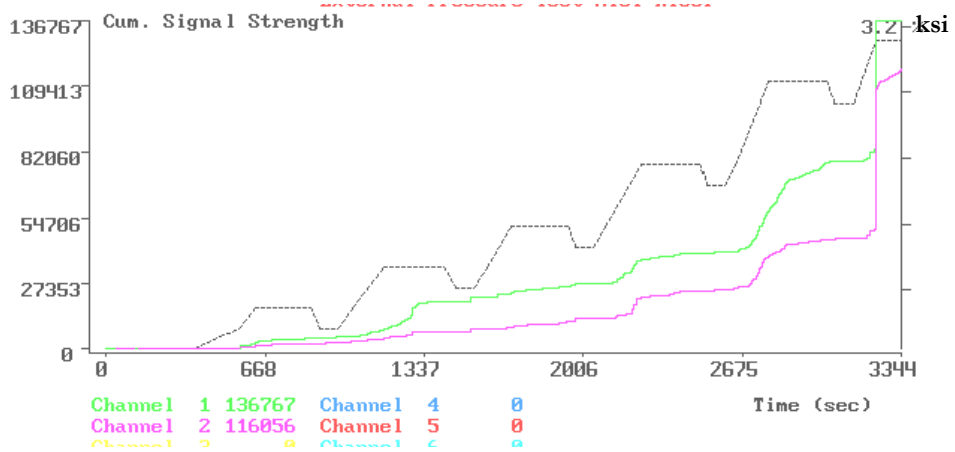

(b) Cummulative signal strength

Figure 2.28 Acoustic emission records for final test for pressures from 1,600 psi to failure

2.4. ANALYSIS AND DISCUSSION OF TEST DATA

Although during the tests some strain gages were lost at different locations, the information was sufficient to provide some useful observations on the specimen behavior. The use of acoustic emission provided additional insights into the specimen's response at various stages of loading. The analysis of the data gathered during the tests will be divided in two sections. First, the strain gage data and the acoustic emission data will be examined. Second, comparisons will be made to various failure criteria. The comparisons will be made at the local material level and at the structural level (elastic buckling of a pipe).

2.4.1. ANALYSIS OF STRAIN GAGE DATA

In the analysis of the strain gage data, calculated principal strains are used. For this test, where the state of stress induced was primarily uniaxial, or in the hoop direction only, the principal strains will correspond to the direction of loading (hoop or Principal 2) and the normal direction (axial or Principal 1) to the loading. Boundary and other conditions however, may affect the direction of the principal strains. For example, the specimen was supported only at discrete points at each end. This introduced the effect of bending in the recorded strains, as will be discussed later. The effect of the bending induced strains on the measured hoop strains was minimal. However, the axial strains were visibly affected by this influence. The result was that the alignment of the Principal 1 (P1) strains is not exactly longitudinal to the specimen, whereas the P2 strains do not change orientation for all practical purposes. Further, errors are unavoidable when placing strain gages in a specimen; therefore alignment is never perfect. Using the principal strains for all the locations instrumented in the specimen facilitates comparisons.

With the data recorded from the strain rosettes, principal strains were calculated for different locations along the length of the specimen. The first objective was to verify

if permanent damage had been generated during the preliminary test to 700 psi. A comparison of the strains calculated for the first test with the strains from the final test calculated at the same level of loading reflect no detectable difference in stiffness (Figure 2.29). There is a small difference noted at the last load stages of the Principal 1 curves. This difference is small and could be attributed to round-off error in the calculation or even in the accuracy of the recording equipment. In addition, at this stage of the preliminary test, the seal had started to fail and maintaining the pressure was difficult. The plot shown in Figure 2.31 does not reflect the actual fluctuations of the pressure at that point. This strain data does not reflect anything conclusive with respect to damage incurred in the resin matrix of the riser. Since extensive matrix cracking will have little effect on the overall stiffness of the component [2.12], the recorded strains may not reflect this. Nevertheless, it can be concluded that no considerable change to the overall stiffness of the specimen was generated at the 700-psi pressure level.

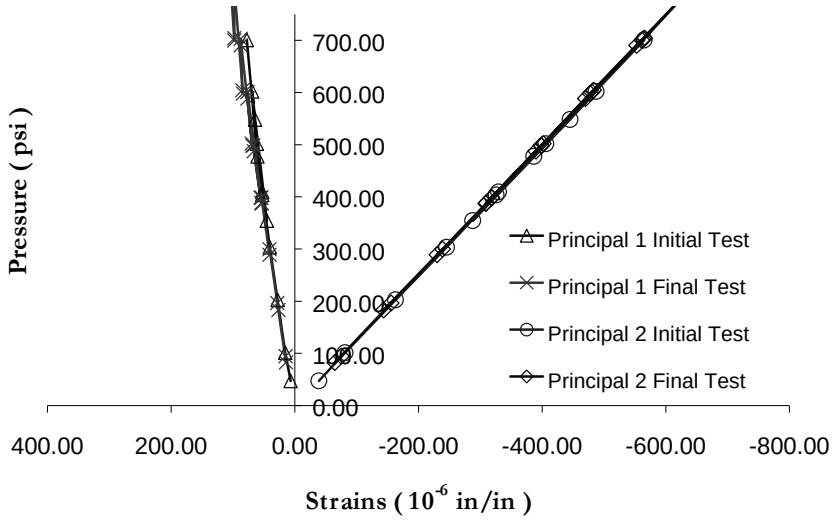

Figure 2.29 Comparison between loadings

Figure 2.30 shows the principal strains as calculated for the interior wall gages for the final test to failure. In the figure, the strains are labeled P1 and P2. These are the minimum principal strain and maximum respectively. The curve for P2 at End A shows

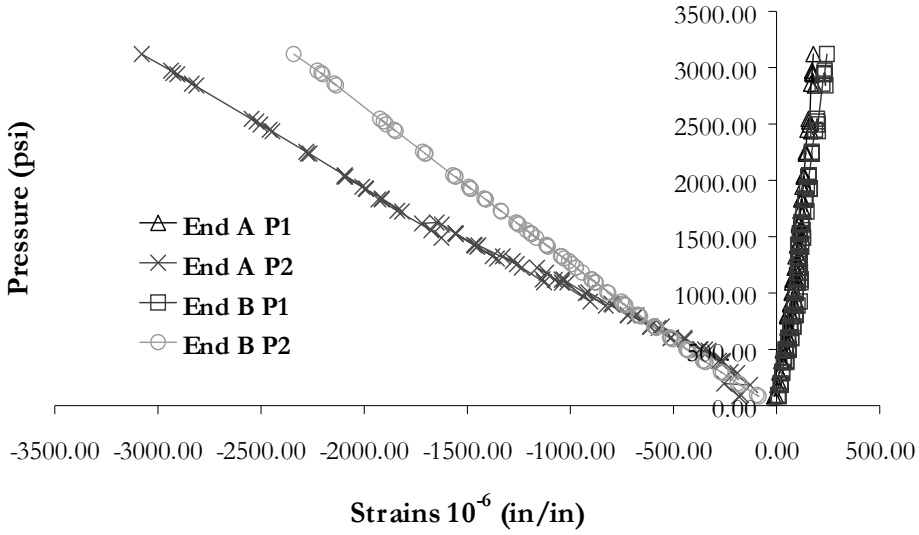

Figure 2.30 Calulated principal strains inside wall

a drift in the plot at about 1,100-psi. As noted in Figure 2.18 (b), at this point water was observed coming out of the gage wire shielding. No other gages showed such a drift in the response. It is therefore assumed that this drift is due only to the change in resistivity produced by the introduction of water into the strain gage wire.

Additional explanation is needed regarding the calculation for P2 at End B. As noted in Section 2.3.1, for the final test, the Delta (+) gage at End B was lost. The other two gages in the rosette remained in good condition for the duration of the test. The data from the preliminary test was used to calculate a relationship between Delta (-) and Delta (+) on this particular rosette since all the gages were active during this test. It was then assumed that this relationship did not change for the final test and, was used to calculate P2 and P1 based on only the axial gage and Delta (+). It is believed that this procedure introduced little, if any, error. As can be seen from this and subsequent strain plots, there were no major changes noted in the trends for any of the calculated strains that would be affected by this assumption.

The calculated principal strains for the exterior surface gages are presented in Figures 2.31 and 2.32. The first figure presents the calculated principal strains at the ends of the specimen and the latter figure shows the calculated strains at the middle and quarter length of the specimen.

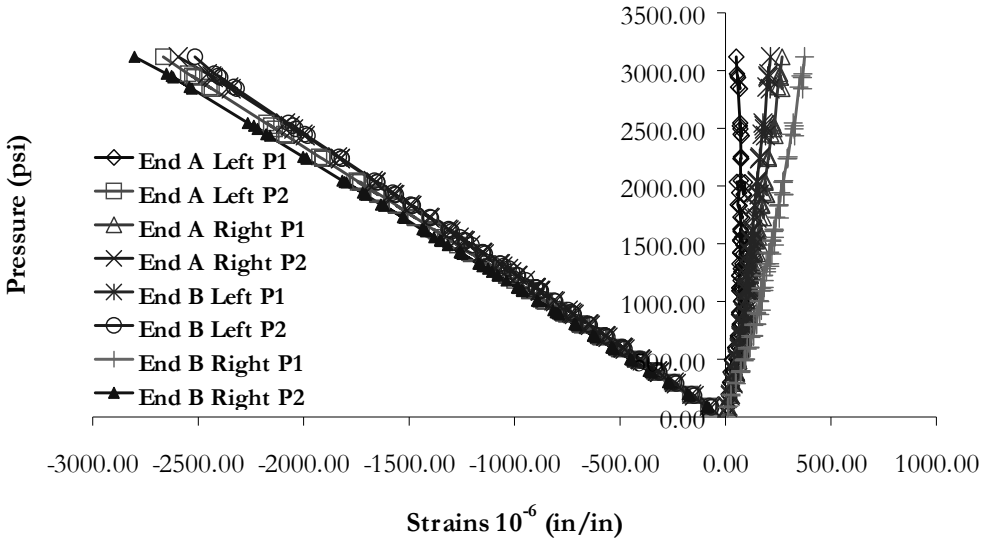

Figure 2.31 Principal strains on exterior ends of specimen

Assumptions had to be made for the calculations of the principal strains at the ends as a result of loosing some of the gages during the test. Looking at the data plots presented earlier in Section 2.3.1 for the end locations, it is apparent that the strains measured by the delta-oriented gages were very consistent to each other at both ends. Most of the noticeable differences were observed in the gages oriented to the longitudinal axis of the specimen. However, even in the case of the longitudinal gages, the differences in the recorded strains are only noticeable because of the small magnitude of the strains measured, which magnifies the differences induced by gage error and alignment differences between them. Therefore, in the case where the missing strain data was from one of the delta-oriented gages, it was assumed that the P2 strains calculated at End A Right were the same for all the locations at the ends of the specimen up to 500-psi. The motivation for using of the low range of pressure for the adjustment

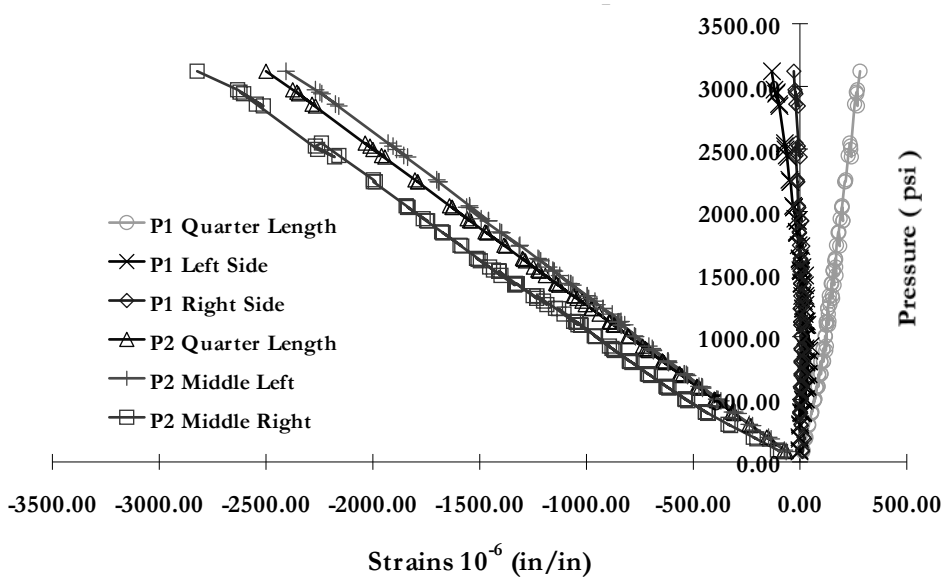

Figure 2.32 Exterior principal strains at middle and quarter locations

came from studying the measured strains in other locations for this same pressure level and noting the linearity in the behavior. With the assumed value of P2, and with the records for the remaining active gages, the misalignment between gages and the principal axis was calculated, with P1 subsequently calculated. The values were compared to the calculated values of end A right, at every load step for verification.

With these calculated values for the principal strains, we note that the P2 strains are very consistent and linear at the ends of the riser as the pressure increases. A departure from the linearity is noted in the P1 strains as calculated. This change will be addressed later.

Figure 2.32 shows the calculated principal strains at locations in the middle and quarter length of the specimen. Differences can be observed in P1 strains between the middle and the quarter length locations. It should be noted that there is a difference in the circumferencial location for gages at the middle and quarter length of the specimen. The gages at the middle of the specimen were located at the middle depth. In contrast,

the gage at the quarter length was located at the top of the specimen. These locations held true when the specimen was placed in the pressure chamber. Both gage locations at the middle of the specimen showed the same behavior, which suggests that the gage readings are valid.

Figure 2.33 shows a comparison of P1 strains for the exterior surface locations. Strains for the Ends A and B were averaged for purpose of this comparison, and so were the strains for the middle gages. Looking at the averaged strains it is clear that at most locations on the exterior surface the data follows a similar trend with increasing nearly linear values of strain. However, the middle strains exhibit a completely different pattern of behavior.

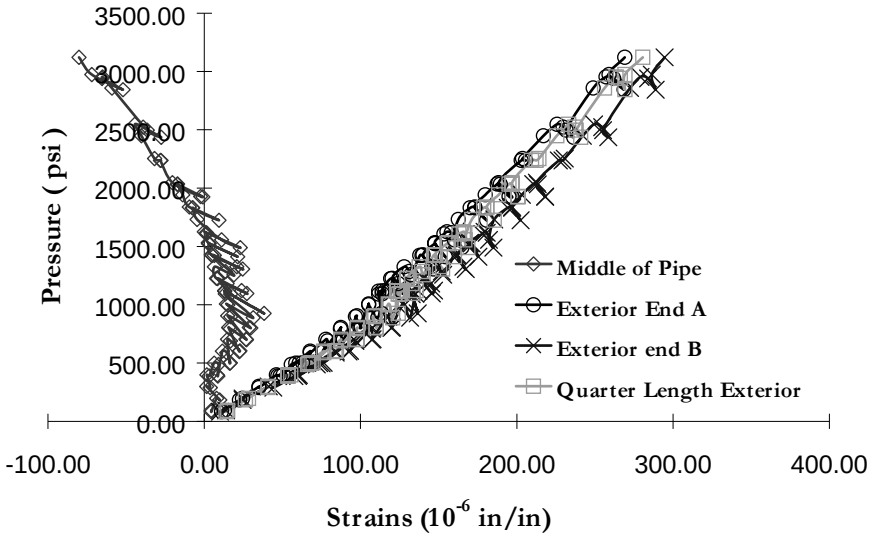

Figure 2.33 P1 strain comparinson at exterior surface locations

Looking at the general profile of the P1 strains in Figure 2.35, two things are immediately evident. First, there is a noticeable change in the slope of the middle P1 strain at the lower pressures between 100 and 400 psi. In addition after 500-psi all the P1 strains significantly deviate from linear behavior and the value of the middle P1

strains reverse in sign. This change in sign occurs even when the applied pressure would create positive P1 strain resulting from the Poisson ratio effect. The resulting change is the likely result of the straightening of the specimen from the curvature induced by the end support condition and the self-weight of the riser as pressure is applied.

In can be verified by analysis including self weight of the specimen that pipe specimens under uniform external pressure have the tendency of straightening from any curvature in their length. Since the specimen was allowed to move freely in the axial direction in the test setup, and it was supported only at the very ends in rolling supports, its own weight created a curvature. As stated before, the gages were zeroed after the specimen was set in the chamber and filler with water. Therefore, the straightening of the specimen would be detected by the gages. This also explains why the unusual behavior is observed only in the middle gages and is not as apparent in the end and quarter length gages. The quarter length gages may have seen some change in its strains, but it was small enough that it is not as obvious as in the middle ones.

The next peculiarity in the strain gage data is the non-linearity in the calculated P1 strains even at locations where the effect of the longitudinal curvature change as explained should not have influenced the behavior. This non-linearity is not as apparent in the P2 strains. Not even effects of ovalization in the radial direction were noticeable in the measured strains in the hoop direction during the test. Unfortunately it is not possible to calculate the true principal strains in the middle of the riser at the inside wall location. As noted in Section 2.3.1, a number of individual gages within the rosettes were lost during handling of specimen. However looking at the recorded strain for the surviving delta gage a few interesting observations can be made on the behavior of the specimen. Figure 2.34 shows the behavior of this gage for the preliminary and final tests.

To help interpret Figure 2.34, Figure 2.35 also presents the recorded strains for gages located on the exterior wall of the specimen for the same load range. It is apparent that the same noticeable change in behavior can be seen in the axial gages shown in the

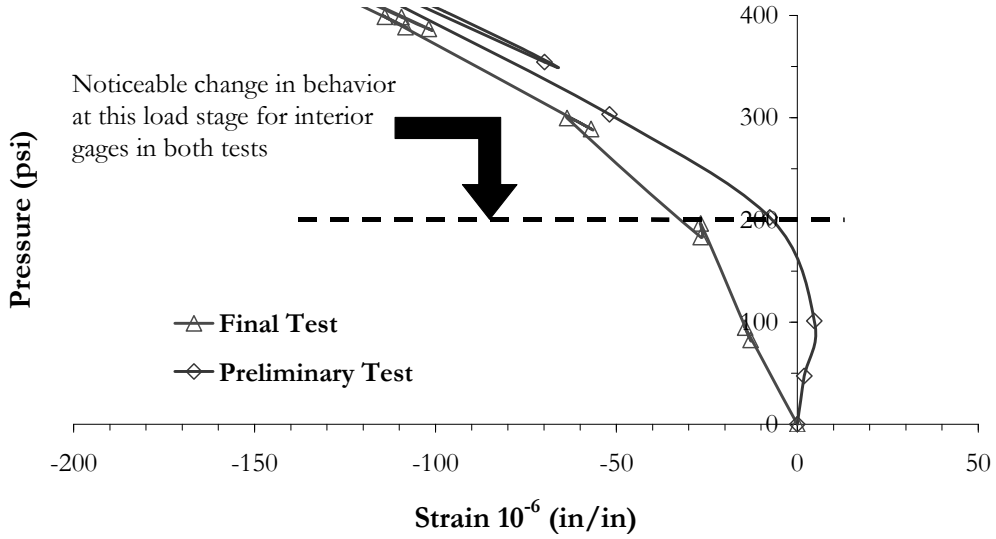

Figure 2.34 Strains recorded for interior wall of specimen

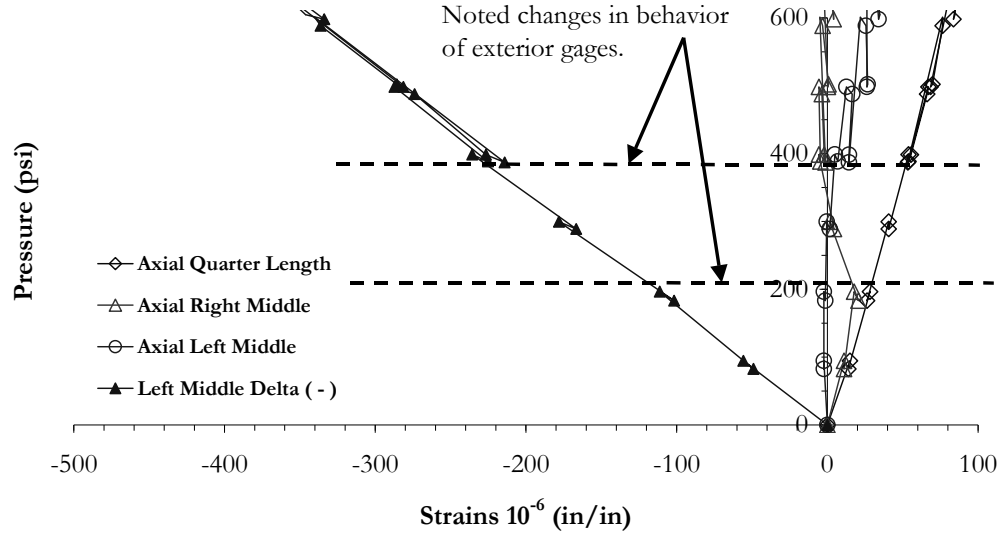

Figure 2.35 Strains recorded at exterior surface of specimen

figure. This change is more visible in the axial gages than in the Delta gages where is virtually nonexistent. Nevertheless, the change in the slope for the axial gages can be seen at about 200 psi. The only delta type gage that showed any change in trend was the

one at the inside wall. This gage showed almost no increase in strains until this point during the preliminary test. The same gage showed a slightly different trend during the final test where it showed minimal strain increase at the initial stages and then started to pickup more after this load point. The reason for this observed change, at this load range, is speculated to be a combination of factors related to the geometry of the specimen and not related to material nonlinearity. Later in this chapter a finite element model is presented that includes the delamination as a gap between two separate cylindrical shapes modeled with contact elements. This model includes an internal ring and an external ring as part of the same specimen separated by the gap created by the delamination. The model will show that, at about this load stage, depending on the separation of the layers at the delamination, both rings are engaged by the reduction in diameter of the external ring which is the one directly exposed to the fluid in the pressure chamber.

This point of contact noted in the plots is not as clear in the final tests as it is in the preliminary test plots. It is speculated that the difference between the preliminary and final tests can be attributed to water filling the specimen between the preliminary and final tests. When the seal failed during the preliminary test, water rushed inside the assembly. This water ended in the inside diameter of the riser and was not emptied between tests since the seals where modified without disassembling the main fixture plates. The weight of the water inside the specimen forced the inside ring into contact across the delamination gap to the outside ring by bending.

As noted earlier, one of the factors influencing the recorded behavior of the specimen was the straightening of the bending curvature induced by the applied pressure. To obtain an estimate of the amount of the axial deformation associated with this phenomenon, a comparison is made, between the surface axial strains measured at the ends and, those measured at the middle locations. Note that the readings from the longitudinal strain gages and not the calculated P1 strains are used for this purpose, since the orientation of the P1 strains was not always to the longitudinal direction as a result of this same effect.

Figure 2.36 shows the difference between the axial gages located at the middle and at the ends of the specimen. In the figure, the absolute difference between the readings is labeled as "axial difference." There will be some error involved in this comparison, since the longitudinal gages in the rosettes are not perfectly aligned with the axis of the specimen. In addition, even when every effort was taken to place the gages in the same diametrical location, this may not have been achieved to perfection. Nevertheless, a reasonable estimate can be obtained of the curvature in the specimen at the beginning of the test. Only the readings recorded immediately after pressure increases were used for calculations shown in Figure 2.36. This was because permanent deformation effects became more significant during loads starting at about 400 psi, and continued until failure.

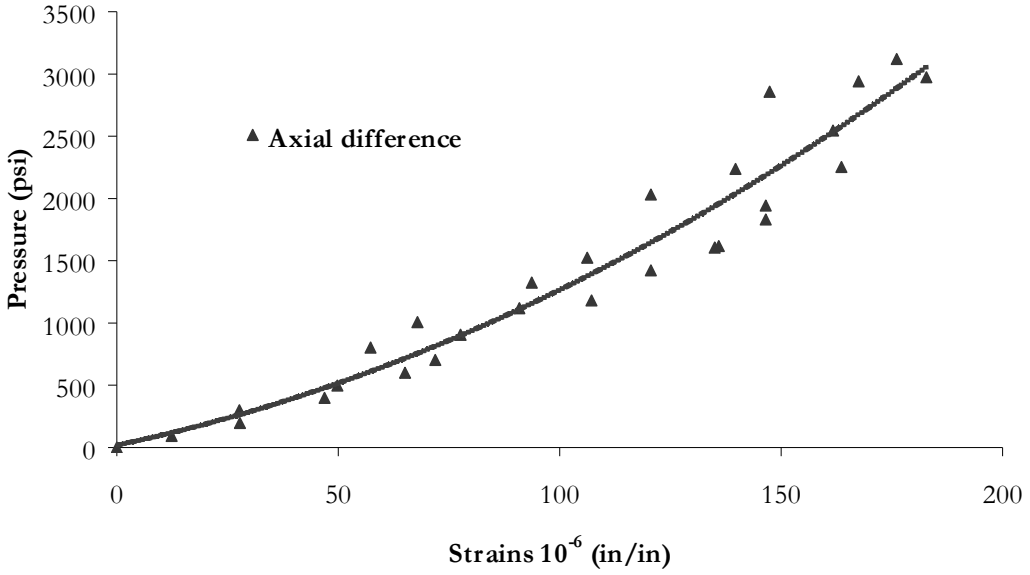

Figure 2.36 Axial strain deviation

As noted in the previous discussion, permanent deformation or indications of creep behavior were recorded in the axial or longitudinal direction during the final test. Figure 2.37 shows the plot of the recorded axial strains at the quarter point location in pressure range of 0 to 1,500 psi. The reason for selecting the quarter points is that this

location showed the least amount of influence of pipe straightening while still keeping the most important aspects of the deformation induced by the applied pressure.

Two numbers are shown in the plot at every location where permanent deformation was noted. The top number indicates the amount of permanent deformation as the difference between the strain readings from two records made at the same pressure level. The first record was made immediately after reaching that pressure level for the first time in the test, and another made during the unloading stage as dictated by the predetermined loading curve. The second number, shown in the bottom of the pair, is the ratio of permanent deformation as a function of the increase in pressure. This ratio was calculated by the following expression:

$$Ratio = \frac{\delta \Delta}{\delta P}$$

Where $\delta\Delta$ is the permanent deformation and δP is the increase of pressure between the maximum pressure previously applied to the specimen at that stage and the pressure at the initial reading.

Figure 2.38 presents the calculated values for stages between 1400 and failure. Comparing Figures 2.37 and 2.38 we see that permanent deformation became noticeable after 500 psi, with a steadily increasing value up to failure. At the time of buckling, the ratio of permanent deformation in the axial direction as calculated in the plots was 0.14.

The permanent deformation in the specimen during loading may play an important role in the prediction of the collapse load and perhaps associated limit states. From the strains that were calculated in the hoop direction it was observed that almost no change was noticeable during the test up to the time of failure.

Determining experimentally the amount of damage that takes place in the resin matrix in a specimen as result of applied load it a difficult process. As noted, this damage will not be readily apparent in the recorded stiffness for the specimen.

However, determination of the effect of damage progression at the matrix level through other properties like the Poisson relationship in the material, may give a relationship between damage in the matrix and specimen properties. Lack of companion specimens and similar tests makes this impossible to extrapolate. Nevertheless, it is a behavioral aspect worth noting for future tests in similar specimens.

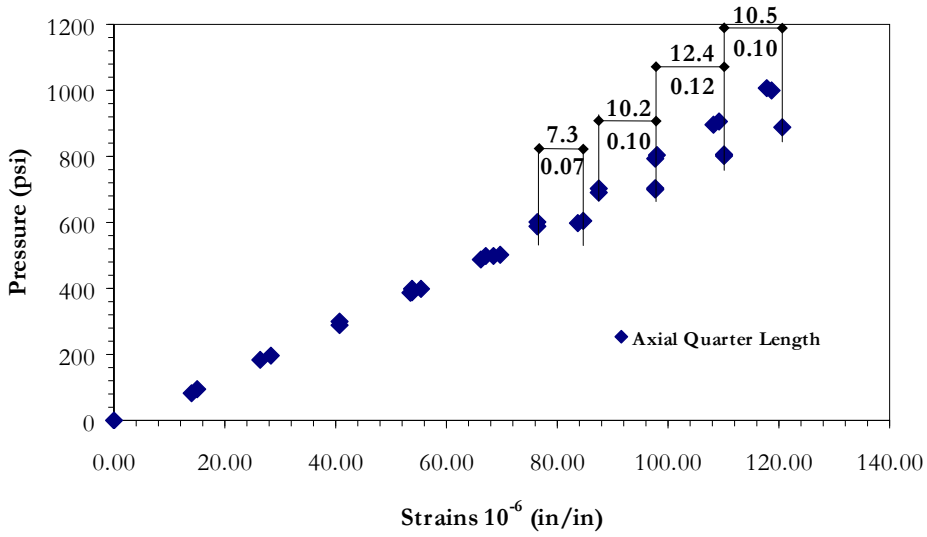

Figure 2.37 Permanent deformation estimates for 0 to 1.5 ksi

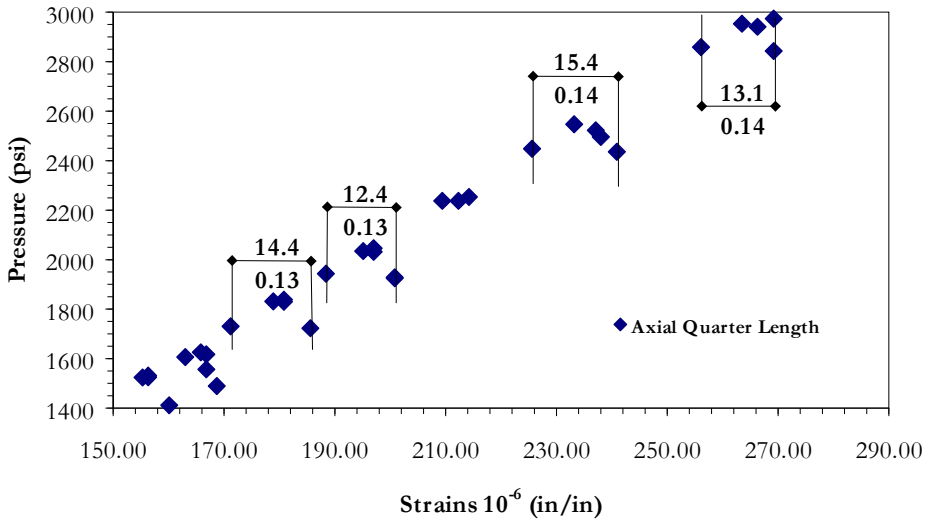

Figure 2.38 Permanent deformation estimates for 1.5 to 3.0 ksi range

2.4.2. ACOUSTIC EMISSION ANALYSIS

As mentioned before, acoustic emission (AE) has been used successfully in the in-service monitoring of fiber reinforced pressure vessels. AE analysis is greatly enhanced when data from several tests of the similar components are available since it would help with the association of AE features to behavioral milestones. For a single test to failure, as was the case here, AE analysis can be supported with the use of other information gathering means like strain gages or similar devices. In this work, the information gathered by AE methods will be used to support some interesting trends observed in the associated data from the strain gages and the followup finite element model.

A comparison of the AE signals, between the preliminary and final test for the pressure range of zero to 600 psi, is in Figure 2.39. Channel 1 and channel 2 as indicated in this and following figures, corresponds to the two AE sensors placed on the specimen. The location of the sensors is shown in Figure 2.9. Channel 1 corresponds to

the sensor near the gate of the pressure chamber or End A in the figure. Channel 2 is the other end or End B. Figure 2.39 shows the beginning of emission at about the same pressure for both tests. However, the total cumulative energy is clearly larger in the final test that in the preliminary. The larger energy in the final test is influenced more by the amount of AE detected in the initial 200 psi of applied pressure than in subsequent applied pressures up to the pre-tested 700 psi. Since no leakage was detected during the initial stages of the final test, the noise may be mechanical in nature.

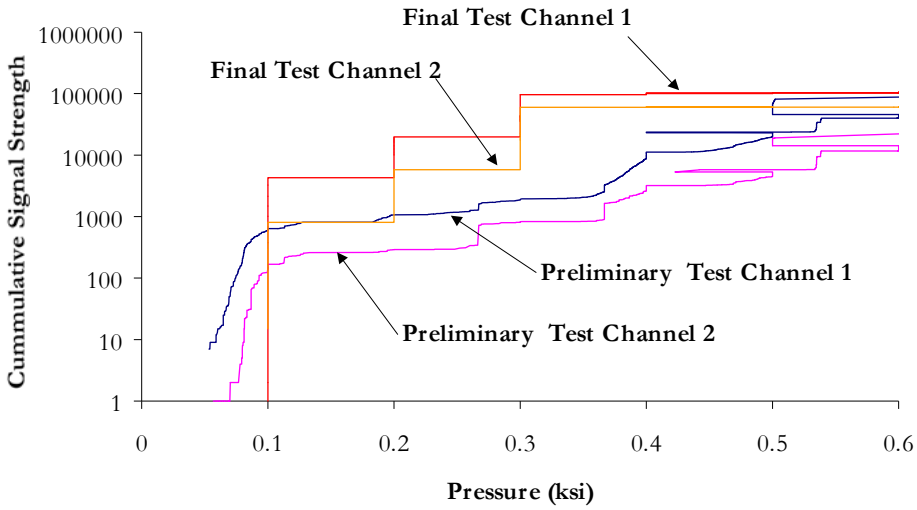

Figure 2.39 Comparison of signal strength betwen tests

Typically a mechanical source of AE emission is referred to an external source that has nothing to do with damage growth in the material. For example, the filler pipe and the specimen, may have rubbed against each other, or the specimen seal may have rubbed against the specimen. Another possibility is movement of the entire assembly inside the pressure chamber. Finally, it could be speculated that the emission can be attributed to the rubbing and contacting of the two cylinders as the void in the delamination is being closed. The source of this emission at this point cannot be determined with certainty. Associated analysis of the AE data obtained from this test will provide with additional information. However, from the strain gage data, where it is seen that a change in stiffness took place a low pressure levels as the result of contact, it

is speculated that the main source of this emission could be the rubbing and contacting at the preexisting delamination in the tube. The fact that the emission is different between the preliminary and final test at very low pressure, suggests that the surfaces could have been in greater contact at the last test than in the preliminary one. In addition, although the emissions were strong at this stage, they took place only while the pressure was increased, with no significant emission detected during the pressure hold. Looking at the plots presented from Figures 2.21 to 2.28, we can see a strong correlation of the AE signatures to the assumptions of initiation of contact and rubbing between the two cylinders at the low pressure levels. Looking at Figure 2.23 for the final tests, it can be seen that at the low levels of about 200 psi, signatures typically associated with mechanical rubbing are present in three occasions. This are further corroborated by the duration plots shown in Figure 2.24 where long duration events were observed at this same location on the time scale. The same trends were present in the plots for the preliminary tests, although somewhat obscured by the leak taking place at the time. The remaining AE data analysis will now concentrate on the emissions obtained during the final test of the specimen.

Looking at the plots presented in Figures 2.21 and 2.22, the following can be noted with respect to duration of events. If the duration of the events recorded during the initial stages up to about 300-psi is neglected, then, a steadily increasing duration value for the events at each of the load stages can be noted. In addition, although most of the emission takes place during the load increases, the amount of emission during load holds increases starting at the 500-psi level and with each increasing load stage. The reason for the large amount of emission recorded during the load increases can be explained by the first loading effect on composites. As discussed before, composites will typically present high amounts of AE emissions when they are loaded for the first time. In this particular case this cannot be specified as the only reason since the specimen was preloaded two previous times. However, the time between tests may have been long enough for the material to recover.

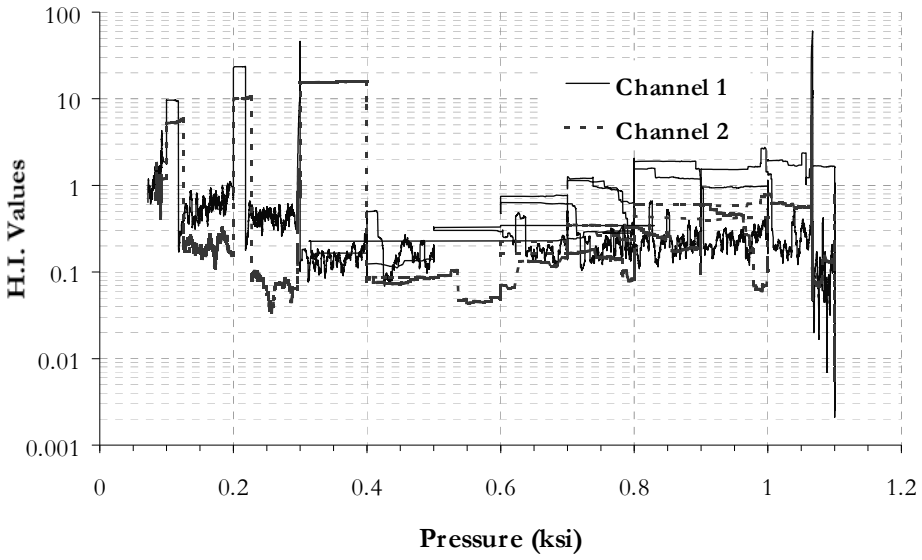

Figure 2.40 Historic index for final test pressures from 0 to 1,100 psi

As defined in Chapter 1 of this dissertation, a common method used to interpret the significance of the AE emission is by the Historic Index (HI). The HI helps determine at what point the emission becomes significant by comparing the energy for each event to the energy of the immediate preceding events. HI calculates a relationship between the slope of the energy plot and the change at each load stage. Figure 2.40 shows the historic index for the pressure stages between 0 and 1,100-psi for the final test. The HI is typically plotted against time. However, in Figure 2.40, HI is plotted against pressure to assist in the evaluation of the data. Because of the difference in HI values calculated through the test, a logarithmic axis was used for the vertical values of the plot.

Some of the more distinguishable features of the plot are the large jumps in HI values at 100, 200, 300, 400 and 1,100 psi. A quieting of the signal occurs from 500 to 600 psi followed by a gradual increase in HI with increasing load. Recall that after 600 psi, the permanent deformation becomes more noticeable in the strain gage data. It is

speculated that this emission is associated with the increase in permanent deformation. Perhaps it could be associated with damage growth at the matrix level, such as delamination or fiber debonding, which are not predictable directly by failure criteria calculations.

Another interesting feature of the AE signals is that after 800 psi the Felicity ratio becomes apparent for the first time. The Felicity ratio is a way to quantify the amount of damage in a composite by calculating the relationship between the previous pressure level in the specimen and the pressure at which emission begins at reloading. Figure 2.41 plots cumulative signal strength against pressures up to 1200-psi. This figure shows that the signal strength curve increases in magnitude after unloadings, even before the previous maximum load is reached. This corresponds to Felicity ratios less that 1.0 suggesting that damage being generated in the specimen is increasing. The indications of permanent deformation that begin to be noticeable at this level appear to support this observation. Unfortunately, it was not possible to compute the Felicity ratio as the specimen approached its maximum load. The amount of unloading allowed during the test was not sufficient to allow the specimen to stop emission during load

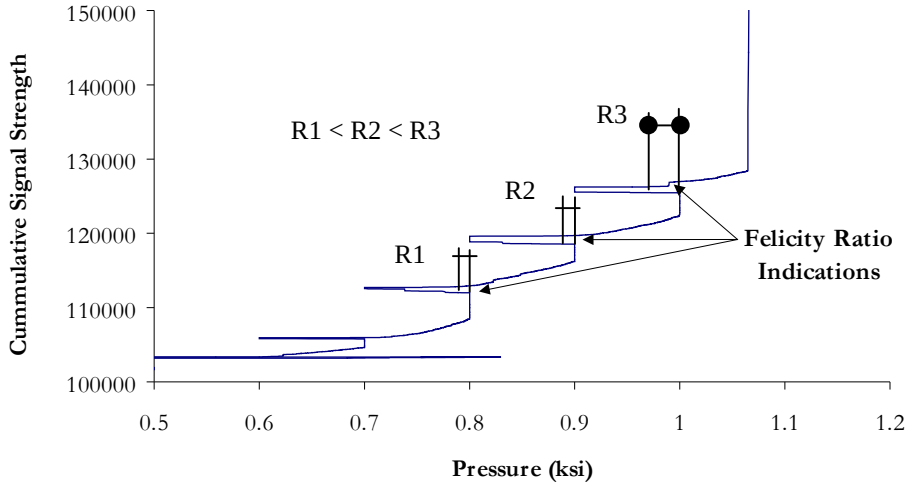

Figure 2.41 Initial Felicity ratio indications

holds, and since emission was continuous during unloading and load holds the Felicity ratio could not be numerically determined. However, it is possible to qualitatively estimate that as the load increased, the Felicity ratio decreased. This is seen by noting that as the load level increased, the amount of emission decay during load holds decreased at every new load. So if the amount of emission during load hold is associated with the Felicity effect, the Felicity ratio must be decaying at every increase of pressure. As can be seen in Figures 2.25 and 2.26 most of the cumulative energy recorded in the final test was generated during the loading stages between 1400-psi and 1600-psi. The source of this emission is unclear.

Finally, the values for the historic index for the final portion of the loading will be presented here. Figure 2.42 shows the historic index for the first load stages from 1,100 to 1,600 psi. Figure 2.43 plots the historic index between 1,500-psi up to failure at 3150-psi. The historic index jumps at about 2.0 ksi and becomes quite active until failure is reached. The historic index values plotted for the initial load stages of the final test, plotted in Figure 2.40 showed the majority of the HI values, other that the spikes, are at least one order of magnitude smaller than the ones recorded immediately after 2.0 ksi. This indicates that the relative change in signal strength between the emissions recorded to that level is greater after 2.0-ksi, indicating that the amount of damage being generated at that stage has higher signal strength levels. This would indicate that the damage as recorded after 2.0 ksi was more critical than the one recorded at lower levels.

Finally, Figure 2.44 shows the calculated severity curves for three separate load stages of the test. Severity, as defined in Chapter 1, is another measure of the importance of the emissions recorded during a test. It is, as the historic index, an indication of the amount of energy recorded by the acoustic emission. The severity plots follow the same trends as discussed above. The relative value of the calculated severity supports the observation that a great deal of the energy was released between pressures of 1,400 and 1,600 psi. If we ignore the energy at the time of failure, there was little indication of imminent failure even at the load hold prior to maximum pressure.

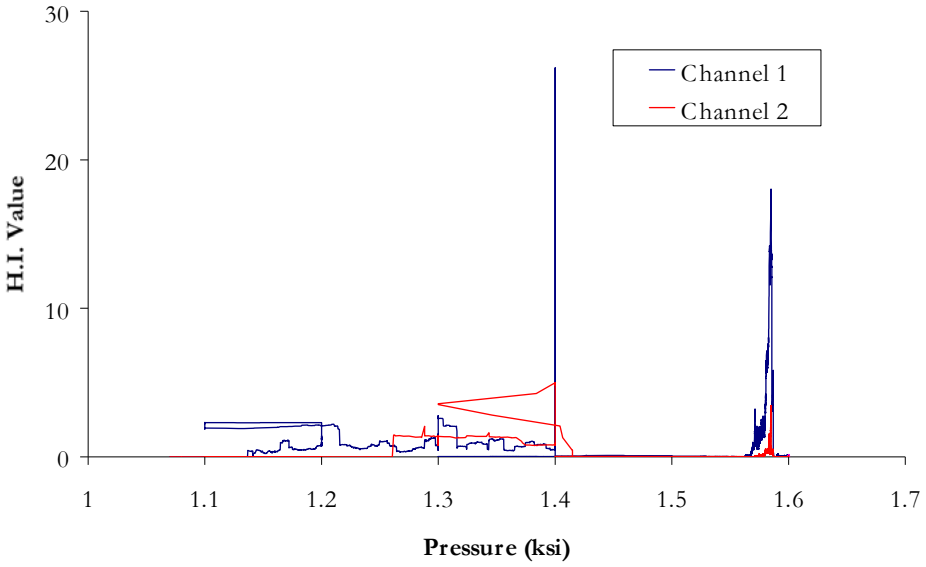

Figure 2.42 Historic Index for Final load stages

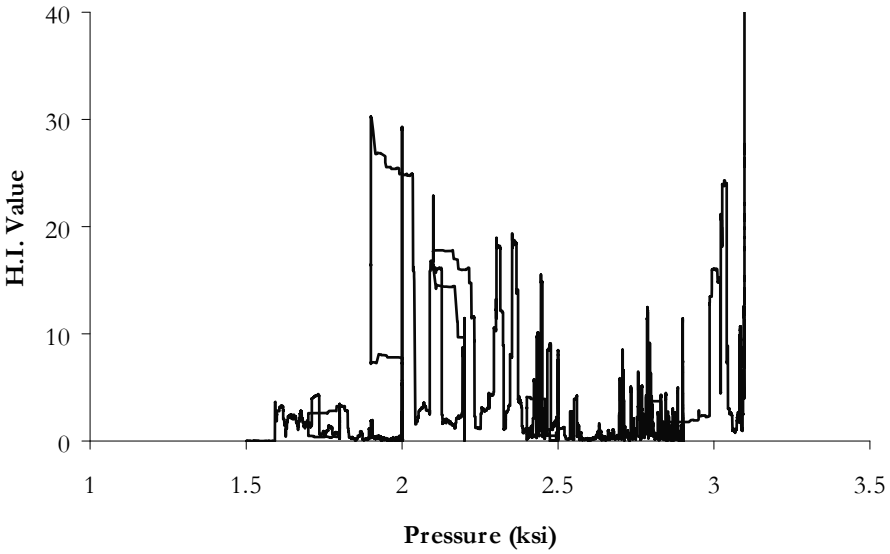

Figure 2.43 Historic Index for Final load stages

The main significant aspects of the previous discussion relate to the type of failure and the possibility of predicting it. The lack of more clear indications of imminent failure suggests the possibility of a failure not driven by progressive material damage. A more extensive damage mechanism would have had progressively growing emissions and intensity as the pressure increased. The AE records of this test suggest that the failure was probably the result of a sudden change in geometry rather than a slow weakening in the material capacity. Damage growth in the specimen was detected by the AE. However, the records did not show clear changes as the pressure increased that would have indicated that failure was approaching. If the failure was the result of elastic instability, this would explain why prediction by means of AE was difficult. Elastic instability would not be the result of damage growth, but of the geometric properties of the specimen, which are not quantifiable by AE.

In addition to the data in figure 2.44, Figure 2.45 shows the correlation plots for the same pressure groups. Generally accepted as a means to verify the validity of the attributes from the AE data, the plots show the data trends and their similarity with typical characteristics as expected from real emission. From the figures shown for the different loading stages, we see no obvious indication that the data may be the result of leakage or any other source that would result in false emission. Even more important, different mechanisms can be seen at play at each of the load stages presented in Figure 2.45. For example, view A shows the long duration events associated with contact at the delamination along with other sources. View B is a completely different mechanism, since it is speculated that by this load stage the contact between the rings was complete. View C in contrast shows a typical profile for the condition where one sensor is closer to the area of damage than the other. This particular condition is supported by the figures shown in Figure 2.46 where the correlation for the sensors is plotted for selected load holds, but each sensor hit is shown separately by a different tick mark. All figures show the condition where one sensor is more active that the other during the particular load holds. However, this difference is minimized as the final load approaches and both sensors begin to receive similar hits.

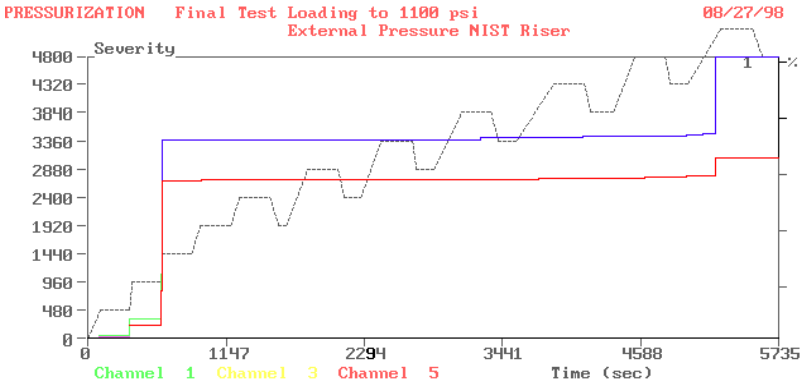

(a) Pressures up to 1100 psi

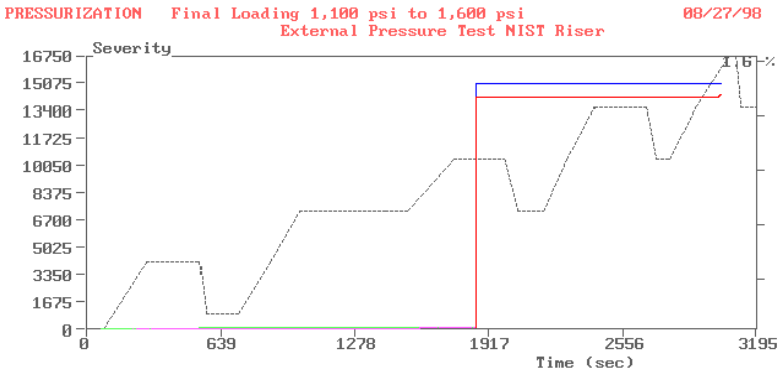

(b) Pressures from 1100 to 1600 psi

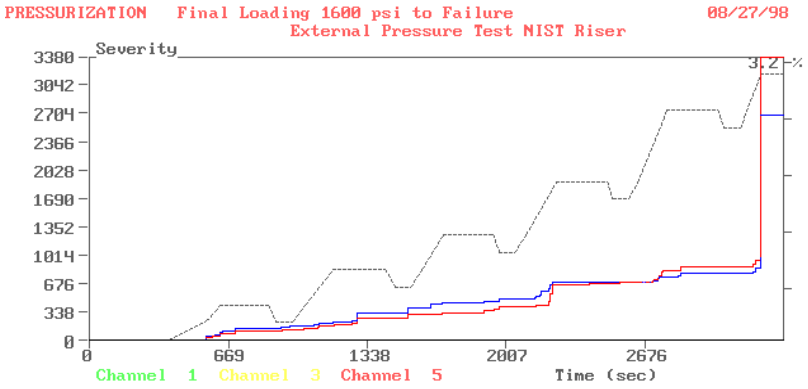

(c) Pressures from 1600 psi to failure

Figure 2.44 Severity plots

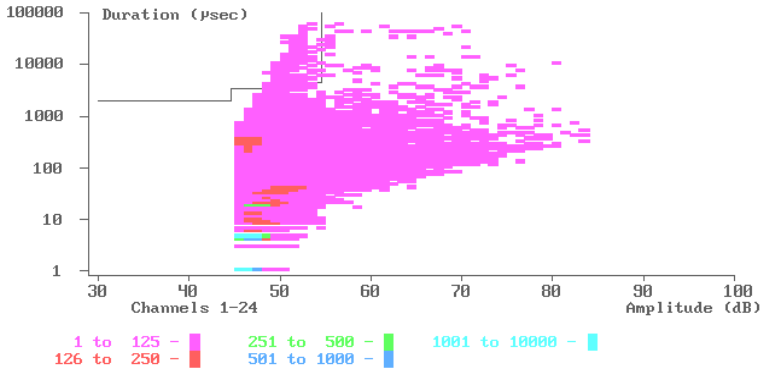

(a) Pressures up to 1100 psi

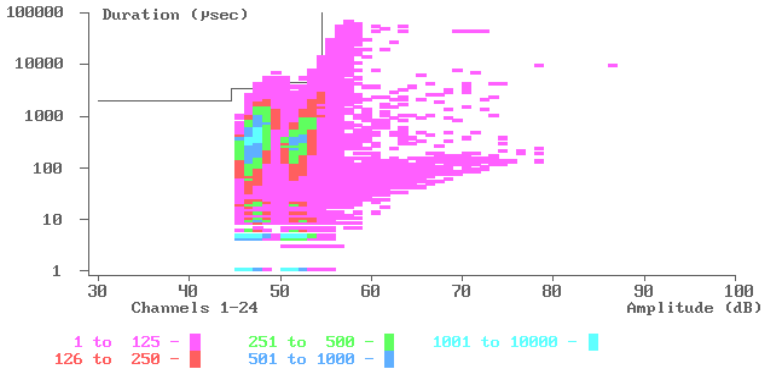

(b) Pressures from 1,100 to 1,600 psi

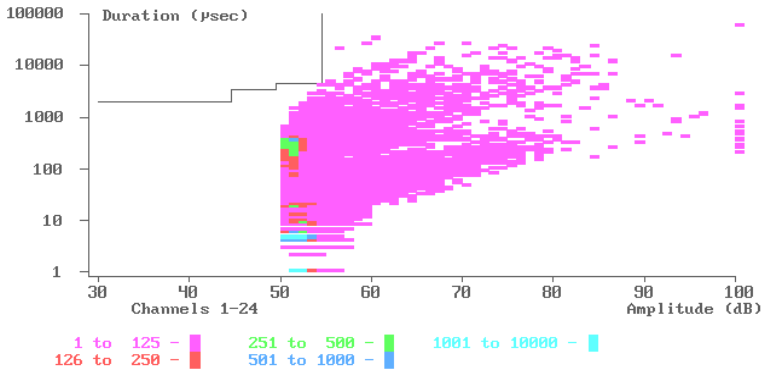

(b) Pressures from 1,600 psi to failure

Figure 2.45 Correlation plots for final test

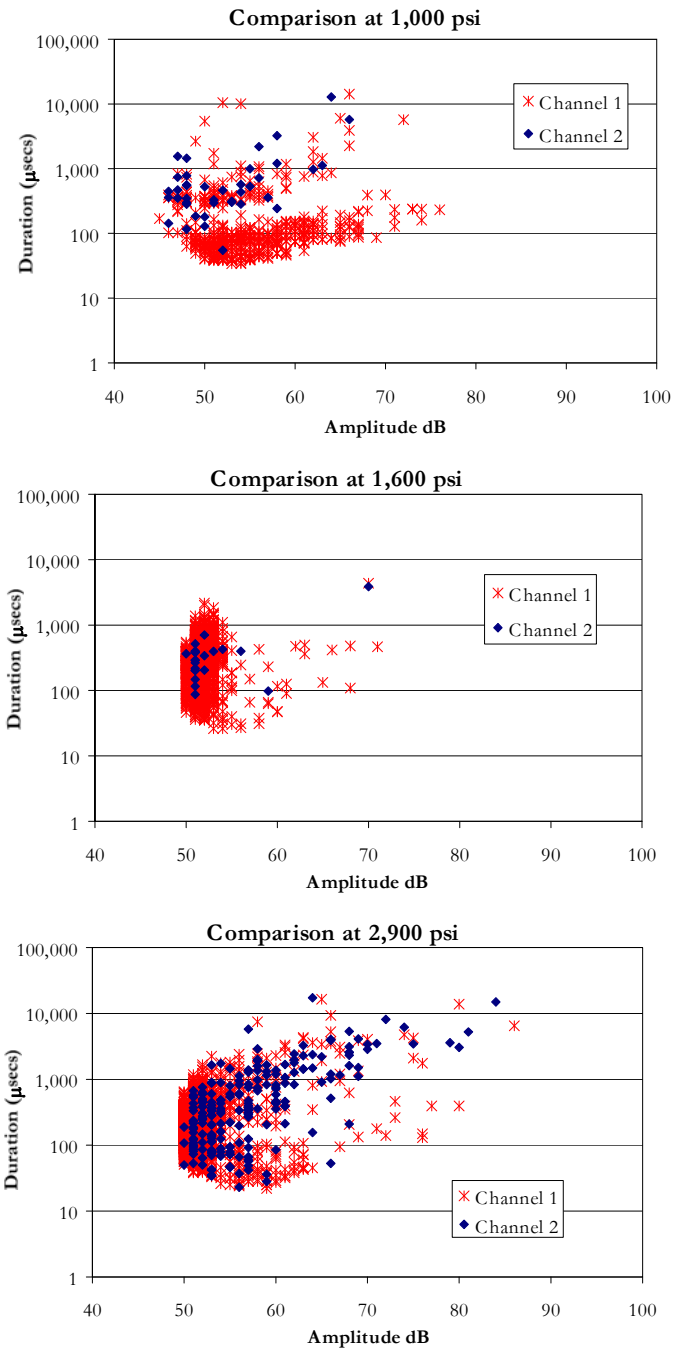

Figure 2.46 Correlation plots for final test

2.5. ANALYTICAL STUDIES OF COLLAPSE PRESSURE

2.5.1. OBJECTIVES OF ANALYSIS

The primary objective of this section is to evaluate the capability and accuracy of various analytical tools for predicting the observed response of the specimen. After the selected methods are presented, observations on the capabilities and limitations of analytical approaches for predicting collapse pressure will be made. Finally, the case of the non-delaminated specimen will be approached analytically in an attempt to assess the impact of the delamination on the behavior of the specimen.

2.5.2. MATERIAL PROPERTIES FOR ANALYSIS

2.5.2.1. RESIN AND FIBER PROPERTIES

A typical approach in defining the stiffness or property matrix of a composite laminate reinforced with continuous fiber is to calculate, or measure, from test elements the properties of each one of the layers forming the laminate. These layers in turn are assembled in a global matrix forming a quasi-homogeneous material representation. The task is then to first estimate relatively accurate properties for the lamina alone, followed by estimation of how these laminae interact when assembled in a thicker profile. Considering that the typical thickness of an individual lamina is about 0.0015 inches then, it is easy to see how assembling layers in thicknesses of 800 times their individual thickness could have an impact on their values.

A more complete introduction of the expressions used in the estimation of the material properties has already been presented in the introduction Chapter of this dissertation. Here, we will just present the ones most commonly used in the forming of the material properties for the lamina of this specimen.

For the fiber direction, properties are calculated using the rule of mixtures. The properties in directions other than the longitudinal were calculated using the Halpin-Tsai equations. Traditionally, the question of accuracy of the rule of mixtures for estimating properties in the direction of the fibers has not been largely debated. Results obtained with this approach are typically accepted as accurate for simplified analysis and design purposes within the elastic range of the structure.

For the purpose of this analysis, properties calculated using the rule of mixtures will be used. Later in the chapter calibrations will be done to the expressions that calculate the properties in the directions orthogonal to the longitudinal axis. There are always questions on the effectiveness of the interlaminar bond and its impact on the material properties. We will assume that the behavior in the in-plane direction will be largely dominated by the fibers in the laminate and their distribution or angle. The resin in the composite dominates interlaminar bond properties and in turn has little or no influence over the fiber behavior. In addition, fabrication practices in continuous winding interlock fiber of different layers with each other. All this added together results in a very low likelihood that, for as long as there are not extensive interlaminar voids or weak links in the composite, the properties in the fiber directions will not be affected by layering.

Table 2.4 presents the values used in the determination of the material properties for the lamina. The values used were obtained from the manufacturer of the component used in the fabrication of the composite. These basic properties were not altered during the calibration process of the finite element model.

The percentage of fiber in the composite laminate was estimated between 55 % and 60 % by volume. Test made after collapse of the specimen showed a volume content of carbon fiber of 58 % for the inside ring as divided by the delamination, and 59 % for the outer ring. An averaged value of 58.5 % was used in the calculations.

MATERIAL PROPERTIES TABLE

	EPOXY RESIN	CARBON FIBER	GLASS FIBER	C-VEIL
Modulus of Elasticity	430 (ksi)	35,000 (ksi)	12,600 (ksi)	650 (ksi)
Poisson Ratio	0.2	0.24	0.22	0.22
Shear Modulus	187.5 (ksi)	14344 (ksi)	5164 (ksi)	266 (ksi)
Density	0.042 lb/in^3	0.0640 lb/in^3	0.090 lb/in^3	0.050 lb/in3
Thermal Coefficient	0.0000033	0.000002	0.000003	0.0000031
Max. Strain Tension	0.048	0.016	0.054	0.050
Max. Strain Comp.	0.020	NA	NA	NA
Tensile Strength	11.3 (ksi)	610 (ksi)	660 (ksi)	12 (ksi)
Compressive Strength	17.4 (ksi)	NA	NA	NA
Flexural Modulus	448 (ksi)	NA	NA	NA
Compressive Modulus	416 (ksi)	NA	NA	NA
Shear Strength	7 (ksi)	NA	NA	NA

Table 2.4 Raw material properties

2.5.2.2. MATERIAL PROPERTIES FOR THE LAMINA

Estimating the material properties for the lamina is an important aspect of the analysis phase. There are several expressions available for this purpose, along with exact solutions that account for fiber size and orientation, geometry etc. In practical analysis, the exact solutions are too cumbersome to use and the values obtained from them assume conditions almost impossible to achieve in real manufacturing. Approximate expressions are a more practical approach, but care must be exercised in their use. Some expressions are very sensitive to certain variables in the composite. Variability in wall thickness and amount of fiber in the fabrication process are factors that influence the accuracy of these expressions.

Looking at the expression for the material property calculation developed by Halpin-Tsai:

$$\frac{M}{M_m} = \frac{1+\xi\eta V_f}{1-\eta V_f}$$

where

$$\eta = \frac{\left(M_f / M_m\right) - 1}{\left(M_f / M_m\right) + \xi}$$

in which

M = composite modulus of interest E_2, G_{12}, or υ_{23}

M_f = fiber modulus E_f, G_f, υ_f

M_m = matrix modulus E_m, G_m, or υ_m

ξ and η = calibration factors for fiber volume content and effective contribution

Traditionally this formula has been acceptably accurate for matrix dominated composites. Nevertheless, its accuracy diminishes in fiber dominated systems like the

one being considered here [2.15]. For use in analysis of fiber dominated systems modifications are required to this expression. To date, the amount of work in this area has been limited. For this work we will used these approximate expressions since it is more likely that a design process will include the use of them rather that trying to find an exact expression.

2.5.2.3. HOMOGENIZATION OF THE LAYERS IN THE SPECIMEN

Once the lamina or individual layer properties have been determined, it is necessary to assemble them in a global stiffness matrix for the analysis of the structural component. This process is commonly known as homogenization of the layers. That is, a system made of several layers of different properties will be modeled as a system with a single layer whose properties are the sum of the properties of all the layers that make it up [2.12]. This process provides for the use of a single global stiffness matrix in the analysis. However, it assumes that strain compatibility through the layers. As it will be shown later, this assumption begins to lose its accuracy as the thickness of the laminate increases. The properties of the specimen as calculated by the homogenization procedure are as shown in Table 2.5.

Laminate properties as calculated by homogenization		
Property Direction	**Value**	**Units**
$E_{longitudinal}$	10,900	ksi
E_{hoop}	13,100	ksi
ν_{lh}	0.22	na
ν_{hl}	0.17	na

Table 2.5 Laminate theoretical properties for specimen

2.5.3. GEOMETRICAL DATA FOR THE ANALYSIS

A finite element model of the test specimen, described in greater detail later, consisted of a symmetrical representation of the middle section of the specimen. Since it had been determined that the end conditions would not have an effect in the behavior, it was assumed that no specific support conditions needed to be included. The quarter ring model allowed for the representation of a symmetrical if not ovalized profile. The specimen had symmetry boundary conditions defined on all the edges. The length of the meshed model was 36 inches, so including the symmetry, the prototype analyzed was 9 feet total length.

Convenience was the main factor in the selection of this length. The pressure was applied uniform to the entire cross-section and therefore the length of the model does not affect the result obtained. Another reason for the limitation of the length and symmetrical representation was that contact elements were used to model the inter-phase of the delamination. These elements connect each node to a target surface [2.21]. Since a symmetrical mesh was used here as well this became extremely taxing on the computer and program memory and limitations. The version of the program used was the academic version that has a limited amount of available wavefront. This limited the number of elements that could be analyzed severely. The use of contact elements added an additional variable in the possible combinations of properties used in the analysis. These will be approached during the discussion of results presented in following sections of this chapter.

There are several issues to keep in mind during the modeling process for the analysis of any structural component. Defects either geometrical or at the material level are possible in any component. In general, the importance of these defects on the strength or general behavior of the components is what is of interest to the designer. Therefore, in a research program, the important steps are the determination of the extent and existence of these defects to be able to assess their importance in the behavior.

Because of the type of loading used in the testing of this specimen and the thickness to diameter ratio, the expected factors affecting the behavior are: out-of-roundness (or ovalization) and large delaminations. For our model, out or roundness was determined using the API [2.6] expressions presented at the beginning of this chapter. This expression defines cross-section ovalization. It does not define local deformations like waviness. Nevertheless, waviness does not affect radial buckling significantly [2.3]. According to API, the maximum out-of-roundness for tubes with walls up to 2 inches should not exceed 1% or ¼ inch. Typically, steel tubes show an out-of-roundness of about 0.5%. During the analysis for this specimen, several values of β were studied along with the measured dimensions, and the results will be presented later.

2.5.3.1. LOCATION OF PRE-EXISTING DELAMINATION

The manufacturer provided the information on the location of the delamination. It places the delamination at about $^1/_3$ of the thickness from the inside diameter. For the case of analysis with code predictions, the delamination was not included in the calculations in any way. The equations were not modified to account for any kind of separations between the rings either.

The finite element modeling did include considerations for the existence of the delamination. In modeling the boundary condition for this specimen, two separate rings were modeled as to constitute the cross section of the specimen. At the gap allowed for the two rings, contact elements were used to model the interface conditions. Allowances were made for the introduction of friction in the interface, in addition to the separation between the rings and the contact stiffness of the elements used.

2.5.4. *ANALYSIS OF COLLAPSE PRESSURE USING CLOSED FORM SOLUTIONS*

There are several approaches for developing analytical predictions for buckling of pipes under external pressure. Closed form solutions have been developed for a variety of cases involving thin-walled pipes [2.11] which have been extrapolated or adapted for thick walled pipes [2.12]. A second approach is the development of numerical solutions using methods such as finite element analysis. Finite element solutions are examined in a following section. A third approach for predicting the collapse pressure of a pipe is the use of simplified equations that can be found in design codes and specifications. These design equations generally involve mechanics based theoretical predictions that have been empirically modified based on experimental observations. These simplified predictions are examined below.

2.5.4.1. *SIMPLIFIED CODE PREDICTIONS*

First, the simplified expressions most commonly used by design codes will be examined. It appears that most common expressions found in codes and specifications for vessels made of composite materials are adaptations of expressions developed for homogenous isotropic materials. In the case of filament wound vessels an attempt has been made to account for the anisotropy by having two separate moduli of elasticity in the expressions. One modulus accounts for the stiffness in the hoop direction and the other for the axial direction.

It will be difficult to compare the collapse pressure predictions from simplified expressions with the specimen in this program since none of the expressions account for a delamination in the pipe wall, as was the case for the specimen. Each expression generalizes the possibility of flaws and geometric imperfections by the use of safety factors in either the collapse pressure calculation or as a multiplier in the final result of

the expression. For the comparisons presented in this section, the modulus of elasticity of the specimen, with no modifications for the delamination, was used.

Simplified equations used to predict collapse that will be considered here include: British Standard [2.13], the French Code [2.17], the American Society of Mechanical Engineers (ASME-ANSI RTP Code, Boiler and pressure vessel code – Section 10) [2.18, 2.19] and the API LFRD Specification [2.15]. Even though the last one was originally developed for steel vessels is adaptable to composite pipes. Table 2.6 shows the general expressions for each one of the codes indicated here. An equation for the critical length or distance between stiffeners is presented along with the equation for the calculation of the maximum collapse pressure. It should be noted that the factors of safety indicated in the Table were not used in the calculation of collapse pressure values presented later. A brief description, of each of these code equations is presented below.

Code Name	**Critical Length L_c**	**P_A if $L \geq L_c$**	**P_A if $L < L_c$**	**Factor of Safety**
British Standard	$L_C = 1.35\, D_O \left(\frac{E_{LAM}}{pF}\right)^{0.17}$	$P_A = \frac{2\, E_{LAM}}{F}\left(\frac{t_m}{D_o}\right)^3$	$P_A = 2.5\, \frac{E_{LAM}}{F}\frac{D_O}{L}\left(\frac{t_m}{D_o}\right)^{2.5}$	**4**
French Code	$L_C = 2.5\, R_O \left(\frac{E_{axial}}{E_{circular}}\right)^{\frac{1}{4}} \left(\frac{R_O}{t}\right)^{\frac{1}{2}}$	$P_A = \frac{3\, E_{circular} I}{R_O^3}$	$P_A = 0.83\, E_e \left(\frac{t}{R_o}\right)^{\frac{5}{2}} \left(\frac{R_o}{L}\right)$	**None specified**
ASTM RTP-1	$L_C = 1.73\, D_O \left(\frac{D_O}{t}\right)^{\frac{1}{2}}$	$P_A = 2.6\left(\frac{E}{F}\right)\left(\frac{D_o}{L}\right)\left(\frac{t}{D_o}\right)^{2.5}$	$P_A = \frac{2.6\left(\frac{E}{F}\right)\left(\frac{t}{D_o}\right)^{2.5}}{\frac{L}{D_o} - 0.45\left(\frac{t}{D_o}\right)^{\frac{1}{2}}}$	**5**
ASTM Section X	$L_C = 1.14\, D_O \left(1-\upsilon_1 \upsilon_2\right)^{\frac{1}{4}} \left(\frac{D_O}{t}\right)^{\frac{1}{2}}$	$P_A = \frac{2\left(\frac{E_2}{F}\right)}{1-\upsilon_1 \upsilon_2}\left(\frac{t}{D_o}\right)^3$	$P_A = \frac{2.42\left(\frac{E_2}{F}\right)\left(\frac{t}{D_o}\right)^{2.5}}{\left(1-\upsilon_1 \upsilon_2\right)^{\frac{1}{2}}\left(\frac{L}{D_o} - 0.45\left(\frac{t}{D_o}\right)^{\frac{1}{2}}\right)}$	**5**
API LRFD	$L_C = 1.13\, D_O \left(\frac{D_O}{t}\right)^{\frac{1}{2}}$	$F_{he} = 2\, C_h\, E \left(\frac{t}{D}\right)$ $C_h = f(M)$ $\quad M = \frac{L}{D}\sqrt{\frac{2D}{t}}$ *where* $L =$ distance of stiffeners		**1**

Table 2.6 Simplified equations for collapse pressure

The British Standard [2.13] provides equations commonly used to determine required wall thickness in vessels made of hand lay-up materials. Therefore it does not make any mention to fiber angles and different modulus at normal directions within the lamina itself. It defines a critical length or spacing between stiffeners (L_c) to account for end restraint conditions. This critical length is dependent on the applied pressure and the diameter of the pipe (D_o). Therefore, an iterative procedure is necessary in order to determine the collapse pressure for a restrained specimen. It then proceeds to present two equations for the determination of minimum thickness, or maximum collapse pressure, depending on the spacing between supports or stiffeners. In both expressions used for buckling calculations, the code uses a safety factor of 4. The main material property is the modulus of elasticity in the directions of interest (E_{LAM}). The rule of mixtures is used in the calculation of the properties. By using this simplified approach to the material properties, the code does not account for the Poisson coupling or other coupling terms in composite laminates.

The French Code [2.17] is designed to cover the case of filament winding in a simplified manner and with respect of the radius of the pipe (R_o). Its particular approach requires the determination of both the hoop and the axial laminate modulus ($E_{circular}$ and E_{axial}). As with the British Code [2.13], this code also accounts for the distance between stiffeners in the component (L_c). However, the definition of the critical length in this case used the ratio between axial and hoop modulus in the expression [2.17]. If the stiffeners are separated farther than the critical length, the collapse pressure is dependent only on the hoop modulus of elasticity and the moment of inertia (I). If, however, the stiffeners are within the critical length, the axial stiffness is part of the expression by means of calculating an apparent effective modulus that includes the effect of the axial and hoop modulus. No specific factor of safety is defined in the code.

The expressions derived by the ASME codes, RTP-1 [2.18] and Section X [2.19] are different from each other even though developed for the same type of vessels. They do, however, have the same safety factor included in the expression (S.F = 5). The critical length is defined almost identically in both specifications (L_c), with only a slight

variation in the expressions, with one of them accounting for the different properties in the normal directions. In addition, although both expressions are intended to be used in filament would vessels, RTP-1 has jurisdiction on vessels up to 15 psi and Section X on vessels above 15 psi. The main difference in the approach comes in the introduction, by Section X of two Poisson ratios ν_1 and ν_2 and in a different constant in the expression. No specific mention is made as to the fabrication tolerances assumed in the expressions for the ASME specification.

The LRFD-API [2.15] expressions were developed for the analysis and design of steel pipes under external pressure. Because it is meant for use in the LRFD format, no implicit safety factor in the equations is used. The safety factor is added at the time of calculating the nominal stress by means of a ϕ factor. As shown in Table 2.8, the API expression calculates the stress in the pipe wall at the time of elastic buckling. To obtain the collapse pressure from this stress, use the following expression:

$$P_e = 2 * F_{he} \frac{t}{D}$$

Where F_{he} is the stress as calculated by the equation in Table 2.8 and P_e is the elastic buckling external pressure; t and D are thickness and diameter respectively. To account for the effects of end restraints, the API-LRFD specifications [2.15] use a parameter M to calculate the value of C_h. This parameter M varies with respect of the distance between the stiffeners or ends of the pipe. Refer to the API specifications [2.15] for more detailed information on the expressions to calculate the parameter M. These expressions were applied for this case with only a slight modification. The modulus of elasticity used in the calculation was the hoop modulus for the composite specimen. It is to be noted that the expression for C_h in the API specification has been calibrated to predict buckling of a geometric shape with an out-of-roundness of 1%.

Table 2.7 shows a summary of collapse prediction values as calculated by each one of the codes mentioned above. In the table calculations are made based on two values for the modulus of elasticity in the specimen. One column shows the predicted

collapse pressure using the theoretical hoop modulus of elasticity as defined by the raw material properties from the manufacturer and accepted classical mechanics of materials elastic calculations, as shown in Table 2.7. The next column is the calculated collapse values using the apparent hoop modulus of elasticity obtained from the strain information recorded during the test, and estimated at 9,900 ksi. The apparent modulus was calculated by comparing the strain-stress curve from the test and then fitting a measure modulus of elasticity based on the lower pressure measurements. The last column presents the ratio of calculated to measured collapse pressure.

PREDICTIONS OF ULTIMATE COLLAPSE PRESSURE				
Specification	***Measured Collapse Pressure = 3150 psi***			
	Predicted Value with $E_{estimated}$ (A)	Predicted Value with $E_{measured}$ (B)	(A) Predicted / Measured	(B) Predicted / Measured
API-LRFD RP2A [2.15]	4.56 ksi	3.45 ksi	1.45	1.10
British Standard [2.13]	4.89 ksi	3.7 ksi	1.55	1.17
French Code [2.17]	5.83 ksi	4.4 ksi	1.85	1.40
ASME RTP Code [2.18]	3.1 ksi	2.34 ksi	0.98	0.75
ASME Section X [2.19]	5.07 ksi	3.83 ksi	1.61	1.22

Table 2.7 Comparison to Simplified Predictions

Looking at the results in the table, it is apparent that some expressions were closer to the measured capacity that others. It is difficult to extrapolate from this observation to other conditions. When comparing to only one test, it is difficult to attribute the result to coincidence or behavioral fact.

The reader is encouraged to look over the references for the detailed description and more detailed information of the expressions for each code.

2.5.4.2. THEORETICAL BUCKLING EXPRESSIONS FOR ORTHOTROPIC PIPES

Calculations based on theory of elasticity including effects of general anisotropy are extremely difficult to deal with intricate expressions and relationships. In order to keep these expressions manageable; simplifications on the relationship between stresses and deformations have to be made. Since most of the laminates and components made with continuous fibers are homogenized for analysis, they can be considered as orthotropic materials at the laminate level. Therefore, we will assume that the following discussion on buckling of isotropic cylinders and its extension to orthotropic materials applies to our riser specimen. First, we will look at the common equation of buckling developed with shell theory for isotropic materials [2.22], and that is:

$$\sigma_{cr} = \frac{kEh}{r\sqrt{3\left(1-\upsilon^2\right)}}$$

where E is the material modulus, υ is the Poisson's ratio, h is the thickness of the shell and r is its radius. The factor k is an empirical constant between 0 and 1. The function of k is to calibrate the expression to account for flaws and imperfections, since it is common that the real buckling load of a specimen is lower than the predicted by the formula.

For anisotropic materials, the differential equation that originates a similar expression to the isotropic one becomes quite involved. However, a more convenient solution can be found if the laminate is considered ortothropic instead of anisotropic. This assumption will induce errors in the final result. However, for most applications, these errors are negligible and the resulting expressions are more manageable than a rigorous anisotripic one. The final expression for orthotropic elements based on shell theory is:

$$P_{cr,shell} = \frac{E_2}{\left(1-\upsilon_{23}\upsilon_{32}\right)}\left(\eta^2-1\right)\left(\frac{h^3}{12R^3}\right)$$

where $R=(r_1+r_2)/2$ is the mid-surface radius, and $h=r_2-r_1$ is the shell thickness. η is an integer value greater than 1.0. The minimum eigenvalue is obtained with $\eta = 2.0$

The similarity with some of the expressions found in the simplified code equation section presented before are immediately apparent. The main difference is that this expression does not account for reductions in capacity induced by imperfections in the geometry. The obvious conclusion is that using the exact expressions would not be any more accurate for a real structure than using one of the simplified equations. If a more accurate prediction than the ones provided by the simplified equations is necessary, or required, the most effective and convenient method would be the use of a finite element model. For large structures with imperfections, calibrations of finite element models and simplified expressions would be more desirable for design versus the use of the more detailed and involved theory of elasticity solution.

2.5.5. FINITE ELEMENT ANALYSIS

2.5.5.1. FINITE ELEMENT MODEL DESCRIPTION

In order to understand the observed behavior of the riser, a finite element model was created. This model included the effects of the delamination but did not include the curvature that was detected by the strain gages during the test. Because the behavior was assumed mostly elastic at the material level, any non-linearity was attributed to the geometry and delamination. No material non-linearity was modeled in the initial trials. The results from the FEA and measured behavior seem to indicate that the assumptions made are acceptable.

The program selected for analysis of the specimen was ANSYS® on a IBM® workstation computer. For the model including the delamination, solid layered elements from the ANSYS® library were used. These elements allowed for the data to be input in terms of the layer properties. The program then proceeds to calculate the global stiffness matrix, effectively homogenizing the layers into an equivalent system. If more information is desired on how this homogenization is accomplished, the reader is referred to Refs. 2.12, 2.20 and 2.21. Figure 2.46 shows the profile of the model as created in ANSYS®.

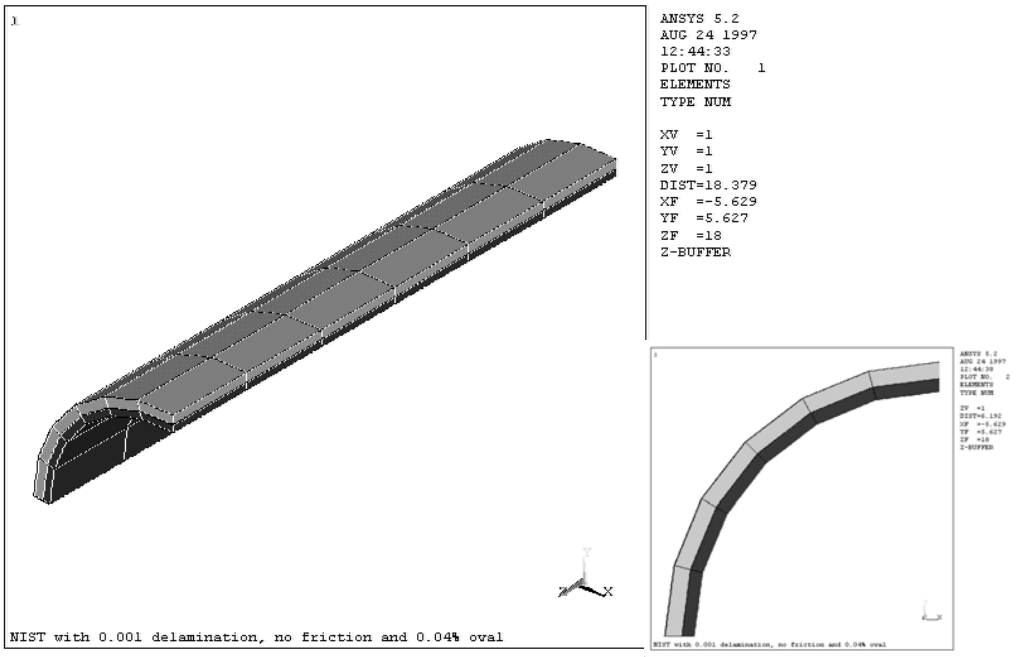

Figure 2.47 Finite element model for specimen

2.5.5.2. MODEL CALIBRATION

The first phase of the analysis was to estimate acceptable values for the material properties in the model. The fact that only one test is presented here makes this a difficult task to verify. However, every effort was taken to maintain the calibration

process as realistic as possible. For the calibration only the results of the recorded strains for the first 500 psi of applied pressure during the test were used.

As it has been discussed in previous sections in this chapter, two tests were performed on this specimen where the pressure reached 500 psi or higher, the preliminary to 700 psi and the final to failure. Also, it was shown that the strains recorded for this stage of pressure showed the same behavior between tests. Therefore it was assumed that no non-linear behavior had been present and calibration based on these strains would be acceptable.

The dimensions used in the calibration process were selected so they would resemble the actual measured conditions of the specimen. Two simplifications were made in the modeling of the riser geometry. The first was that the same out-of-roundness was assumed for the inner and outer diameter of all the rings in the specimen. The second simplification is related to the way in which the geometry of the riser was defined for the model. In modeling an oval system, an elliptical equation was used to define the locations of the nodes in the perimeter of the model. The top and side dimension were defined to meet the API definition of out-of-roundness and the nodes in between were filled using the ellipse equation. Because of the small amount of out-of-roundness measured in the riser, this approximation was not believed to be critical in the resulting analysis.

The main factors in the Halpin-Tsai expressions are the variables ξ and η. The first one accounts for geometry and distribution of the reinforcement in the composite while the latter is meant to account for the difference in material properties in the composite. Generally accepted values for ξ are 1.0 for the calculation of E and as determined by the expression:

$$\xi = 1 + 40 V_f^{10}$$

Where V_f is the volume fraction of fiber and is used for the determination of G and ν. These will be the values to be calibrated using the results of the finite element model and the preliminary test on the riser.

Figure 2.48 shows the comparison between the two main properties affected by the calibration process. The figure shows the results for the Halpin-Tsai equations as specified and results for the calibrated expressions keeping in mind that the values of G and ν are affected by the same expression. Therefore the variation noted for G also affected the Poisson's ratio. The calibration was performed by comparing the results of the finite element model to the recorded strains in the test. The volume percentage used was obtained from testing of sections of the failed specimen. Each of the components in the calibration process is analyzed here. For the value of ξ plotted in Figure 2.49, the multiplier β and the fiber volume fraction were varied. The only difference with the equation previously shown is that the 40 multiplier has been changed by β for sensitivity analysis. From the plot we can see that only a difference of 9% in the value of ξ is

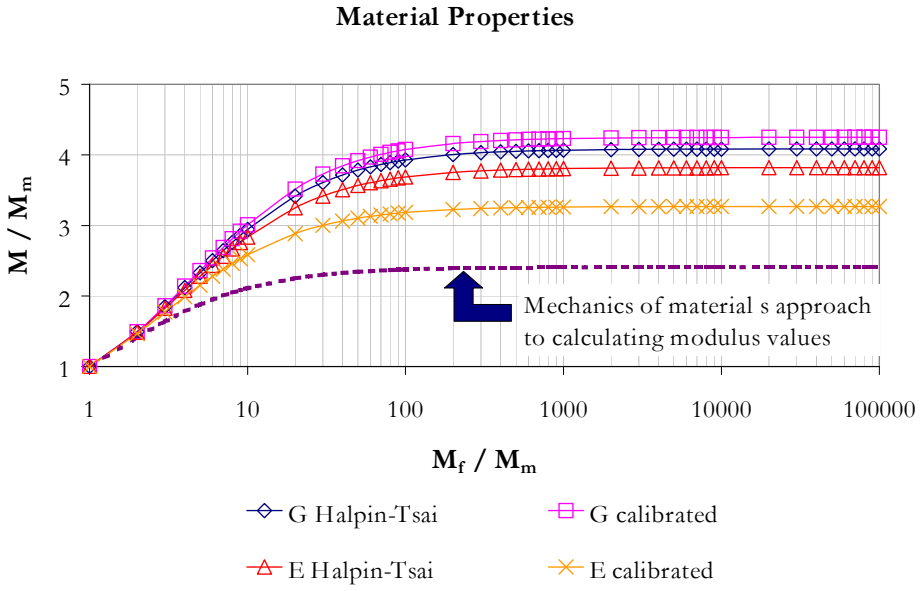

Figure 2.48 Material properties calibration

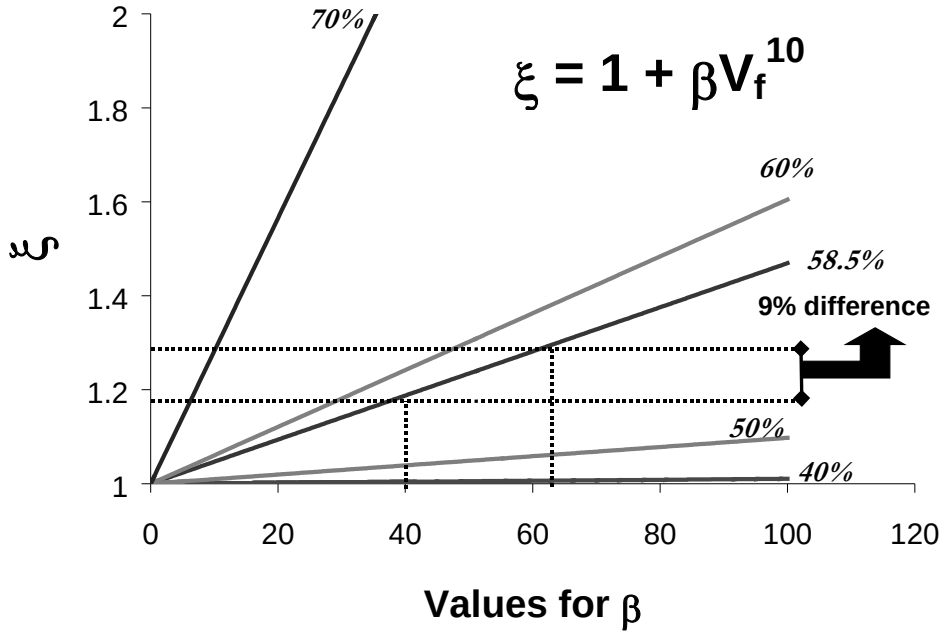

Figure 2.49 Sensitivity of calibrated values

obtained between the theoretical value and the calibrated one for the ranges in this specimen. To see how this change affected the associated material property prediction, the two most affected properties are plotted next.

As it can be seen in the figure 2.48, the difference between the expressions for the modulus E is the one more affected by the calibration. The mismatch seems to be more forgiving for the values of G and v that for E. The final values for the variable ξ in the analysis were:

$$\xi = 0.57 \ \textit{for } E$$

$$\xi = 1 + 65V_f^{10} \ \textit{for } G \textit{ and } \nu$$

The sensitivity of the material properties to the modified variable values is approached next. Figure 2.49 shows the variability of the expression for the values of ξ.

The figure presents the values for the ξ variable used in the calculation of G and ν plotted for separate percentages of fibers in a composite element. In addition the curve for the percentage as found for the specimen is added to the figure. We can see that the difference between the calibrated values and the recommended ones is of about 9 %.

To study the impact of the difference of 9% in the calculated properties, a sensitivity analysis was carried out for two properties. Figure 2.50 shows the changes in the shear modulus G_{12} as the result of changes in ξ. As seen in the figure, the difference between the value obtained with the original expression versus the calibrated one is only 3%. We can therefore presume that, for this particular property calculated using the expression, the calibration, although providing more accurate predictions based on the

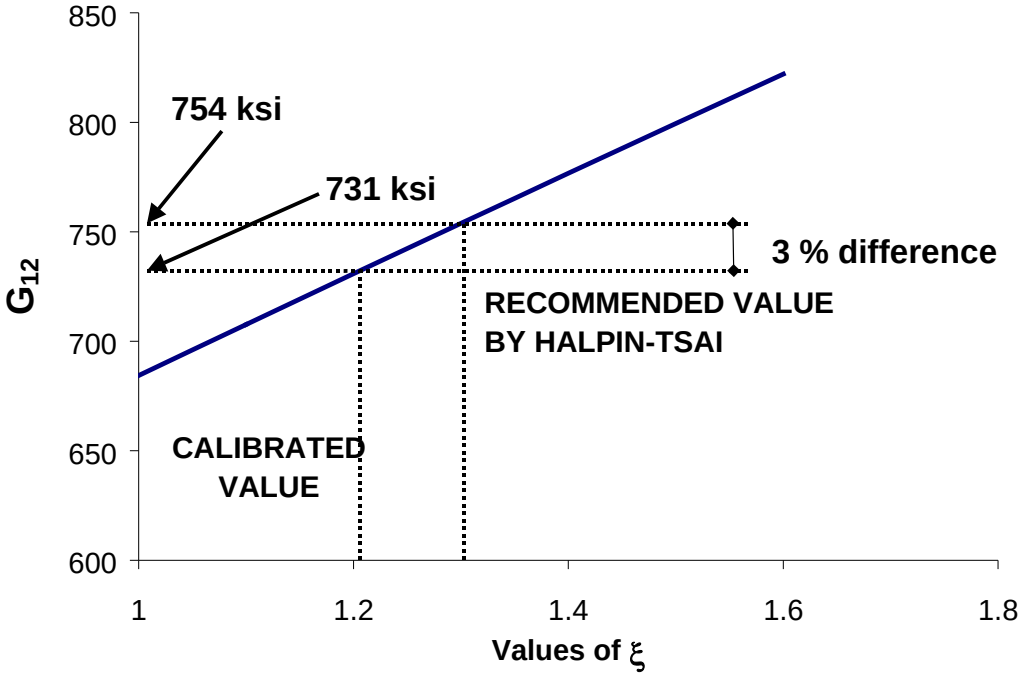

Figure 2.50 Calculated values for G_{12}

specimen tested, would not be a necessary step in the formation of an acceptable model.

Looking at the values for the modulus of elasticity in the direction perpendicular to the fibers, we can see that this variable is the one most profoundly affected by the calibration process. The importance of the accuracy of the prediction of this property in the design phase, could vary depending on the loading case and structure being analyzed. In the case of this specimen, the impact was noticeable and did seem to affect the predictions. Lack of experimental data on similarly constructed and tested specimens makes extrapolation of this characteristic unreliable. We will simply state the differences but will not try to justify the behavior in any way other than the fact that the analytical model behaved in a very similar way to the experimental results. Figure 2.50 show the calculated values for E_{22} using the calibrated expression and the suggested one.

We can see that the difference for E_{22} is 17% with a difference of the ξ value of 50% between suggested the by Halpin-Tsai and the calibrated one. This appears to

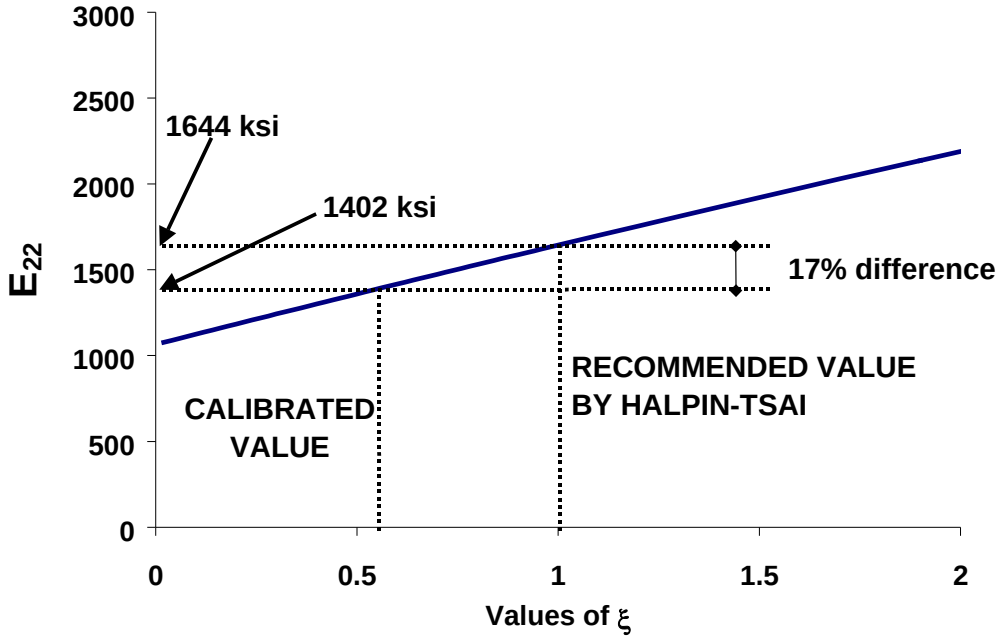

Figure 2.51 Results for transverse modulus of elasticity

indicate that for thick walled composites the fibers do not influence the transverse properties in the same proportion as observed with thinner specimens.

All the properties resulting from this calibration are valid only for the particular test presented and cannot be extrapolated beyond it. Nevertheless, the data presented here provided some interesting trends that may be used to support observations developed in other programs with more extensive testing.

2.5.5.3. COMPARISON OF FEA RESULTS TO EXPERIMENTAL DATA

After a good match was obtained between calculated and measured strains at the lower pressures of the preliminary test, the next step was to estimate the analytical buckling pressure for the specimen. The most important question was to determine if the non-linearity observed in the strain gages was due to the geometrical or material nonlinearities. Material nonlinearities affect the constitutive properties of the model and complicate the process of buckling pressure estimation.

Looking at the recorded strains in the final test, we notice a maximum strain at failure of 0.3% which is well below the failure strains for either of the materials as shown in Table 2.5. In addition, the behavior of the fibers is elastic up to fracture, therefore any material non-linearity would have to come from the matrix behavior. It is well known that a large part of any observed non-linear behavior in composite materials comes from the shear stress-strain behavior. Based on the loading condition and the boundary supports provided during the test, it was assumed that the shear stresses would be the less critical that the normal stresses induced. Therefore, it was assumed that the material maintained a linear behavior throughout the loading and up to failure.

The measured tolerance for the inside diameter was assumed equivalent to about 0.04% as defined by API. It was decided to use the inside diameter for defining the geometry of the riser since a large component of the dimension variations in the outer diameter could be due to waviness. The other factor of interest is deciding how far apart

are the layers at the delamination inter-phase. This was a variable that was not possible to measure and probably would be difficult to assess accurately with any non-destructive evaluation method. The separation used for the analysis was equal to the typically assumed thickness of a single lamina. Therefore, a separation of 0.0015 inches was used for the delamination gap.

Figure 2.52 presents the calculated strains up to the pressure immediately before predicted collapse pressure for the specimen. The predicted collapse pressure is 2.93 ksi which is 94% of the measured collapse pressure. This was judged as an acceptable estimate since a number of simplifying assumptions were made in the process as described before in this section.

Before continuing with the discussion on the results for the finite element model, it necessary to describe where in the models the readings come from. Figure 2.53 has a schematic representation of the analytical model with the nodes used for the results plots highlighted. The locations were selected in an attempt to match the location of the strain gages in the real specimen. During the discussion of the results is necessary to keep in mind that the effect of the straightening as discussed in the strain gage section was not included in the model. This is partially responsible for the non-linear behavior of the P1 strains as shown before.

Some interesting trends that support the conclusions made during the strain gage data analysis can be seen in the finite element model. The first comparison made is to the overall magnitude of the principal strains as recorded and calculated for common pressure levels. Figure 2.54 View A presents the calculated principal strains during the load history in the FEA, View B show the principal strains as calculated using the strain gage data recorded during the test.

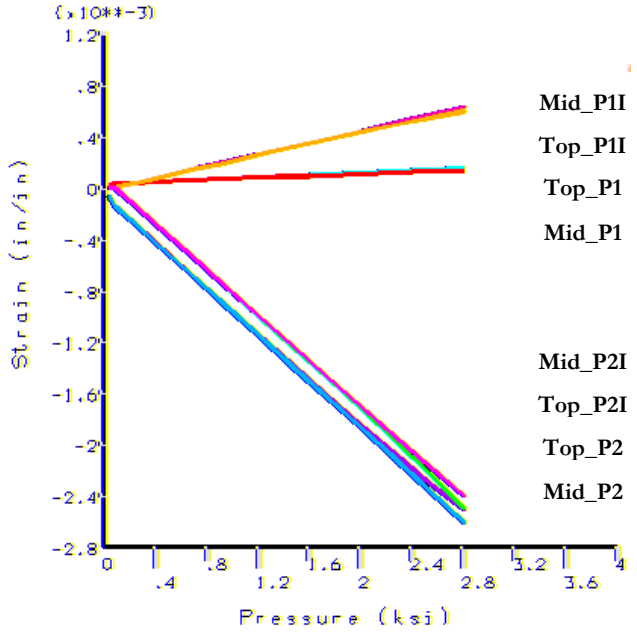

Figure 2.52 Calculated strains for FEA model

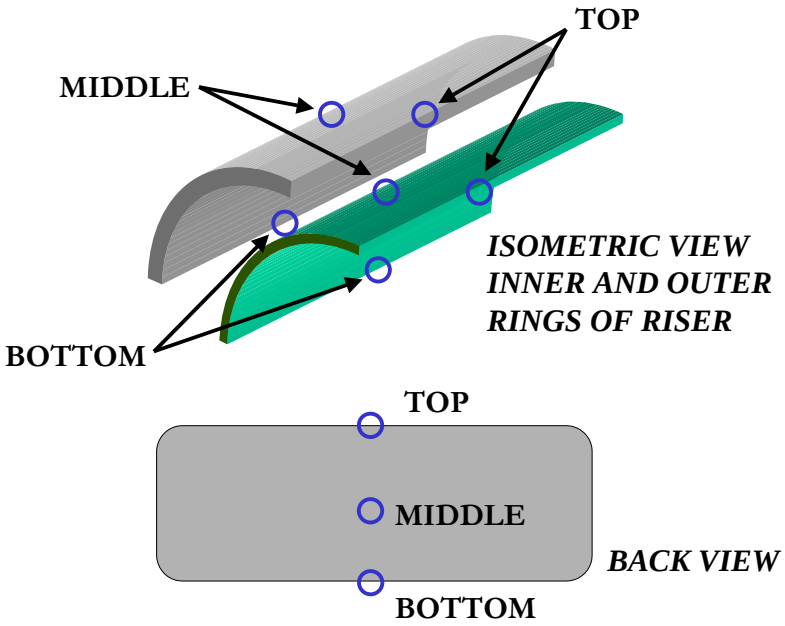

Figure 2.53 Locations for nodal results in the FEA model

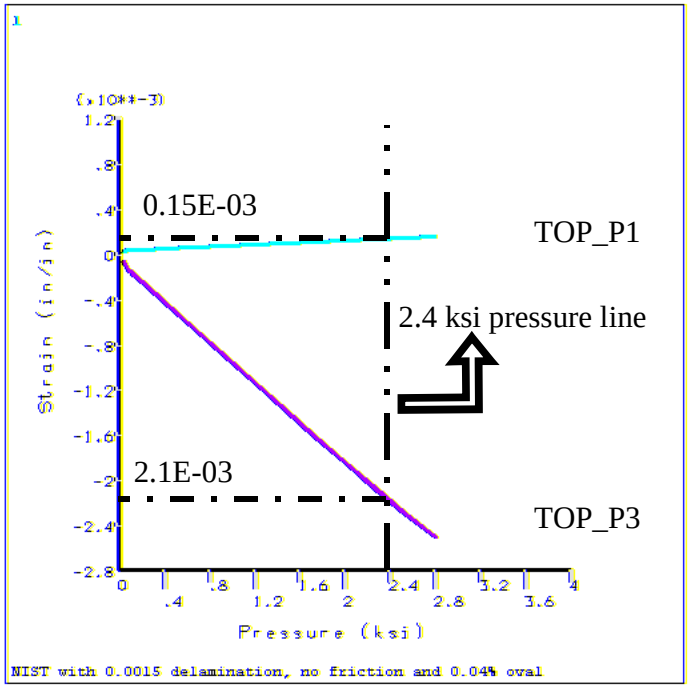

(a) FEA Results

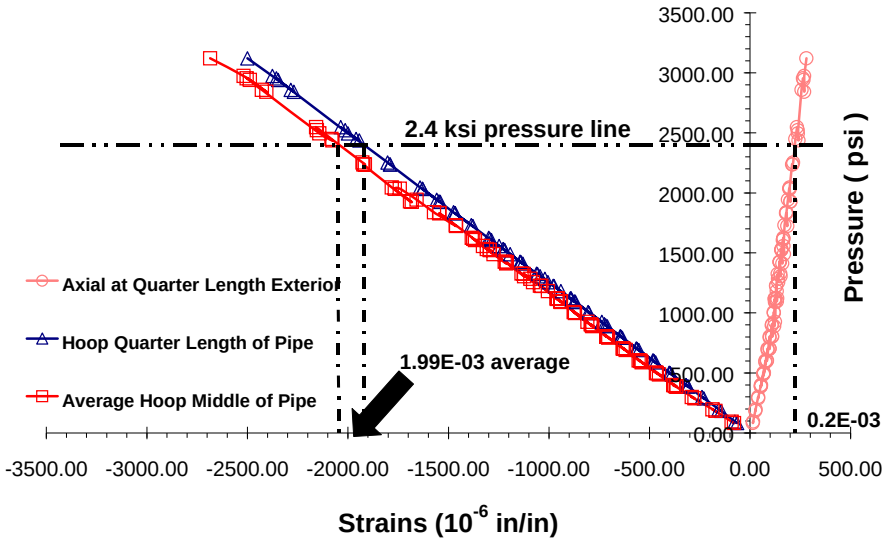

(b) Strain gage data results

Figure 2.54 Strain comparisons

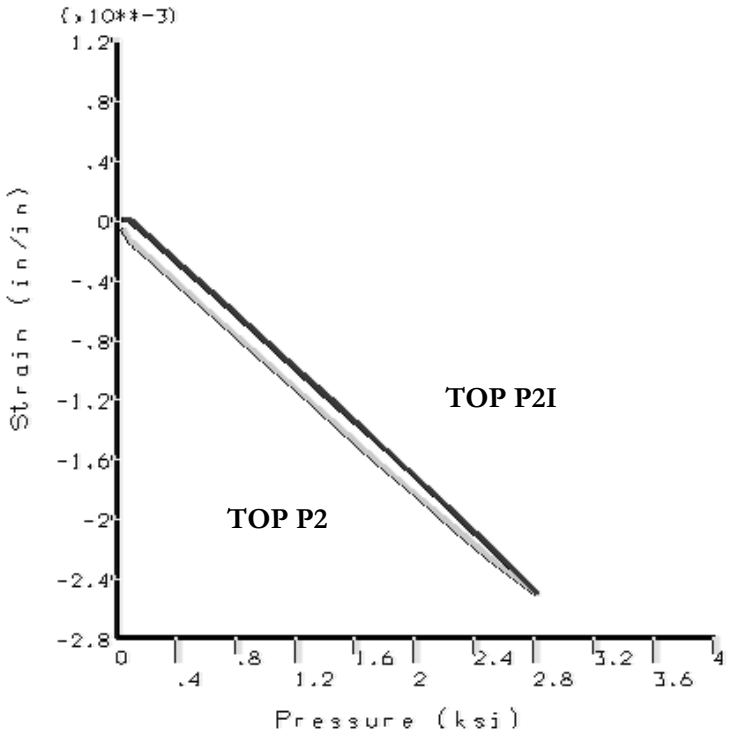

Figure 2.55 Comparison of ring strains

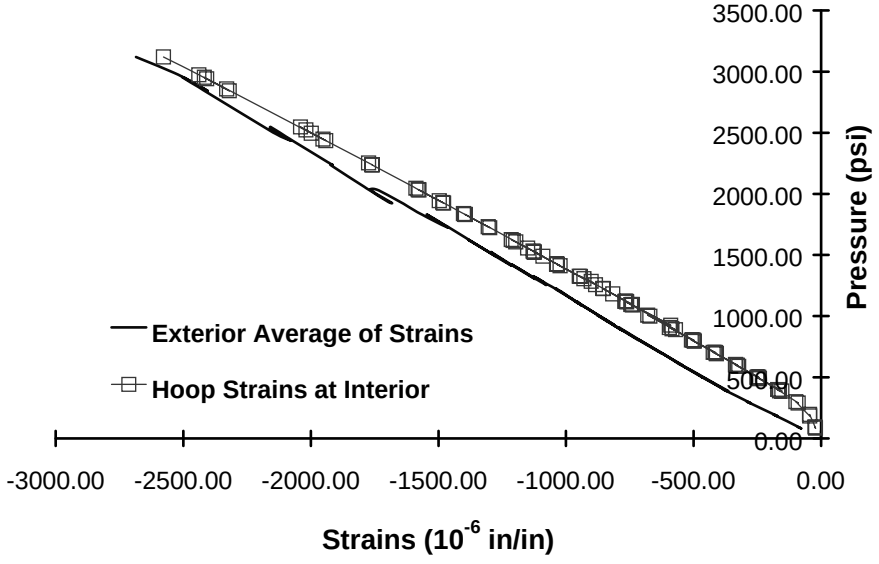

Figure 2.56 P2 strain comparison for measured strains

The more reliable comparison comes from the P2 strains between the models. These were the least noticeably affected by the straightening of the specimen during the experimental phase. Selecting three separate pressure stages and comparing the strains to each other, we see that the error between curves is less than 5% with the measured data being smaller that the predicted. The axial strains of the quarter length location were used to compare to the calculated ones since they were not extensively affected by the curvature straightening. The average of the two rosettes placed in the middle portion of the pipe at the surface was used for the comparison. The resulting strains are very much in agreement in both models. The strains in the analytical model are greater that the measured ones but the predicted collapse for the analytical model was lower that the measured. Remembering that we are looking at an elastic buckling value, the original stiffness in addition to the initial deformation is a critical part of the result. The analytical model had a lower stiffness that the one observed during the test. This results in slightly higher strains per pressure stage and a lower buckling load. The calibration could have been continued to the point where the values matched more closely. However, it was deemed unnecessary to carry this calibration any further since only the general tendency of the material property prediction model was desired.

One additional point to make is in relation to the axial strain comparison between the analytical model and the measured values. First notice that the compared values are the quarter length rosettes. These gages were located in the top of the specimen as it was placed in the test chamber. Thinking how the axial strain distribution would be in the case of the pipe with a flexural curvature, we can see that as the specimen lost this curvature the axial strains at the top of the specimen would be increased. Strains due to the applied pressure would be positive, strains in the top part of a recovering specimen would also be positive therefore adding their effects together. The difference between the measured and calculated strains is about 25% with the measured strain being the higher value. Looking at the values that were estimated for the change in curvature we can see that this difference can easily be the result of this condition. Attempting a more in depth analysis may prove futile and probably

impractical since first the value of the axial strains is in general so low and no backup specimen is available. There is no way to reliably estimate how much of the difference is due to error in the measurement and how much is influenced by the curvature.

Comparing the P2 strains in the inside wall of the specimen to the outside strains we can see the effect of the delamination and the interaction of the two rings. Figure 2.57 show the calculated strains for locations in both the inside and outside ring of the analyzed specimen. In the figure we can see that the P2 strains initially acted separately, but that after a certain pressure the interior ring P2 strain did begin a tendency to match the external ring strains. This tendency continued up to the point of buckling where the strains almost match in value.

To compare this behavior with the recorded strains in the tested specimen, we must make some estimates about the principal strains on the interior wall of the specimen. Since not all the gages in the middle of the riser survived during the test, we must use the recorded strains in other locations within the inside wall to calculate the P2 strain at this location. First since only one of the delta gages survived the test we will say for this estimate that the gages were perfectly aligned with the longitudinal axis of the pipe. Second since the axial gage did not survive either we will assume that the axial gages measured at the ends are the same as those in the middle. Because of the difference on magnitudes between the axial and the delta gages this assumption will have a very small effect on the calculated strains. The numbers obtained from this calculation, and presented in Figure 2.56 will be used only for general comparison and trend observations.

In the Figure 2.56 we can see a similar trend in the behavior of the strains as the one predicted by the finite element model. Based on the results of rosettes that had all the gages active, the confidence on the alignment of the gages in the specimen is fairly high. Even though perfect alignment may have not been achieved, a fairly close orientation was noticeable in all of the other gages. Therefore, the error for the interior gage is probably small. In addition, the axial strains do not contribute considerably to

the magnitude of the strains so the error in using the end strains is small. The trends observed in the rosette, as the result from this calculation, is considered valid.

2.5.5.4. FAILURE CRITERIA ANALYSIS

There is a large body of work directed towards the development of the reliable failure criteria for composite materials. There has been however, little agreement in a single criterion that describes the behavior of all the possible loading combinations. Two reasons are probably the main causes of this discrepancy or disagreement:

- The criteria are not well established or verified with experimental results and,
- There is a lack of good quality and well established strength data base for composite materials

The main problem with establishing reliable criteria and the reason for the sometimes-sporadic behavior of composite materials is the variability in construction and the natural complexity of behavior of composites. Flaws are very common in composites and assessing their impact in the capacity of the component is a very complicated process. The need for a reliable database is even more obvious in trying to determine the approach that more accurately will not be sensitive in its prediction to flaws in the material.

Of the failure criteria approaches mentioned in the first chapter of this dissertation two were selected for use in this program. One of the criteria is an intra-ply failure criterion and the other is an interactive failure criterion. Of the intra-ply criteria, the maximum strain failure criterion was selected. The selection of maximum strain and not maximum stress criteria is that in the case of stability behavior it is not expected that the specimen will be able to reach the level of stresses necessary to achieve maximum stress values for any of the components of the composite. Fiber failure was not expected until the postbuckling deformation stages, and matrix failure is more of a combined

effect that will be checked with the use of the interactive criteria selected. The interactive criterion was the modified Tsai-Hill failure criteria. The final version of the criteria used was as defined in the ANSYS analysis program. If during the application of the failure criteria a large amount of failed layers was detected during the loading for the test specimen, a more in-depth study will be developed of the failure criteria. The analysis results from ANSYS were used in the verification of the failure criteria since it was possible to do a criteria check as the loading was gradually increased in the analysis. This way if there was any accumulation of damage with the pressure increases it would be simple to track in the model. The confidence on this approach is high since the values of strains obtained in the finite element model were well matched to the strains developed during the test. In addition there would be no difference in the results from the failure criteria if applied by hand calculation since these would be based on the strains measured. In addition, failure criteria would also be easily used during the finite element verification phase.

The maximum allowable values used for the failure criteria verification will be presented next, in the tabulation of values x-axis corresponds to the fiber direction in the layer. These values were obtained from characterization tests performed in specimens built with same materials and fiber distribution. Negative values for normal stress are for capacity in compression and positive values are for tension.

ε_{max} = 0.04 in/in (based on matrix maximum strain in tension)

σ_{xt} = 240 ksi

σ_{xc} = -180 ksi

σ_{yt}, σ_{zt} = 4 ksi

σ_{yc}, σ_{zc} = -28 ksi

τ_{xy}, τ_{xz} = 13.6 ksi

τ_{yz} = 4 ksi

The expression used for the failure criteria is defined by ANSYS as a strength index, and is defined as:

$$\xi = A + B$$

where A and B are defined by the expressions:

$$B = \left(\frac{1}{\sigma_{xt}^{f}} + \frac{1}{\sigma_{xc}^{f}}\right)\sigma_{x} \quad + \quad \left(\frac{1}{\sigma_{yt}^{f}} + \frac{1}{\sigma_{yc}^{f}}\right)\sigma_{y} \quad + \quad \left(\frac{1}{\sigma_{zt}^{f}} + \frac{1}{\sigma_{zc}^{f}}\right)\sigma_{z}$$

and the expression

$$A = -\frac{(\sigma_{x})^{2}}{\sigma_{xt}^{f}\,\sigma_{xc}^{f}} - \frac{(\sigma_{y})^{2}}{\sigma_{yt}^{f}\,\sigma_{yc}^{f}} - \frac{(\sigma_{z})^{2}}{\sigma_{zt}^{f}\,\sigma_{zc}^{f}} + \frac{(\sigma_{xy})^{2}}{(\sigma_{xy}^{f})^{2}} + \frac{(\sigma_{yz})^{2}}{(\sigma_{yz}^{f})^{2}} + \frac{(\sigma_{xz})^{2}}{(\sigma_{xz}^{f})}$$

$$\ldots\ldots + \frac{C_{xy}\,\sigma_{x}\,\sigma_{y}}{\sqrt{\sigma_{xt}^{f}\,\sigma_{xc}^{f}\,\sigma_{yt}^{f}\,\sigma_{yc}^{f}}} + \frac{C_{yz}\,\sigma_{y}\,\sigma_{z}}{\sqrt{\sigma_{yt}^{f}\,\sigma_{yc}^{f}\,\sigma_{zt}^{f}\,\sigma_{zc}^{f}}} + \frac{C_{xz}\,\sigma_{x}\,\sigma_{z}}{\sqrt{\sigma_{xt}^{f}\,\sigma_{xc}^{f}\,\sigma_{zt}^{f}\,\sigma_{zc}^{f}}}$$

where:

C_{xy}, C_{yx} and C_{xz} – are coupling coefficients for the criterion. A good conservative value for these coefficients is 1.0.

σ^{f} – is the strength of the laminate in the specified direction

In none of the load cases studied including the modeled specimen was the failure criterion exceeded prior to buckling failure. In the only instance where the criteria was exceed before buckling was achieved was in the model with the large initial imperfection of 1%. Here, 110% or 1.1 times of the allowed maximum criteria was exceeded is some layers at the time the maximum stable pressure was reached.

In most of the model conditions the maximum strain criteria was the one with the closest ratio to one during the load steps. Nevertheless, this was not exceeded either up to the time of instability

2.5.5.5. EVALUATION OF SENSITIVITY OF MODEL TO SELECTED PARAMETERS

As part of the general study of the analytical model a simple variable sensitivity study was carried out on the final model. The main aspects of the behavior of the tested specimen were identified as:

i. Initial imperfection level
ii. Existence of any internal flaws
iii. Separation at the delamination
iv. Location of the delamination in the wall thickness
v. Level of friction at the delamination surfaces

Of the issues presented before, the last two were not studied in detail for this model. The variable of friction was approached by assuming for the analytical model in this program that no friction developed at the surfaces. The second bullet refers to an existence of an internal flaw of importance. The level of flaw that should be considered as critical and the development of reliable methods to detect them are part of a number of research studies. For our model only two conditions are studied, either a complete delamination exists or no delamination is present. This last point will be addressed in the following section of this chapter.

Table 2.7 presents the results of the finite element model prediction of buckling load as some of the variables are modified in the analysis. The tabulated buckling pressure is a percentage in terms of the calculated pressure for the specimen that had the properties closest geometrical and material characteristic to the tested specimen. This is highlighted in the table by a shade in the line.

VARIABLE SENSITIVITY STUDY FOR RISER MODEL				
Delamination (inches)	**% of Ovalization**	**VonMises Stress Max.**	**Maximum P3 strain**	**Buckling %**
0.0010	0.02	56.40	0.310 %	110 %
0.0010	0.04	52.04	0.296 %	106 %
0.0015	0.04	52.00	0.290 %	100 %
0.0010	0.08	46.60	0.266 %	83.4 %
0.0010	0.20	37.43	0.213 %	65.2 %
0.0010	0.30	34.93	0.199 %	58.6 %
0.0010	0.40	29.80	0.170 %	48.9 %
0.0010	1.00	63.70	0.300 %	32.6 %
0.0020	0.04	49.52	0.280 %	93.2 %
0.0050	0.04	48.00	0.270 %	71.8 %
0.0050	0.40	23.62	0.130 %	43.2 %

Table 2.7 Varaible sensitivity study results

From the results it is apparent that ovalization has the strongest effect on the buckling load. The results also seem to implicate that the assumption of elastic buckling being the mode of failure on our particular test specimen is reasonable. Two failure criteria were checked during the analysis, both the maximum strain and modified Tsai-Hill criteria. Remembering the results presented in the section on failure criteria we know that none of the criteria had been exceeded during the analysis of the model simulating the tested specimen. For this study, none of the criteria was exceeded at the time of collapse until the maximum out-of-roundness of 1% was analyzed. For the model in which criteria was exceeded at the time of collapse both the maximum strain as established in the model and the Tsai-Hill were exceeded at one time.

The effect of the gap between the delaminated surfaces is noticeable not only in the calculated collapse pressure but also in the calculated strain profiles in the specimen. Figure 2.57 shows the plot of the P1 strains for the finite element model for both the interior and exterior rings.

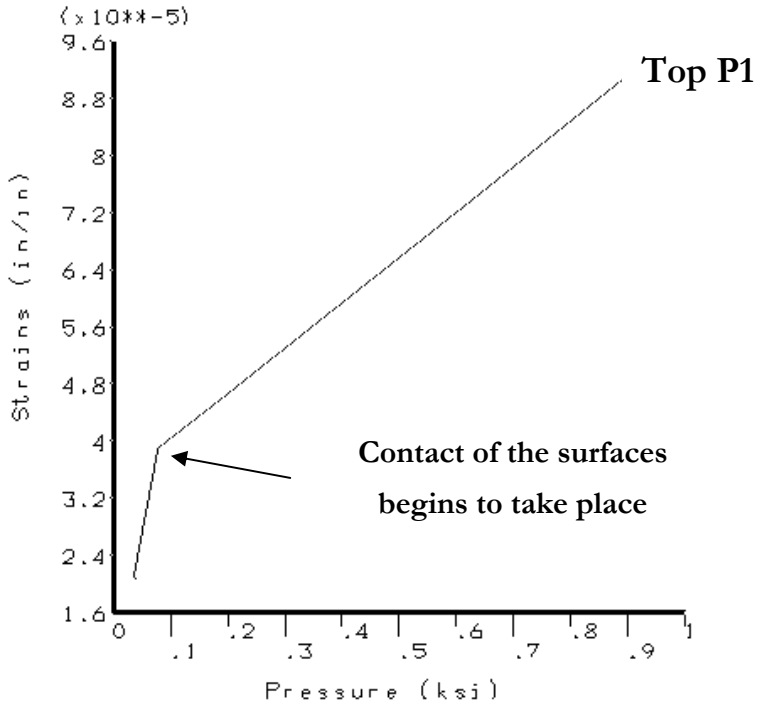

Figure 2.57 Delamination contact time

We can see the change in stiffness of the exterior ring at the time of contact. The point at which contact takes place is dependent on the separation of surfaces. If comparing to the experimental results, it is necessary to keep in mind that several factors could affect the exact moment of contact. First, the model assumes the same gap throughout the perimeter at the delamination. In addition, it also assumes that at the time of first contact this is perfect in the sense that there are no ridges or features that could affect the effectiveness of the contact. These are physical conditions that could have been different in the experimental model. Nevertheless, the change of stiffness at the recorded strain gages is clear and the behavioral tendencies observed follow those of this model.

A final comment in this section will be addressed to the contact stiffness (K_t) used with the analytical model. Rasheed [2.8] suggests a contact stiffness of 5,000

kips/in/in for contact convergence and minimizing numerical penetration in the surfaces. He finishes by suggesting that a value of 1,000 kips/in/in would be a good compromise to ensure fast convergence and accuracy.

In the model used for this study it was found that contact stiffness values had a somewhat noticeable effect in the calculated collapse pressure. Even though this effect was in the order of 10% maximum depending on the value of contact stiffness used, there was a definitive computational cost saving associated with the selection of contact stiffness values. A suggestion would be that if accuracy can be sacrificed, for as long as is a conservative estimation, the value of 5,000 kips/in/in will ensure good convergence with a difference of about 5 % in the predicted pressures. However, if more accurate estimation is needed the contact stiffness should be brought as high as possible without forcing numerical instability in the solution. For our model a contact stiffness of 8,500 kips/in/in was used. Higher values of K_t were found to become unstable when the delamination gap or the out-of-roundness were increased to values higher than 0.001 inches and 0.05 % respectively.

2.5.5.6. PREDICTED COLLAPSE WITHOUT DELAMINATION

As a final step in the analysis phase of this program, using the material properties and the same geometry definition a model of the riser was created that did not include a delamination. This model included the same out-of-roundness than the model that predicted a very close collapse pressure to the delaminated model. Also, the same calibrated material properties were used for the model that will be referred to as solid model. Two different values of out-of-roundness were analyzed in the solid model. The first was the same value as the tested specimen 0.04% and the second was the maximum expected value of 0.4% as stated at the beginning of the chapter. No other modifications were made between the delaminated and solid models. Figure 2.57 shows the results for the model with 0.04% out of roundness, View A has the deformation of the top edge at the time of collapse, and View B has the strains as calculated right before collapse.

The main characteristics of interest in these results are that, first the delamination does appear to have an effect on the capacity of the riser, and second, coincidentally if using the maximum expected out-of-roundness by API the resulting capacity is the same as the one measured for the specimen. The increase in capacity for the model of the tested specimen calculated by the finite element is of 80% or 1.8 times the measured one. Failure criteria was not exceeded for this model either. The difference in capacity between the delaminated FEA model with 0.4% oval (Figure 2.58) and the solid model with the same level is 106% difference with the solid model being higher. This indicates that if the collapse was governed by elastic instability as assumed the delamination had a strong effect on the capacity.

The stiffness of the solid model was as expected higher than the delaminated. However the solid model with the large out of roundness exhibited strains very similar to the tested specimen. This would raise question on the behavior of the tested specimen as of how important the delamination really was in the behavior. The fact that the FEA model, with similar geometric characteristics that the ones measured for the test specimen, tracks the behavior recorded during the test, supports the conclusions as made.

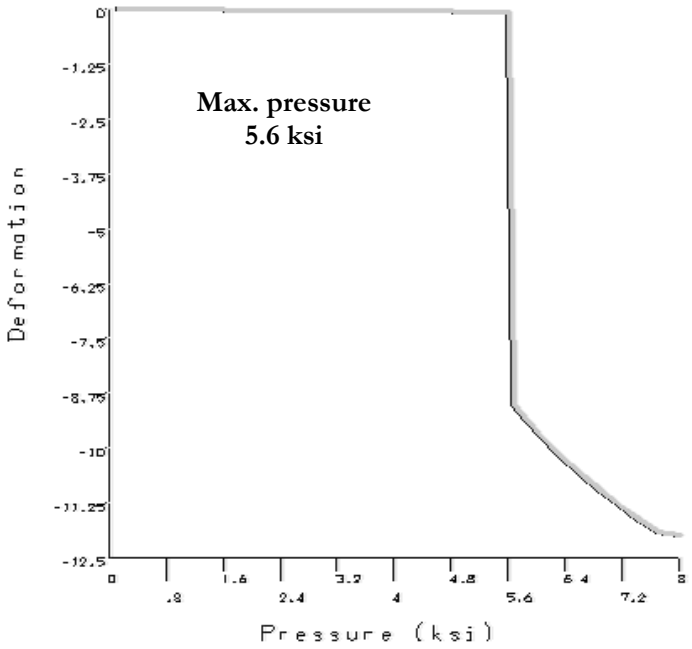

(a) Deformation at collapse

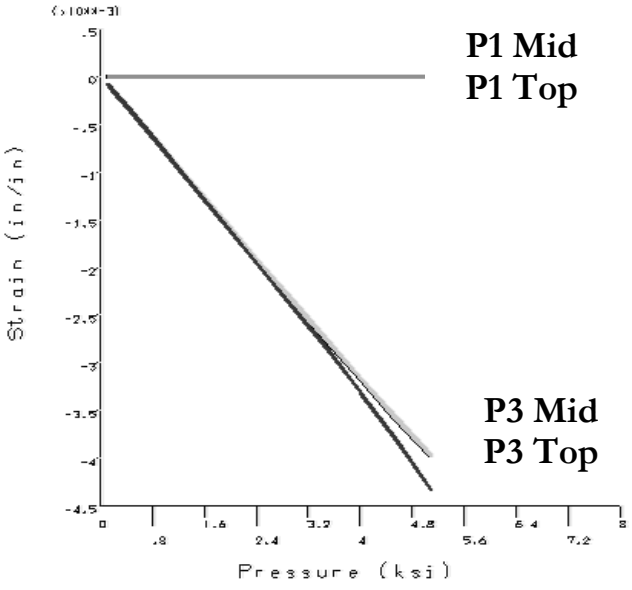

(b) Strains in solid model

Figure 2.58 FEA results for solid model 0.04% oval ratio

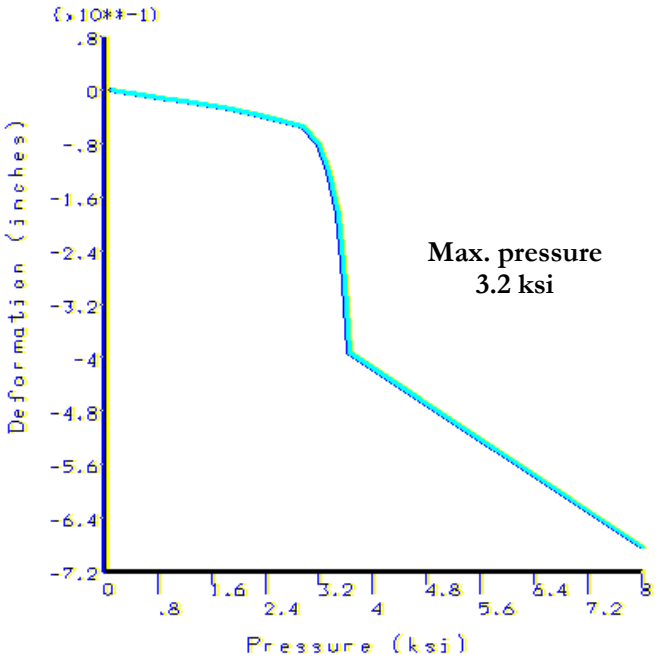

(a) Deformation at collapse

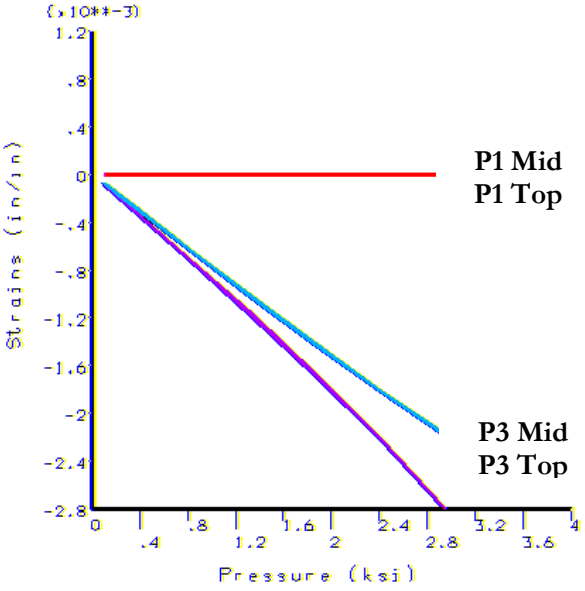

(b) Strains in solid model

Figure 2.59 Solid model FEA results for 0.4% oval ratio

2.6. SUMMARY AND CONCLUSIONS

A unique large-scale composite pipe was tested under external pressure up to collapse. Because of unexpected circumstances, a circumferantial delamination was created at about 1/3 the thickness of the specimen, as measured from the inside diameter. The maximum pressure recorded was 3150 psi. This corresponds to a predicted capacity by the use of a finite element analysis using the ANSYS® code with a model that includes the delamination. During the analysis of the recorded strains and the associated stresses, in addition to the finite element model results, a check on the failure criteria was performed. The results seem to indicate that no material failure was produced during this particular test. This could indicate that the failure observed was one of elastic buckling alone.

The analyses of the recorded strains indicate a behavior, mainly elastic, which is expected in fiber dominated composites where no fiber failure is detected. This elastic behavior remains apparent even if matrix cracking has taken place since fibers provide most of the stiffness to the composite. This appears to support the results of the finite element model that predicts the collapse pressure by pure elastic behavior. Using this same model, a second analysis was made on a similar geometry, but without the delamination in order to evaluate the effect of the delamination in the capacity of the specimen. A peculiar trend was that a permanent deformation was increasingly recorded during the test at load drops. However, no change was noted in the stiffness as the loading continued past the previous maximum load. There is a strong possibility that the permanent deformation was just the result of the movement between the two separate rings and friction at the delamination surfaces not allowing it to recover. The lack of additional specimens makes any further conclusion difficult to support.

The analysis of the acoustic emission data was used to support to the observed behavior in the strain gages. This support is provided by means of increases in the measured activity at the time a behavioral milestone was reached. As presented, the data does not provide a clear picture of the mechanisms at play during the complete test.

This type of analysis was not intended in this work and will be approached by others. There is, however, a clear statistical trend of increased activity as the maximum pressure was reached.

Using the same material properties and geometry as defined for the delaminated model a second model was developed. This model did not have a delamination and was subjected to the same loading and boundary conditions. The resulting predicted collapse pressure was of 5.6 ksi, about 81% more that the recorded and calculated collapse pressure for the delaminated model. This indicates the strong possibility that the delamination did have an effect on the behavior of the specimen. This is intuitively correct since by having a practically frictionless surface separating the thickness of a component, it becomes essentially two different pipes fitted one inside the other. This fact also makes the direct use of theoretical solutions for delamination buckling failure not reliable. The stress profile at the delamination would be different for a partial delamination than for this case. Tests are still necessary in this area for verification of the results and trends seen here and in other conditions.

CHAPTER 3

INTERNAL PRESSURE TESTS ON COMPOSITE TUBES

3.1. INTRODUCTION

3.1.1. DESCRIPTION

This chapter describes an experimental program conducted on fiber reinforced composite tube specimens, subject to static and cyclic internal pressure. The program was aimed at refining current design approaches and design criteria for composite pipes, tanks and pressure vessels that contain fluids. This experimental program was also intended to explore the possibility of using acoustic emission data as basis for establishing allowable strain values for design of these and similar components.

Current design procedures for fiber reinforced pipes and pressure vessels in the US are based largely on empirical rules, or statistical sampling, combined with long term cyclic testing. Components are subjected to cyclic pressure testing to determine the relationship between strain at failure and the number of cycles at failure. This data is then extrapolated to estimate the strain at failure of the composite at a number of pressure cycles that a component is expected to see in its service life. ASTM D2992 specifies the requirements for such testing and for the extrapolation of the data. In order to qualify new designs or new material systems according to ASTM D2992, generally more than a year of testing is required to establish the fatigue life of a component. The need to conduct such long term testing programs can provide a deterrent to the development of new designs or the use of new material systems.

A long term cyclic test program, as described above, was conducted by A.B. Isham [3.1] in the 1960's to establish safe strain limits for use in the design of fiberglass

chemical storage tanks. Based on these tests, which will be described in greater detail later, Isham recommended a design strain limit of 0.1 %. This value is still used today in the design of fiberglass tanks as specified by ASME-RTP-1 committee [3.2]. Resins currently used in the construction of fiberglass tanks are substantially different than those used by Isham, and may be capable of sustaining substantially higher strains. Nonetheless, the 0.1% limit is still widely used for design.

3.1.2. PROGRAM OBJECTIVE

The purpose of the tests described in this chapter is as follows:

i. Using test methods similar to those employed by Isham, determine if design strain limits for fiberglass can be safely increased above 0.1% when typical current resin systems are employed.
ii. Determine if acoustic emission testing can be used as a basis for establishing design strain limits, without the need for long term fatigue testing.

The results from the tests performed by Isham, were the basis for the development of the design limits specified by the codes regulated by the ASME. Materials have improved in the past 30 years and, as a result, design limits developed with earlier systems may not reflect the benefits of the newer materials systems. This program is partly aimed at comparing the behavior of specimens manufactured with these new materials as they relate to the results of the older tests.

The specimens tested were built following the guidelines from ASME RTP-1 committee [3.2]. These guidelines apply to tanks that may contain corrosive or chemically active materials. They include a protection barrier meant to inhibit exposure of the structural layers, which are fiber wound on top of the barrier. This protection layer is typically a resin rich glass mat chopped layer with a low structural strength when compared to the winding layer. The design of this layer is included in the guidelines for the entire tank or vessel and is based on strength ratios between the structural winding and the barrier. The participation of the barrier in the capacity of the vessels has been a

source of discussion in the development of the guidelines. This program will evaluate the amount of participation of the barrier in the structural behavior of the specimen.

As discussed before, the long test time requirements are a source of problem in the application of composites in the area of civil engineering. The nature of most of the structures in civil works calls for unique one-time design and use specimens. It is obvious that the testing requirements developed for pressure vessels could prove to be impossible to carry on in the case of single-use applications. An example is the use in offshore applications where composites are being used in production and drilling risers. These are essentially pressure vessels that will vary in load requirements and dimensions, along with maybe forming materials, from project to project. The sheer size and cost of production makes the fabrication and testing of prototype specimens for each one of these components cost prohibitive. And even if performed, due to the variability issues discussed before, this would not ensure that the final product would behave in the same way as the tested prototype once is placed. The development of non-destructive methodologies for the testing of these structures could prove to be invaluable for predicting capacity and life of the component. This program approaches the possibility of developing such methodology with the use of acoustic emission (AE) technology. Acoustic emission monitoring can be used for both proofing and prediction of capacity in the same test without having to destroy the component.

Determination of fatigue or cyclic life is an issue of great importance in the design of a structural component. Here also, composites have demonstrated a scattered behavior more so than other materials typically used in structures. The use of large safety factors has been the common practice in dealing with this problem. The use of AE is explored in this phase as a possibility for predicting cyclic behavior in composite materials subject to internal pressure. Measurements at the beginning of the load history will be compared to measurements during the history and final loading to failure. The possibility of using AE records in determining the cyclic life characteristics for composite pipes will be assessed during this program.

3.1.3. PERFORMANCE CRITERIA

A large number of the composite structures in service are standard sizes with a preset maximum service pressure determined by code; between 5-psi and 15-psi [3.2 and 3.3]. This approach generated standard applications and sizes that manufacturers were able to certify by the use of a long term testing program that included creep and fatigue testing. Once a maximum life was determined the design for a particular application would be developed based on this information and linear regression curves as by ASTM-D2992. Currently, a manufacturer following this specification must proof-test any new component for approximately 1.5 years before being able to proceed with commercial development. Current applications and needs in the civil engineering field makes this type of testing impractical and uneconomical. The development of new materials and systems has forced the need for change in the policies for design and manufacturing.

The American Society of Mechanical Engineers has two committees dedicated to the regulation of design and construction of fiberglass pressure vessels. The committees for the Section X Code and RTP-1 specifications provide design and fabrication criteria based on empirical experience and experimental research results. These are the basis for the design of composite vessels or components in applications other than those originally covered by the codes. This is apparent in the design of composite components for offshore applications, where the use of these standards as the preliminary sources of design criteria is very common. However, because of the uncertainty associated with the design limits, large prototyping is a main part in the design phase. Development of design criteria and evaluation procedures that have more general applications is critical for the development of economical systems using composite materials for the offshore industry. Details of these design criteria will be approached later in the chapter.

Composite materials are quite complicated to analyze in precision due to their layered nature and the variability in construction. Variability in composite components is an important design issue. Assessing the properties of a component fabricated using

high performance composites with NDE methods is a way to confront the variability effects. However, this assessment must be practical and economical.

3.1.3.1. FAILURE MODES FOR INTERNAL PRESSURE SPECIMENS

Several modes of failure are possible when testing composite specimens under internal pressure. The stages of behavior can typically be separated in the following steps:

- Non-linearity of stress strain curve
- weeping or leakage
- loud emission of cracking noise and isolated fiber breakage
- burst or total failure

These forms of failure will, in many cases, appear in this sequence. This is not, however, always the case. For example, non-linearity may not be apparent before weeping or leakage is detected. Or, isolated weak fibers may break at low load levels when compared to burst and even before leakage. When looking for signs of non-linearity, the best source it to look at the axial strains in the tested tube. In the case of a structure under pure hoop stresses, the axial strains are very small compared to the hoop strains. They respond to the Poisson's ratio effects, and in composites, depending on the winding angle this relationship can have a very small value between hoop and axial.

For undamaged structures, laminate and shell theories have proven to be reliable in calculating strain stress relationships. These theories however, assume a perfect condition and bond in all the layers. Real measurements start deviating from theory at first ply failure. For predicting the onset of non-linearity, Spencer and Hull [3.4, 3.5] used the following expression to predict non-linearity:

$$1 = \frac{\sigma_T^2}{Y\,Y_C} + \sigma_T \frac{Y - Y_C}{Y\,Y_C} + \left(\frac{\sigma_S}{S}\right)^2$$

In this expression Y and Y_c are the strengths in the direction for the particular laminate transverse from the fibers, with Y_c being the compressive strength of the laminate. The shear strength is incorporated by the term S in the expression. The term σ_t is the applied tensile stress in the axial direction of the pipe. This expression has found good agreement in tests performed on pipes with winding angles varying from 35^o to 75^o.

Following the point of non-linearity is the point of leakage or weeping. Tests have shown that leakage is independent of the shear stress [3.5]. This could indicate that a growth of cracks in the interface between fibers and resin is necessary for the liquid to find its way to the outer wall. At this point, a non-lined pressure vessel will be considered failed. If a liner is added, then the vessel will continue to hold fluid until burst. Typically this liner will be made of flexible material that will gap the cracks holding the fluid from moving through the wall of the vessel. In these cases, failure will be controlled by fiber capacity. The procedure for determining this level is similar to the one followed for the onset of non-linearity. A progressive failure of layers or plies is calculated until the last one is reached at this point. A common way to calculate this degradation of layers is by the expression:

$$E_i^* = (DF)\, E_i$$

Where "i" can be either, longitudinal, transverse or shear modulus. And E_i^* is the degraded modulus, and DF is between 0 and 1.

The use of non-flexible liners like in the case of RTP-1 vessels, place leakage loads somewhere in between the weepage as estimated by these expressions and burst. However, it is still quite a bit smaller than the burst pressure capacity.

Other failure criteria are available in the literature for the determination of failure of laminates under combined loading. Some of the more common are Tsai-Hill, Tsai-Wu, and Hashin, all of which have already been treated in detail in the first chapter of this dissertation. All criterions have demonstrated good agreement with some tests and poor correlation with others with different loading conditions. For as long as no general agreement is reached in the application of failure criteria, support methods for determining capacities of as-built structures and components are needed.

Ultimate behavior of fiber reinforced composites has been researched extensively. The linear nature of the fiber during their load histories makes prediction of fiber breakage quite reliable. The same applies to the behavior of the resin used in the formation of the matrix for the composite. The difficulty comes when trying to predict the interaction of all this components. Flaws and imperfections in the material form during the fabrication or are created during their in-service condition. A number of applications for fiber reinforced composites do not depend on the ultimate capacity of the fibers but on other behavioral states. For example pressure vessels depend on leakage which as been found to be at a much lower level than burst, or fiber failure. Load levels at the beginning of matrix cracking in a fiber composite depends on several factors like fiber angle, applied loads and existing either initial or generated material flaws. These factors are difficult to measure and predict in real structures and are critical in the service life of a structure. They do not reflect in the stiffness of the material since this is dominated by the fiber which remains elastic and linear to the point of failure. This does not imply that composite material components do not show non-linear behavior. It does, however, imply that in some cases this non-linearity is very difficult to detect and even when noticed it may not indicate the nearing of a limit condition. This program will concentrate in the development of methods of predicting the factors that will be referred to as serviceability limit states.

Acoustic emission (AE) has been successfully used in the in-service monitoring of pressure vessels and tanks. As a global monitoring system, AE can monitor the behavior of the complete structure at the time is being loading. This global monitoring

provides with information of the state and condition of the structure without regards to specific identification of problems. Presently there is considerable research work being made in the use of AE for identification and specific location of damage mechanisms. However, a large amount of research is still required for the development and verification of reliable methods for identification and location of AE originating sources. Nevertheless, parametric or statistical AE is a mature and proven technology to the point that, if used properly, can provide reliable benchmarks on the capacity and expected behavior of a composite material component, without determining the specific failure mechanisms at play. The typical methodology for testing with AE follows this procedure: the specimen is tested under pre-determined loading conditions while monitoring with AE at the same time. If the amount or the intensity of the emission is more that preset thresholds or limit values, the specimen is judged unsuitable for service and a more in-depth inspection is then performed. One of the biggest obstacles to the acceptance of AE as a design tool has been the policy of trying, unsuccessfully, to associate specific parameters of the emission to a particular type of damage mechanism. The common practice of using resonant sensors in the monitoring of structures, although acceptable for a number of applications, makes identification of mechanisms difficult. In addition, the complicated nature of wave propagation properties in composite materials forces a more in-depth analysis of the captured signal than what it is possible by the use of resonant information. When the details of the mechanisms at play are so difficult to define, a method that looks at the global influence of the different mechanisms at play could prove to be more useful.

Using a simple state of stress makes the analysis and interpretation of results clear and reliable. In addition, when looking at cyclic behavior it is necessary to have a predictable state of stress and strain that will remain in the same relationship to the applied loads during the extent of the test. The objective of trying to calibrate non-destructive methods to predict the behavior and capacity of a structure also benefits from the analysis of a simple state of stress. More complicated state of stresses will be easier

to understand and model if, the simpler conditions are well understood. A tube under internal pressure provides for such a simple state of stress.

3.1.4. REVIEW OF TESTS PERFORMED BY A. B. ISHAM

In the late 1960's, A. B. Isham developed a research program with the objective of determining acceptable design limits for fiberglass reinforced plastic vessels [3.1]. ASTM had specifications already in place for the determination of design limits for reinforced plastic pipe (ASTM D2143-63T and the methods of analysis prepared by Section XVIII B of ASTM D-20). It was, however, felt that the strain conditions generated by the tests were not applicable to large storage plastic tanks. Tanks had a lower level of axial strains induced by the applied pressures than those generated on a pipe by a hydrostatic pressure test. Isham modified his test setup to allow for the free movement of the end cap plates during the pressurization. This produced a state of stresses of pure hoop tension as produced by the applied internal pressure.

The test specimens used in the Isham program were 9 ¼ inch I.D. with wall thicknesses equal to a full-scale construction vessel. Figure 3.1 shows the typical profile of the specimens used for this program. Each sample had a "leak detector" embedded in the pipe wall. This detector consisted of a narrow strip of fine mesh bronze screen placed at the interface of the chopped strand and filament wound layers. During the cyclic test, any crack in the interior layer that extended to the interface, would allow fluid to come in contact with the bronze, therefore closing an electrical circuit. When this took place during the cyclic tests, the specimen was considered to have failed.

Tests were controlled in terms of the strain in the outer wall of the specimen at the target pressure. Maximum internal pressures of 400 to 1,000 psi were used in the tests. The pressure was cycled between normal water pressure of 35 psi and the desired maximum. Cyclic rates between 700 and 900 cycles per hour were used, based on the capabilities of their equipment. The material used for the internal chopped strand layers

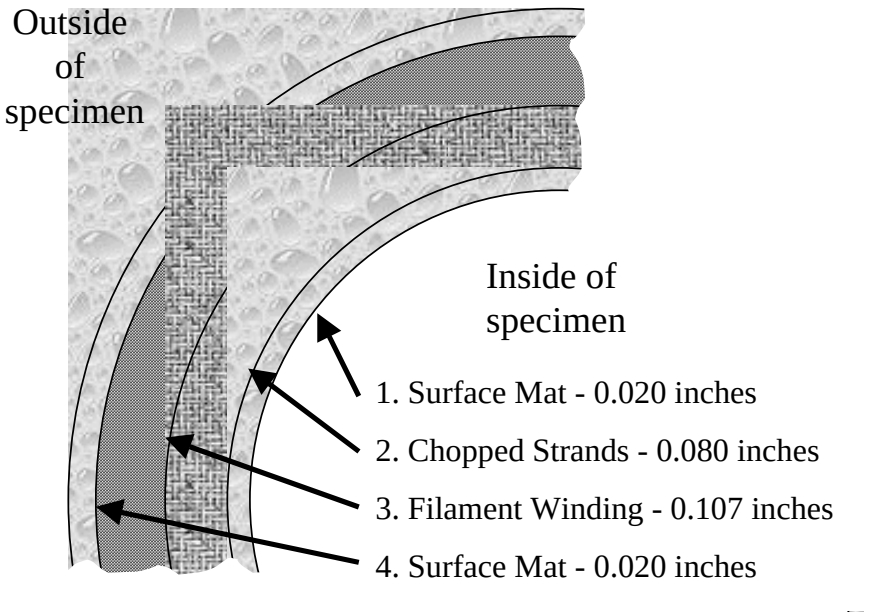

Figure 3.1 Specimen profile for Isham tests

was Atlac 382 vinylester resin, reinforced with 25% OCF M710 mat. No information is provided as to the materials used for the other layers that were part of the specimen.

The maximum static capacity of the specimens was determined first as the starting point of the cyclic tests. This capacity was determined at 0.4% strain, which was considerable lower than the published strain limit (1.7 %) for the resin alone. The longest test part of the program lasted for 335,000 cycles at a strain level of 0.2% and was used for the calculation of extrapolated capacities. This specimen, however, did not fail during testing. The test of the final specimen was stopped without failure due to the need of using the testing facilities for a different program.

Results were presented in a log strain versus log time plot and linear regression analysis was performed and plotted. Figure 3.2 shows the plot of results as presented in the paper referenced. Long-term design strain was determined by extrapolating the plot to 15 years (131,500 hours). Even when the data available for this estimation was

extremely limited, these values were used in the discussion of design limits. A confidence limit of 95% was used in the determination of the statistical data for design limits. An arbitrary safety factor of 1.57 was selected for the long-term data to account for the degradation in the material as a result of exposure to the environment and the fluid contained. The final value determined for design was of 0.093 % of strain. The thickness of the corrosion barrier was determined by design rules in effect at the time and based on experience of tank manufactures. The typical barrier thickness was of 0.10 inches, and was used in the specimens tested in the program. A final surface mat on the exterior was added for a total of 0.12 inches of non filament wound structure.

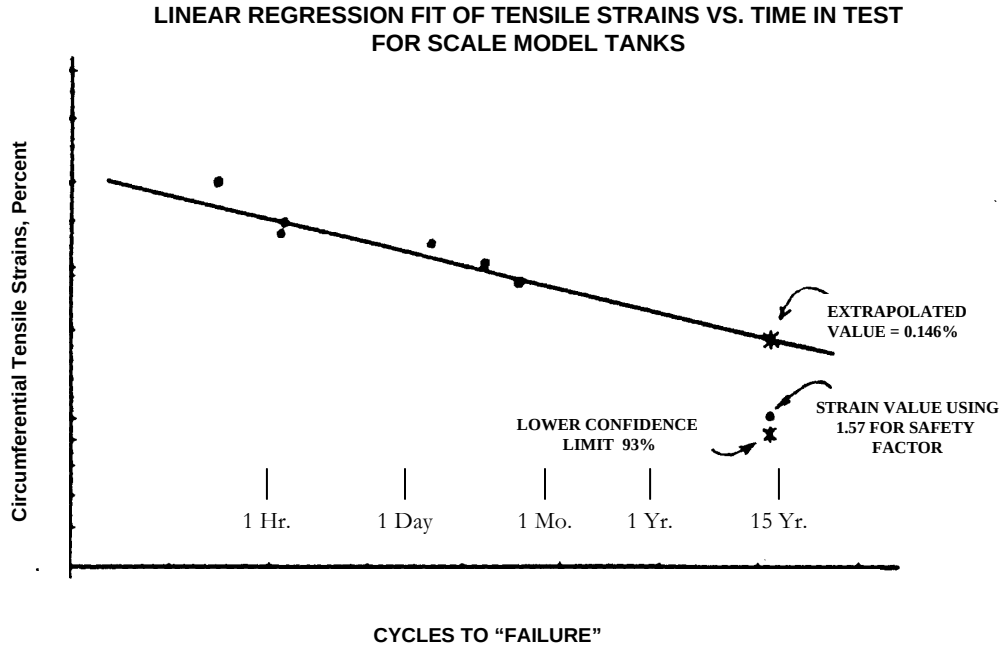

Figure 3.2 Isham tests results [From Ref 3.1]

3.1.5. CURRENT DESIGN CRITERIA FOR PRESSURE VESSELS

Eckold [3.6] describes in his book the steps in the design process for composite materials. The initial steps, independent of the design methods to be used are:

i. Functional specification: what are the functions and working requirements for the component to be designed
ii. Materials of construction: decide what materials to use in the manufacturing. A very complicated process in composite construction due to the number of options and combinations available
iii. Design and analysis: analysis of an anisotropic material like a layered composite is quite different from an isotropic material like steel. This step is the focus of this section.
iv. Fabrication limitations: properties in composites are very dependent on the fabrication process used. These differences should be kept in mind when proceeding with the design.
v. Reliability requirements: selection of safety factors still an area of need of extensive research
vi. Cost considerations: still the biggest obstacle for the development of composite materials. Cost of composites should be compared to other conventional construction in terms of durability and performance.

For the design step, there are at present a number of approaches that are widely acceptable. In general, their application is not mandated or regulated in any manner. Manufacturers are free to select which design and verification process they are to follow, and for as long as they follow the requirements of each, the designs are deemed acceptable. The main approaches for design is:

- Empirical Design
- Deterministic Design
- Probabilistic Design
- Fracture Mechanics

Of these approaches, the ones more suited for civil engineering applications are the deterministic and the fracture mechanics approach. The nature of the single component design and application of civil structures calls for the development of reliable and economical design methods. The cost implications of the empirical and probabilistic approaches make for an impractical use of them on the design process for civil applications.

In the deterministic approach there are three main bodies of specifications in the United States for the design and manufacturing of fiberglass or fiber reinforced plastic pressure vessels. Two of these come from the American Society of Mechanical Engineers (ASME), and they are the RTP-1 committee standards and the Section X committee [3.2 and 3.3]. The other comes from the American Water Works Association (AWWA) Standard [3.7]. Each of these standards has a limited scope in their application and make provisions for extrapolation beyond these limits. Moreover, reflecting the inconsistency in the design philosophies in the manufacturing area, the standards provide with alternate design approaches in their specifications. Typically these will be either an empirical or rules based design or a stress-based design. This rules based design is what limits the scope of each of the specifications so severely. These specifications will not be presented in detail here, for additional information of the procedures and formulas used the reader is directed to the references indicated previously. We will, however, enumerate the main areas of influence for the standards and their intended application.

3.1.5.1. ASME RTP-1 STANDARD (REINFORCED THERMOSET PLASTIC CORROSION RESISTANT EQUIPMENT)

Developed for use in the design of tanks operating at pressures not higher than 15 psig over hydrostatic head or, 15 psig of external pressure, and containing corrosive or otherwise hazardous materials. ASME developed this specification in response to the absence of one by ASTM. Structures made of laminates fabricated via contact molding

or continuous winding are covered by this specification. However, only vessels fabricated using glass fibers for reinforcement are allowed in the specification. Several loading conditions are covered by the specification (internal pressure, collapse, axial load, etc.); we will concentrate on the specifications relating to the internal pressure loading. There are two main design methods allowed by the specification, the first one is design by rules and the second design by stress analysis. In both methods, failure of the vessel is defined as leakage of the fluid through the vessel wall.

The first design method called SUBPART 3A DESIGN BY RULES, is based on the homogenization of the laminate to an average property value in the direction of interest (hoop or axial). With this average value and a maximum predetermined value of strain and stress the required thickness of the wall is calculated. The specification also provides the necessary guidelines to determine the limiting strain and strength values. It also provides values for the design factor values to be used in the design of vessels. If the form of manufacturing to be used is hand lay-up the safety factor is 10. For filament winding, regardless of the angle of fibers in the laminate, the design is determined by a maximum strain of 0.1% for hoop direction loading and a combination of allowable stress and design factor of 10 for axial loading. In any case, the minimum thickness for any vessels shall not be less than 0.22 inches. The formulas for filament winding are:

Hoop Loading

$$t_h = \frac{PD_i}{2(0.001\ E_h)}$$

Axial Loading

$$t_a = \frac{N_{ax}}{S_a / F}$$

where:

D_i = inside diameter, in

F = Design factor = 10

N_{ax} = axial force per circumferential inch of shell, lbs/in

P = total internal pressure, psig (internal pressure plus hydrostatic head)

S_a = ultimate axial tensile strength, psi

S_h = ultimate hoop tensile strength, psi

t_a = total wall thickness, in., for axial stress

t_h = total wall thickness, in, for circumferential stress

E_h = hoop tensile modulus

The wall thickness of the shell would be the thicker of the two calculated values for t. This particular approach does not allow for the use of the corrosion liner as part of the structural wall. It accounts only for the filament winding as the structural component of the vessel.

The second design method SUBPART 3B DESIGN BY STRESS ANALYSIS, allows for design using elasticity theory and a recognized failure criteria in the design of the layers of the vessel wall. In addition, the specification allows for the use of alternative mathematical techniques. However, these techniques must be shown to be more accurate or conservative that the ones indicated in the specifications. The use of stress ratios is the key to this method. Stress ratios are determined by the use of failure criterions as applied to individual layers. To obtain the strength ratios, maximum stresses are determined using these failure criteria relationships and then, they are compared to the stresses induced by applied loads in the layer. In contrast to SUBPART 3A, this section allows for the inclusion of the internal corrosion barrier layer as part of the structural component of the vessel. It does, however, apply more restrictive allowable strength ratios to the inner layers than to the structural winding. The requirements for strength ratios for the inner layer, veil and glass mats are as follows:

(a) For vessels which are designed using a combination of Subparts 3A and 3B rules, the minimum strength ratio shall be ten

(b) For vessels designed entirely by Subpart 3B rules, the minimum strength ratio shall be nine

(c) For vessels designed entirely by Subpart 3B rules and for which acoustic emission examination by Appendix M-10 is performed, the minimum strength ratio shall be eight

(d) For vessels in critical service as defined by the specification, the minimum strength ratios in (a) through (c) above shall be multiplied by 1.25. And finally,

(e) For the other layers in the vessel not in critical service, that is the filament winding for our case, the strength ratio shall be 1.6. If the vessel is on a critical service, the ratio will be 2.0.

It is readily apparent that the application of these design specifications can be quite involved and complicated depending on the amount of refinement desired at the time of determination of the requirements. In addition, the specifications are very specific as to the cases they cover; any deviation from these conditions is not included and cannot be designed using these methods. Development of more consistent design criteria is necessary for the application of these or other specifications to cases where the stress profiles are more complicated than the ones covered.

3.1.5.2. SECTION X OF THE ASME BOILER AND PRESSURE VESSEL CODE

These specifications were developed for the design of vessels not used to store, handle, transport or process of hazardous or lethal fluids as is the case with RTP-1 designed vessels. It therefore establishes minimum requirements for the design of thermosetting plastic components for general service. It also sets limitations on the service conditions and defines specifically what vessels are not covered by its rules. Different from the aforementioned RTP-1, this specification allows for the use of fibers other than glass fibers for reinforcement purposes. It defines two methods of design qualifications, Class I and Class II, and the differences are:

Class I – Qualification of a vessel through the destructive test of a prototype

Class II – Mandatory design rules or design by stress analysis and acceptance by nondestructive testing

Procedures outlined in Class I method are non-mandatory, whereas procedures in Class II are mandatory. Each of the classes outlined by the specifications also includes sub-methods for the design of vessels. Additional specifications, procedures and rules are outlined in the code for fabrication and design of components.

Covered pressures vary depending on a combination of design Class used and method of fabrication and sub-method of design used. For example, vessels designed using the Class I method have a maximum pressure of 150 psig for bag molded vessels, centrifugal cast, and contact-molded vessels; 1,500 psi for filament-wound vessels with cut filaments and, 3,000 psi for uncut filament vessels that have ports only in the axis of rotation. For Class I vessels requirements for proof testing are outlined. A cyclic test to 100,000 cycles at the service or design pressure, followed by a static test up to six times the design pressure without failure is required.

Class II method is subdivided in two sub-methods for design, Method A and Method B. The former is a design rules based method, with the latter being a discontinuity stress analysis based method. Vessels designed with Method A can have a maximum service pressure limit up to 75 psi. Vessels designed following Method B can have a maximum design pressure up to 200 psi. There are also other associated limitations related to dimensions and algebraic product of dimensions to internal pressure. Maximum external pressure is limited to 15 psi, regardless of the method of design used. The only other limitation is in Method B where the shear design factor is 10 and the maximum allowed strain is 0.1% in any direction. The expressions used in the determination of shell thickness by the Class II design method A are:

Longitudinal Stress

$$t_1 = \frac{PR}{2(0.001E_1 - 0.6P)}$$

Circumferential Stress

$$t_2 = \frac{PR}{2(0.001E_2 - 0.6P)}$$

where:

E_1 = tensile modulus in longitudinal direction

E_2 = tensile modulus in circumferential direction

R = inside radius, inches

P = internal pressure, psi

t_1 = structural wall thickness for longitudinal stress

t_2 = structural wall thickness for circumferential stress

For design based on discontinuity stress analysis (method B), the specification requires a detailed stress analysis. The only point of interest is that the method specifically states that the interlaminar shear between the lamina does not need to be considered. It also states that the failure criterion to be used in the design by this method is the quadratic interaction criterion (Tsai-Wu). All strength ratios are calculated based on this criterion. Design strength ratio is 6 for all load combinations in this method.

3.1.5.3. AWWA STANDARD FOR FIBERGLASS PRESSURE PIPE

The scope of this standard is for among other things the design, fabrication and testing of nominal 1-in through 144-inch fiberglass pipe for use in above or below ground water systems. The way the standard specifies the design limits is by first defining what a pressure class is. Pressure classes are typically designated as half of the leakage capacity of a pipe. Therefore, as this specification covers the pressure classes of 50, 100, 150, 200 and 250 psi, the corresponding maximum pressures for each class are 100, 200, 300, 400 and 500 psi respectively. There are also provisions for extending the standard to cover pressure classes other than the ones specifically referenced. It also includes design specifications for pipes with an internal liner similar to the RTP-1 specification. The specifications also include requirements for minimum stiffness for pipes. The stiffness is to be determined by sample testing of pipes in terms of deflection

tests during a fabrication run. The measured deflections or calculated stiffnesses must be compared to allowable values stated in design tables. Similarly, statistical sampling with frequent test of fabricated pipes is required for approval. The sampling is subject to the following expression:

$$F = \frac{S_i}{S_r}(P\,r)$$

Where:

F = required minimum hoop tensile strength, in pounds-force per inch of width

S_i = initial design hoop tensile strength, psi

S_r = hoop tensile stress at pressure class, psi

P = specified pressure class from a table in AWWA

r = nominal pipe radius, in inches [(OD – single wall thickness)/2]

Rational and empirical methods are used in the design of fiberglass pipe. Most performance limits are established from long-term strength characteristics. Design stress or strain limits are obtained by reducing the strength limits with appropriate design factors. These factors are designed to cover any variability in material and load, in addition to account for long-term performance issues. This is one of the few specifications that allow for the design of pipes based on two approaches. The pipe can be designed based on stress, as the hydrostatic design bases as outlined by ASTM D2992 procedure A. In addition, a maximum strain basis can also be used based on the same ASTM standard. The expressions for this specification are as follows:

For stress basis HDB

$$P_C \leq \left(\frac{HDB}{FS}\right)\left(\frac{2t}{D}\right)$$

For strain basis HDB

$$P_C \leq \left(\frac{HDB}{FS}\right)\left(\frac{2E_H t}{D}\right)$$

Where:

P_C = pressure class in psi

HDB = hydrostatic design basis, in pounds per square inch for stress basis or inches per inch for strain basis

FS = minimum design factor, 1.8

t = thickness of pipe reinforced wall per ASTM D3567, in inches

D = mean pipe diameter in inches as follows:

For inside diameter (ID) series pipes (Tables 1 and 2, AWWA C950)

$D = ID + 2t_L + t$

For outside diameter (OD) series pipes (Tables 3, 4, 5, and 6, AWWA C950),

$D = OD - t$

Where:

t_L = thickness of liner (when used), in inches

ID = inside diameter, inches

OD = outside diameter, inches

E_H = hoop tensile modulus of elasticity for the pipe, in psi

A complication with the HDB approach is that it may be defined in terms of reinforced wall hoop stress, apparent glass fiber stress, or hoop strain on the inside surface, depending on the product and type of construction used. To facilitate interpretation, the relationship between HDB in terms of composite stress and reinforcement stress is:

$$HDB = \left(\frac{t_R}{t} \right) (HDB)_R$$

Where:

t_R = effective thickness of hoop reinforcement adjusted for helix angle (Annex A1, ASTM D3517) in inches

$(HDB)_R$ = hydrostatic design basis in terms of reinforcement stress, psi

In this specification, there are two main factors included in the design. The first is included in the determination of *Si* and *Sr*. These reflect a minimum design factor of 4.0 on first load or initial hydrostatic strength. The second factor is the ratio of HDB to hoop stress or strain at pressure class P_c. This factor assures that the stress or strain due to sustained working pressure does not exceed the long-term hoop strength of the pipe wall as defined by HDB. For fiberglass pipe design, this design factor is 1.8. The main limitation with this approach is that it treats all pressure ranges with the same safety factor. It does not differentiate between specimens of different fiber types, or with different fiber content. The stiffness values are for ring deformation under external loads, not for internally applied pressures, therefore, specimens with high stiffness values are not allowed to carry higher pressure levels that those with lower stiffness but the same pressure requirements. Stiffer specimens will limit the amount of deformation under internal pressure, the statistical sampling used in the design does not reflect this.

3.2. EXPERIMENTAL PROGRAM DESCRIPTION

The program consisted on a series of tests on fiberglass reinforced pipe specimens built in accordance to RTP-1 guidelines. The loading profile would be of simple hoop stresses as applied by internal pressurization with water. Both static and cyclic loading will be presented, in addition to static tests on hybrid pipes fabricated by winding similar to the fiberglass specimens with an additional winding of carbon fibers in the surface. The loading was produced by the use of an air driven water system, in a

test tank designed and built during this program to contain the specimen in case of burst. Figure 3.3 show a schematic representation of the test tank setup.

Acoustic emission will be recorded during the tests for both the monotonic and cyclic phases. Parametric AE will be used in the evaluation of the behavior of the specimens. Work in source identification, or identifying the originating mechanism for the AE events recorded, is being done by others [3.8]. AE parameters will be compared to recorded strains for the tests and between different tests. The purpose is to estimate the possibilities of using AE for proof testing of composite pipes either for series production or for single application. The static tests will provide information on the strength ratios between the corrosion barrier and the structural winding.

Hybrid construction has acquired increased interest in recent years. Combining the high stiffness from carbon fibers with the low cost of the glass fibers along with the high strength of their combined action, is very attractive. Because of the stiffness

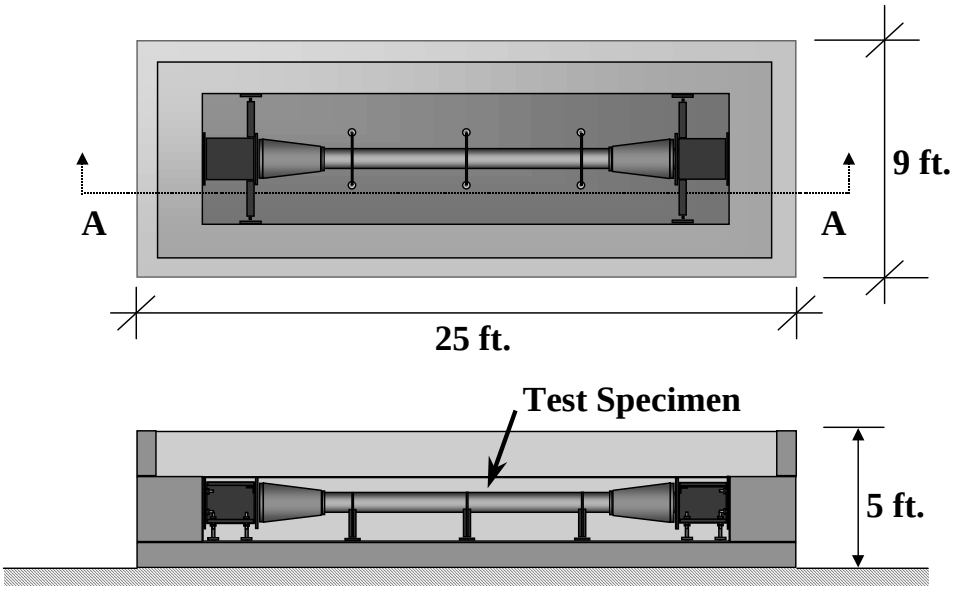

Section A-A

Figure 3.3 Blast containment tank

mismatch in the fibers the effectiveness of their combined action has always been questioned. Two separate hybrid specimens will be tested in this program under static monotonic load to failure in an attempt to approach this question as a basis for future work.

3.2.1. SPECIMEN DESCRIPTION

This program was based mainly on fiberglass specimens. However, two identical hybrid specimens were also tested. These specimens are the initial stages for a follow-up study, and their descriptions and results will be presented here.

3.2.1.1. FIBERGLASS SPECIMENS

As stated at the beginning of this chapter, the specimens were built to meet the guidelines of RTP-1 committee for tanks. The construction was made of a series of mat layers for the corrosion barrier and a structural glass fiber continuous winding in the outer shell. Figure 3.5 presents a description of the cross section for the non-hybrid elements.

The figure presents the construction sequence for the specimen. First, a C-veil

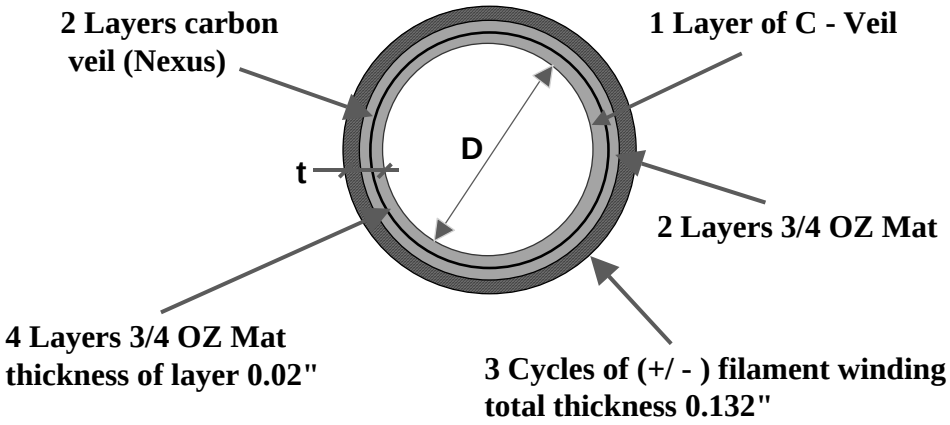

Figure 3.5 Cross section of internal pressure specimen

was placed as the first layer, followed by three layers of chopped glass mat layers. Typically, there would be no interruption of the mat layer all the way up to the continuous winding. However, in this case a leak detection system was implemented in the test program. Because of the leak system, an electrically sensitive layer was necessary between the mat layers. This layer consisted of a nexus carbon veil of very low stiffness. The layer is wound integral with the pipe of a thickness of no more than 0.04 inches. After the nexus layer, the remainder mat layers are placed for a total thickness of the corrosion barrier of 0.18 inches. The fiber angle in the winding portion of the specimen was measured at 60 degrees from the longitudinal axis of the pipe.

Typical nomenclature of fiber manufactures refers to the process in which the winding machine moves up and down the spinning mandrel as a "cycle". The angles in the winding are therefore laid out as the winder moves in one direction and the other. For example the trip down the mandrel would be considered positive angle and the return the negative. A difficulty arises when truing to analyze this type of components. During the construction of the pipe there are no assurances that the cycle will lay out a complete ply since gaps may be left between bands of fiber. These gaps are then covered when the return part of the cycle passes through the same area. At this point the only things to do is to estimate the volume content for the total thickness of the winding and assume that the distribution is symmetrical between the angles. For this specimen three cycles were part of the continuous winding layer for a total thickness of 0.132 inches. This makes the total theoretical thickness of the specimens of 0.312 inches. The materials used for the specimens were Hetron 922 vinylester resin with the glass reinforcement provided by Vetrotrex Certainteed type E.

In the preceding specimen description, a reference was made to a leak detection layer wound integral with the specimen. This leak detection layer based on a system developed by Anderson Consulting developed for detecting in-service deterioration of the corrosion protection barrier. The name for this system is Corrosion Resistance Barrier Deterioration and Damage Detection ($CRBD^3$). It works by providing a conductive layer to the wall of the vessel. This layer is then connected to an electrical

circuit that has separate contacts to both ends of the layer and contacts to the fluid inside the vessel. When the protection barrier is cracked and fluid reaches the sensitive layer, a circuit is closed and a reading is detected in the monitoring equipment.

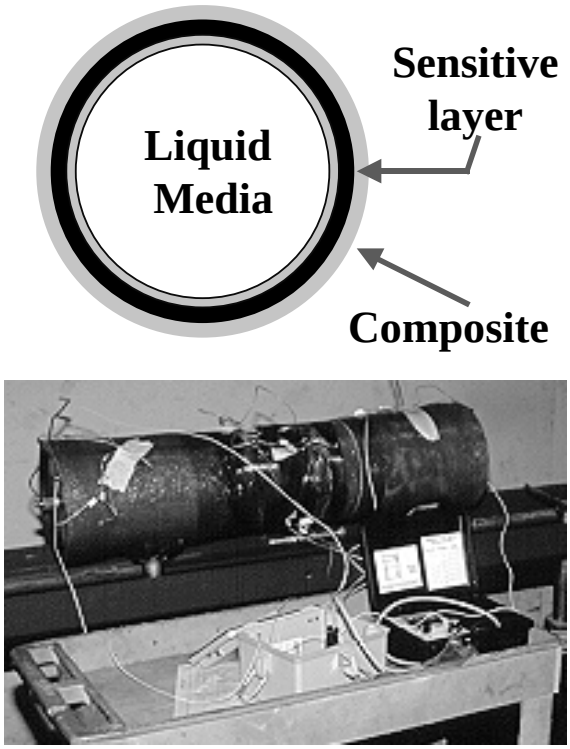

Figure 3.6 Leak detection system

Figure 3.6 shows a schematic representation of the system and the implementation as used in this experimental program. There are a number of advantages to a system like this one for monitoring the behavior of a layered material. It allows for the monitoring of the condition of the layers through the thickness of the specimen, as the specimen is being tested or loaded. This is something not accomplished by any other technique, since most do not allow for a through thickness inspection and those that do require for an active monitoring after the damage has occurred. To be able to determine the load at which the damage takes place would require the constant load stopping and active monitoring of the specimen. This makes the process too long and involved, whereas this system is a passive monitoring that does not require any special loading sequence, and after the contacts to the layers are made, no access to the specimen is necessary. Like any other system this one also has certain disadvantages. The first one being that it requires coordination with the manufacturing process, since the sensitive layers need to be placed integral with the structural winding. A suitable conductive material must be used, which could result in interaction problems with other

types of reinforcement. Finally, if done too often, these conductive layers could impact the material properties of the laminate. The information extracted from this system is quite basic, the barrier either is or is not compromised. The system has not been developed to a more advanced point yet. However, at this point it is its simplicity that makes it easy to use and understand.

After the specimens from the first batch were received at Ferguson Laboratory, measurements for the wall thickness at the ends of each specimen were made. In addition, the diameters were also measured at the ends. Results from the interior diameter measurements can be seen in Figure 3.7. As seen in the figure, the variations in the ID are very small and values are also very consistent. There is a general trend towards a smaller diameter specimen starting with TP-1 and all the way to TP-8.

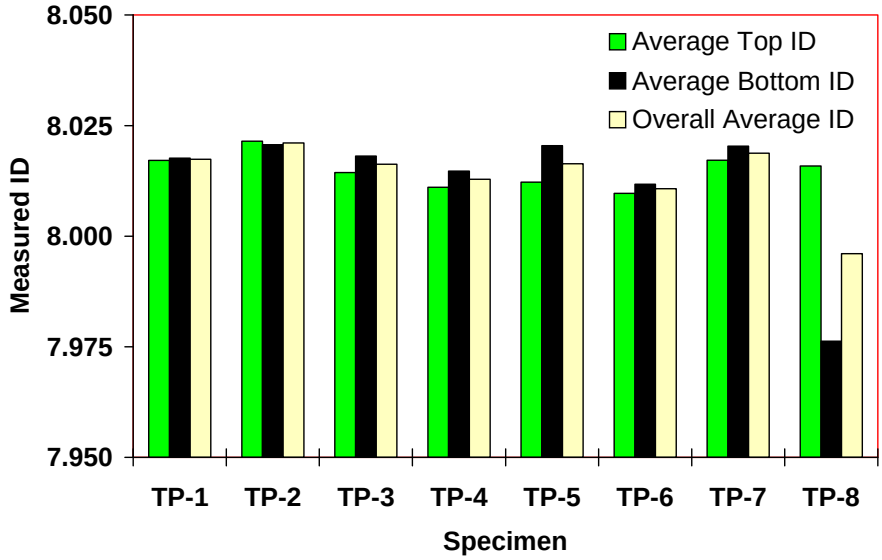

Figure 3.7 Internal diameter measurements first batch

Remembering the way these specimens were manufactured and the requirements for removal of the inside mandrel this variation is expected. The figure presents the average of four measurements at each end of the specimen and the average of both. The large variation noted in specimen TP-8 is the result of this being wound on the last part of the

mandrel. This is the end that is pulled to remove the specimen from the winding mandrel. This is why only one of the ends is off the average of the diameters.

Figure 3.8 shows the measurements at both ends for each of the specimens for wall thickness. The measurements were made with calipers in four separate locations and averaged. This is the only batch where this was possible since the proceeding ones had an end reinforcement integral at the time they were manufactured at the plant. For the next specimens, TP-9 and on only isolated sampling was performed since measurements could not be done until after the specimen was tested. After testing some of the specimens from each batch were cut in half and thickness measurements made at the middle of the pipe. Due to the nature and localized forming of failure modes, it was not expected that large changes in thickness took place during testing. Unfortunately, a

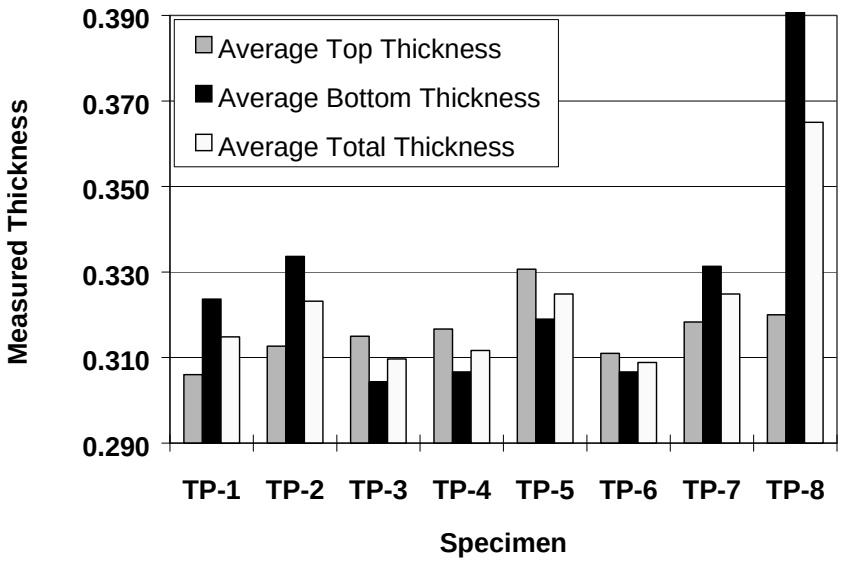

Figure 3.8 Wall thickness measurements first batch

more complete sampling of the specimens was not possible, therefore possible changes in thickness will have to be kept in mind during the interpretation of the results.

As observed on the figure, variations in the thickness are larger that for the internal diameters in the same specimen. The variations were noted more in the inner

liner layers that in the fiber winding. This is easily explained by looking at the construction methods for each of the layers in the specimen. The inner layers are made of chopped strand mats, these are typically placed by hand and therefore more prone to variations due to human error. The wound layers are computer controlled in most cases, and were for these specimens, and therefore less likely to show variations in thickness. This is not to say that there will not be any variation, since there is still a component of randomness in the way the layers will fit with each other. However, this variation will be in a small

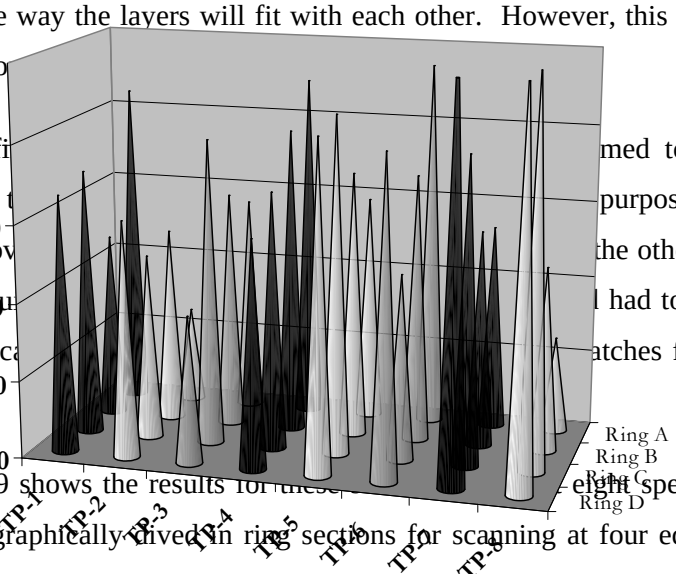

For the fi med to sample the variations in wall t purposes alone, this ultrasonic test prov he other specimens. The ultrasonic equ had to be returned. This is why the sca atches from the pipe manufacturer.

Figure 3.9 shows the results for these eight specimens. The specimens were graphically divided in ring sections for scanning at four equally spaced locations. Three readings were taken on each ring at equal spaces in the perimeter, these then were averaged to form the ring reading.

Figure 3.9 Results from the UT scan of first batch of specimens

From the scanning is apparent that there is a large variation of thickness within the diameter and length of the pipe. Even though the values predicted by the UT scan may be not exact due to the nature of composites, the relative variations are obvious. This was later confirmed by sectioning the specimen TP-8 after testing. Sections of the specimens were cut at every six inches and measurements were made only in the areas where no failure surface was noticed or formed. The measurements showed that a large part of the deviation was due to changes in the inner layer thickness and not in the winding.

3.2.1.2. HYBRID SPECIMENS

The structural profile of these specimens was made of two parts. The first part was exactly the same as the fiberglass specimens used in this program. The second part was the addition of a final winding layer with carbon fibers. Grafil Inc. provided the fibers used in the final winding of the hybrid specimens. They were aerospace carbon fibers with structural properties very similar to AS-4D fibers. The resin used for the hybrid specimens was the same as the fiberglass components. The thickness of the carbon winding was designated as a "one-cycle" thickness. It was the intention to provide with the carbon fibers a layer equivalent in stiffness to all the glass fibers layers in the fiberglass specimens. Based on the properties of the constituent components and the predetermined percentage of fiber in the composite, a single cycle of carbon fibers was roughly equivalent to 3 cycles of fiberglass composite. Because of the limitation of having a single pass in each direction, special care was taken in not allowing gaps in the band of fiber in each direction. This slowed the winding process considerably, but the final product showed no signs of banding as highlighted by gaps in the fibers. The final thickness for the carbon layer was designed to be 0.025" (+/- 0.005). The same mandrel as for the fiberglass specimens was used in the hybrid fabrication. Therefore, the internal diameter remained the same as the fiberglass specimens.

3.2.2. SPECIMEN PREPARATION AND SETUP

The dimensions for the specimens were eight inches average inside diameter; the end to end length was between four feet six inches and five feet two inches. The specimens were fabricated in three separate batches from two different plants. All of the specimens were fabricated by winding a 40-foot long pipe and cutting to specimen length after removal from the mandrel. The specifications for the specimens were the same and the raw materials used were also the same.

Before program testing began, it was necessary to consider the requirements for the end conditions of the specimens. Composite materials are highly sensitive to stress concentrations and boundary conditions. This is also true for internal pressure specimens [3.9]. The use of pipe specimens has become quite regular in composite materials because the edge conditions are eliminated. However, the end conditions of an

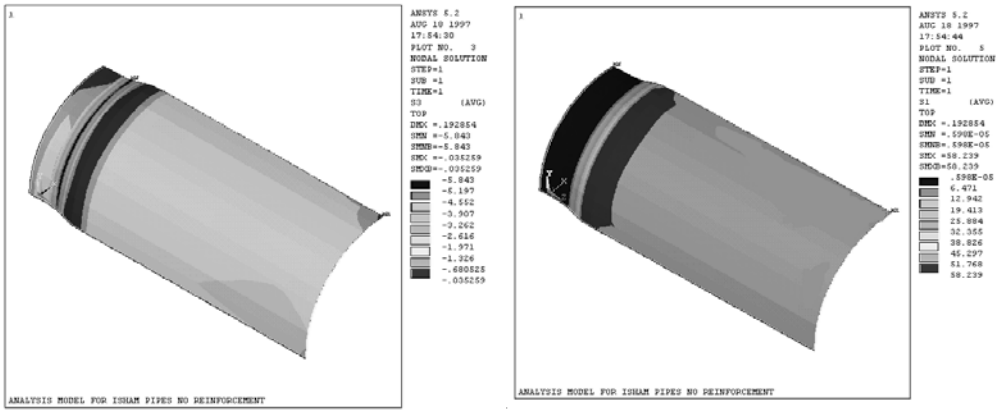

Figure 3.10 Finite element results for non-reinforced pipes

internally pressurized specimen generate a stress concentration that if not dealt with could force a failure zone in an area where the stresses and strains are difficult to predict. Figure 3.10 show the finite element results of the analysis of an non-reinforced specimen subjected to internal pressure. Because of the location of seal plates at the ends of the specimen, a stress concentration is generated at the point where there is no internal pressure applied.

The figure presents the results of an analysis made to an applied unit pressure level (1 ksi). Looking at the two main principal stresses from a three dimensional analysis, we see that a concentration is generated at the location of the seal plate. Even when the seal system is designed to allow for axial movement, axial stresses are generated as the result of bending at the seal location. Shear stresses are also generated at the location of the seal in the two main directions for the pipe. This increases the non-linear behavior of the material even more, concentrating this behavior at the seal

vicinity. These conditions would make interpretation of analysis results extremely difficult since at stress concentration regions the state of stress is very complicated.

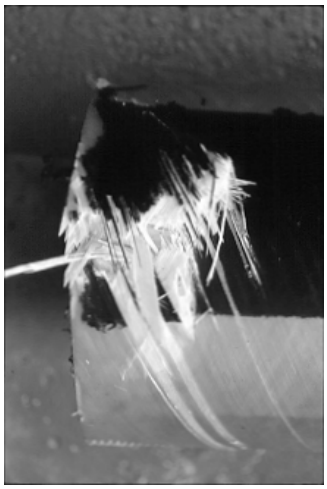

Figure 3.11 Failed surface of pipe

A test on a fiberglass specimen, that did not have the ends specially reinforced to control stress concentrations caused by the seal plates, was performed to verify the result obtained from the finite element model. The specimen tested was a ½ inches thick and four feet six inches long. Figure 3.11 show the failed specimen after burst. The failure was sudden with no previous indication except of the immediate ones. The energy released in the failure was enough to completely separate the specimen from the test fixture and flip it for a 180-degree turn. An important note to make is that later similar specimens showed a mode of failure dominated by leakage and almost no fiber breakage. Therefore confirming that the effect of the seal plate was a noticeable increase in the stress profile. This test highlighted the need for a reinforcement profile in order to move the failure surface from the boundary or seal location to the intended test gage. In order to simplify the interpretation of test results it is necessary to move the failure zone to an area where the stress and strain profile are known and controllable. Swanson and others [3.9] have had success moving this failure plane by using a tapered buildup at the end of small-scale specimens. This buildup was made by the use of an epoxy casting with no other reinforcement. In large-scale testing, this type of reinforcement is inadequate for reasons of strength and deformation.

For large-scale systems, is necessary to use a stronger reinforcement scheme, there are several options that can be explored for this purpose. The use of a metal reinforcement is attractive for the isotropy of the material and the simplicity of calculating its effects with respect to the specimen. Unfortunately, the side effect to a metal reinforcement is ensuring contact and effectiveness during testing. Non formed

exterior surfaces, like the one on a fiber glass pipe, show a number of irregularities that would be very difficult to match with a machined surface. If the possibility of machining the exterior of the specimen is not acceptable then the use of metal reinforcement is non-practical. Even when machining is possible, if several specimens will be tested in a short amount of time, this type of preparation would increase the cost and time associated with the testing considerably.

Another possibility is the use of additional layers of fiber and epoxy reinforcement on top of the designed specimen. This solves some of the problems indicated for the metal buildup, however it has some limitations of its own. The first limitation is the required coordination during fabrication if this is to be done at the time of manufacturing. This may increase the price of the specimens considerably. This is important in large scale testing of composites, since manufacturing facilities are not small or simple. An alternate option is to reinforce the specimen after it has been manufactured. When using this scheme, the question to answer is how sensitive is the design to the fabrication tolerances. Winding of individual specimens could be an intensive hand labor task, even when in some cases an automatic winding machine may be used. Deciding how important manufacturing tolerances are to the design of the reinforcement is critical in the manufacturing costs of the reinforcement, or in the possibility of performing the reinforcement in house. In simple internal pressure specimens, the function of this reinforcement is to gradually increase the stiffness and provide additional strength at the ends. The additional strength required is not as important as the stiffness needs for the seal tolerance. In the case of internal pressure specimens, a hoop only winding will provide the necessary reinforcement. As the loading conditions change a more elaborate fiber pattern may be required, however this can be verified by the use of a finite element model.

The initial specimens as received from the manufacturer did not have any special end reinforcement. A finite element model was analyzed with different end reinforcement schemes to evaluate their effect on the stress profiles. The final profile and results of the selected reinforcement profile are shown in Figure 3.12. The results shown in the right of the figure are the VonMisses stresses.

It is very difficult to model in detail all the conditions in the tapered profile like this one. Even when the taper comes to an almost zero thickness in the finite element model, this is difficult to represent in a preliminary model. Moreover, the percentage of fiber content in the reinforcement will change as the taper reduces to zero. All of this will produce an error in the estimation of the stress values. However, with an adequate model, these will be small and can be ignored. The final profile dimensions are shown in the Figure 3.13 along with the implementation in the plant. As noted, the placement of the end reinforcement was a manual operation. This resulted in considerable variation of dimensions from the specified values. This, however, did not prove to be critical as

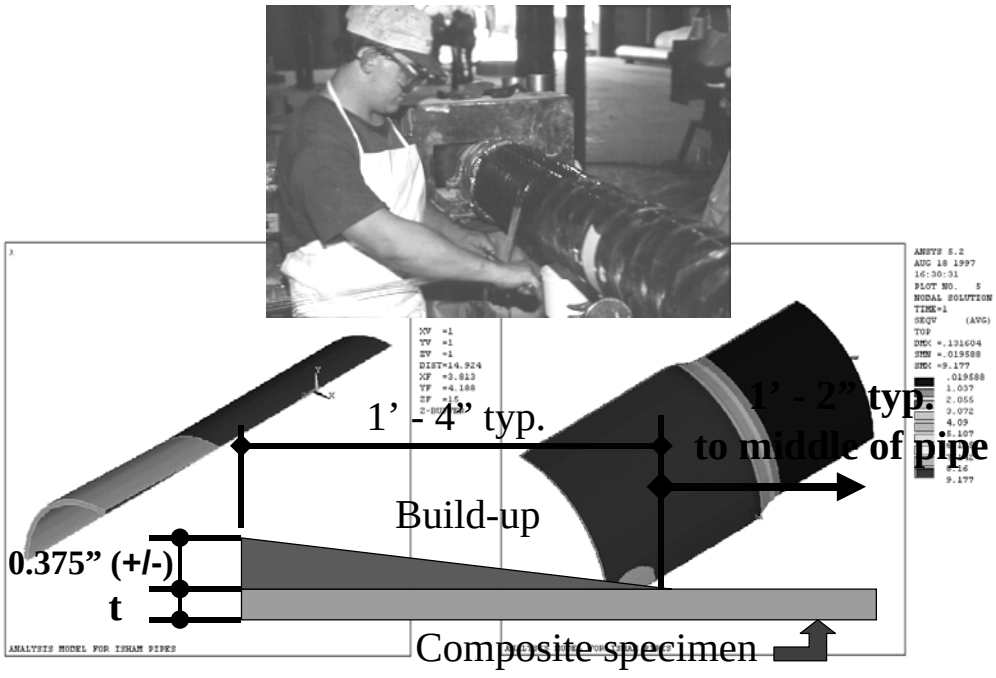

Figure 3.13 End reinforcement profile and implementation

the results will show later in this chapter. The implications are that, as long as a gradual change in stiffness is ensured, the behavior is not overly sensitive to the actual dimensions of the reinforcement as long as they are more than the minimum specified.

The next step in the program was the design and detailing of the sealing system. The system was designed to allow for axial movement of the specimen as result of the applied pressure. The selection of the seal profiles is critical for the proper sealing of a piston type application like the one in this program. The definition of piston application refers to the use of the seal in the setup. The internal sealing plate as designed will act in a similar way to a piston inside the composite pipe. It will move up and down the interior wall while keeping a seal.

The options for sealing, as stated in the introduction chapter, are either an o-ring profile or a chevron type seal. For this application, since the interior walls are expected to grow away from the seal plate as result of the applied pressure, the chevron profile is

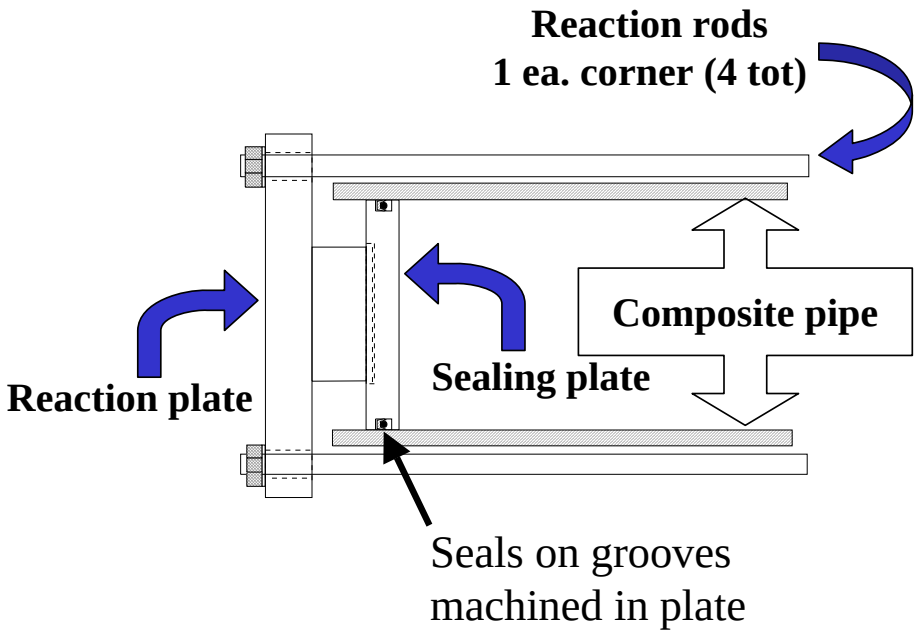

Figure 3.14 Seal system internal pressure tests

selected. Figure 3.14 shows a schematic representation of the seal system implemented for these tests.

After the seal system was designed, the next step was to verify the tolerances between seals and pipe wall. There are no general guidelines for tolerances in seal design. Each seal profile has different and very specific dimensional tolerances. The manufacturers will provide these tolerances as they apply to each one of their seal dimensions and profiles. The difficulty arises when these tolerances have to be applied to a composite filament wound specimen. As indicated in the introductory chapter, there are certain requirements for the surface roughness to ensure a good seal. Typically this roughness will be met by the interior surface of a fiber wound pipe. However, in some cases modifications must be made to either meet the dimensional tolerances or roughness requirements.

In this test program, the most common adjustment needed was for the difference in diameters from end to end of the pipe. When building a composite pipe by winding fibers over a mandrel, the mandrel is tapered to facilitate pipe removal by sliding the mandrel out. This taper can be large enough to affect the tolerance requirements of the seals. In addition, if the specimens are inventory specimens from a manufacturer, the diameters will be different from specimen to specimen, and end to end. The solution used in this program was machining the inside walls of the pipes with a carbide bore. Figure 3.15 shows the required machine for the preparation of the inside diameter of the specimens. The only modification necessary was the addition of an elbow attachment and the carbide bore (both not shown). When done properly, this solution proved

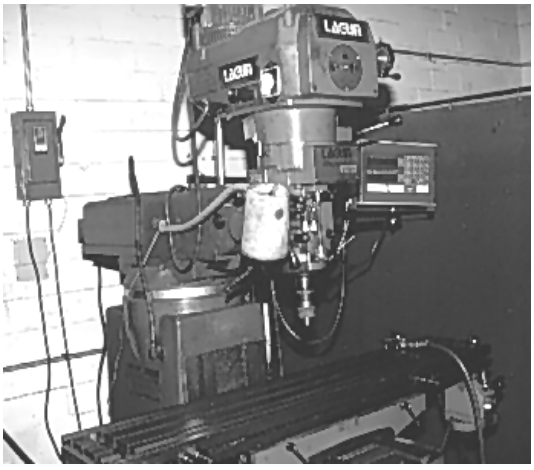

Figure 3.15 Machine for ID polishing

adequate and, it simplified the seal system allowing for the fabrication and design of a single set of seal plates for all the specimens.

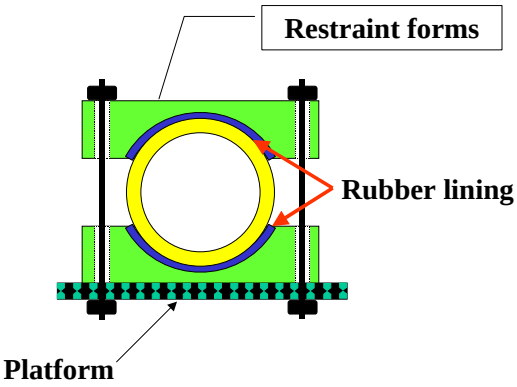

Figure 3.16 Pipe support setup

One precaution that must be followed when machining specimens like these is their tendency to ovalize when placed on the machine platform. If using a flat surface to apply pressure between the surface and the platform, the specimen will deform to conform to the flat surfaces. If the system ovalizes extensible after the bore machines a perfect round surface, it will be oval when released. The system used for these specimens was the use of circular rubber lined supports, as shown in Figure 3.16. A top and bottom form are placed around the specimen and tightened together. These forms are also secured to the platform by means of bolts. The rubber lining is to ensure that the specimen will not rotate as the bore passes through the inside diameter. The lining also allows for securing of the specimen without the use of excessive pressure, and it will adjust for any surface irregularity in the external diameter. The tolerances achieved on the machined ID of the specimens in this program with this technique were consistently of 0.002 inches or better.

Ferguson Laboratory at the University of Texas did not have facilities for the pressure testing of pipe specimens. A test facility was designed and built for this program (Fig 3.3). In addition an air driven water pressurization system was developed for testing to pressures up to 30,000 psi. Figure 3.17 presents a picture of the overall setup for tests performed in this tank.

Figure 3.17 Internal pressure tests setup

The specimen is fitted inside the containment tank, and for tests where high pressures were expected, the tank is filled with water to contain debris in case of an explosion. A rotating mirror was fitted on top of the tank, so that the specimen would be in sight during the entire test without endangering the researcher.

The long walls at the concrete containment tank are post-tensioned in order to minimize cracking due to applied stresses during test or creep and shrinkage. The short walls are designed to act as a support for end reactions from the specimen inside if necessary, in addition to an overpressure wave equivalent to $^{2}/_{3}$ lbs of TNT. Figure 3.18 is a picture of a specimen in the tank ready for test.

For the cyclic tests where no burst was expected the setup was a hydraulic oil closed loop system. This system is capable of faster loading rates than the air driven water pump. The fluid used for pressurization in this setup was low viscosity hydraulic oil. Specimens tested in this system will be indicated in the results section, however, general characteristics of the testing were as follows:

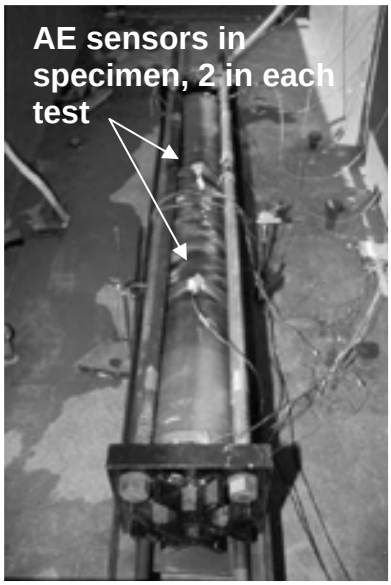

Figure 3.18 Pipe in tank

- Maximum loading rate was 2Hz
- Maximum test oil temperature was 110^{o} F for all specimens except TP-11 and TP-7 whose oil temperatures during testing was 125^{o} F
- All specimens were allowed to cool before the static AE tests were performed

Instrumentation for all of the tests consisted of a pair of delta profile strain rosettes located at opposite ends in the middle gage of the pipe. In addition to the strain gages, pressure was recorded by the use of a SC-200 data acquisition unit manufactured by Sensotec Inc. This unit was connected to a pressure transducer and was able of refresh rates every one mili-second. In addition, it was capable of recording the maximum pressure from all channels at the same rate. As indicated before in the specimen description the leak detector was implemented during the test. Finally, acoustic emission sensors were used for all the tests. The sensors were place on the test gage as defined by the ends of the buildups. The sensors were placed in the same side of the pipe and at equal distances from the center. Only the emissions from the test gage are of interest, so any emission from the ends can be identified with this sensor placement and therefore eliminated. Figure 3.18 also shows the location of the sensors for all the tests. The sensors were attached to the specimen with duct tape, and silicon vacuum grease was applied between the sensor plate and specimen surface.

The loading profile for tests performed in this setup were monotonic to failure, as defined by leakage or burst. Because of the AE monitoring, a series of downloads were performed during the test, but no more than three downloads were made in any non-cyclic test. The profile followed for the cyclic tests is show in Figure 3.19. The

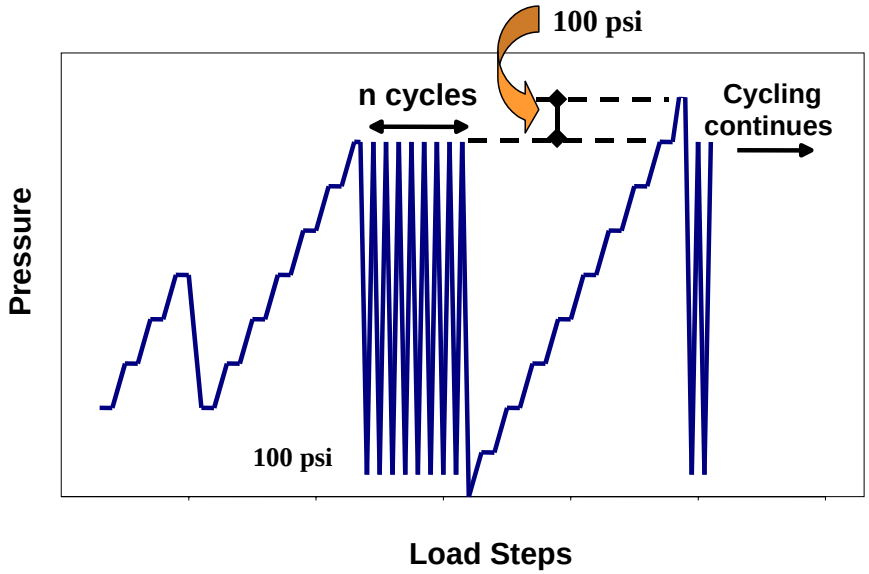

Figure 3.19 Load profile for cyclic tests

initial load was up to the target pressure. After that, the cycles started between 100 psi and the target pressure. The AE monitoring made during the cycling phase were done by monotonically loading the specimens to a level 100-psi higher than the target pressure. The objective of the overload was to assess the amount of damage accumulation at the target pressure. The purpose of overloading was to study the relation of a variant to the felicity effect to a previous service load and a load beyond that service level. The hardware used of the AE data acquisition consisted on an old version of the Transportation Instrument by PAC. The settings on the instruments were of 24dB gain at the instrument, antialiasing banpass filters for 100 and 300 kHz. Hit definition time is set at 400 μsecs.

3.3. TEST RESULTS

In this section the results for the fiberglass and hybrid specimens will be presented. Results from both the strain gage measurements and acoustic emission monitoring are shown. Strain rosettes in a delta pattern were used in the monitoring.

The angle between the rosette gages was 120^{o}-degrees as is typical on this pattern. The location of the rosettes was at the middle of the specimen and diametrically opposite to each other. In a few of the specimens, a 45^{o}-degree rosette was used and those will be flagged as such in the presentation of the results. In all of the specimens one of the gages in the rosette was aligned to the longitudinal axis of the specimen. This will be referred to as the axial gage. Figure 3.20 shows a schematic of the profile of the rosettes used and the designation given to each one of the gages in the plots.

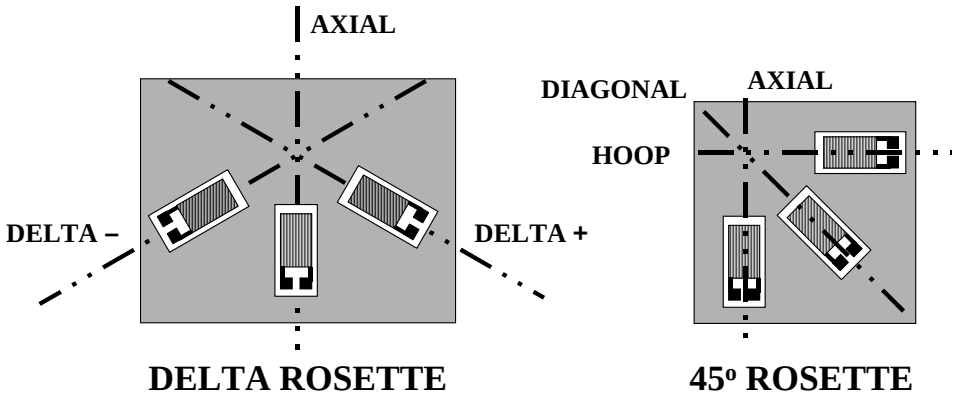

Figure 3.20 Gage direction labeling

All rosettes used were 120 Ohm, manufactured by Measurements Group Inc. The bonding agent used was AE-10 epoxy also by Measurements Group Inc. In some of the tests there were gage failures and in some cases the gages failed between cycles. In these cases, only the surviving gages in a complete rosette were used in the analysis of strains. The rosettes with an incomplete set of gages were not used unless no other option was available. In the cases where a complete set on a rosette was not available in a specimen, the information available from the remaining gages was combined. This introduces a slight error in the estimation of the principal strains, since the alignment of the gages was not exact. Even though the errors were minimal, these cases will be flagged in the presentation and analysis of the results. However, in all the specimens the axial strains were measured with surviving gages.

A total of 22 tests were performed on fiberglass reinforced specimens and two on the hybrid variant. Figure 3.21 shows a summary of the tests for the fiberglass specimens alone. The results of the hybrid tests will be presented later in this chapter.

In Figure 3.21, two elements of information are shown. The first is the test pressure for each specimen shown in the front bar with the values on the top of each bar. The second is the number of cycles it went through before leakage was recorded, shown in the back bar with the logarithmic vertical axis on the left. The final leakage cycle is included in the count. Therefore, for the static specimens, the pressure shown is the maximum pressure at leakage. For the cycled specimens, pressure shown is the target pressure during the cycling test as show in Figure 3.19. The order of the test as shown in Figure 3.21 is set with the static tests first starting from the right of the figure and moving left with decreasing test pressure. Specimens in the cyclic phase were tested at 2100, 1800, 1600, 1400 and 1200-psi. Therefore, after the static tests, the next group is specimens cycled at 2100-psi, followed by 1800-psi, and so on.

As previously indicated, all cyclic tests were performed with the pressure varied from 100 psi to the target pressure. During the cyclic tests, two differences exist in some of the tests. The cyclic tests for the target pressures of 2100-psi and 1600-psi were performed with the air-driven high-pressure water system. All the remaining cyclic tests were performed with a hydraulic oil closed loop system. The difference was the rate at which the specimens could be tested. With the water based system the load rate was 1 cycle every 40 seconds. In contrast the rate with the closed loop system was 2 Hz for all tests at or lower than 1600-psi and 1 Hz for tests at 1800-psi. A transition specimen was tested at 1600-psi to determine if the change of rate would have an effect on the results.

A common factor in the behavior of all fiberglass specimens was the failure mechanism and appearance. All fiberglass specimens failed by leakage at a load hold as required by the AE. As soon as the internal liner cracked, water forced its way through the layers of the fiber winding and found its way to the surface. On the inside surface of the specimens, a single longitudinal crack was visible immediately under the failure surface of the specimen. No other signs of damage were visible on the inside surface. On the exterior surface of the specimen the difference was the extent of delamination observed for each test. Even when the mechanism was the same in all the tests, the observed extent of the delamination changed. Figure 3.22 shows a set of images that represent a typical failure surface and cross section for the fiberglass specimens.

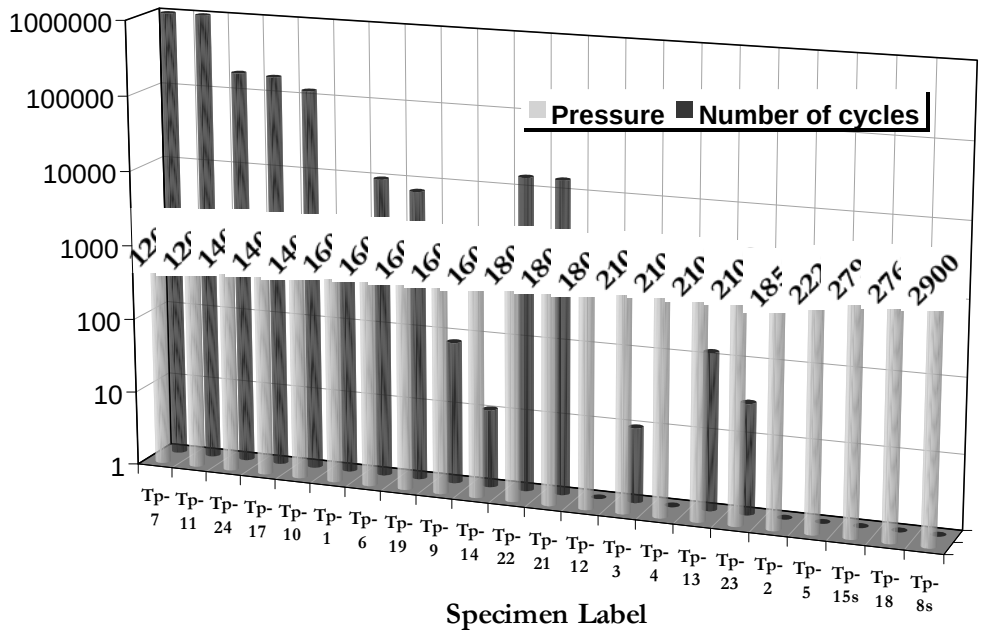

Figure 3.21 Summary of fiberglass test results

The images come from the same specimen, the cross section shown in the smaller image came from sectioning the specimen in a band saw. The cut was made through the failure surface of the specimen. The cutting process produced no additional damage in the surrounding area to the section. As seen, a single crack crosses the inner mat, or corrosion barrier layers. Once the crack reaches the interface between the

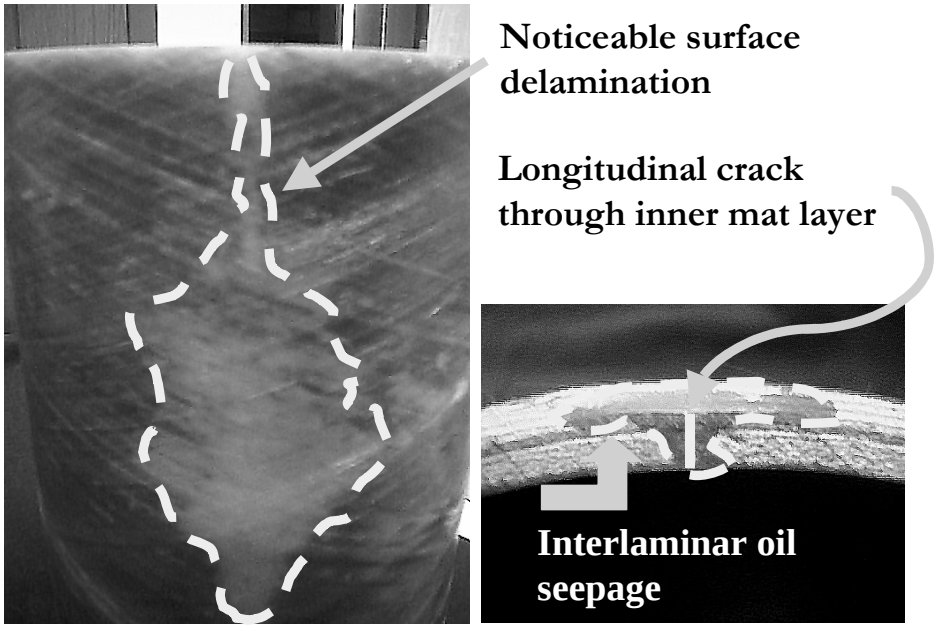

Figure 3.22 Failure surface details for fiberglass pipes

corrosion barrier and the beginning of the continuous winding, the crack progresses in the perimeter of the specimen at that point. In addition, liquid continued to seep in the radial direction through the winding layers to the surface. The figure shows the area of influence of the seeping liquid in its path to the outside. This area varied with each specimen and with the level of pressure applied at the time of failure.

To verify the extent of this delamination within the area of influence, an additional section was cut in some of the specimens. This section came from the damaged portions of the specimen. For verification purposes, an alternate cut was performed in the same specimen but in a non-delaminated section after the test. This alternate cut did not show any signs of damage or separation between the layers. Some cracking was observed in the matrix at the winding surface, however, the layers maintained their integrity. Figure 3.23 show an image of the sections obtained from the failed surface.

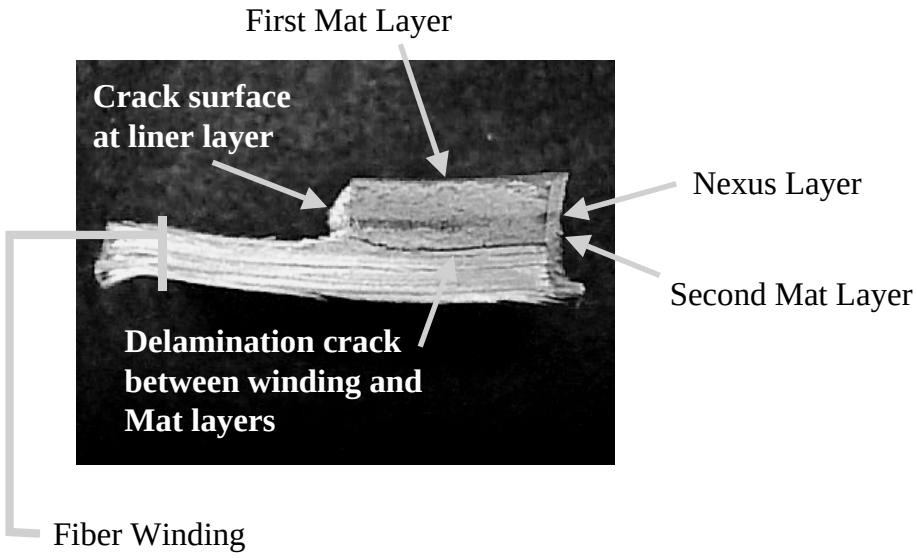

Figure 3.23 Failure surface section

It is clear that the radial crack observed in the inner layers did not propagate in to the outer fiber wound portion of the specimen. Rather, delamination was the most apparent form of damage in the outer filament would layers. A combination of transverse matrix cracking and gaps between fibers and surrounding matrix epoxy possibly provided the path for the water to find its way to the outer surface of the specimen. It also points to the possibility that the winding alone might have leaked at a lower pressure had the inner liner not been in place.

The performance of the leak detector during all the tests in this program supports the possibility of prior winding matrix failure as indicated above. During the static and cyclic loading of the specimens, the system did not register leakage. This indicates that the inner liner did not fail until the time where the final pressure was reached. In other words, cracking of the inner layers was immediately followed by leakage of the system. Figure 3.24 show a typical plot of the performance of the leak detector in a test.

In the following sections, results strain gage and acoustic emission monitoring will be presented. The presentation of results will be grouped in the same way as presented in Figure 3.21. The results from the static tests will be presented first, followed by the cyclic tests in decreasing target pressure magnitude.

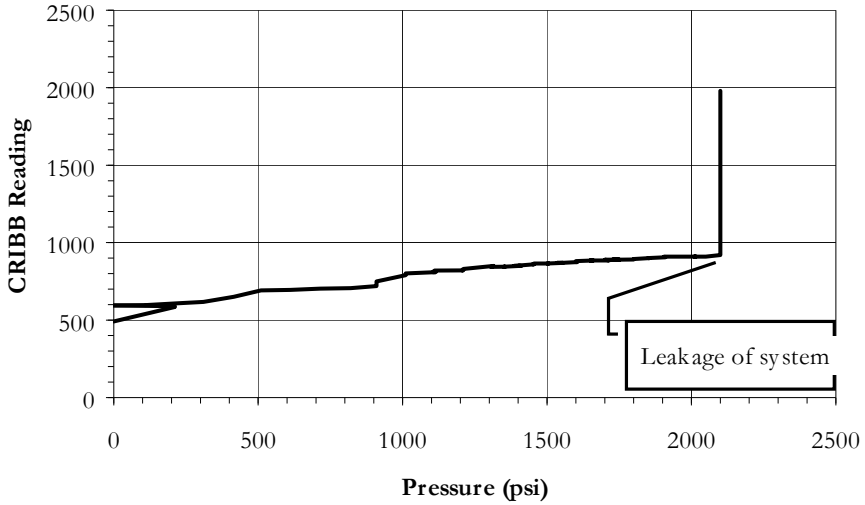

Figure 3.24 Leak detector performance

3.3.1. STRAIN GAGES RECORDS

As stated at the beginning of the chapter, some of the strain gages in the rosettes were damaged during the tests. These gages were damaged either at the beginning of a static test or after a number of cycles had been performed. Whenever possible, these will be indicated during the presentation of the results. In addition, a description of the steps taken in the adjustment of the remaining gages will also be explained.

3.3.1.1. STATIC TEST RESULTS

Of the specimens indicated in the previous summary figure, the ones tested under monotonic pressurization to leakage were Tp-2, Tp-5, Tp-15s, Tp-18, and Tp-8s. The designation "s" corresponds to "short", indicating that these specimens were shorter that the other typical length ones. The shorter length came from the way they were cut after fabrication. As previously indicated all the specimens were fabricated by winding a single large component and cutting equal length sections out of it. Typical sections were five feet long, where the specimens designated short were approximately four feet. The reason for the short length was that out of a standard 40-foot mandrel, the ends are always wasted after the winding. This reduces the usable length of the mandrel usually by about two to three feet less.

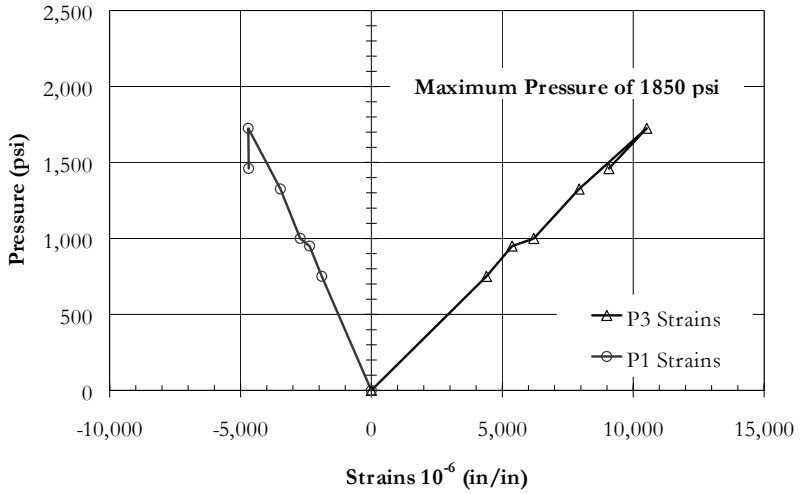

Figure 3.25 Recorded strains for TP-2

Figures 3.25 to 3.29 presents the recorded strains for the static tests performed in the static phase of this program

Designations P1 and P3 in the figures refer to principal strain directions. Direction P1 is the direction in which compressive strains are at a maximum, and P3 is the direction where tension strains are at a maximum. Therefore, the P1 strains are associated to the axial deformation of the pipe, where the P3 strains are associated with the hoop direction. P2 was skipped as a label since that is associated with the strains in the radial direction of the specimens. Even though these were not measured or calculated they are referenced to in the text and therefore included in the strain-labeling scheme. An additional benefit of the labeling is that the measured strains can be easily referenced to the finite element results without having to re-label either one of the plots.

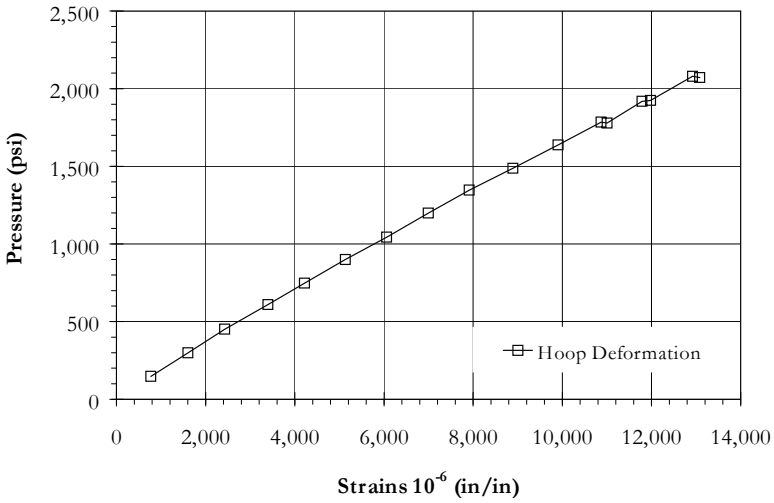

Figure 3.26 Recorded strains for TP-5

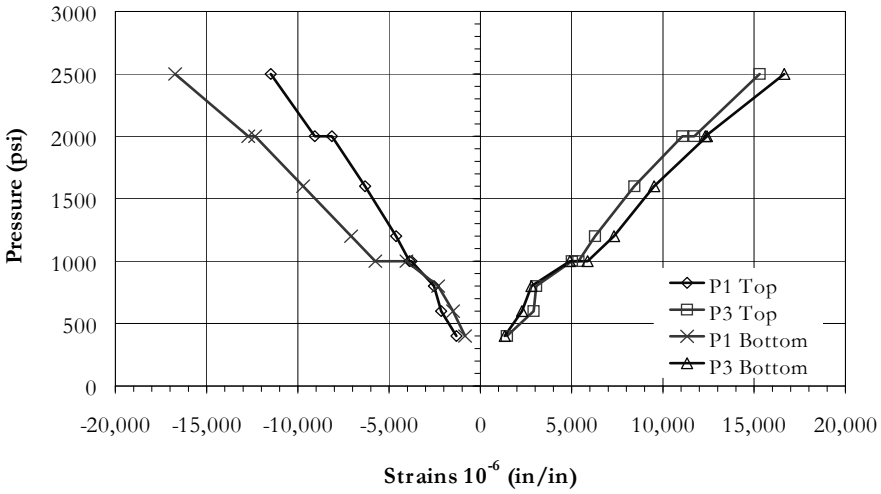

Figure 3.27 Recorded strains for TP-8

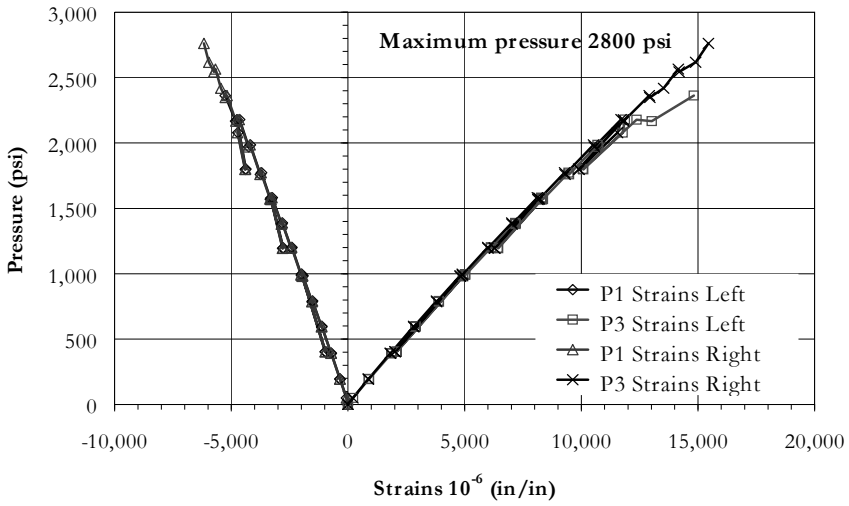

Figure 3.28 Recorded strains for TP-15

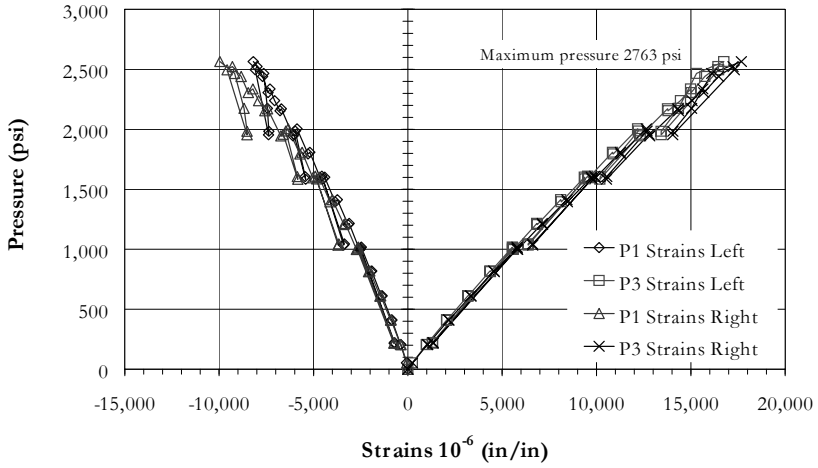

Figure 3.29 Recorded strains for TP-18

The gages for TP-5 were lost during the test leaving only one gage in a rosette available. The gages used in the specimen were the 45°-degree type. The surviving gage was aligned to the hoop direction of the specimen, which should provide a reasonable representation of the P3 strain, allowing for minor misalignment of the gage.

In all the observed strain plots an apparent non-linearity is visible in the axial or P1 strains. This is not so in the hoop or P3 strains. Except for the irregular strain records seen in TP-8, strains in the P3 direction for all the other specimens showed few signs of non-linearity. Another aspect of the behavior was the permanent deformation recorded in the specimens during the unloading as required by the AE testing. These signs of permanent deformation were clearly noticeable in all tests where unloading were part of the pressurization profile. As expected for continuous fiber composites, the stiffness in the specimen is dominated by the fibers with a very small contribution from the resin. There are no clear signs of cracking in the resin by looking at the P3 strains. The P1 strains appear to be a better indicator of damage by virtue of the change in the Poisson's ratio relationship between P3 and P1. The stiffness in the direction of the loading (hoop) did not change considerably during the loading to failure. Maximum pressures were different in all of the tests. In addition, maximum recorded strains were also different for each specimen. Nevertheless, the order of magnitude of the P3 strains was the same in all the static tests even when the final values were different when compared. The axial or P1 strains were not as similar to each other in the tests. No correlation is apparent between the tests in the P1 deformations recorded. Differences were on the order of 100% between the lowest recorded strains and the highest one.

Figure 3.30 shows the failed profiles for the specimens tested in this phase. The extent of damage at the time of leakage varied with each specimen. The short specimens

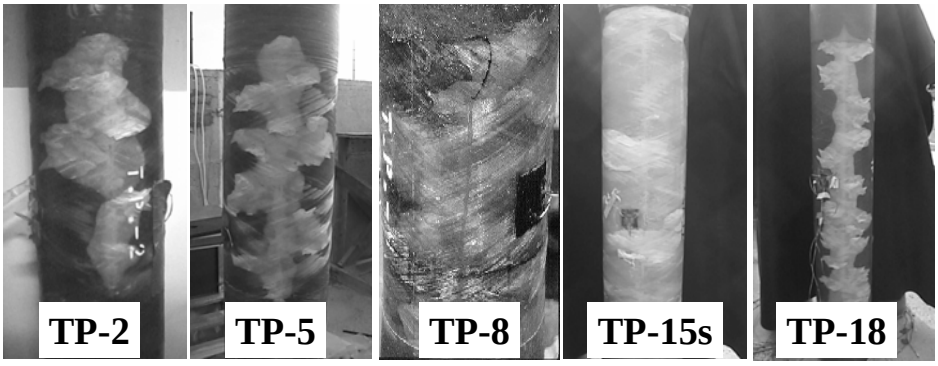

Figure 3.30 Failure zones of specimens in monotonic load phase

TP-8 and TP-15 showed the largest extent of visible change. Also, the specimen with the lowest failure pressure did have the least extensive delamination. Another interesting point is that the specimen end reinforcement seemed to work as designed since most of the failure was centered between the end buildups, within the gage section of the specimen.

3.3.1.2. CYCLIC 2100-PSI TEST RESULTS

Figures 3.31 to 3.33 show the recorded strains for specimens subjected to cyclic pressure at 2100-psi. In total, four specimens were tested at this pressure range. However, strains are only available for three of them. The specimens tested were TP-3, TP-4, TP-13, TP-23. The specimen labeled as TP-3 is the only one with no strain data.

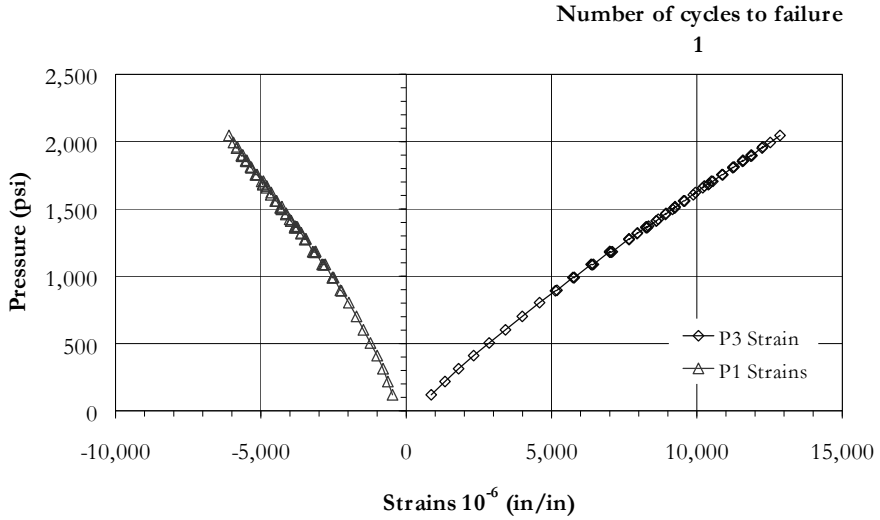

Figure 3.31 Recorded strains for TP-4

For specimen TP-4 only one strain rosette was used in the test. This rosette was placed in the middle of the gage of the specimen. Principal strains were calculated based on the readings of all three of the rosette gages. The specimen failed at the first loading to target pressure. This specimen also showed the largest recorded P3 strain at near the

target pressure. The P1 strains in contrast were not the largest recorded ones, although they were very close to this value as recorded by TP-23.

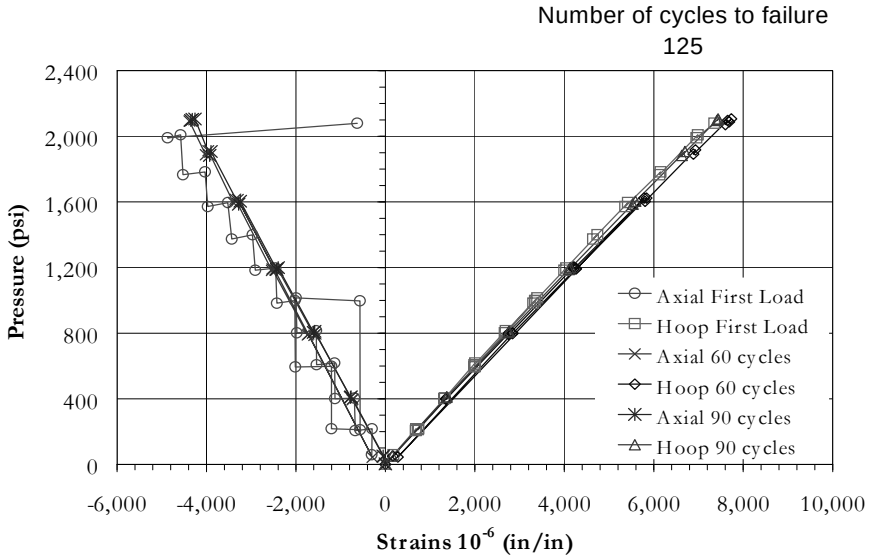

Figure 3.32 Recorded strains for TP-13

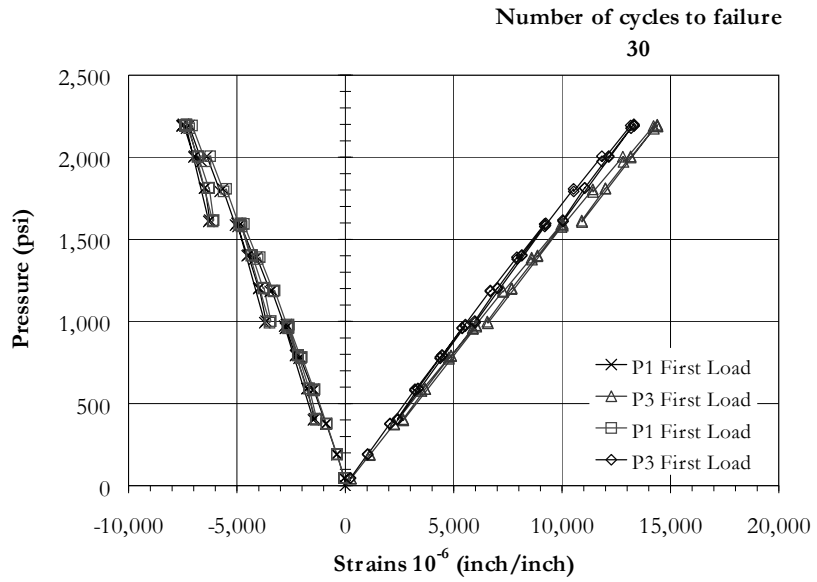

Figure 3.33 Recorded strains for TP-23

TP-13 is the only specimen where data points beyond the first cycle were recorded. The strains shown in the plot do not include probable permanent deformation accumulated during the tests since gages were zeroed between static tests. In addition, 45^{o} degree strain rosettes were used in this specimen. Of these, the diagonal gages were lost for both tests, leaving only hoop and axially oriented gages. As in other cases, perfect alignment cannot be assured. However, several interesting behavioral points can be noticed. The first one is in the axial strains recorded at the initial load versus other loads.

During the load holds, the axial gages showed signs of creep. This tendency did not repeat itself as clearly in the subsequent loading steps. The possibility of this observation being an experimental error has not been eliminated. Nevertheless, this observation will be compared against results of subsequent tests at smaller pressure amplitudes. In addition, the system used for all the tests in the data recording was the same, connections remained in place during the cycling and no modifications were made to the specimen setup between cyclic and static loading.

Figure 3.34 show a diagram representing the amount of permanent strain recorded in the specimen after the end of each static loading from the two active gages in the strain rosettes. This permanent deformation was calculated by measuring the residual strain measured at the end of the unloading stage (zero pressure) during the AE monitoring. The values for hoop strains on the second group for loading other that the initial were not possible to calculate. The hoop gage in the rosette for this group was also lost during cycling. The plotted values for the axial strain were obtained from the surviving axial gage in the rosette. The error in the values is likely small since alignment to the specimen axis has been quite accurate in most of the rosettes placed in the specimen.

An interesting trend in Figure 3.34 is how the permanent deformation at first loading was in general less than the one during the middle life of the specimen. The permanent deformation then drops between the middle life and the monitoring at 75% of

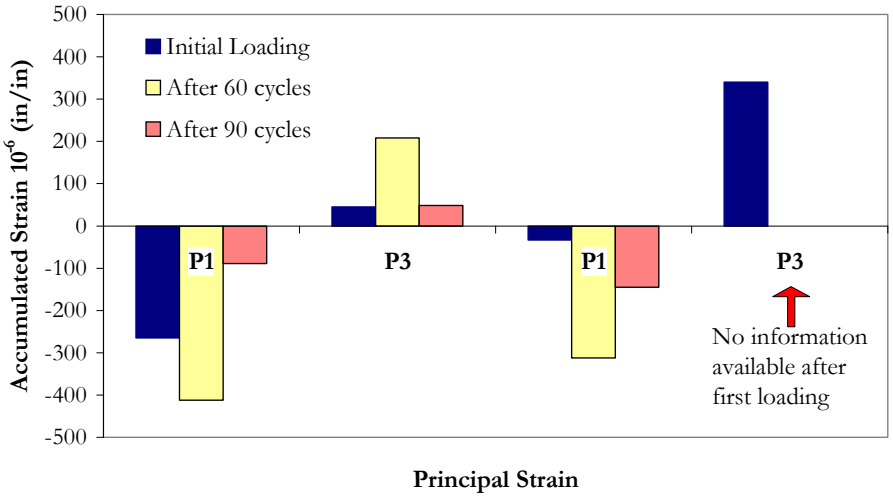

Figure 3.34 Strain recovery loss for TP-13

the life. This will be compared to results from following tests at different amplitudes. In all though, the stiffness of the specimen did not seem affected during the test to the point of leakage.

Figure 3.35 show the profiles of delaminated specimens that were part of this load phase. The smaller of the areas belongs to TP-3 with almost no difference between

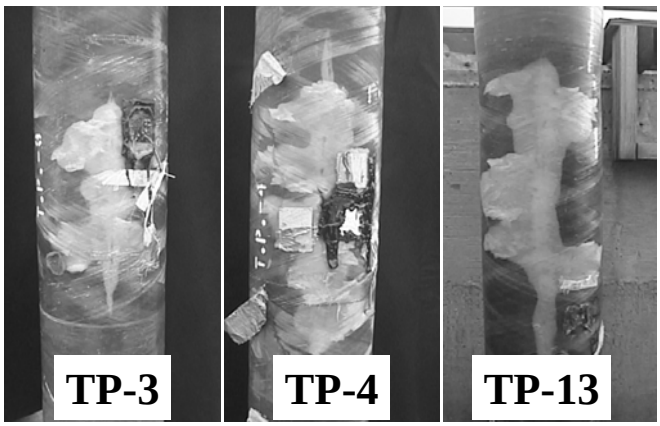

Figure 3.35 Failure surfaces for specimens in 1600-psi phase

TP-4 and TP-13. No image is available for TP-23 but the damage area was very similar to TP-3.

3.3.1.3. CYCLIC 1800-PSI TEST RESULTS

Figures 3.36 to 3.38 show the recorded strains for specimens subjected to cyclic pressure at 1800-psi. Due to the number of cycles in some of the tests, plots are separated for P1 and P3. Three specimens were tested at this pressure amplitude. The labels for the specimens were TP-12, TP-21 and TP-22. The first specimen came from a different batch than the following two specimens. Because of the number of cycles in the tests, strains were separated in the plots. Also, for comparison purposes with the trend observed in the 2100-psi specimens, accumulated strains are also plotted.

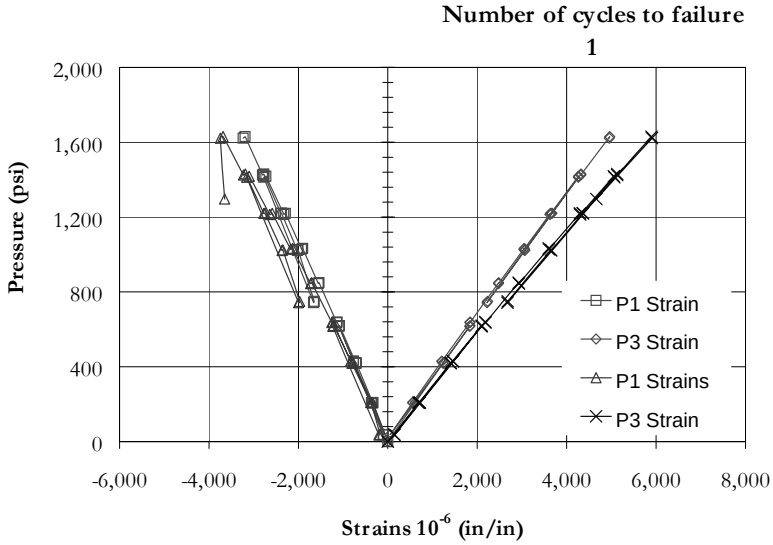

Figure 3.36 Recorded strains for TP-12

Specimen TP-12 failed in the initial load to 1800-psi without the need for cycling. All the gages were intact for this test. Therefore, the principal strains P1 and P3 are used in the plots. The maximum strains recorded for this specimen were about 0.005 for P3 and 0.003 for P1. Like other tests, there was no clear indication of stiffness

reduction. P3 strains show very little signs of changing stiffness and permanent deformation is almost not existent during unload. The P1 strains, on the other hand, show clear signs of permanent deformation after 1,400-psi in addition to a slight deviation from linear behavior. No other indications are noted in the plot as failure the pressure is nearing.

Specimen TP-21 failed after 15,000 cycles at 1,800-psi. The first obvious aspect of the behavior is the change in stiffness between the first loading and the following static loads. However, after the drop in stiffness from the first load, no apparent trend is apparent in the strains. The P1 strains do not have a clear tendency to lose stiffness as the final cycle nears. If anything, the stiffness recorded at 1/10 of the life is the largest of the ones recorded. The P3 strains on the other hand, do show a consistent tendency of reducing stiffness as the cycles increase. The lowest value for the stiffness was recorded at the final static test. Unfortunately, no other indication is apparent since the drops of stiffness were almost identical between static tests. Looking at the final plot presented in Figure 3.37, which are the permanent deformations, no clear trends are apparent. From the first load, a decreasing amount of permanent deformation is recorded at final point in the static tests after cycling. This decrease is reversed after the 5,000 cycle readings where the permanent deformation recorded takes a jump higher that the previous one. Following this jump the records drop again down to the lowest values recorded during the test. The final jump in the plot may be deceiving since this was the static step that caused failure (leakage) and the final reading in the plot was recorded after leak.

Specimen TP-22 failed after 15,000 cycles at 1,800-psi. As with the previous specimen in this section, no apparent sings of significant non-linearity are seen in the strain data. P1 strains show the most consistent behavioral tendency. From the first load, stiffness drops consistently up to the test after 7,500 cycles where the stiffness is larger than in the previous cycle tests. After this point, the specimen appears to recover some axial stiffness as the number of cycles increase. P3 strains do not show a tendency as clear as the axial strains. There is some apparent loss of stiffness as the cycles are

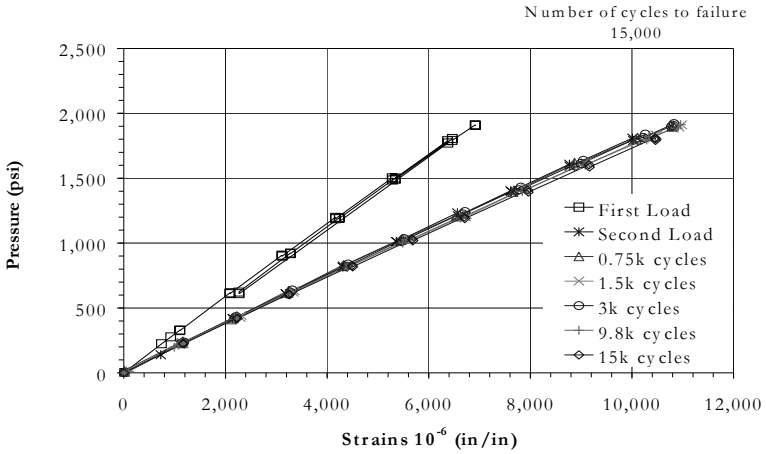

P3 Strains Plot

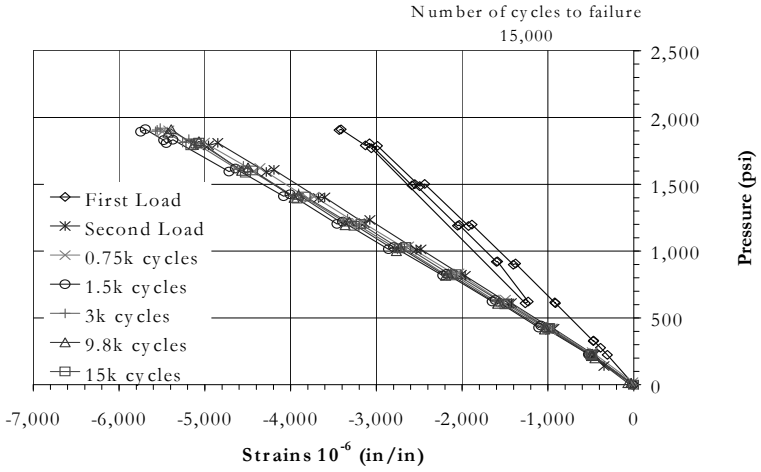

P1 Strains Plot

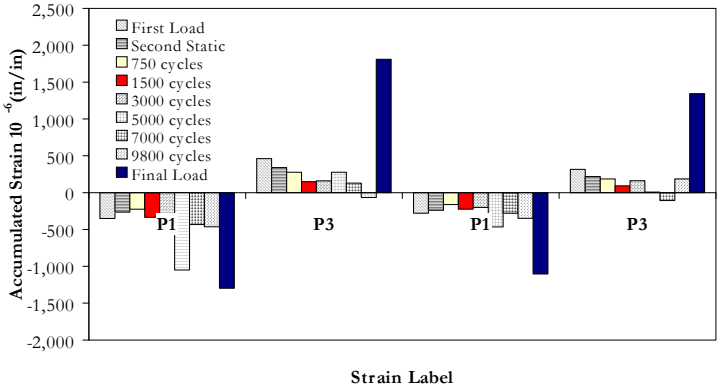

Figure 3.37 Recorded and accumulated strains for TP-21

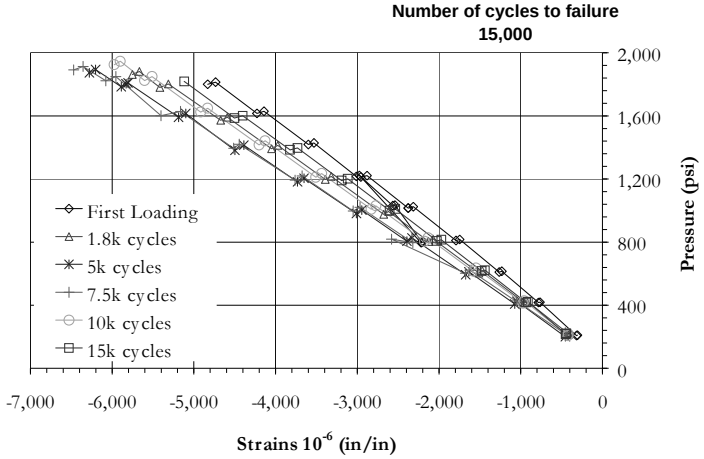

P1 Strains Plot

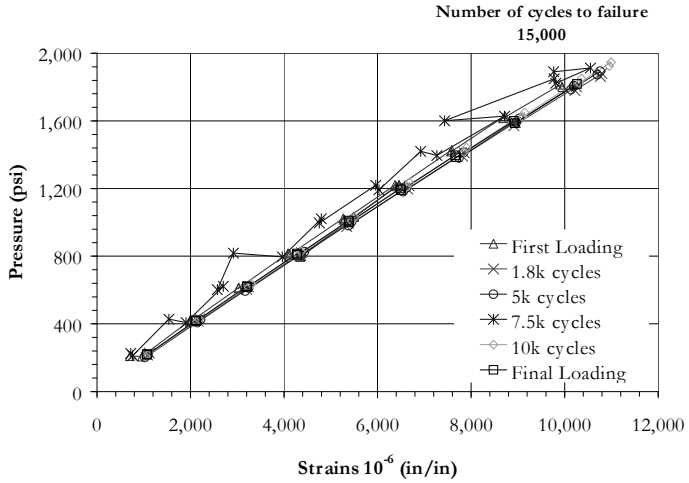

P3 Strains Plot

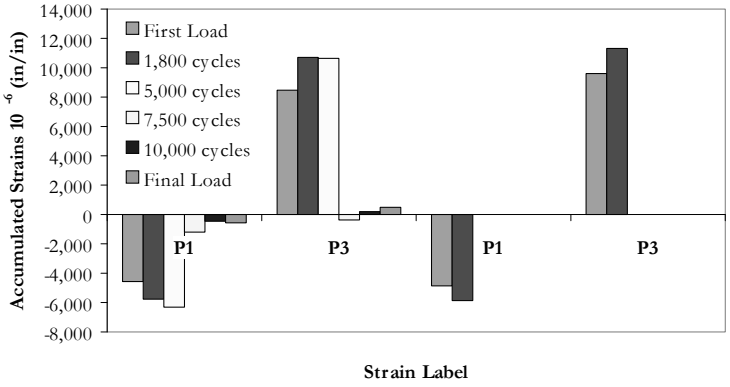

Accumulated Strains

Figure 3.38 Recorded and accumulated strains TP-22

completed. Nevertheless, this change is not clear enough to derive a correlation between failure and stiffness. The permanent deformation plot similar to the one presented for TP-21 shows an interesting similarity to the previous one. The permanent deformations take a large jump at the monitoring done at 5,000 cycles. Following these cycles, the permanent deformations drop to much lower values. Remembering TP-21, a similar jump was noticed in the plot. Unfortunately one of the rosettes was lost during the cycling of the specimen. The readings for this rosette are in the right side of the plot.

A noticeable difference between the failure surfaces for the specimens (Figure 3.39) in this phase as compared to the specimens in the previous phases is the extent of the delamination. Here we see that the delamination did not extend very far from the location of the main longitudinal crack. This trend was observed in all the specimens tested at this amplitude regardless of the number of cycles at failure. The image for TP-21 has a high level of contrast and this makes finding the failure area difficult. However, it is very similar to the TP-22 specimen.

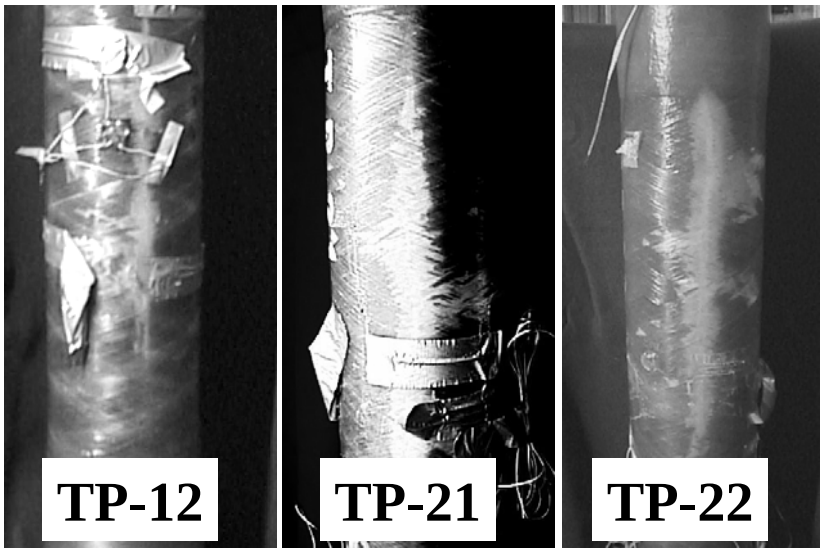

Figure 3.39 Failure surfaces for specimens in 1800-psi phase

3.3.1.4. CYCLIC 1,600-PSI TEST RESULTS

Figures 3.40 to 3.43 show the strain data for specimens subjected to cyclic pressures at 1600 psi.

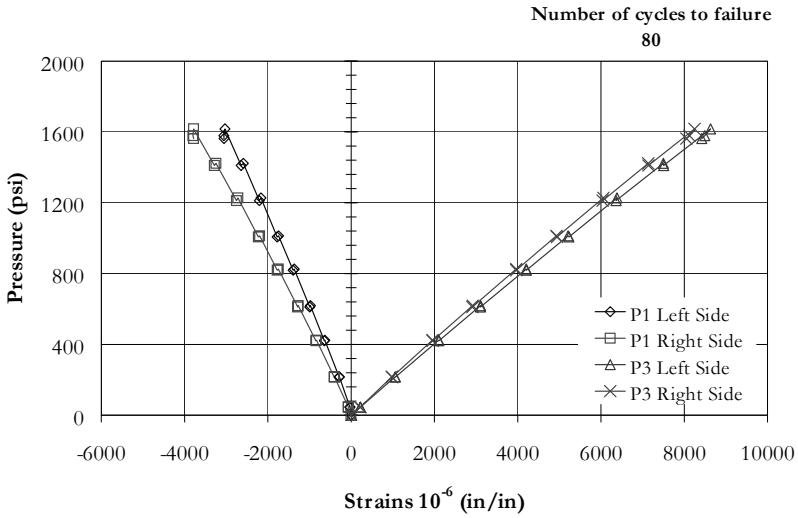

Figure 3.40 Recorded strains for TP-9

As with the previous group, the strains in some cases have been separated into P1 and P3 strain plots. In addition, the accumulated strain will be presented in the figures. For this phase, a total of five specimens were tested. Specimens TP-1, Tp-6, TP-9, TP-14 and TP-19 were tested at this pressure amplitude. Figure 3.44 shows the profile of the delaminated specimens after failure by leakage is reached.

No strain records are available for specimen TP-1 that failed after 500 cycles at an amplitude of 1600-psi. The strains for TP-6 (Figure 3.41) show no signs of stiffness degradation in the P3 strains. The P1 strains show a gradual reduction of the slope in the curve. However, this reduction is not consistent with the number of cycles applied to the specimen. In addition, the change is small enough to make a definite conclusion difficult. A slight indication of non-linearity is also apparent in the P1 strains. The amount is also very small suggesting that only a very limited amount of damage to the

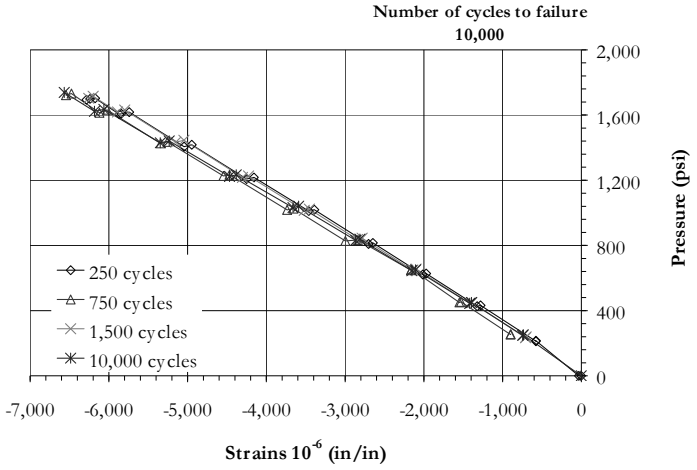

P1 Strains Plot

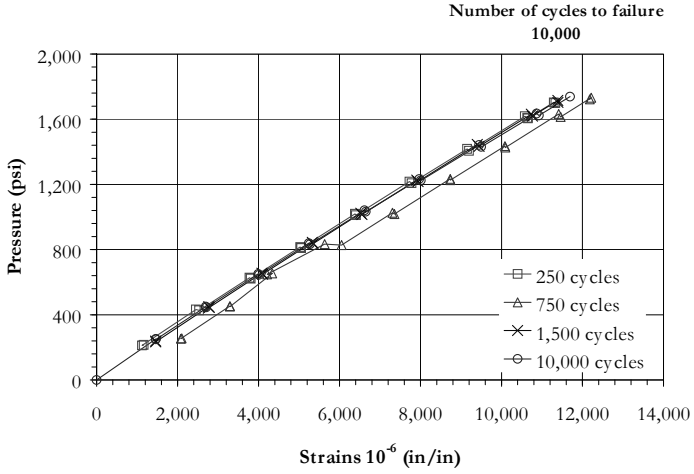

P3 Strains Plot

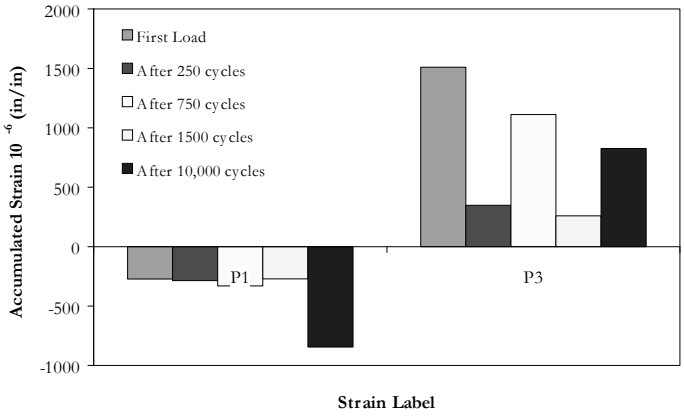

Figure 3.41 Recorded strains for TP-6

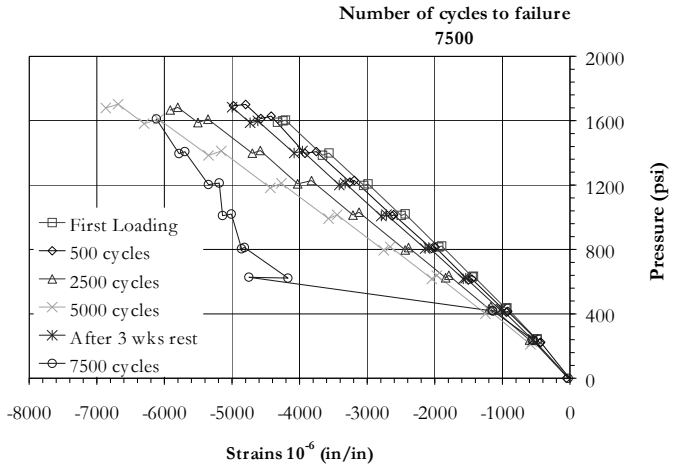

P1 Strains Plot

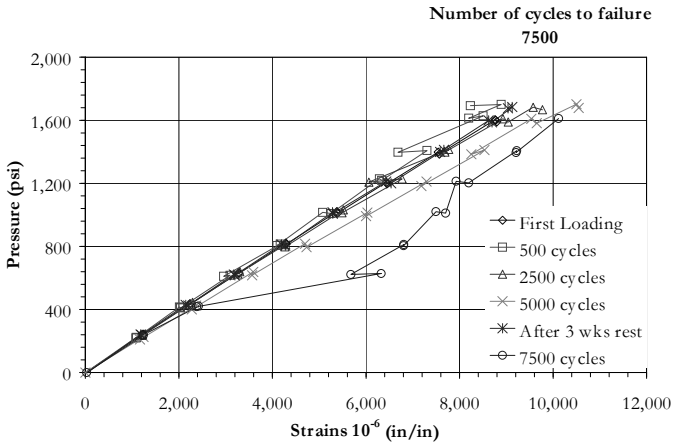

P3 Strains Plot

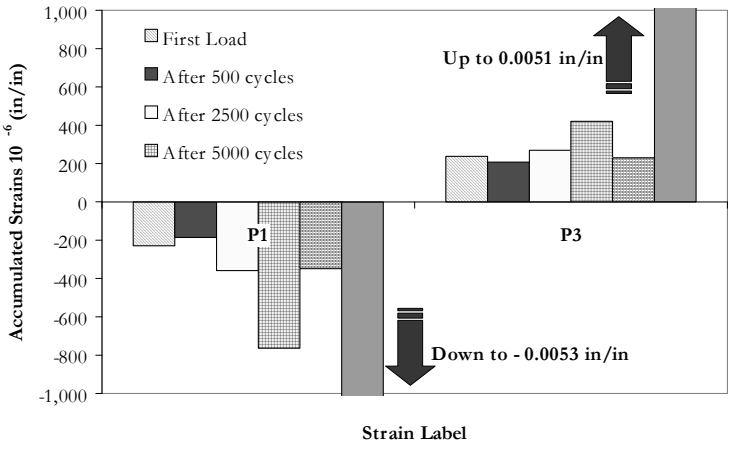

Figure 3.42 Recorded strains for TP-19

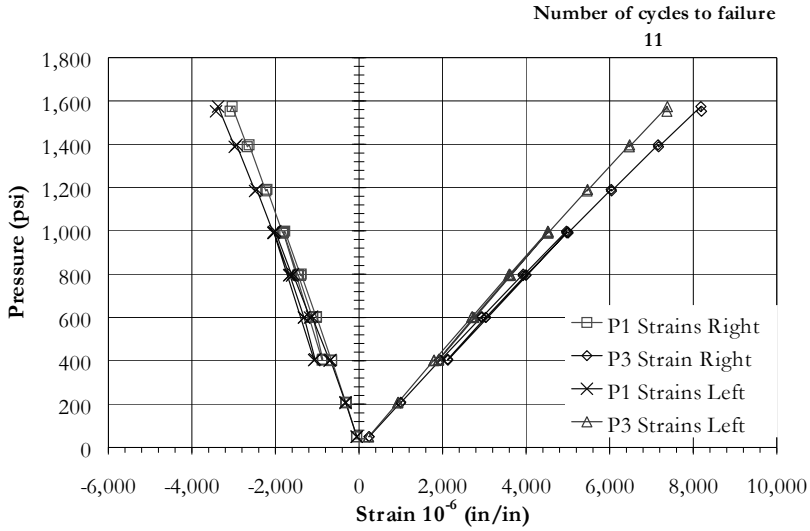

Figure 3.43 Recorded strains for TP-14

matrix had been done. An odd behavior is noted at the static monitoring after 750 cycles in both the principal strains. The reason for the irregularity in the strain data is not clear. One possibility is that this was the result of error in the data acquisition system. Following comparisons to other specimens and associated forms of monitoring (e.g. AE) will provide more insight to the behavior. No other changes are apparent in the strains, not even at final loading to leakage did the plots showed any kind signs of damage.

On the permanent deformation graph a similar tendency as observed in other specimens is noted. However, the number of cycles separating the last monitoring at final loading and the immediately previous one is quite large. Comparing the deformation between those two stages alone would be difficult. However, comparing to the behavior of a similar specimen provides some interesting points of comparison. The tendencies shown in TP-6 would be almost identical to the ones seen in TP-19 if we ignore the records at 750 cycles. It would seem that an error in the records was very possibly encountered when monitoring after 750 cycles throwing the measurements off. Therefore, if we neglect the readings at 750 cycles, a tendency of decreasing residual deformation with increasing number of cycles is noted at the initial cycle stages.

Looking at the strains recorded for specimen TP-9 (Figure 3.42) we note a similar trend to the ones observed in other cyclic specimens in this program. P1 strains show a slight tendency towards non-linearity, whereas very little is noticed in the P3 strains. The maximum recorded strains at the target pressure at the first loading in the P3 directions was in the order of 0.85% and for P1 was about 0.30%. No other monitoring is available since the specimen failed at 80 cycles. This was also another of the specimens tested in the air-driven water system. Again, this could explain the discrepancy between the number of cycles in this specimen and the others in the same group. No information is available for residual deformations since only one stage was monitored.

Strains for specimen TP14 are almost identical to TP-9. P3 strains were smaller at 0.8% at first loading. Maximum number of cycles at failure was 11 making it similar to TP-9. Trends in the behavior were the same as described for TP-9 so they will not be described again. Failure occurred during a loading portion of the test. This is contrary to specimens tested in the closed loop system, where failure occurred during the AE testing and at the load hold at target pressures.

Records for TP-19 show a decreasing stiffness with increasing number of cycles. An interesting aspect was how the stiffness seemed to recover after 5000 cycles and 3 weeks rest. Strains measured in the first test after 5000 cycles show the drop in stiffness expected from the increased number of cycles. However, the specimen was allowed to rest for 3 weeks before performing another static test. The results of this test show an increase in the stiffness in both the P1 and P3 strains. Strains measured at final load, which occurred after 7500 cycles, show a progressive deterioration of the stiffness during the loading process. The recovery noticed in the tests after 5000 cycles indicate that permanent deformations are partially recoverable. This recovery was the reason why the plots of residual deformations presented in the results were created with the strains immediately after the static tests.

Figure 3.44 shows the profiles of the specimens for this phase after testing. There appears to be a correlation between the total number of cycles and the extent of

the delamination encountered at failure. Specimens TP-1, TP-6 and TP-19 had the largest number of cycles to failure of the set and, as observed, the smallest areas of delamination at failure. On the other hand specimen TP-9 did have a larger number than TP-14 showing a less extensive delamination when compared to TP-14. It should be noted that specimen TP-1 was one of the few cyclic specimens tested using the air-driven water system. This system had a slower rate of loading than the closed loop hydraulic system used in the following specimens. The slower rate provided by the water system may have allowed for a creep-influenced failure. This will be noted for further interpretations of results in the following sections.

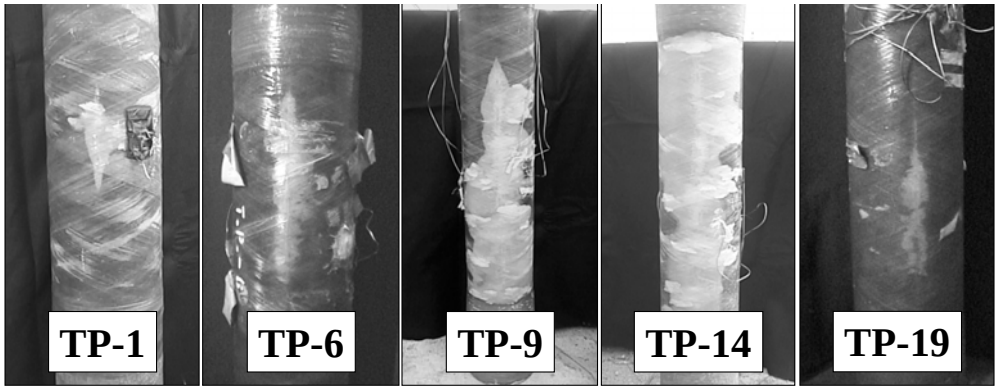

Figure 3.44 Surface condition after leakage for 1600-psi

3.3.1.5. CYCLIC 1400-PSI TEST RESULTS

Figures 3.45 to 3.47 show the strains gage data for specimens subjected to cyclic pressures at 1400 psi. Three specimens were tested for this group: TP-10, TP-17 and TP-24. All three failed in the same characteristic way as the other specimens tested in the closed loop system. Leakage took place at the load hold at the target pressure during the AE monitoring. The behavior of these specimens followed the trend of little to no stiffness loss during the cycling as noted in previous tests. If anything, a change into stiffer response was noted in the specimens with the longer cyclic life. A point to keep in mind is that this "stiffer" behavior was noticed in the P1 strains that are not in the

direction of the applied stress. Strains in the P1 direction are the response of the specimen to the Poisson's relationship. Strains in the P3 direction showed almost no change in behavior between the initial load and the final one. Specimen TP-10 with the lowest number of cycles to failure showed no change at all in the stiffness. In addition, it was the specimen with the stiffer response at initial loading of the group. A very interesting behavior aspect of the specimens was that, in the final loading, both TP-17 and TP-24 values for P3 approximated the values for TP-10. For the values of P1, the correlation appears to be in that the specimen with the smallest value for P1 for the target pressure failed at the lowest number of cycles. By looking at P1 values for the specimens we see that TP-10 had 0.30% strain at 1400-psi, where the values for TP-17 and TP-24 were in excess of 0.36%. General trends in all of the specimens included a slight departure from linearity noticed in the P1 strains during all of the tests. In the plot of residual deformation after each test, the same trend as in other groups was noticed. The residual deformation increased with the first cycles, but after reaching a peak level in decreased as it approached the final cycle. This was observed in all the specimens belonging to this group.

Finally, Figure 3.48 show the profiles of the damaged sections for the specimens after the tests were completed. The trend observed in the previous group, as it relates to the diminishing size of the delamination, is observed here. The specimens with the longest cyclic life showed the smallest delaminated area at failure, whereas specimenTP-10, which failed at a lower cyclic life, showed two failure areas. This was the only case where more than one crack formed on the internal liner of the specimen. Typically, only a single longitudinal line had formed at the time of failure. Here, two lines of cracks formed next to each other. These two zones of damage have been circled in the image for easy reference. The extent of the delamination around these damage areas was in the same proportion to the one noted in the other specimens in this group. No other damage mechanism was immediately apparent in any of the specimens.

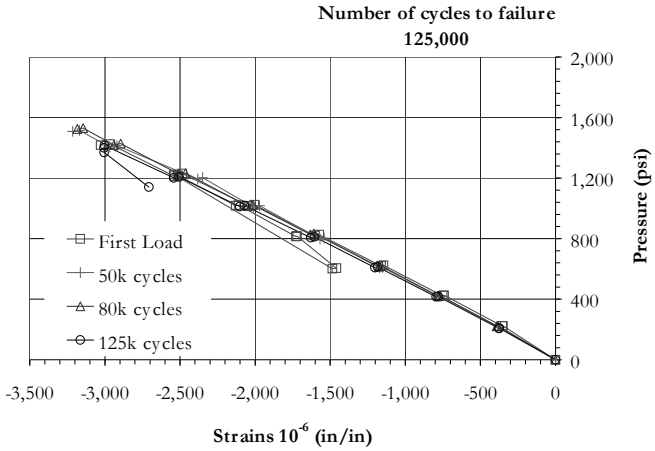

P1 Strains Plot

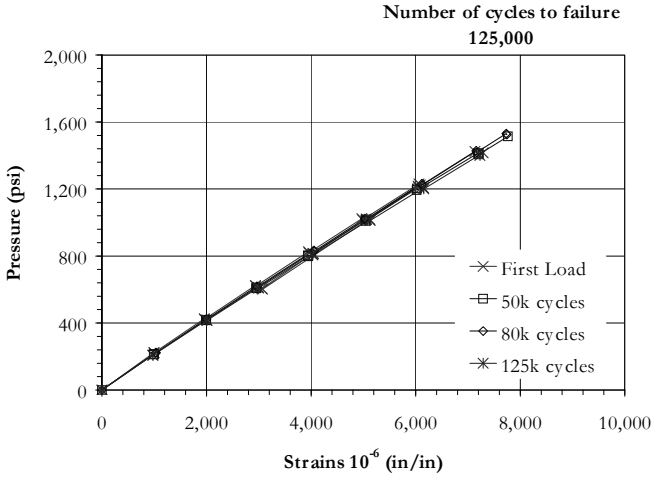

P3 Strains Plot

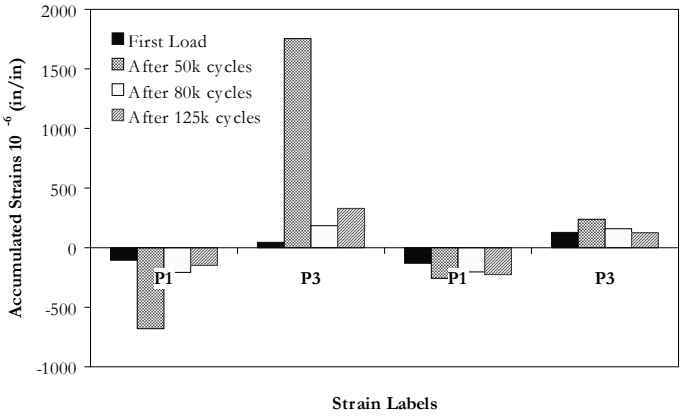

Figure 3.45 Recorded strains for TP-10

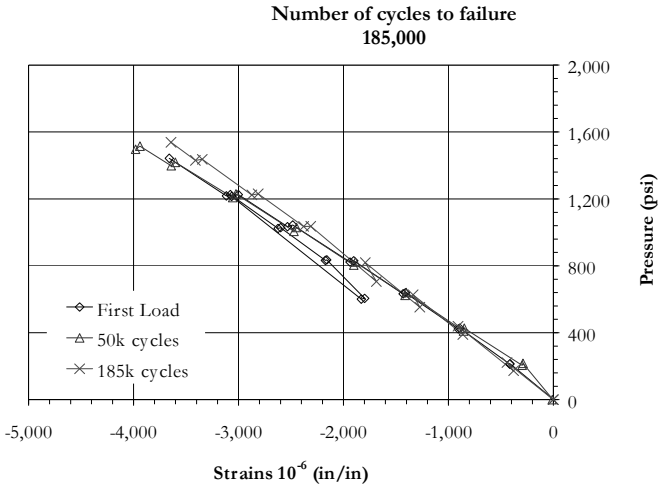

P1 Strains Plot

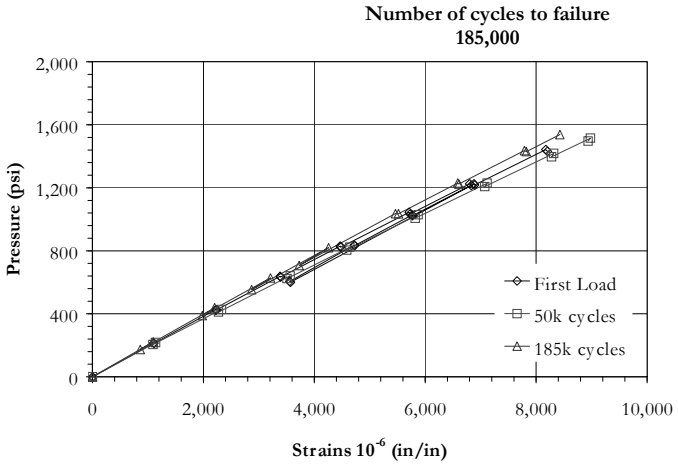

P3 Strains Plot

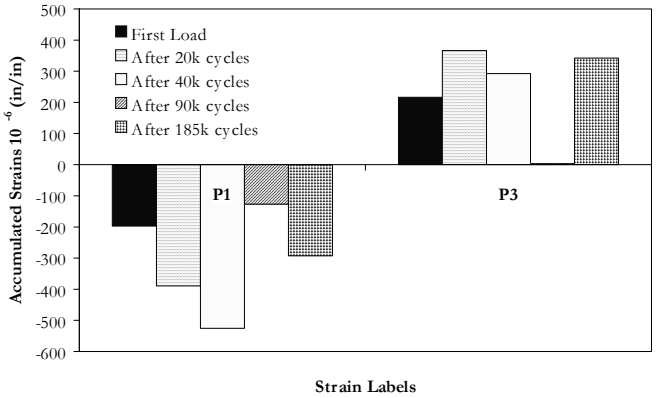

Figure 3.46 Recorded strains for TP-17

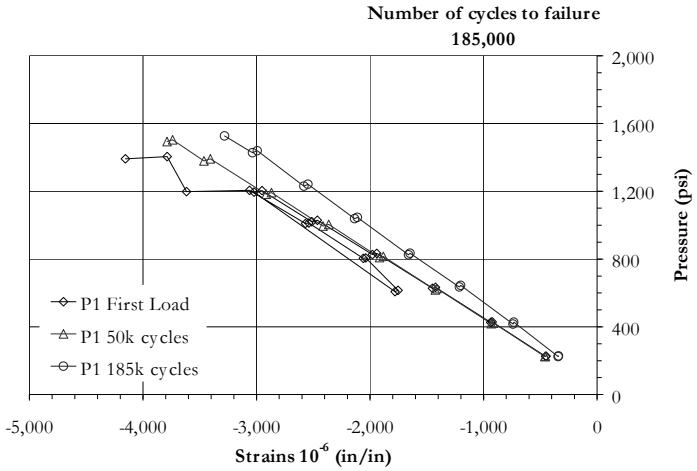

P1 Strains Plot 1

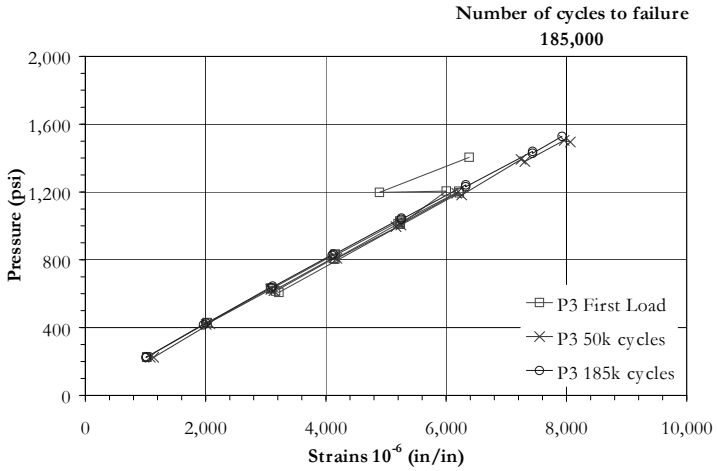

P3 Strains Plot 1

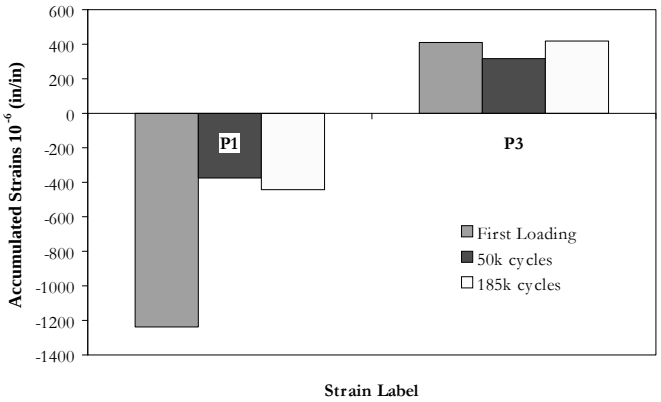

Figure 3.47 Recorded strains for TP-24

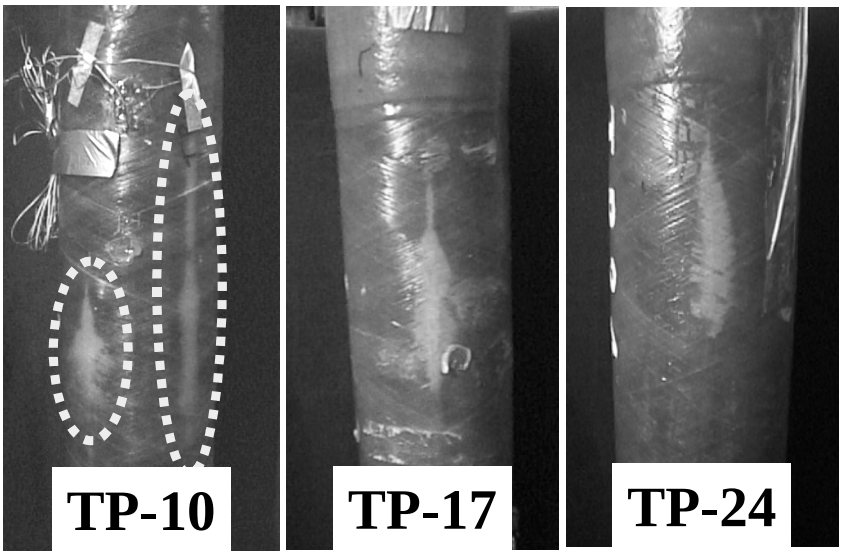

Figure 3.48 Failure surfaces for specimens in 1400-psi range

3.3.1.6. HYBRID SPECIMENS STRAINS DATA

Two hybrid specimens were tested under static load to failure. Specimens were labeled HTP-1 and HTP-2. The end preparation was the same as used in the fiberglass specimens. Strain gage data is shown in Figures 3.48 and 3.49.

The main difference in the behavior between the hybrid specimens and the pure fiberglass, tested under the same conditions, was the mode of failure. The hybrid specimens failed by bursting at maximum pressure. There were no prior indications of failure or damage visible on the exterior of the specimens. No leakage was noticed and, no visible change in the strain gages was recorded as failure was nearing. Failure pressures were of 3277 psi for HTP-1 and 3,435-psi for HTP-2, indicating an increase in the capacity as compared to the TP specimens. The cost of this increase, however, was a sudden and catastrophic mode of failure.

In general terms, the behavior of the specimens was similar. That is, no indications were noticeable in either one that failure was about to take place. In addition, both failed by a sudden burst of water and high-energy release.

From the strain plots, we can see that the specimen with the lowest capacity was the one with the most difference between gages. Different apparent stiffnesses were recorded at two locations for specimen HTP-1. Both rosettes were located at the middle of the specimen but at diametrically opposite locations. P1 strains recorded were practically identical in both locations. P3 strains, however, showed a marked difference in the records. There is a good possibility that the records of HTP-1 are correct since the recorded P1 strains for both locations were in good agreement. A slight difference was recorded in the P3 strains at opposite sides for the final loading in HTP-2. The difference was not as marked as with HTP-1.

Because of AE monitoring, during the testing for HTP-2, the specimen was loaded four separate times to gradually increasing pressure levels. As it can be seen in Figure 3.48, no change in stiffness was noted between the records of the separate tests. This makes prediction of failure or leakage based in stiffness measurements extremely difficult. Specimen HTP-2 was the first one tested in this group. For HTP-1 only one test was carried out. However, several unloading steps were included in the profile. In the strain plots for HTP-1 residual deformation can be noted at every unloading. As with the fiberglass specimens the residual deformation is more noticeable in the P1 strains than in the P3 direction. It is noted that this residual strain increases as the maximum pressure nears the final value. These same trends were indirectly observed in specimen HTP-2 between the separate tests performed. These are similar to the trends observed in the fiberglass specimens. Unfortunately, the information available on these specimens may not be sufficient to draw a final conclusion.

This concludes the presentation of the strain data recorded during the tests. As was seen, in most cases this data was inconclusive and ambiguous at best when it came down to relate it to data from other tests in the same group, and even to data from the

same experiment at different stages. The gap left by the ambiguities in the strain data is expected to be bridged by the acoustic emission monitoring. In the next section the results of the acoustic emission will be presented.

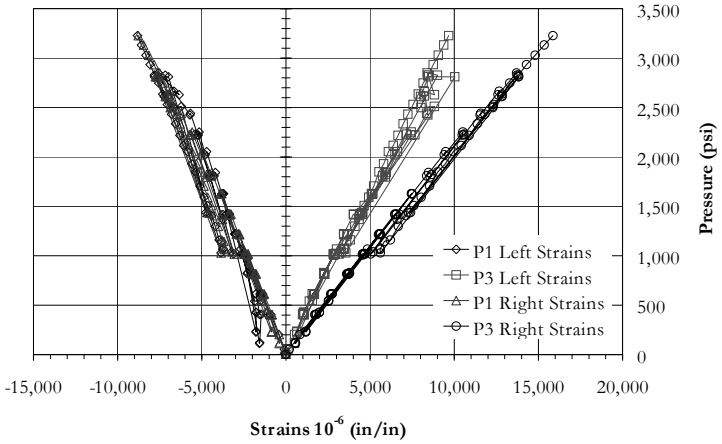

View Principal Strains

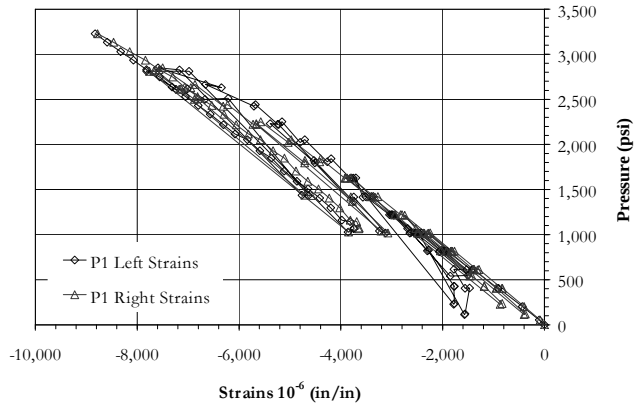

P1 Strains Plot

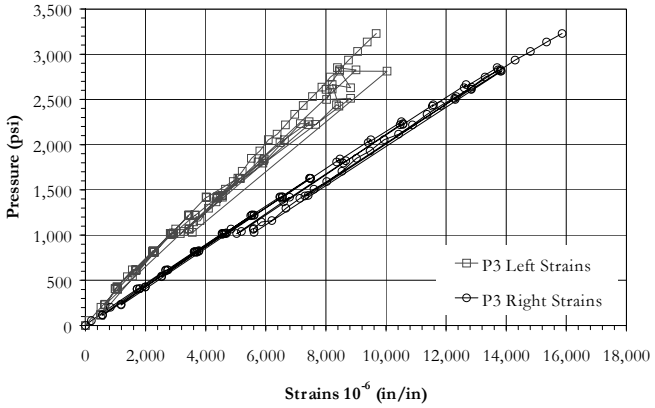

P3 Strains Plot

Figure 3.48 Recorded Strains for HTP-1

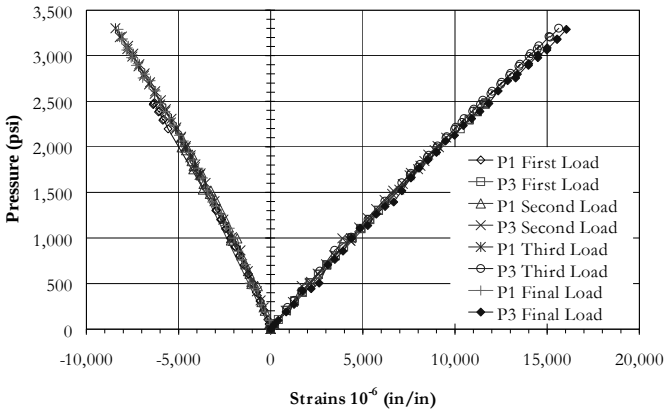

View Comparison between loadings

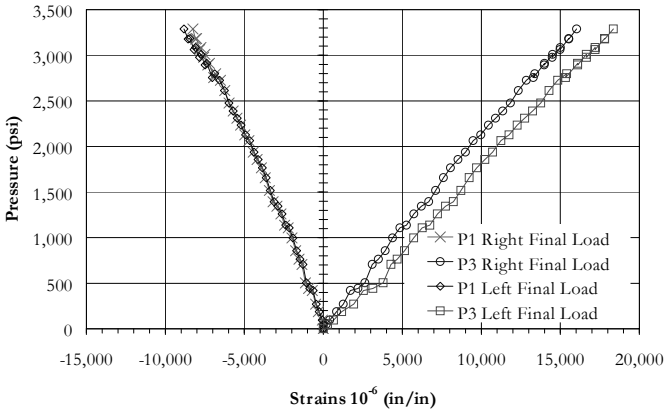

View Principal strains at final loading

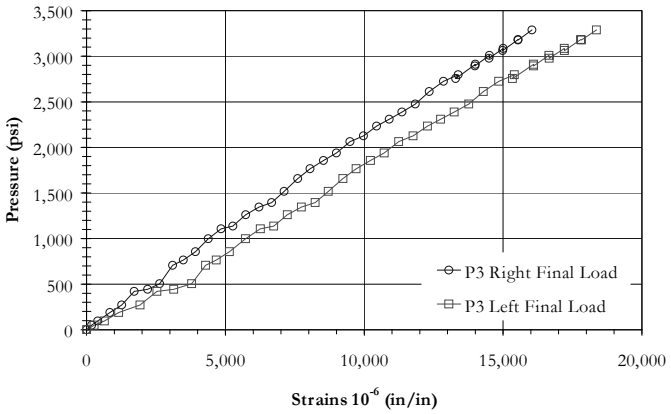

P3 Strains Plot at final loading

Figure 3.49 Recorded strains for HTP-2

3.3.2. ACOUSTIC EMISSION RECORDS

Acoustic emission records were obtained with the use of traditional feature extraction data acquisition equipment. The R15I resonant sensors were used for the AE monitoring. Two sensors per specimen were typically used, although in the initial tests up to four sensors were used.

In the history of the development for attribute based AE, several attribute comparison plots have been developed. Each of these plots finds an application depending on the type of test and the specimen in question. AE has proven itself reliable in predicting the general condition of structures monitored using this technology. The complicated nature of composite material mechanisms provide for an environment where statistical approach to capacity prediction based on as-built nondestructive monitoring could prove practical and extremely useful. It is because of this approach that the information presented in this description of the AE records is based on the statistical nature of the emissions and not on the identification of the specific damage mechanisms at play.

The selected features for presentation and analysis were the recorded amplitude, duration, and the accumulated signal strength. For the definition and description of each one of these parameters, the reader is directed to ASTM specification 1316 and the CARP Recommended Practice in addition to the Chapter 1 of this dissertation. Follow-up information presented in this chapter that relates to the acoustic emission analysis was calculated based on these individual features or a combination of them. As with the strain data, results records will be grouped based on the pressure magnitude used in the testing. It should also be noted that the loading profiles selected during the monitorings included several load drops and load holds to account for the possible redistribution of load paths as discussed in Chapter 1.

3.3.2.1. MONOTONIC TEST DATA

Figures 3.50 to 3.54 present three of the most relevant aspects of the AE records during the tests. As presented before, the specimens for this phase were TP-2, TP-5, TP-8, TP-15 and TP-18. All were tested to failure as defined by leakage of the fluid used in the pressurization. The static tests were the first tests performed in this experimental phase for the internally pressurized specimens. During this phase, the seal system was still being developed and tuned. This development phase resulted in some of the tests having an odd looking load profile, or more than one loading in the records. Because of the sensitivity of the AE monitoring to extraneous and mechanical noise, the test had to be stopped and restarted when leakage through the seals was detected. In addition, the load holds, as required by the AE, were not consistent in one of the specimens in this group.

Each of the following AE data figures is plotted against time. Time is the horizontal axis in the figures with the units of seconds. The starting point in the time axis was at the beginning of the tests after line pressure from the water outlet was allowed into the specimen (approximately 50-psi). The reason for allowing the line pressure before AE monitoring began was the elimination of seal seating noise. After the pressure inside of the specimens reached balance with the line pressure, AE monitoring began. For specimens tested in the closed looped system, an initial line pressure of 50-psi was applied prior to the beginning of AE monitoring. All pressure values shown in this program include the pre-monitoring pressure of 50-psi, and therefore no adjustments are required in the pressure logs. The applied pressures are plotted as a dashed line. On the right of each of the plots an axis representing the applied pressure is shown with units of kips per square inch. Finally, the left axis in the plots represents the parameters of interest. The units depend on the parameter in question. Amplitude is presented in decibels, the duration in microseconds and, in a logarithmic scale, and signal strength in consistent of volts and time unit.

TP-8 was the first specimen tested in this series of the experimental program. It is easy to see how the sealing system had not been finalized at this point. Load holds were inconsistent with continuous leaks noted at the end plates. Even when these leaks did not generate detectable emissions they made interpretation of results difficult. Without consistent load holds no reliable comparisons can be made to other tests. Emissions during load holds are an indication of the extent of damage incurred in a structure. If the load holds are not stable, it is difficult to determine how the AE responded to them. If the emissions dropped it could be due to minimal damage occurring in the structure, or the load dropping below the level where damage is taking place. At any rate, the recorded emissions do indicate at which load level the amount of emissions increased when compared to the previous load levels. So even when determination of damage based on load hold emissions is not possible, it is still possible to asses the load at which significant emissions, and perhaps damage, started during the load history of the specimen.

Because of limitations encountered during the analysis, it was necessary to divide the AE results for specimen TP-8 in two separate files. The results of these files are shown in Figures 3.52 and 3.53. The most noticeable feature of the AE in Figure 3.52 is the increase in AE energy as the result of the increase in the recorded duration of the events at time 1400-sec. In comparison, the amplitude recorded did not show a significant increase at this time. If anything, it showed decay in the decibel value at this same time. The pressure at this time was 1000-psi. An interesting feature is how the cumulative signal strength shows an increase at the time of maximum pressure but levels out after that. There is a notable increase in the slope of the cumulative signal strength at 1400-psi (1867 secs), which is also the maximum pressure achieved in this first test. Figure 3.53 shows the results for the second test on this specimen. The AE records take a noticeable jump when the previous pressure is exceeded; as noted at time 1112 in the second test where the pressure of 1400-psi was passed. In addition, the same trend was observed as with the first test where the duration plot shows a noticeable increase in

activity, but the amplitude plot does not show the same significant change. There is a constant record of low amplitude emissions, with virtually no high amplitude events.

Specimen TP-2 was the second tested in this program, and the results are shown in Figure 3.50. This was one of the lowest recorded leak pressures of the specimens tested under static load. In this test, the plots show the complete records of the monitoring from beginning to final pressure. The plots indicate that this was the second loading of the specimen. However, the first loading did not reach pressures greater than 150-psi before it was suspended due to a problem with the leak detector system used. After the problem had been solved, the test was restarted following the same profile as described at the beginning of this section. The most notable feature is how the amplitudes seem to reach a maximum at time 1500-sec, with a gradual decay in following load steps until an increase in the final loading was reached. The point of maximum amplitude coincides with the first notable jump in the signal strength. This occurred at about 1000-psi of applied pressure. A feature that is hidden by the scale of the plot influenced by the final stages of loading is that emission started at 700-psi, and that the first noticeable jump in the signal strength took place before the jump at 1000-psi at about 850-psi. The duration plots showed continuous activity during the test, with few events with duration greater than the average until final loading. The last behavioral feature that will be highlighted is a band of silence detected in the duration plot in the final stages of the life of the specimen. This quiet band could be the result of equipment malfunction, like a full buffer on the systems, or could be a real feature of the specimen and its behavior. This will be revisited at the end of the section.

Next is the TP-5 specimen, with the results shown in Figure 3.51. Main features include the gradual increase in the amplitude recorded from initial loading to final pressure. Amplitude reached a maximum at about 1988 seconds, which corresponds to about 1100-psi in the loading curve. Duration also appears to distribute more evenly at about the same time and the cumulative signal strength also begins to show a change at 1988 seconds. In actuality, the change in signal strength was first detected at an earlier time; at about 800-psi, but emissions during load hold are more noticeable. One of the

channels in the specimen recorded a large increase in emission at 2982 seconds and about 3500 seconds, with the remaining channels maintaining a consistent behavior. At these same times, the duration plots show a localized increase in the plot. This seems to indicate that the changes in the duration plot are the result of the increased activity in only one of the channels.

The last specimens shown in the plots are TP-15 and TP-18. Data for these specimens is presented in Figures 3.54 and 3.55. Their behavior was so similar to each other that they will not be treated separately here. The leakage pressures were 2790-psi and 2763-psi respectively. Their respective AE plots were also similar to each other. In both specimens the initial signs of AE occurred at 400-psi and the first noticeable change in slope took place at 1200-psi. The amplitudes had a gradual increase in magnitude reaching a peak at about 1200-psi also. The distribution of the event duration was well distributed from the beginning of the records to right before the failure.

This completes the presentation of AE data for the static tests to failure. Some interesting trends were noticed in the plots that could indicate that there is the possibility of associating AE results to the leakage capacity of the specimen. These records will be compared later to the behavior recorded by strain gages in the specimens. The interesting point in the comparison with the strain information will be assessing if extensive fiber damage was present in the specimen during testing. During the monitoring of these specimens a number of high amplitude short duration events were recorded, these typically indicate that fiber breakage did take place during the test. However, after inspection of the specimens post-leak, very few indications of fiber breakage were observed.

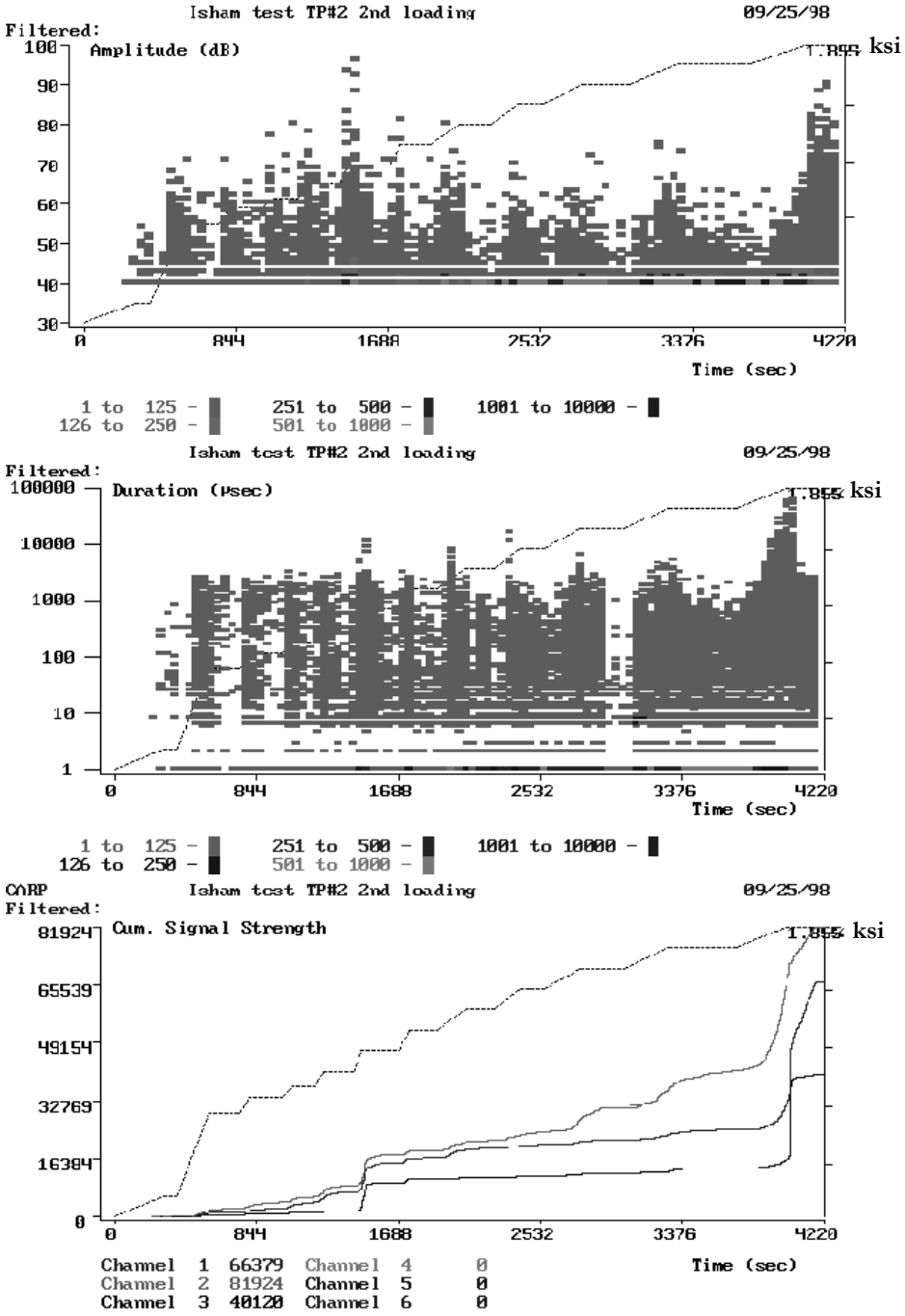

Figure 3.50 AE data recorded for TP-2

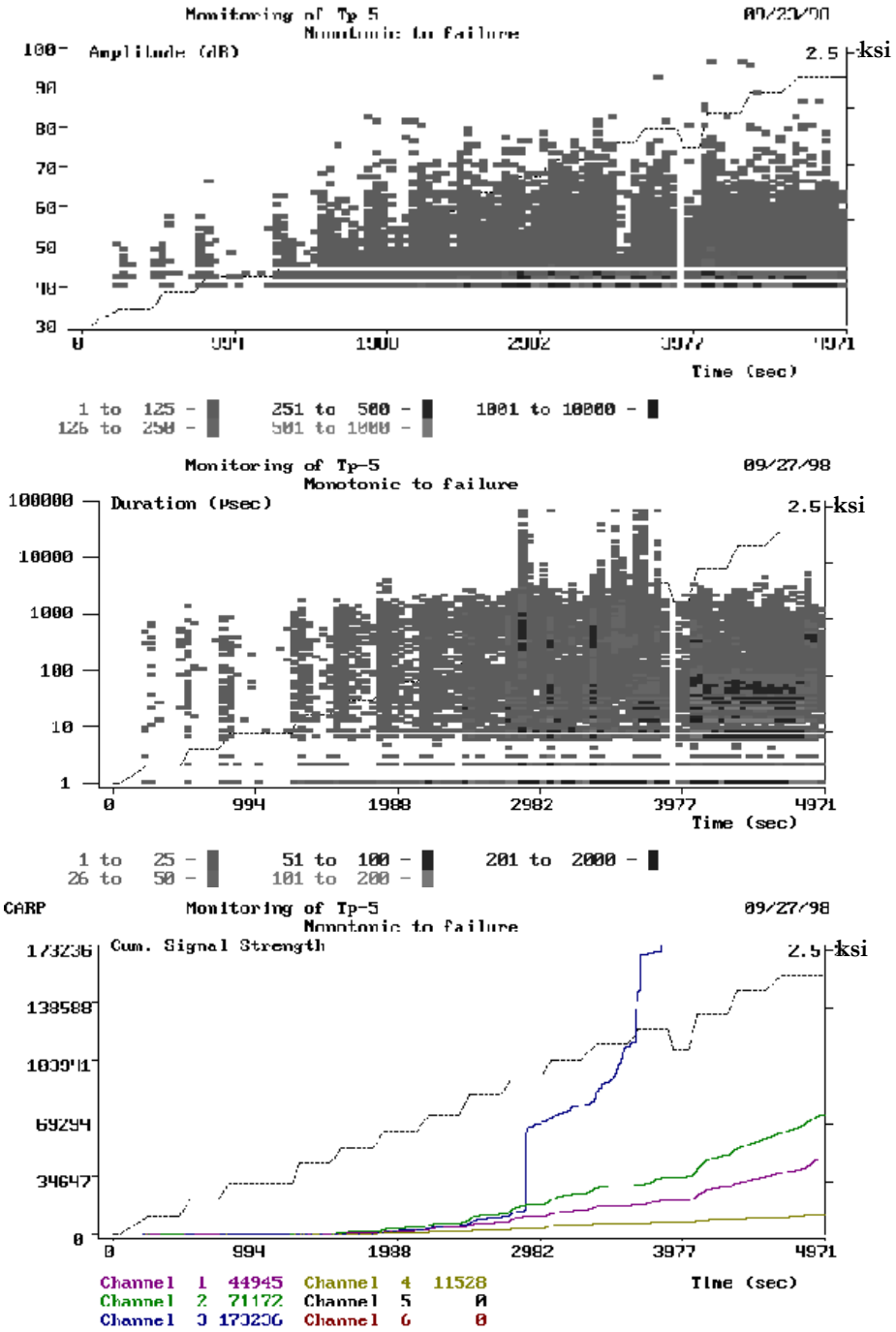

Figure 3.51 AE data recorded for TP-5

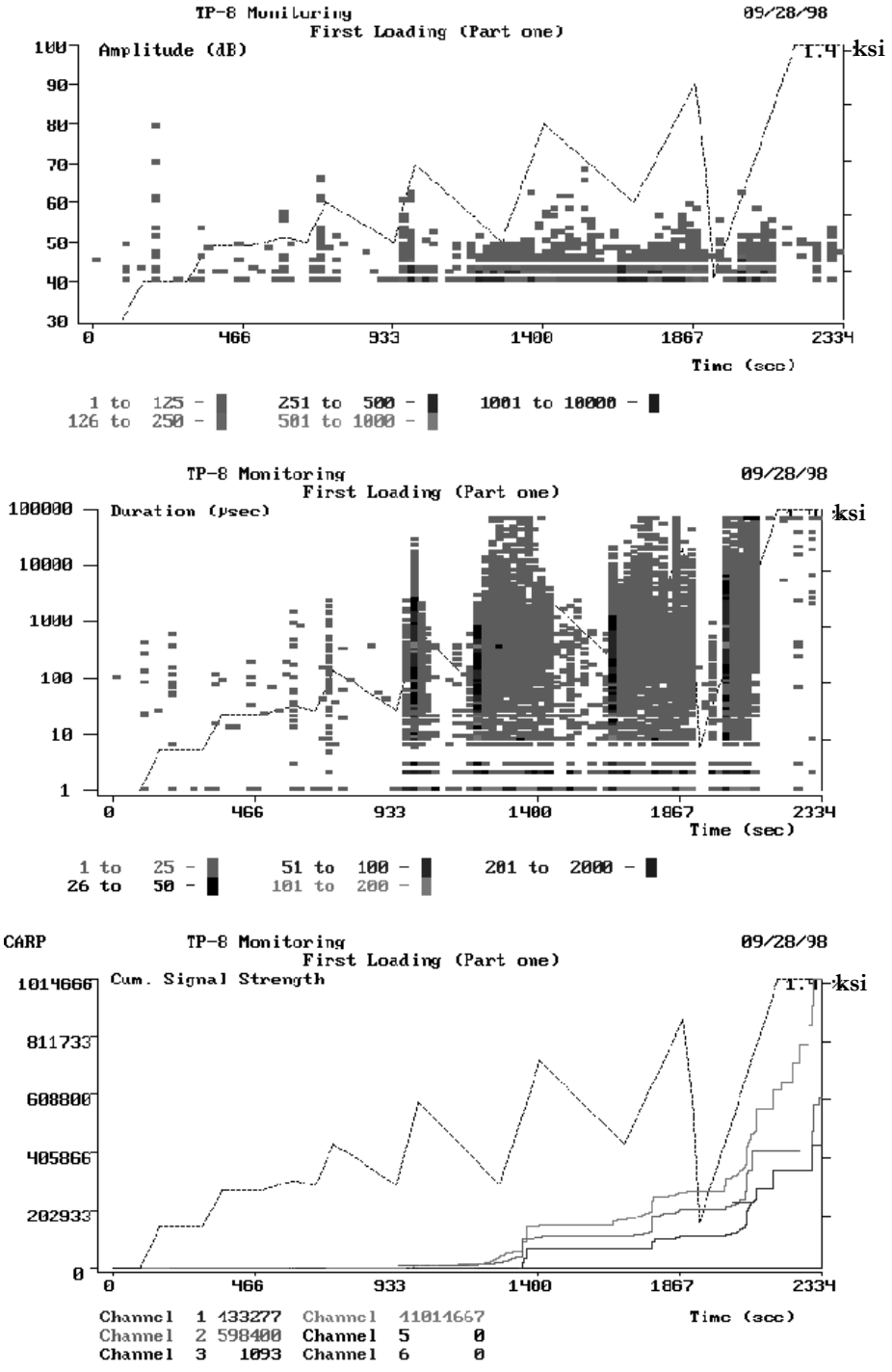

Figure 3.52 AE data recorded for TP-8 first stage

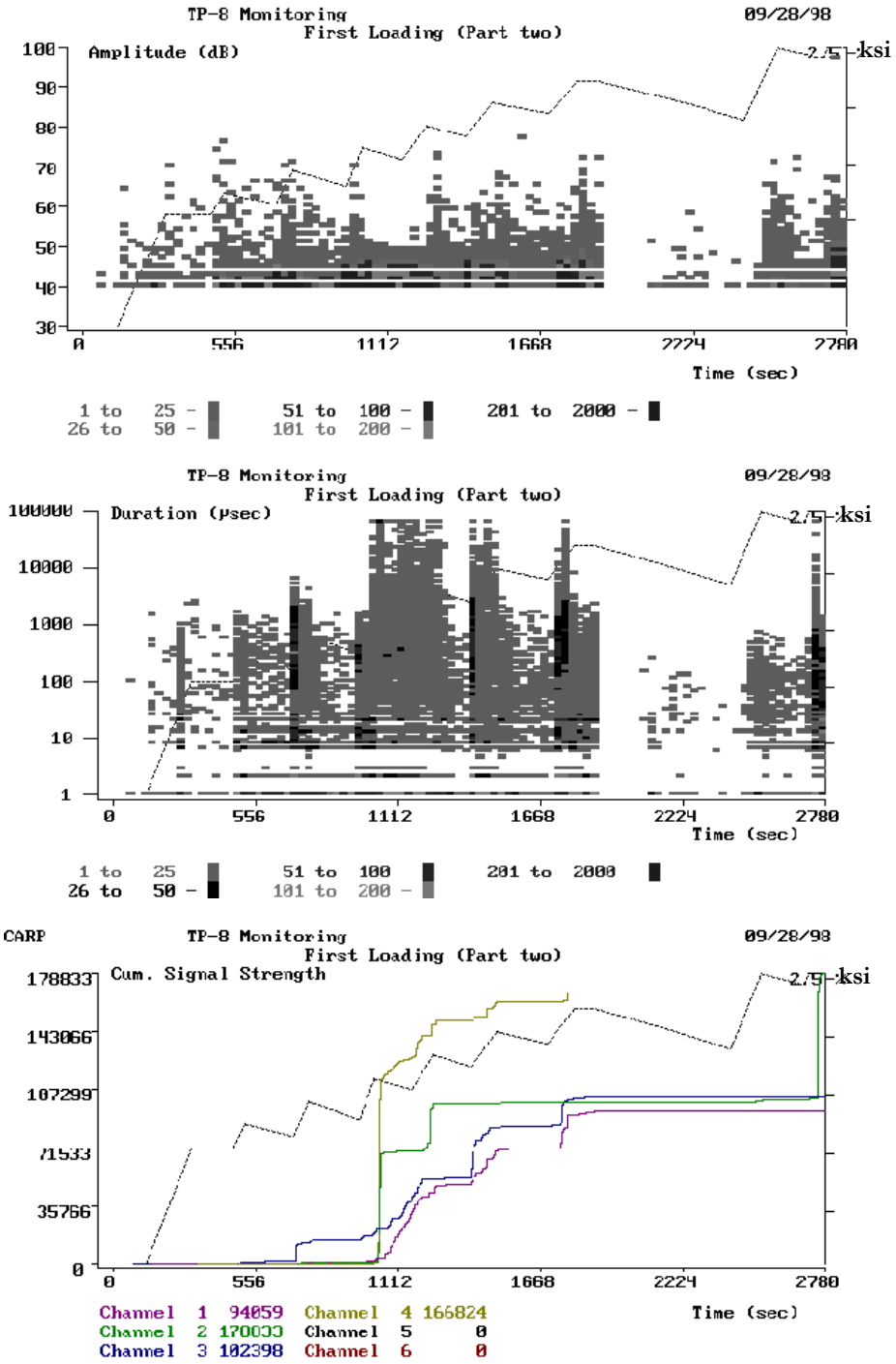

Figure 3.53 AE data recorded for TP-8 second stage

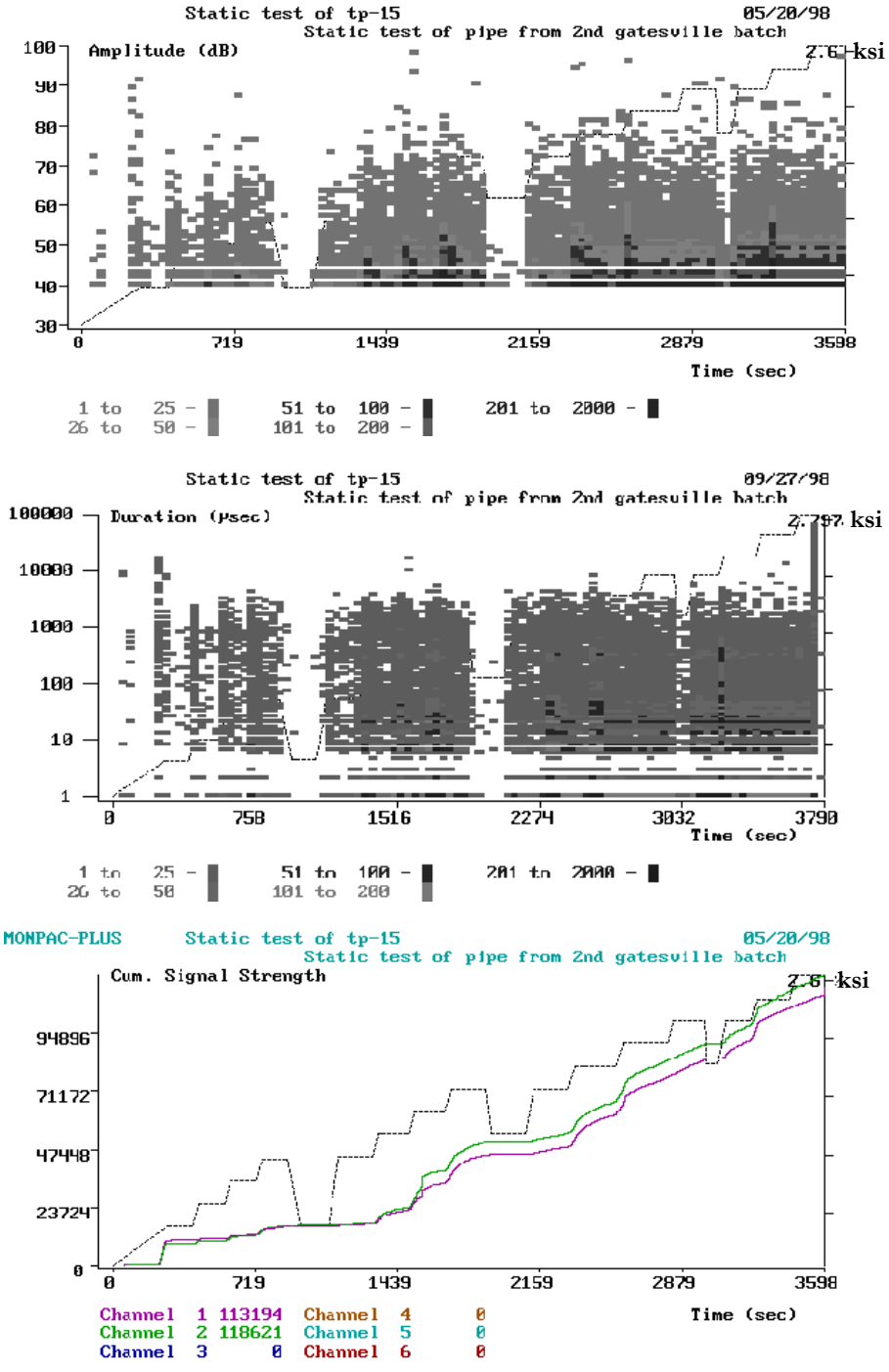

Figure 3.54 AE data recorded for TP-15

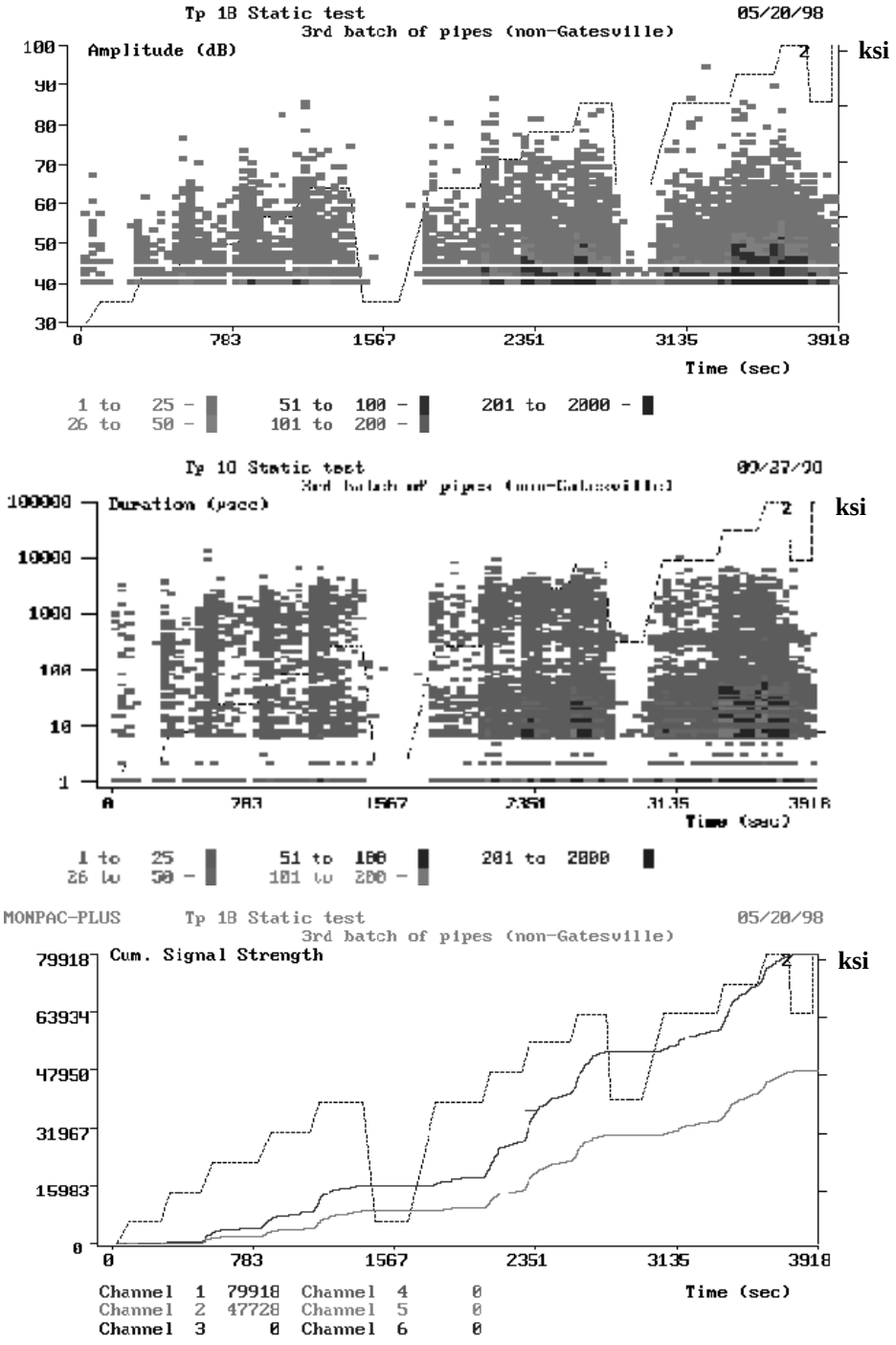

Figure 3.55 AE data recorded for TP-18

3.3.2.2. RESULTS FOR CYCLIC TESTS AT 2100-PSI

A difficulty that will be encountered in presenting the data for the cyclic tests is the amount of records available from AE. This will be more noticeable as the pressure range is lowered and the number of cycles increases. In some cases the number of cycles to failure was low enough that only one AE monitoring was performed before failure took place. In contrast, there were some specimens where between the first and last monitoring more than four intermediate records were obtained. The results will be presented, when possible, in the following way: first loading, one intermediate scan and final scan. The same parameters as the ones used for the static tests will be used here. During the analysis of results section, some additional data will be presented as it is judged relevant.

Figures 3.56 to 3.61 show the records of AE for the specimens in this pressure amplitude. A total of four specimens were part of this phase, TP-3, TP-4, TP-13 and TP-23. This indicates that two specimens from the first batch, one from the second and one from the third were tested. This differentiation will be useful in comparing the results to the static capacity of the specimens since there appears to be a difference in capacity between the specimens from different production batches.

The first specimen in the figures, TP-3, lasted for a total of 10 cycles at a pressure range of 100-psi to 2100-psi. The obvious features of the AE plots are the gradual increase in activity from the initial to target pressure. AE activity in the signal strength plot started at about 300-psi with events being recorded at every increase in pressure. However, the most noticeable change in slope was not recorded until the load step between 1000-psi to 1200-psi. A second change in the slope of the signal strength was noted at 1200-psi. Isolated jumps from the average were noted in both the amplitude and duration plots during the pressure steps. The general trend, however, was very consistent in both amplitude and duration.

The next specimen, TP-4, failed after one cycle at 2100-psi. That is in the first cycle immediately after the AE monitoring leakage took place. Because of equipment difficulties monitoring was only possible up to 1115-psi. Also, the specimen had been preloaded to 500-psi in a previous test. The pre-load condition is clear by looking at the lack of activity recorded by the AE in the initial load stages. Nevertheless, a clear characteristic that is noticeable in the signal strength plot is the marked change in the slope at 900-psi, 200-psi below what it had been observed in the previous test. A second sharp jump is observed at 1100-psi in the same signal strength plot.

Specimen TP-13 lasted for 125 cycles at the target pressure. Unfortunately no AE data is available for the final cycle for this specimen. The last monitoring took place after 90 cycles. Because of the amount of data available, the data was separated in three figures. Figures 3.58, 3.59 and 3.60 show respectively the amplitude, duration and signal strength records during four separate loading stages of the specimen. In some of the monitoring, the Felicity ratio was estimated by providing download stages during the tests. In those where no downloads were produced, the ratio was calculated based on the previous record available. Looking at the amplitude plots in Figure 3.58 we note a marked change between the first load and subsequent ones. At first loading, AE activity was noted from initial pressures of 200-psi, whereas in the following monitoring no consistent activity was recorded until after higher pressures that varied depending on the cycle stage. In the amplitude plots presented here it is seen that after 15cycles the first emissions were detected after 800-psi, after 60 cycles this moved up to 1200-psi. Finally, after 90 cycles some emissions were noted at 800-psi again with the more consistent emissions taking place at 1200-psi. The magnitude of the amplitudes showed a drop from the first test to the monitoring after cycles.

On the duration plots for TP-13 we note a drop on the average duration recorded for events during monitoring from the first load records to the records after 90 cycles. The number of events of more than 1000 μsec were significantly reduced by the time the specimen had gone through 90 cycles.

The last plots for this specimen are the cumulative signal strength curves. For this specimen, at first loading the first considerable accumulation of signal strength takes place at 200-psi, which agrees with the observations made in the amplitude plots. The first considerable change in the slope took place at 1200-psi, with the second taking place at 1400-psi. For the following records, changes in slope were first detected at 1200-psi with two more jumps at 1600-psi and at 1900-psi. An important issue is to determine which of the changes in slope in the signal strength curve is relevant to the capacity of the specimen. Each one of the jumps indicates that some type of significant damage is taking place. Determining what kind of damage and its relationship to the capacity could be critical in predicting the life of the specimen.

Specimen TP-23 was the last one tested in this group with a life of 30 cycles. Looking at the only monitoring made for this specimen we can see the same trends observed in other specimens during the first load. The AE emissions started at low levels of pressure. Even though the figure shows a single constant slope line from 50-psi, the load was stepped at every 200-psi. The limitations in the software used for the AE analysis made for a small number of load steps that can be plotted in the figures. That is why the initial load steps were simplified. That said, it is apparent that the emissions during load holds began at 800-psi for this specimen. This was concluded because at this time, the signal strength plot shows a constant gradient on the slope through the load hold. The flat areas in the curve are the results of the download to previous pressure levels and may obscure the slope changes in the plot.

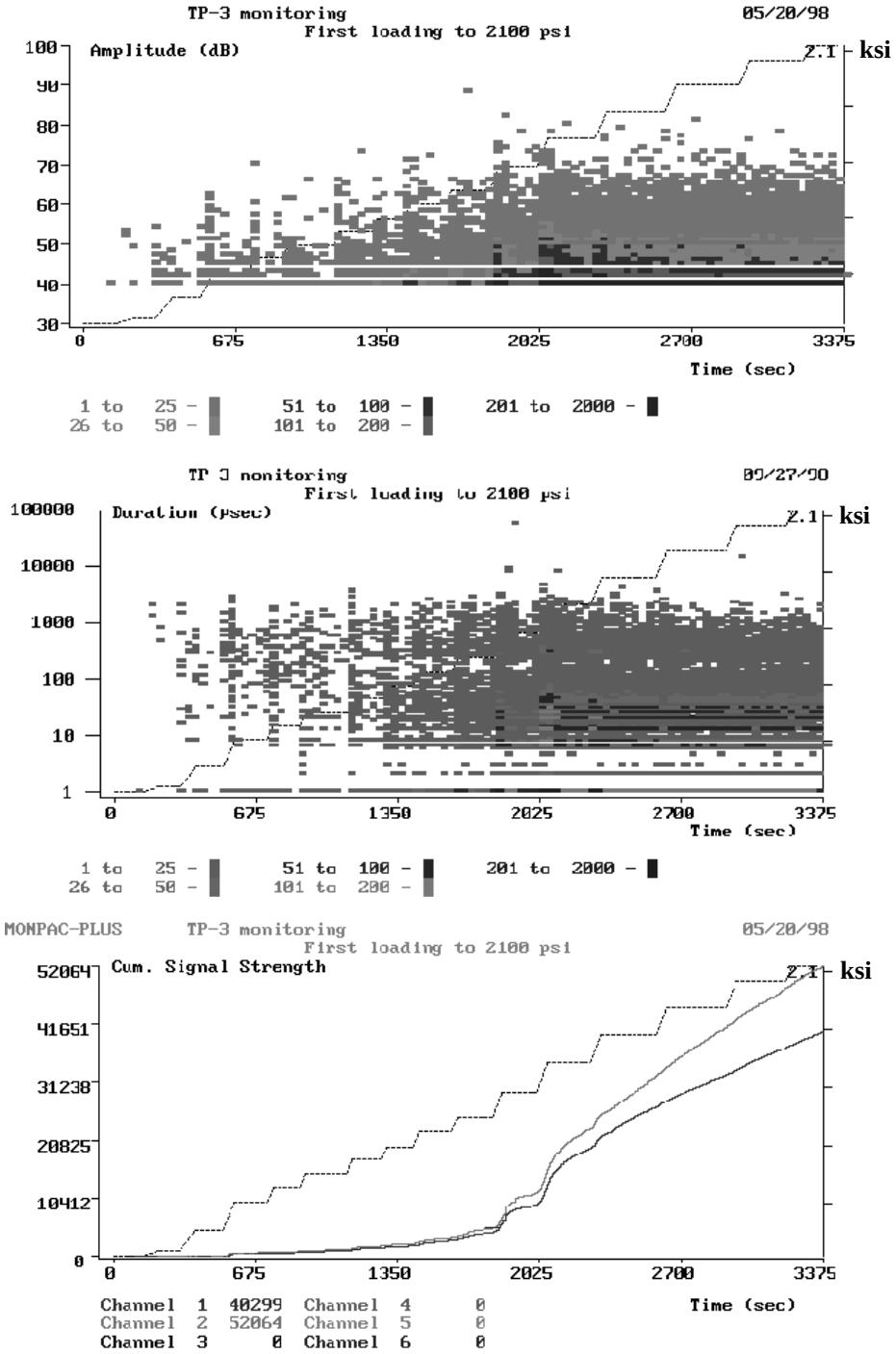

Figure 3.56 AE data recorded for TP-3 First Load

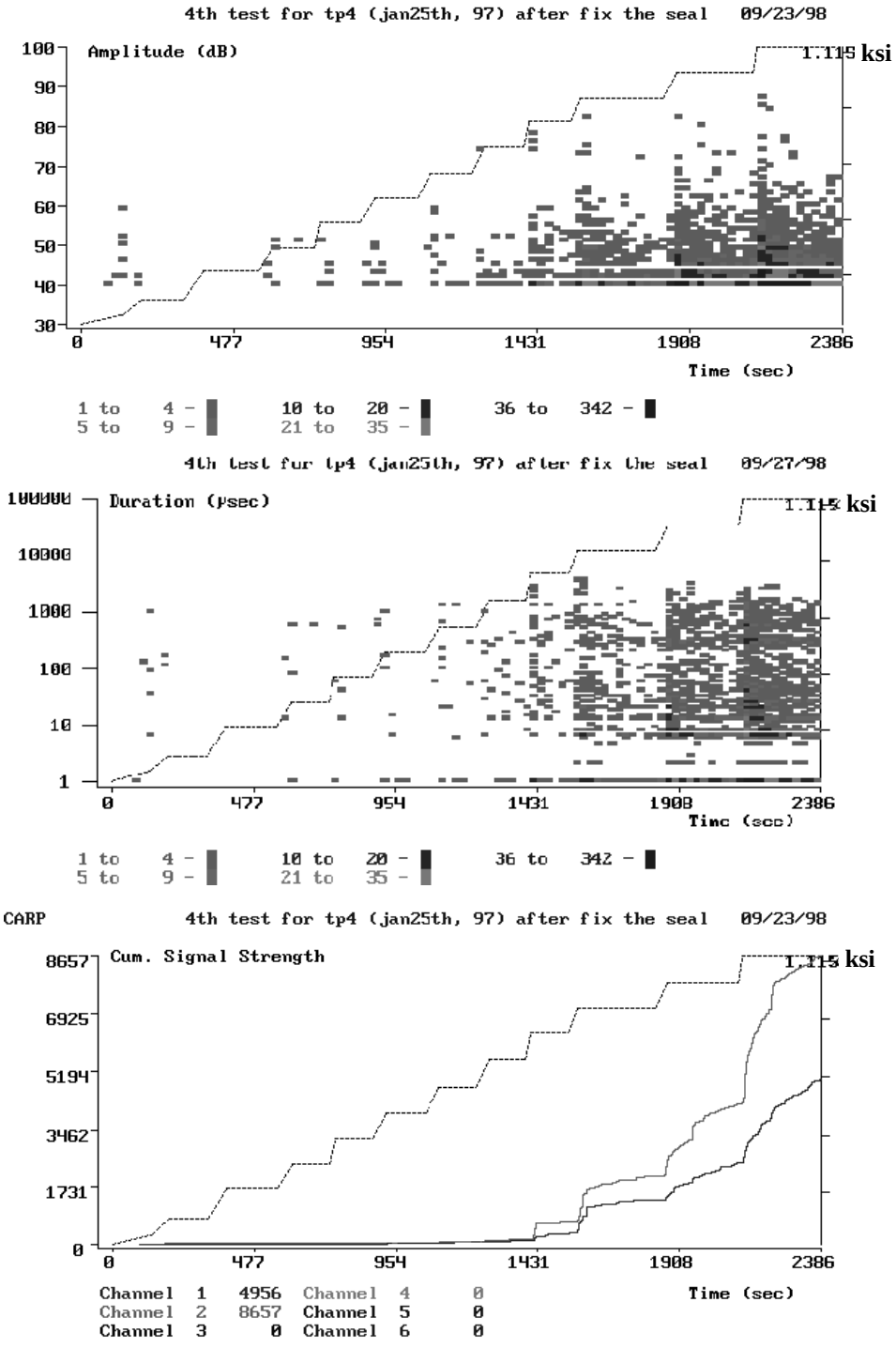

Figure 3.57 AE data recorded for TP-4 First Loading

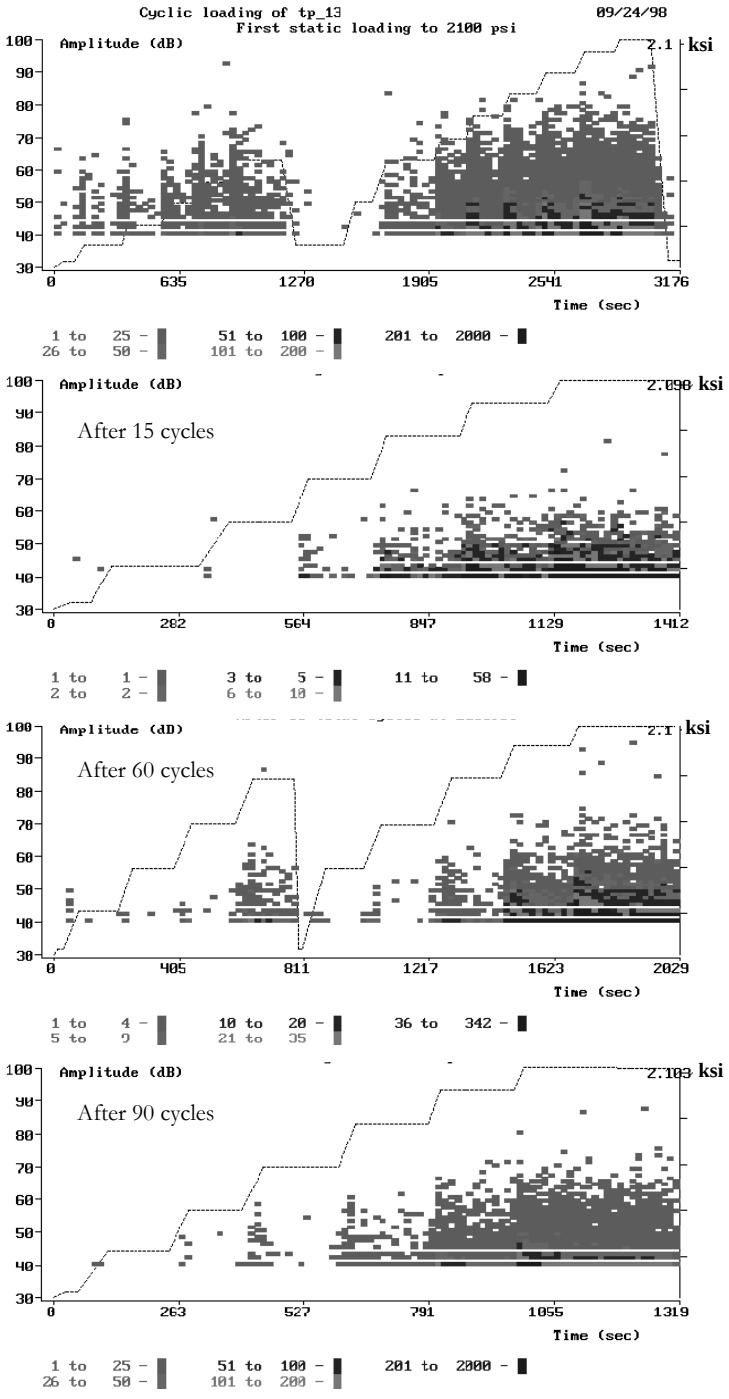

Figure 3.58 Selected AE amplitude data recorded for TP-13

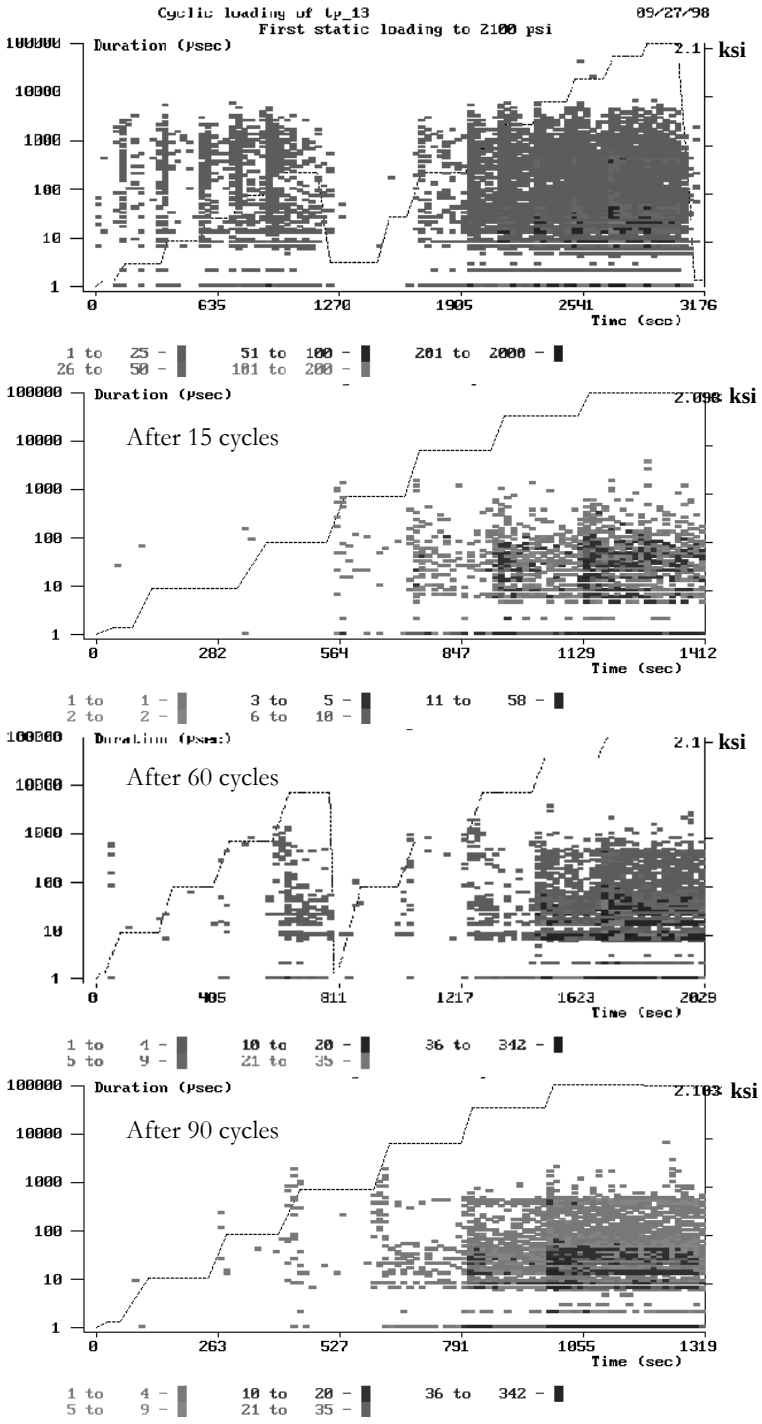

Figure 3.59 Selected AE duration data recorded for TP-13

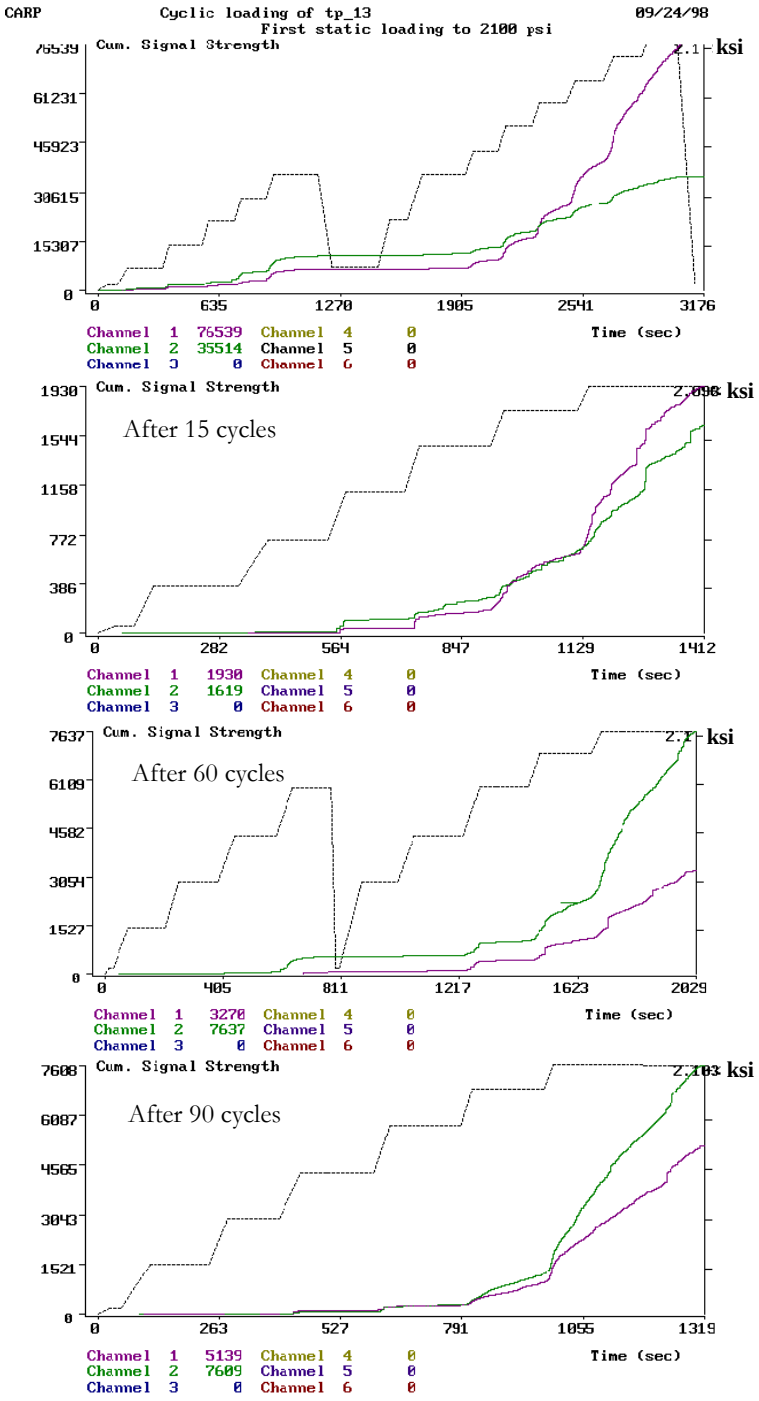

Figure 3.60 Selected AE energy data recorded for TP-13

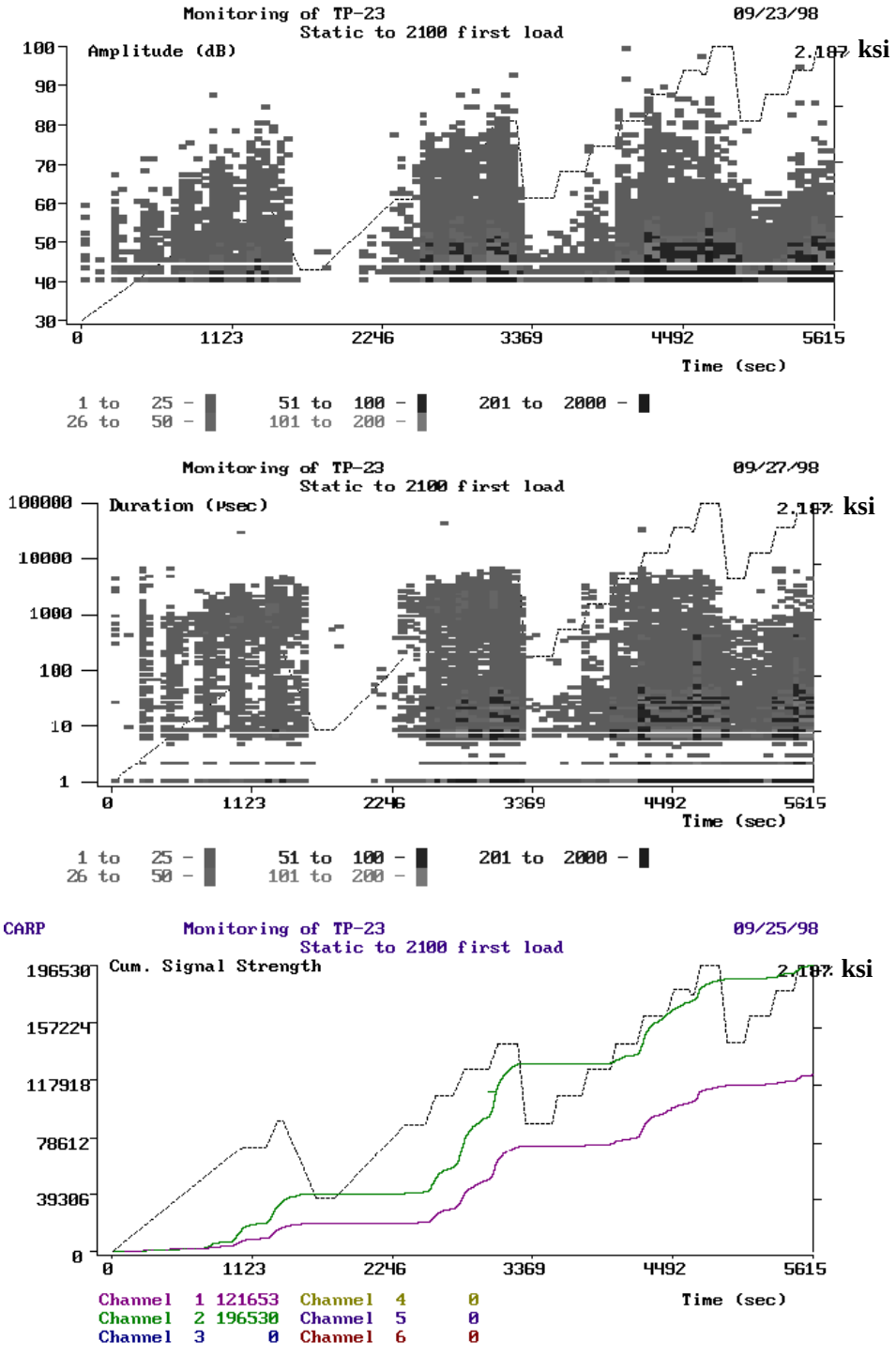

Figure 3.61 AE data recorded for TP-23 First Loading

3.3.2.3. RESULTS FOR CYCLIC TESTS AT 1800-PSI

Figures 3.62 to 3.68 show the records of AE for the specimens tested at this pressure amplitude. A total of three specimens were part of this phase, TP-12, TP-21, and TP-22. This indicates that one specimen from the second batch and two from the third were tested. The difference between the specimens from the two different batches was considerable. Whereas the two specimens from the last batch lasted more than 10,000 cycles each before failure, the single specimen from the second batch failed during the initial static loading at the target pressure. As presented earlier in this chapter, the strain gage information did not show any indications of a large difference in stiffness between the specimens. Hopefully the AE records will help in the interpretation of these results. As with the previous section, the plots in the figures will be separated in groups for amplitude, duration and signal strength where multiple monitoring was done for the same specimen.

Figure 3.62 shows the AE records for the initial and only monitoring for specimen TP-12. The specimen was initially loaded to 600-psi before the resetting of the seal plates generated a loud noise. This kind of event obscures the AE data making interpretation difficult. The specimen was unloaded and the test restarted from 50-psi. Data from this monitoring is not presented here. Nevertheless, emissions were noted from 200-psi at every load step. No emissions, however, were noted during load holds at this stage. From the plots in Figure 3.62 it can be noted that activity began prior to reaching the 600-psi mark previously achieved in the first test. Even when the activity is not dense, it did give an indication of damage accumulation since typically the specimen would not have shown signs of activity until after the previous load had been reached. This is verified by the proportionally high jump in activity observed at pressures slightly higher than 600-psi. As with the other specimens a second significant change was observed at 1100-psi where the slope of the signal energy curve showed positive gradient. The second most visible feature is at the download phase where the AE activity showed signs of significant damage by the Felicity Ratio [3.10]. The previous

pressure before unload had been 1400-psi. When the pressure was increased again, the AE activity was recorded at 1200-psi, which indicated a ratio of 0.85. Other than these indications no other visible changes were noted for TP-12 during the loading stages.

AE data for specimen TP-21 is shown in Figures 3.63 to 3.65. The specimen had a life of 15,000 cycles at a maximum target pressure or 1800-psi. It is very difficult to associate any of the indications or emissions as seen in the plots to the possibility of failure. The only clear association that can be made is to the pressure at which activity begins and the associated Felicity ratio. It is clear in the amplitude plots (Fig. 3.65) that emission during load hold at final monitoring started 200-psi before than in the previous plots for 3,000 and 12,000 cycles. The main feature during initial loading is the significant increase of activity at 1,200-psi, which also happens to be the maximum plotted pressure in the figure. A more detailed analysis will be made in a following section of this chapter.

Finally for this group, specimen TP-22 is shown from Figures 3.66 to 3.68. The cyclic life of this specimen was identical to TP-21. Both specimens were part from the same batch and were in continuous sections in the main pipe that was cut. The behavior of this specimen was similar to that of the previous TP-21. The same trends were observed in all plots as they related to Felicity ratio and distribution of amplitudes. No other indications are apparent in the records, the general tendency during cycling is to quiet down and maintain a gradual increase in activity as the target pressure is approached.

No further observations will be made until after the specimens at lower pressure amplitudes are presented for comparison purpose.

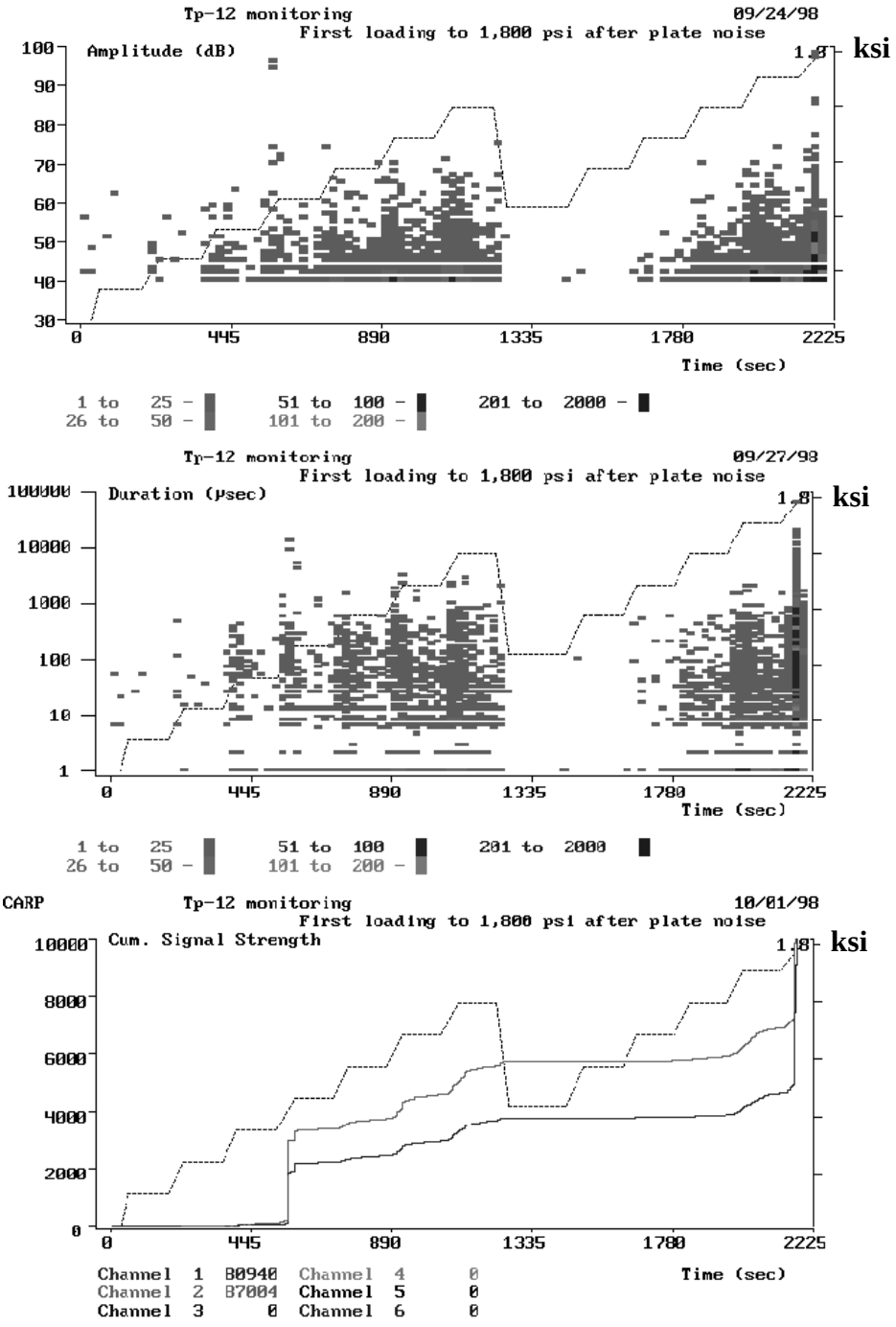

Figure 3.62 AE data recorded for TP-12 First Loading

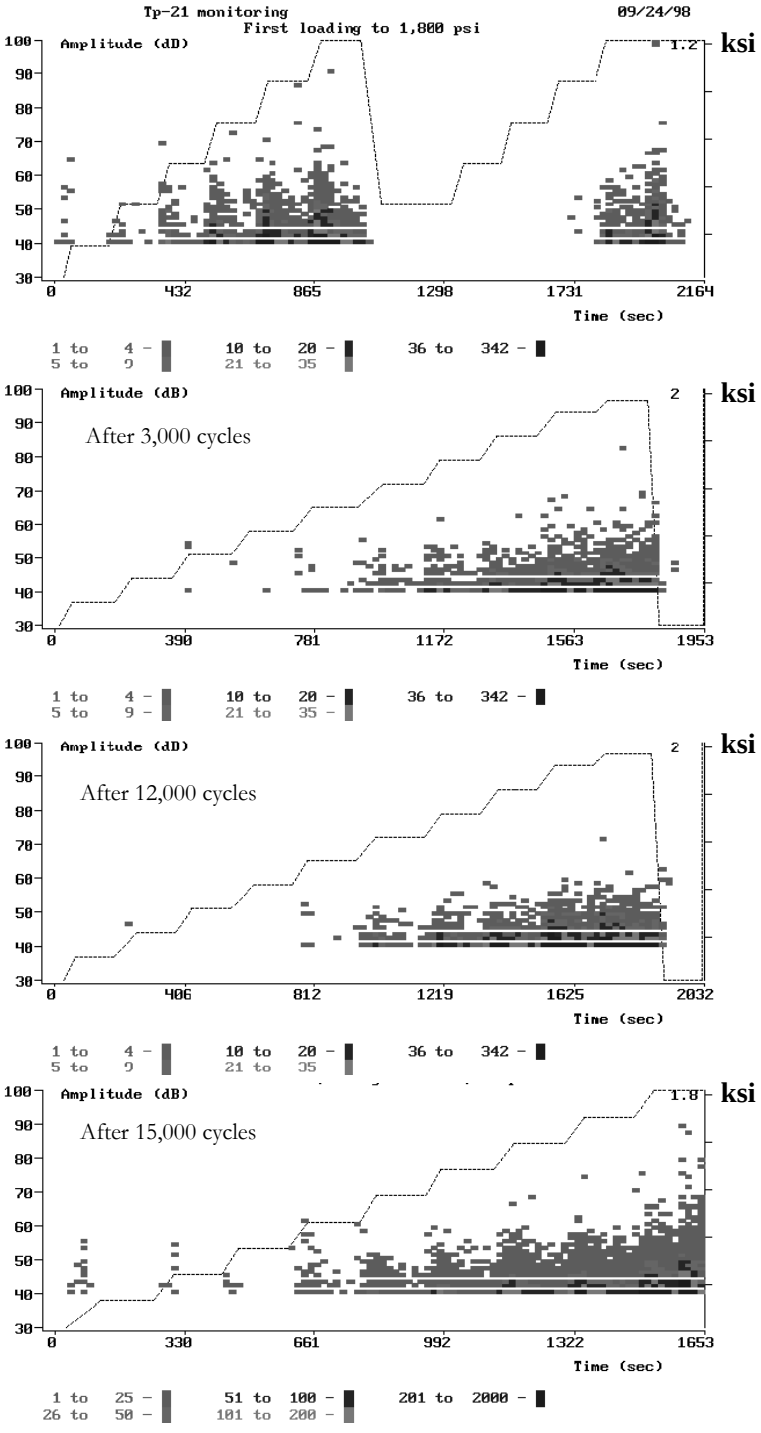

Figure 3.63 Selected AE amplitude data recorded for TP-21

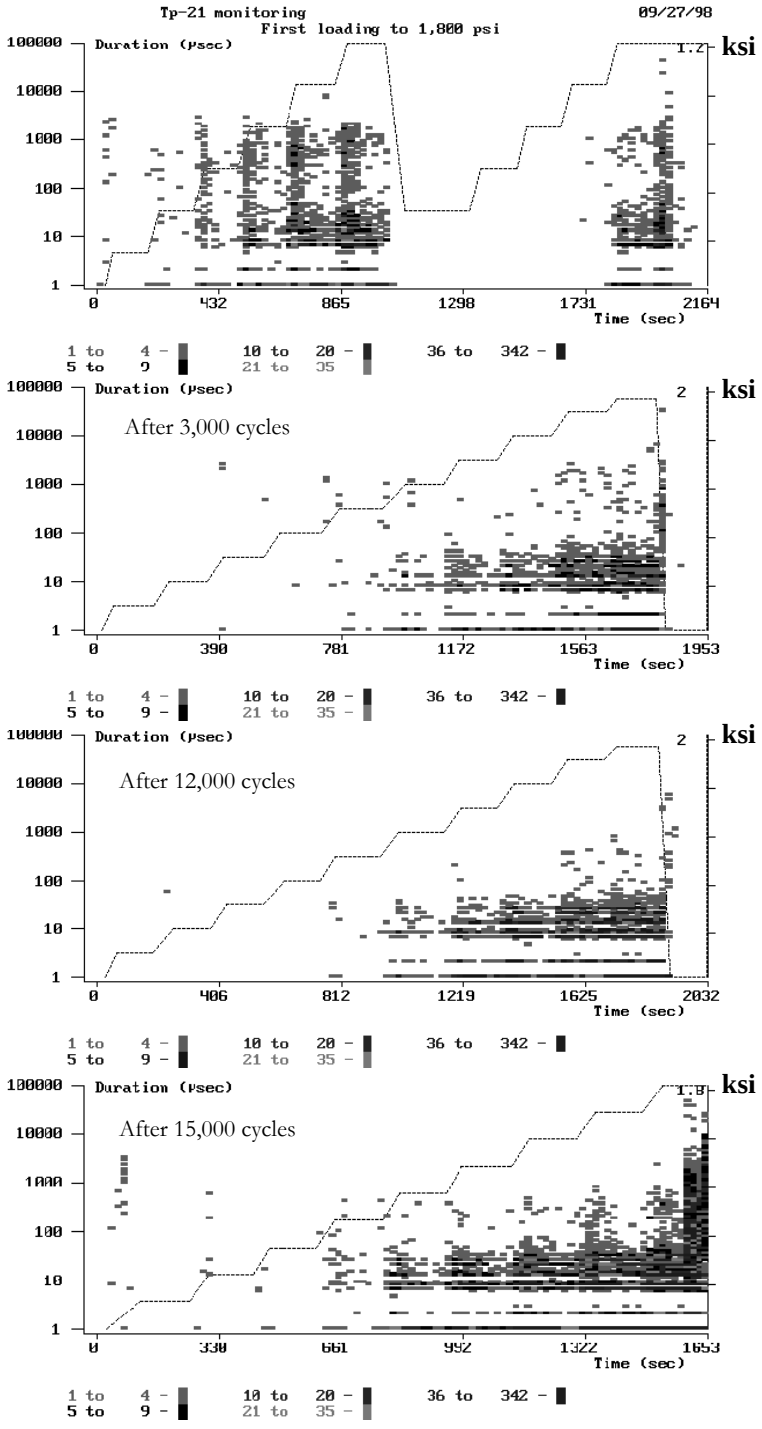

Figure 3.64 Selected AE duration data recorded for TP-21

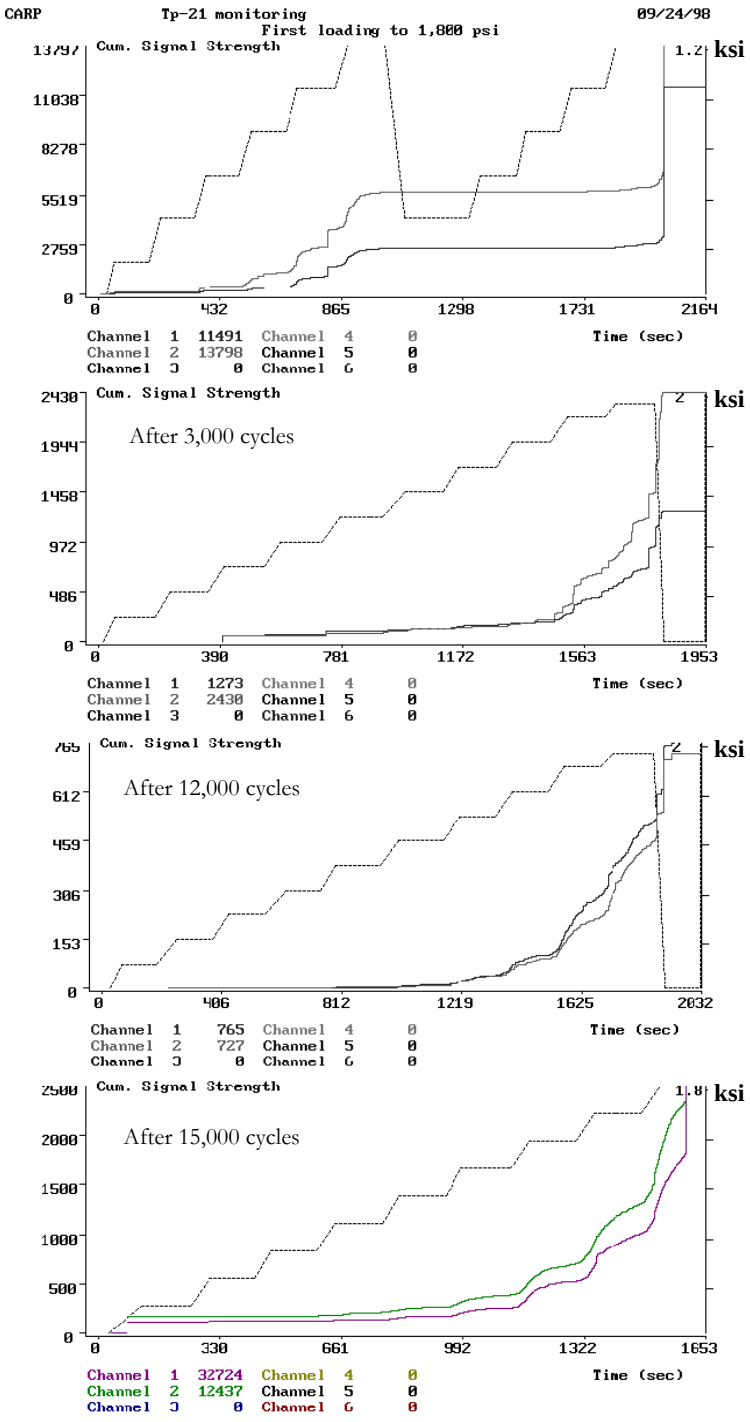

Figure 3.65 Selected AE signal strength data recorded for TP-21

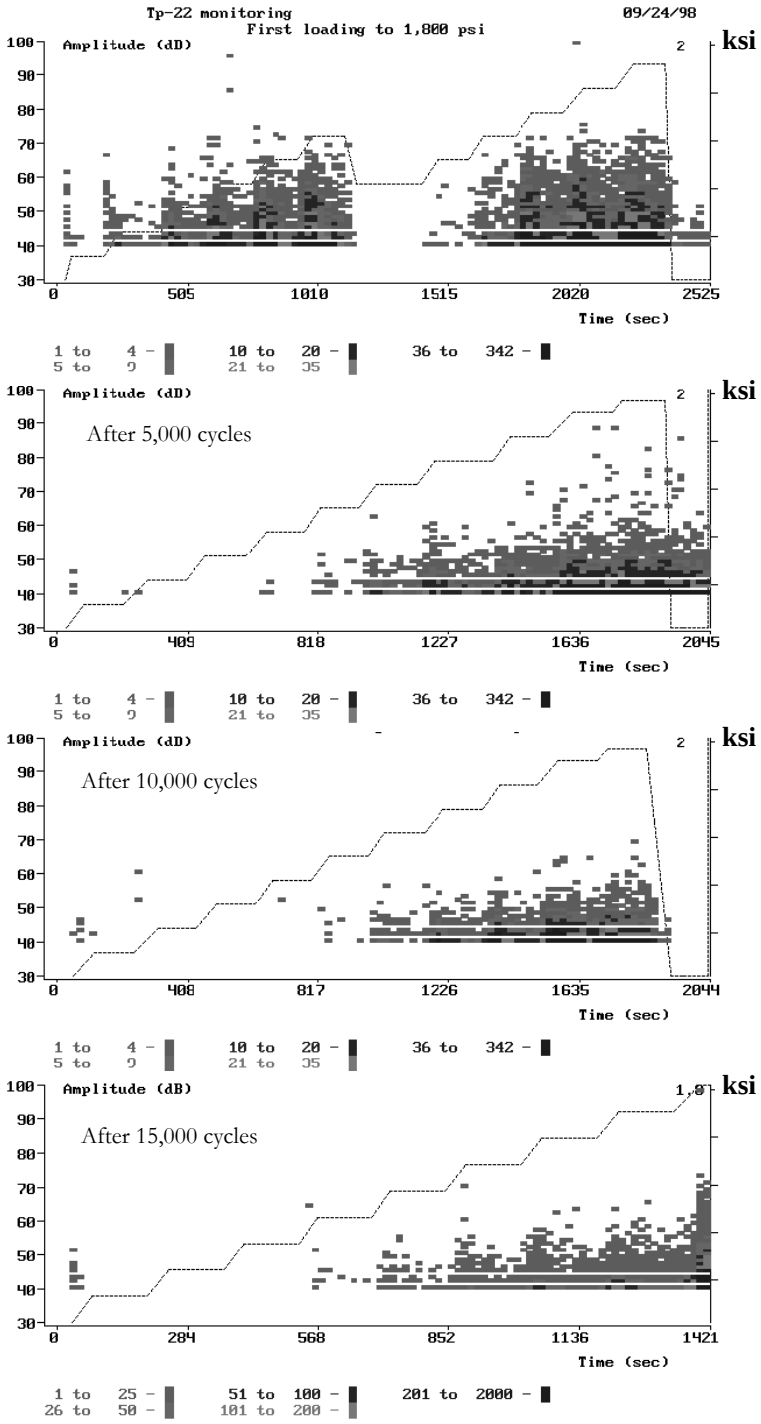

Figure 3.66 Selected AE amplitude data recorded for TP-22

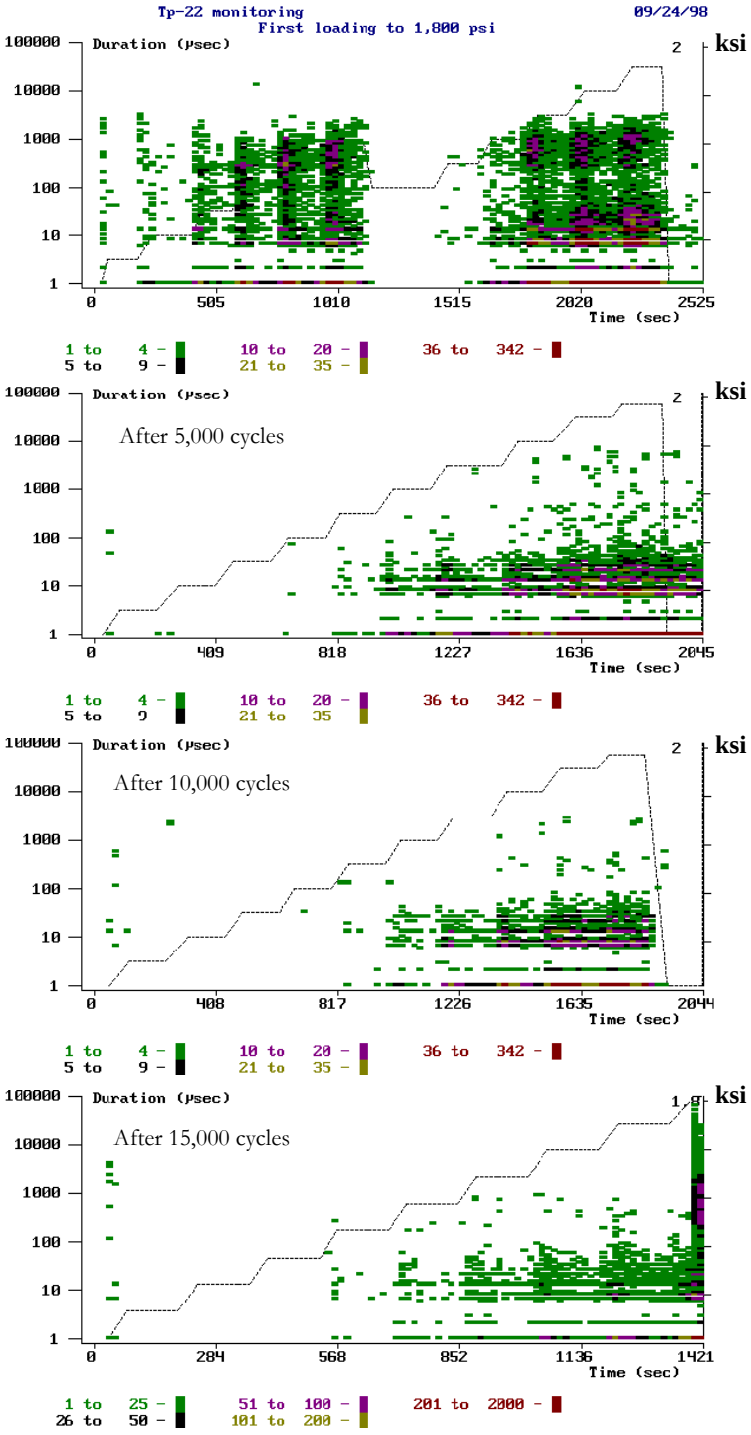

Figure 3.67 Selected AE duration data recorded for TP-22

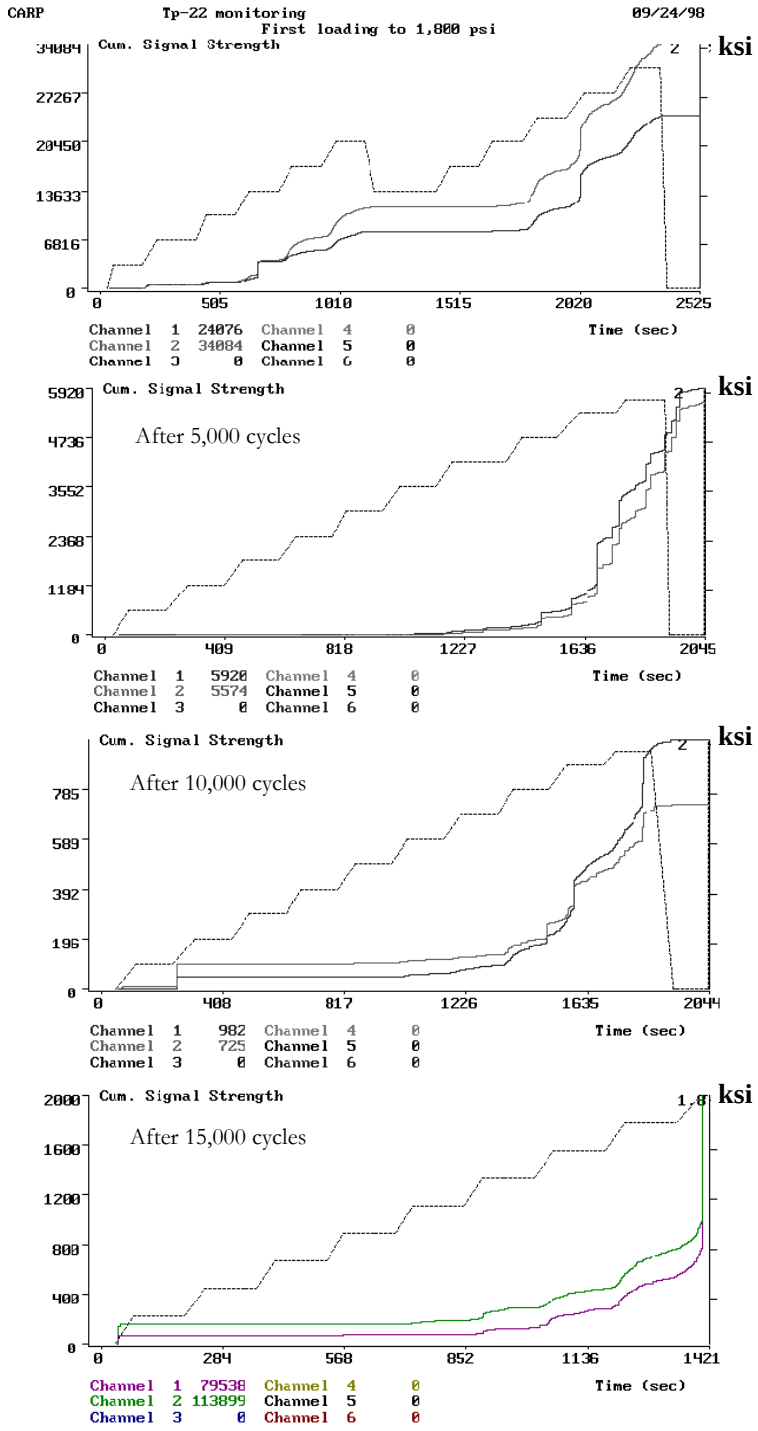

Figure 3.68 Selected AE signal strength data records for TP-22

3.3.2.4. RESULTS FOR CYCLIC TESTS AT 1600-PSI

This group consisted of five specimens tested to a target pressure of 1600-psi. The cyclic life of these specimens showed a large variation. Specimens from all three batches were tested at this range, and showed no specific trends related to the batch itself. It should be noted that there were wide differences recorded in tolerances and quality each batch. The specimens that were part of this group were TP-1, TP-6, TP-9, TP-14 and TP-19. Unfortunately, no AE information is available for specimen TP-1; therefore no discussion will be presented here.

Figures 3.69 to 3.71 show records for specimen TP-6 in terms of amplitude, duration and signal strength. The life of TP-6 was 10,000 cycles at a target pressure of 1,600-psi. Failure took place during the 100-psi overload applied to all the specimens in the AE monitoring phase. These records do show differences in the AE behavior of the specimen between life cycles. In the amplitude plots in Figure 3.69 a clear sign of activity in the lower pressure stages is visible at the final cycle in the life. This is compared to the limited activity noted at 1500 cycles. In addition the Felicity ratio in the emissions has clearly dropped from the behavior noted in the initial loading where emissions during load hold were noted at 400-psi, and significant increase in emission noted at 800-psi. The duration plots shown in Figure 3.70 also show this change in behavior between the intermediate AE monitoring and the one at the final cycle. A clear distribution of several different duration hits is noted at the final cycle at low pressures. In contrast, during the intermediate loading only isolated duration events were noted. The signal strength plots in Figure 3.71 show that the change in slope in the curve did not take place until after 1000-psi, although there was activity noted at the lower pressure as stated before.

Figure 3.72 and 3.73 relate to emissions from specimen TP-9. Specimen TP-9 failed after only 80 cycles at the target pressure of 1600-psi. This was one of the few cyclic specimens tested in the air driven water system. The fact that it had such a short

cyclic life may indicate that the rate of loading in this case may have had some effect in this group.

For TP-9 AE activity was noted starting at 200-psi with the first clear signs of emission during load hold detected at 600-psi. Two separate load tests were made in the specimen at the beginning of the cycling. The first one at 1200-psi and the following to the target pressure of 1600-psi. In the first test, it is very clear that after reaching 1200-psi and unloading, no significant emissions were detected during the following load increases up to 800-psi. On the second loading however, we can see that significant damage was generated in the first loading since emissions were detected at a pressure below 1000-psi which is less than the previous load of 1200-psi. Coincidentally, it was the pressure of 1200-psi that appears to have the largest influence in the change of gradient in the signal strength plot.

Figure 3.74 show the records for specimen TP-14 in the first loading. The specimen had a life of 11 cycles at target pressure of 1600-psi. This specimen as TP-9 failed during the load up step in the last cycle. No AE record other than the initial loading was taken. The feature that immediately comes to attention is the activity at the beginning of the test. It is difficult, by just looking at the plots here, to define at which level the emissions during load hold became significant. It would appear they took place between 600 and 800-psi. Also, the first load curve was stopped at 1000-psi and the second load increase phase did not show signs of significant Felicity ratio drop.

Figures 3.75 to 3.77 show the AE information for specimen TP-19. This specimen failed after 7,500 cycles at the target pressure. Like specimen TP-6, it also failed at the overload stage in the static monitoring for AE. Looking at the information obtained during the AE monitoring, it is notable how there were no signs of impending failure during the final monitoring. The specimen was unusually quiet during the loading process. This is contrary to what is usually expected with AE monitoring as failure is near. It will be interesting to compare this behavior with the recorded strains during the test. The lack of activity indicates no damage growth detected by the AE

throughout the test up to the final pressure where the main longitudinal crack in the liner formed. This would support the statement made before in the chapter that extensive damage had already been generated in the winding by the time the liner had failed. Therefore if the liner did not exist in this specimen, it would have likely leaked before the final registered cycle.

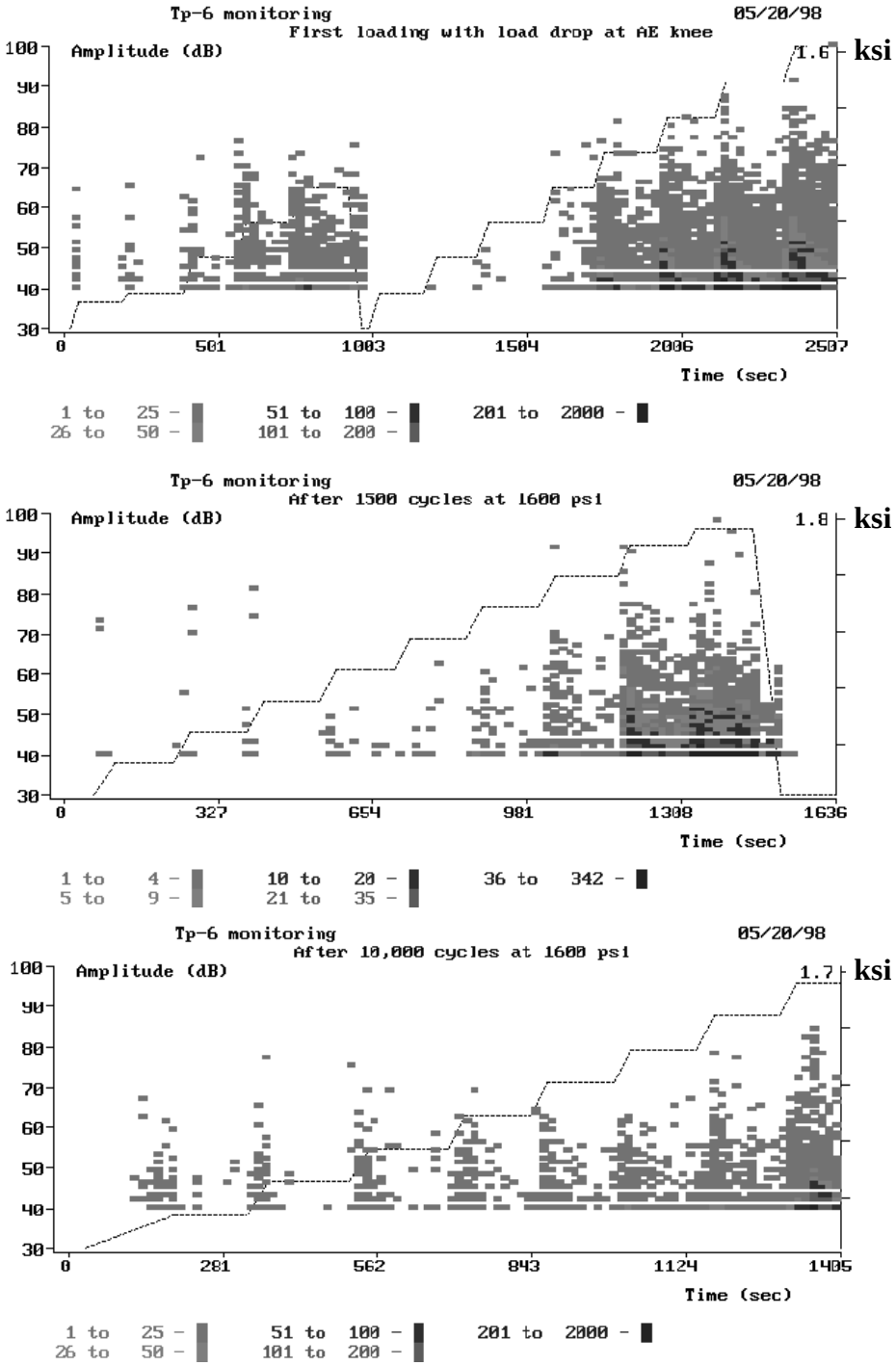

Figure 3.69 Selected AE amplitude data records for TP-6

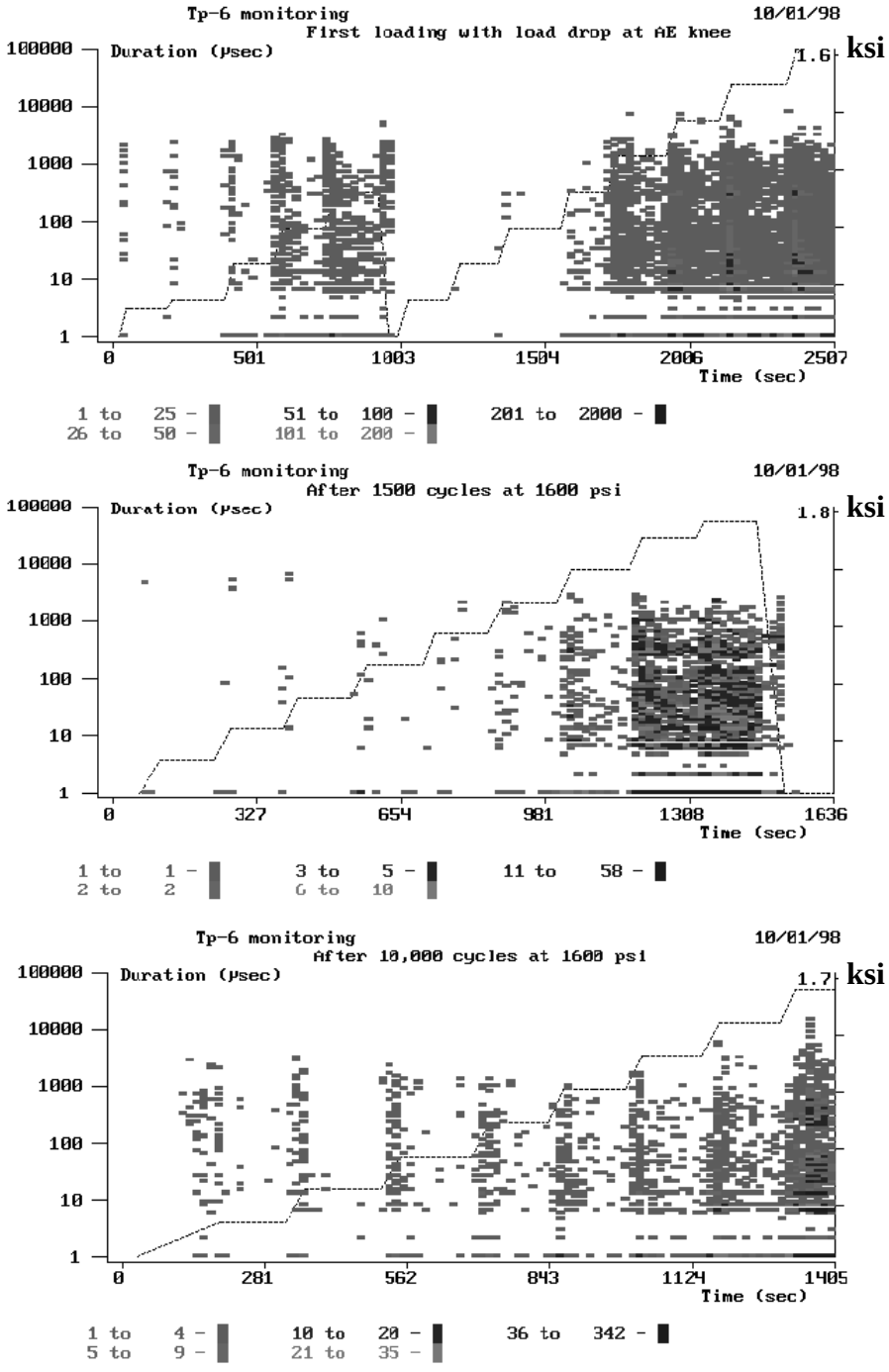

Figure 3.70 Selected AE duration data records for TP-6

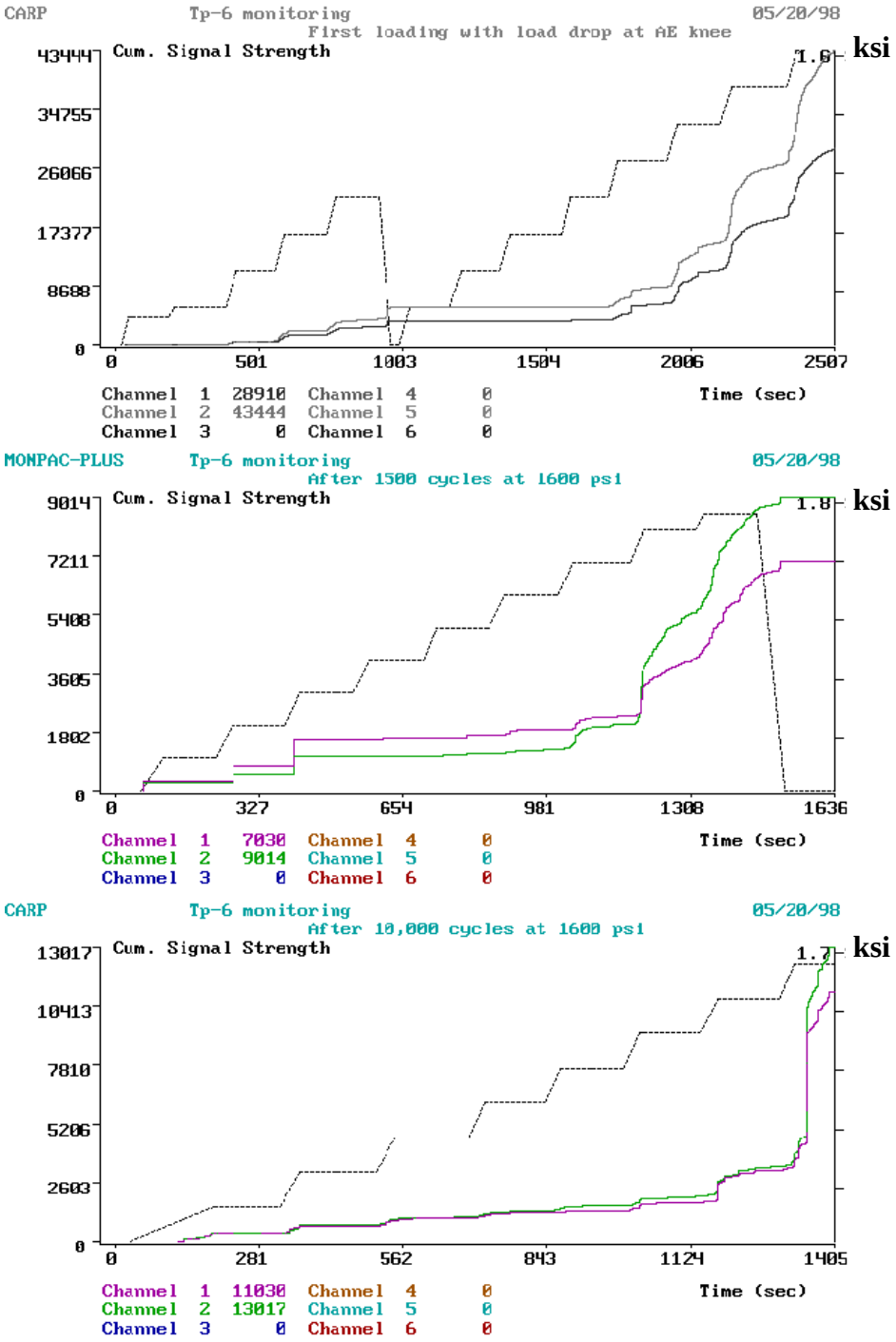

Figure 3.71 Selected AE signal strength data records for TP-6

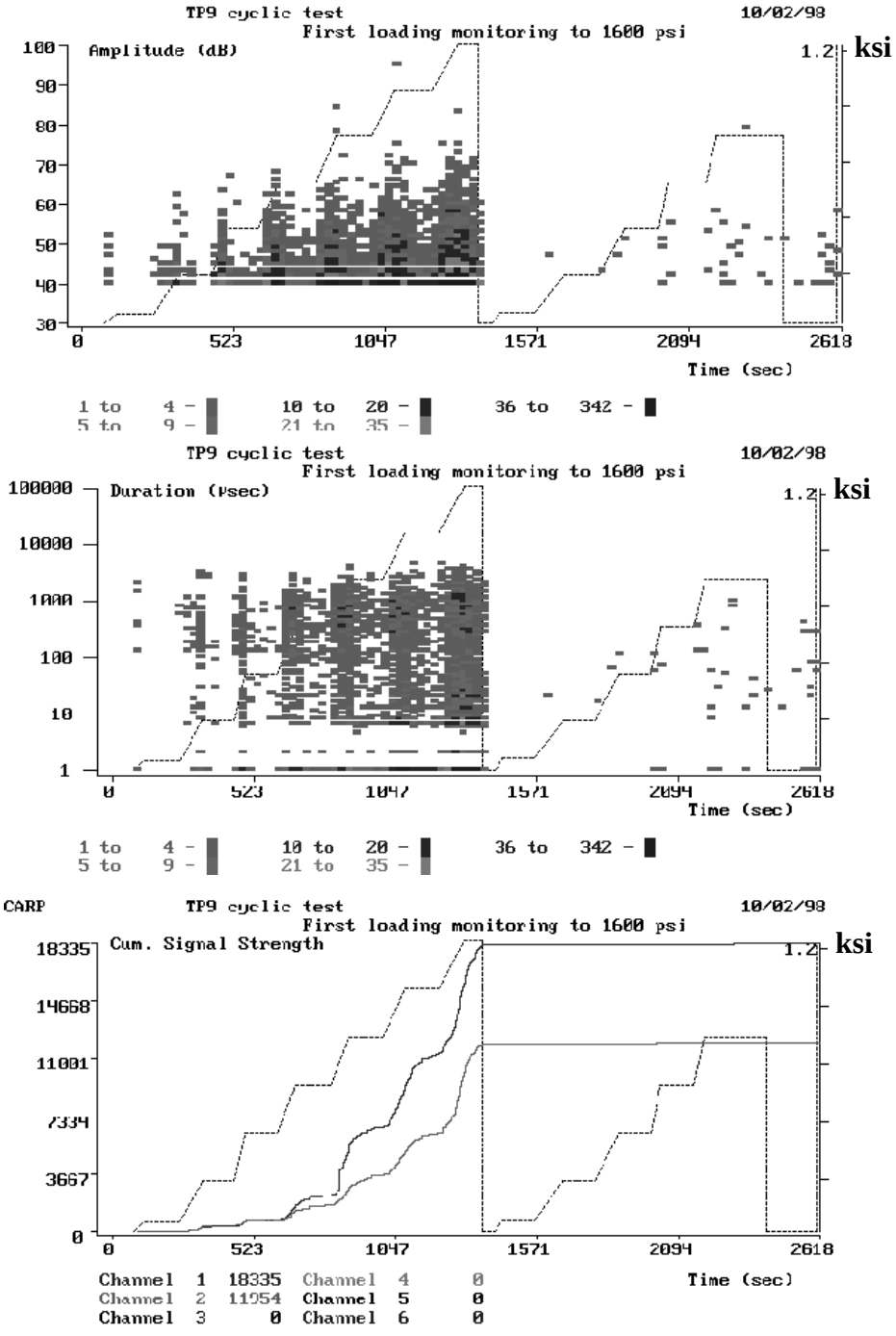

Figure 3.72 AE data records for TP-9 First Load to 1200-psi

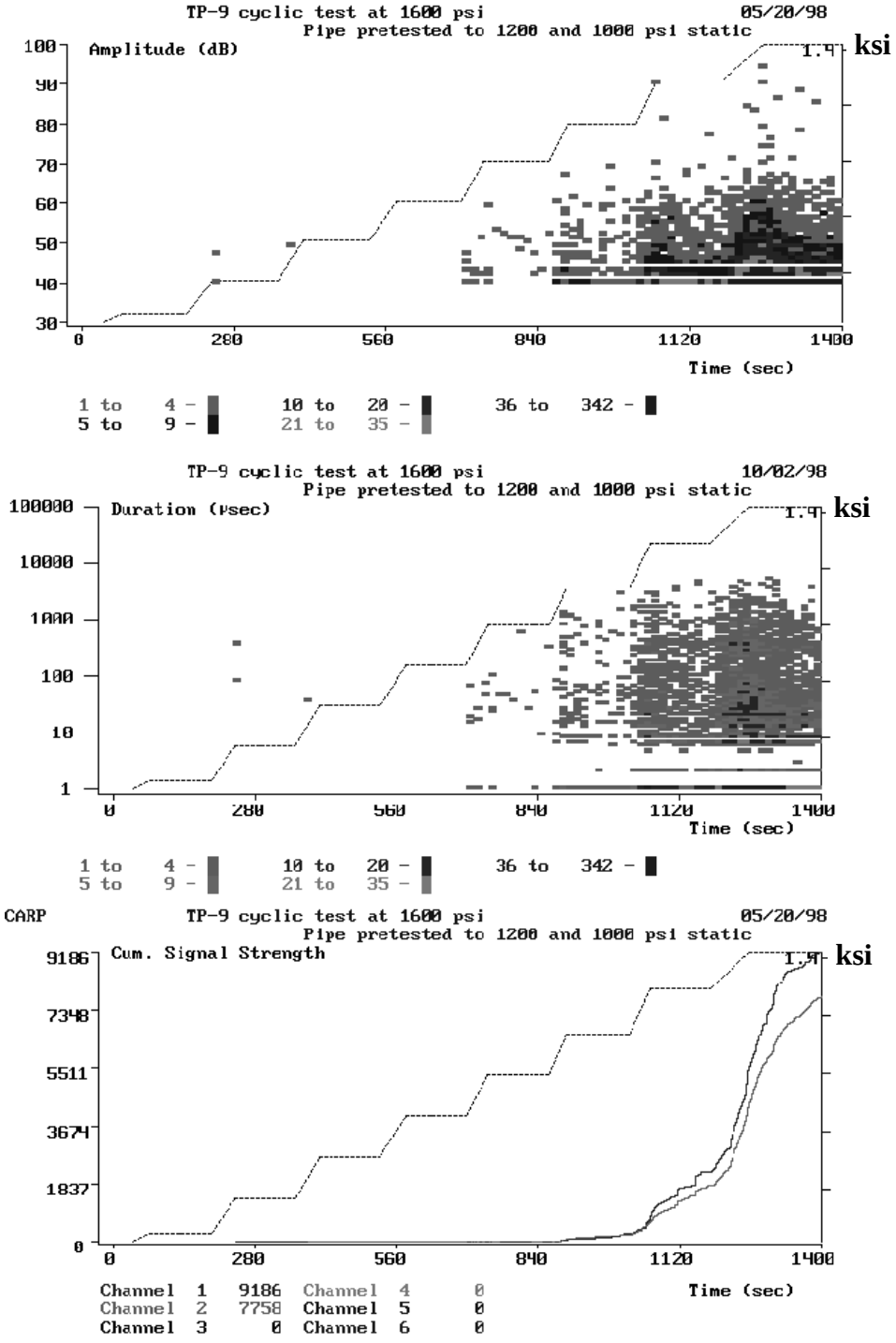

Figure 3.73 AE data recorded for TP-9 Second Loading

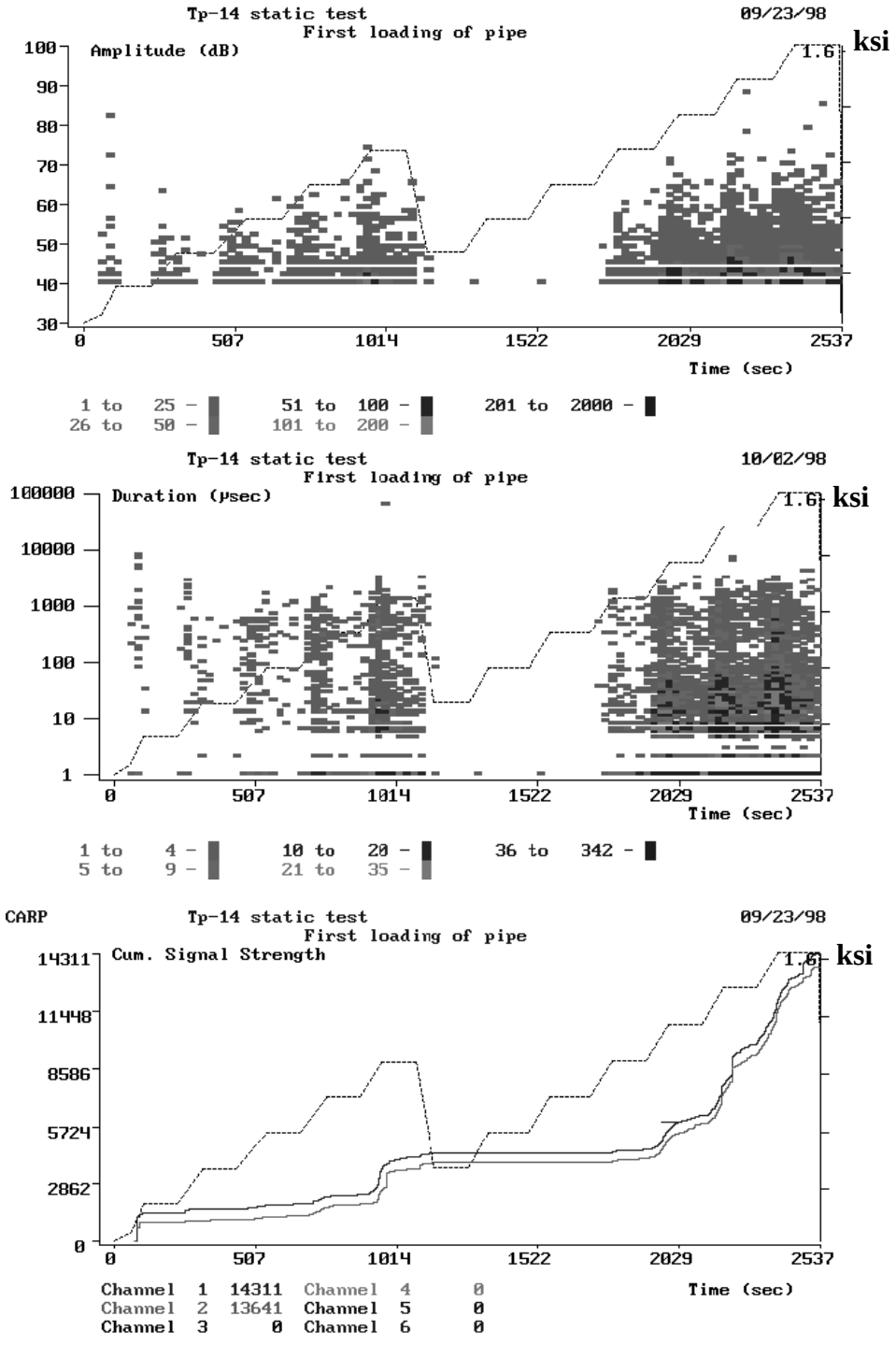

Figure 3.74 AE data recorded for TP-14 First Loading

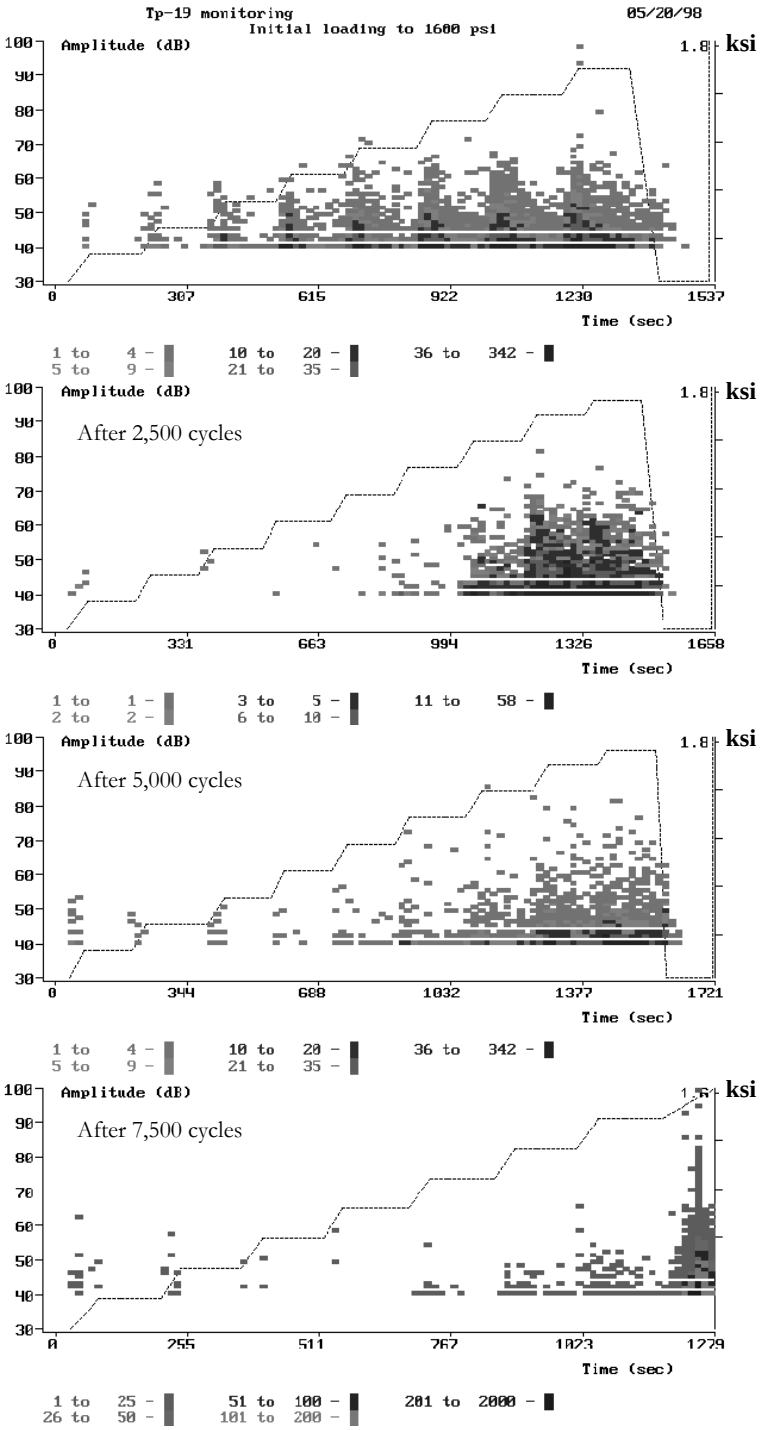

Figure 3.75 Selected AE amplitude data recorded for TP-19

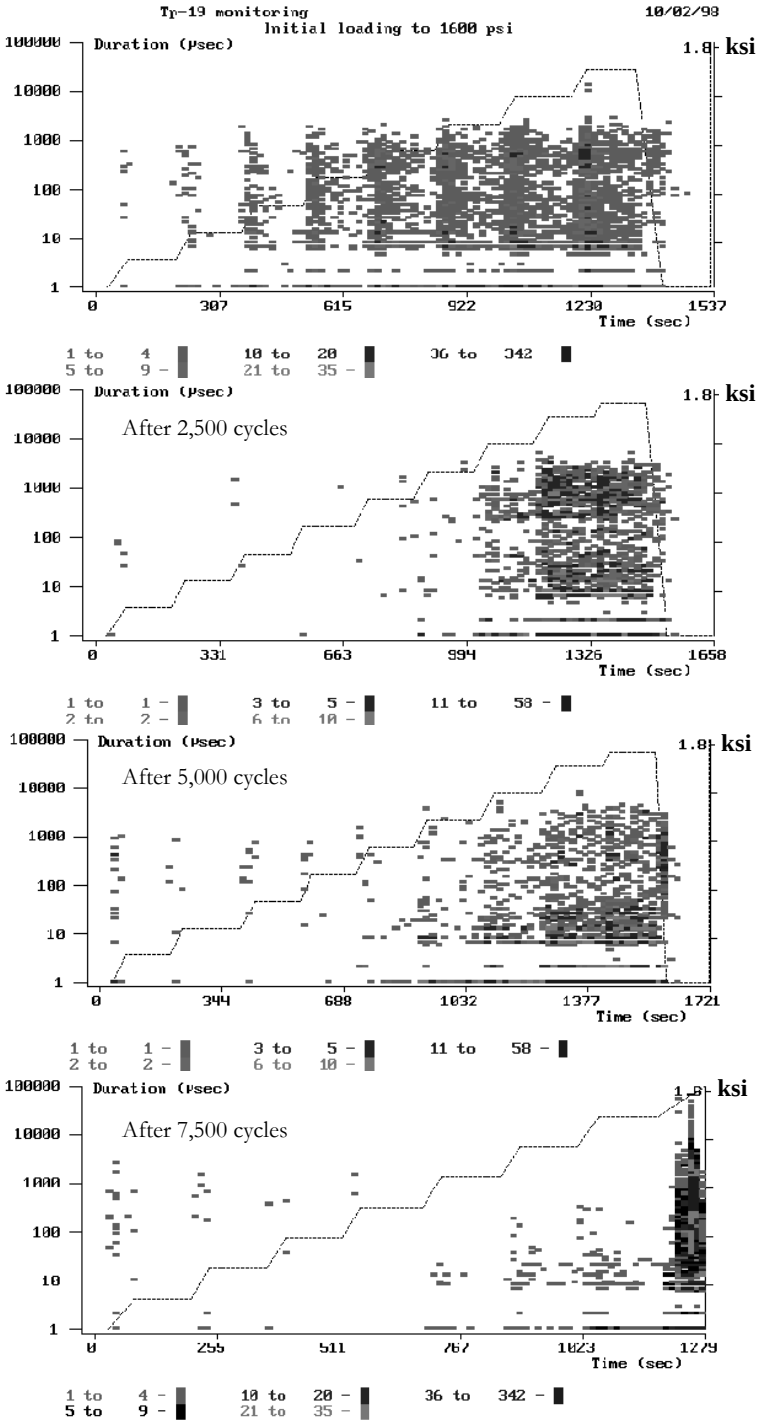

Figure 3.76 Selected AE duration data records for TP-19

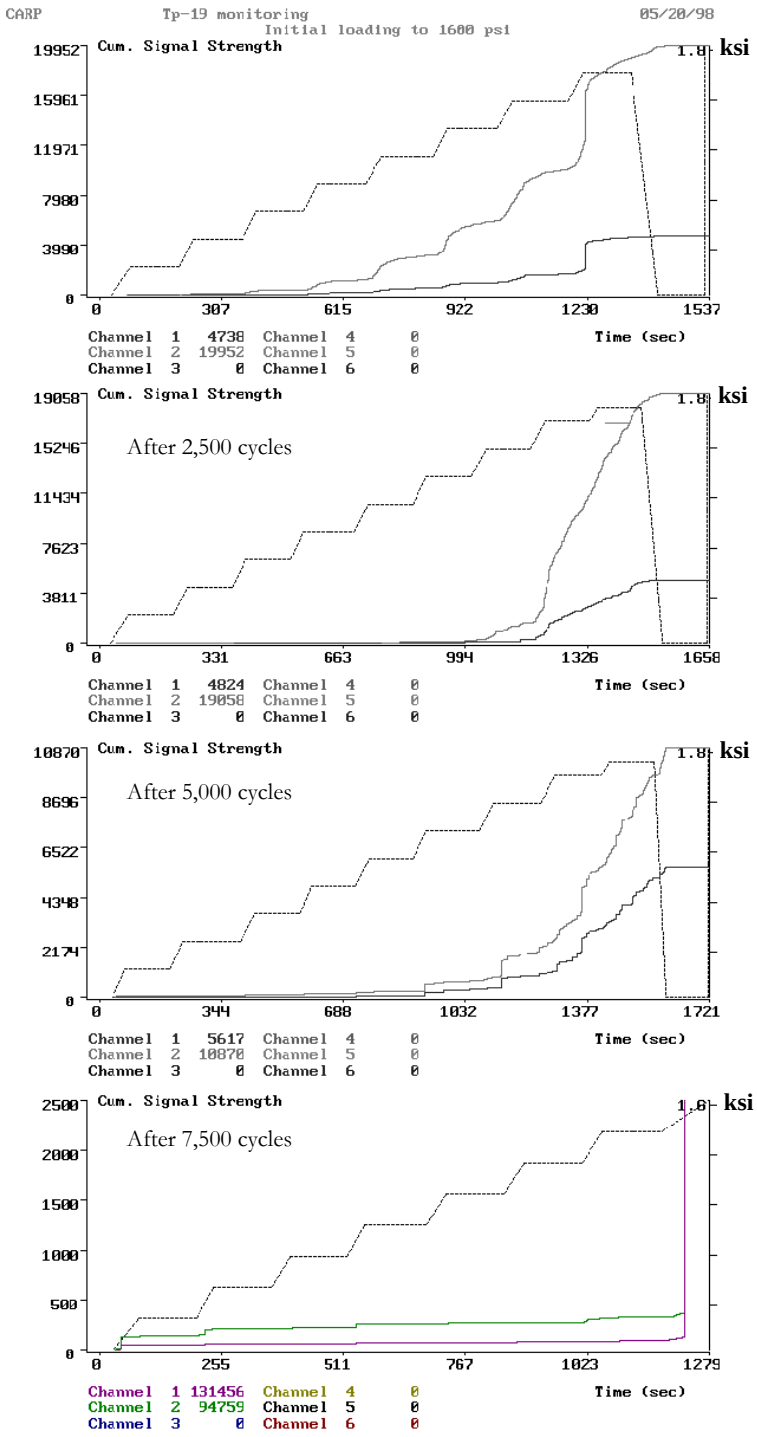

Figure 3.77 Selected AE signal strength data records for TP-19

3.3.2.5. RESULTS FOR CYCLIC TESTS AT 1400-PSI

Specimens TP-10, TP-17 and TP-21 were cycled at 1400-psi. Figures 3.78 to 3.86 show the recorded acoustic emission information for this group. This was the first group in which some consistency was noted in the results. All three of the specimens failed between 100,000 and 200,000 cycles. One specimen from the second batch and two from the third one were tested. A difference in the behavior associated with the batch was noted in the results. Both pipes from the third batch failed within 5 % of each other, while the specimen from the second batch had about a 30 % lower life. Failure was during the overloads while performing the AE monitoring, as was the case of the previous group.

The first group of figures is for specimen TP-10, which had a life of 125,000 cycles. The monitoring made at 50,000 cycles was obscured by a loud noise that generated AE records resulting from the seal plates resetting at about 1250-psi. This plate adjustment generated a number of events that can be seen as a concentrated line of points in both the amplitude and duration plots. In addition, the plot in the signal strength group shows a large jump at this time. If this event were eliminated from the plots, then a very low quantity of emissions would be noted at this time. All three plots show a tendency towards a distributed and low quantity of emissions. As was the case for the 1600-psi group, there is no clear indication during the final monitoring that failure was about to take place. If anything, the specimen did not seem to have any significant emission during the last monitoring up to the time of failure. From the first monitoring, however, the feature of interest was the point, at which emission during load hold became apparent, which was 1000-psi. A last interesting point is the detection of high amplitude hits during the load hold at the target pressure. This same phenomenon took place in all the specimens in this group. For easy reference they have been highlighted in the figures.

Specimens TP-17 and TP-24 showed the same general trends as TP-10. The pressure level at which emission during load hold became significant enough to affect

the slope of the curve was about 1100-psi for both specimens. No other clear signs were noted from the raw data. If anything, it appears that a high number of cycles will reduce the number of AE events on the material.

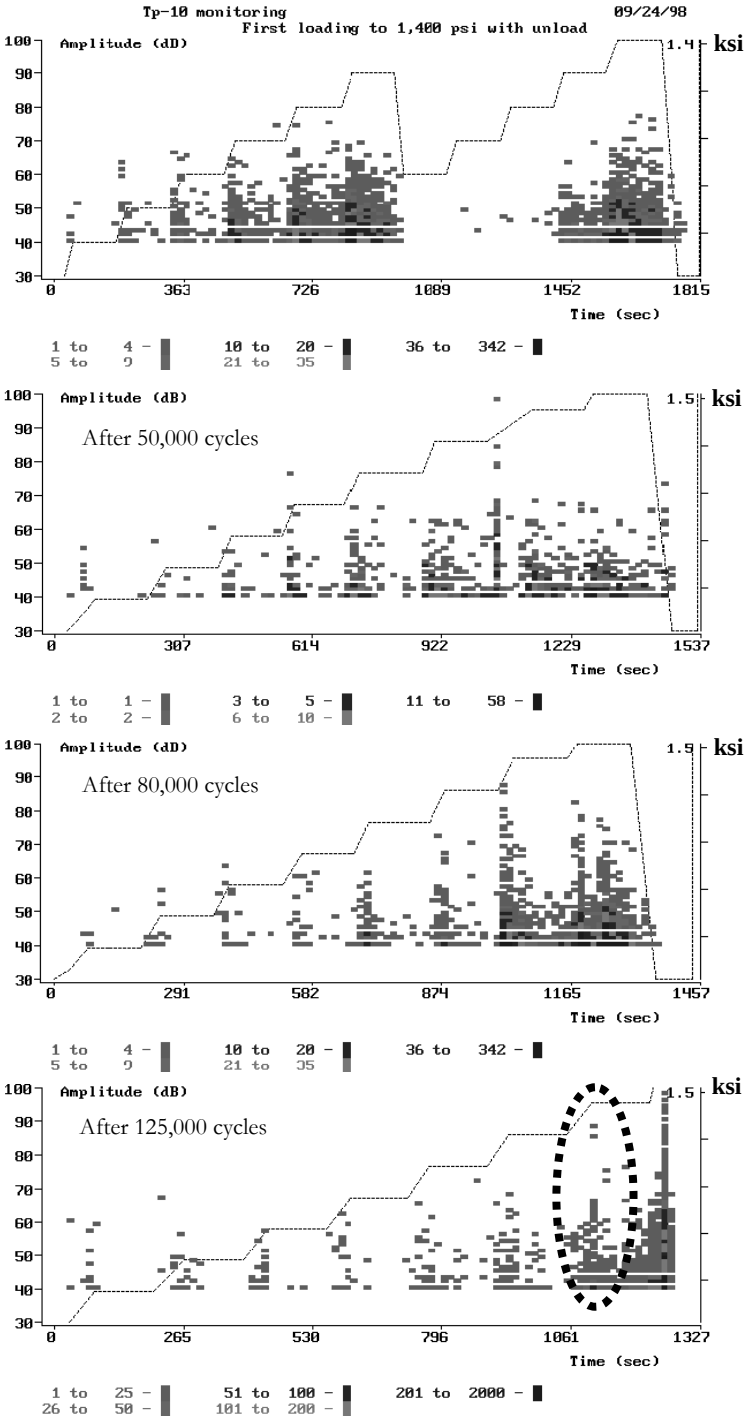

Figure 3.78 Selected AE amplitude data records TP-10

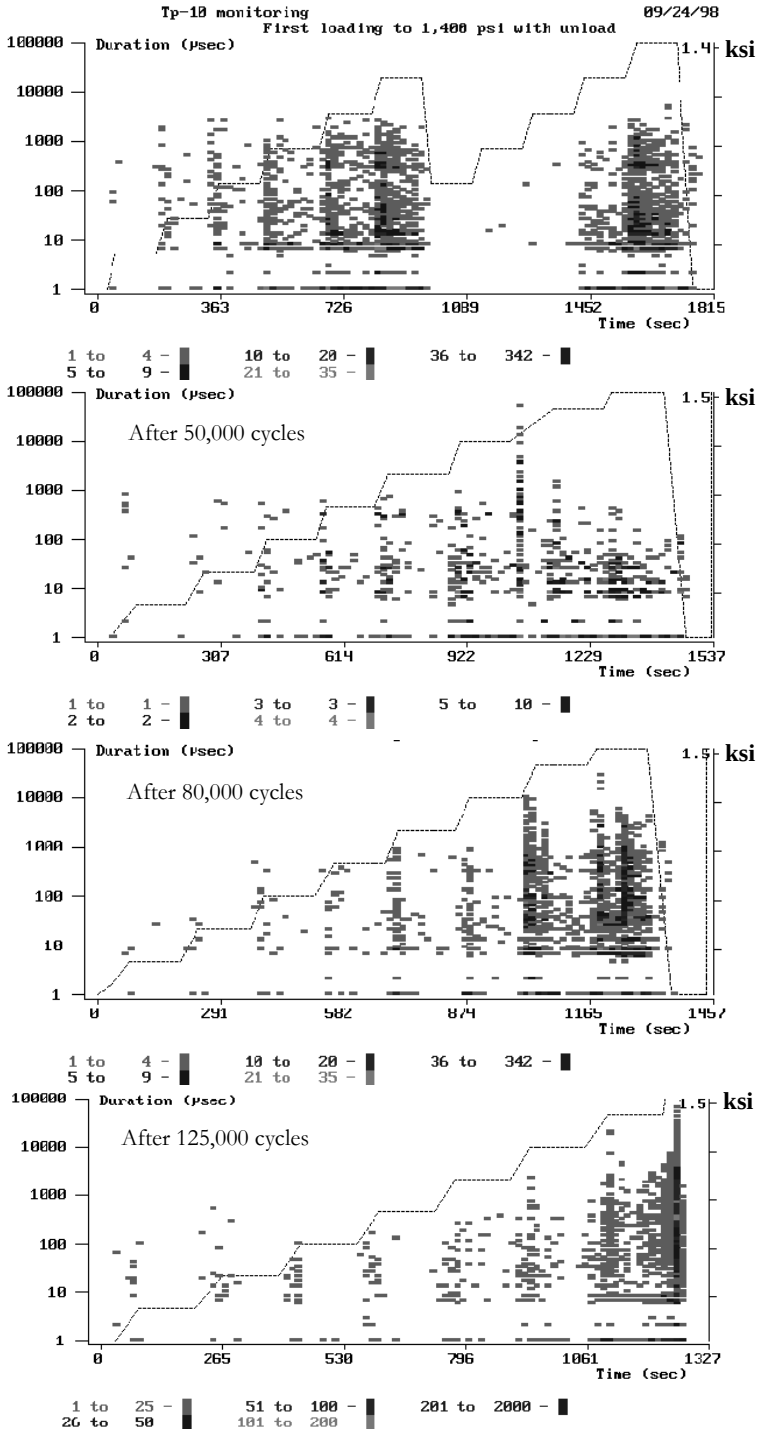

Figure 3.79 Selected AE duration data records for TP-10

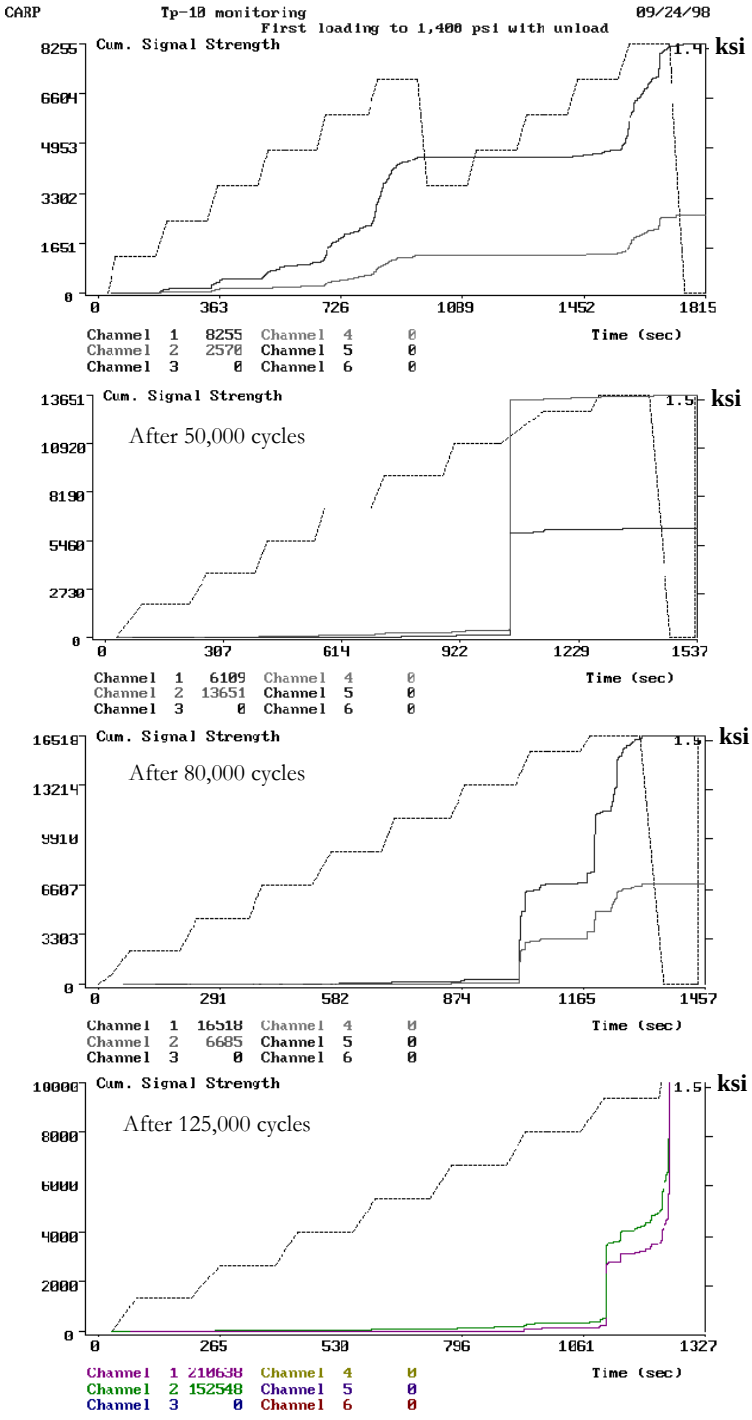

Figure 3.80 Selected AE signal strength data recorded for TP-10

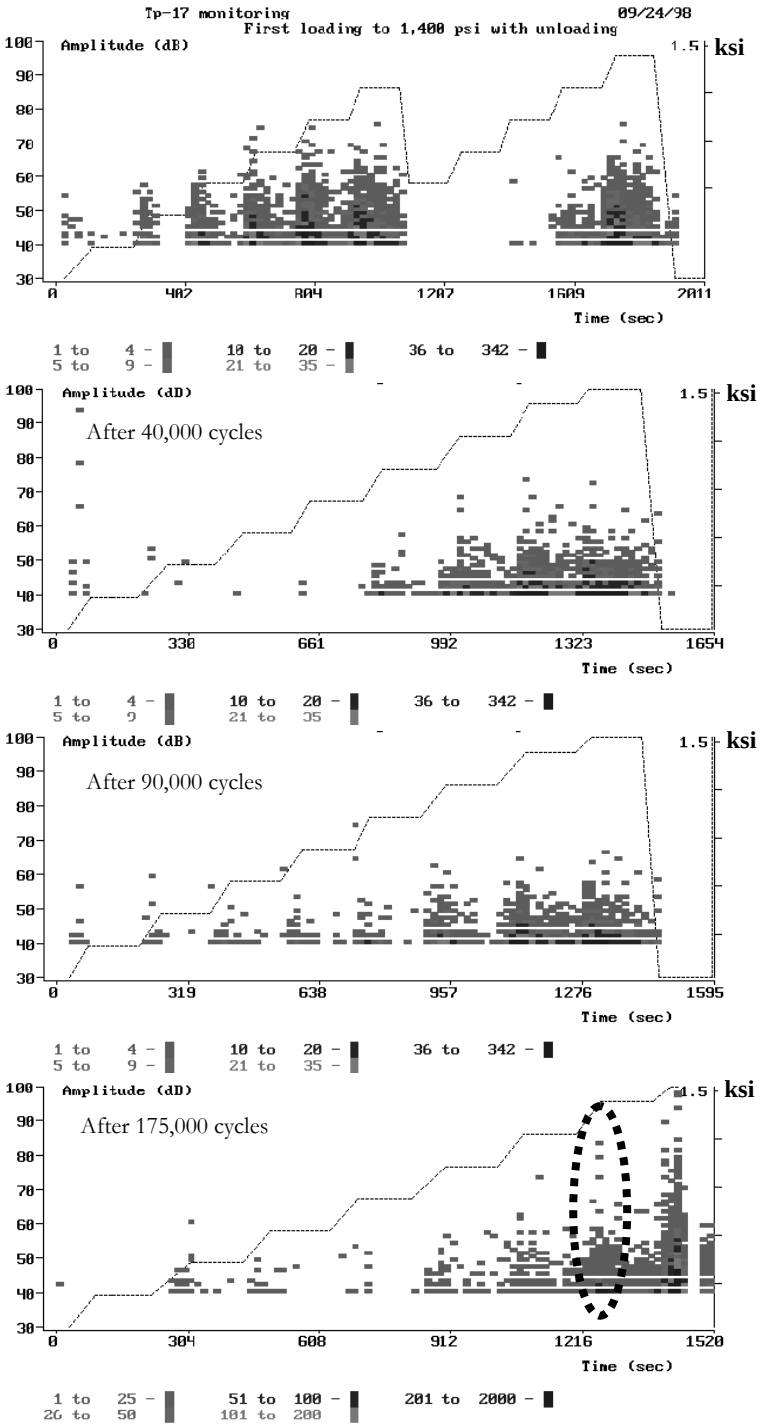

Figure 3.81 Selected AE amplitude data records for TP-17

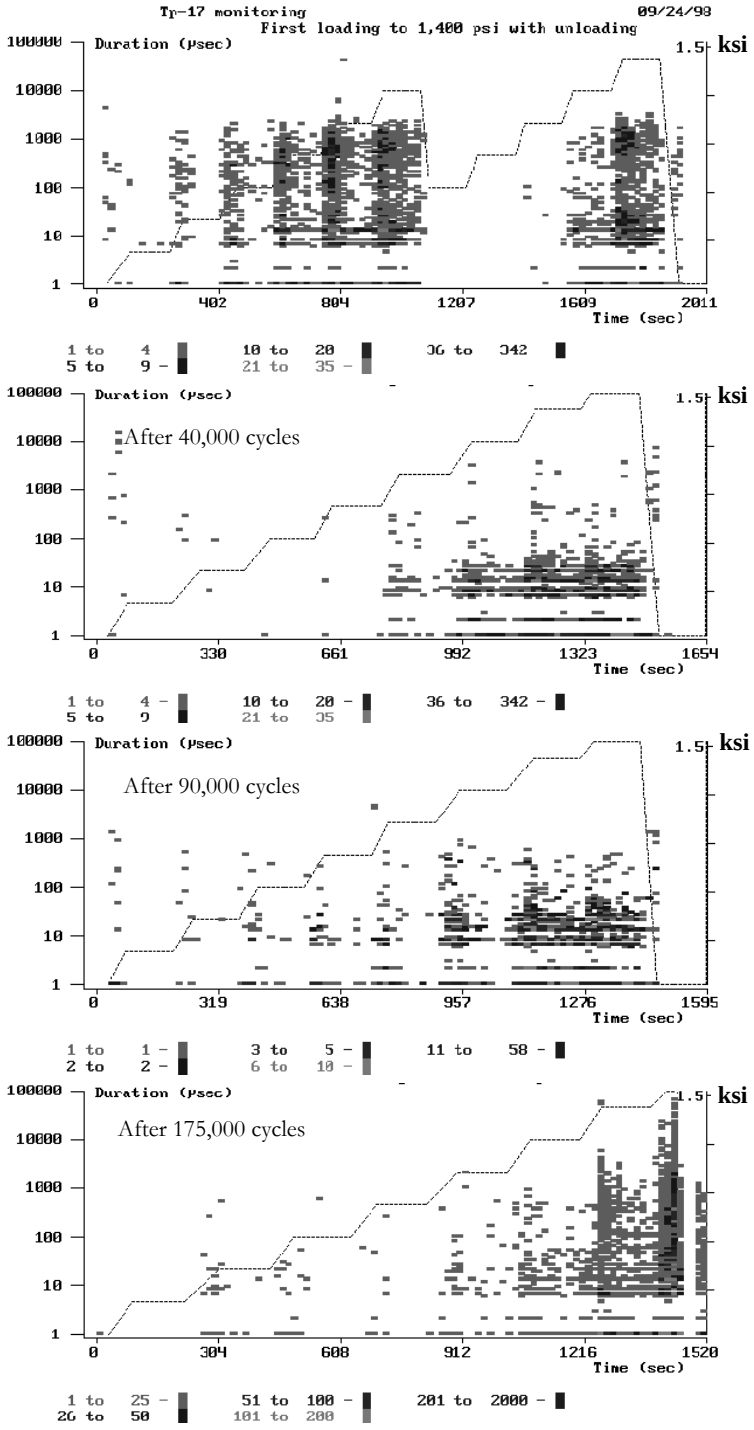

Figure 3.82 Selected AE duration data records for TP-17

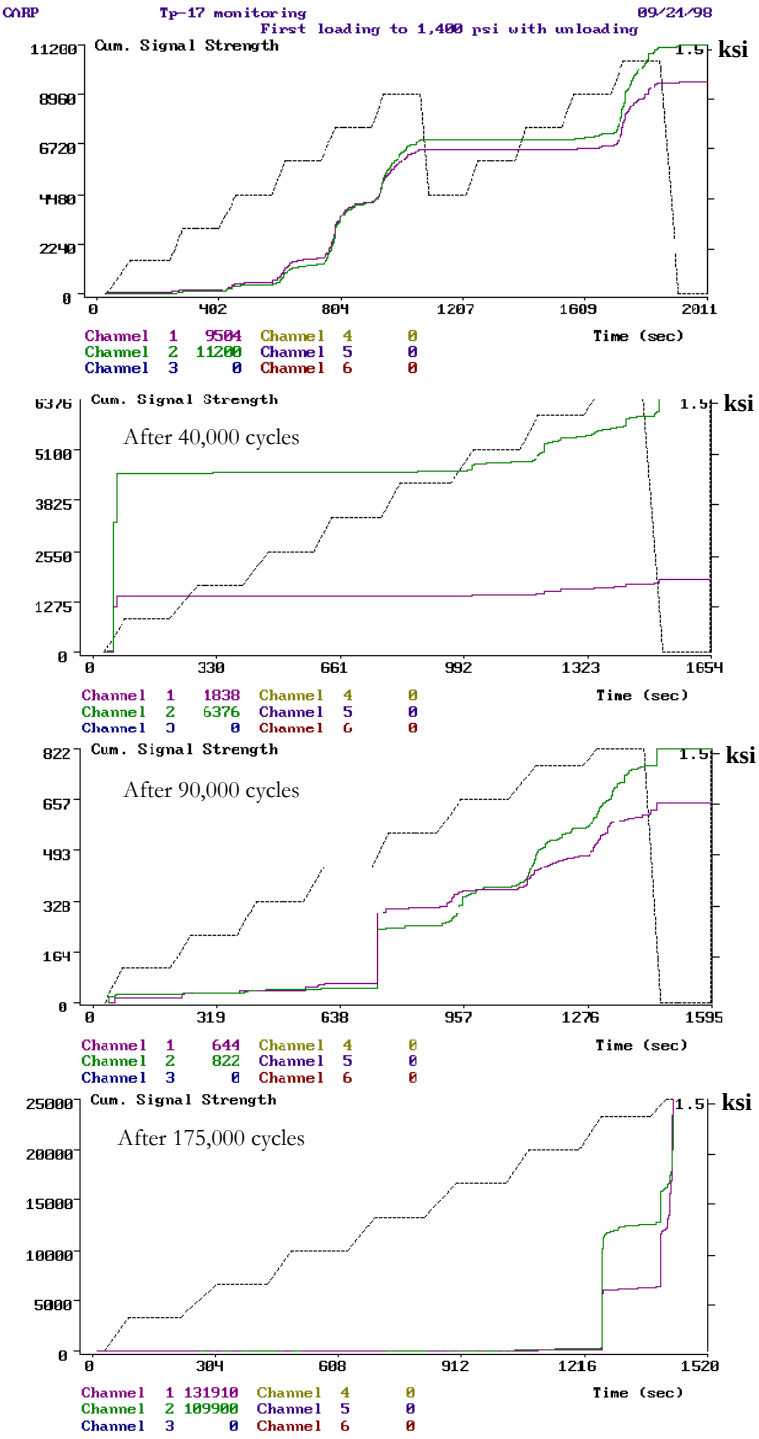

Figure 3.83 Selected AE signal strength data records for TP-17

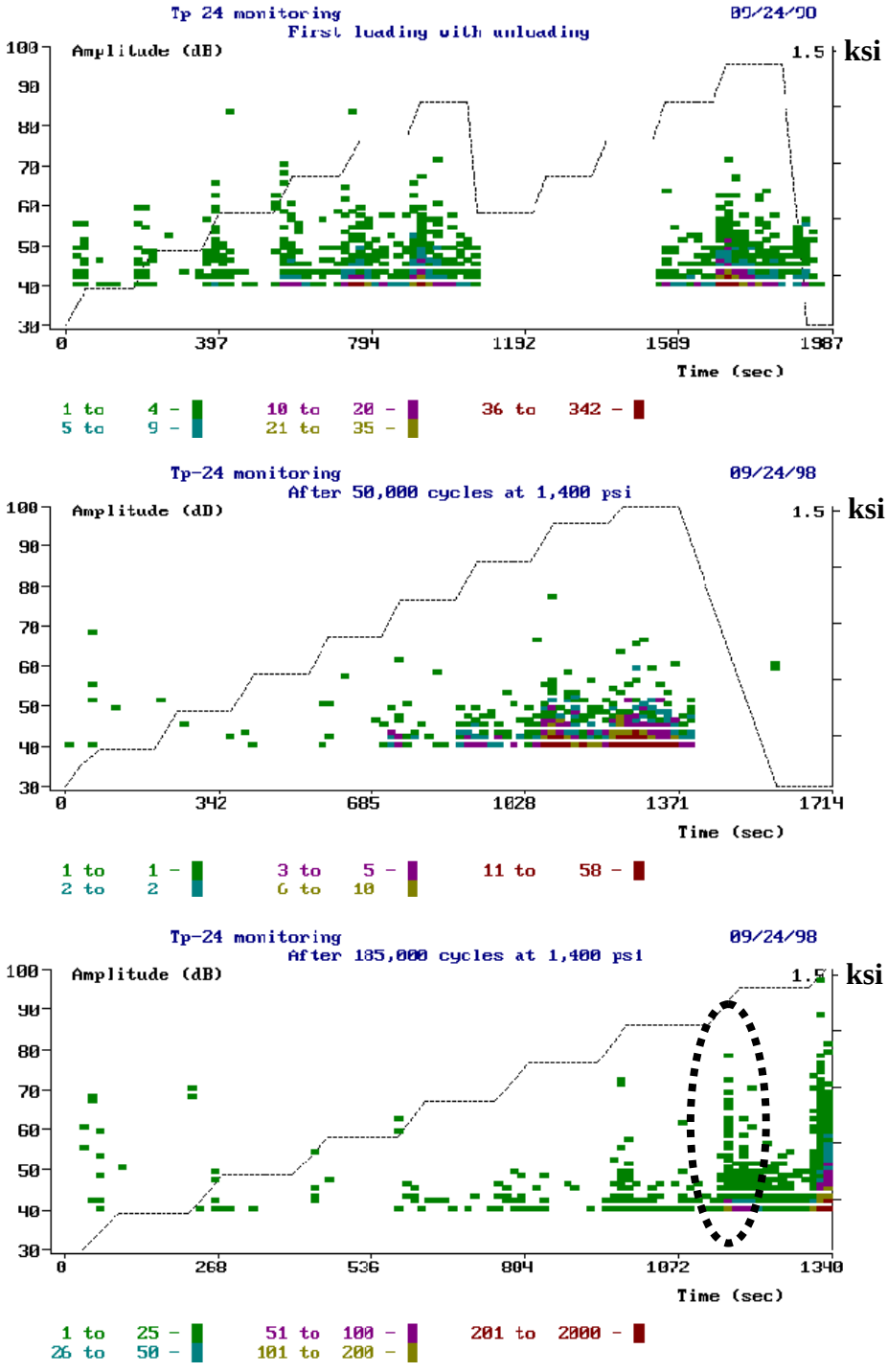

Figure 3.84 Selected AE amplitude data records for TP-24

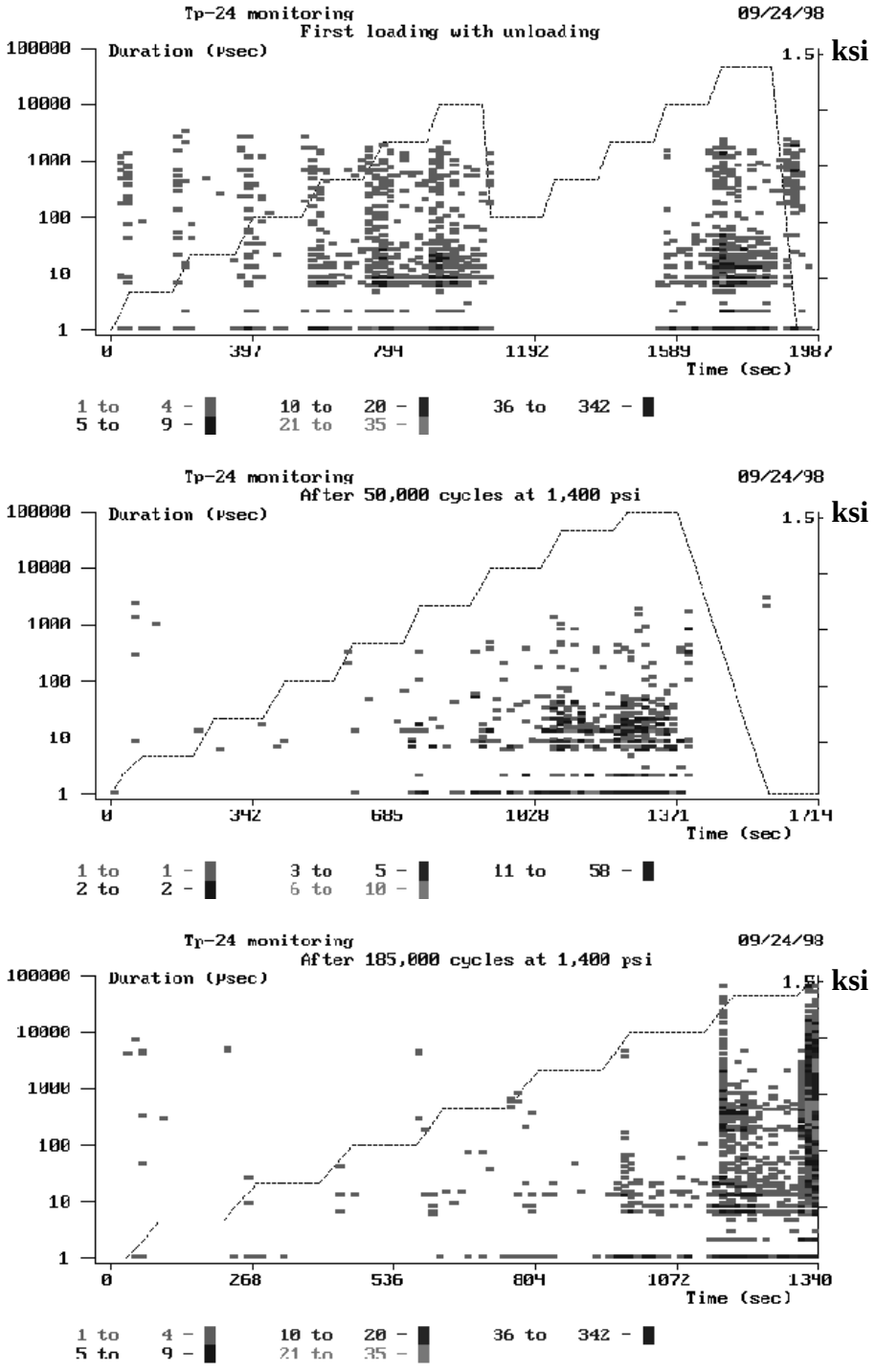

Figure 3.85 Selected AE duration data recorded for TP-24

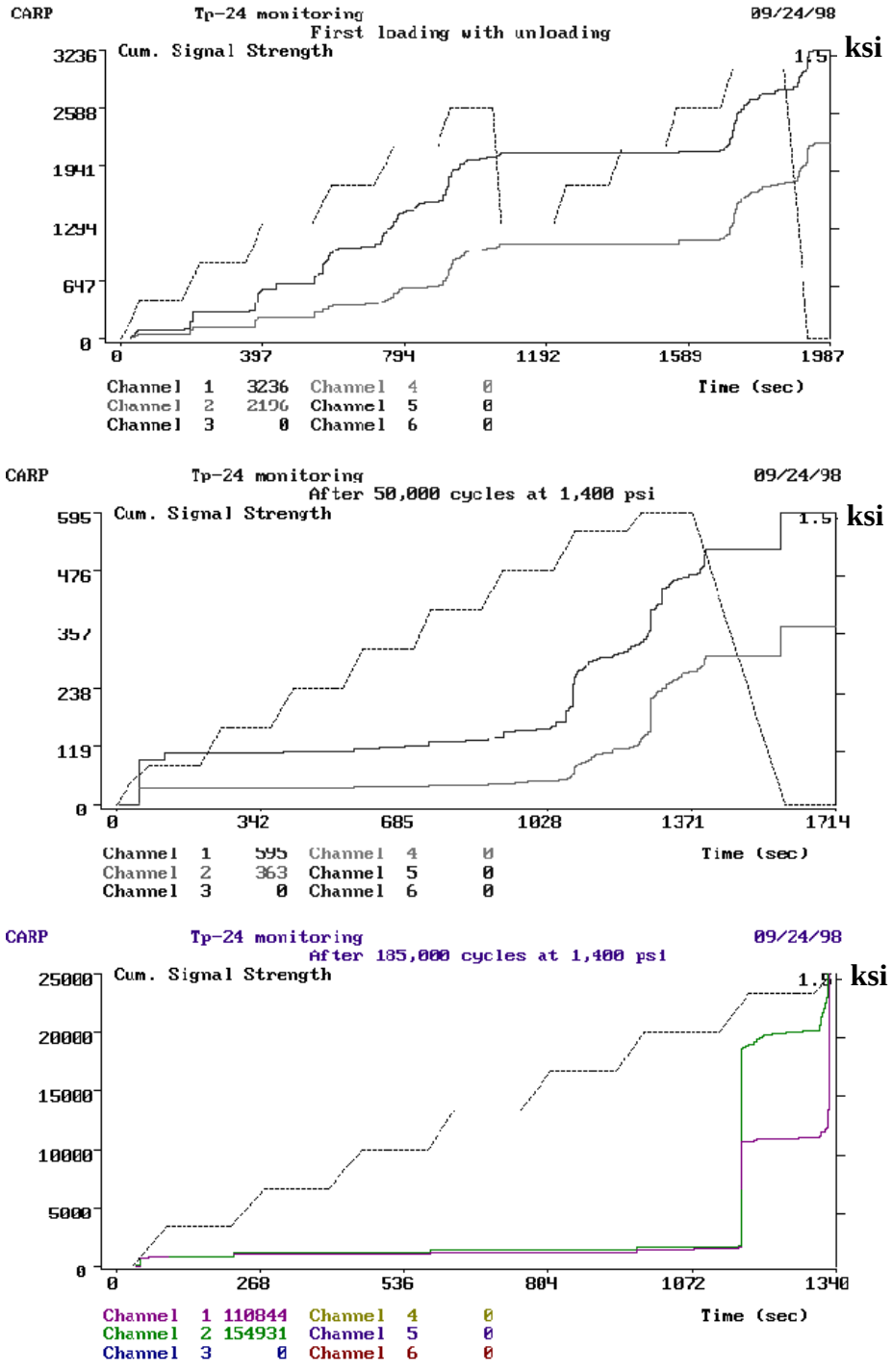

Figure 3.86 Selected AE signal strength data records for TP-24

3.3.2.6. RESULTS FOR CYCLIC TESTS AT 1200-PSI

Three specimens were tested in this group. The difference between this group and the others tested in the program was that none of them failed during the cycling and monitoring with AE. In order to assess the extent of damage incurred during the cycling for these specimens two of them were tested to failure after 1,000,000 cycles at the target pressure. The specimens tested were TP-11 and TP-7. In order to compare the AE records with the ones obtained with specimens tested in the program, results of the monitoring up to the highest level achieved in the closest previous group will be shown. In addition a follow up monitoring after that will also be presented for additional comparison.

Figures 3.87 to 3.89 show AE data for specimen TP-11. Again we can see the emission reduction trend observed in the 1400-psi group. This is even more noticeable at the final loading where almost no emissions were detected at the 1200-psi level. The 1200-psi pressure was close to the pressure where the slope of the cumulative signal strength plot begins to show a positive gradient during the load holds.

The duration plot also shows this "quieting" trend towards the target pressure. The specimen was allowed to rest one day between the completion of the cyclic phase and the static monitoring for AE. Therefore, the recovery behavior noted for other tests was not observed in this specimen. A longer rest period would be necessary in order to reliably evaluate the recovery characteristics of this specimen after cycling.

Signal strength characteristics during cycling do not reveal any behavior trends that would separate the monitorings from each other. It is obvious that the signal strength decreases with each monitoring as related to the first loading. Attempting to build a relationship between cyclic stage and the value of the signal may prove difficult. The value would change depending on the number of sensors and their location in the specimen. Even when there is a clear general trend towards signal strength decay in the

emissions associated with the number of cycles at the target pressure, there is not enough information to develop a consistent relationship between them.

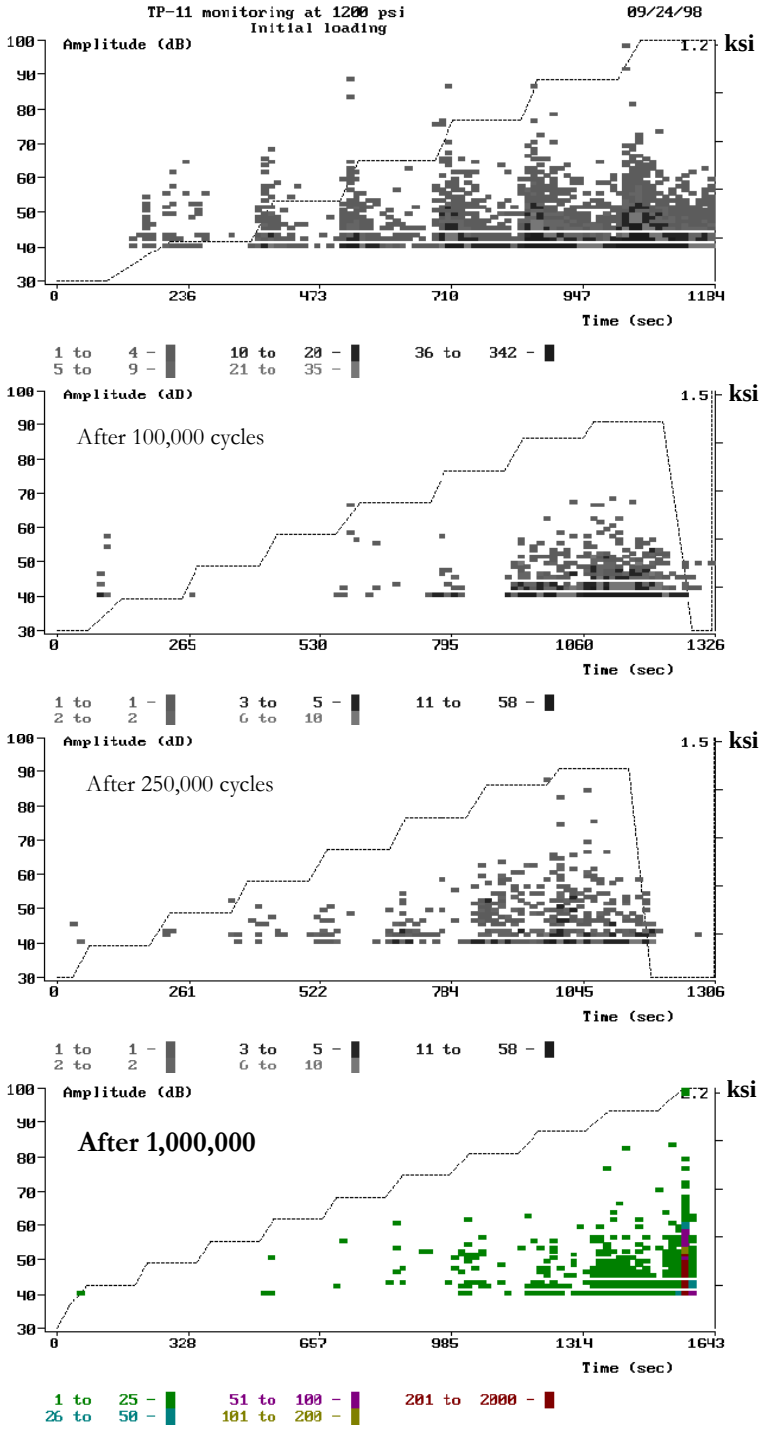

Figure 3.87 Selected AE amplitude data recorded for TP-11

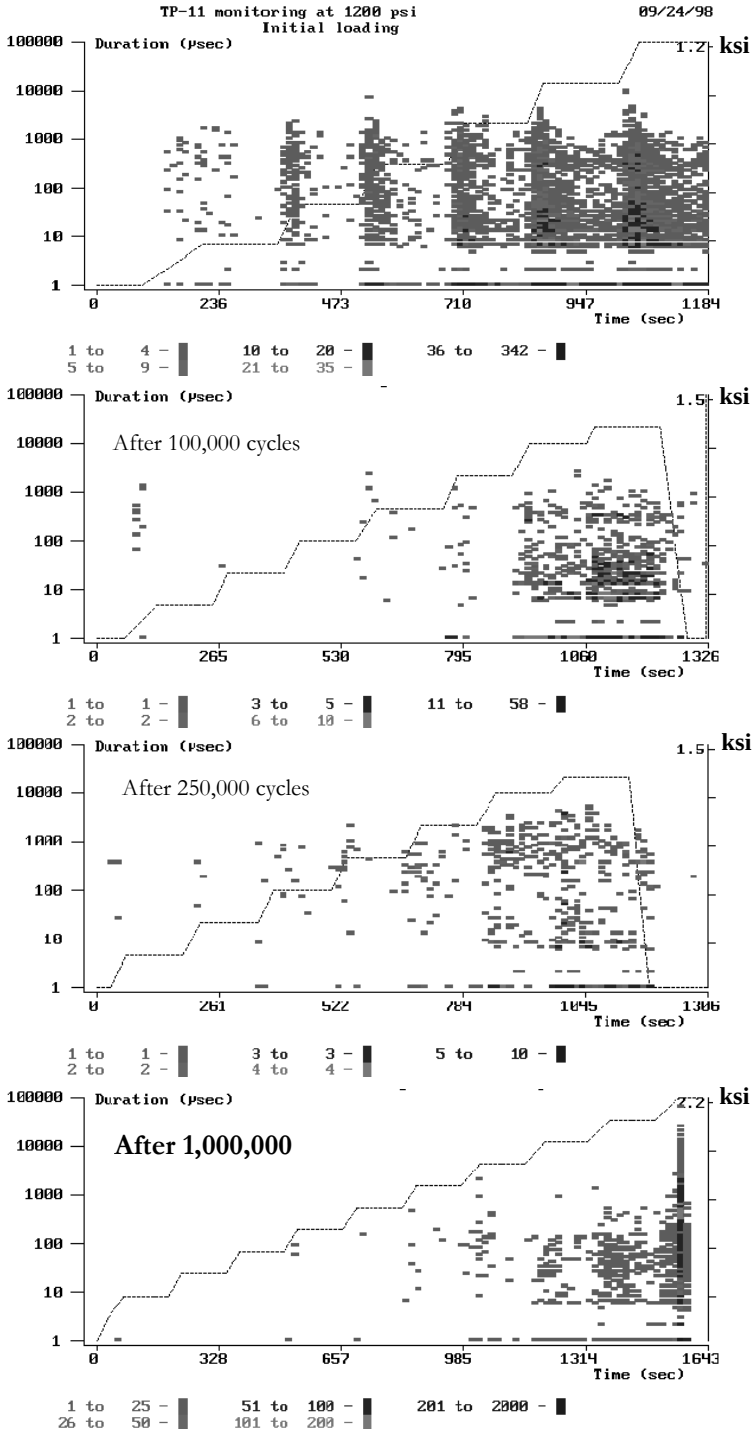

Figure 3.88 Selected AE duration data records for TP-11

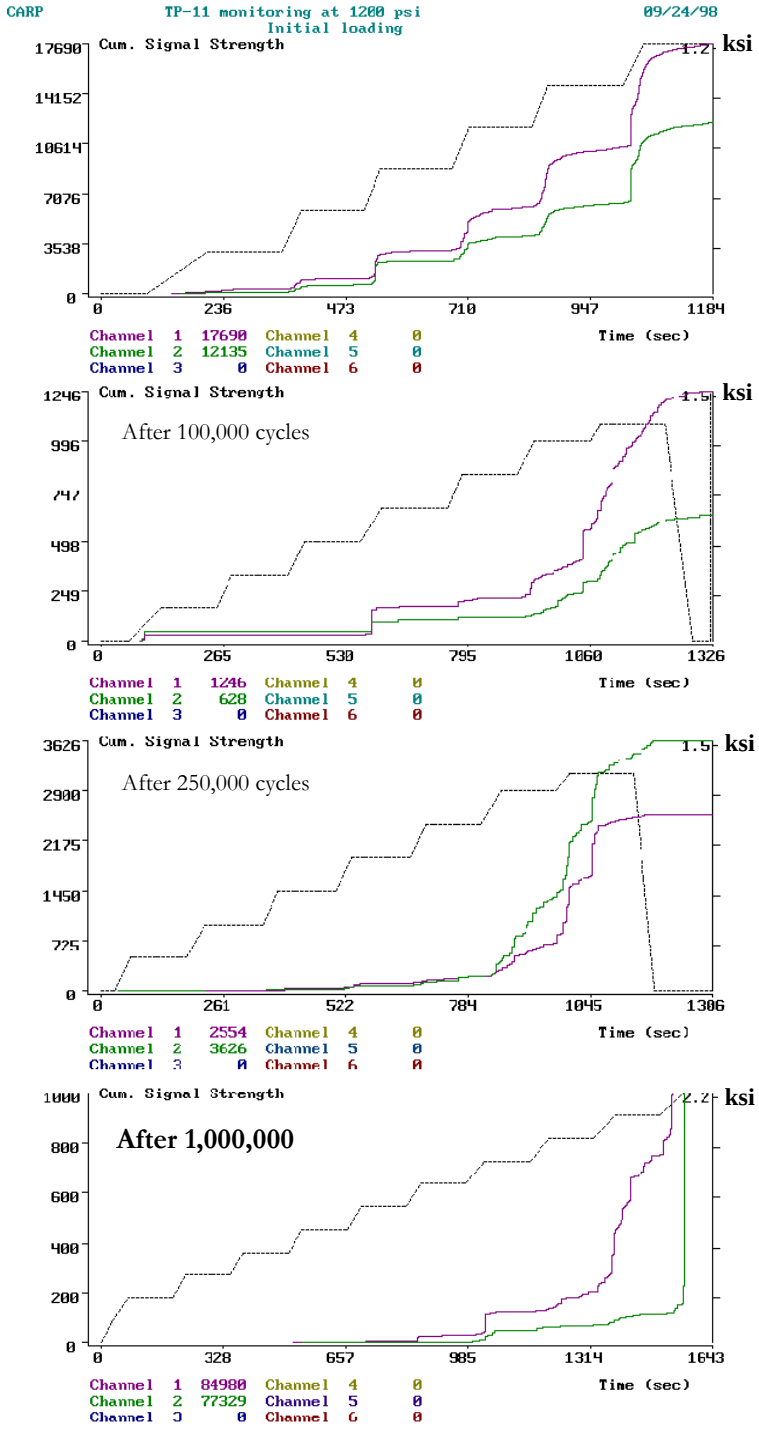

Figure 3.89 Selected AE signal strength data records for TP-11

Figure 3.90 shows a comparison between two of the pipes tested for 100,000 cycles at this pressure range. The recorded data was almost identical in both specimens. The drop in the amplitude magnitude is very similar in both, with very few hits to almost none greater than 60 dB.

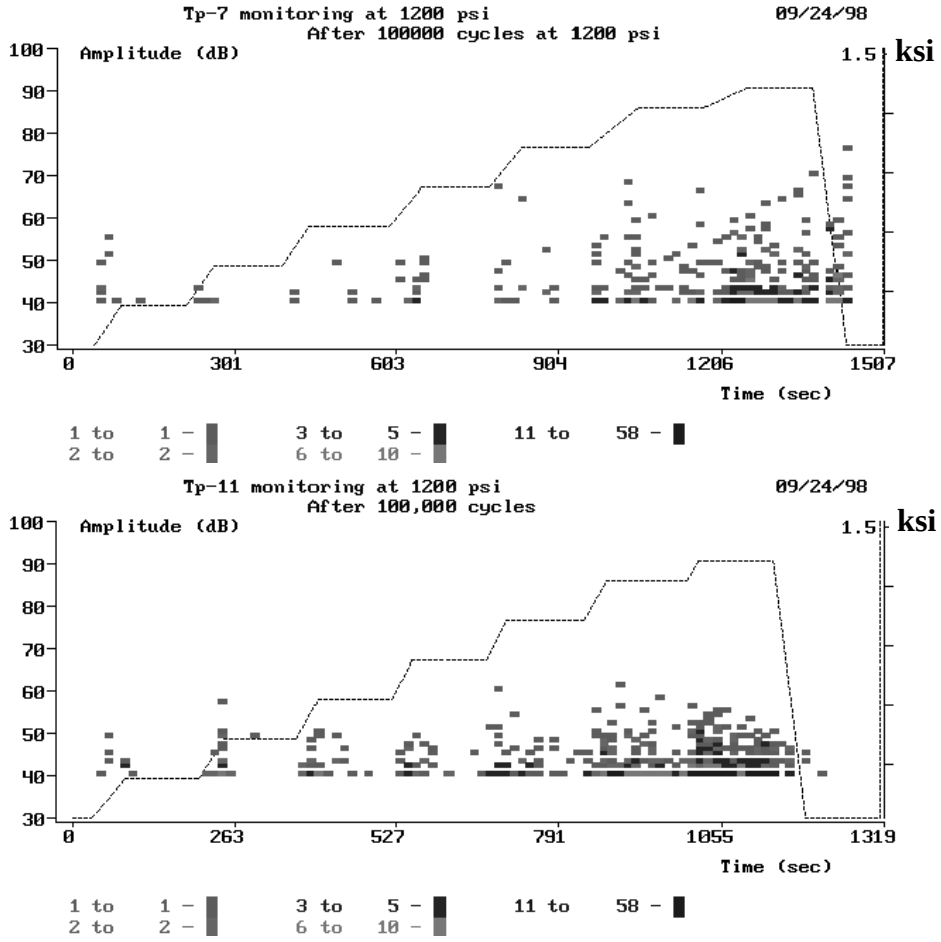

Figure 3.90 AE data comparison between TP-7 and TP-11

Figure 3.91 shows the same two specimens compared after each has gone through about 200,000 cycles. Again, a very consistent behavior between the two specimens is observed. The amount of activity towards the end of the pressure history in this monitoring appears denser than in the previous monitoring at 100,000. However, considering that this is not even half the life of the specimen and that at the final loading

to failure even less activity than this was recorded, no clear extrapolation can be made from this.

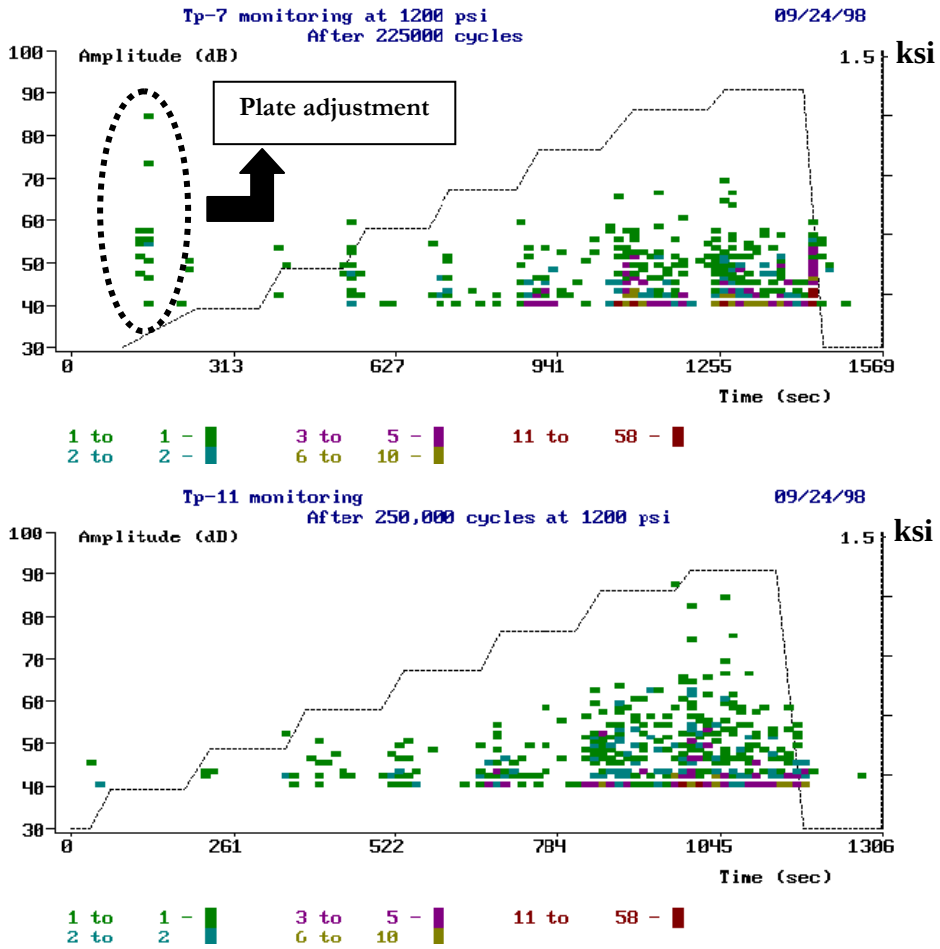

Figure 3.91 AE data comparison at 250,000 cycles for TP-7 and TP-11

The initial activity seen for TP-7 in Figure 3.91 is due to a setting of the seal plates when the initial increase in pressure was applied. If we eliminate the emission generated by the plate, the plots could almost be interchangeable with each other. So even when both pipes belonged to different batches in the fabrication process, the behavior was the same at this lower pressure level. The residual capacity of the pipe when tested after cycling was of 2100-psi. which is still similar to the results for non cycled specimens.

3.3.2.7. AE INFORMATION FOR HYBRID SPECIMENS

Two specimens were tested monotonically to failure in this group. As previously indicated, these pipes consisted of an inner core build to the same specifications as the fiberglass specimens and an outer ring, or shell, of carbon reinforcement. The specimens tested in this phase were labeled HTP-1 and HTP-2. The acoustic emission records will be presented in that same order.

Figures 3.92 to 3.94 show the records for specimen HTP-1. This specimen failed at about 3270-psi. For each one of the features selected for plotting there were two loading phases that are represented. The first phase consisted of pressurization to 1000-psi with a following load drop to 200-psi. From this drop, the pressure was again increased to 1200-psi. The load was then dropped to zero before a final monitoring began. This first phase is represented in the top view in the figures. The next phase consisted of a pressurization to 2200-psi followed by another drop to 200-psi and a final monitoring to 2800-psi before the AE sensors were removed and the specimen pressurized to failure. The loading curves in the final phase had to be separated in two files. The remaining two views in the figures are the same AE data plotted with the two different load curves superimposed. The middle view has the curve from zero to 2200-psi and the bottom view the same AE information but with the curve from 200-psi to 2800-psi superimposed.

The first feature noticed in the AE plots is the drop of the Felicity ratio after the first pressurization to 1000-psi. On the second reload, emissions during load hold were apparent immediately after 800-psi. This results in a ratio of 0.8 between the previous load and load at first emission. This ratio dropped as the load was increased past 1200-psi. The final calculation of the ratio was after the pressure was dropped from 2200-psi. On the reload, the Felicity ratio was calculated at 0.65. The duration plots shows a consistent distribution of duration for the events recorded. This consistency was noted from the initial loading to the final monitoring. As the maximum load was approached in the test, it would seem that the AE activity diminished. No large amplitude events

were recorded during this monitoring even when 2800-psi was reached. The signal strength plots at the final figure reinforce the observations made here.

At this time it is necessary to comment on the reliability of the determination of the point at which significant emissions is declared. Traditionally, the cumulative signal strength plot has been used for this purpose. The point at which significant emission is declared is when a change in the slope in this curve is severe enough to form a "knee". In most practical, and in a number of research applications, this methods has proven difficult to apply since most structures present AE activity from the beginning. Others will not show a change in the slope severe enough to facilitate the declaration of significant emission. A more effective method for determining the point of significant, or onset of, emission will be used in the next section of this chapter.

The main characteristic in the behavior of these specimens was that failure was not defined by just leakage through the matrix and fibers, but by total burst of the specimen. Even at pressures 85% of the ultimate, no emissions typically associated with fiber breakage were recorded. It is estimated that little or no fiber breakage took place until the maximum pressure was reached. This indicates that first ply failure in the fibers may constitute complete failure of the component.

Figures 3.95 to 3.97 are the AE parameters recorded for HTP-2. Maximum pressure for this specimen was recorded at 3400-psi, only about 100-psi higher than the HTP-1 specimen. This consistency is probably the result of the mode of failure in both specimens. Fiber strength is easier to determine and less likely to suffer from reductions as the result of flaws.

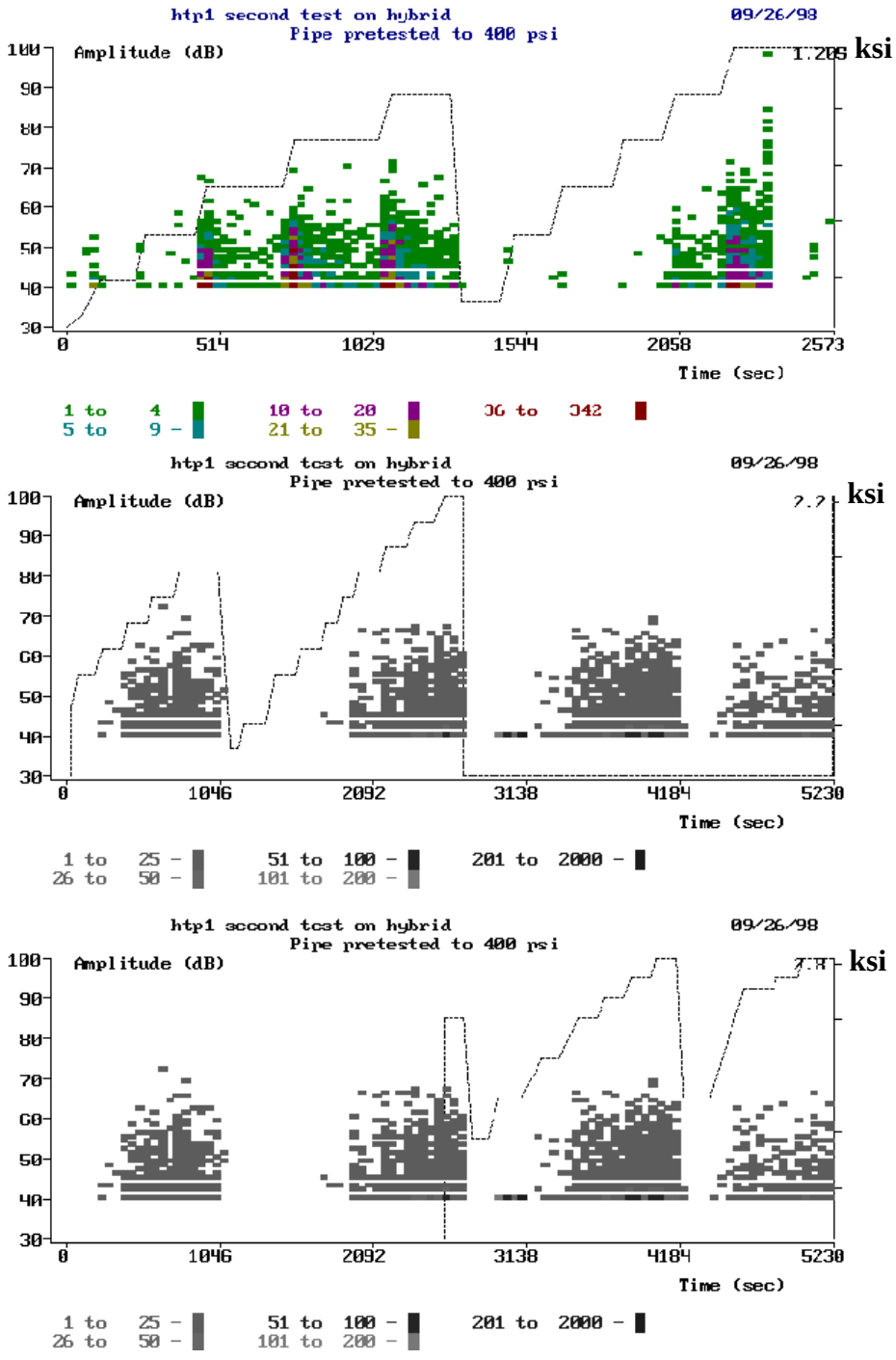

Figure 3.92 Amplitude records for HTP-1

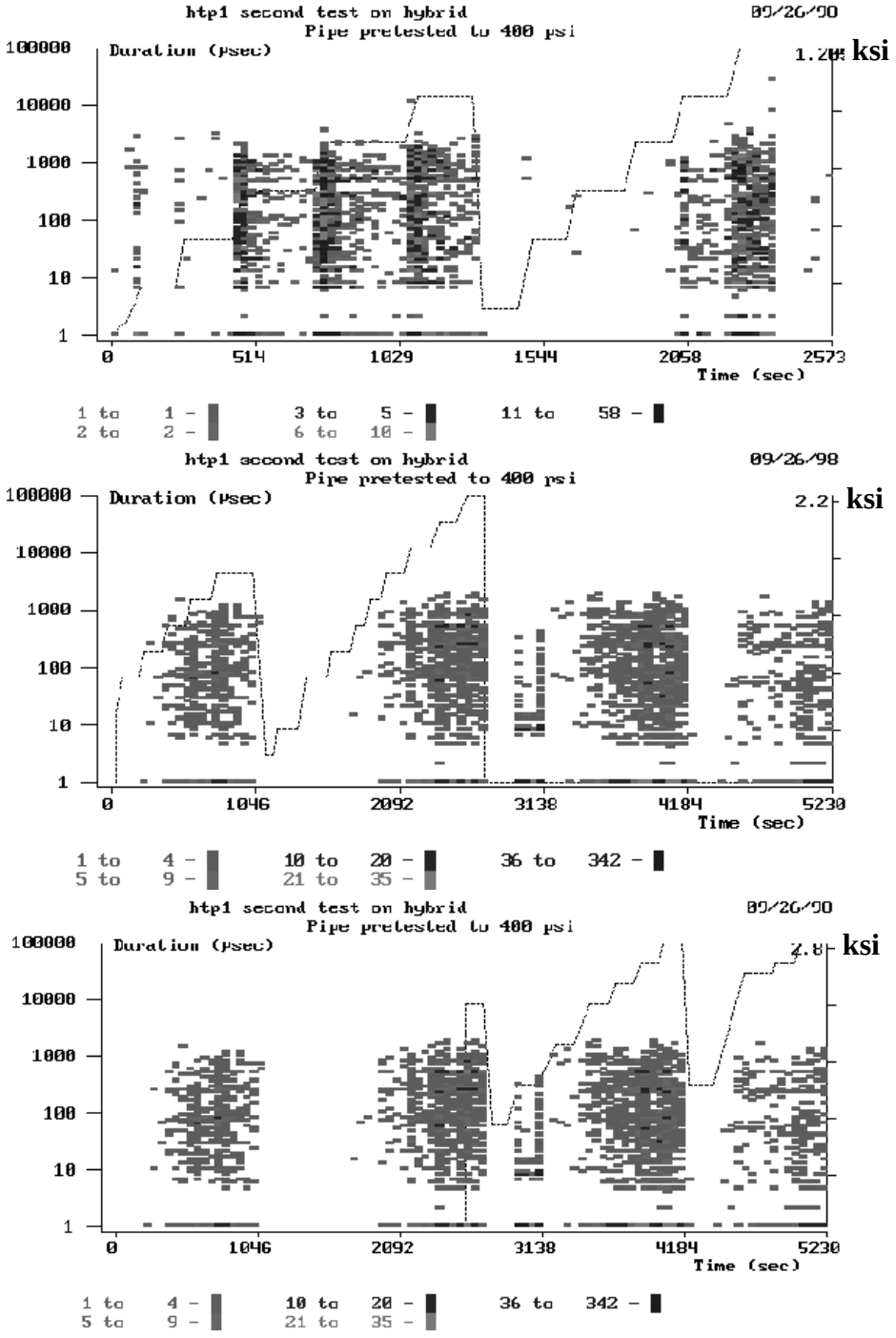

Figure 3.93 Duration records for HTP-1

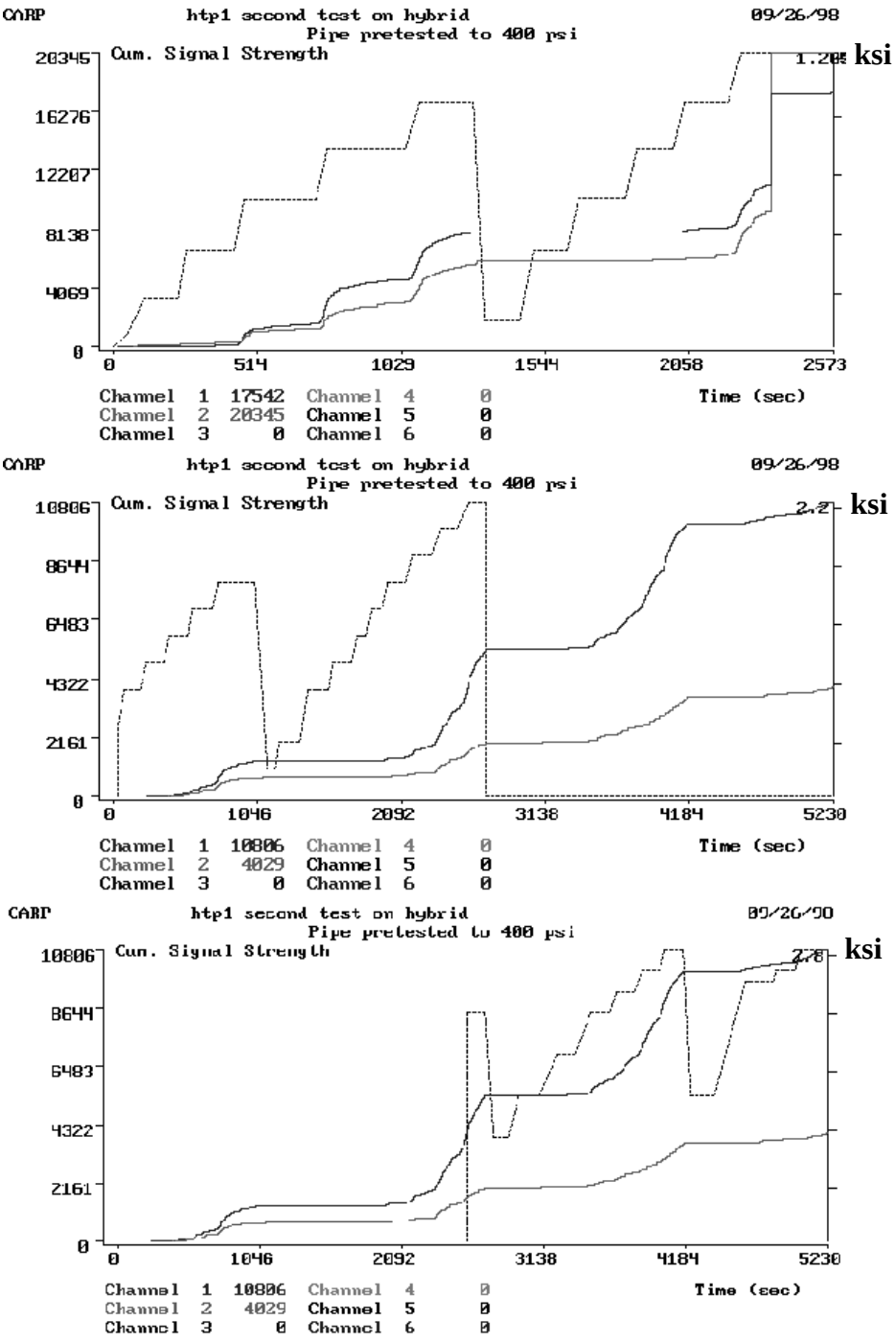

Figure 3.94 Signal Strength records for HTP-1

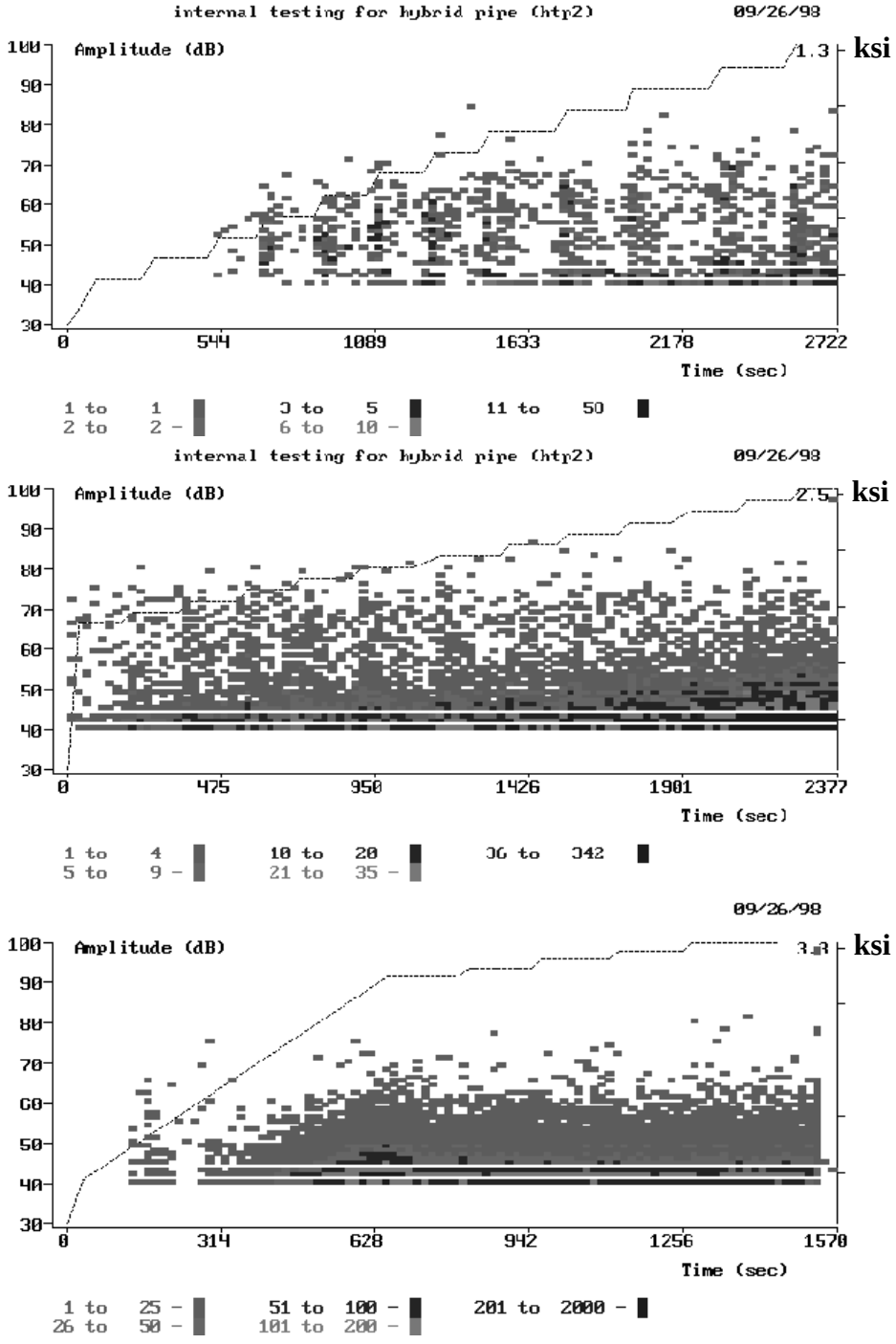

Figure 3.95 AE amplitude data records for HTP-2

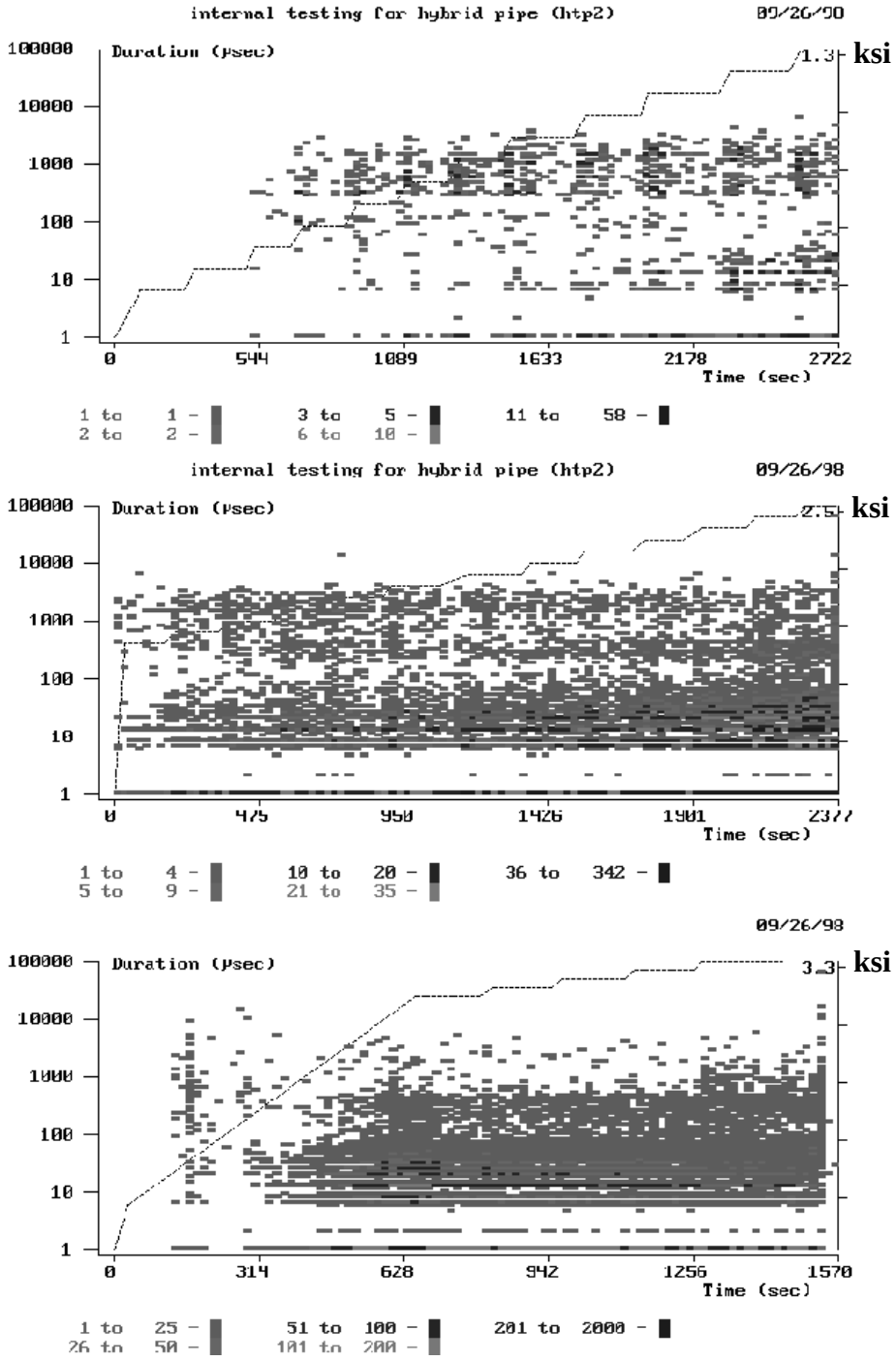

Figure 3.96 AE duration data records for HTP-2

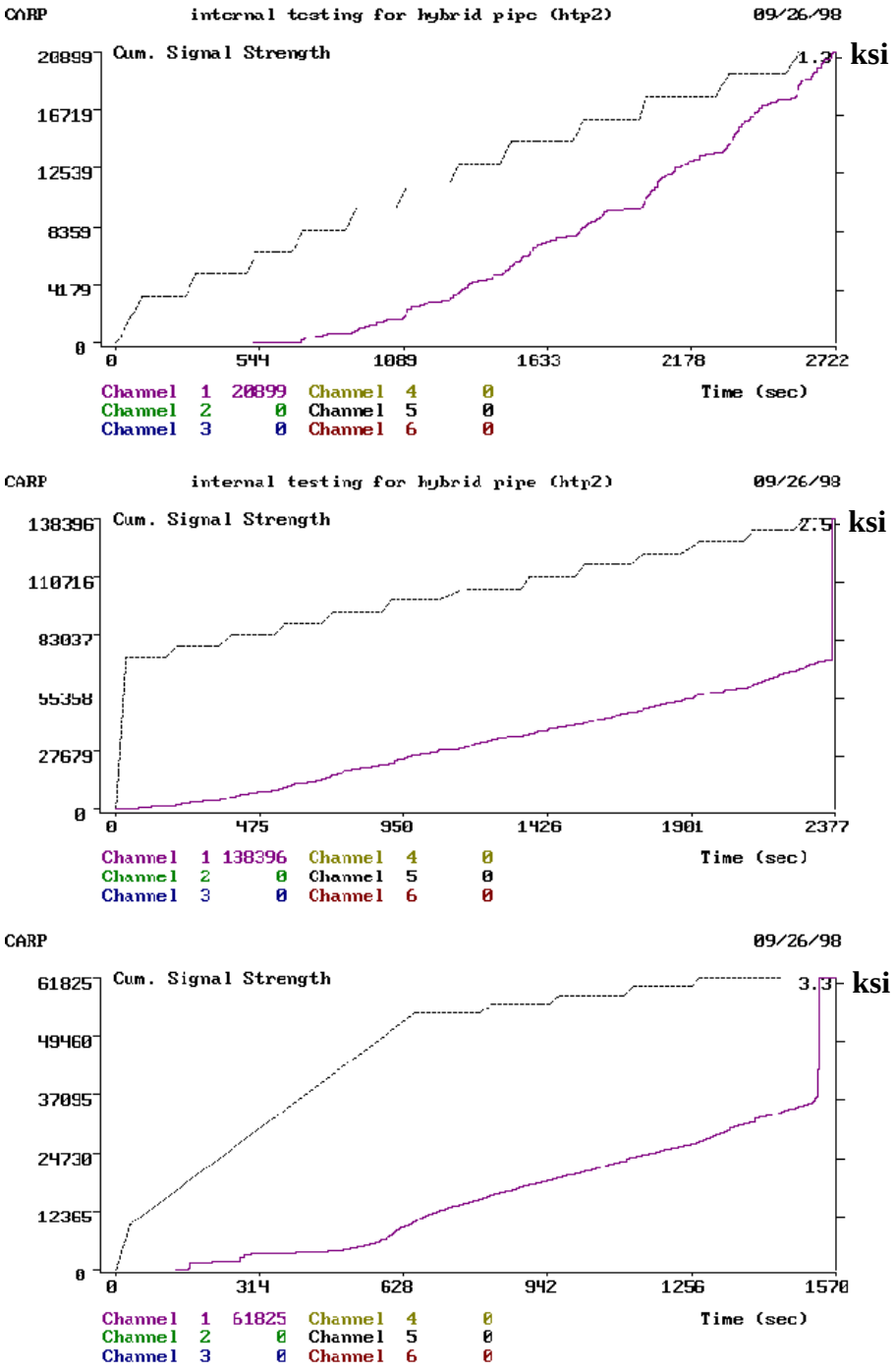

Figure 3.97 AE signal strength data records for HTP-2

The figures for HTP-2 show three load stages in the test of the specimen. The first stage was from zero to 1400-psi. The second stage from 1400-psi to 2500-psi and the third and final stage from zero to 3300-psi. The specimen was downloaded to zero after the second stage prior to the final load to failure.

The most notable feature in the AE records is the tendency of the amplitude parameter to drop in magnitude as the final pressure approaches. In addition, the events tend to populate densely at the lower amplitude levels. The event duration plot also shows a clear change during the loading phases. At initial AE activity most of the recorded hits take place in the range of 1000 microseconds with lower duration events starting to make an appearance as the load increased. An almost clear banding is visible in the first 2/3 of the second load phase, one concentrated around 1000 microseconds and a second band around 50 microseconds. Towards the end of the phase the banding is starting to disappear and in the third stage is no longer clear. Duration of the recorded events is well distributed throughout the plot. Considering that throughout the test only one sensor was left in the specimen and it was left in place without adjusting, this could be a clear indication of the AE signature of this type of specimen as it approaches failure.

From the signal strength plot we can see how specimens with carbon fiber tend to be quite active in the emission of AE activity. Unlike the fiberglass specimens, this particular specimen showed considerable activity from the beginning of its load life. This is due to the carbon fibers since it has been found that carbon fiber specimens are more active that glass specimens when monitoring with AE sensors. There are two relatively clear points of change detected in the signal strength plot. The first is at 800-psi where the cumulative energy begins to have considerable values. The second point is at 2500-psi where the biggest change other than failure takes place in the curve. Other than these two places, the gradient of the energy curve is quite consistent and the plot smooth through the test. The next part of this chapter will deal with the interpretation of the results presented here. The AE records will be combined with the strain measurements and final pressures obtained.

3.4. FURTHER EVALUATION OF EXPERIMENTAL DATA

Data recorded during the test and presented in the preceding sections will be further evaluated here. General trends in behavior will be indicated along with the interaction between acoustic emission records and strain measurements. Again, it will be noted that the analysis shown here is only a preliminary look at the AE data recorded. Further analysis in the area of damage identification will be carried out at a later date.

3.4.1. STRUCTURAL BEHAVIOR

The plot in Figure 3.98 presents a summary of the results from the tests performed in this program. The vertical axis presents the pressure in pounds per square inch, and the horizontal axis is a logarithmic scale of the number of cycles to leakage.

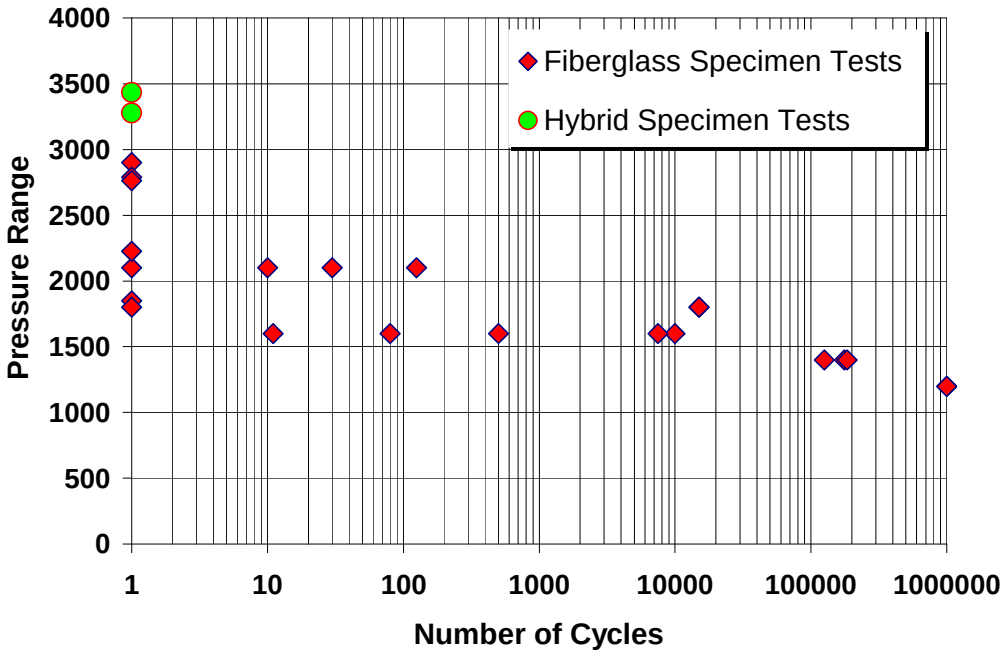

Figure 3.98 Test Results for Internal Pressure Specimens

The hybrid specimens were added as a reference to the increase in capacity when compared to the fiberglass ones. Note, however, that the mode of failure for these two specimens was different than that of the fiberglass, where leakage was the mode of the latter, burst was the mode of the former.

The first noticeable feature in the plot is the scatter of the results at the static or single cycle failure. We can note a difference of up to 1100-psi between the lowest static specimen and the highest one. This constitutes a difference of more than 60% of the lowest recorded pressure in the measured capacity. Considering that both specimens were built to the same specifications of material and mix, this is a significant difference.

Another apparent aspect is how the groupings tend to become tighter in the plot as the pressure span drops. That is, a relative consistency is created by a large number of cycles during testing of the specimens. Specimens tested at all pressure groupings were combined from different batches to avoid biasing the results as much as possible.

3.4.1.1. FIBERGLASS SPECIMENS

The first step in the interpretation of the results for the fiberglass specimens was determining the theoretical values for stiffness and deformation expected for the specimens. Later, these theoretical values will be compared to the measured response of the tested elements.

3.4.1.1.1. ANALYSIS RESULTS

Making use of the results from the finite element model presented at the beginning of this chapter, it was assumed that the response of the element would be dominated by the properties within the test gage. Strain and stress calculations shown here are for an infinitely long pipe with no end restraints. The raw material properties used were as provided by the manufacturer of each individual component used in the composite.

The calculated properties used in the analytical model are as presented in Figure 3.99. No modifications were made to the properties to match measured values. The reinforcement weight was of 1.27 lbs/sq-ft, with a laminate weight of 2.54 lbs/sq-ft. The fiber content in the winding portion of the specimen was established at 70% by weight with the mat layers calculated at ¾ oz as presented at the beginning of the chapter. For the results presented in the following figures, the directions are defined as longitudinal or along the length of the pipe, transverse or hoop direction and normal or radial direction.

Tensile		Modulus		Ult. Strength	
- Longitudinal	=	1,275,363	psi	11,020	psi
- Transverse	=	1,663,111	psi	29,930	psi
- Normal	=	1,049,674	psi	1,405	psi
Flexural					
- Longitudinal	=	1,206,038	psi	24,460	psi
- Transverse	=	1,413,524	psi	25,181	psi
Shear					
- L-T (Inplane)	=	620,394	psi	12,145	psi
- L-N	=	368,975	psi	3,865	psi
- T-N	=	352,051	psi	4,504	psi

Poisson ratios - Load direction / Strain direction

- L/T = -0.32	T/L = -0.42
- L/N = -0.26	N/L = -0.21
- T/N = -0.25	N/T = -0.16

Neutral axis (measured from the centroid)

- Longitudinal	= -0.017	in
- Transverse	= -0.043	in

Figure 3.99 Material properties for fiberglass specimens

Using an internal diameter of 8 inches and a total wall thickness of 0.312 inches the response shown in Figure 3.100 was obtained. Note that no allowances were made for nonlinear behavior of the material. The values obtained here will be compared to measured ones next. During the development of this section, references will be made to the AE knee from the acoustic emission records. Typically, in acoustic emission technology, the location of this knee is associated with the term "onset of significant emission" and, in turn, to the beginning of important damage induced in the material. Defining where this AE knee takes place is mostly a subjective matter. During the

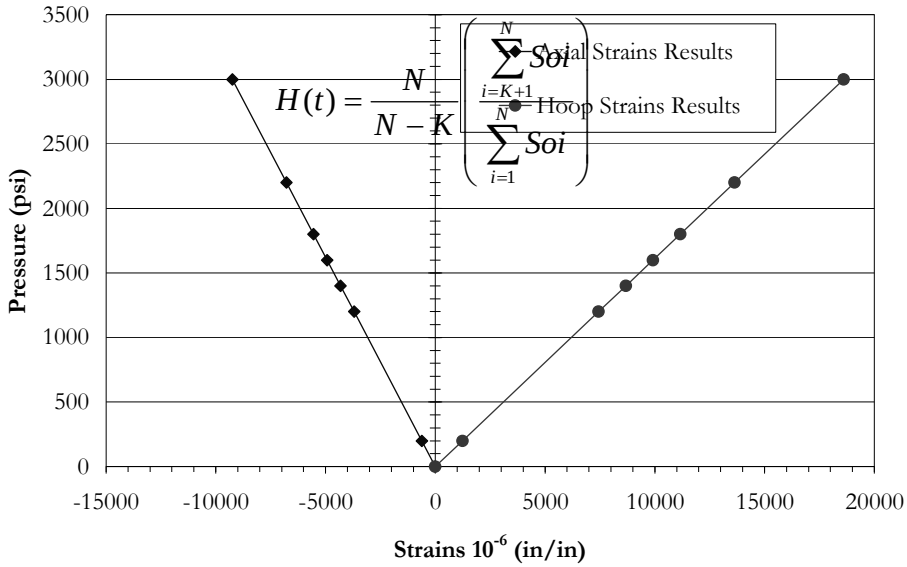

Figure 3.100 Calculated response of fiberglass specimens

loading history of a component several "knees" can be noted in the AE signature. All of these indicate damage being generated with increasing stress levels. However, no clear definition as to their importance in the behavior or capacity is available. In addition, clearly defining at which stress level these knees begin to form also presents difficulties. One of the most accepted methods of finding the knee in the curve has been the use of the cumulative signal strength in the AE records. Not without its problems, this method has been used with relative success in the inspection and acceptance testing of pressure vessels. Because cumulative signal strength is always additive, the scale obscures occasionally important signals, or events.

An alternative to the signal strength value is the use of the "historic index". This approach estimates the change in slope of the emissions and plots it against time. The equation for the calculation of the historic index is as follows:

Where

N ~ Number of hits up to time (*t*)

$S_o i$ ~ Signal strength of i^{th} hit

and for composites, the value of K is defined by the following table [3.13, 3.14]:

# OF HITS	**K**
Less that 100	Not applicable
101 to 500	0.8 * N
> 500	N - 100

The values for K change depending on the type of material in question, the ones shown here are specifically for composite materials. Even though this approach is also empirical, it does provide a good estimate of the change in the signal strength slope. In this discussion we will be using the historic index approach to determining the location of the AE knee. A note of interest is that, as with the case of signal strength, the historic index (or HI) also shows more that one location for the AE knee. Its usefulness comes in the fact that it is easier to determine if the AE knee is due to scale of the plot or due to real damage taking place.

The data used in the following analysis is related only to the first AE monitoring made to the specimen. The goal was to explore the possibilty of finding AE features obtained during this first time monitoring that could be related to the capacity of the specimen. This would open the possibility of predicting capacity of a fabricated specimen without having to perform an extensive testing program to failure of several specimens.

Now that a way of determining the location of the AE knee has been selected, it is important to define which one of all the possible knees is the one of interest or

importance in the behavior of the structure. When looking at the information on the AE records presented previously in this chapter, we can say that there is inconsistency in the level at which emission begins to take place. In some cases emission begins only after a certain level of pressure is reached, whereas in others emission appears to begin at the start of the loading profile. Eliminating the cases where the sources of the emission at the beginning of the load profile were known to be non-structural would still leave a considerable number of specimens where the emission is considered genuine.

Figures 3.101 and 3.102 show typical plots of AE records for two of the specimens tested in this program obtained during the first time monitoring, and the corresponding historic index (HI). In the figures, the plots for cumulative signal strength are also shown for reference to estimate at what pressure the AE knee took place.

The two specimens show in Figures 3.101 and 3.102 are representative of all the fiberglass specimens tested in the program as it relates to AE records. It is clear that determining the location of the "onset of significant emission" would be a difficult task if using only the amplitude or cumulative signal strength records. In addition, each specimen responds slightly differently to load when looking at the AE records. It should be noted that, the case represented in Figure 3.101, was the most common case observed in the specimens tested. Only a few of the specimens showed the trends described in Figure 3.102. However, because this could be the case encountered in a real application it is also presented here for information.

The most common trend observed was a first knee in the signal strength record at lower loads with little or no emission during the load holds of 2 minutes and represented in the figures by a square box. The next was a second AE knee observed in the vicinity of, or right at the location where emission during load hold was noticed and where an increased activity was noted in the Historic Index (HI) plot. In most cases a clear spike in the HI value would be seen in the plot, followed by the HI fluctuation representative of emission during load hold. This spike would be either right at the beginning of the fluctuation or a few moments later followed by a drop to the previous

levels of HI. In a few cases however, there would be no clear spike in the HI, only the beginning of a strong activity in the plot. Specimens TP-15 and TP-18 represent each one of these cases. In TP-15 (Fig. 3.101) the spike is clearly visible and marked by an elliptical shape, and in TP-18 (Fig. 3.102) only activity is noted and, also marked. It should be noted that in most of the cases a series of unloadings were part of the loading profile use in order to possibly avoid the potentially misleading information resulting from the shakedown period. The success of this attempt will be explored in a following chapter of this dissertation

Looking at the amplitude records for the specimens similar to the one shown in Figure 3.102, at the time of the second AE knee, it is noticed that the number of hits, at the lower amplitude level increases, as show by the darker patches of points in the figures. The distribution of the higher amplitude remains essentially the same at this point and through subsequent load increases. We also note that from this point forward, the quantity of emission during load hold begins to increase and the Felicity ratio gradually drops in the cases where load drops and reloading were recorded. This was used to help identify the location of the second AE knee that would correlate well with the knees observed in other specimens. Therefore, for these few specimens, the second AE knee was determined by looking at the HI plot for the location of continuous fluctuation and within that area finding the time at which the hits at the lower amplitude level began to increase significantly. The significance of these AE knees will be approached later in the prediction chapter of this dissertation.

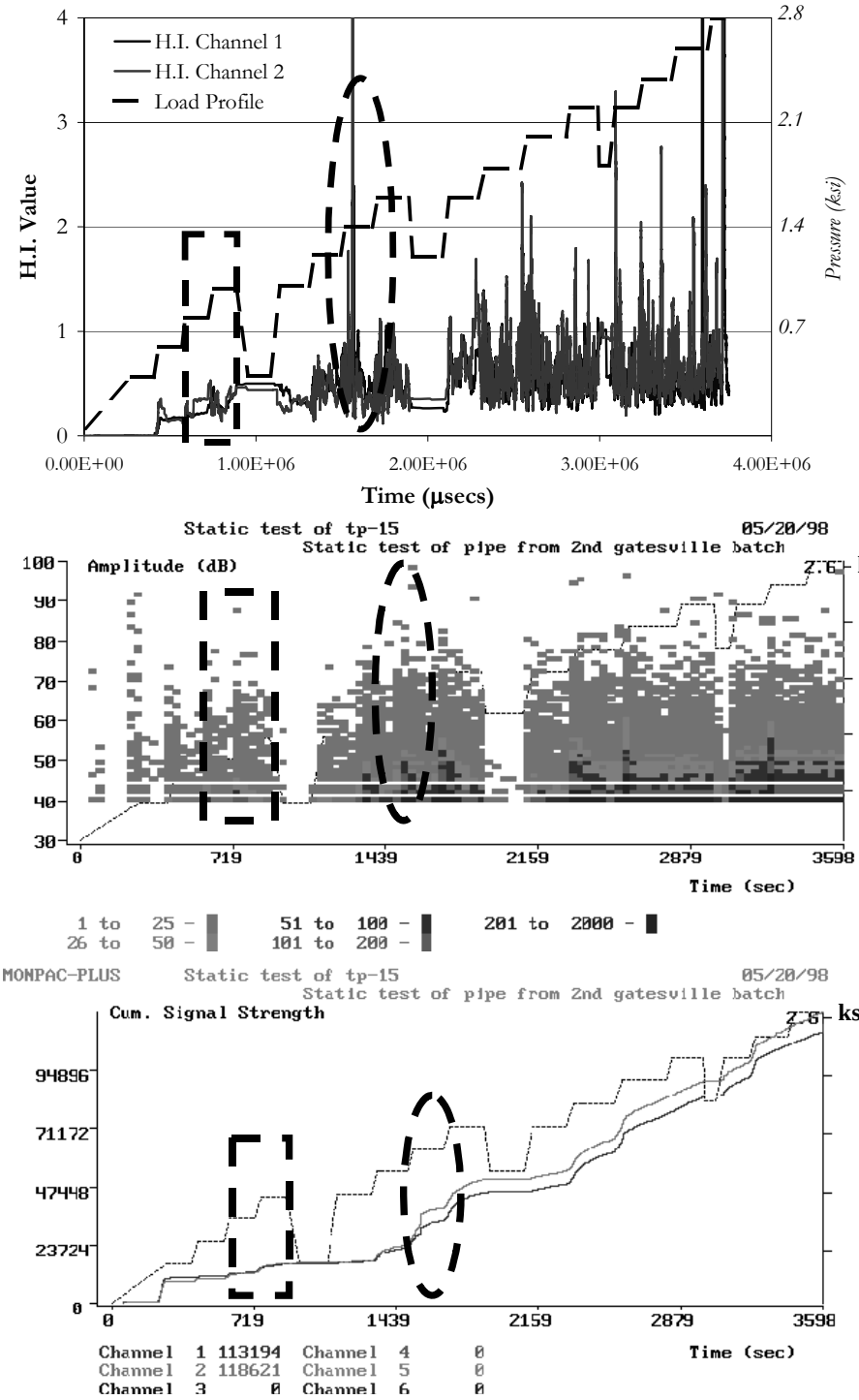

Figure 3.101 Determination of AE knee for TP-15

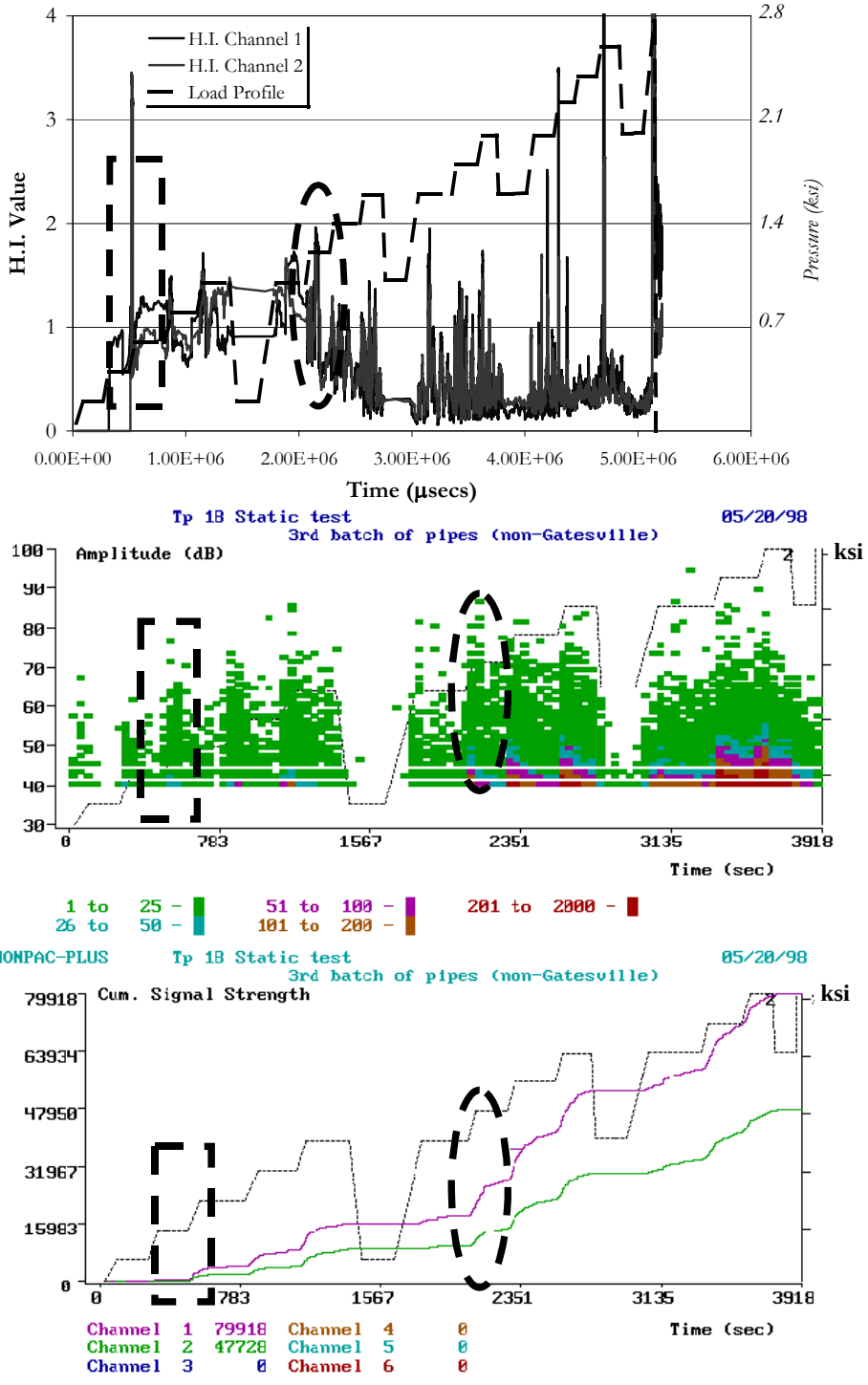

Figure 3.102 Definition of AE knee for TP-18

3.4.1.1.2. MEASURED RESPONSE DURING STATIC LOADING

Figure 3.103 presents the recorded principal strains for the specimens tested. It is noted that the prediction of the deformation in the direction of the loading (hoop) was in relative good agreement with the recorded strains. However, the measured values for the axial strains were not in as good of agreement. In addition the error between the measured and estimated strains varies from specimen to specimen. In one specimen the Poisson's ratio was smaller than estimated, in another larger and in two of them in very good agreement. Since the same type of strain gage was used for all, the possibility of measurement error is reduced. In addition, this reflects the same tendency observed during the external pressure test presented in Chapter two of this dissertation. Unfortunately, there does not seem to be a relationship between the recorded behavior and the leakage pressure observed for the specimens. The three highest capacity specimens are each on different locations of the plot as it relates to the theoretical result.

The strains recorded at the time of leakage were also different for each of the specimens. The hoop or load direction strains had values between 1.5% and 1.7% at the time of leakage. The strains in the opposite direction had values between 1.1% and 0.6% at the time of leakage. Non linearity was noted in the axial strains and almost not perceptible in the hoop strains. Looking at the failure appearance of each specimen in this group, it is apparent that the specimens with the largest recorded capacity are the ones with the more extensive delamination. It is possible that this profiling did not have to do with the damage present in the specimen at the time of failure. Because the pressure in the fluid was higher in some specimens at the time of failure that in others, fluid had different levels of energy at the time of leakage. The ones with the higher pressure were capable of delaminating the layers more noticeably that the ones with lower pressure. When the fluid found the final path to the exterior, all energy due to pressure was lost and delamination stopped in the specimen. This would indicate that the levels of pre-exiting damage in the winding shell were almost the same for all specimens at the time of failure.

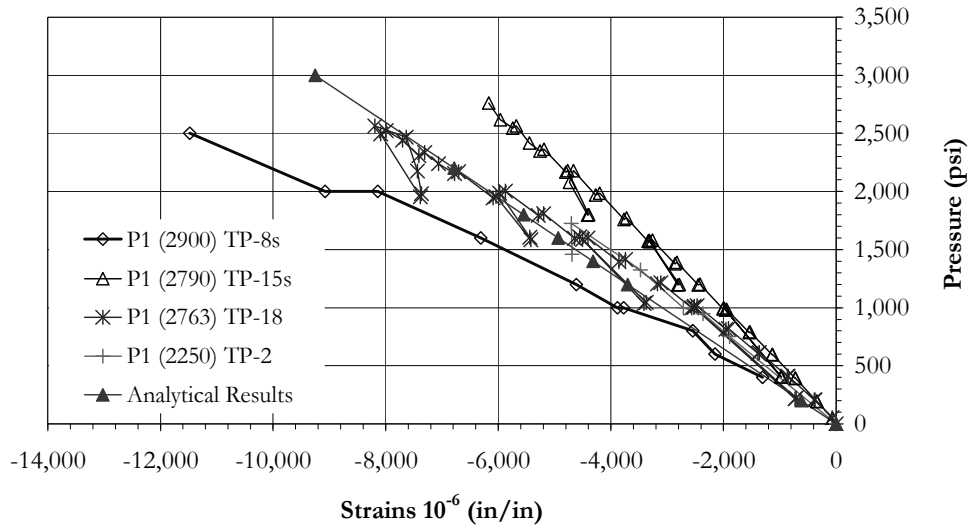

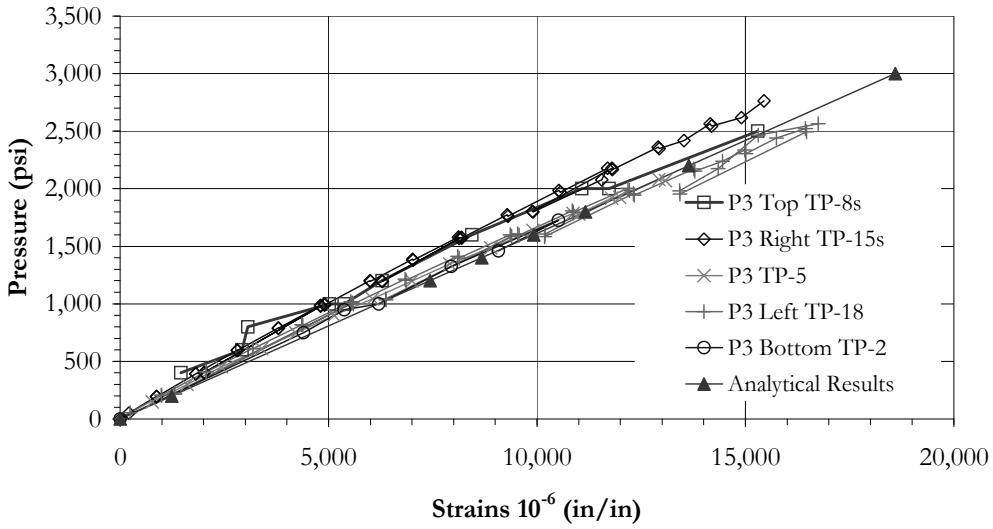

Figure 3.103 Recorded strains for static tests

3.4.1.1.3. MEASURED RESPONSE DURING CYCLIC LOADING

Since there was almost no extensive fiber breakage noted during the cyclic tests in this program, it is very unlikely that the strain records would show any clear indications of the behavior of the specimens. Regardless of the pressure span used in the testing of the specimens, no apparent loss in stiffness was recorded as result of damage incurred in the cycling of the specimens. Even the initial changes of the Poisson's ratio did not seem to have an effect on the capacity of the specimen under cyclic pressure. Figures 3.104 and 3.105 show the recorded strains for specimens in each of the pressure groups tested in the program. Typically the records from the first loads were selected since no loss of stiffness was noted in the specimens during the cyclic testing phase. In some cases records for additional cycles are also shown for information purposes.

The inconsistency of the results is such that no clear conclusions can be inferred from the data. The variability of the results obtained during the tests could be attributed to the amount of initial flaws in the material prior to loading. A note should be made that the differences in thickness of the layers and specimens recorded are considered as part of these initial flaws. A justification for including the thickness variations as part of the flaws comes from the inherent difficulty of accurately estimating as built thickness of fabricated specimens or structures made with fiber composites. As it was seen previously, even within the same component there is the possibility of considerable thickness variations. These variations may not be critical in the ultimate capacity (burst) of the specimen since they are mostly due to resin rich layers and not to increase in fiber content. For the case of leakage, however, such verifications may be of greater importance

There is always the argument that the specimens failed at different cycles because the strains were different for the same pressure, and that if the strains had been kept the same, there would be more consistency in the results. Unfortunately, the results of this program appear to indicate that there was no direct correlation between the strain level at target pressure and the endurance.

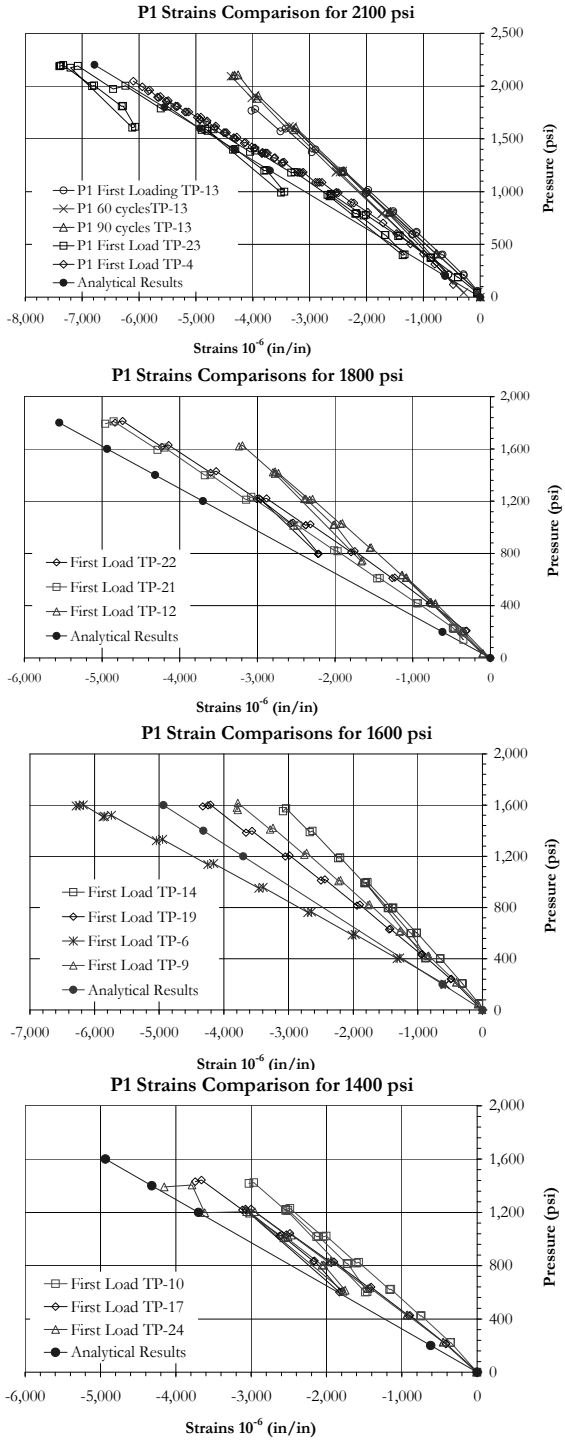

Figure 3.104 Axial strains comparison for fiberglass cyclic specimens

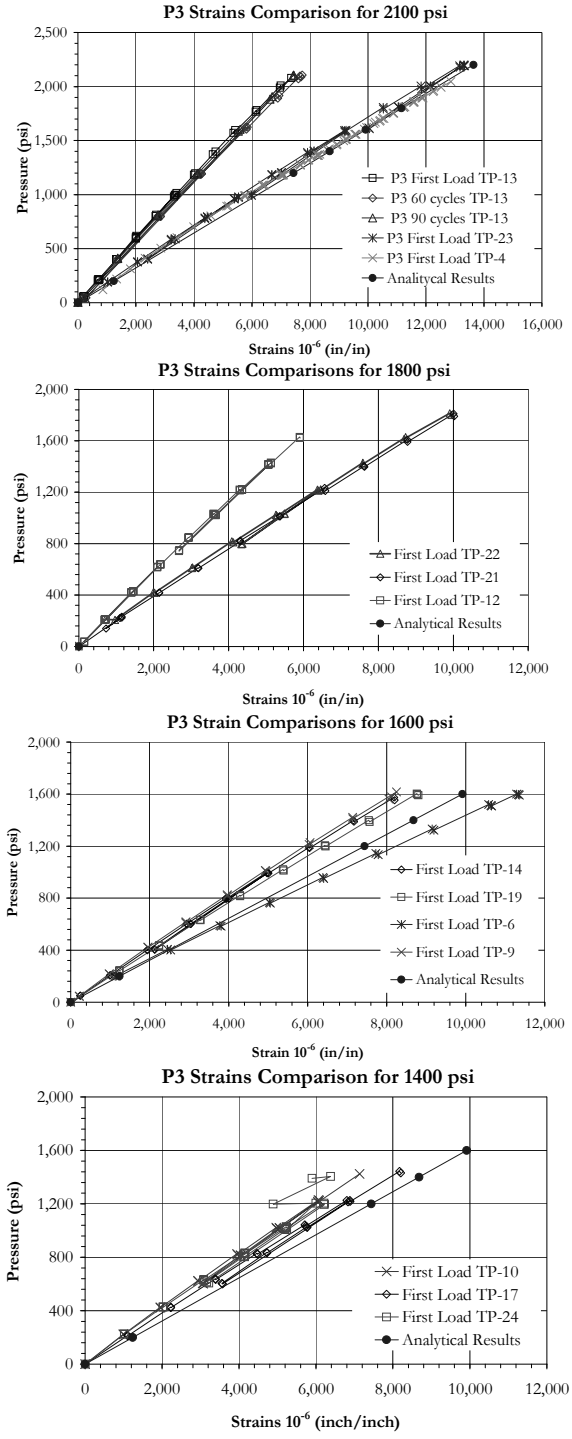

Figure 3.105 Hoop strains comparison for fiberglass cyclic specimens

In some cases the specimens with the higher value of strains at initial loading were the ones with the longer life. There is no debating that a consistent strain level would provide with a more accurate comparison for the results. However, as it was postulated at the beginning of the chapter, there is the possibility that the capacity is more directly related to the liner tolerance to deformation than to the winding strength or stiffness.

3.4.1.1.4. ACOUSTIC EMISSION RECORDS

As stated at the beginning of this section, there were two separate AE knees defined for the specimens. Figures 3.106 shows the pressure at the first and second AE knees respectively for each of the fiberglass specimens. Again, the variability in quality of the specimens is apparent by looking at the 1st knee plots. Remembering that specimens were fabricated in three separate batches we can almost identify the batches by looking at the consistency of levels of pressure that caused the 1st AE knee. Specimens TP-1 to TP-8s were part of the first batch and the most inconsistent ones. Specimens TP-9 to TP-17 were part of a second batch made in the same plant and even though they show the lowest pressure at 1st AE knee, they are quite consistent. Last set from TP-18 to TP-24, were from a different plant belonging to the same company, and probably the most consistent set of the program. The consistency was evident in the results during the life endurance test and also in the pressure for the 1st AE knee.

The information in Figure 3.106 also shows the pressure at which the second AE knee was estimated. As in the case of the first knee plots, the consistency of the specimens can be seen the figure. Specimens from the third and last batch show an extremely good consistency both in the AE records and in the strains and life endurance measurements. The differences are negligible when compared with the other two batches.

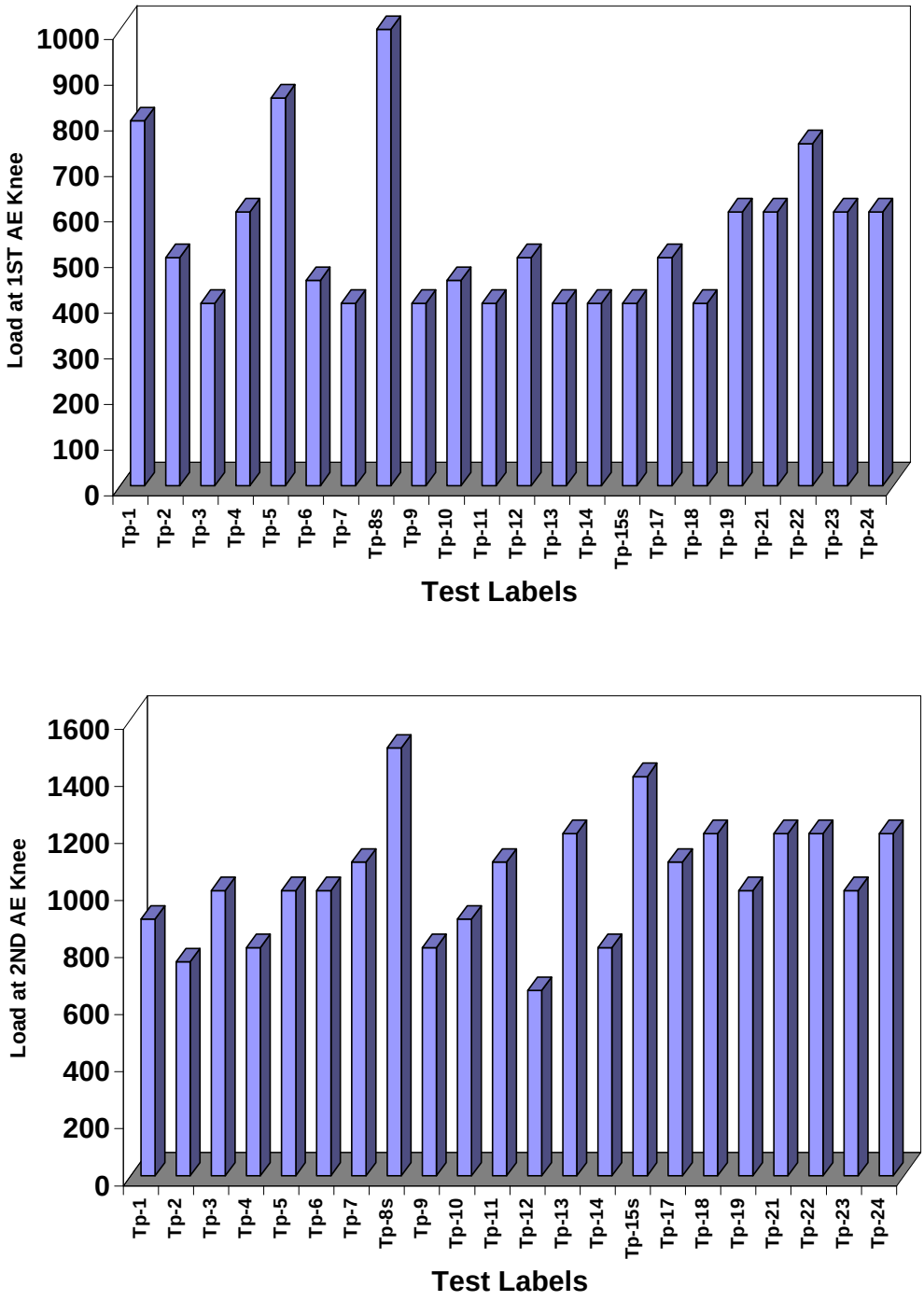

Figure 3.106 AE records summary for fiberglass specimens

3.4.1.2. HYBRID SPECIMENS

In order to develop preliminary data on the effect of adding a carbon layer to the fiberglass construction, two hybrid specimens were tested under static loading to failure or leakage. The additional carbon fiber winding was a single cycle of the winder, or equivalent to one layer of glass fibers.

3.4.1.2.1. ANALYSIS RESULTS

The main question in these specimens was the effectiveness of the carbon layers when combined with the glass pipe. As it was noted in the fiberglass specimens, there was good success in estimated the properties of the material in the direction of the loading. The same type of agreement was not seen for the direction normal to the loading (axial deformation or Poisson's relationship). The properties as calculated for the hybrid pipe are as shown in Figure 3.107. These properties assume a perfect bond between the layers of glass fibers and carbon fibers.

Tensile		Modulus		Ult. Strength	
- Longitudinal	=	1,338,508	psi	10,384	psi
- Transverse	=	1,951,369	psi	35,208	psi
- Normal	=	1,139,865	psi	1,541	psi
Flexural					
- Longitudinal	=	1,262,950	psi	25,713	psi
- Transverse	=	1,625,732	psi	25,716	psi
Shear					
- L-T (Inplane)	=	730,175	psi	17,024	psi
- L-N	=	400,589	psi	3,938	psi
- T-N	=	377,103	psi	4,684	psi

Poisson ratios - Load direction / Strain direction

- L/T = -0.32 T/L = -0.46
- L/N = -0.25 N/L = -0.22
- T/N = -0.23 N/T = -0.14

Neutral axis (measured from the centroid)

- Longitudinal = -0.023 in
- Transverse = -0.067 in

Figure 3.107 Calculated properties for hybrid pipe

3.4.1.2.2. MEASURED RESPONSE DURING STATIC LOADING

Figure 3.108 shows the measured strains for both hybrid specimens. In addition to the measured strains, theoretical values obtained using the properties shown in Figure 3.107 are added to the plot.

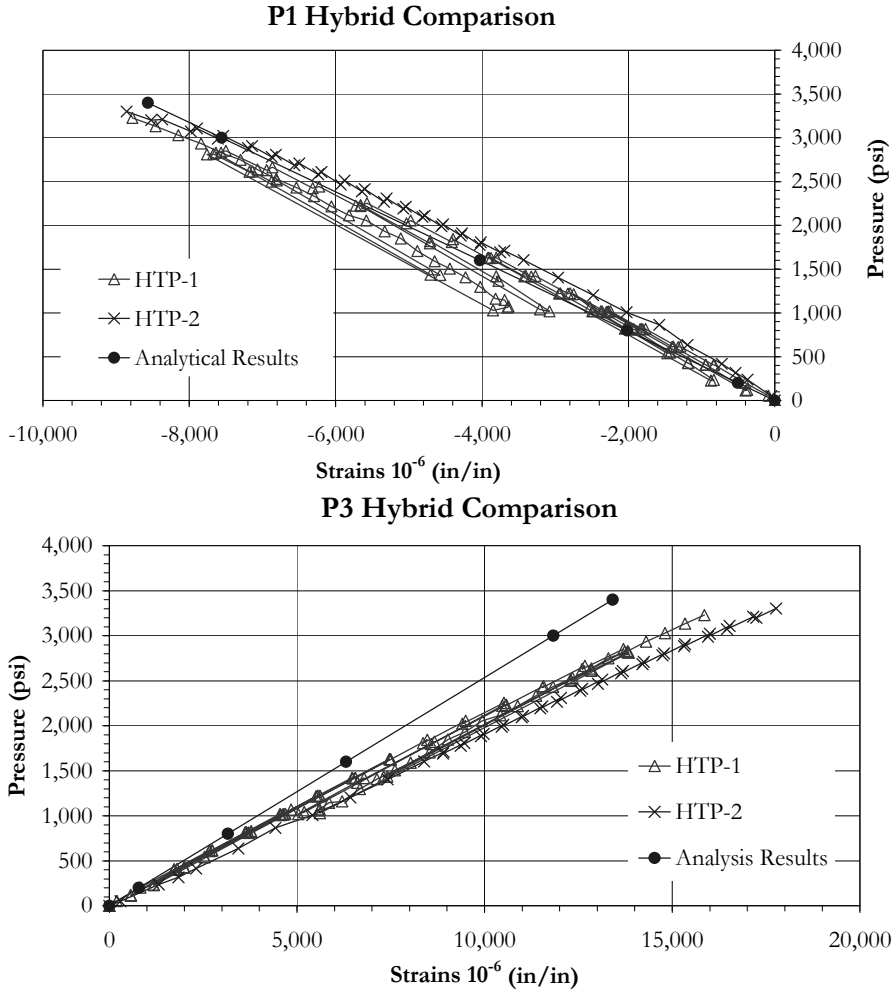

Figure 3.108 Measure strains for hybrid specimens

As seen, there was very good agreement between the tested specimens in the measured strains. Both the axial and the hoop strains show this agreement. They do not, however, show the same agreement with the calculated strains for the direction of the

loading. It is apparent that the participation of the carbon fiber in the overall stiffness of the composite was not as assumed in the analysis.

Another side effect of the use of carbon fibers was the mode of failure for both specimens. As indicated before in the chapter, instead of leakage, these specimens exhibited burst as the mode of failure at maximum pressure. This type of failure will have serious implications in the determination of factors of safety for pressure vessels under internal pressure. The maximum strains recorded for these hybrid specimens were 1.6% to 1.8% in the hoop direction and of 0.9% in the axial direction. These strains were approximately the same as those recorded for the fiberglass specimens at the time of leakage but at lower pressures. Therefore, there was an increase in stiffness between the fiberglass and the hybrid specimens between 20% and 30%. However, this is still less than the estimated change in stiffness using the theoretical values for the hybrid action. The estimated increase in stiffness between hybrid and fiberglass specimens had been of about 45% over the stiffness of the fiberglass specimens. This suggests a partial interaction between the layers of a hybrid specimen as the result of the mismatch of properties between the glass and carbon fibers.

3.4.1.2.3. ACOUSTIC EMISSION ANALYSIS

A previously observed trend for specimens with carbon fiber reinforcement was found here. Carbon specimens tend to be extremely active in the generation of AE, quite more than fiberglass specimens. For the hybrids, once AE activity was recorded it continued during all load holds and increased during part of the loading profile. This makes interpretation of parametric data extremely difficult. Even in the plots for the HI, no clear indications were noted. Therefore, in the case of hybrid specimens only one AE knee is recorded and that is the first one as defined by the HI plot. Figure 3.109 shows the HI plots for specimens HTP-1 and HTP-2.

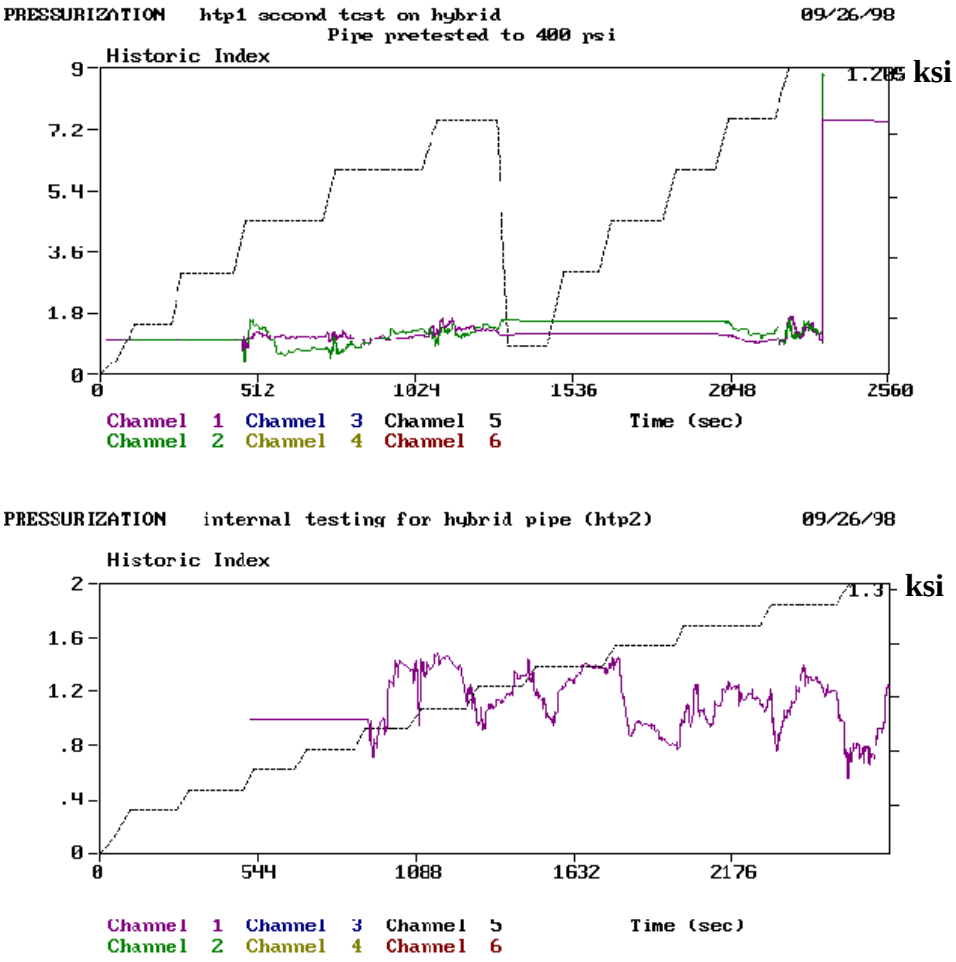

Figure 3.109 Historic index plots for hybrid specimens

As noted in the figure, the location for the onset of significant damage was determined at 1200-psi for HTP-1 and 1100-psi for HTP-2. This correlates with the recorded failure pressures since the pressure for HTP-1 was higher than for HTP-2. Unfortunately with only two specimens, extrapolation of this characteristic is difficult. Unfortunately, as it was seen in the presentation of the results section, emissions were very high in number after this point was reached, obscuring any other possible observation in relation to the AE profile and maximum pressure.

3.4.1.2.4. INTERACTION BETWEEN LAYERS IN HYBRID SPECIMENS

As seen in the strain records between the theoretical values and the recorded ones, only a partial interaction between the layers of carbon and glass fiber existed. To determine the amount of interaction lost in the hybrid specimen, look back at the measured versus calculated strains. Figure 3.110 shows the same strain plots as presented before, only in this case a fourth line has been added to represent the theoretical value of a reduced interaction between layers.

The material properties used in the partial hybrid plot are presented in Figure 3.102. The apparent reduction in stiffness is about 23% of the full active hybrid system. Or in other words, the carbon layer is only about 75% effective in improving the stiffness of the specimen. Considering that 1/3 of the number of cycles used for the fiberglass winding were used for the carbon winding with an effective increase in stiffness of only about 20%, the value of the carbon layer is questionable. The change in failure mechanism between hybrid and fiberglass specimens is another point of concern.

3.5. DESIGN CRITERIA COMPARISONS

Using the design criteria presented at the beginning of this chapter the estimated design capacity of the fiberglass specimens tested here will be determined. This will provide insight into the adequacy of the existing limits of design most commonly used.

3.5.1. FIBERGLASS SPECIMENS

The two main approaches available for commercial design of pressure vessels are given by the American Society of Mechanical Engineers [3.2 and 3.3]. They are the RTP-1 committee specifications and the Section X specifications. First, we will look at the RTP-1 specifications and then at the Section X.

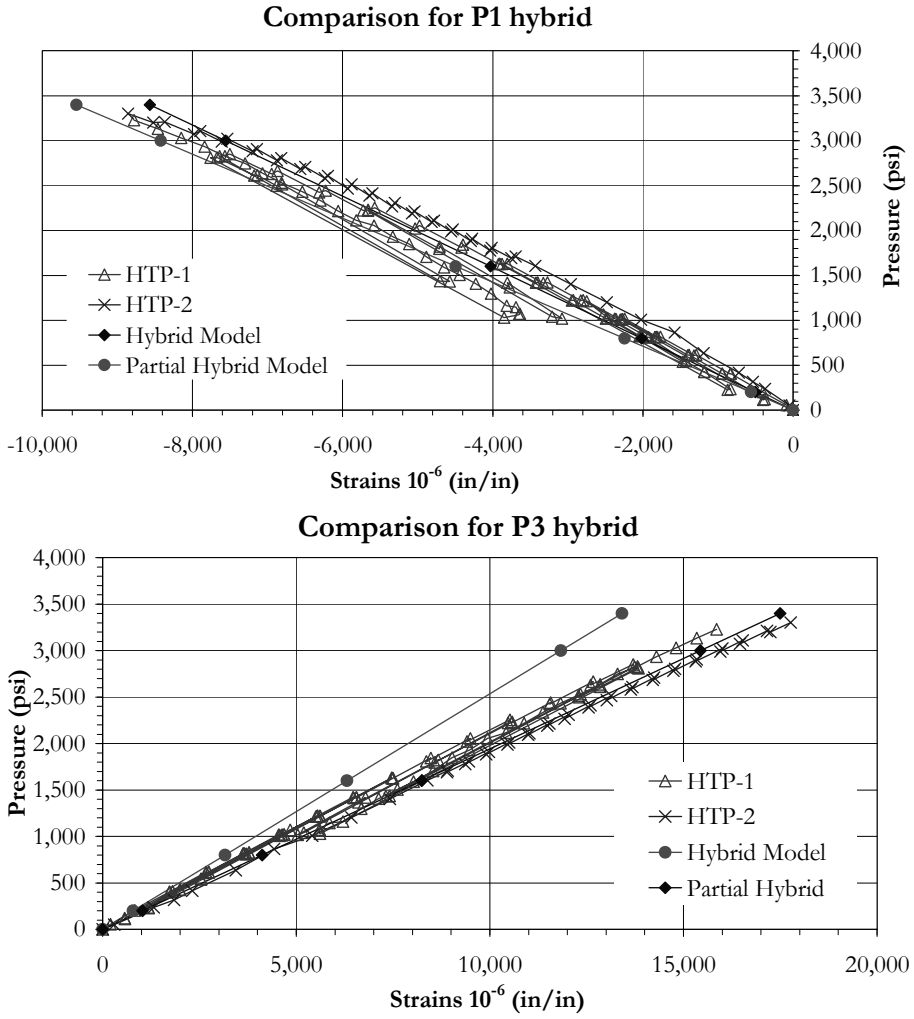

Figure 3.110 Partial interaction between layers

As noted in the beginning of this chapter, RTP-1 provides two different design approaches available for the engineer. Subpart 3A Design by Rules and, 3B Design by Stress Analysis. Using the expressions for the design by rules approach, the maximum allowable pressure for a vessel with the same characteristics as the one tested here would have been 55-psi. Looking at the values calculated using the theoretical properties for the fiberglass specimens, we see that using a maximum strain of 0.1% would correspond to a pressure of 160-psi. Even with a safety factor of 2, this would still be 80-psi. This

indicates the importance of the liner in the structural behavior of this type of construction. The design by rules as established by RTP-1 appears to be overly conservative not on the allowable pressure itself, but on the participation of the liner as a structural component.

Adopting the specifications of subpart 3B of the RTP-1 specifications would allow for the use of the internal liner as a structural component. It does penalize the liner by applying a more strict safety factor in its design. For purpose of comparisons we will use the more strict of the safety factor in the calculations (SF=10). Using this factor the allowable pressure of the specimen as detailed here would have been 260-psi for the internal liner dimensions. For the fiber winding, using the factor of safety of 1.6 results in an allowable pressure of 1600-psi. At the time of the leakage in the statically tested specimens with the lowest pressure (1800-psi), the strength ratios as calculated for each layer were 1.33 for the liner and 1.45 for the winding layers. In the case of the highest recorded static pressure, the strength ratios were 0.86 for the winding and 0.83 for the liner. This seems to indicate that, at least for the static capacity of the specimens, the safety factors associated with the winding are not sufficient and for the liner are too conservative. Assuming that the endurance limit of the specimen is associated with the pressure at which the AE knee is recorded results a pressure of about 1000-psi. For this pressure, the safety factors in the liner and winding were 2.4 and 2.5 respectively.

Section X has a higher allowable operational pressure for vessels designed using the specifications part of its code. The main difference between sections X and RTP-1 is the use of a safety factor of 2 in RTP-1 that is not present in Section X. The Section X expression uses the inside radius where RTP-1 used the diameter and then divides by 2. The only other difference in the expressions for the allowable internal pressure for the hoop stress only case is the addition of a 0.6P term as reduction factor. Using this expression, the allowable pressure in a vessel like ours would be of about 105-psi. Section X also allows for the use of a stress analysis approach with a safety factor of 6. The pressure allowed for this approach would be of about 450-psi.

In general it would appear the maximum allowable strain of 0.1% is too conservative. Tests indicated that if a specimen is loaded below the point of AE emission, no endurance limit would be probably found. In most cases this point of the AE knee was above 1000-psi. Using this as a limit, it is possible to estimate that a maximum strain of at least 0.3% could be safely used.

3.5.2. HYBRID SPECIMENS

At this time there are no established design criteria for hybrid specimens similar to those discussed in the previous section. Most of the hybrid components in use today are subjected to a series of proof tests to determine their acceptability for their intended application. Developing an acceptable design criterion requires more than the two specimens tested in this program. Future work in similar specimens will provide with the required additional information in order to develop reliable criteria.

3.6. SUMMARY AND CONCLUSIONS

A number of tests were performed for this internal pressure program. Static tests were conducted to assess the typical variability seen in commercial composite construction. Following the static tests, a series of cyclic pressure tests were performed on similar specimens. The tests did not follow the specifications of ASTM 2992 D by design. The purpose was to determine is there exists the possibility to estimate the capacity of a pipe specimen without having to perform the long term cyclic testing required by the specification. In addition, the tests were aimed at re-evaluating the design specifications in the two ASME codes, RTP-1 and Section X. The use of AE was explored as means of determining allowable stress values in as-made specimens or components.

Strain data in experimental programs has been a regular and reliable source of information as to the behavior of a component or structure. In the case of ultimate

behavior of fiber reinforced composite materials, it has proven mostly reliable. However, in the determination of less catastrophic limit states, sometimes strain data does not provide with a clear indication of behavior changes. The resulting loss of stiffness associated with matrix cracking in composites is not readily apparent when looking at the deformations measured in the direction of the loading [3.11]. The influence of the fiber reinforcement on the overall stiffness of the material is so high, that the drop in the contribution of the matrix is imperceptible. In cases where considerable flaws are generated at the location of the measuring device (in our case strains rosette), these present themselves as jumps in the strains. However, the overall stiffness of the component could remain virtually unchanged. Estimating the importance in the behavior of the localized flaw is also difficult since it depends, in most cases, on the expected loading or stress profile and the structural function of the component. In addition, the uncertainty of the extent and size of the flaws in a structure is a big part of the design process and safety factor determination in composite structures.

The static test showed large variability in the leakage capacity of specimens tested during this loading phase. Pressures ranged from 2900-psi to 1800-psi for specimens fabricated to the same specifications. The resulting records of strain measurements did not seem to show a clear pattern in relation to the leakage capacity. They did show, however, that estimates for the properties in direction other than the loading direction are inaccurate using current models. Not enough information is available to generalize an expression for determining these properties, but the obvious trend was towards underestimation of the stiffness and Poisson's ratio.

The strains recorded during the tests at the time of failure were almost 20 times larger than that allowed by design codes. This does not account for long term effects in the component under sustained loading. However the cyclic tests performed were designed to approach the question of damage accumulation. Results at pressures above 1600-psi were inconsistent as to the number of cycles required for failure or leakage. Strain measurements showed no apparent loss of stiffness as a result of cycling. In

addition, residual deformations recorded at the end of each static monitoring were mostly recovered in one day of rest.

Acoustic emission records showed some interesting trends during the monitoring of all the tests. Some of these relationships will be explored in more detail in the following chapter in this dissertation. There was also an observed relationship between the cyclic endurance and the AE knee that will also be explored. The lowest pressure where this second AE knee was recorded was 800-psi; the results of the cyclic test suggest that this could be the endurance limit of the specimens. Tests at 1200-psi of load span showed that the specimens suffered minimal damage after one million cycles. These specimens had the second knee recorded at 1100-psi, slightly lower than the maximum pressure. Using this AE milestone as the endurance limit, we can see that allowable strains of up to 0.3% or more may be possible in the design of vessels in the direction of the loading. This would result in an improvement of up to 300% over the previously accepted limit.

The mode of failure of the fiberglass specimens does raise some concern over the philosophy in the design of lined vessels. The maximum pressure was reached during the static loading used for the AE monitoring. Once the failure of the internal liner was achieved, complete leakage was generated until the pressure inside the specimen equilibrated the ambient pressure. No previous indications were visible before failure, which would make prediction based on visual methods very difficult. Typically, internal liners are not included in the design of the vessel and when they are the are penalized with a very high safety factor. This could make the liner sometimes stronger than the winding shell. The side effect is that when failure of the liner is reached by stress or deformation the fluid contained in the vessel will be sprayed to the outside. Tanks built with this system are used in containing corrosive or hazardous materials. The possibility of having a failure where the material is suddenly released is of concern. Failure for this type of tank should be controlled to generate a small amount of weeping rather than a sudden release.

Promising indications of prediction of life by use of non-destructive methods were observed and will be presented later. The need for methods for determining capacity of a vessel based on non-destructive monitoring was also reinforced by the variability of the results presented here.

CHAPTER 4

STUDIES ON IMPACT DAMAGED TUBES

4.1. INTRODUCTION

Fiberglass tubes my be subject to impact damage sometime during their service life. Such damage may affect the tube's capacity to sustain internal pressure and other types of loading. Non-visual methods of evaluation for determining the damage extent and residual capacity are of interest. The difficulty with providing an accurate evaluation of damage based on a purely visual inspection can be seen in Figure 4.1.

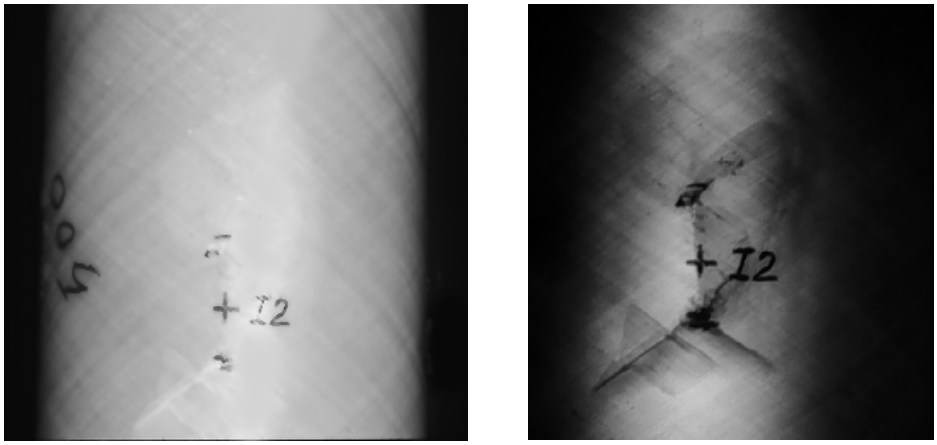

(A) **(B)**

Figure 4.1 Visual Evaluation of Impact Damage

This figure presents two views of the same impact damage on a fiberglass tube specimen. View (A) shows the surface as it would be seen in a well-lighted environment. As can be seen, the indication of damage is barely visible, with some surface delamination noted as a result of the slight de-coloration. View (B) shows the same damage area with an interior light source. Here the extent of delamination is more noticeable along with deep cracking as depicted by the darker lines. This type of

inspection would provide some additional information as to the extent of damage. Nonetheless, even this more revealing view does not permit an evaluation of the loss of structural capacity due to the impact damage. There is a need for a global inspection method that will provide with information on the presence of impact damage, residual strength and location of damage.

4.1.1. PREVIOUS RESEARCH WORK

Relatively few publications exist where studies of impact damaged pipes and the significance on their capacity is presented. Initial studies were by Manders and others (1979), who performed studies of impact damage in fiberglass composite tubes. The main features resulting from this study were that failure of the tubes consisted mainly of matrix microcracking followed by delamination, and resulting from fiber microbuckling. They observed the formation of large cracks through the wall of the specimen in addition to considerable local fiber damage, at which point the specimen began to loose capacity under internal pressure loading. Lloyd and Knight (1986) confirmed that fiber fracture was the dominant factor that results in the degradation of burst capacity. Delamination and transverse matrix cracks will have an effect on the shear capacity and compressive strength, but they will have a minimal impact on the burst capacity of the pipe.

In another work, Anderson and Evans [4.18 and 4.19] studied mechanisms and the progression of failure in filament wound glass/epoxy composite pipes under static and impact loads. The main conclusion was that, even when the nature of the damage was similar under the static and impact loadings, the extent of the delamination is much larger for the impact loading than for the static one. This would appear to indicate that the fracture strength of the interface is rate-dependant, because the deformation resulting from impact is more localized that that developed by an identical magnitude of normal force applied statically. Another interesting feature reported in this work was that apparently the level of damage during impact was larger for a pipe resting on a hard surface in comparison to similar specimens resting in cradle-type supports.

Matemilola and Stronge [4.13] performed follow-up work, associated with impact damage on composite vessels, where results of low velocity impact tests in carbon fiber reinforced pressure vessels was reported. Their specimens were of 0.39 inches wall thickness, 12 inches in diameter and a length of 38 inches. Both static and impact tests were performed on the specimens, followed by burst pressure tests. The results indicated that observed damage included fiber microbuckling, matrix cracking and delamination. The results also indicated that burst pressure of a damaged vessel decreased with the ratio of axial length of damaged fibers l, to vessel wall thickness h, up to a ratio l/h = 3; where beyond this length of damaged section the burst pressure was independent of length of damage. Measurements of strain at regions near loading points showed that damage related to fiber microbuckling is sensitive to strain rate. In locations where impact damage was predominantly due to fiber microbuckling, the failure strain measured was about six times the strain measured for the same mechanism during static loading.

Matemilola and Stronge's experimental program included the determination of the effects of the shape of the impactor and the amount of energy imparted to the structure. Figure 4.2 shows two of the most important results as recorded by their research program. View (A) shows a distribution of the impact forces used in the tests. View (B) shows a summary of the results of the burst tests. Burst pressure of the damaged pressure vessels decreased with an increase in the axial extent of the damage to the fibers. The results were plotted normalized to the ratio of length of fiber damage to wall thickness (l / h). Results presented in View (B) are for both types of impactors used in the testing. In the figure, the dash-dot line represents the effect on burst capacity of uniform removal of the outer laminate. The other curves are obtained by calculating the capacity of the specimen using expressions developed from the ones obtained by Timoshenko and Woinowsky-Krieger [4.35] and modified by Matemilola and Stronge [4.13].

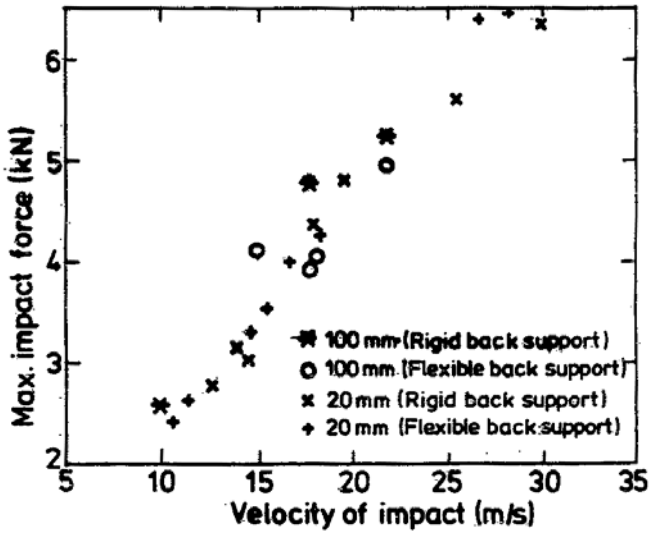

Variation of maximum impact force with incident velocity for impactors with 20 and 100-mm-dia noses, each having a mass of 2 kg. For each impact, the pressure vessel has either a rigid or flexible back support.

View A

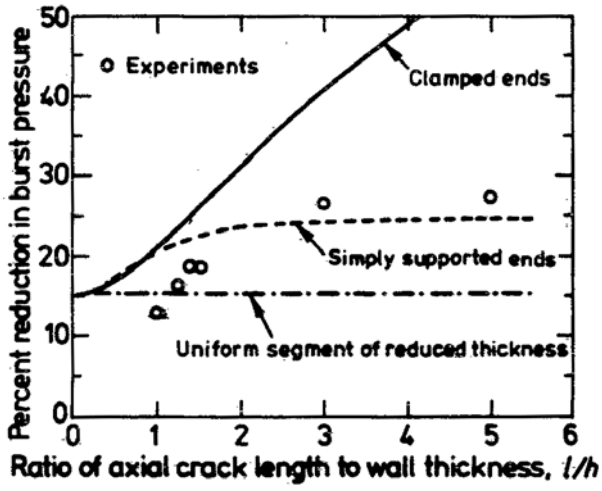

Effect of fiber crack length on the reduction in burst pressure of a filament-wound composite pressure vessel

View B

Figure 4.2 Test results from Matemilola and Stronge (4.13)

The expression developed resulting from this research program for the prediction of burst pressure is as follows:

$$\frac{P}{\tilde{P}_b} = \frac{Cos^2\tilde{\theta}}{Cos^2\theta}\left\{\frac{\left(\frac{\tilde{r}_o^{\,2}}{\tilde{r}_i^{\,2}}-1\right)+\left(\frac{\tilde{r}_o^{\,2}}{\tilde{r}^{\,2}}+1\right)\left(\frac{\tilde{r}_o^{\,2}}{\tilde{r}_i^{\,2}}-1\right)^{-1}\tan^2\tilde{\theta}}{\left(\frac{r_o^2}{r_i^2}-1+\frac{l^2/r_i^2}{2\left(r_o/r_i-1\right)^2}\right)+\left(\frac{r_o^2}{r^2}+1\right)\left(\frac{r_o^2}{r_i^2}-1\right)^{-1}\tan^2\theta}\right\}$$

Where the tilde denotes undamaged pipe properties, those without tilde are the damaged pipe properties for the same locations. The term r_o is the outer radius, r_i is the inner radius, and r is the radius or the laminae with the maximum fiber tension. The angle θ is the angle of the fibers with respect to the longitudinal axis of the pipe at the laminate with the most fiber tension. This angle could be different between the damaged and undamaged pipe. The term l denotes the length of the annulus that will cover the damaged area, i.e., it is the length of the damaged section with respect to the longitudinal axis. Finally, term P denotes the internal pressure (burst) capacity of the specimen. Therefore, the expression is developed to determine the ratio of reduction between the undamaged and damaged specimen.

A significant limitation of the expression presented above is that it is proved valid only for cases where the damage induced by the impact does not extend beyond the second layer of the composite wall. The expression does not account for the depth of the damage only for the extent of fiber damage in the longitudinal direction of the pipe. In addition, the expression was developed for carbon fiber specimens, and may not be necessarily valid for fiberglass pipes. Nevertheless, the work presented by the authors present a rational approach for the determination of extent of damage of impacted pipes. Accounting for the depth of damage and including it in the expressions would complete this approach to account for most possible conditions.

4.1.2. PROGRAM OBJECTIVE

This program was aimed at studying several issues in the assessment of impact damage in composite materials. The first objective was to explore methods for monitoring the progression of impact induced damage with the use of non-intrusive techniques.

In the area of strength evaluation, the next objective of the program was to assess reduction in capacity based on non-destructive evaluation methods. The convenience of evaluating the severity of the damage and its influence on the capacity of the structure as it remains on site would be valuable. Therefore, this objective was to explore the possibility of developing in-situ methods for evaluation of composite tubular structures subjected to impact damage

4.1.3. MONITORING THROUGH NDE METHODS

Traditionally acoustic emission (AE) has been successfully used in the monitoring of in service pressure vessels and railroad tank cars among other applications. The development of high fidelity broad band sensors and digital capturing equipment provide AE with additional digitized information in conjunction with the features traditional extracted [4.1, 4.2]. On itself, the use of broadband sensors has limitations associated to their performance. In general, broadband sensors are less sensitive than the resonant type, as a result, in some cases these sensors will not detect emissions that would be detectable with the use of resonant sensors. This new data however in addition to the feature extraction and analysis of AE may provide a reliable tool that not only will identify the damage and its effect on the capacity but also its location.

An additional nondestructive evaluation technique used in this program was thermal emissions monitoring. Figure 4.3 shows the SPATE™ (**S**tress **P**attern **A**nalysis through **T**hermal **E**missions) system as used in this program. The system consisted of a

camera aimed at the specimen. Controlling this camera was a PC-based system. Unfortunately at the time of the testing for this phase, the system suffered a malfunction in its ability to download data either to an external data disk or to a hard copy. Most of the images used here were obtained by taking digital screen shots of the data from the PC monitor.

One of the advantages of using a thermal system is its ability to study the localized region of concentrated damage. There are, however, disadvantages to keep in mind when planing to use a thermal monitoring system. One of them is the difficulty in determining the real state of stress in conditions with complicated loading. Thermal changes in the material are related to the sum of the principal stresses at that point. In a material like fiber reinforced composites, determining the exact state of stress at a particular point is difficult. Therefore, in most cases the usefulness of the thermal monitoring will be limited to a qualitative evaluation.

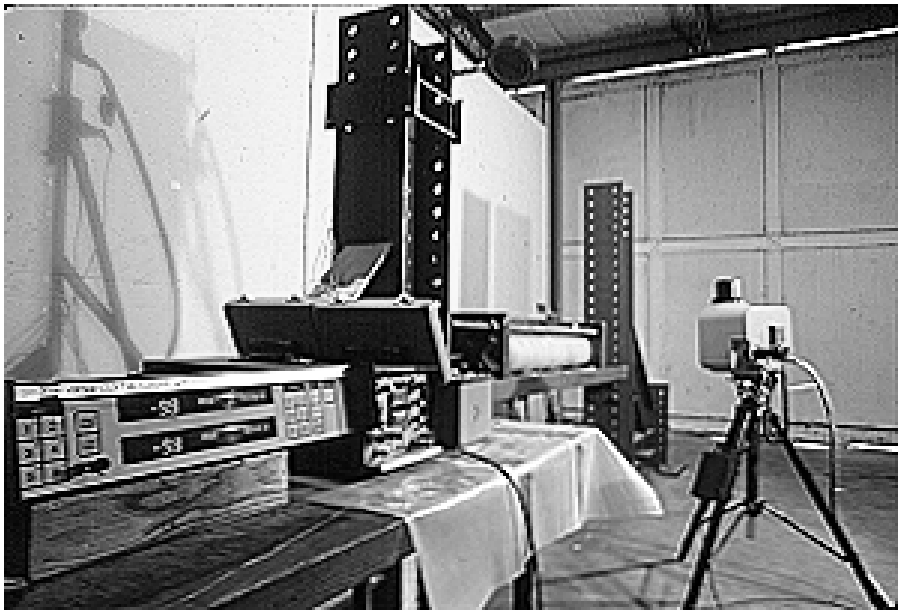

Figure 4.3 SPATE monitoring setup for impact specimens

Geometry is another constraint in thermal monitoring. It is very difficult to account for changes in the geometry in the structure at the time of the monitoring. Circular surfaces provide a difficult geometry for reliable area scans since each point within the area is at a different distance from the monitoring camera. This is a problem that could be solved with modifications and additions to the controlling software for the equipment. Finally, flaws that are not near the surface may be difficult to detect by thermal emissions.

4.2. EXPERIMENTAL PROGRAM

4.2.1. SPECIMEN DESCRIPTION AND PREPARATION

The specimens used in this program were fiber reinforced epoxy pipes made by the continuous winding process. The reinforcement was E-Glass with 60% content by volume and a winding angle of ±60 degrees. The proportions of fiber in the specimens were verified by chemically digesting the resin, with a deviation in the results of less than 5%. Three sets of specimens were used in this test program. The difference between the sets is the wall thickness of the pipes. The wall thicknesses were 0.13 inches, 0.37 inches and 0.52 inches for the three sets of pipes. The inside diameter of all the pipes was 5.95" with a total length of 3 ft each. To avoid variability in fabrication typical in composite materials, specimens of the same thickness were obtained from a single longer pipe. Each one of the longer pipes were 14 ft in length. Before testing, the specimens were reinforced by providing a tapered buildup at the ends. This was to avoid the premature failures, typical in composite materials, of the specimens to be pressurized after impact loading. The buildup was provided by means of additional winding of glass/carbon fibers that tapered from zero at 8" from the end to a thicker profile at each end of the pipe.

4.2.2. TEST SPECIFICATIONS AND SETUP

The program consisted of three phases of testing. The first test phase was a static punch series where three separate punch profiles were used. One profile was a round punch of ½ " of diameter with a spherical head. The other profiles were a rectangular narrow punch with dimensions 3/16" x 1½", and a long one of ¼ x 6". The static tests were aimed to help determine the AE signature of the failure mechanisms associated with each punch, along with the maximum load at failure. In addition, deformation readings were taken in order to compare later with readings from the low velocity impact tests. A picture of the setup for the static tests can be seen in Figure 4.4.

Figure 4.4 Static punch setup

The dynamic impact was performed with a cylindrical weight setup in a pendulum type setup. The energy of the impact could be controlled by adding weight to the end of the pendulum, or increasing the release height. Figure 4.5 shows the frame used for the impact testing along with the AE acquisition equipment.

The readings taken during impact were of deformation of the pipe in the outer and inner diameter with the use of Direct Current Displacement Transducers (DCDT). Deformation at the punch was measured with the use of strain gages (four each punch).

Figure 4.5 Low velocity impact setup

The data was recorded with the use of a National Instruments board based Data-Logger at a rate of 5 kHz. At the fast rate used in the acquisition, some electronic noise is to be expected in the system. This noise was filtered with the use of a wavelet based de-noising routine and MatLab® software applied to the data after recording. In order to maximize the use of each specimen, the pipes were damaged in two separate locations with two different impact profiles. As show in Figure 4.6, each impact was made at about 1/3 of the length of the pipe and at diametrically opposed locations and ends.

The acoustic emission system used in the test program consisted of two separate units and sensor types. Both 150 kHz resonant sensors and high fidelity broad band sensors were used to acquire AE data. Although for most of the test, only feature extraction hardware described at the transportation instrument was used. The data acquisition systems used are manufactured by Physical Acoustics Inc (PAC). These were the Transportation Instrument for the resonant sensors and the Mistras-2000 for the digital information. The settings on the transportation instrument were the default settings as provided by the manufacturer. In the Mistras system, the threshold was set to 40 dB, with a gain of 40dB on the preamplifier and a pretrigger timing of 100 μsec in order to capture the complete waveform.

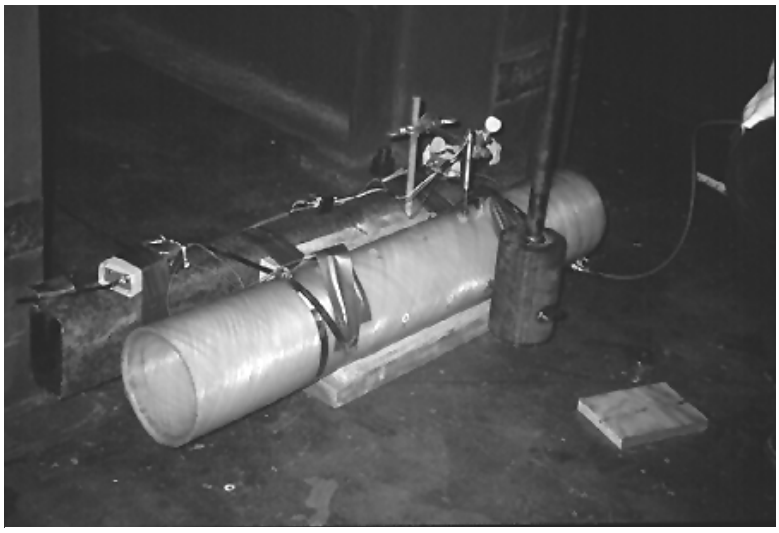

Figure 4.6 Location of impact regions

After impact testing the pipes were subjected to internal pressure. The intent was to determine the reserve leak/burst capacity after impact. The tests were monotonic loading to failure. During the static pressure testing, regular monitoring sessions with the SPATE™ equipment were carried out. The use of the SPATE™ machine generated the need to apply a cyclic load while making the thermal scans. Because it was desired to avoid damage growth due to fatigue as much as possible, the cycles were made at the lowest pressure level possible. It was decided to keep the maximum pressure under the rated service pressure for each of the three thickness tested. As it will be shown later in this chapter, these service ratings were well below the static leak capacity of each pipe. The seal system selected allowed for axial deformation of the specimen while maintaining a constant pressure. The loading was in stages to leakage/burst, with regular load holds for AE monitoring.

4.3. TEST RESULTS

The program consisted of two phases of tests. The first phase consisted of a series of static penetration tests with the same punch profiles as would be used in the low

velocity impact tests. The second phase was to test pipes under low velocity impact followed by internal pressure tests. Strain gage readings were kept only for the control specimens for each of the thicknesses tested. No strain data was obtained from the impacted pipes.

4.3.1. STATIC PUNCH TESTS

The results from the static punch tests are shown in Table 4.1. Tests were performed in specimens of all three thicknesses for damage mechanism identification. As indicated before, three separate punch surfaces were used in the test. The specimens labels are H5, H15 and H20 to represent respectively the 0.13", 0.37" and 0.52" specimens. The AE sensors were placed on the top surface of the specimen in all the tests. Failure loads were determined as the loads where the deformation of the loading head increased without any increase in the measured load. The tests were repeated in separate areas of specimens to verify results.

Specimen	Thickness	Punch Dimensions	Max. Load
H5	0.13"	½" round	0.5 kips
H5	0.13"	¼" x 1 ½"	0.8 kips
H15	0.37"	½" round	1.8 kips
H15	0.37"	¼" x 1 ½"	4.4 kips
H20	0.52"	3/8" round	4.0 kips
H20	0.52"	¼" x 2 ½"	8.5 kips
H20	0.52"	¼" x 4"	14.0 kips
H20	0.52"	¼" x 6"	19.0 kips

Table 4.1 Static Punch Results

Before performing the tests presented here, a series of static tests were performed in a separate set of tubes to determine the most critical punch size and orientation for the specimens used here. It was determined that the use of the round punch and the longer one oriented along the pipe axis would provide two common

damage mechanisms that may be encountered as a result from impact. The round punch presented a considerable amount of surface damage followed by fiber breakage and finally delamination at the higher loads. On the other hand, the longer punch caused almost imperceptible surface damage and extensive delamination of the interior layers. This trend was confirmed by the low velocity test that showed that same damage profile for the two punch surfaces in all of the tests. The only difference was the extent of damage observed after each impact level, but the mechanisms remained the same. Figure 4.7 shows the general damage profiles for the two punch areas used.

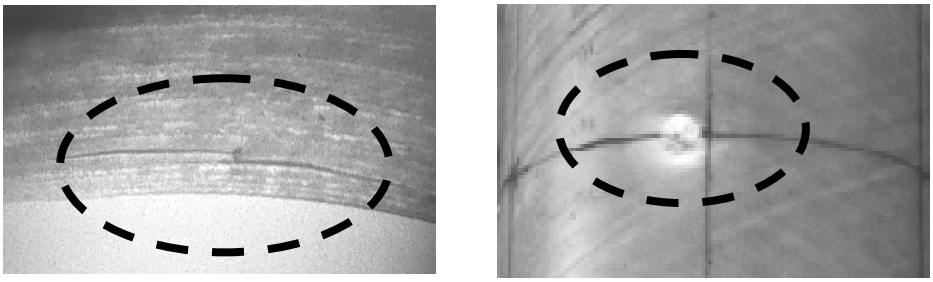

Long Punch Tests **Round Punch Tests**

Figure 4.7 Damage mechanisms for static and impact tests

4.3.1.1. DEFORMATION MEASUREMENTS

Two different displacement measurement points were used during the static punch tests. One displacement gage was placed at the location of the loading head, the other at 6 inches from the loading point at the top surface of the pipe. Results will be presented by pipe type from thinner to the thickest of the specimens.

For the thinner specimens of the H5 group, the round punch did not produce as an extensive penetration as with the others (Figure 4.8). Matrix cracking and interior layer delamination were the primary damage mechanisms. Cracking at the internal diameter of the pipe was also noted immediately after the maximum load had been reached. With the rectangular punch surface, almost no surface damage was noted and maximum load came when the interior layers began to delaminate. Once the first load

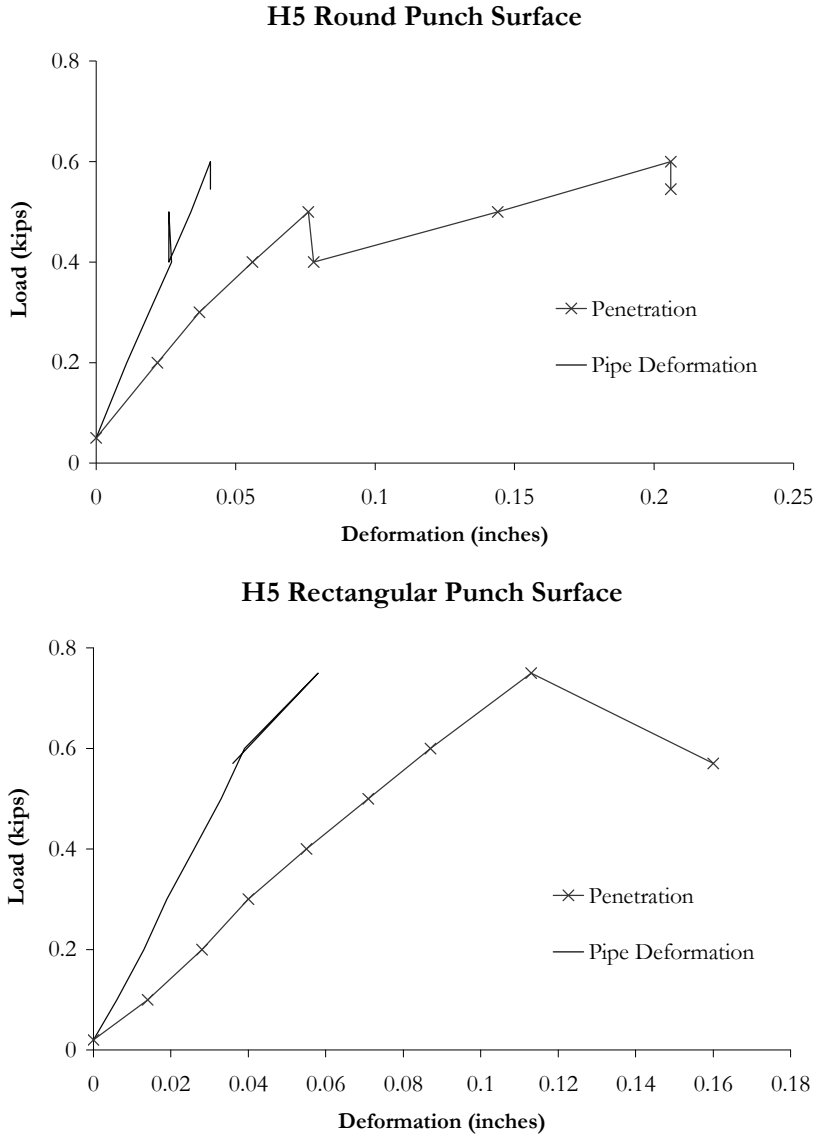

Figure 4.8 Static punch tests for H5

drop was reached, subsequent load increments were not able to reach the previous level.

The most notable feature for the H15 tests is in the results for the rectangular punch surface (Figure 4.9). At the time of failure, as defined by the load drop in the testing machine, a recovery is noted in the pipe deformation. In the round punch for the H5 specimens no real recovery was recorded at the gage 6 inches from the loading point. For all of the specimens in the measured pipe deflection with the rectangular punch, at

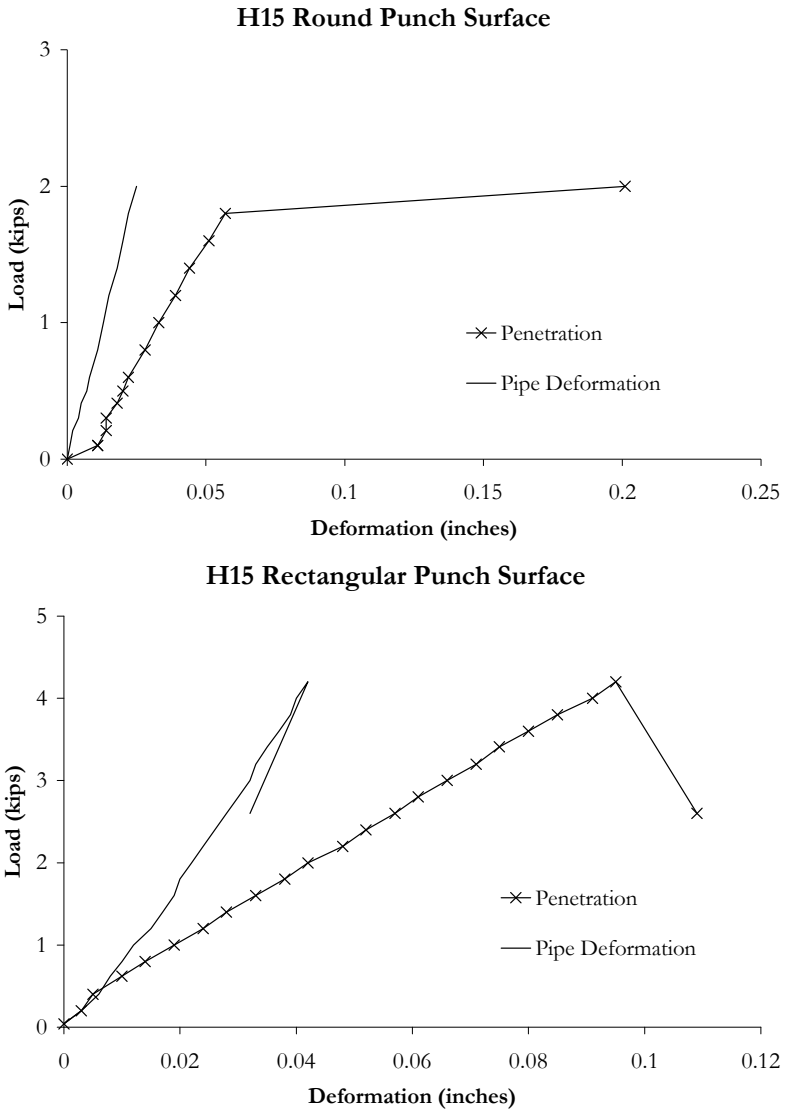

Figure 4.9 Static punch tests for H15

the time of failure there is an apparent recovery in the geometry. This would indicate that delamination of the interior layers played a critical role in the behavior of this specimen with this punch surface. For this specimen, the failure load for the rectangular punch was double the one for the round.

The deformation behavior recorded for the thicker of the pipes in the group was not too different from the H15 pipe (Figure 4.10). For the round punch, almost no change in the stiffness is noticed until the point where the first load drop took place. The

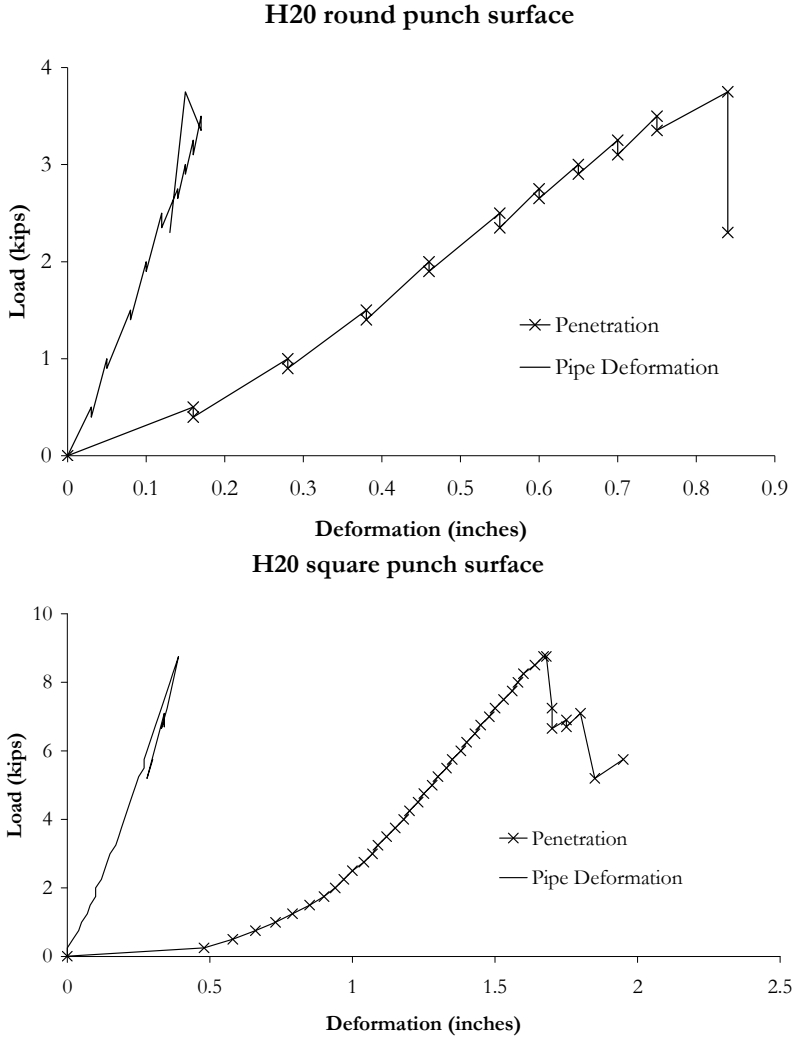

Figure 4.10 Static punch tests for H20

small drops in deformation noted during the test took place at load holds performed due to the AE monitoring. After the first load drop was reached, no subsequent loads were higher, and the deformation increased.

Different behavior was recorded for the rectangular punch test. There was a large amount of deformation recorded at the initial load stages. The gage placed at the pipe 6 inches away does not show any difference from the records or trends observed in the previous tests. This larger initial deformation is probably due to seating of the loading head in the machine. After the adjustment was complete, then the readings took a more normal behavioral trend. If the initial behavior is ignored, then the behavior of the H20 specimens followed the exact same trend as those for the H15 specimens.

4.3.1.2. ACOUSTIC EMISSION RECORDS

Acoustic emission records were made during the static punch tests. These records were made using a Transportation Instrument manufactured by Physical Acoustics Inc. This is an old instrument capable of storing only the traditional parameters of AE signatures as recorded with resonant sensors. Sensors used were R15I sensors also manufactured by PAC. These sensors are resonant to frequencies between 100 kHz and 250kH with theoretical peak sensitivity at 150 kHz.

Figure 4.11 shows the records made for the H5 series pipes for both the round and rectangular punch surfaces. As previously noted, the specimen tested with the round punch showed a large amount of damage in both surfaces after the test was concluded. Cracking in both the internal and external surfaces was noted and a large amount of delamination observed. The AE records support this by showing a considerable amount of activity distributed after the first significant emission was recorded. Also, bursts of emission were recorded in subsequent load increments. Looking at the loading curve superimposed for the round punch records we see that the distributed emission took place during a load hold after the first load drop was recorded. However, in subsequent load increases, tightly grouped burst of emission were the dominant records for this pipe.

The records for the rectangular punch in the H5 pipes showed little emission until the maximum load was reached. In contrast to the round punch, once maximum load was reached, no more increases in load were possible.

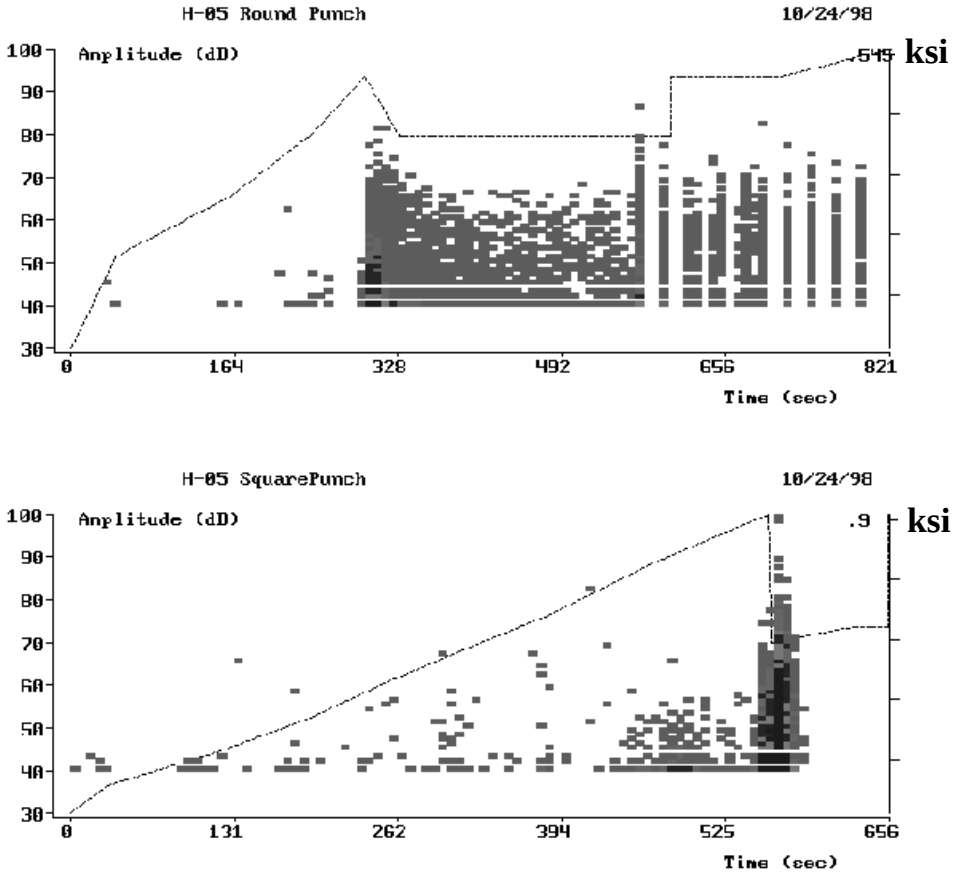

Figure 4.11 AE records for static tests for H5 specimens

Figure 4.12 show the records for the H15 pipes under static punch tests. They show a behavior that appeared as a reduced version of the H5 pipes. The records for the round punch show almost no activity during the initial load stages until maximum load was reached. However, the same bursts of emission are noted in the end of the records similar to the ones observed in the H5 pipe round punch. The records for the rectangular punch showed almost no difference from the ones recorded for H5.

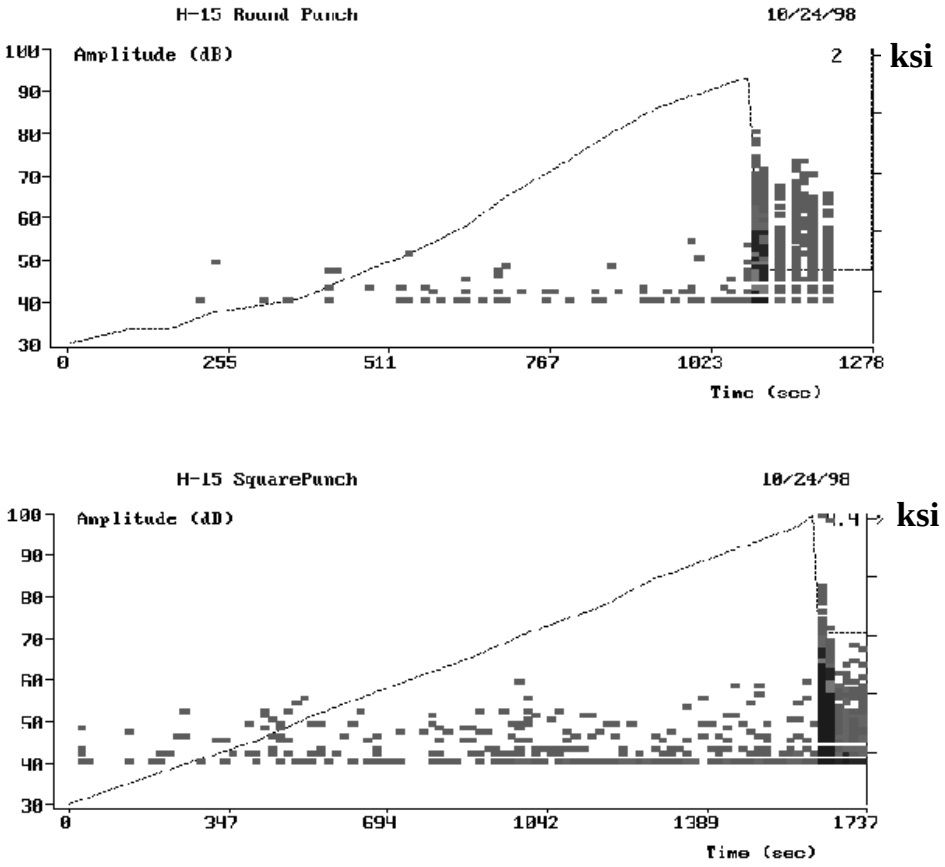

Figure 4.12 AE Records for static test for H20 specimens

Figure 4.13 show the AE records for the H20 pipe under static load. Like the case for H15, no significant emissions are noticeable for the round punch until the maximum load is reached. Once the maximum was achieved, further attempts to reach a load higher than the previous one at a similar loading rate were not successful. After maximum load, all subsequent records during loading attempts were characterized by a burst followed by continuous emission. As noted in the figure, every burst in the AE records is associated with an attempt to increase the load. Even when the load dropped, continuous records of AE are apparent in the plot.

Records for the rectangular punch tests are no more revealing in this case. At the beginning of the test, large bursts of emission with distributed amplitude are noticed. As stated in the previous section this could be attributed to mechanical noise resulting from the loading head adjusting. Neglecting the records at the beginning, the AE profile at maximum load is very much the same as the one for the round punch.

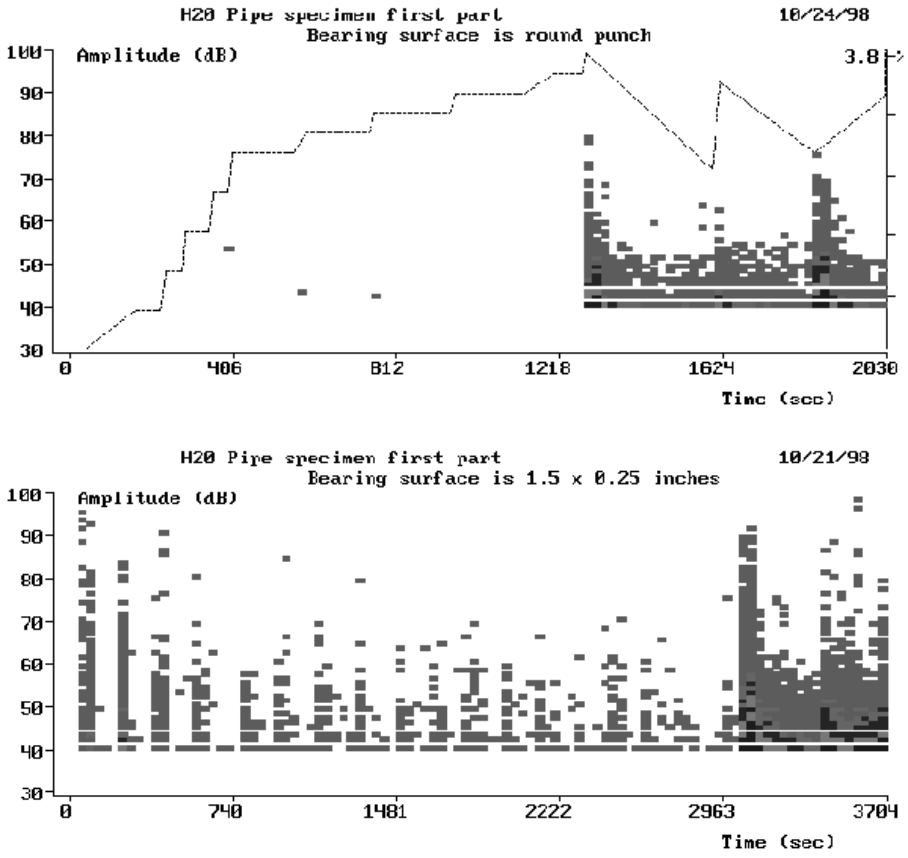

Figure 4.13 AE records for static tests for H20 specimens

4.3.2. LOW VELOCITY IMPACT TESTS

Instrumentation during the low velocity impacts consisted of broadband acoustic emission sensors and linear potentiometers at the interior and exterior diameter of the pipe. Initially there was an attempt to measure the force at the time of the impact by using strain gages on the punch. Unfortunately, during the impacts the punch penetrated more than expected into the pipe. This caused some friction to be generated at the surface of the strain gages making their readings unreliable. Figure 4.14 show a schematic representation of the setup as used during the tests. One of the displacement transducers used in the program was a direct current displacement transducer (DCDT). This transducer was typically placed 90 degrees from the impact point to measure pipe deformation due to bending.

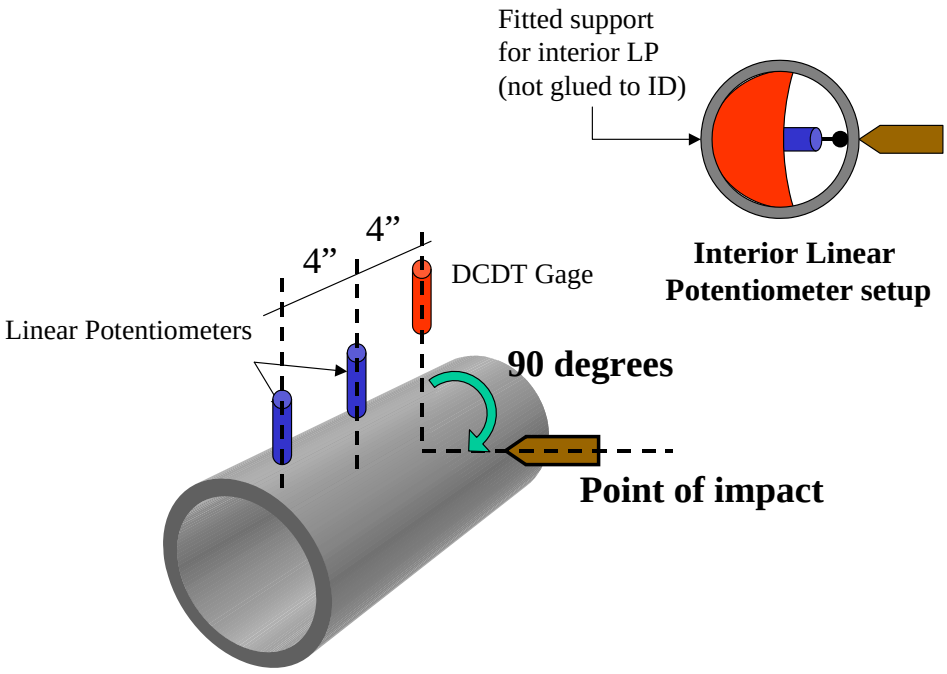

Figure 4.14 Setup for displacement measurements impact test

In some of the tests an interior linear potentiometer (LP) was used in system. This transducer was placed inside of the pipe by means of a fitted support that was machined to fit with a very tight tolerance inside the ID of the pipe. This was left in place by friction with the interior wall and stabilized laterally by the use of extended supports that were also not rigidly attached to the surface. In all of the tests a second LP was placed in the same longitudinal line with the DCDT at 8 inches from the location of the impact in order to estimate the extent of the area of influence of the impact in the overall geometry of the specimens. In later tests, this LP was augmented by a second LP placed at half the distance from the impact region.

Figure 4.15 shows the filtered result for the measurements during impact of pipe 1H5. The impact energies were selected based on results of previous work found in the references. A low level of impact energy, sufficient to cause surface damage, but not enough to cause immediate leaking was selected as the initial level and incremented based on the test results. This pipe was tested under 40 Joules of energy in the round punch and 80 Joules of energy in the rectangular punch. The plot shows the information in milivolts in the vertical axis and number of records in the horizontal axis. The number of records is directly related to the time spanned during the test by the acquisition rate of the machine as indicated at the beginning of this chapter. The interesting feature of this test was the difference in amount of deformation recorded by the external DCDT. The readings from the internal LP seem to indicate a difference in the amount of deformation recorded at the punch or impact location. The records for the rectangular punch surface are larger than the ones for the round punch. This would apparently agree with the energy of impact imparted in the tests. The records from the DCDT, however, indicate that the overall deformation in the pipe resulting from the impact was greater in the case of the round punch than in the case of the rectangular one. The difference between readings for the round and rectangular punches is of almost a factor of two.

It should be noted that some measurement error may occur while measuring dynamic displacements. DCDT gages however, are not as sensitive to these effects as are linear potentiometers. Of the LP gages used in other locations of the same pipe, the springs were removed from the shafts to avoid the dampening influence of the spring.

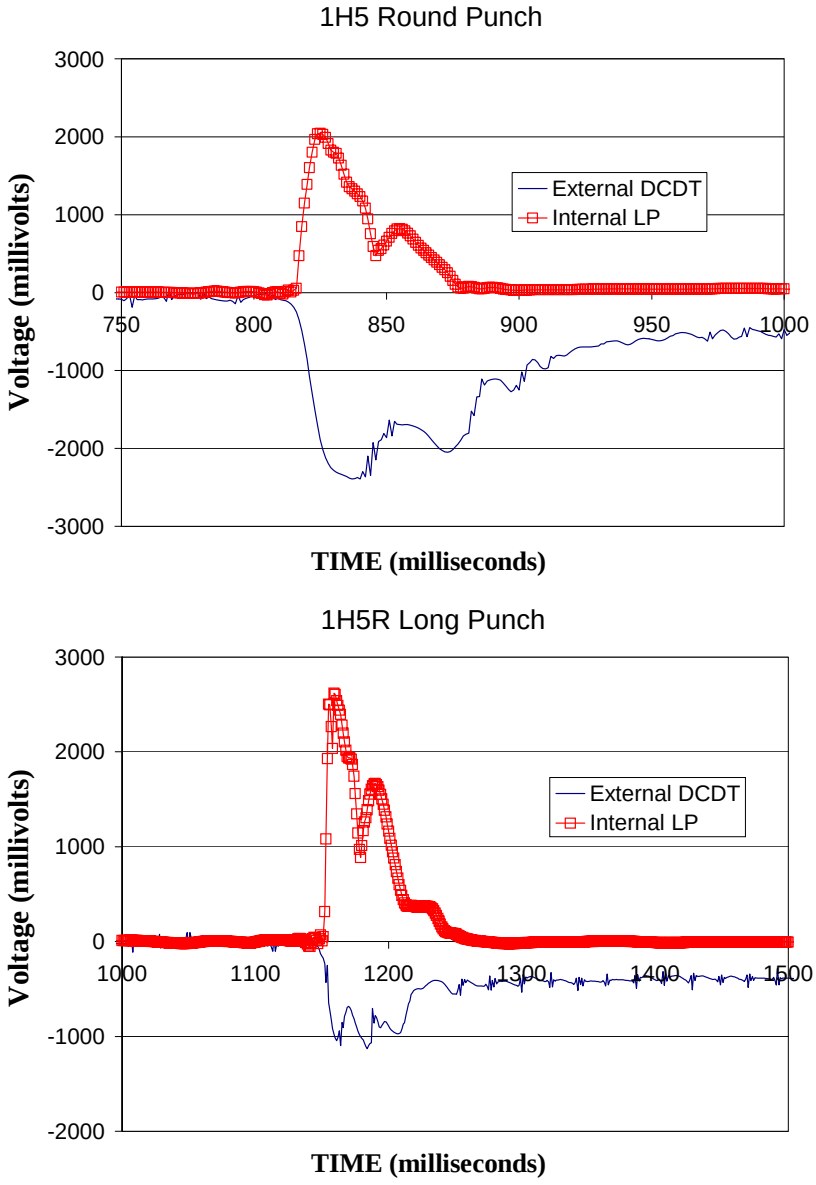

Figure 4.15 Impact records for 1H5 pipe

Although the behavior observed indicates the possibility of error during the readings, this cannot be verified until after the readings from the other tests are presented in the section. However, even agreement in the case of the internal LP will be difficult to confirm without doubt. In contrast to the records for 1H5, Figure 4.16 shows the records for the test of the pipe labeled 2H5. This pipe was also tested with a round and a square punch on opposite sides. The energy levels used were 60 Joules for the round punch and 180 J for the rectangular.

The records for 2H5 show trends that mimic those observed for 1H5. The first trend is that of the deformation recorded at the DCDT gage. In this specimen, the DCDT also indicated that the deformation recorded in the pipe was smaller for the rectangular punch surface than for the round punch. This could reinforce the validity of the DCDT records from this test phase since the stress applied by the punch is distributed over a longer length of pipe thus providing for a longer effective length in the pipe at the time of the impact. Here the readings for the internal LP in the round punch showed a larger deformation than the rectangular one. The difference in the amount of deformation was very small in comparison to the scale of the total readings.

For the specimen 3H5, the energy of impact for the round punch was 130 Joules and for the rectangular punch was 220 Joules. For this specimen the readings for the interior LP show for the first time a larger deformation recorded in the rectangular punch than in the round punch (Figure 4.17). The difference, although, noticeable in the plot is small as in 2H5 when compared to the scale. The implications of this difference will be studied in the analysis of results later in this chapter. The DCDT again, as in the case of 2H5 showed a small amount of deformation in the case of the rectangular punch and a larger one for the round punch. For this specimen a second external LP was placed in the specimen. This was at eight inches from the area of impact. The records indicate no deformation recorded by the LP at this location.

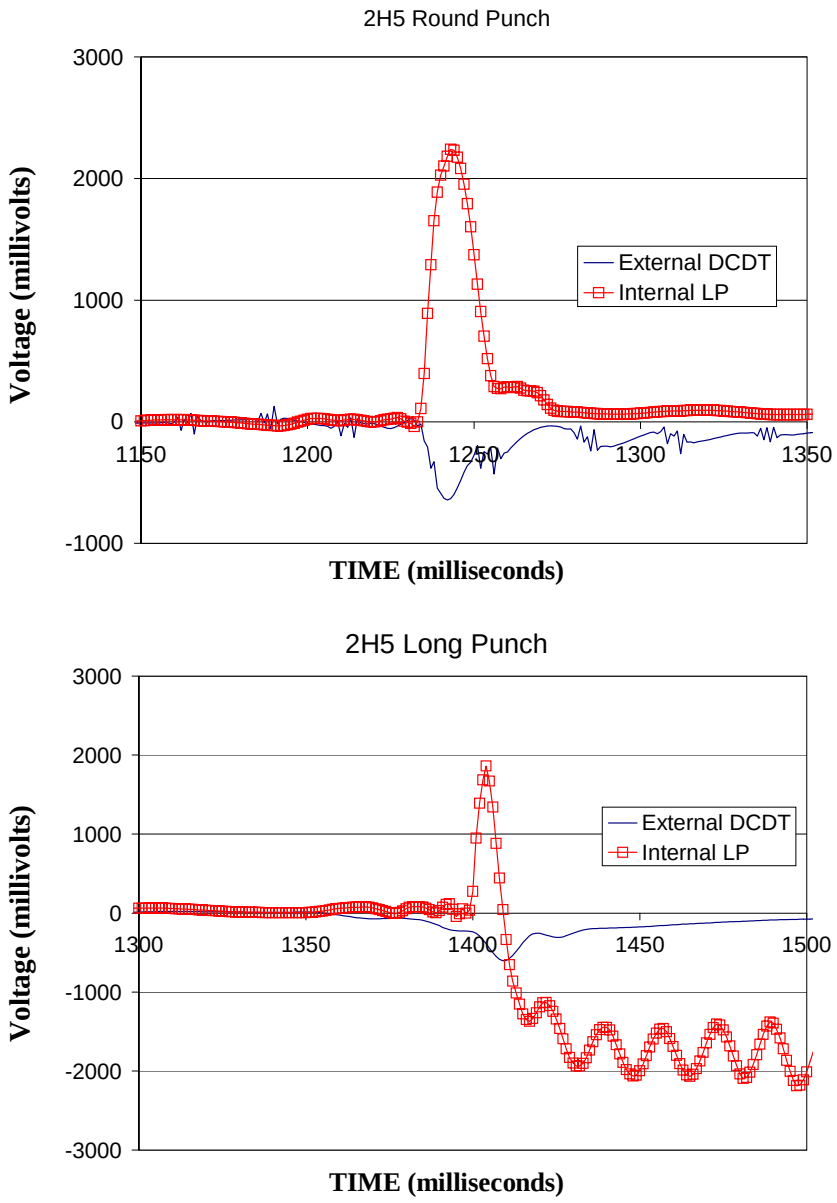

Figure 4.16 Impact records for 2H5 pipe

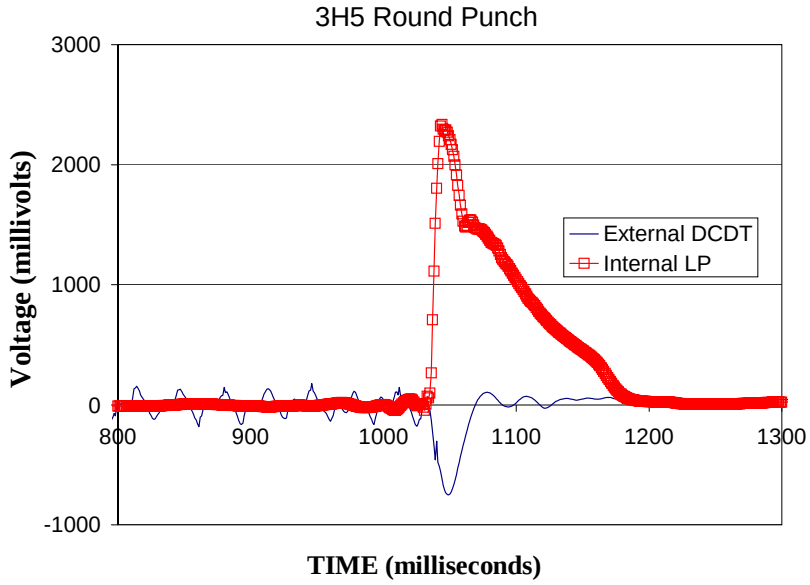

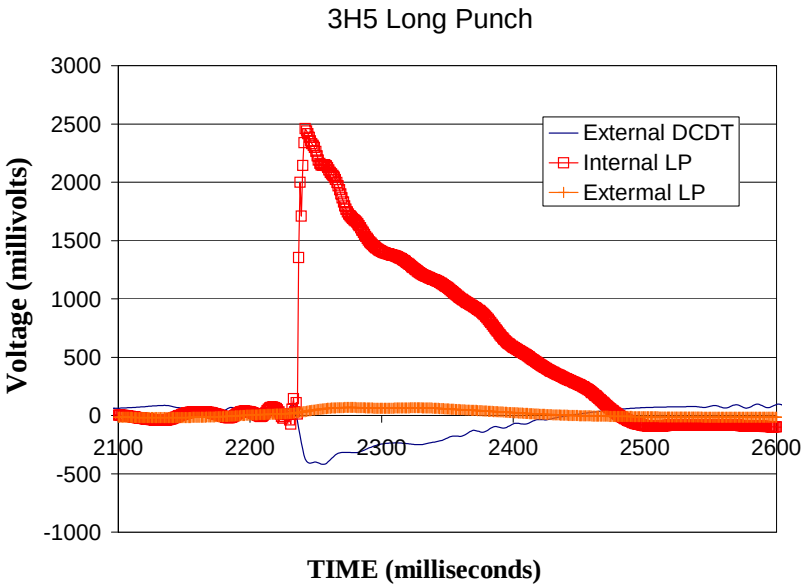

Figure 4.17 Impact records for 3H5 pipe

Figure 4.18 shows the results for the first of the medium thickness pipes, specimen 1H15. As with the H5 specimens, these pipes were subjected to the two

profiles for the punch surfaces. For this specimen the energy at the time of impact was selected to be 130 Joules for the round punch and 190 Joules for the rectangular punch.

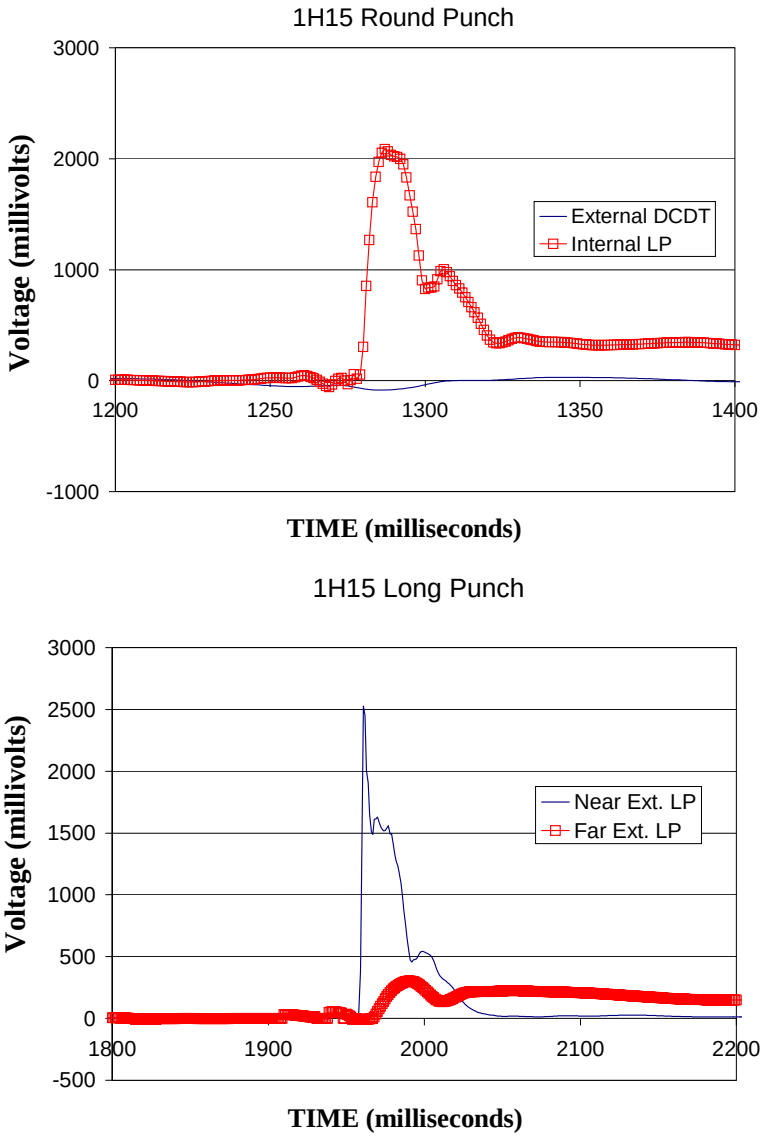

Figure 4.18 Impact records for 1H15 pipe

From the resulting records shown in the figure we can see that for the round punch the internal gage showed the same deformation as the previous test in 3H5. After

this pipe records in the interior diameter of the specimens were no longer acquired. The DCDT showed almost no amount of deformation at the time of impact for the round punch.

In the case of the rectangular records a significant amount of external deformation is noted in the near LP. The far LP recorded some deformation also, but at a much smaller scale. Because of equipment malfunction, no reliable records for the DCDT were available for the rectangular punch for this pipe.

Figure 4.19 shows the records for the 2H15 specimen. For this specimen no interior LP readings were made at any of the punches and the DCDT was again used. Readings made reflect an error in the setup at the time of testing. The measuring potentiometers were not properly attached to the pipe at the time of impact. Therefore after the first deformation of the specimen was recorded a permanent reading can be seen in the channels. This does not affect the relative maximum values observed since the error took place at the time of the recovery of the specimen where the attachment failed to retract the shafts of the potentiometers. The energies used for this specimen were 350 Joules for the round punch and 700 Joules for the rectangular punch. The deformation readings for this specimen reflect a difference in the same proportion and the difference in impact energy. Even when it is not expected that the error during the test would reflect in the maximum values for the deformation, there is a possibility that the proportions in the deformation between round and rectangular punch tests are not the correct ones. The readings from the next specimen will help resolve this situation. The proportional difference between the round and rectangular punch for 3H15 will be the same as for this specimen.

Figure 4.20 shows the records for specimen 3H15 at the time of impact. As tested, the energies selected were 400 Joules for the round punch and 800 Joules for the rectangular punch surface.

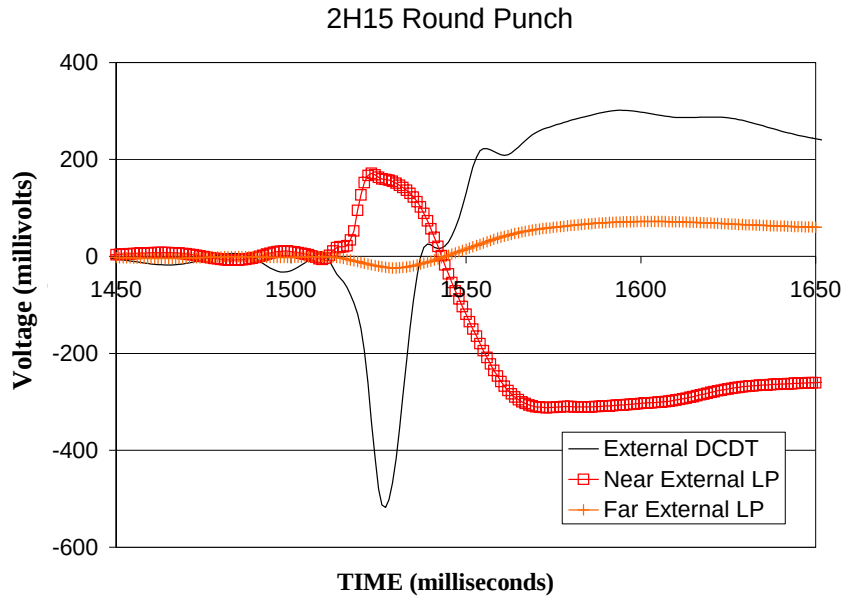

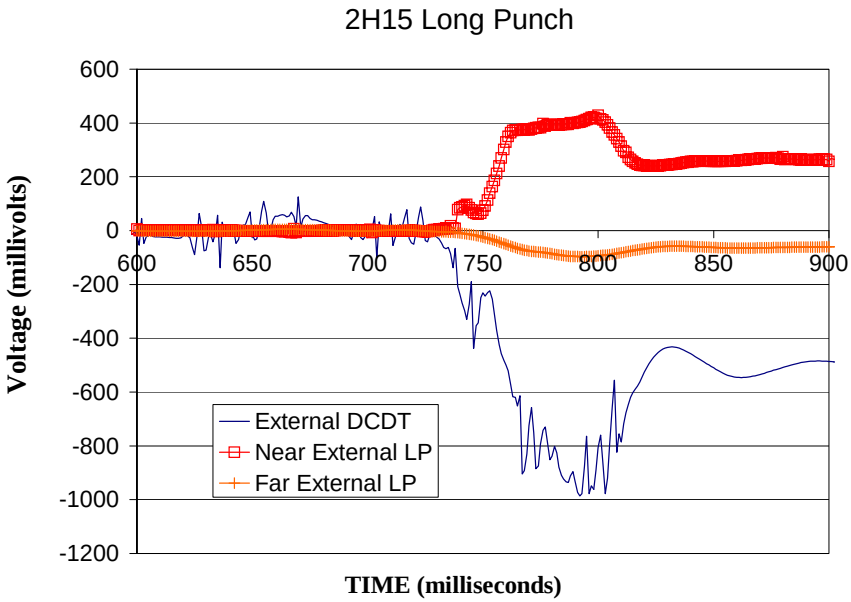

Figure 4.19 Impact records for 2H15 pipe

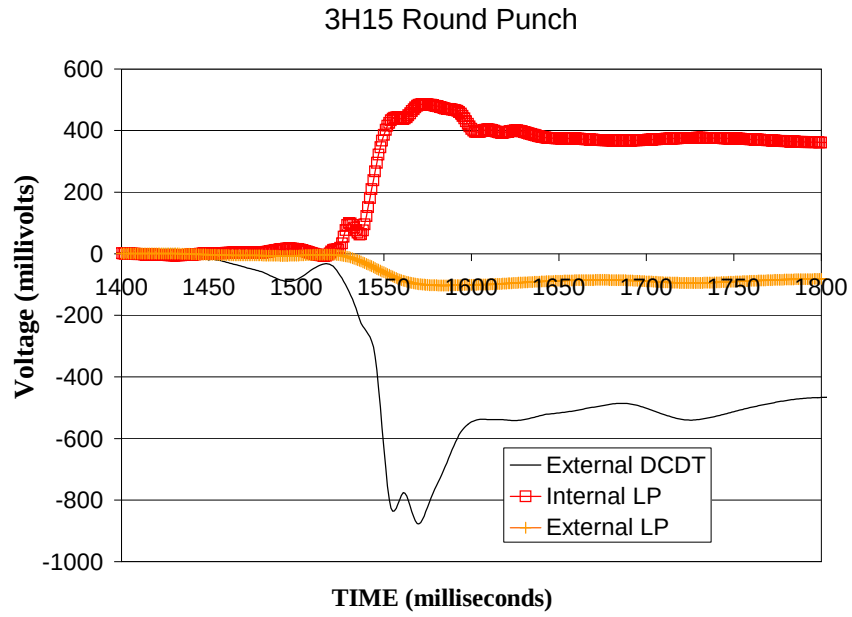

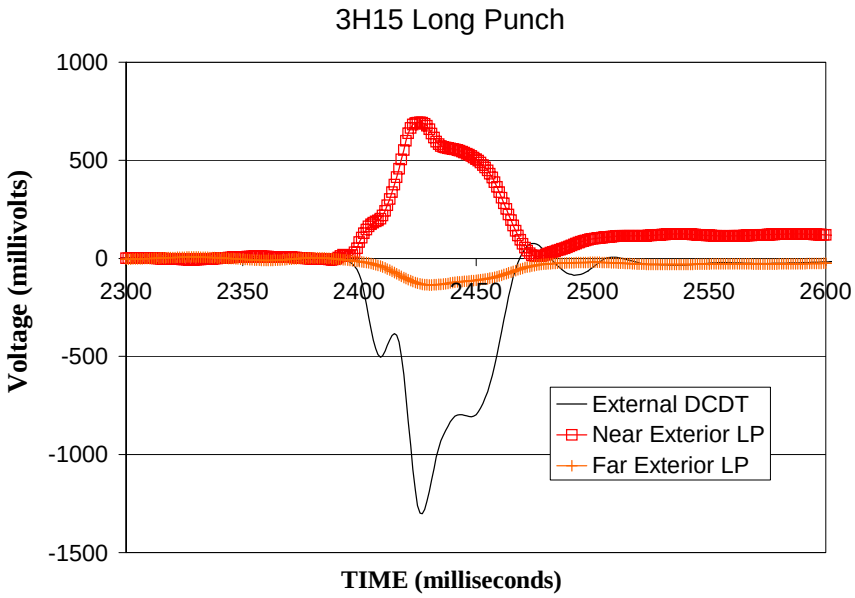

Figure 4.20 Impact records for 3H15 pipe

The same problem as with the readings in specimen 2H15 is noticeable in readings for the round punch. The proportional increases in maximum deformations recorded for both round and rectangular punch, however, appear to provide support for the validity of the 2H15 readings and the round punch of this pipe. There is a difference between the deformations recorded for the round and rectangular punch for this pipe, with the rectangular punch providing the largest of the values. Another odd characteristic is that the far LP appears to record a reversal in the curvature of the pipe. This would appear to indicate that the far LP was placed at the edge of the area of influence of the pipe in reaction to the punch or impact.

Finally the records for specimen 1H20 are presented next. This was the thickest of the specimens in the program, and even though three specimens were tested, the impact records for only one are presented. The other two specimens were impacted with the same level of energy and punch profile. In addition, these specimens were tested only with the round punch surface. During initial trial runs for this thickness, it was determined that the

amount of energy required in the rectangular punch to achieve a more than negligible level of damage was beyond the capabilities of the test setup. As it was, the setup failed at the connection between the pendulum and frame after the last test was performed at this level of energy. The energy used for the impact was 840 Joules with the round punch. Figure 4.21 shows the records for this test.

The measured deformation in specimen 1H20 shows very clearly the zone of influence for the punch. Both the near and far LP record deformation at the time of impact along with the DCDT. In addition, they show the same amount of time for recovery after impact in all of the gages or potentiometers. This was a trend not typically observed in other specimens with exception of 3H15 rectangular punch. The voltage change recorded in the DCDT was also the largest of the group as expected for the higher level of energy in the impact. Because of the information in the far LP

channel, we can also determine that the effective width for these tests was larger than the 8 inches used in the spacing of the potentiometers.

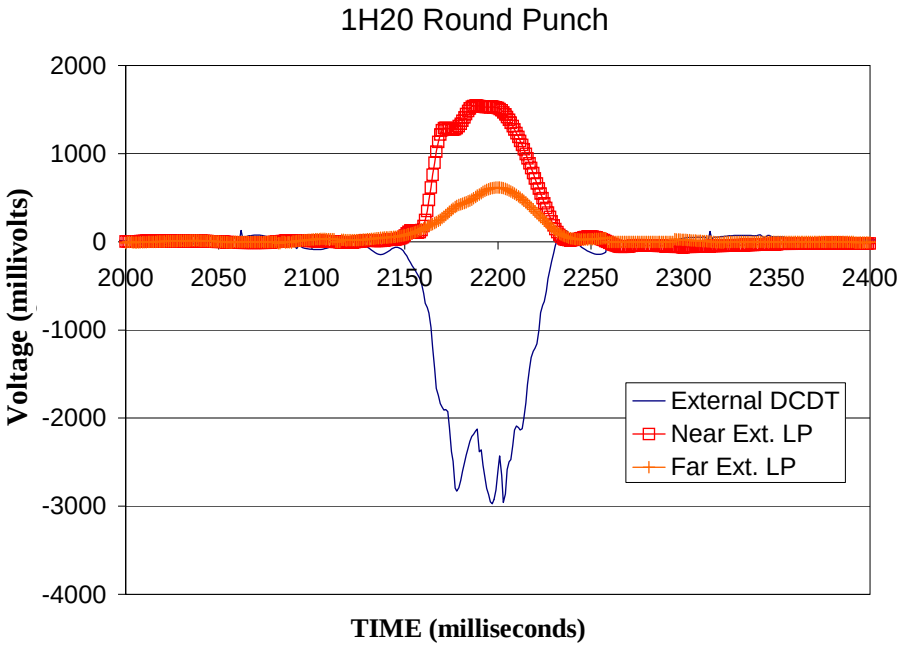

Figure 4.21 Impact records for 1H20 pipe

4.4. INTERNAL PRESSURE TESTS RESULTS

Before testing of the damaged specimens, control tests were performed on similar pipes for each one of the thicknesses tested. These control tests were done on specimens that had no impact damage generated at the laboratory. They would serve in the evaluation of capacity reduction as induced by the impact. The specimens were fabricated in the same winding as the impact damaged pipes. They are all part of a longer pipe and cut to sections for testing. Each one of the series H5, H15 and H20 are made this way.

4.4.1. UNDAMAGED CONTROL SPECIMEN

4.4.1.1. H5 CONTROL SPECIMEN

Figure 4.22 shows the strain data recorded for the undamaged specimen in this group. The maximum pressure at leakage was 2100-psi with limited fiber damage observed in the failure zone. During the loading of this specimen several load holds and unloading stages were performed. Strain records made during these stages are cluttered and are therefore shown in two separate plots in the figure. One of the plots is the full-scale graph of the data, the other is a reduced scale at the first 1200-psi of applied pressure. The test however was to failure with no long stops other than required for the AE monitoring.

One of the characteristics of this pipe is the Poisson's relationship. From the plots it would appear that the ratio has a value greater than 1. This is not uncommon in composite specimens where researchers have reported values of almost 4 in experiments [4.36]. Another feature was that creep was more noticeable in the axial strains than in the hoop direction. This is due to the influence of the resin or matrix on the behavior in that direction. A final note is made in the permanent deformation recorded in the axial strains at the time of the unloading. As the maximum pressure was approached, this permanent deformation became increasingly large. The records show that at the level of 1800-psi or 85% of the maximum pressure, this permanent deformation was 40% of the final strain at failure.

The acoustic emission records for the control specimen are show in Figure 4.23. A very typical plot can be seen in the figure. The first jump in AE activity took place at about 450-psi. The second most noticeable increase in emission occurred at about 950-psi. This distinction will be important, as noted in the previous chapter of this dissertation. Another feature of interest is the number of high amplitude events recorded

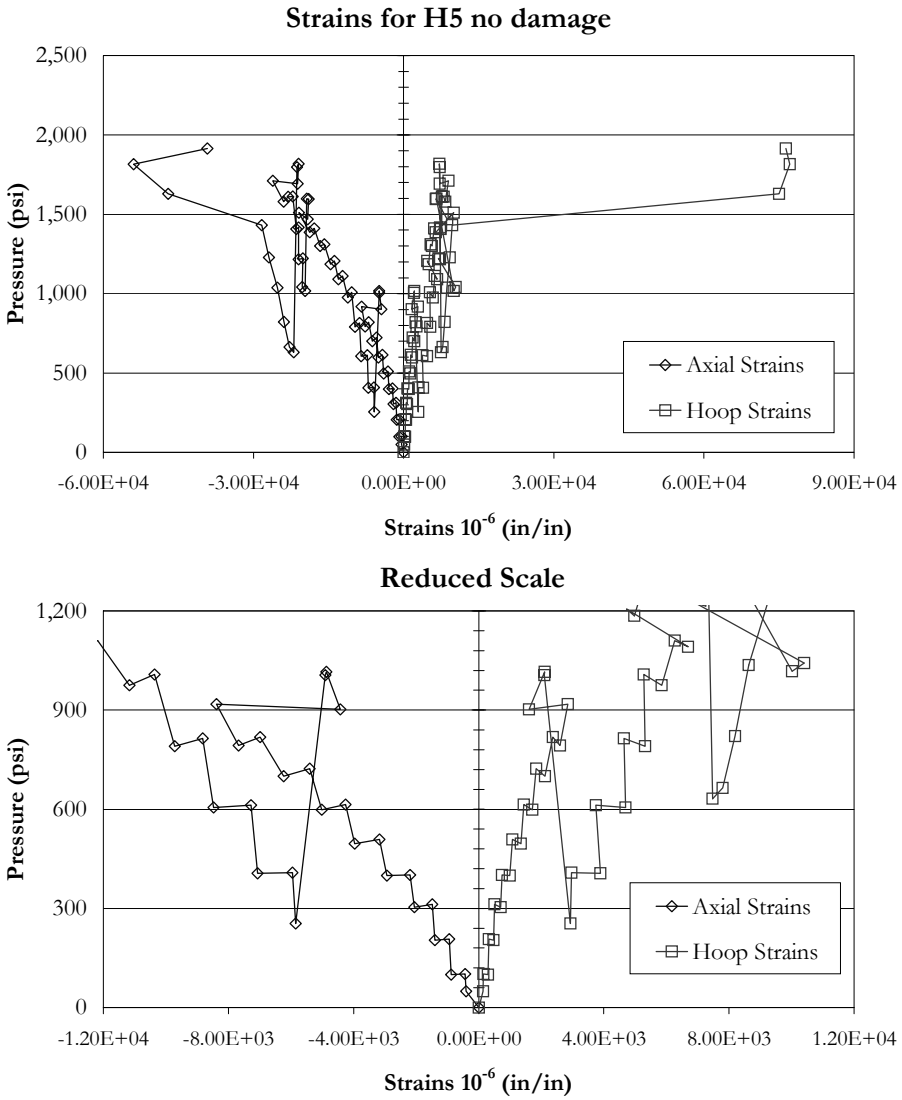

Figure 4.22 Strain data for specimen H5 no impact

at the time of the first knees of AE. This again demonstrates the problems in using the amplitude level as means of identifying damage mechanisms. Typically this type of emission along with short duration would be partially attributed to fiber breakage. As noted in the AE records, the duration for the events was distributed from short to long for some of these high amplitude events. This makes association of events to the

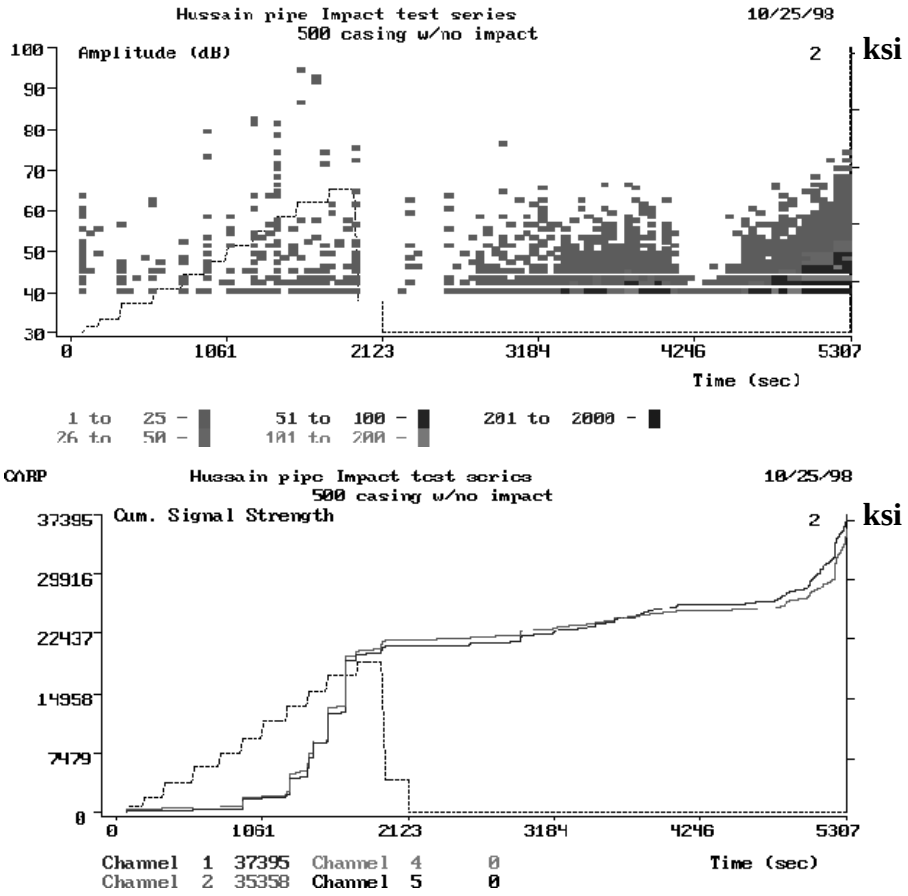

Figure 4.23 Acoustic emission records for H5 no impact

particular mechanism of fiber breakage difficult and subjective. No extensive fiber breakage was apparent at the time of leakage. A more detail analysis of the importance for these two AE knees will be presented in a following chapter.

4.4.1.2. H15 CONTROL SPECIMEN

Figure 4.24 shows the strains recorded during the test for this control specimen. Due to a seal failure, this specimen was pressurized twice. Strain records for both tests are shown in the figure. In addition, during the final test, the specimen was loaded to a predetermined level before unloaded to remove the AE sensors to avoid damage to the

equipment. A third plot is added to the figure that has the strains measured at this third pressurization stage. All of the plots were left at full scale since the behavioral trends of interest can be observed from that point of view.

The specimen failed by leakage at 5500-psi. As with the previous control specimen, no fiber failure was detected at the failure zone. Water worked its way from the inside diameter between the fibers. At the time of failure cracking was audible from the specimen. The failure zone was concentrated in a small portion of the specimen with no other leakage or apparent delamination areas detected visually elsewhere.

The strain records show a strong non-linearity in the axial strains almost right from the beginning of the loading history. The hoop strains also show this non-linearity, but is not as readily apparent until after considerable pressure. The non-linearity in the axial strains appears clearly after 1000-psi of applied pressure. In addition, traces of permanent deformation, or slow recovery, are seeing in every unload step in the test. Axial strains at the time of failure are very similar to the ones recorded for the H5 control specimen. The hoop strains however are almost double the recorded ones for H5. The apparent Poisson's ratio in this specimen was almost one, which is smaller than the one observed for the thinner specimen H5. The last plot in Figure 4.24 shows the strains after the specimen was loaded again once the AE sensors were removed. Strain records appear to have a larger amount of permanent deformation as recorded during load holds. Unfortunately no backup gage was available in a separate section of the specimen to confirm this. The gages were also lost before maximum pressure was achieved.

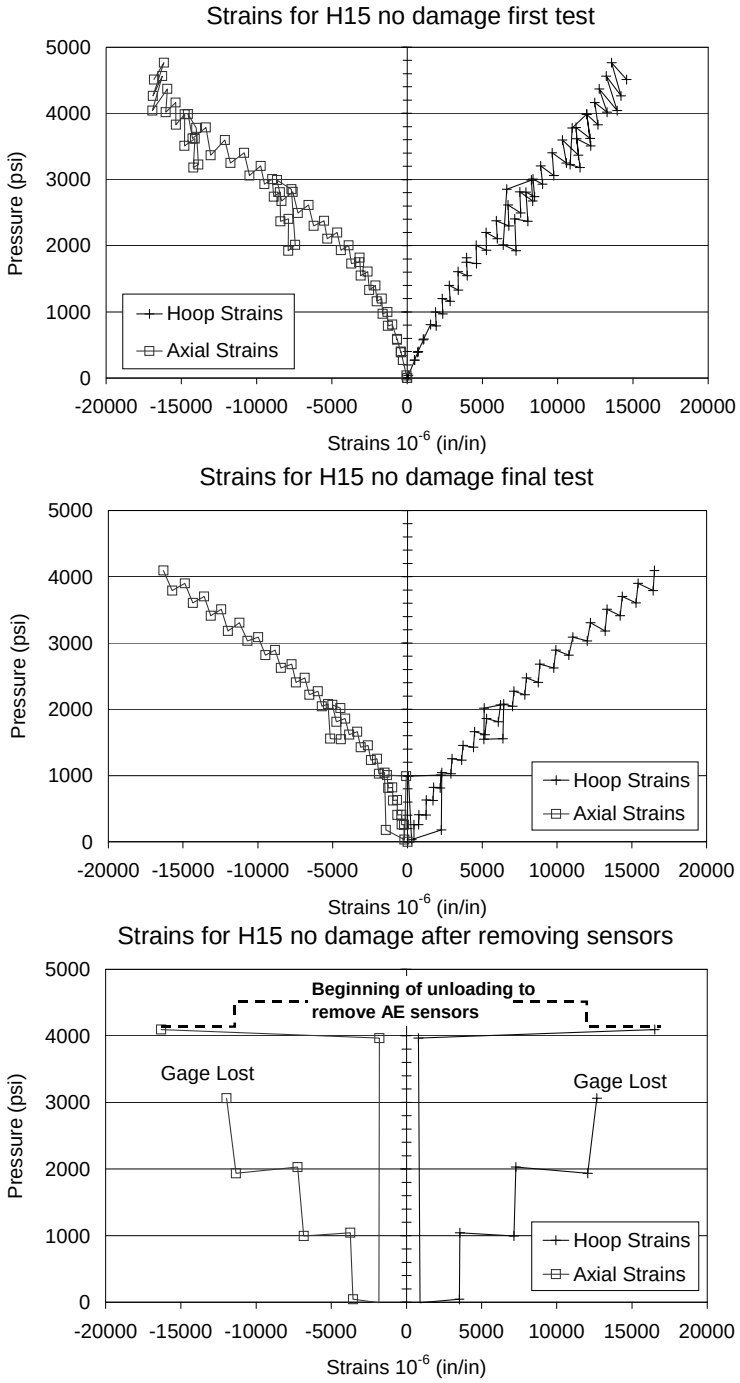

Figure 4.24 Strain data for specimen H15 no impact

Figure 4.25 shows the AE records for this specimen. The plots presented in the figure were the amplitude and cumulative signal strength. It is rather clear in the figure that emissions during load hold became apparent at about 3-ksi of applied pressure. The emission, however, was of low amplitude and not very active at the higher amplitude

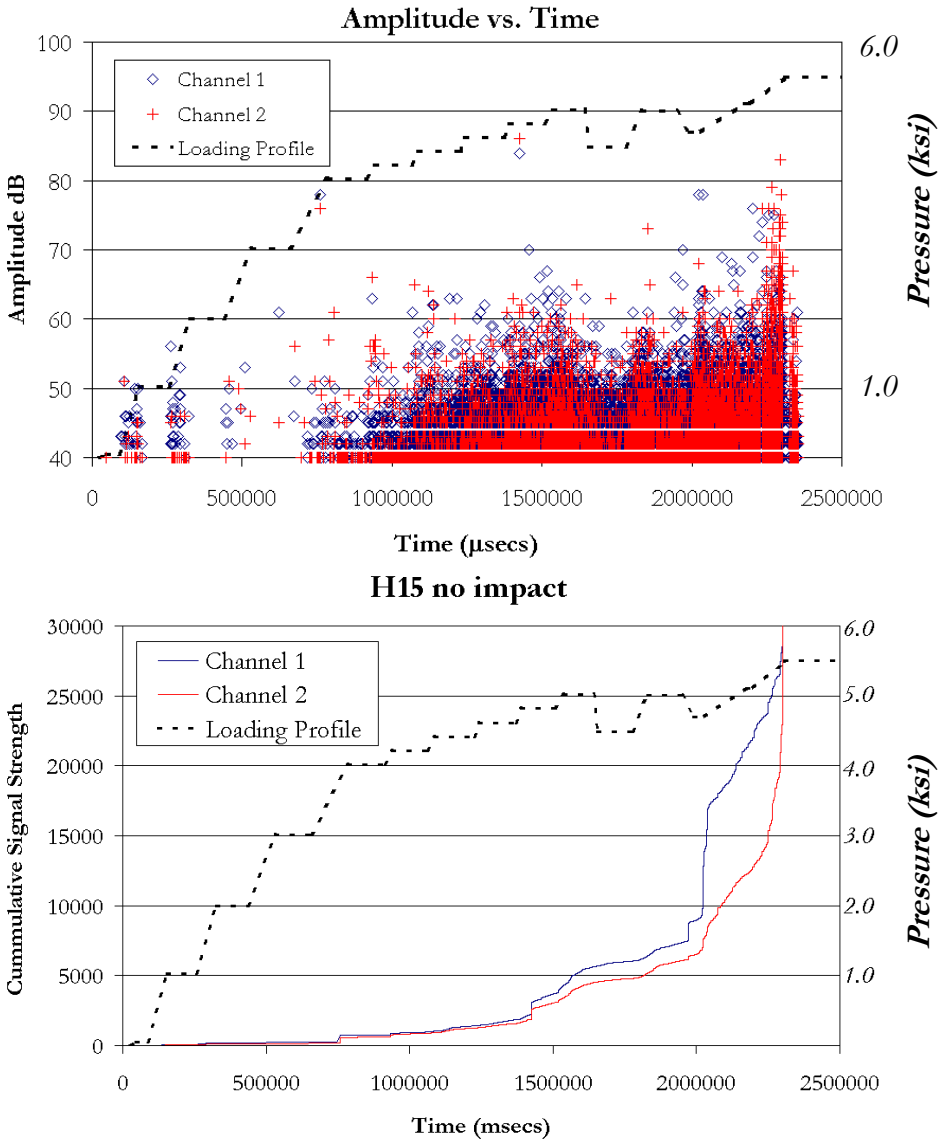

Figure 4.25 Acoustic Emission records for H15 no impact

levels. More considerable emission above 50 decibels starts taking place at a pressure of about 4-ksi and above. Looking at the cumulative signal strength plot, we note the first noticeable jump in the AE at about this level. However, a more drastic change was observed at a slightly higher pressure of above 4600-psi.

4.4.1.3. H20 CONTROL SPECIMEN

Figure 4.26 shows the strain records for the control specimen of the thickest pipe tested in the internal pressure program. The wall thickness of the pipe was of 0.52" on average. The maximum pressure at leakage was 12,000-psi, with failure been mainly leakage through the resin matrix and fiber interface. In contrast to the other specimens tested in the program, this specimen did exhibit some fiber breakage at the time of failure. The fiber damage was not extensive, but the pressurizing fluid separated the fiber bands and broke isolated sections as it leaked out of the specimen.

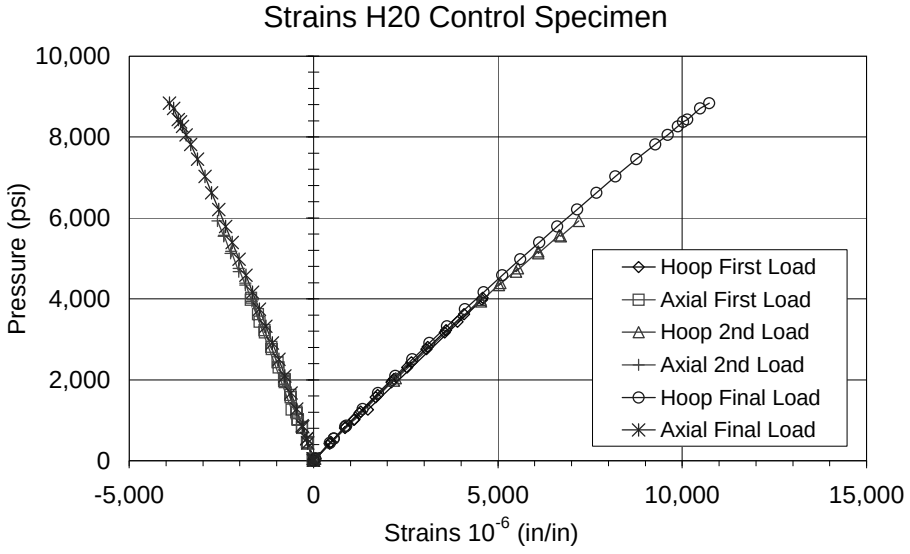

Figure 4.26 Strain data for specimen H20 no impact

In the strain plots three separate loading results are shown. It was determined that the instrumentation would be removed from the specimen after a predetermined pressure level was reached. In order to retain the largest amount of information possible, the specimen was tested several times at increasingly large target pressures. The last strain gage records correspond to the pressure level of 8,500-psi. As can be seen in the figure, no considerable damage was accumulated during the loading stages that resulted in stiffness loss. In addition, the behavior was very linear as shown by the plots.

Figure 4.27 shows the AE records for the H20 control specimen with reinforced ends. Because this was the first specimen that reached pressure levels higher than preciously encountered, instrumentation was removed after a predetermined pressure level to avoid damage. This is the reason why the strain and the following AE records do not show the pressure levels at the time of failure. Acoustic emission sensors were removed at an earlier pressure than the strain gage acquisition equipment. At 4,000-psi the load was dropped and the AE equipment removed.

Although AE activity was detected from the beginning of the test, the first considerable jump in the records took place at a pressure level of 2,400-psi. After this level, emission during load hold was also continuous with no drops at the end of the load hold. A second large change in the AE activity was detected at 4,000-psi of pressure. However at this point is when the sensors were removed from the specimen making further comparisons extremely difficult to develop.

4.4.2. IMPACT DAMAGED SPECIMENS

For testing of the impacted damaged specimens no strains records were acquired. Only acoustic emission and in selected specimens, thermal emission records were obtained. Results are presented below for the three pipe thicknesses tested.

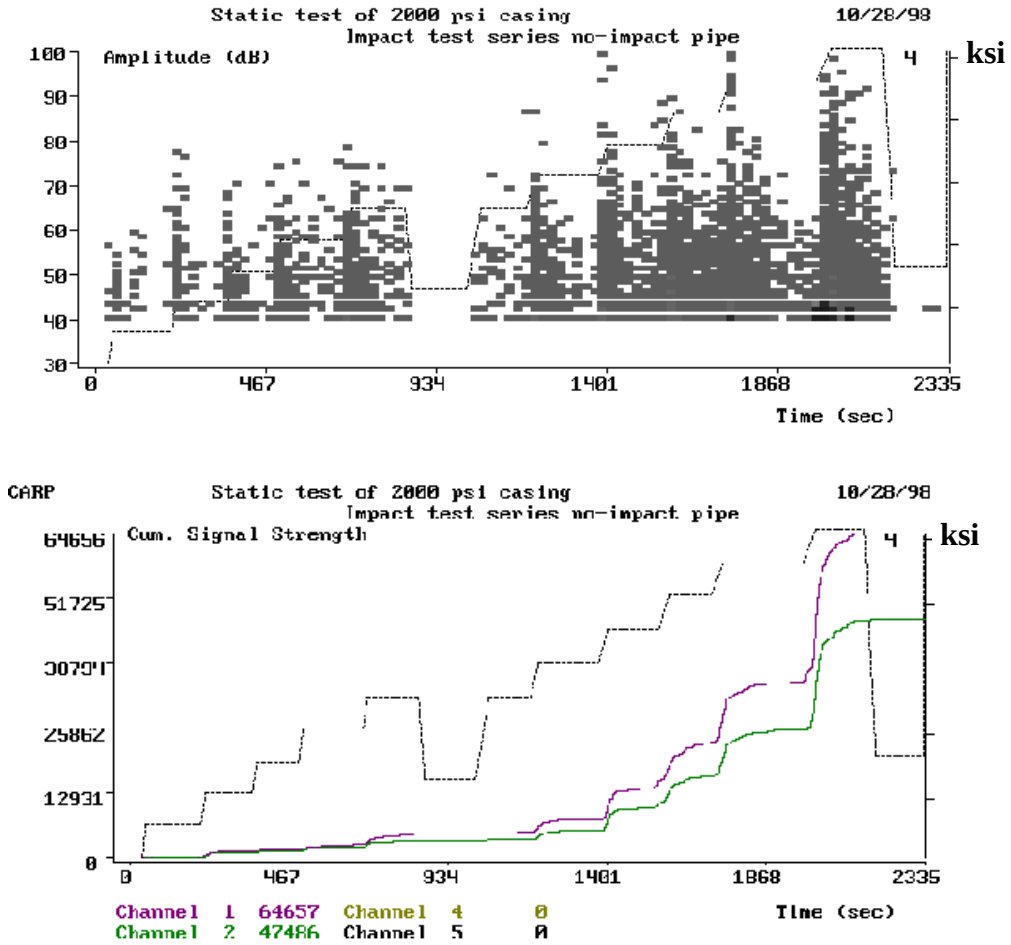

Figure 4.27 Acoustic emission records for H20 no impact

4.4.2.1. H5 IMPACT DAMAGED SPECIMENS

Table 4.2 show a summary of the results obtained during the internal pressure testing of the impacted pipes belonging to this group. As a reference, the control specimen has been added to the table. As indicated before, two different punch surfaces were used in the testing of these specimens. The table shows at which of the punch locations the leakage or failure took place if at all. The energy of impact specified in the table is in the units of Joules.

Label	Energy Round	Energy Long	Maximum Pressure	Location of Failure	Type of Failure
H5	NA	NA	2100	Middle	Leak
1H5	40	80	1500	Long Punch	Burst
2H5	60	180	800	Long Punch	Burst
3H5	130	220	400	Round Punch	Soft Leak

Table 4.2 Results for specimens H5 under internal pressure

The first notable feature of the impact tests was that all that did not leak immediately after application of water pressure, failed by burst. Specimen 3H5 showd slow leakage at line pressure of about 50-psi, however, it was possible to increase the pressure inside the specimen. Therefore, pressure was applied until the rate of leakage exceeded the rate of the pump at 400-psi. Figure 4.28 shows a typical view of the burst failure surface after pressurization. This was the same mode regardless of the type of

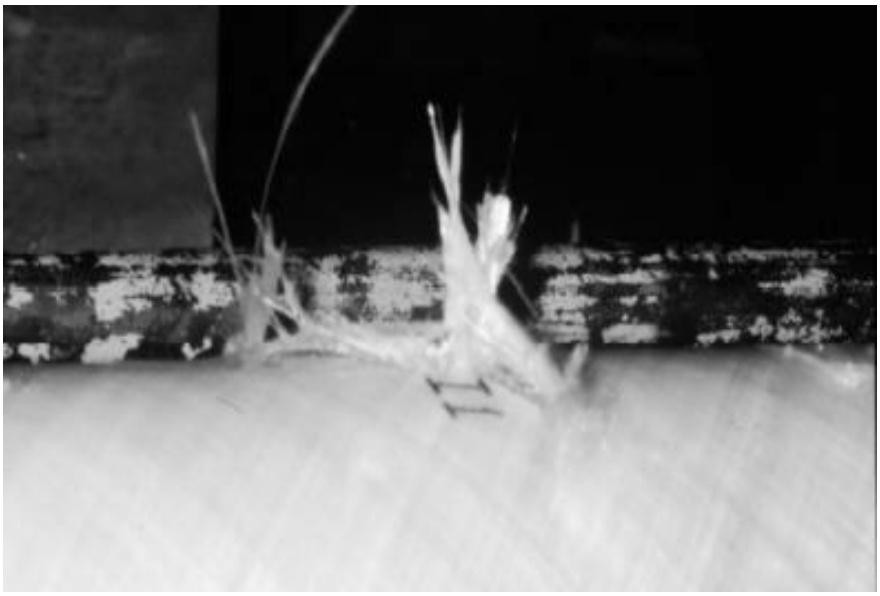

Figure 4.28 Failure surface impact zone

impact that caused failure and of the specimen thickness tested.

Figure 4.29 shows the AE data from specimen 1H5. Failure of this specimen took place at the location of the long or rectangular punch. The features of interest at this point are the amount of emission during load hold that was apparent at about 300-psi

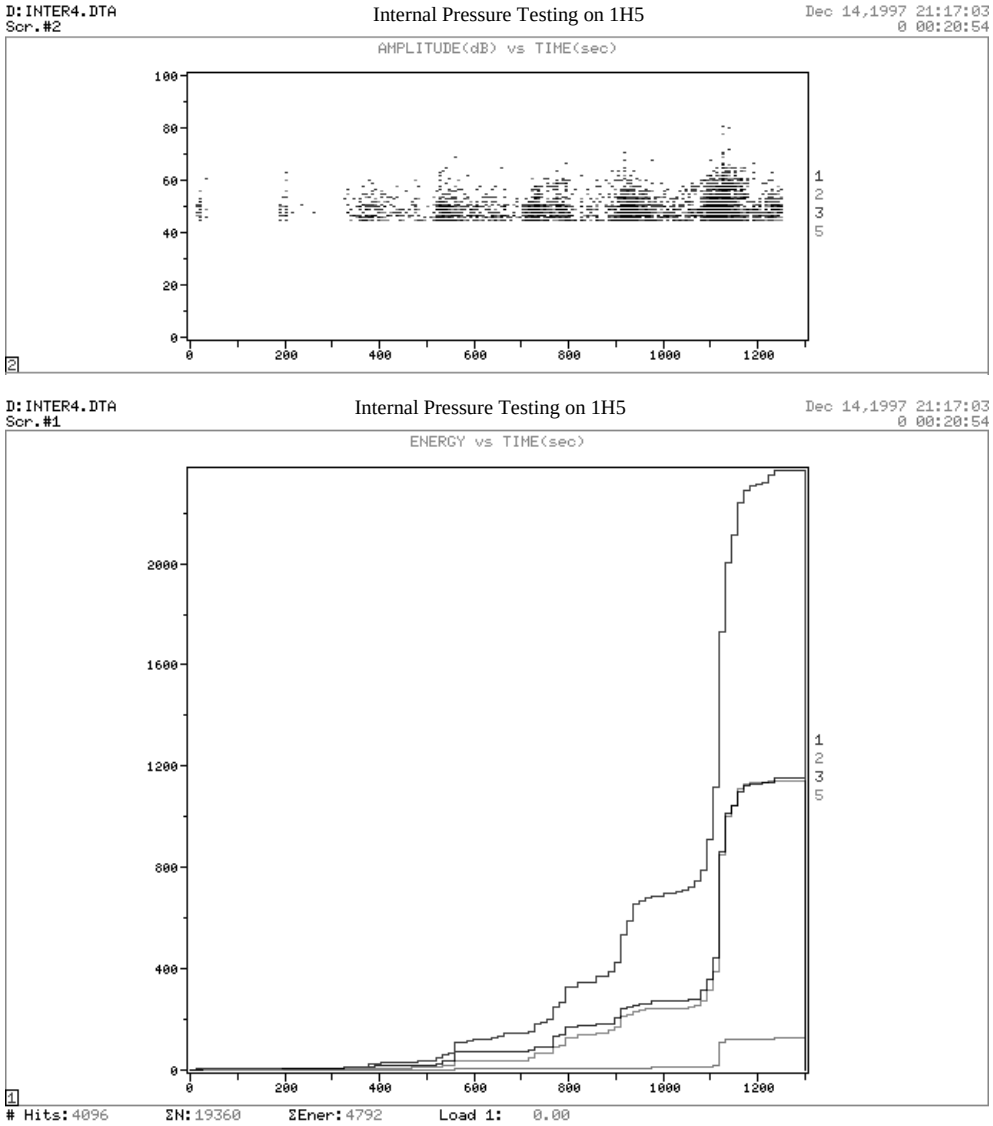

Figure 4.29 Acoustic emission records for 1H5

or 500 microseconds in the horizontal axis of the plots. The second large jump noted in the figure was the recorded emission during the bursting of the pipe. There were not AE records for specimen 2H5 due to equipment error. This specimen failed at an applied pressure of 800-psi at the location of the long or rectangular punch.

Figure 4.30 show the AE records for specimen 3H5. As stated before, the failure mode for this specimen was different from the other two. The location was the round punch area where the impact force was sufficient to crack the internal diameter of the specimen and produce seepage at very low pressures. The specimen was tested anyway to determine if additional pressure was possible after leakage was detected at low levels. The specimen was pressurized to 400-psi before the amount of water leaking

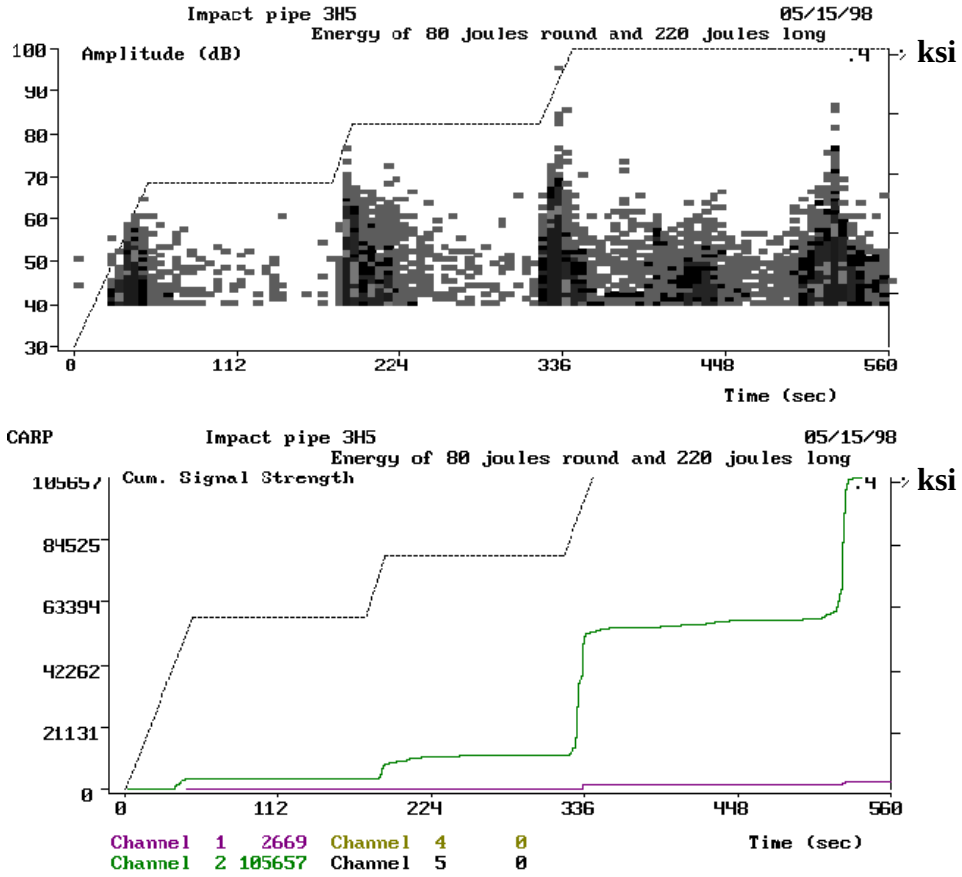

Figure 4.30 Acoustic emission records for 3H5 impact specimen

through the damaged area was more per minute than the rate of loading by the pump.

The records in this case are misleading because of the scale in the cumulative signal strength plot is dominated by the emission at the final load stage. Emissions during load hold were noted at a pressure of 200-psi. Although leakage was apparent from the beginning of the test, it did not generate detectable emissions until after 100-psi of pressure.

4.4.2.2. H15 IMPACT DAMAGED SPECIMENS

Table 4.3 shows a summary of the results obtained during the internal pressure testing of the impacted pipes belonging to this group. As a reference, the control specimen has been added to the table. The energy of impact specified in the table is in the units of Joules.

Label	Energy Round	Energy Long	Maximum Pressure	Location of Failure	Type of Failure
H15	NA	NA	5500	Middle	Leak
1H15	130	190	5500	Round Punch	Burst
2H15	350	700	4100	Round Punch	Burst
3H15	400	800	3900	Round Punch	Burst

Table 4.3 Results for specimens H15 under internal pressure

All impacted specimens in this group failed by burst at the location of the round punch. The acoustic emission records for specimen 1H15 to 3H15 are in Figures 4.31 to 4.32 with the former showing the amplitude against time plots and the latter the cumulative signal strength plots for each of the specimens in ascending order. The most notable aspect of the AE signatures of the specimens was the general distribution of amplitudes, between the specimen that did not show any reduction in strength as compared to those that did.

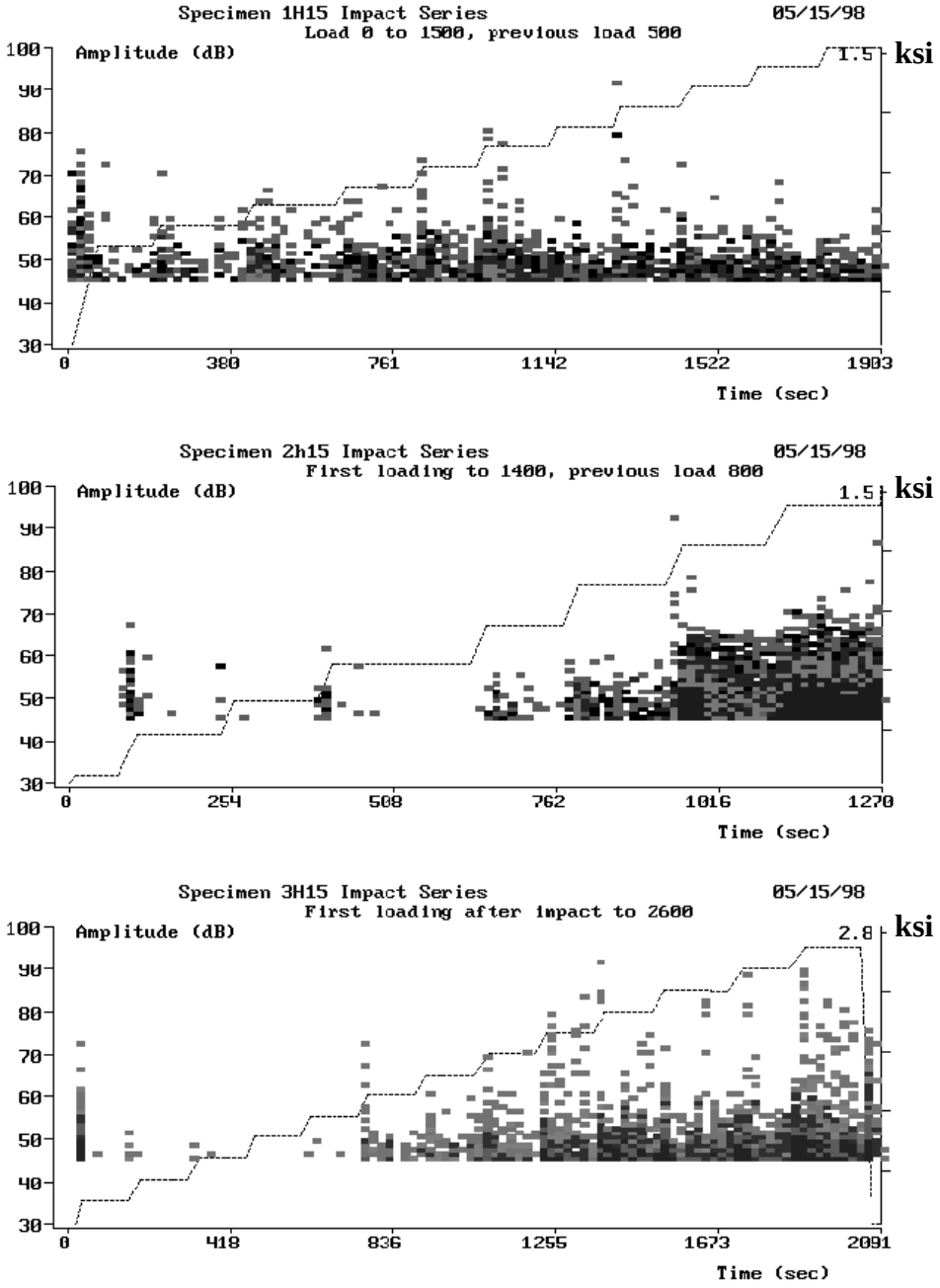

Figure 4.31 AE amplitude records for H15 specimens

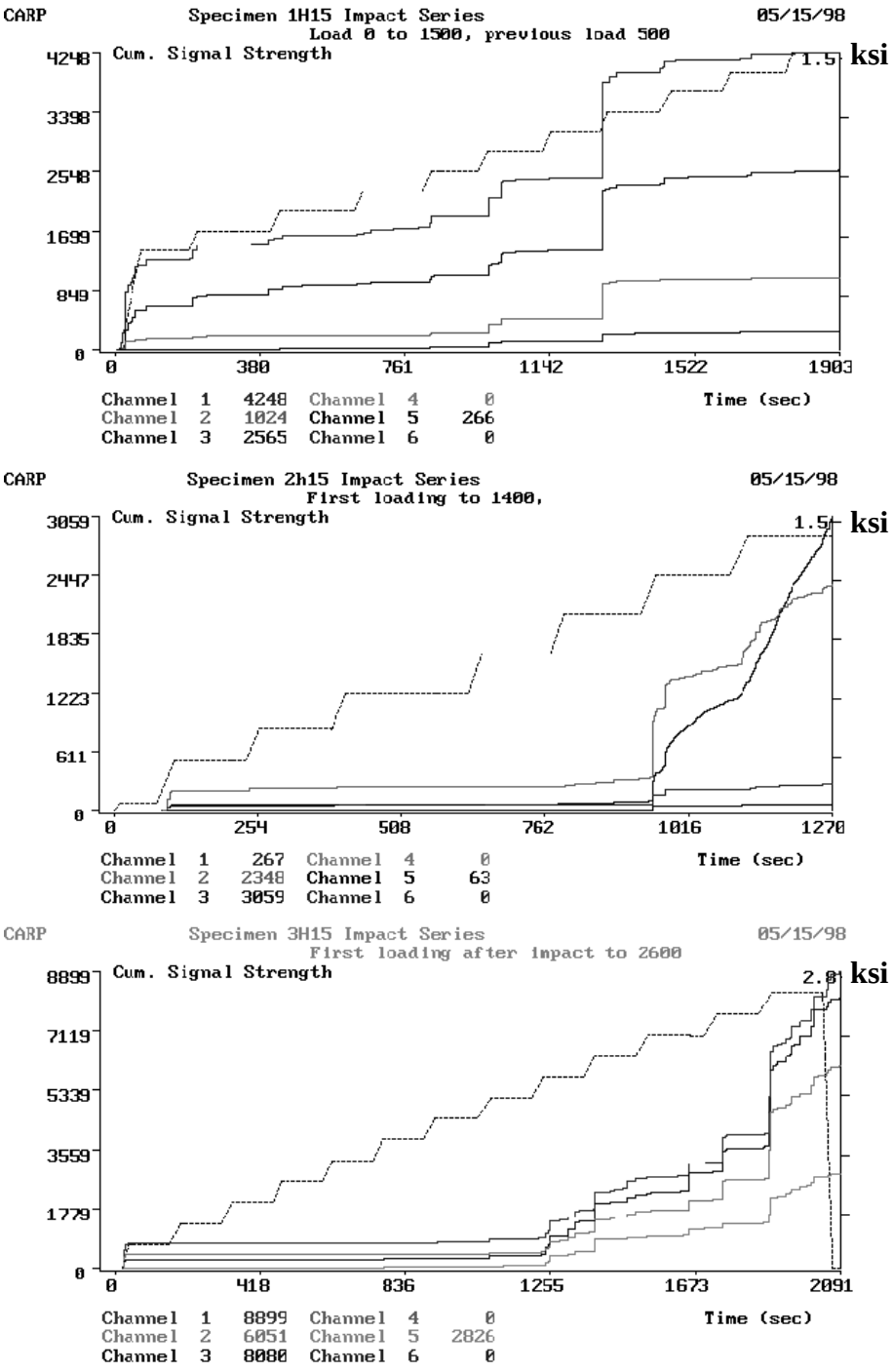

Figure 4.32 AE signal strength records for H15 specimens

For specimen 1H15 that showed no significant reduction, the amplitudes were in the range below 60 dB with very few hits in the larger amplitude ranges. For the specimens that did show some reduction in capacity, the number of events recorded at the higher amplitude levels were more significant. In addition, damaged specimens showed a less gradual increase in the AE activity. Whereas the undamaged control specimen showed limited but noticeable emission during the lower load levels, damaged specimens appeared to be relatively quiet until the point where significant emission was first reached. At this point the slope of the AE signal strength curve changed in to a relatively steep angle.

4.4.2.3. H20 IMPACT DAMAGED SPECIMENS

Although two specimens were impacted with the same energy in this group, only one was taken to failure statically. The other specimen was reserved for cyclic loading tests and monitoring using thermal emissions. The results from the cyclic specimen will not be shown here.

Specimen 1H20 was damaged with the impact of the round punch with release energy of 840 Joules. No impact was made with the long punch since 840 Joules was the highest energy achieved by the test setup. In addition, preliminary tests, on a spare specimen, had shown that the rectangular punch at that energy level did not create significant damage in the same wall thickness.

Figure 4.33 show the AE records for the impacted specimen tested to failure under internal pressure. As with the undamaged specimen, the instrumentation was removed after the same pressure level was reached (4,000-psi). The specimen failed at 10,000-psi of pressure, roughly 84% of the undamaged capacity. The AE signature of the damaged specimen showed an extensive amount of activity at the beginning of the loading history. However, the energy of these emissions was relatively low. We can note the same trend as those in the H15 series in which once significant emission was

detected, the slope of the curve for the cumulative energy is considerably higher than the one observed in the undamaged specimen.

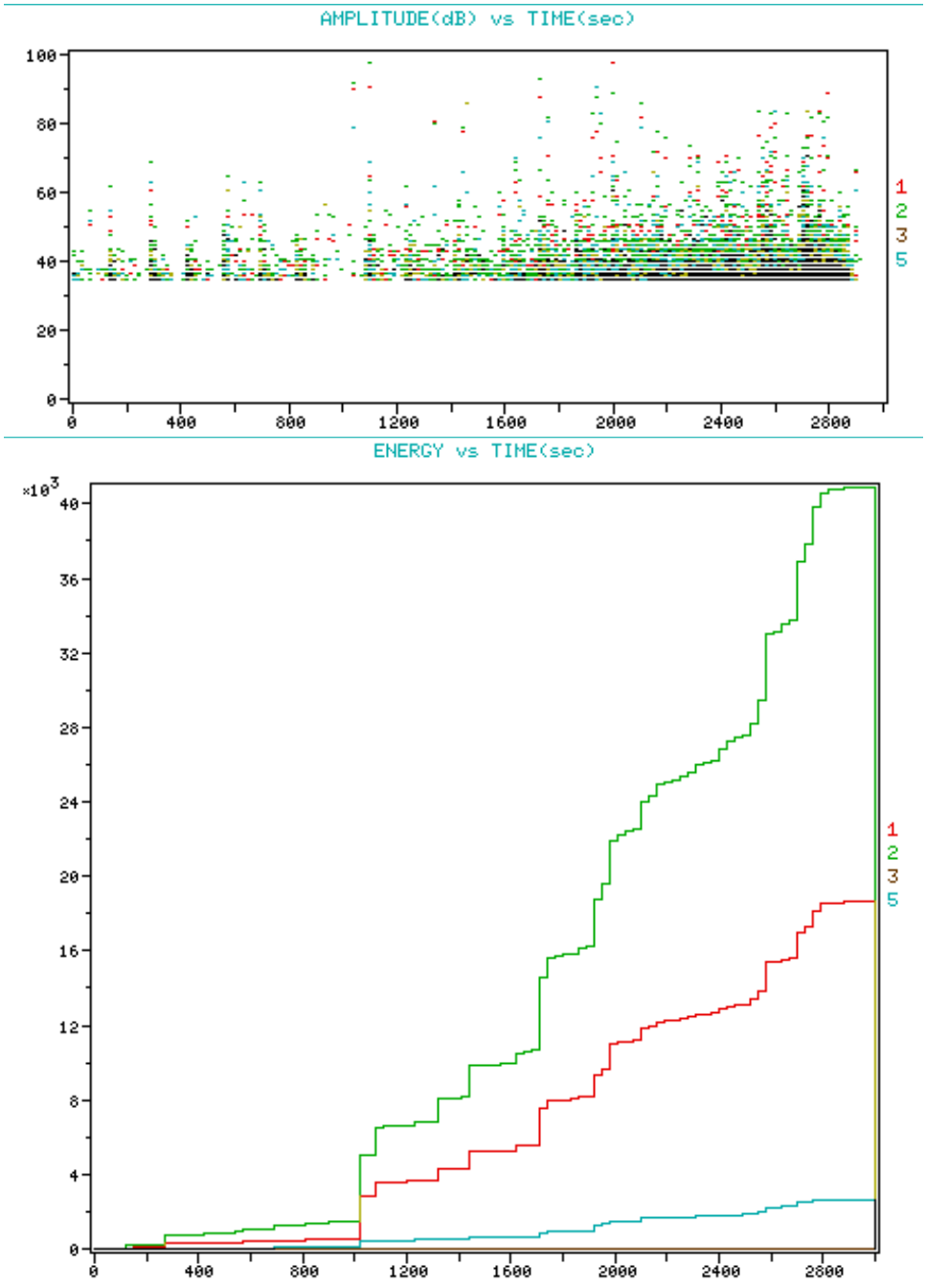

Figure 4.33 AE records for impacted specimen 1H20

4.5. ANALYSIS OF RESULTS

4.5.1. THERMAL EMISSION MONITORING

Of the sets of pipes tested in the impact evaluation program, the H15 group was selected for monitoring with the use of the SPATE™ thermal system. For the specimens pressurized after impact, where thermal emission monitoring was to be performed, a pre-loading to the level designated for the thermal monitoring was made. This target level was increased as the thermal monitoring was completed. This was to ensure that the cycling of the pipe at this level would not produce leakage.

Looking at the results from the H15 series that are shown in Table 4.3, we can notice the correlation between the thermal monitoring results and the results of the pressure tests. From the table it is clear that the impact in 1H15 did not have a considerable effect in the capacity of the pipe. Figure 4.34 shows the screens from the first of the thermal scans made through the damaged area. As we can see in the figure, both the round and long impacts do not have a noticeable thermal signature. This profile did not change considerably during the load stages. This was in agreement with the behavior of the specimen that did not suffer a reduction in its capacity as a result of the impact.

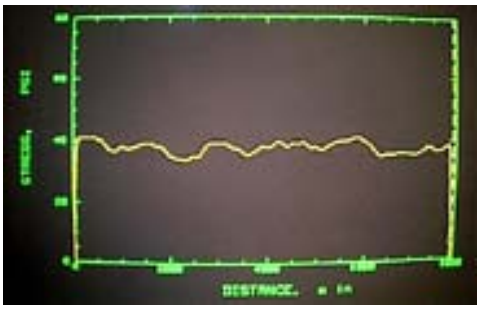

Long Punch

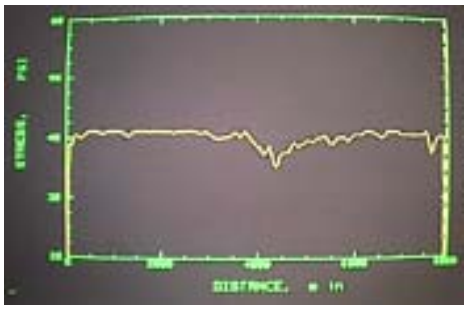

Round Punch

Figure 4.34 Thermal Readings for 1H15

Looking towards specimen 2H15, we can see that the reduction in its capacity indicated in the table was about 25%. Failure occurred suddenly and by fiber failure, which is different from the mechanism of an undamaged pipe. Typically, failure is characterized by leakage as a result of matrix cracking with little or no fiber breakage. As seen in Figure 4.23, the failure is catastrophic and with no warning. It also highlights the importance of being able to predict the capacity after impact damage. Where the previous mechanism does not involve significant fiber breakage allowing for reserve capacity, after the impact the difference between leakage and fiber breakage is reduced to zero. The difference is also noticeable in the thermal readings obtained from this specimen. As seen in Figure 4.35, the readings show a more significant effect in the thermal signature for both the round and the long punch areas.

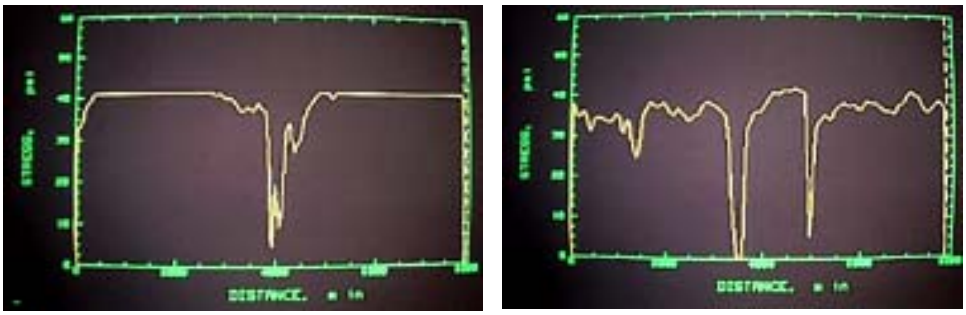

Round Punch **Long Punch**

Figure 4.35 Thermal Readings for 2H15

The change in the readings was proportionally similar between both scans, and this was reflected in the failure mechanisms where both areas failed simultaneously. The noticeable change in the thermal scans for the long punch happened at the edges of the punch area. Initially, the thermal scan had shown no distinguishable changes in the readings, but after the first load increment the signal cleared to the level presented in the figure. In the case of the specimen labeled 3H15, the scans looked similar to the ones from 2H15 (see Figure 4.36). This similarity is also reflected in the leak pressure that was very close to that previously recorded for specimen 2H15.

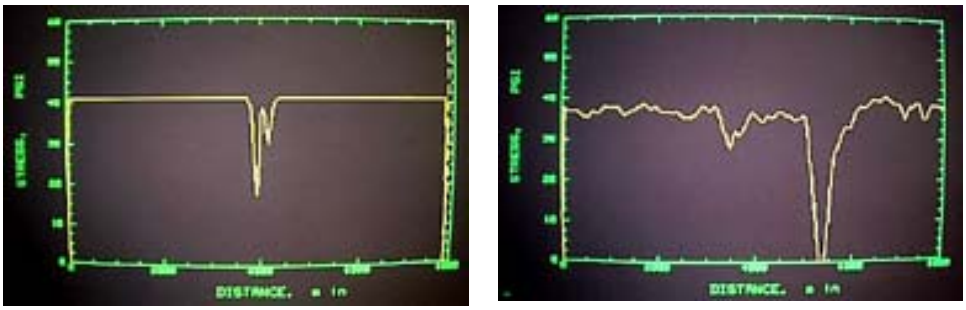

Round Punch **Long Punch**

Figure 4.36 Thermal Readings for 3H15

4.5.2. CAPACITY REDUCTION ANALYSIS DUE TO IMPACT DAMAGE

Comparing the results of the groups tested against each other is a difficult task. Even when the internal diameters of the specimens were the same, the thicknesses and therefore the outside diameters were different. In addition, determining the type of damage and its importance that was generated by the two punch profiles used is very important.

During the testing of the impacted specimens it was determined that the round punch generated the most critical type of damage for the same amount of energy. This by itself is not difficult to determine subjectively since the stress per unit area is larger in the round punch than in the rectangular one. The question is how a layered element like a fiber wound composite will dissipate the impact energy and if the particular mechanism would change depending on the thickness or diameter of the specimen. Another question is how important is each of the mechanisms generated in the capacity reduction and general behavior of the impacted pipe. A typical damage profile that was generated by the round punch is shown in Figure 4.37, along with the profile for the rectangular punch.

Here we see that almost no delamination was generated and large cracking radiated from the point of impact. The limited amount of delamination observed occurred along the path of the cracks that were the main dissipation mechanism in the round punch. In contrast, the damage for the rectangular punch was dominated by delamination in an area that extended completely around the point of impact. In the same Figure 4.37 we see the common profile of damage generated by the rectangular punch.

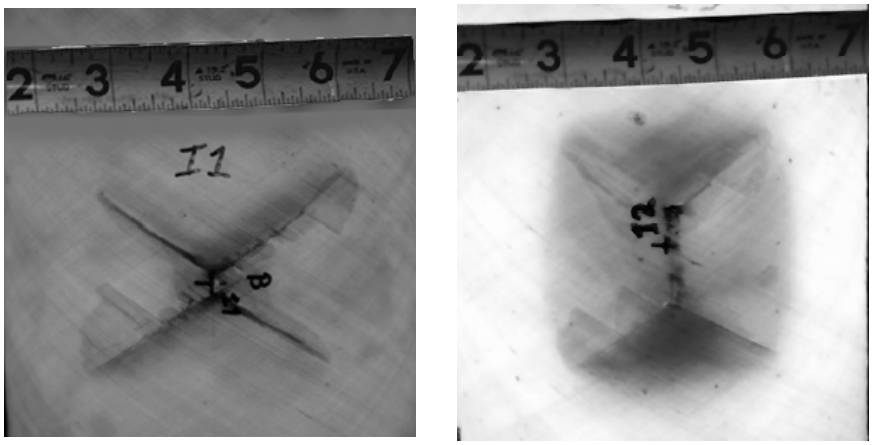

Round Punch **Rectangular Punch**

Figure 4.37 Generated damage for punch profiles

The specimens in Figure 4.37 were backlit to enhance the effects of the impact through the thickness of the specimen. The darker surfaces indicate extensive delamination that extended through more than a couple of layers. The rectangular punch produced this type of damage along with some surface cracking that radiated from the corners of the punch. It was determined that a difference in the energy between the round punch and the rectangular one used in the program of 2.5 times would result in similar capacity reduction. In addition, the results from the static tests indicated that once the stress is distributed in essentially a linear profile as in the case of the rectangular punch, then the width of the punch does not play as an important role as the

length. Calculating the required stress for initiation of damage for a rectangular punch of different lengths is a matter of relating a measured or predetermined load to the length of the punches only. The same type of relationship does not apply to the round punch. In the case of a round or polygon of equal sizes, the type of damage and load required to generate it varies depending on the curvature of the pipe and size of the punch.

Figure 4.38 shows the results of pipes tested in this program along with the results obtained for similar pipes tested by Oden [4.37]. In order to compare the results of the tests directly, the energies have been normalized to the longest dimension of the punches and the square of the pipe thickness. In the case of the round punch the value of the diameter was used in the normalization. In addition, the measured capacity of the pipes has been related to the residual capacity as compared to the control specimens. This was found to work better than the areas of the punches as would be expected from the results of the static punch tests with different sizes.

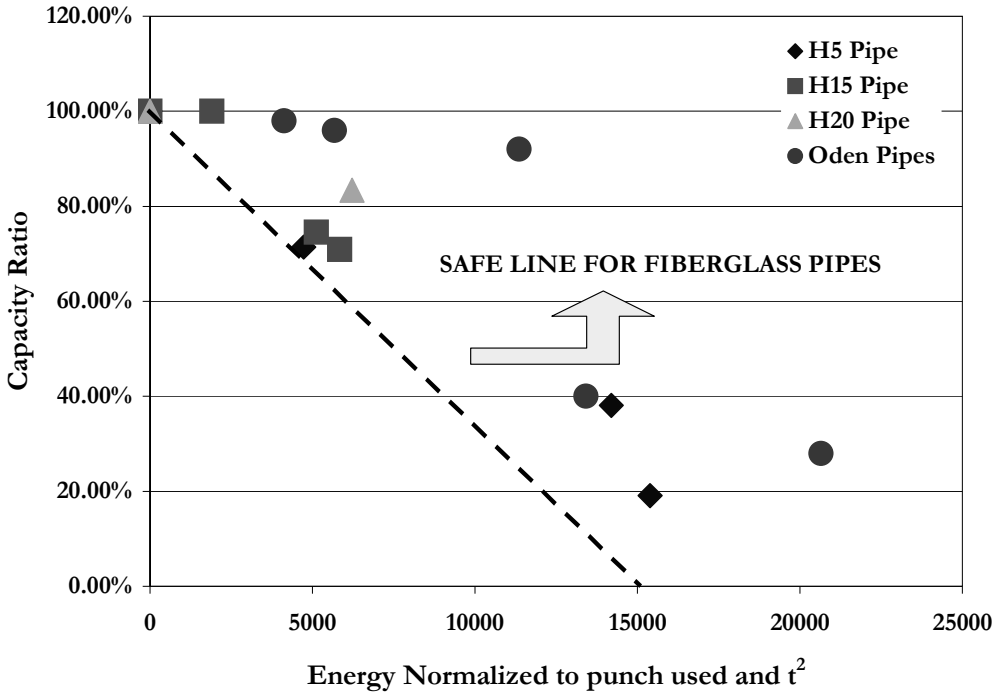

Figure 4.38 Normalized capacity reduction

From the results as plotted in Figure 4.38 there appears to be a relationship between the capacity of the pipes to leakage or burst and the energy of impact. A note is made that the energy as shown in the figure is in terms of Joules. A line was added to the plot to define a "safe zone" between the energy and leakage pressure determination or capacity reduction. This line was drawn as a lower bound for the data points in the plot. It is obvious that a low impact energies there will be no reduction in capacity, however this has been neglected in the plotting of the safety area in the figure.

In some cases, the impact force was large enough to cause immediate damage in the internal diameter of the specimen and therefore result in leakage at very low pressures. This happened in pipes tested in this program and in the ones by Oden [4.37]. These tests negatively influence the location of the safety zone since after the level of energy required to produce internal cracking is reached, any additional energy will only increase the amount of cracking without reflecting on the recorded leak pressure.

4.5.3. ACOUSTIC EMISSION ANALYSIS

Based on the results of the tests performed in this program, it was observed that the AE signature of damaged specimens is noticeably changed in comparison to the undamaged ones. This change, however, is relatively subjective and difficult to quantify if the profile of an undamaged similar specimen is not known. In addition, if the specimen impacted has already gone through a load history, the acoustic emission signature analysis can be complicated. In chapter 3 of this dissertation we have seen that fiberglass specimens that have gone through extended load histories without failing tend to have their AE signature attenuated at the low-pressure levels. Determining, without knowing if an impact has occurred, if the signature is the result of damage or regular load life can be a difficult task.

If the zone of impact is known, then sensors can be placed around that area for analysis of AE signature. The records obtained from the damaged specimens in this phase indicated that a damaged zone like the resulting area around an impact point have

effects on emissions recorded in the immediate vicinity. Table 4.4 shows the results obtained from the AE monitoring of these specimens. Where possible, after a pressure level was reached where consistent emission during load hold was detected, load was dropped and increased again in order to determine the Felicity ratio for the specimen. In the case of 2H5 where leakage was detected even before pressurization took place the Felicity ratio was impossible to determine and therefore is labeled as NA.

Specimen	Pressure	AE Knee at First Loading	Felicity Ratio
H5	2100	600	1.0
1H5	1500	200	0.5
2H5	800	NA	NA
3H5	400	100	0.1
H15	5500	3200	1.0
1H15	5500	1100	1.0
2H15	4100	1000	0.8
3H15	3900	1000	0.6
H20	12000	4000	1.0
1H20	10000	4000	0.95

Table 4.4 Acoustic emission results for impact specimens

In the table we see how the pressure at which the first significant emission is detected is affected by the impact blow. The amount of reduction shows a relationship to the energy at the time of the impact. The most telling aspect of the AE signature as it relates to the reduction in capacity appears to be the value for the Felicity ratio. In the undamaged specimens, since the first knee of the AE curve was reached following download revealed that the felicity ratio had not been reduced to less than one. From the table we see that there is an apparent relationship between the level of capacity reduction and the Felicity ratio at first detection of significant AE emission. Typically, this value will be of one at the time of first knee, and will deteriorate as the load is increased beyond this point. However, if load is reduced and increased around the location of the first knee, it would take a high number of cycles before the ratio is noticeably affected. In the case of the impacted specimens, this tendency was changed. As soon as

significant emission was detected, if the load was dropped and immediately increased, the pressure at which this emission would be detected will be lower providing ratios of less than one.

4.6. SUMMARY AND CONCLUSIONS

A series of impact tests on tubular specimens were performed for this phase. The results showed promising indications of the possibility of using AE/NDE methods for the damage monitoring and strength prediction in composite pipes. The main characteristic of the method selected is its ability to inspect large areas in a short amount of time. In addition to providing indications of the existence of damage, AE showed promise in the determination of residual capacity after damage is created. A parallel study using the same impact specimens is aimed towards the development of source location techniques based on AE. The results of this study will be presented elsewhere, but they have shown very promising results. Follow-up tests are designed to determine the possibility of monitoring damage growth in pipes under cyclic loading at the service levels for which the specimens are designed. This would present a useful tool for monitoring the damage progress in a particular location once a zone is identified.

The main effect of an impact into a fiber composite pipe is the reduction of the ultimate capacity. All specimens that were affected by the impact in this program failed by bursting with the associated fiber failures. These same specimens had failed only by leakage at higher pressures than those recorded after impact. This is a critical result since it shows that any residual capacity associated with first leakage is eliminated by the impact damage. Results indicate that specimens will either be not affected by the impact, or their ultimate capacity will be severely affected by displacing fiber breakage stress to below leakage stress levels. The level of this reduction is related to the energy of the impact, the shape of the impacting surface and the wall thickness of the specimen.

There appears to be a correlation between the measured felicity ratio and the residual capacity of the damaged pipes. This relationship will be studied in detail in the next chapter of this dissertation.

CHAPTER 5

SUMMARY AND FURTHER EVALUATION

OF ACOUSTIC EMISSION DATA

5.1 INTRODUCTION

This chapter provides a summary and further analysis of acoustic emission (AE) data collected throughout this research program. This includes AE data collected in the external pressure test reported in Chapter 2, the internal pressure tests reported in Chapter 3, and the tests on impact damaged pipes reported in Chapter 4. In particular, the data will be examined to evaluate correlation between the AE data and the experimentally measured capacity of the various test specimens. No attempts are made to associate specific damage mechanisms to the AE information. Additional analysis is underway and required in order to establish relationships between AE data and damage mechanisms.

Acoustic emission has been widely used in the nondestructive evaluation (NDE) of fiber composite pressure vessels for a number of years. A significant amount of literature exists from researchers that have developed several correlations between AE data and the strength of pressure vessels at burst or leakage. Typically these correlations have been developed from AE data recorded during rising pressure curves and/or load holds sustained at different pressure levels. An important analysis concept used in these correlations has been the Felicity ratio as developed by Fowler, et.al., [5.4, 5.5]. Other researchers have also made use of the Felicity ratio in the development of prediction models for burst capacities [5.24, 5.25].

Other correlations between AE and structural capacity based on data obtained during load holds have also been available in the literature. Some of the concepts

include the use of the rate moment [5.25, 5.26], and the quantity of all events or of long duration events [5.6, 5.21 and 5.22].

A few researchers have published results using other AE characteristics as the rate of emission during unloading with some success [5.7, 5.27]. Hamstad et.al. [5.7], developed the concept of the Shelby ratio, which is an adaptation of the Felicity ratio used on data obtained during unloading cycles in a pressure vessel. This proved successful in determining damage on graphite/epoxy vessels. It did not, however, predict the amount of reduction in the specimen after damage was detected. In addition, the specimens tested had an internal aluminum liner, which would make comparison of AE to the capacity of the fiber composite portion difficult.

Most research had been focused on determination of capacity as controlled by fiber breakage. Prediction of other failure modes like leakage and stability, using AE methods have not been as extensively researched to this date.

The remainder of this chapter will summarize and further evaluate the AE data for each of the experiments conducted in this research program. The external pressure test will be considered first, followed by the internal pressure tests and the tests on impact damaged pipes.

5.2 EXTERNAL PRESSURE TEST

A static external pressure test to collapse was conducted on a large-scale carbon fiber reinforced epoxy tube, as reported in Chapter 2. The specimen had an initial delamination flaw through the complete perimeter and along the entire length of the tube, located at approximately 1/3 of the wall thickness from the inside surface. The maximum pressure at collapse was 3150-psi. Figure 5.1 shows the specimen after testing.

Figure 5.1 External Pressure Specimen after Testing

Results from the strain gages indicated a non-linearity produced by the delamination in the recorded axial strains. The hoop strains did not appear to be as highly influenced by the delamination or any damage produced during the load increments up to the point of failure. Failure was sudden and was centered in the gage of the specimen between the supports provided. Reasonable agreement was found between the measured collapse pressure and a finite element model that accounted for the delaminated condition. The use of contact elements with no friction included provided reasonable predictions of behavior when compared to the tested specimen. These results, however, cannot be extrapolated with complete certainty since only one specimen of this scale was tested under these conditions in the program.

Acoustic emission data was recorded throughout the external pressure test from two resonant sensors mounted on the outside of the specimen. Analysis of this data was conducted with one objective in mind. This objective was to determine if the acoustic emission data could provide an indication of impending collapse before the actual occurrence of collapse. Initial analysis of the AE data suggests that the acoustic emission monitoring of this specimen provided immediately clear of impending collapse.

The correlation plots similarly showed no clear indications of impending collapse either. Although they provided with promising indications that damage identification from additional analysis is possible but difficult. Plots in Figure 5.2 show the typical correlation plot used in the analysis of AE data for three separate stages in the

loading of the specimen. In Figs. 5.2(a) and 5.2(b), records typically associated with fiber breakage can be noted with a number of high amplitude (>75dB) events recorded. As indicated in Chapter 2, no loss in stiffness was observed in the strain measurements during these stages of the test. In addition, since the critical stresses in the specimen wall were of compressive nature as the result of the external pressure, the occurrence of considerable fiber breakage in the specimen is questionable. The high amplitude events recorded during these stages of loading may not be confidently associated with fiber damage.

To further examine the AE results, Figures 5.3 and 5.4 show data for selected load holds during the testing of the riser. Figure 5.3 show the amplitude versus time plot of events that had signal strength with levels of at least one volt-millisecond and,

NIST Riser between 0 and 1,100 psi

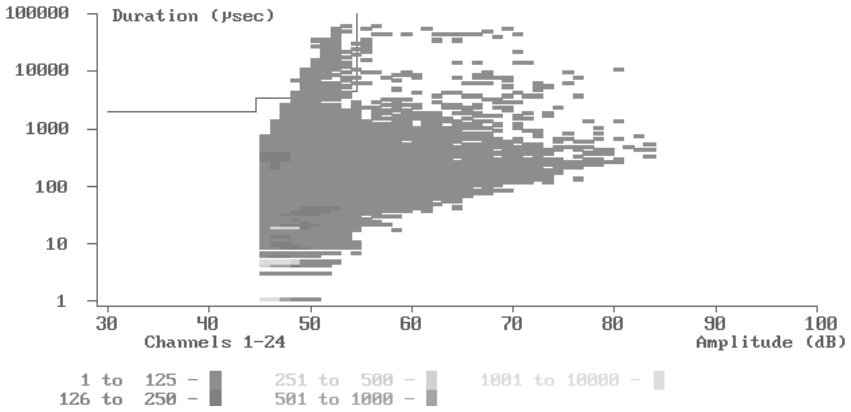

NIST Riser between 1,100 and 1,600 psi

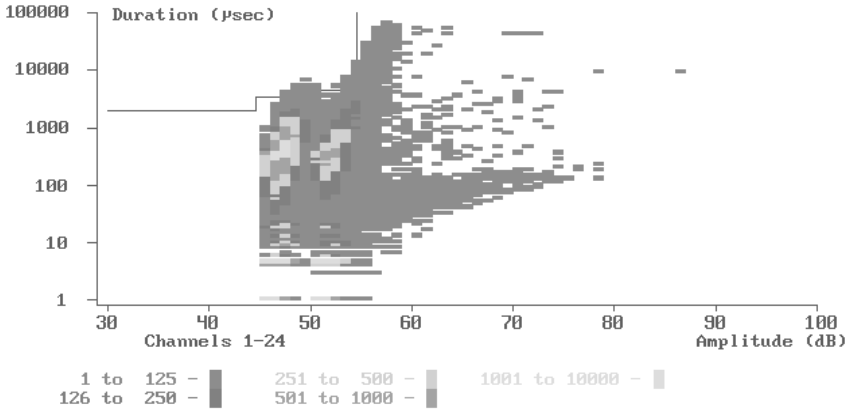

NIST Riser between 1,600 psi to failure

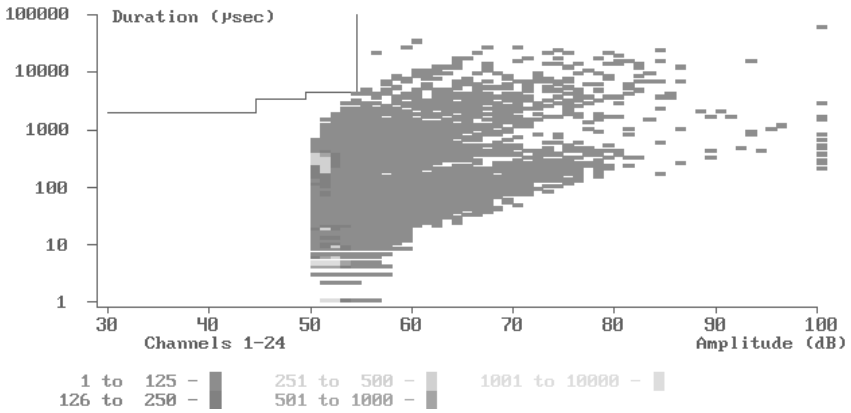

Figure 5.2 Correlation plots for the external pressure specimen

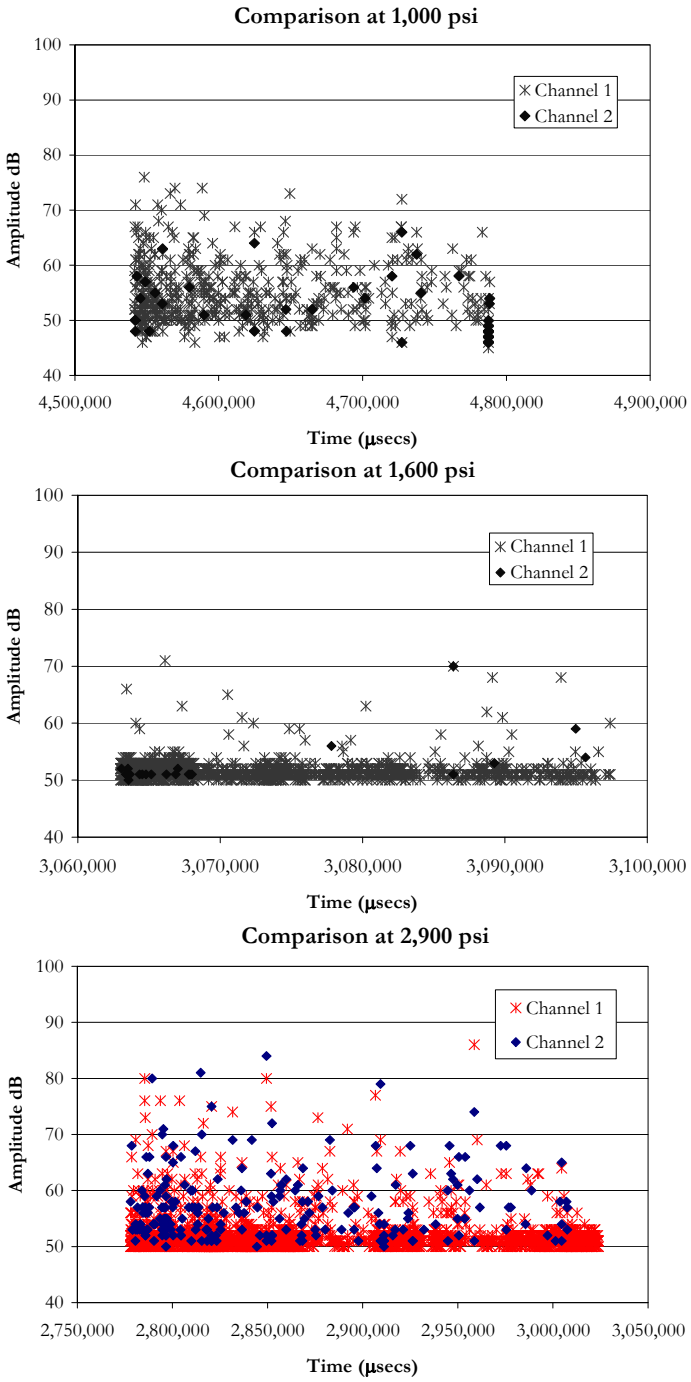

Figure 5.3 Selected amplitude data during load holds

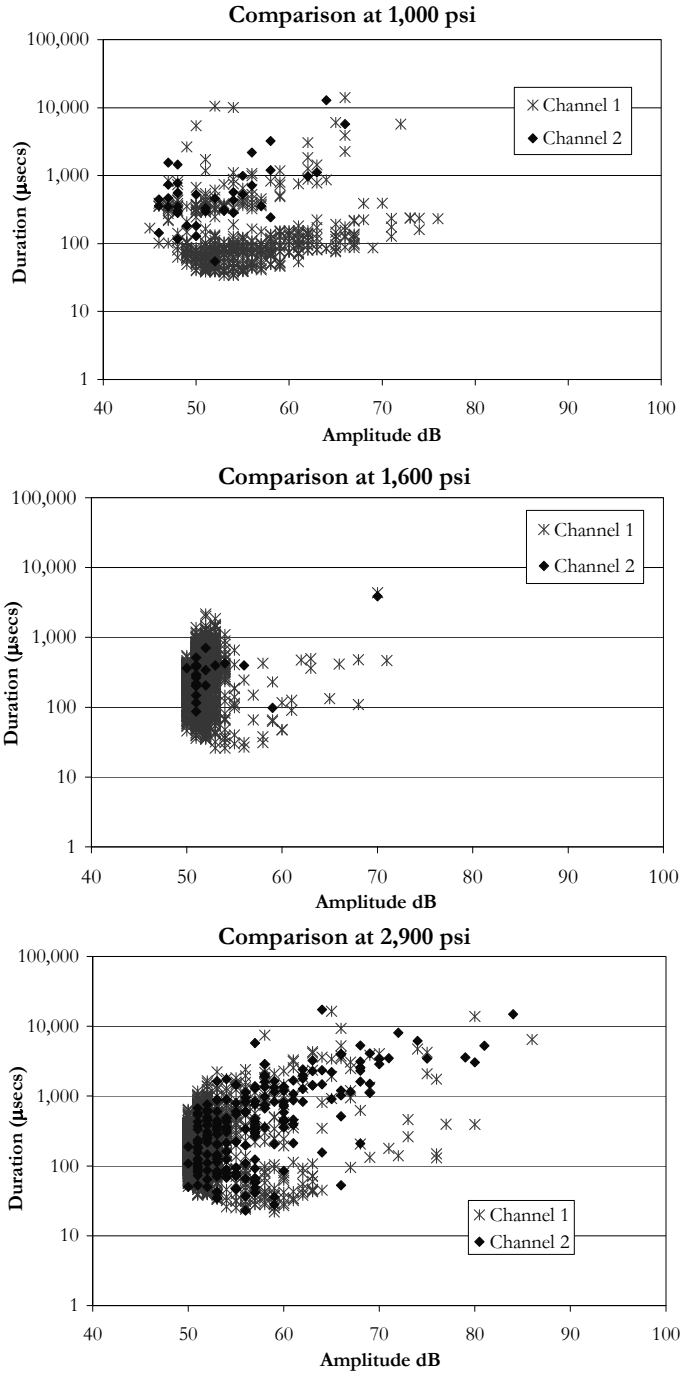

Figure 5.4 Correlation plots during load holds

duration as recorded of one millisecond or more. Two features are apparent in these plots. The first is that a large amount of the data recorded in the tests was associated with one of the sides of the specimen. As it can be seen, for the same time period, on of the sensors showed a lot more activity than the other. This will be of critical nature when additional analysis is made on the data in an effort to identify damage mechanisms. Even though the sensors were calibrated before the test, this calibration only assures that the sensor will detect events within its area of influence. Information gathered during the calibration is seldom used in the signal interpretation of the AE data. Unless the specific source of the event is located or known, typical calibration data cannot be used in signal interpretation.

As an example of the difficulty in identifying individual damage mechanisms from the AE data from a single specimen, Figure 5.4 shows data from load holds at three different pressure levels. The first is a load hold at 1,000-psi, less than a 1/3 of the ultimate capacity. The second is a load hold at 1,600-psi, approximately 50% of the capacity and, the third one is a load hold at 2,900-psi, the last load hold before failure by collapse. Noting that the plots are shown in the same order as the incremental pressures, it appears that the initial load hold was more critical than the one at 1,600-psi. The amount of activity recorded during the load hold of 1,000-psi and the number of the high amplitude events would seem to indicate that more critical damage was being generated at this point than at 1,600-psi. Keeping in mind that for the final test, no leakage of the seals was recorded at any pressure level, it is assumed that the data presented can be considered as real emission from the specimen. Without additional supporting data, it would be difficult to associate any kind of damage mechanism to the data recorded based on the information shown.

The correlation plots of Figure 5.4 also do not provide an immnediate clear picture as to the sources of the emissions. As with Figure 5.3, correlation data for the load hold at 1,600-psi appears to be less critical than at 1,000-psi. Data for the lower

load hold suggest fiber breakage, whereas data for the high pressure load hold suggests events associated with matrix cracking. This sequence of damage seems doubtful.

Overall, the initial analysis of AE data for this external pressure test did not provide with immediate indications that collapse was imminent. Analysis would be greatly facilitated if additional information from similar tests was available as part of the same testing program. More extensive testing of such specimens is needed to develop correlations between the AE data and the observed response of the specimens.

5.3 INTERNAL PRESSURE TESTS

A series of static and cyclic internal pressure tests were conducted on 22 tubular fiberglass specimens manufactured in accordance with the ASME RTP-1 Committee specifications. Two additional static internal pressure tests were conducted on tubular specimens of hybrid construction. The hybrid specimens were identical in construction to the fiberglass specimens, except that they were over-wrapped with several layers of carbon fibers. The internal pressure tests were reported in Chapter 3.

The internal pressure tests were conducted with two objectives in mind. The first was to determine if the current design strain limit of 0.1% typically used for fiberglass tanks could be safely increased. The second objective was to investigate correlations between AE data and the pressure capacity of the specimens under static and cyclic internal pressure loading.

5.3.1 FIBERGLASS SPECIMENS

A total of 22 nominally identical fiberglass specimens were tested to failure under internal pressure. The specimens were constructed with a resin rich corrosion barrier on the inside of the tube, and a filament wound structural layer on the outer portion of the tube. Failure of all specimens occurred by leakage of the internal fluid.

Even though the same manufacturing company built the specimens to the same specifications, a large scatter was observed in the results for both static and cyclic tests to leakage. For the most part, specimens failed during load holds as required by the AE monitoring.

Strain gage data showed very little loss in stiffness in the specimens up to the point of leakage. That is, the relationship between pressure and strain was typically nearly linear up to leakage. This is corroborated by the fact that little or no fiber damage was observed in the failed specimens. Once the inner barrier was penetrated, as indicated by the leak detection layer in the specimen, fluid immediately found a path to the exterior. This path was a combination of delamination and seepage through the interface of fiber and resin. This suggests that the strain limit associated with leakage was first reached in the outer filament wound layers. When the strain limit of the inner corrosion barrier was then finally reached, fluid was able to immediately penetrate the outer layer.

Extensive acoustic emission monitoring was conducted on the internal pressure test specimens. As noted earlier, an objective of this monitoring was to search for correlations between the AE signature of the specimens and the actual internal pressure capacity of the specimens. This objective was based on the hypothesis that damage critical to fatigue endurance is first generated, in the composite material, at low-pressure levels. As the pressure is increased, this damage grows up to the point where failure (leakage in this case) occurs. Acoustic emission monitoring is capable of detecting this damage at its early stages of development. It may therefore be possible to use AE data generated at low-pressure levels to predict the ultimate capacity of the composite tubular member. This possibility was investigated for both the monotonic and cyclically loaded specimens in this program. First, it is necessary to evaluate if the AE emissions obtained during the initial monitoring of the specimens would have the same characteristics as emissions typically classified as “real emission”. In order to evaluate this, the correlation between duration and amplitude were plotted for monotonic cases and a

typical cyclic specimen. Figure 5.5 show the correlation plot for two of the specimens that failed during the first cycle to the target pressure, Tp-5 and Tp-23. Although no attempt is made to identify different damage mechanisms from this correlation plots, we can still see that the general characteristics are of emissions obtained from material behavior and not mechanical noise. Plots show indications of large influence from neither leakage nor rubbing type emissions. Figure 5.6 shows the correlation plot for one of the cyclic specimens of the program, Tp-10. The correlation is plotted for three different stages during the cyclic portion, first monitoring, after 50,000 cycles and after 125,000 cycles or final cycle. Again most emissions fall within the frame of real emission, although slight differences are noted in the mechanisms at play during the different stages. Future analysis will show if this changes can be reliably related to the load history and therefore to the residual capacity of the specimen.

In either case, the challenge was to determine at what point in the load history of the specimen did the AE data indicate the onset of significant damage. One approach to correlating AE data with significant damage is to search for “knees” in a plot of cumulative signal strength versus time. Knees in the cumulative signal strength plot indicate an increasing rate of emission, and can be indicators of significant damage occurring in the material. However, such plots can often show many knees of varying intensity. Consequently, identifying the AE knee that corresponds to the onset of significant damage and which correlates with the actual leak capacity of the specimens was an objective of this test program.

In the case of the statically loaded specimens, analysis of the AE data indicated that a significant “knee” in the AE could be identified by evaluating the historic index combined with an evaluation of AE during load holds. More specifically, it was found that a pressure level of significance corresponded to the point at which the historic index has a maximum and at which emission during load hold is present. This point in the AE record will be referred to as the “RAM” knee. The pressure or strain in the specimen at this point will be referred to as the RAM pressure or strain.

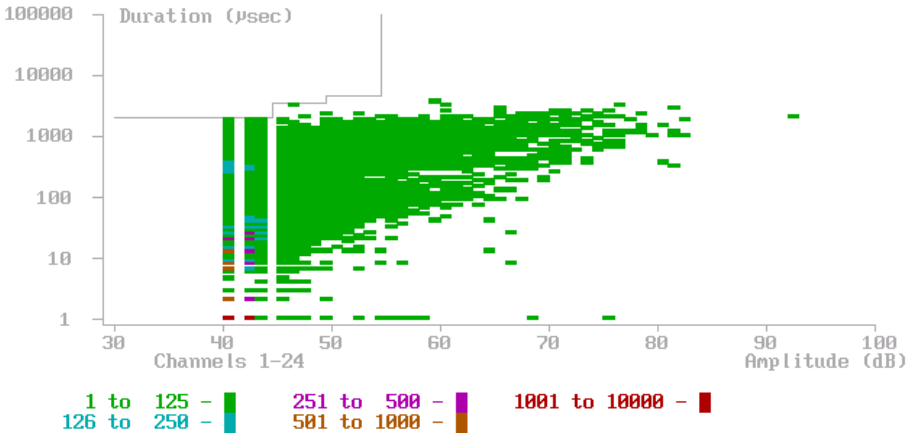

(A) Speciment Tp-5

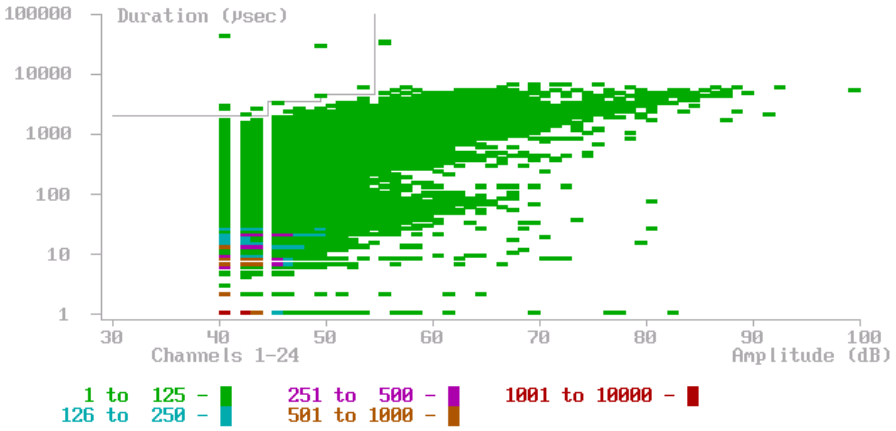

(B) Speciment Tp-23

Figure 5.5 Correlation plots for monotonic specimens

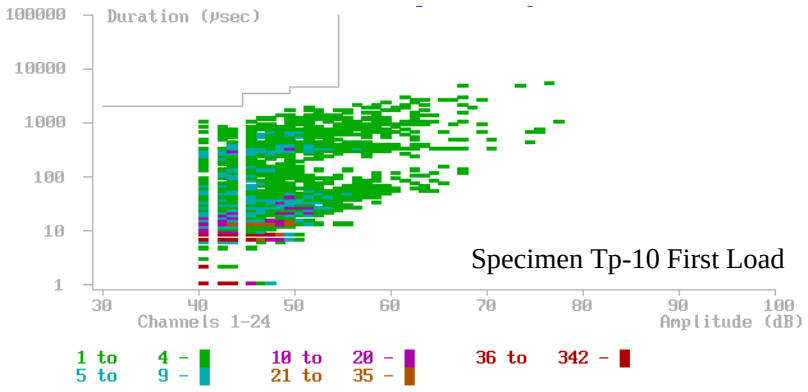

(a)

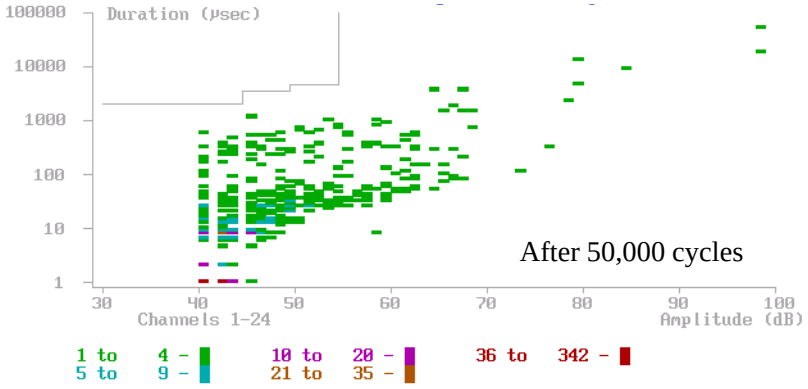

(b)

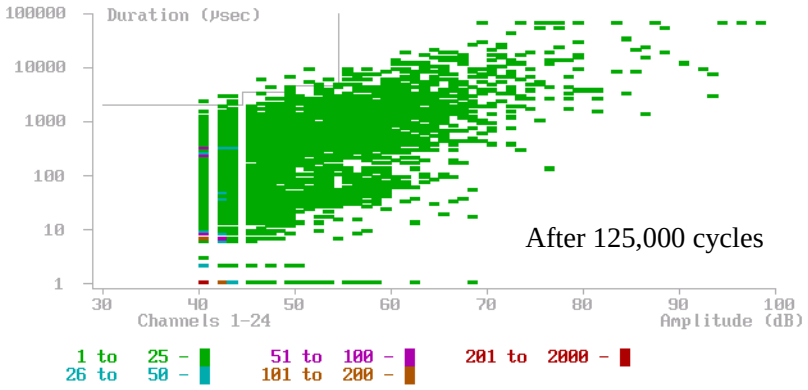

(c)

Figure 5.6 Correlation plot for cyclic specimen Tp-10

Figure 5.7 shows the leakage pressure for the specimens tested under static load and the value for the RAM pressure as determined using the AE records. As is apparent from this plot, there is a strong correlation between the RAM pressure and the pressure capacity of the specimen at leakage.

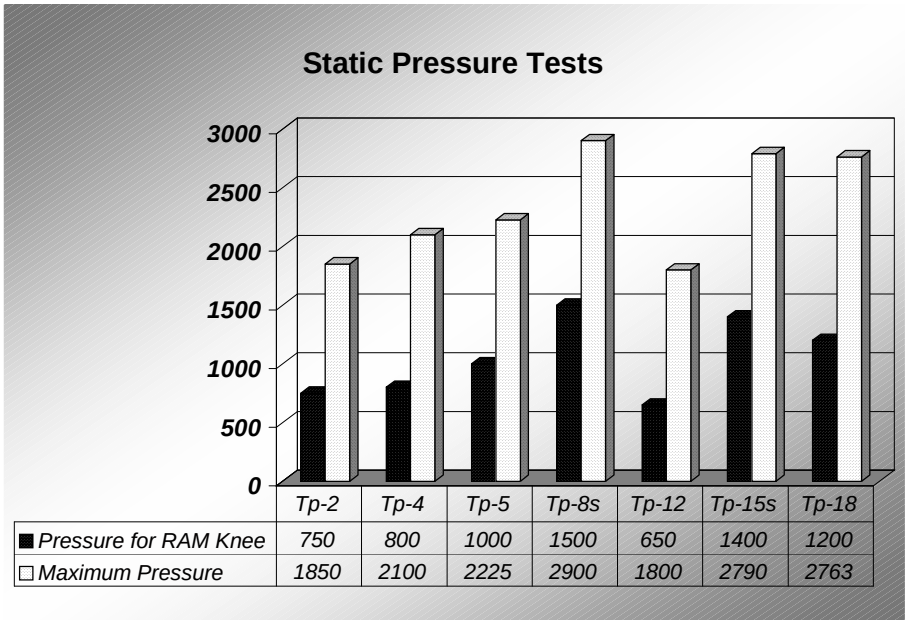

	Tp-2	Tp-4	Tp-5	Tp-8s	Tp-12	Tp-15s	Tp-18
Pressure for RAM Knee	750	800	1000	1500	650	1400	1200
Maximum Pressure	1850	2100	2225	2900	1800	2790	2763

Figure 5.7 Static pressure tests: Pressure at Leakage vs. Pressure at RAM Knee

It is apparent from the Figure 5.7 that even though the individual tests showed considerable variability in the leak pressure, the RAM pressure tracked this variability quite closely. The same relationship is observed in the strains recorded during the tests. Figure 5.8 shows the strains at leakage and those recorded at the time the RAM knee was detected in the AE data.

Figure 5.9 shows the difference between the RAM pressure and the leak pressure for the statically loaded specimens. The difference between the RAM and leak pressures in Figure 5.9 ranges from 1100 to 1500 psi. The average difference is 1,300-psi with a standard deviation of 200-psi. This corresponds to a coefficient of variation of 15 percent. When comparing this error to the typical scatter of the data it can be seen

that a good correlation can be inferred between the RAM knee derived from the AE and the leak pressure.

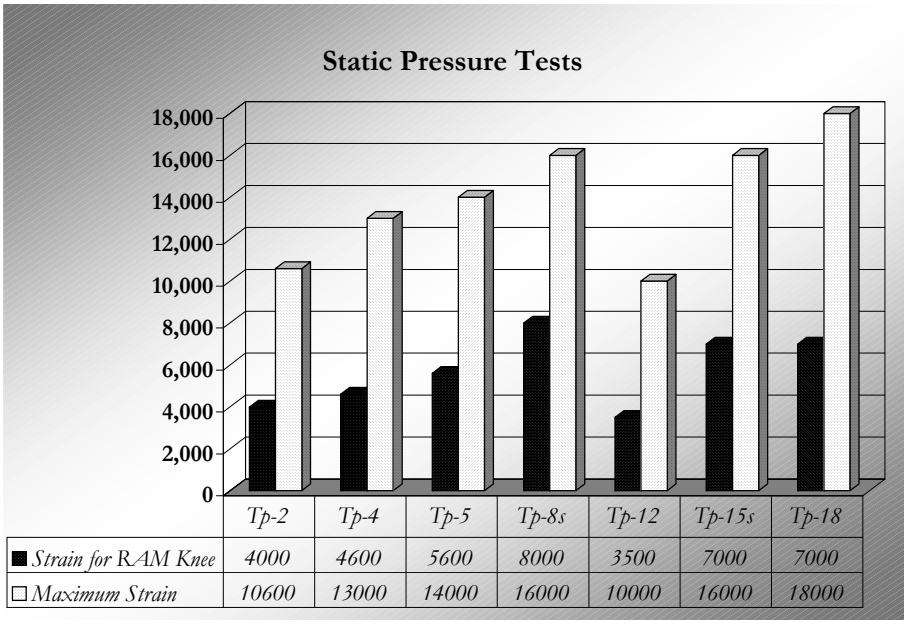

Figure 5.8 Static pressure tests: Strain at Leakage vs. Strain at RAM Knee

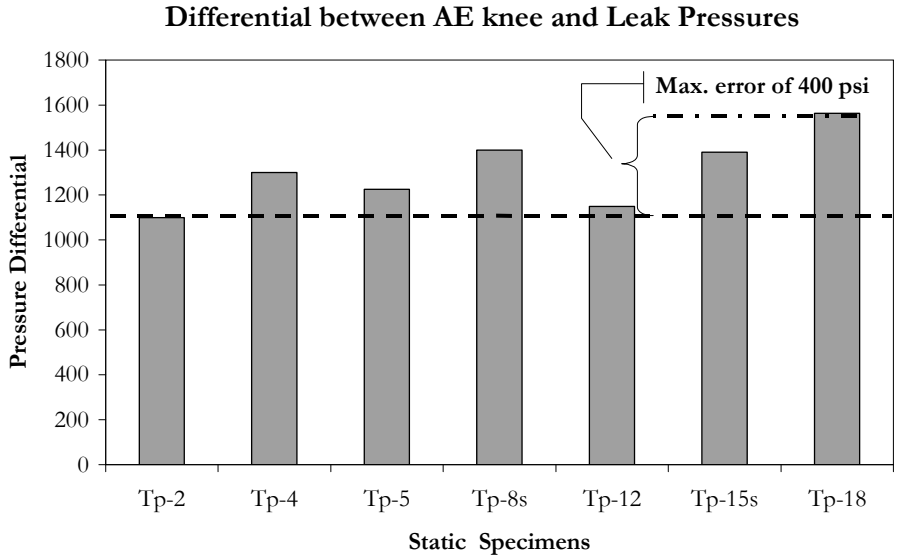

Figure 5.9 Difference between RAM pressure and pressure at leakage

For the cyclic tests, the tubes were cyclically pressurized to a pre-determined pressure level. The number of applied pressure cycles up to leakage of the tube was then determined. Like the static tests, there was considerable variability in the test results. That is, there was a significant variation in the number of cycles to failure for each pressure range. Figure 5.10 plots the number of cycles to failure for each specimen against the pressure at the RAM knee determined from the AE data. The RAM knee was determined in each case during the first cycle of pressurization. The data in Fig. 5.10 is plotted to a log-log scale. A general correlation between the RAM pressure and the cyclic life of the specimens can be observed. The data shows that a lower cyclic life corresponds to a lower pressure at the RAM knee. This seems reasonable in that specimens with a lower cyclic life likely had a greater number of defects or more severe defects than specimens with a longer cyclic life. Specimens with a larger number of defects or more severe defects would likely show earlier significant AE, i.e. a lower pressure at the RAM knee. Further, for each of the pressure ranges an almost linear relationship can be fit between the cycles to failure and the value of the RAM pressure for the specimen. For the specimens tested at 1600, 1800 and 2100 psi, there further

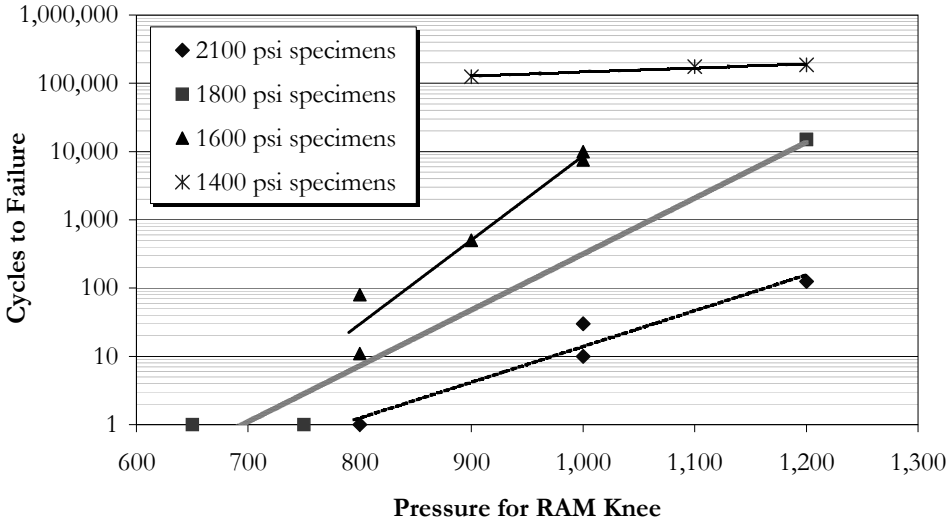

Figure 5.10 Cyclic pressure tests: Cycles to Failure vs. Pressure at RAM Knee

appears to be a trend that the slope of the line decreases with increasing pressure. Unfortunately, the line for the 1400-psi specimens contradicts this trend. Nonetheless, the data in Fig. 5.10 suggests a correlation between the pressure at the RAM knee and the cyclic life of the specimen.

The results of the cyclic loading tests are also plotted in Fig. 5.11. This plot shows the strain at the target pressure level vs. the cycles to failure. The target strains are plotted on a natural scale and the cycles to failure are plotted on a logarithmic scale. In this figure, a line has been fit to the data following an exponential formula. This plot shows a rather large scatter in the test results, although the degree of scatter appears to be smaller at the lower levels of applied strain.

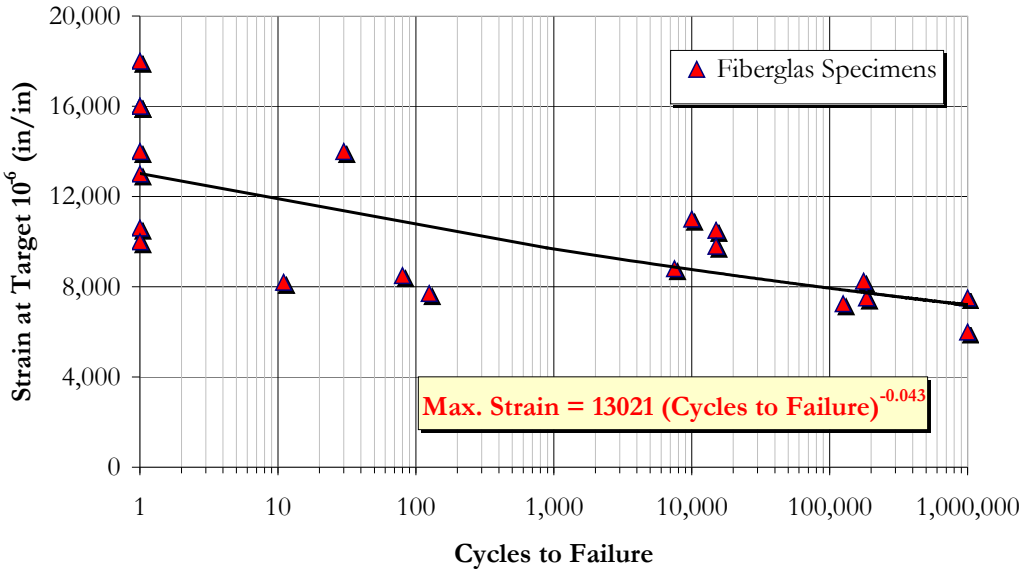

Figure 5.11 Cyclic pressure tests: Cycles to Failure vs. Maximum Strain

The correlation between acoustic emission data and the cyclic life of the specimens is further examined in Fig. 5.12. The difference between the strain at the RAM knee and the maximum applied strain (i.e., the strain above the RAM strain) is plotted on the horizontal axis, and the cycles to failure is plotted on the vertical axis. As with Fig. 5.11 a line has been fit to the data. Note that there is considerably less scatter

in Fig. 5.12 as compared with Fig. 5.11. Another interesting feature is that the line in Fig. 5.12 tends toward an infinite number of cycles as the difference between the maximum strain and the RAM strain tends toward zero. This suggests that the strain or pressure at the RAM knee may correlate with the endurance limit of the specimen. These same trends can be seen in Fig. 5.13, where pressure rather than strain is plotted on the horizontal axis. In this figure, the difference between the maximum applied pressure and the pressure at the RAM knee is plotted.

In general, data from the cyclic loading tests suggests a correlation between acoustic emissions during first loading of a specimen and the specimen's ultimate life under cyclic loading. In particular, the pressure or strain at the RAM knee appears to be a significant indicator of a specimen's cyclic life.

In the analysis considered above, AE data collected during first monitoring of a virgin specimen showed correlation with cyclic life of the specimen. However, no clear trends were observed in the AE data recorded during the cyclic testing of the specimens that would indicate imminent failure. Additional analysis will be required in order to determine if the possibility of prediction based on a monitoring of an in-service specimen is achievable. The general tendency, for specimens with more than 1000 cycles, was towards reduction of emissions at pressures lower than the target pressure. No significant AE events were observed during monitoring at the final cycle prior to failure for these specimens. Those that failed at less than 1,000 cycles showed a Felicity ratio of less than 0.85 at the final loading. However, this was not consistent since some showed this ratio during the initial loading stages and not only at the final cycle. The scatter in the data, however, would indicate that for pressure levels exhibiting a Felicity ratio of less than 0.85, failure is to be expected at very low levels of cycling. Therefore, during the first loading, stress levels should be kept below the point where the Felicity ratio becomes 0.85 or less. If this ratio is less than 0.85 for the pressure level of interest, it may be concluded that the vessel will not tolerate this level of stress during repeated use.

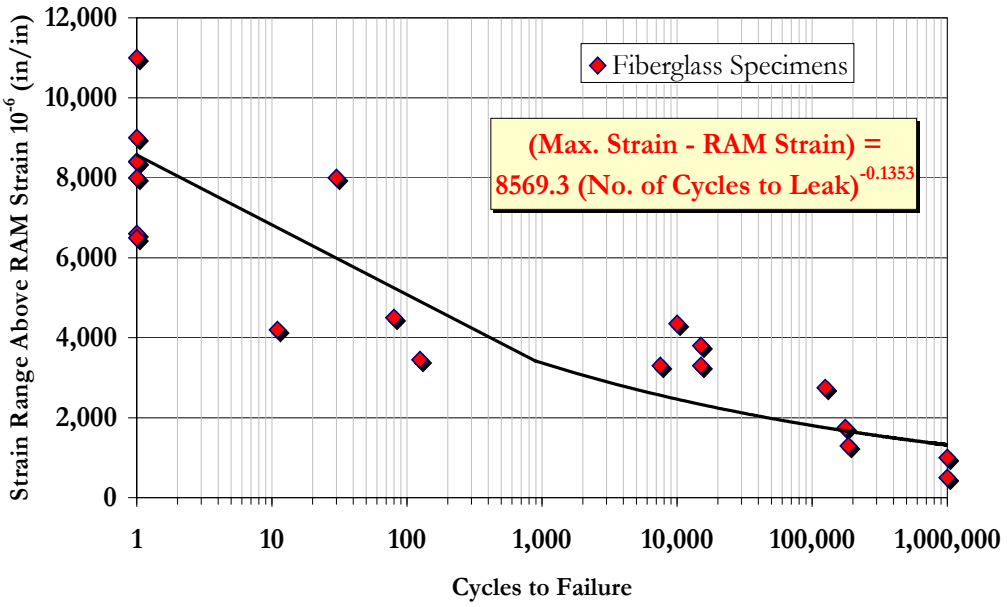

Figure 5.12 Cyclic pressure tests: Strain above RAM Strain vs. Cycles to Failure

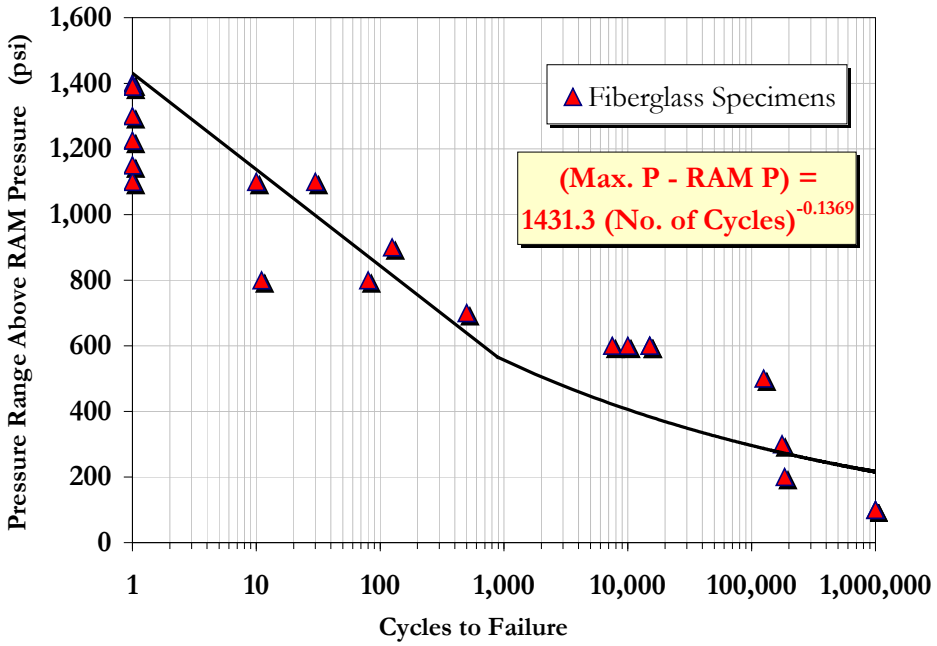

Figure 5.13 Cyclic pressure tests: Pressure above RAM vs. Cycles to Failure

5.3.2 HYBRID SPECIMENS

Two glass-carbon hybrid specimens were tested to failure under statically applied internal pressure. In comparison with the fiberglass specimens, all of which failed by leakage, the two hybrid specimens failed by burst. As shown in Chapter 3, the acoustic emission records for the hybrid pipes showed large amounts of activity from the initial stages of the test. This activity had a mixed parametric profile that made association with damage mechanisms difficult. The partial interaction observed in the strain measurements between the carbon fibers and the glass fibers indicates that a large number of the AE hits may have been due to delamination between the glass and carbon windings. Overall, however, no clear trends were found that would suggest a correlation between the AE data and the ultimate capacity of the specimens. A primary difficulty in interpreting the AE data for these tests was the fact that only two specimens were tested, making it difficult to identify trends. More extensive testing of hybrid specimens is needed to correlate emissions with pressure capacity.

5.4 TESTS ON IMPACT DAMAGED TUBES

In this portion of the research program, fiberglass tubes were subjected to impact damage and then tested under internal pressure. The objectives of these tests were to correlate the loss in pressure capacity with the type and energy of impact, and to further correlate loss of pressure capacity with the AE signature of the damaged tubes. Three sets of specimens of the same construction but different wall thickness were tested in this program.

The results of these tests showed a relationship between the impact energy, profile of the impacting surface and thickness of the specimen. All specimens tested had the same fiber angle in their construction. Therefore, no data was collected on the influence of fiber angle to reduction in capacity due to impact. Static punch tests

however indicated that the orientation of the fiber with respect to the impacting surface does have an effect on the damage mechanisms induced by the punch.

Table 5.1 shows the summary of results for the acoustic emission monitoring for the impact damaged specimens. Specimens that had no impact damage are designated as "control" in the table. In general a correlation was noted between the Felicity ratio and the residual capacity of the specimen after impact. For specimens with reductions in capacity of more than 15%, the Felicity ratio was less than one. The Felicity ratio was determined by comparing the pressure at significant emission at first loading after impact against the pressure required for significant AE in subsequent loading. Similarly, as with the internal pressure cyclic specimens, the AE knee was determined by using the historic index information and the emission recorded during load holds. After significant AE was reached, the pressure was dropped back to zero and the specimen was then re-pressurized while monitoring with AE.

The implication for real structures is that the damage would have to be located first with respect to the sensors. Information from sensors located in the immediate vicinity of the damage could then be used to evaluate the structural significance of the impact damage. For pipes damaged during handling, this should provide no difficulty. Application of this criterion to structures in service cannot be extrapolated until more testing is done for verification. The specimens in this program were damaged while empty. The effects of a pressurized fluid in the specimen at the time of impact, in addition to the changes in AE signature as the result of load history must be considered.

Specimen	*Pressure at Failure*	*AE Knee at First Loading*	*Felicity Ratio*
H5 control	2,100	600	1.0
1H5	1,500	200	0.5
2H5	800	NA	NA
3H5	400	100	0.1
H15 control	5,500	3,200	1.0
1H15	5,500	1,100	1.0
2H15	4,100	1,000	0.8
3H15	3,900	1,000	0.6
H20 control	12,000	4,000	1.0
1H20	10,000	4,000	0.95

Table 5.1 AE comparison table for impact specimens

CHAPTER 6

CONCLUSIONS AND RESEARCH NEEDS

6.1 OVERVIEW

During the course of this research program, three separate test series were conducted on composite tubular members subject to external or internal pressure loading. The aim of the program was to develop a better understanding of the behavior of large scale composite tubes under pressure loading, to develop improved experimental methods for large scale composite tubes, and to asses several methods for NDE for evaluation of composite tubes.

All of the three test series required the development of specialized sealing systems to permit the application of internal or external pressure. Further, in the case of the internal pressure tests, reinforcement of the tube ends was needed in order to prevent premature failure of the tubes at the seal regions. The development of successful seal systems and the development of appropriate end reinforcement techniques represented a major effort in this research program. In all three test series, finite element analysis of the tube ends combined with a significant number of laboratory trials were needed before successful tests were obtained. In many of the initial tests, failure of the seal system or failure of a tube end at the seals was encountered. Recommendations for sealing systems and end reinforcement schemes for internal and external pressure testing of large size composite tubes are provided in Chapter 2, 3 and 4 of this dissertation.

Various methods of NDE were used throughout this research program. This included acoustic emission (AE) monitoring, thermal emission monitoring, the use of leak detection layers embedded in the tube wall, and limited use of ultrasonic scanning. Of these methods, AE monitoring was used most extensively in this test program, and showed a number of useful results, particularly for the internal pressure tests. AE

monitoring provided an aid in evaluating damage mechanisms as they developed in the tubes under increasing load. Moreover, promising results were obtained that indicated that AE monitoring may be capable of predicting the ultimate capacity of tubes subjected to internal pressure. This was the case for the tubes both with and without initial impact damage. For the fiberglass tubes without initial impact damage, correlations were found between the AE signature of the specimens under low-pressure levels, and the ultimate capacity under static and cyclic loading. Perhaps most interesting among these results was a correlation found between AE and the endurance limit of the tubes under long term fatigue loading. A correlation was also found between AE and the loss of internal pressure capacity of an impact-damaged tube. Overall, the AE monitoring proved to be a highly useful technique for evaluating damage and predicting the static and cyclic capacity of fiberglass tubes under internal pressure.

Other NDE techniques were also used to a more limited extent in this test program. Thermal emission monitoring conducted with the SPATE device provided useful qualitative behavioral information on the tubes under internal pressure. Thermal emission monitoring was particularly useful in evaluating the presence and severity of stress concentrations in the sealed regions at the ends of the tubes subjected to internal pressure. This data was useful in designing end reinforcements for the test specimens. Thermal emissions were also useful in monitoring the extent of damage for tubes subjected to various types and intensities of impact damage. The leak detection layer that was embedded in the wall of some internal pressure specimens also provided useful information. This leak detection system provided an indication of the level of applied internal pressure at which the internal fluid in the tube had penetrated the tube wall at the point where the leak detection layer was located. This information was useful in diagnosing the sequence of events that lead to the failure of these specimens. Finally, limited use was also made of ultrasonic NDE methods. Ultrasonic methods were used to evaluate the location and extent of the pre-existing delamination in the external pressure specimen. Ultrasonic methods were also useful for evaluating variations in tube wall thickness.

The following sections provide a brief summary of key findings from each of the test series conducted as part of this research program.

6.2 EXTERNAL PRESSURE TEST

This was a single specimen with the particular characteristic of containing a complete delamination at near mid-thickness of the tube wall, which covered the length and perimeter of the specimen. The lack of a non-damaged specimen makes some of the observations preliminary at best. However, some interesting comparisons can be made based on finite element models that contain the delamination and a control model that does not contain the delamination. The model was calibrated to the strains measured during the test of the delaminated structure. The dimensional tolerances on out-of-roundness used in the model were based on the field measurements performed on the specimen prior to testing. The measured out-of-roundness was far less than the minimum acceptable out-of-roundness criteria set by API, and much less than out-of-roundness values typical of steel tubes.

Based on the finite element results, the model predicted that elastic buckling of the cross section of the specimen caused the collapse. In addition, it predicted that the delamination had an effect on the collapse capacity of the specimen. Based on the results from the model, the measured collapse pressure of 3150-psi was approximately 45% of the predicted capacity on elastic buckling for a non-damaged or unflawed specimen. Based on the model's prediction for maximum strain and stress combined with the Tsai-Wu failure criteria, no material failure was apparent until after the elastic buckling load was reached and the deformation produced the observed fiber breakage. A follow up sensitivity analysis reflected that material failure for this specimen would not have played an important role until after the initial out of roundness exceeded the level of 1.0% as defined by API. However, this analysis also indicated that the collapse pressure is highly sensitive to the tube's initial out-of-roundness. This suggests that out-of-roundness must be carefully controlled during manufacturing of tubes in order to

maximize external pressure capacity. It appears that finite element modeling can be useful guide in establishing acceptable out-of-roundness limits.

The use of contact elements at the delamination in the model provided for reasonable predictions with the observed behavior during the test. During analysis, limiting penetration by the contact elements to the target surfaces provided with the most accurate predictions. Using the largest value of contact stiffness that will result in a stable numerical solution appeared to provide the best combination of predicted deformation and measured capacity. This observation agrees with conclusions made by Rasheed [2.8].

The analysis also indicated that the location of the delamination in the wall thickness would have played a role on the measured capacity. An additional variable that was included was the gap between the layers at the delamination surfaces. It revealed that the separation between the layers would have played a marginal role in the capacity for as long as the total distance between layers was not more than the estimated thickness of a fabricated layer of the laminate.

Overall, the acoustic emission data collected for this specimen proved difficult to interpret in this first analysis. In addition, the fact the tube was constructed largely with carbon fibers also contributed to difficulties in interpreting AE data by extrapolation. The historical database relating damage in composites with AE is established largely for glass fiber composites. Less historical data is available for carbon fiber composites, making the interpretation of such data more difficul. Nevertheless, AE did provide some useful data for the external pressure test that appeared to corroborate predictions of the analytical model. Ultimately, a larger experimental database of AE for carbon fiber tubes under external pressure is needed to develop more useful correlations with damage mechanisms and tube behavior.

6.3 INTERNAL PRESSURE TESTS

This was the largest component of the research program. Two separate groups were tested under this sequence. The first and largest group of specimens consisted of fiberglass pipes fabricated to the requirements set by the ASME RTP-1 committee for pressure vessels. A second and much smaller group of specimens consisted of hybrid construction made with the same specifications as the first group with the addition of an external winding of carbon fibers. Only preliminary static tests were performed on the hybrid specimens.

The need for methods for determining capacity of a vessel based on non-destructive monitoring was reinforced by the variability of the results presented here. Even though these were simplified tests, they provided useful information on the behavior and design of fiberglass tubes and pressure vessels.

6.3.1 STATIC PRESSURE TESTS ON FIBERGLASS SPECIMENS

The static tests showed large variability in the leakage capacity of specimens tested during this loading phase. Pressures at leakage ranged from 1800 psi to 2900-psi for specimens fabricated to the same specifications. The resulting records of strain measurements did not seem to show a clear pattern in relation to the leakage capacity. They did show, however, that estimates for the properties in direction other than the loading direction are relatively inaccurate using current models. Not enough information is available to generalize an expression for determining these properties, but the obvious trend was towards underestimation of the stiffness in the direction normal to the fibers and in the Poisson's ratio.

The strains recorded during the tests at the time of failure were almost 20 times larger than the allowed by current design codes. This, however, does not account for long term effects in the component under sustained loading. Results indicated that the

internal corrosion barrier as designed under the RTP-1 specifications played an important role in the measured capacity of the specimen.

Acoustic emission records showed some interesting trends during the monitoring of all the tests. There was an apparent relationship between the load at which the AE knee was recorded and the leakage failure pressure. A very consistent difference between the pressure at significant AE emission and leakage pressure was found. Even when the variation in this value was on the order of 10% it still provided with a more consistent estimate than the current specifications. The stress level, designated as the RAM stress, at which significant emission and emission during load hold take place at the same time was a consistent milestone from where leakage could be determined within an acceptable range of accuracy.

The mode of failure of the fiberglass specimens does raise some questions over current philosophy in the design of lined vessels. Once the failure of the internal liner was achieved, complete leakage was generated until the pressure inside the specimen equilibrated the ambient pressure. No previous indications were visible before failure, which would make prediction based on visual methods very difficult. Typically, internal liners are not included in the design of vessels or, when they are, the are penalized with a very high safety factor. This could result in a liner sometimes stronger than the fiber winding shell itself. The side effect would be that when failure of the liner is reached by stress or deformation in tanks designed for higher pressures, the fluid contained in the vessel will be suddenly sprayed to the outside. Tanks built with this system are used in containing corrosive or hazardous materials. The possibility of having a failure where the material is suddenly released is of concern. Failure for this type of tank should be controlled to generate a small amount of weeping rather than a sudden release.

6.3.2 CYCLIC PRESSURE TESTS ON FIBERGLASS SPECIMENS

Results of cyclic tests at target pressures above 1600-psi were relatively inconsistent, within common groups, as to the number of cycles required for failure or leakage. Strain measurements generally showed no apparent loss of stiffness as the result of cycling. In addition, residual deformations recorded at the end of each static monitoring were mostly recovered in one day of rest. Tests performed at a target pressure of 1200-psi lasted for a total of one million cycles before being tested to leakage. The results indicated that little or no reduction in the capacity was recorded after the cycles.

Acoustic emission during first loading of the specimens indicates that prediction of the fatigue endurance limit based on this NDE technique is possible. Data from these tests indicate there is a correlation between the RAM stress and the expected life to leakage of the specimen in tests between zero and the target pressure. The lowest pressure where this second AE knee was recorded was 800-psi; the results of the cyclic test suggest that this could be the endurance limit of the specimens. Following the results of tests at 1200-psi of load span we note that these specimens had the second knee recorded at 1100-psi, slightly lower than the maximum pressure. Using this AE milestone as the endurance limit, we can see that allowable strains of up to 0.3% or more may be possible in the design of vessels in the direction of the loading. This would result in an improvement of up to 300% over the previously accepted limit.

Acoustic emission, however, was not fully approached in an attempt to find indications during the cyclic phase that would help in the prediction of remaining life. Cursory evaluation of the data shows that this may be a difficult task if the loading history or the structure is not known. The general tendency of the specimen was to reduce the amount of emission at pressures lower than the target pressure as the number of cycles increased. In the cases of specimens at pressures above 1600-psi, at the time of leakage, the Felicity ratio was 0.85 or lower. This does not apply to the specimens tested at target pressures under 1600-psi where, after a number of cycles, no clear

acoustic emission was apparent until the target pressure was reached. A possibility of predicting remaining life is apparent in these cases but only if the complete load history of the specimen is known beforehand.

6.3.3 STATIC PRESSURE TESTS ON HYBRID SPECIMENS

The use of an external layer of carbon fibers provided for an increase in the leakage capacity and stiffness of the specimens when compared to the fiberglass components. The failure mode was also different for the hybrid specimens. Whereas first failure in the fiberglass pipes was that of leakage, failure of the hybrid specimens was by burst. No leakage was detected in the internal layers prior to complete failure of the pipe.

The contribution of the carbon fibers to the stiffness was not 100% effective, based on comparisons between simplified analysis of the specimen and measured strain values. The measured stiffness was lower than the predicted one based on the individual properties of each of the layers. The mismatch of stiffness at the interface between the fiberglass winding and the carbon winding resulted in delamination generated by the applied pressure that limited the effectiveness of the carbon.

Acoustic emission showed the tendency of carbon fibers of producing a high level of emissions at low stresses. Records of AE events were apparent from the beginning of the load history of the specimen. However, the response to unloading was similar to the one noted in the pure fiberglass specimens, where a relative low AE activity was recorded at pressures previously seen by the specimen.

6.4 TESTS ON TUBES SUBJECT TO IMPACT DAMAGE

This test series consisted of static penetration tests followed by low velocity impact and pressurization tests on fiberglass pipe specimens. Three different wall

thicknesses were part of the program. In addition, different profiles of punching surfaces were used in the tests. After impact, specimens were pressurized internally to determine the residual capacity after damage. Some of these specimens were monitoring with the use of the SPATE™ or thermal emission monitoring system, in order to determine if the extent of the surface damage can be evaluated with this measurement technique.

The importance of properly determining the extent of damage resulting from an impact was highlighted by the change in mode of failure observed in the test specimens. Non damaged specimens failed under internal pressure by leakage. Impacted specimens not only failed at lower pressures than the undamaged pipes, but the failure mode was burst instead of leakage.

Acoustic emission showed good results in predicting residual capacity on specimens after impact. A correlation was found between Felicity Ratio and residual capacity.

These tests also indicated that the tolerance of empty specimens to impact could be evaluated by static punch tests. The orientation of the penetrating surface with respect to the fiber direction and with respect to the orientation of the tube had an important effect of the type and extent of damage produced by the impact. For penetrating surfaces extending along the length of the specimen, the main mechanism of damage was delamination. In contrast, the smaller penetrating surfaces produced more bearing failures and fiber breakage.

6.5 FUTURE RESEARCH NEEDS

A number of questions remain unanswered by this program and, in general, in the area of behavior of large-scale composite components.

More data are necessary for external pressure tests of large-scale composite tubes. Most analytical models available today have not been calibrated to cases with a variety of flaw dimensions and distributions. The test performed in this program was an extreme case of delamination. Intermediate conditions must be explored in order to build confidence in available models.

The sensitivity of the AE to the thickness of the corrosion liner in the internal pressure specimens needs to be studied in more detail. In general, an apparent dependency on the maximum recorded pressure to the capacity and strength of the liner was noted, more so than to the winding itself.

Results indicate that an endurance limit can be found for a specimen based on the AE signature at first loading. This must be verified by long term testing of specimens following the demanding specifications of ASTM D2992, or by statistical sampling of specimens from different manufacturers at first loading that were fabricated after passing the cyclic endurance test as specified by the same standard.

In the case of hybrid construction more research is required in order to develop a better understanding of the interaction between the two materials. The mismatch of stiffness in windings where no stacking of material is provided proved to be a hindrance to the strength of the hybrid system. Alternate methods and forms of combining the two materials must be explored.

In the area of impact damage evaluation, more research is needed to determine the effect of an impact in a filled pipe. For the most part, the common dissipation mechanism is that of delamination in the internal layers at the time of the impact. The tests performed in this program cover only the condition where impact has been generated in a pipe during handling. Thus allowing free deformation of the surface at the time of impact. Filled pipes under pressure will limit this delamination from taking place changing the importance of punch penetration and fiber breakage. Further, more

data and analysis are needed for correlating AE with the loss of capacity in impact damage pipes.

References:

Chapter 1

1.1 F.J. Fischer, K.H. Lo and Su-Su Wang, "Material Requirements for Risers", ASME International Conference, Dallas, Texas 1998.

1.2 The American Society of Mechanical Engineers, "Reinforced Thermoset Plastic Corrosion Resistant Equipment", ASME RTP-1

1.3 The American Society of Mechanical Engineers, "Fiber Reinforced Plastic Pressure Vessels – Section X", ASME Boiler and Pressure Vessel Code

1.4 American Water Works Association, Standard C950, "Fiberglass Pressure Pipe", American National Standard

1.5 The American Petroleum Institute, Specifications 15LR, 15HR, 15 TR, "Specifications for Fiberglass Tubing", Draft Revision, May 5, 1994

1.6 The Composites Institute of the Society of Plastics Industry, "Recommended Practice for Acoustic Emission Testing of Fiberglass Reinforced Plastic Resin (RP) Tanks/Vessels", Published by the Committee for Acoustic Emission from Reinforced Plastics (CARP)

1.7 The American Society of Testing Materials, Specifications D2992 "Obtaining Hydrostatic or Pressure Design Basis for Fiberglass Pipe" and, D2837 "Obtaining Hydrostatic Design Basis for Thermoplastic Pipe Materials"

1.8 Sims, G. D., "Development of Standards for Advanced Polymer Matrix Composites", Composites, Vol. 22, 267, 1991

1.9 Military Handbook of Polymer Matrix Composites (in editing), Department of Defense, Vol. 1. And Vol.2

1.10 Swanson S. R., Christoforou, A.P., et al. "Biaxial Testing of Fiber Composites Using Tubular Specimens", Experimental Mechanics. 1988

1.11 Parker Seals, Catalog PPD3700, Parker Seal Group packing division, (801) 972-3000

1.12 Vishay Measurements Group, Micromeasurements Division, Technical Notes TN-505 and TN-515, Bulletins B129 and B137

1.13 American Society of Non-Destructive Testing, "Non-Destructive Testing Handbook", Vol. 5, 2nd Ed. Columbus Oh.

1.14 Society of Experimental Mechanics, "Handbook on Structural Testing", The Fairmont Press Inc, Bethel, Conn.

1.15 Ian G. Scott, "Basic Acoustic Emission (Nondestructive Testing Monographs and Tracts, Vol. 6)", 1990, Gordon & Breach Science Pub; ISBN: 2881243525

1.16 Fowler T.J. and Scarpellini, "Use of Acoustic Emission in the Design of Glass and Carbon Fiber Reinforced Plastic Pipe", Proceedings 2nd International Symposium on Acoustic Emission from Reinforced Composites", Montreal, Canada, July 21-25 1986, pp. 153-158

1.17 Fowler T.J., "Acoustic Emission of Fiber Reinforced Plastics", Journal of the Technical Councils of ASCE, December 1979, pp. 281-289

1.18 Kline R.A., "Acoustic Emission in Composites", Manual on Experimental Methods for Mechanical Testing of Composites, Society for Experimental Mechanics, Bethel, Conn.

1.19 Bakis C.E. and Reifsnider K.L, "Adiabatic Thermoelastic Measurements", Manual on Experimental Methods for Mechanical Testing of Composites, Society for Experimental Mechanics, Bethel, Conn.

1.20 Society for Experimental Mechanics, Inc., "Handbook on Experimental Mechanics", Prentice-Hall, Inc.

1.21 Anderson T.F., "Detection of Deterioration and Damage of Corrosion Resistance of Thermoplastic and FRP Barrier", Business Report, Anderson Consultants, 535 Oak Drive, Lake Jackson, TX 77566

1.22 Timoshenko, S. and Woinowsky-Krieger, S., "Theory of Plates and Shells", second edition, 1987, McGraw-Hill Book Company, New York.

1.23 Agarwal, B. D. and Broutman, L. J., "Analysis and Performance of Fiber Composites," second edition. 1990, John Wiley and Sons, Inc., New York.

1.24 Bert, C. W. and Birman, V. "Parametric study of thick, orthotropic circular cylindrical shells." Acta Mechanica, vol. 71, pp 61-76,1988.

1.25 Bert, C. W. and Kumar, M., "Vibration of cylindrical shells of bi-modulus materials." Journal of Sound and Vibration, vol. 8, 1982, pp107-121.

1.26 Chandrashekhara, K. and Schroeder, T., "Nonlinear impact analysis of laminated cylindrical and doubly curved shells." Journal of Composite Materials, vol. 29, 1995, pp. 2160-2179.

1.27 Flugge, W., "Stresses in Shells", second edition, 1973, Springer-Verlag, Berlin, Heidelberg, New York. Gerald, C. F, and Wheatley, P.O. (1989) Applied Numerical Analysis, fourth edition. Addison-Wesley Publishing Company, Menlo Park, CA.

1.28 J. Highton and P.D. Soden , "End Reinforcement and Grips for Anisotropic Tubes," Journal of Strain Analysis, Vol. 17, No 1, pp. 31-43 1982, IMechE

1.29 G. Dilintas, "Investigation of a Composite Tubing Connection Performance," Journal of Energy Resources Technology, Vol. 113, pp. 40-48, March 1991, Transactions of ASME

1.30 B.E. Spencer, "The design and application of high performance filament wound composites," 1987 OMAE, pp. 1-6, 1987, OMAE

1.31 Sparks, C.P., Odru, P., Bono, H., and Metivaud, G., "Mechanical Testing of High Performance Composite Tubes for TLP Production Risers," Proceedings, Offshore Technology Conference, OTC 5797, Houston Texas, pp. 191-198.

1.32 Eckold, Geoff, "Design and Manufacture of Composite Structures", McGraw-Hill, Inc.1st Edition, 1994

1.33 Swanson, J., "Introduction to Design and Analysis with Advanced Composite Materials,' Prentice Hall, 1998.

1.34 Hahn, H.T., Erikson, J.B., and Tsai, S.W., "Characterization of Matrix/Interface-Controlled Strength of Unidirectional Composites, in Sih, G.C. and Tamuz, V.P. (eds): Fracture of Composite Materials," 1982, Martinus Nijhoff Publishing, pp.197-214.

1.35 Hashin, Z. and Rotem, A., "A Fatigue Failure Criterion for Fiber-Reinforced Materials," Journal of Composite Materials, 1973, Vol 7, No. 4, pp. 448-464

1.36 Yamada, S.E., and Sun, C.T., "Analysis of Laminate Strength and its Distribution," Journal of Composite Materials, Vol 12, pp. 275-284

1.37 Kim, R.Y., and Soni, S.R. (1984) "Experimental and Analytical Stud-ies on the Onset of Delamination in Laminated Composites," Journal of Composite Materials, Vol.18, pp.70-SO.

1.38 Kim, R.Y., and Soni. S.R., "Failure of Composite Laminates due to Combined Interlaminar Normal and Shear Stress, in Kawata, K., Umekawa, S. and Kobayashi, A. (eds.): Composites'86: Recent Advances in Japan and the United States," Proceedings, 3rd Japan- U.S. Conference on Composite Materials, Tokyo (Japan), 1986, pp.341-350.

1.39 Chang, F.K., and Springer, 0.8. (1986). "The Strength of Fiber Reinforced Composite Bends," Journal of Composite Materials, Vol.20, pp.30-45.

1.40 Brewer, J.C., and Lagace, P.A. (1988). "Quadratic Stress Criterion for Initiation of Delamination," Journal of Composite Materials, Vol.22, pp.1141-1155.

1.41 Hashin, Z., "Failure Criteria for Unidirectional Fiber Composites," Journal of Applied Mechanics, ASME, 1980, Vol.47, pp.329-334.

1.42 Hashin, Z., "Analysis of Composite Materials: A Survey," Journal of Applied Mechanics, ASME, 1983, Vol.50, pp.481-505.

1.43 Hashin, Z., Bagchi, D., and Rosen, B.W. "Nonlinear Behavior of Fiber Composite Laminates," NASA Report, 1974, CR-2318.

1.44 Veavesley, P. J. and Knight, C. E., "An Analytical Model of Strength Loss in Filament Wound Spherical Vessels," Journal of Pressure Vessel Technology, Trans of ASME, Vol.109, August 1987, pp.352-356.

1.45 Chang, J. B., et al., "Enhanced Technology for Composite Overwrapped Pressure Vessels, Program Plan," The Aerospace Corporation, Revised Edition, 9 August 1993.

1.46 Whitney, J. M., Daniel, I. and Pipes, B., "Experimental Mechanics of Fiber Reinforced Composite Materials," Revised Edition, Society for Experimental Mechanics Monograph No.4, 1984.

1.47 Coulter, B. A., "Three Dimensional Elastic Constants for Composite Laminates," AIM No. 90(5530-04)-3 1, The Aerospace Corporation, 8 March 1990.

1.48 Chiu, S. T., Shu, J. C. and Chang, J. B., "Evaluation of Analysis Methods for Composite Overwrapped Pressure Vessels," The 1994 JANNAF NDE and Structures & Mechanical Behavior Joint Meeting, Hill AFB, Utah, 24-28 October, 1994.

1.49 Swanson, S.R., and Christoforou, A.P. (1986). "Response of Quasi-Isotropic Carbon/Epoxy Laminates to Biaxial Stress," Journal of Com-posite Materials, Vol.20, pp.457-471.

1.50 Swanson, S.R., and Christoforou, A.P. (1987). "Progressive Failure in C&-bon/Epoxy Laminates under Biaxial Stress," Journal of Engineering Ma-terials and Technology, Vol.109, pp.12-16.

Chapter 2

2.1 E.D Valenzuela, and W.F Anderson et all, 1993. Comparative Performance of a Composite Drilling Riser in Deep Water. OTC 7263, Offshore Technology Conference.

2.2 Garala, H.J. "Structural evaluation of 8-inch diamter graphite-Epoxy Composite Cylinder Subjected to External Hydrostatic Compressive Loading", Davit Taylor Research Center report DTRC-89/016, Bethesda MD, 1989

2.3 Telegadas, H.K. and Hyer, M.W., "The influence of layer waiviness on Failure of hydrostatically loading thick composite cylinders", Proceedings, First Joint Mechanics Meeting of ASME, ASCE and SES, Mechanics of Thick Composites, AMD-Vol. 162, American Society of Mechanical Engineers, 1993, pp.183-196.

2.4 Abdallah, M.G., Cairns, D.S. and Gascoigne, H.E., "Experimental Inverstigation of Thick Walled Graphite/Epoxy Rings under External hydrostatic Compressive Loading", Proceedings of the SEM Spring Conference on Experimental Mechanics, pp 626-631, Milwakee, Wisconsin, June 1991.

2.5 API Specification 2B (1990). "Specifications for the Fabrication of Structural Steel Pipes", American Petroleum Institute Wahington, D.C., Fourth edition, 10pp

2.6 Sparks, C.P.; Odru, P.; Bono, H. and Metivaud, G., "Mechanical testing of High-Performance Composite Tubes for TLP Production Risers," Proceedings, Offshore Technology Conference, OTC 5797, Houston, Tx, pp.467-472.

2.7 Ouellette, P.; Hoa, S.V.; Sankar, T.S., "Buckling of Composite Cylinders under External Pressure", Polymer Composites, vol.7, No.5, pp 363-374

2.8 Rasheed, Hayder A., "Behavior and Strength of composite Tubes Considering Delamination and other Defects", Doctoral Dissertation, The University of Texas at Austin, Department of Civil Engineering, 1997.

2.9 Al-Hassani, S.T.S. ; Darvizeh, M.; Haftchenari, H., "Analytical study of buckling of composite tubes with various boundary conditions", Composite Structures v 39 n1-2, Sept-Oct 1997 Elsevier Science Ltd, Oxford Engl, p 157-164

2.10 Yang, Chihdar; Pang, Su-Seng; Zhao, Yi, "Buckling analysis of thick-walled composite pipe under external pressure", Journal of Composite Materials v31 n4 1997, Technomic Publications Co. Inc., Lancaster PA, p 409-426

2.11 Anastasiadis, J.S.; Simitses, G.J. "Buckling of Pressure-Loaded, Long, Shear deformable, Cylindrical Laminates Shells", Composite Structures, vol.23, pp.221-231

2.12 Jones, Robert M.., "Mechanics of Composite Materials", Hemisphere Publishing Corp., 1975

2.13 British Standard for Design and Construction of Vessels and Tanks in Reinforced Plastics, BS4994-1987

2.14 SPI Composites Institute, Recommended Practice for Acoustic Emission Testing of Fiberglass Reinforced Plastic Resin (RP) Tanks/Vessels.

2.15 API RP 2A-LRFD "Planing, Designing and Constructing Fixed Offshore Platforms", Load Resistance Factor Design, 1993, Section D, Cylindrical Member Design, pg.49-54

2.16 British Standard for Design and Construction of Vessels and Tanks in Reinforced Plastics, BS4994-1987.

2.17 Code de Construction des Appareils Chaudronnes en Plastique Arme, Commission Chaudronnerie, Genie Chimique du Syndicat General de L'Industrie du Plastique Arme, France, December 1976.

2.18 American Society of Mechanical Engineers, Boiler and Pressure Vessel Code, Section 10, New York, 1989.

2.19 Reinforced Thermoset Plastic Corrosion Resistant Equipment. The American Society of Mechanical Engineers, ASME-ANSI-RTP-1989.

2.20 S.V. Hoa, Analysis for Design of Fiber Reinforced Plastic Vessels and Pipings.

2.21 ANSYS Theory , Elements and Procedures Manual, Version 5.0

2.22 Timoshenko, S.,"Theory of Elastic Stability", Second Edition, McGraw-Hill Publishing Company, 1961

2.23 Kardomateas, G.A.; Chung, C.B.,"Buckling of a thich orthotropic cylindrical shell under external pressure including hygroscopic effects", Mechanics of Thick Composites, Edited by Rajapakse, Y.D.S., AMD-Vol 162, The 1st joint mechanics meeting of ASME, ASCE, SES, 1993, Charlottesville Va.

2.24 Fowler T.J. and Scarpellini, "Use of Acoustic Emission in the Design of Glass and Carbon Fiber Reinforced Plastic Pipe", Proceedings 2nd International Symposium on Acoustic Emission from Reinforced Composites", Montreal, Canada, July 21-25 1986, pp. 153-158

2.25 Michael R. Gorman, "Modal AE: A New Understanding of Acoustic Emission".

2.26 Fowler T.J., "Acoustic Emission of Fiber Reinforced Plastics", Journal of the Technical Councils of ASCE, December 1979, pp. 281-289

2.27 Ian G. Scott, "Basic Acoustic Emission (Nondestructive Testing Monographs and Tracts, Vol. 6)", 1990, Gordon & Breach Science Pub; ISBN: 2881243525

2.28 Barnes, C. Andrew, Doctoral dissertation in progress at the University of Texas at Austin

Chapter 3

3.1 Isham, A. B.,"Design of Fiberglass Reinforced Plastic Chemical Storage Tanks", 21st Annual meeting of the Reinforced Plastics Division, Chicago Illinois, The Society of the Plastics Industry, Inc.

3.2 Reinforced Thermoset Plastic Corrosion Resistant Equipment. The American Society of Mechanical Engineers, ASME-ANSI-RTP-1989.

3.3 American Society of Mechanical Engineers, Boiler and Pressure Vessel Code, Section 10, New York, 1989

3.4 Hull, D., Legg, M.J. and Spencer, B.,"Failure of Glass/Polyester Filament Wound Pipe," Composites, January 1978, pp.17-24.

3.5 Hull, D. and Spencer, B.,"Effect of Winding Angle on the Failure of Filament Wound Pipe," Composites, October 1978, pp.263-271.

3.6 Eckold, Geoff, "Design and Manufacture of Composite Structures",McGraw-Hill, Inc.1st Edition, 1994

3.7 American Water Works Association, Standard C950, "Fiberglass Pressure Pipe", American National Standard

3.8 Y. Promboon and T. J Fowler, "Report of Work in Progress, Source Location on Fiber Reinforced Composite", AECM-12, Proceedings, San Antonio, Texas, May 1998

3.9 Swanson S. R., Christoforou A.P., et al. "Biaxial Testing of Fiber Composites Using Tubular Specimens", Experimental Mechanics. 1988

3.10 Fowler T.J., "Acoustic Emission of Fiber Reinforced Plastics", Journal of the Technical Councils of ASCE, December 1979, pp. 281-289

3.11 Fowler T.J. and Scarpellini, "Use of Acoustic Emission in the Design of Glass and Carbon Fiber Reinforced Plastic Pipe", Proceedings 2nd International Symposium on Acoustic Emission from Reinforced Composites", Montreal, Canada, July 21-25 1986, pp. 153-158

3.12 Jones, Robert M.., "Mechanics of Composite Materials", Hemisphere Publishing Corp., 1975

3.13 The Composites Institute of the Society of Plastics Industry, "Recommended Practice for Acoustic Emission Testing of Fiberglass Reinforced Plastic Resin (RP) Tanks/Vessels", Published by the Committee for Acoustic Emission from Reinforced Plastics (CARP)

3.14 MONPAC Plus evaluation criteria

Chapter 4

4.1 Michael R. Gorman, "Modal AE: A New Understanding of Acoustic Emission", Digital Wave Corporation, Eglewood CO.

4.2 Michael R. Gorman, "New Technology for Wave Based Acoustic Emission and Acousto-Ultrasonics, AMD-Vol. 188, Wave Propagation and Emerging Technologies, ASME 1994

4.3 P.D. Soden, etal, "Strength and Long-Term Behavior of Impact Damaged GRE Pipes", Proceedings, CMOO-2 conference, Houston Texas, October 1997.

4.4 Michael R. Gorman, "Some Connections Between AE Testing of Large Structures and Small Samples", Non-Destructive Evaluation, 1998, Vol. 14, pp.89-104

4.5 Fowler T.J. and Scarpellini, "Use of Acoustic Emission in the Design of Glass and Carbon Fiber Reinforced Plastic Pipe", Proceedings 2nd International Symposium on Acoustic Emission from Reinforced Composites", Montreal, Canada, July 21-25 1986, pp. 153-158

4.6 Fowler T.J., "Acoustic Emission of Fiber Reinforced Plastics", Journal of the Technical Councils of ASCE, December 1979, pp. 281-289

4.7 British Standard for Design and Construction of Vessels and Tanks in Reinforced Plastics, BS4994-1987.

4.8 Code de Construction des Appareils Chaudronnes en Plastique Arme, Commission Chaudronnerie, Genie Chimique du Syndicat General de L'Industrie du Plastique Arme, France, December 1976.

4.9 American Society of Mechanical Engineers, Boiler and Pressure Vessel Code, Section 10, New York, 1989.

4.10 Reinforced Thermoset Plastic Corrosion Resistant Equipment. The American Society of Mechanical Engineers, ASME-ANSI-RTP-1989.

4.11 Y. Promboon and T. J Fowler, "Report of Work in Progress, Source Location on Fiber Reinforced Composite".

4.12 Harding, J., Ruiz, C., "Mechanical behavior of composite materials under impact loading", Key Engineering Materials, v 141-143 n pt 2, 1998 Trans Tech Publ Ltd, Uetikon-Zuerich, Switzerland, pp 403-426

4.13 Matemilola, S. A., Stronge W. J., "Low-speed impact damage in filament-wound CFRP composite pressure vessels", Journal of the Pressure Vessel Society, Transactions of the ASME, November 1997, vol 119, pp 435-443

4.14 Matemilola, S. A., Stronge W. J., "Impact response of composite cylinders", International journal of solid structures, vol, 34, No.21, pp 2669-2684, 1997

4.15 Matemilola, S. A., Stronge W. J., "Impact induced dynamic deformations and stresses in CFRP composite laminates", Composites Engineering, Vol. 5, No. 2, pp 211-222, 1995

4.16 Downs, K. S., Hamstad, M. A., "Acoustic emission from depressurization to detect/evaluate significance of impact damage to graphite/epoxy pressure vessels", Journal of Composite Materials, vol 32, No. 3, 1998, p 258-307

4.17 Alderson, K. L., and Evans, K. E., 1992, "Failure Mechanisms During the Transverse Loading of Filament-Wound pipes Under Static and Low Velocity Impact Conditions," Composites. Vol.23 (3), pp.167-173.

4.18 Alderson, K. L., and Evans, K. E., 1992, "Low Velocity Transverse Impact of Filament-Wound pipes: Part 1. Damage Due to Static and Impact Loads." Composite Structures, Vol.20, pp.37-45.

4.19 Alderson, K. L., and Evans, K. E., 1992, "Low Velocity Transverse Impact of Filament-Wound Pipes: Part 2. Residual Properties and Correlations with Impact Damage." Composite Structures, Vol.20, pp.47-52.

4.20 Budianstry, B., and Fleck, N. A., 1993, "Compressive Failure of Fibre Composites." Journal of Mechanics Physics and of Solids. Vol.41(l), pp.183-211.

4.21 Christoforou, A. P., Swanson, S. R., Ventrello, S. C., and Beckwith, S. W., 1987, "Impact Damage In Carbon/Epoxy Composite Cylinders," 32nd Annual SAMPE Symposium, Sampe Publishing, Corvina USA, pp.904-973.

4.22 Christoforou, A. P., and Swanson, S. R., 1988,"Strength Loss in Composite Cylinders Under Impact," ASME Journal of Engineering Materials and Technology, Vol.110, pp.180-184.

4.23 Christoforou, A. P., and Swanson, S. R., 1990, "Analysis of Simply Supported Orthotropic Cylindrical shells Subjected to Lateral Impact loads," ASME Journal of Applied Mechanics, Vol.57, pp.376-382.

4.24 Clark, G., 1989, "Modelling Of Impact Damage in Composite Laminates," Composites, Vol.20 (3), pp.209-214.

4.25 Hahn, H. T and Williams, J. G., 1986, "Compression Failure Mechanisms in Unidirectional Composites, Composite Materials: Testing and Design, Seventh Conference, ASTM STP 893, J. M. Whitney, ed., American Society for Testing and Materials, Philadelphia, PA, pp. 115-139.

4.26 Lloyd, B. A., and Knight, G. K., 1986, "Impact Damage Sensitivity of Filament-Wound Composite Pressure Vessel," JANNAF Meeting, New Orleans, LA, pp.7-15.

4.27 Goldsmith,W. "Impact: The Theory and Physical Behavior of Colliding Solids." 1960, Edward Arnold (Publishers) Ltd., London.

4.28 Gong, S. W., "A study of impact on composite laminated shells." PhD dissertation, National University of Singapore, 1995, pp.125-145.

4.29 Lee, E. H., "The impact of a mass striking a beam," ASME Journal of Applied Mechanics, vol. 62, 1940, Al 29-i 38.

4.30 Matemilola, S. A. and Stronge, W. J., "Impact micro-damage in resin transfer molded (RTM) carbon fiber composite plates." In Impact and Dynamic Fracture of Polymers and Composites, ESIS 19 (eds J. G. Williams and A. Pavan), 1995, Mechanical Engineering Publications, London, pp.371-381.

4.31 Qian, Y. and Swanson, S. R., "A comparison of solution techniques for impact response of composite plates." Composite Structures, vol. 4, 1990, 177-192.

4.32 Ramkumar, R. L. and Thakar, Y. R., "Dynamics response of curved laminated plates subjected to low velocity impact." ASME Journal of Engineering and Material Technology, vol. 109, 1987, 67-71.

4.33 Tan, T. M. and Sun, C. T. (1985) "Use of static indentation law in the impact analysis of laminated composite plates." Journal of Composite Materials, vol. 52, 1985, pp. 6-12.

4.34 Yang, S. H. and Sun, C. T., "Indentation law for composite laminates." Composite materials: Testing and Design (Sixth Conference), ASTM STP 787, 1982, pp.425-449.

4.35 Timoshenko, S., and Woinowsky-Krieger, S., "Theory of Plates and Shells," 1970, Second edition, McGraw-Hill Book Company, New York, pp. 4-20.

4.36 Jones, Robert M.., "Mechanics of Composite Materials", Hemisphere Publishing Corp., 1975

4.37 Oden, J.P., "Structural testing of impact damaged fiberglass pipes", CMOO-2, Houston, Texas, October 1997.

Chapter 5

5.1 Michael R. Gorman, "Modal AE: A New Understanding of Acoustic Emission".

5.2 Michael R. Gorman, "New Technology for Wave Based Acoustic Emission and Acousto-Ultrasonics, AMD-Vol. 188, Wave Propagation and Emerging Technologies, ASME 1994

5.3 Michael R. Gorman, "Some Connections Between AE Testing of Large Structures and Small Samples", Non-Destructive Evaluation, 1998, Vol. 14, pp.89-104

5.4 Fowler T.J. and Scarpellini, "Use of Acoustic Emission in the Design of Glass and Carbon Fiber Reinforced Plastic Pipe", Proceedings 2nd International Symposium on Acoustic Emission from Reinforced Composites", Montreal, Canada, July 21-25 1986, pp. 153-158

5.5 Fowler T.J., "Acoustic Emission of Fiber Reinforced Plastics", Journal of the Technical Councils of ASCE, December 1979, pp. 281-289

5.6 Gorman, M. R., "Burst-Prediction by Acoustic Emission in Filament-Wound Pressure Vessels," Journal of Acoustic Emission, 9(2):131-139, 1990.

5.7 Hamstad, M.A. and Downs, K.S., "Acoustic Emission from Depressurization to Detect/Evaluate Significance of Impact Damage to Graphite/Epoxy Pressure Vessels", Journal of Composite Materials, Vol. 32, No. 3, 1998.

5.8 MIL-STD-1522A, Standard General Requirements for Safe Design and Operation of Pressurized Missile and Space Systems," 28 May 1984.

5.9 "Computer Program for the Analysis of Filament-Reinforced Metal-Shell Pressure Vessels," NASA CR-72124, May 1966.

5.10 Chen, M. C., "Computer Analysis of Filament-Reinforced Metallic-Spherical Pressure Vessels," Second National Symposium on Computerized Structural Analysis and Design, Washington, D. C., 29-31 March 1976.

5.11 Veavesley, P. J. and Knight, C. E., "An Analytical Model of Strength Loss in Filament Wound Spherical Vessels," Journal of Pressure Vessel Technology, Trans of ASME, Vol.109, August 1987, pp.352-356.

5.12 Chang, J. B., et al., "Enhanced Technology for Composite Overwrapped Pressure Vessels, Program Plan," The Aerospace Corporation, Revised Edition, 9 August 1993.

5.13 Whitney, J. M., Daniel, I. and Pipes, B., "Experimental Mechanics of Fiber Reinforced Composite Materials," Revised Edition, Society for Experimental Mechanics Monograph No.4, 1984.

5.14 Coulter, B. A., "Three Dimensional Elastic Constants for Composite Laminates," AIM No. 90(5530-04)-3 1, The Aerospace Corporation, 8 March 1990.

5.15 Chiu, S. T., Shu, J. C. and Chang, J. B., "Evaluation of Analysis Methods for Composite Overwrapped Pressure Vessels," The 1994 JANNAF NDE and Structures & Mechanical Behavior Joint Meeting, Hill AFB, Utah, pp. 24-28, October, 1994.

5.16 Fuchs, H. O. and Stephens, R I., "Metal Fatigue in Engineering," p.76, John Wiley & Sons, 1980.

5.17 Chang, J. B., et al., "Experimental Evaluation of Space Flight Composite Overwrapped Pressure Vessels," The 1994 JANNAF NDE and Structures & Mechanical Behavior Joint Meeting, Hill AFB, Utah, 24-28 October, 1994

5.18 Schulz, J. C., " Netting Analysis of Filament Wound Pressure Vessels," ASME paper 63-WA-223, November 1963.

5.19 Press, W. H., Flannery, B. P., Teukoisky, S. A. and Vetterling, W. T., "Numerical Recipes, The Art of Scientific Computing," Cambridge University Press, 1989.

5.20 Whittaker, J. W., W. D. Brosey and M. A. Ramstad, "Correlation of Felicity Ratio and Strength Behavior of Impact-Damaged Spherical Composite Test Specimens," Journal of Acoustic Emission, 9(2): 84-90, 1990.

5.21 Gorman, M.R. and T. H. Rytting, "Long Duration AS Events in Filament wound Graphite Epoxy in the 100-300 KHz band Pass Region,': proceedings, First International Symposium on Acoustic Emission from Reinforced Composites. San Francisco, CA: July 9-21 1983, New York: Society of the Plastics Industry', Inc.

5.22 Russell. J. C. and M. R. Gorman, "Acoustic Emission Prediction of Burst Pressures in Twenty-Inch Diameter Filament wound Graphite/Epoxy Bottles." Proceedings. First International Symposium on Acoustic Emission from Reinforced Composites. San Francisco, CA, July 19-21. New York Society of the Plastics Industry. Inc, 1983

5.23 Whittaker, J. W., W. D Brosey and M. A Hamstad, “Correlation of Felicity Ratio and Strength Behavior of Impact-Damaged Spherical Composite Test Specimens, "Journal of Acoustic Emission, 9(2).8~90, 1990.

5.24 Whittaker, J. W., W. D. Brosey and M. A. Hamstad, “Felicity Ratio Behavior of Pneumatically and Hydraulically Loaded Spherical Composite Test Specimens," Journal of Acoustic Emission 9(2);75-83, 1990.

5.25 Hamstad,M. A., J. W. Whittaker and W. D. Brosey, "Correlation of Residual Strength with Acoustic Emission from Impact-Damaged Composite Structures under Constant Biaxial Load," Journal of Composite Materials, 26(15)2307-2328, 1992.

5.26 Downs, K. S. and MA. Hamstad, "Correlation of Acoustic Emission Felicity Ratios and Hold-Based Rate Moments with Burst Strengths of spherical Graphite/Epoxy Pressure Vessels," Journal of Acoustic Emission, 13(31); 45-55, 1995.

5.27 Shiwa M., M. Enoki, T. Kishi and S. Kohara, “Acoustic Emission during Tensile. Loading-Holding and Unloading-Reloading Testing in Fiberglass-Epoxy Composites," Proceedings 2nd International Symposium on Acoustic Emission from Reinforced Composites, Montreal, Canada, July, 21-25 New York: The Society of the Plastics Industry, Inc., pp .44-49.

5.28 Awerbuch, J. and S. Ghaffari, “Effect of Friction-Generated Emission on Monitoring Damage in Composite Laminates through Acoustic Emission," Proceedings, Progress in Acoustic Emission III: 8th International Acoustic Emission Symposium. K Yamaguchi, K. Aoki and T. Kishi (eds.), Tokyo, Japan, October 21-24, pp 638-652, 1986

5.29 Awerbuch, J. and S. Ghaffari, “Monitoring Progression of Matrix Splitting during fatigue Loading through Acoustic Emission in Notched Unidirectional Graphite/Epoxy Composites," Proceedings. 2nd International Symposium on Acoustic Emission from Reinforced Composites, Montreal, Canada, July2l-25, New York; The Society of the Plastics Industry, Inc., pp.5l-58, 1986.

5.30 Downs, K S. and M. A. Hamstad, "Correlation of Regions of Acoustic Emission Activity with Burst Locations for Spherical Graphite Epoxy Pressure Vessels," Journal of Acoustic Emission 13(311): 56-66, 1995.

5.31 Hamstad, M. A. and C. M Fortunko, "Development of Practical Wide-band High Fidelity Acoustic Emission Sensors." Proceedings. Non-Destructive Evaluation of Aging Bridges and Highways, S. Chase (ed.), SPIE, 2456:281-288, 1995.

5.32 Hamstad, M. A and K. S. Downs, "On Characterization and Location of Acoustic Emission Sources in Real Size Composite Structures - A Waveform Study," Journal of Acoustic Emission, vol. 3(l-2):3l, 1995.